Internal and Interface Shear Strength of Geosynthetic Clay Liners (GCLs)

by

John Scott McCartney, M.S.
Jorge G. Zornberg, PhD, P.E.
Robert H. Swan, Jr., P.E.

Geotechnical Research Report

Department of Civil, Environmental and Architectural Engineering

At the University of Colorado at Boulder

May 2002

McCartney, John S., Zornberg, Jorge G., and Swan, Jr., Robert H.

Internal and Interface Shear Strength of Geosynthetic Clay Liners (GCLs)

Geosynthetic Clay Liners (GCLs) are prefabricated geocomposite materials used as an alternative to compacted clay liners in hydraulic barriers. They often offer hydraulic performance equivalent to that of compacted clay liners with lower costs, easier constructability and less space requirements. However, the internal and interface shear strength of GCLs is known to be significantly lower than that of compacted clay liners, so their use in a landfill cap or base liner system requires a careful shear strength assessment. Because of the significant time and effort involved in GCL shear strength testing, clear understanding of shear strength data collected for this material may provide insight that complements often limited project-specific testing conducted for engineering design. This report investigates the mechanical behavior of GCLs by providing a state-of-the-art review of internal and interface GCL shear strength testing to date, providing new information through the analysis of a significant database of GCL internal and interface direct shear test results, and the impact of variability in shear strength data on stability of liner systems. A reliability based design methodology is also proposed to address the effect of shear strength variability and field loading conditions on the stability of clay liners.

The shear strength test results from the database are sufficient in scale to develop probabilistic descriptions of the peak and large-displacement internal and interface shear strength for different GCL conditions that may be found in the field. The wide range of test conditions present is suitable for quantification of the effects of normal stress during shearing, normal stress during hydration, time of hydration, time of consolidation and shear displacement rate on GCL shear strength. The water content at failure and the displacement at peak shear strength are also discussed.

In general, it was found that the internal GCL shear strength increases with increasing normal stress during shearing, normal stress during hydration, time of consolidation and shear displacement rate (at low normal stress), and decreases with increasing time of hydration and shear displacement rate (at high normal stresses). The interface shear strength between a GCL and a geomembrane is consistently below the internal GCL shear strength. Analysis of the results indicate that the interface shear strength increases with increasing time of hydration and hydration normal stress, and is unaffected by time of consolidation and shear displacement rate. Observed changes in GCL shear strength behavior can be attributed to the swelling of sodium bentonite, pore pressure generation during shearing, extrusion of sodium bentonite from the GCL, fiber reinforcement rupture, fiber reinforcement pullout from the GCL carrier geotextiles, and GCL-geomembrane interlocking.

1 Introduction 1
1.1 Motivation of this Study 1
1.2 GCL Internal and Interface Shear Strength Database 2
1.3 Important Issues on GCL Shear Strength Addressed in this Report 2
1.4 Report Organization 4
2 Materials and Test Methods 6
2.1 Introduction 6
2.2 Materials 7
2.2.1 Sodium Bentonite Clay 7
2.2.2 Geosynthetic Clay Liners (GCLs) 7
2.2.3 Geomembranes 10
2.3 Overview of Shear Strength Testing on GCLs 12
2.4 Characterization of Shear Strength Envelopes of GCLs 13
2.5 Laboratory Test Methods 15
2.5.1 Background 15
2.5.2 Direct Shear Testing 15
2.5.3 Ring Shear Testing 19
2.5.4 Verification of Direct Shear and Ring Shear Device Test Results 19
2.5.5 Other Test Methods 21
3 State-of-the-Art Review of Shear Strength Testing of GCLs 30
3.1 Introduction 30
3.2 Shear Strength of Sodium Bentonite Clay 31
3.2.1 Introduction 31
3.2.2 Effect of Sodium Bentonite Swell 32
3.2.3 Non-Linear Failure Envelope 34
3.2.4 Residual Shear Strength of Sodium Bentonite Clay 34
3.3 Internal Shear Strength of GCLs 35
3.3.1 Background and Significance 35
3.3.2 Hydration History of Sodium Bentonite Clay in GCLs 35
3.3.3 Effect of GCL Hydration 36
3.3.4 Effect of Sodium Bentonite Swelling 38
3.3.5 Effect of GCL Consolidation 39
3.3.6 Effect of Normal Stress 41
3.3.6.1 Effect of Hydration Normal Stress 41
3.3.6.2 Effect of Normal Stress Used During Shearing 42
3.3.7 Effect of Shear Displacement Rate 43
3.3.8 Peak Shear Displacement Magnitude 46
3.3.9 Failure Plane Location 47
3.3.10 Effect of GCL Reinforcement 47
3.3.11 Effect of Specimen Size and Confinement Procedures 49
3.4 Interface Shear Strength between GCLs and Geomembranes 51
3.4.1 Background and Significance 51
3.4.2 Effect of GCL Swell 52
3.4.3 Effect of Normal Stress 54
3.4.4 Effect of Shear Displacement Rate 54
3.4.5 Peak Shear Displacement Magnitude 54

3.4.6 Effect of Internal GCL Reinforcement 55
3.4.7 Effect of Geomembrane Texturing 56
3.4.8 Effect of Geomembrane Polymers 58
3.5 Conclusions 58
4 Internal Shear Strength of GCLs 61
4.1 Overview of the Database of Internal Shear Strength of GCLs 61
4.1.1 The GCLSS Database 61
4.1.2 Information Included in the GCLSS Database 61
4.1.3 Shear Strength Test Procedures 61
4.2 Shear Strength Test Results and Preliminary Analysis 64
4.2.1 Histogram Analysis 64
4.2.2 Equivalent Friction Angle Analysis 67
4.2.2.1 Background 67
4.2.2.2 Effect of GCL Reinforcement 71
4.2.2.3 Effect of GCL Test Conditions 80
4.3 Internal GCL Shear Strength Analysis 82
4.3.1 Typical Shear Force-Displacement Curves 82
4.3.2 Effect of Test Conditions on Failure Envelopes 83
4.3.2.1 Analysis of GCL A 84
4.3.2.2 Analysis of GCL B 90
4.3.2.3 Analysis of GCL C, D and E 92
4.3.2.4 Analysis of an Unreinforced GCL (GCL F) 95
4.3.2.5 Analysis of Other GCLs 96
4.3.2.6 Comparisons between Failure Envelopes 98
4.3.3 Shear Displacement Rate Analysis 101
4.3.4 Time of Hydration Analysis 103
4.3.5 Time of Consolidation Analysis 104
4.3.6 Variability Analysis 105
4.3.7 Final GCL Water Content Analysis 108
4.3.8 Analysis of Displacement at Peak Shear Strength 111
4.4 Summary and Conclusions 113
4.4.1 Summary 113
4.4.2 Conclusions 114
5 Shear Strength of GCL-Geomembrane Interfaces 222
5.1 Overview of the Database of Interface Shear Strength of GCLs 222
5.1.1 The GCLSS Database 222
5.1.2 Information Included in the GCLSS Database 222
5.1.3 Shear Strength Test Procedures 222
5.2 Shear Strength Results and Preliminary Analysis 223
5.2.1 Background 223
5.2.2 Histogram Analysis 225
5.2.3 Equivalent Friction Angle Analysis 225
5.3 Internal GCL Shear Strength Analysis 233
5.3.1 Shear Force-Displacement Curves 233
5.3.2 Effect of Test Conditions on Failure Envelopes 236
5.3.2.1 Textured HDPE Geomembrane Interfaces with GCL K 236

5.3.2.2 Textured HDPE Geomembrane Interfaces with GCL C 238
5.3.2.3 Textured HDPE Geomembrane Interfaces with GCL A 239
5.3.2.4 Textured HDPE Geomembrane Interfaces with GCL B 242
5.3.2.5 Textured VLDPE Geomembrane Interfaces 243
5.3.2.6 Textured LLDPE Geomembrane Interfaces 245
5.3.2.7 Smooth HDPE Geomembrane Interfaces 246
5.3.2.8 Smooth VLDPE Geomembrane Interfaces 247
5.3.2.9 Smooth LLDPE Geomembrane Interfaces 248
5.3.2.10 PVC Geomembrane Interfaces 249
5.3.2.11 Test Results Reported from Other Studies 250
5.3.2.12 Comparisons between Failure Envelopes 251
5.3.3 Shear Displacement Rate Analysis 255
5.3.4 Time of Hydration Analysis 256
5.3.5 Time of Consolidation / Hydration Normal Stress Analysis 258
5.3.6 Variability Analysis 259
5.3.7 Analysis of the Final GCL Water Content 261
5.3.8 Analysis of Displacement at Peak Shear Strength 262
5.4 Comparisons between Internal and Interface GCL Shear Strength 263
5.5 Summary and Conclusions 265
5.5.1 Summary 265
5.5.2 Conclusions 265
6 Application to Geotechnical Design 363
6.1 Introduction 363
6.2 Conventional Approach to Infinite Slope Design 363
6.3 Introduction to Probability and Reliability Based Design Concepts 365
6.3.1 Background 365
6.3.2 Random Variables 366
6.3.6 Limit State Analysis 367
6.3.7 The Reliability Index 367
6.4 Reliability Based Design/Analysis of Infinite Slopes 368
6.4.1 Background 368
6.4.2 Definition of Variables 369
6.4.3 Formulation of Infinite Slope Problem 370
6.7 Conclusions 372
7 Summary and Conclusions 379
7.1 Summary 379
7.2 Conclusions on Internal GCL Shear Strength 380
7.3 Conclusions on GCL-Geomembrane Interface Shear Strength 381
7.4 Suggestions for Laboratory Procedures 382
References 384

Table of Tables

Table 2.1: GCLs in the GCLSS Database Tested for Internal Shear Strength Listed by Product Name; with Labels and Reinforcement Description 23
Table 2.2: GCLs Tested for GCL-Geomembrane Interface Shear Strength Listed By Product Name; with Labels and Reinforcement Description 23
Table 2.3: Definitions of the Different Geomembrane Polymer and Surface Characteristics..... 24
Table 2.4: Geomembranes Tested for GCL-Geomembrane Interface Shear Strength Listed by Manufacturer; with Labels and Polymer Types Manufactured 24
Table 2.5: Comparison between Different Test Procedures for Sodium Bentonite Clay and GCLs 25
Table 3.1: Triaxial Cell Shear Strength Test Results for a Sodium Montmorillonite Clay reported by Mesri and Olson (1970) 59
Table 3.2: Failure Envelope Data for Different Levels of Confining Pressure for Sodium Montmorillonite Clay 59
Table 4.1: Definition of Variables used in the GCLSS Database..... 118
Table 4.2: Sets of GCLs in the GCLSS Database..... 118
Table 4.3 Results of Direct Shear Tests on GCLs A and F (Fox *et. al.*, 1998) 119
Table 4.4: Results of Ring Shear Tests on GCL A (Eid and Stark, 1999)..... 119
Table 4.5: Results of Direct Shear Tests on a Needle-Punched GCL (Berard, 1997) 119
Table 4.6: Results of Direct Shear Tests on a Needle-Punched GCL (GCL A) Reported by Gilbert *et. al.* (1996)..... 120
Table 4.7: Equivalent Friction Angles for Different GCL Sets with Standard Deviation, Upper Bound and Lower Bound 120
Table 4.8: Effects of Test Conditions on the Shear Strength of GCL A 121
Table 4.9: Failure Envelopes for All GCLs in the GCLSS Database..... 122
Table 4.10: Failure Envelope for GCL A (FE A1: t_H = 24 hrs, t_C = 0 hrs and SDR = 1.0 mm/min); *Baseline Failure Envelope*..... 123
Table 4.11: Failure Envelope for GCL A (FE A2: t_H = 24 hrs, t_C = 0 hrs and SDR = 0.5 mm/min)..... 124
Table 4.12: Failure Envelope for GCL A (FE A3: t_H = 48 hrs, t_C = 0 hrs and SDR = 1.0 mm/min)..... 125
Table 4.13: Failure Envelope for GCL A (FE A4: t_H = 72 hrs, t_C = 0 hrs and SDR = 1.0 mm/min)..... 125
Table 4.14: Failure Envelope for GCL A (FE A5: t_H = 168 hrs, t_C = 48 hrs and SDR = 0.1 mm/min)..... 126
Table 4.15: Failure Envelope for GCL A (FE A6: Staged Hydration and Consolidation, SDR = 0.0015 mm/min) 127
Table 4.16: Failure Envelopes for GCL A (FE A7a and A7b: t_H = 24 and 60 hrs, respectively, t_C = 12 and 24 hrs, respectively, and SDR = 1.0 mm/min) 127
Table 4.17: Failure Envelope for GCL A (FE A8: t_H = 0 hrs (Dry), t_C = 0 hrs and SDR = 1.0 mm/min) 127
Table 4.18: Failure Envelope for GCL B (FE B1: t_H = 24 hrs, t_C = 0 hrs and SDR = 1.0 mm/min); *Baseline Failure Envelope*..... 128

Table 4.19: Failure Envelope for GCL B (FE B2: t_H = 48 hrs, t_C = 0 hrs and SDR = 1.0 mm/min)..... 128
Table 4.20: Failure Envelope for GCL B (FE B3: t_H = 96 hrs, t_C = 0 hrs and SDR = 1.0 mm/min)..... 129
Table 4.21: Failure Envelope for GCL B (FE B4: t_H = 168 hrs, t_C = 48 hrs and SDR = 0.1 mm/min)..... 129
Table 4.22: Failure Envelope for GCL C (FE C1: t_H = 24 hrs, t_C = 0 hrs and SDR = 0.5 mm/min); *Baseline Failure Envelope*..... 129
Table 4.23: Failure Envelope for GCL C (FE C2: t_H = 24 hrs, t_C = 0 hrs and SDR = 0.2 mm/min)..... 130
Table 4.24: Failure Envelope for GCL C (FE C3: t_H = 168 hrs, t_C = 48 hrs and SDR = 0.1 mm/min)..... 130
Table 4.25: Failure Envelopes for GCL D (FE D1, D2 and D3)..... 130
Table 4.26: Failure Envelopes for GCL E (FE E1 and E2: No Consolidation, SDR = 1.0 mm/min)..... 131
Table 4.27: Failure Envelopes for GCL F (FE F1 and F2)..... 131
Table 4.28: Failure Envelope for GCL G (FE G1: t_H = 24 hrs, t_C = 0 hrs and SDR = 1.0 mm/min)..... 131
Table 4.29: Failure Envelopes for GCL H (FE H1, H2 and H3)..... 132
Table 4.30: Failure Envelopes for GCL I (FE I1 and I2)..... 132
Table 4.31: Failure Envelope for GCL J (FE J1: t_H = 24 hrs, t_C = 0 hrs and SDR = 1.0 mm/min)..... 132
Table 4.32: Best-Fit Friction Angles and Adhesive Values for the Peak and Large-Displacement Shear Strength Failure Envelopes..... 133
Table 4.33: Effect of Shear Displacement Rate on the Shear Strength of GCL A; Low and High Normal Stresses (50 kPa and 517.1 kPa, respectively)..... 134
Table 4.34: Effect of Shear Displacement Rate on the Peak Shear Strength of GCL C; Normal Stress of 50 kPa..... 134
Table 4.35: Effect of Shear Displacement Rate on the Shear Strength of an Unreinforced, Unhydrated GCL (GCL F); Normal Stress of 275.8 kPa..... 134
Table 4.36: Effect of Time of Hydration on the Peak Shear Strength of GCL A (a) Data Grouped by Normal Stress Level, (b) Data Grouped by Time of Hydration..... 135
Table 4.37: Effect of Hydration Procedure on GCL A..... 135
Table 4.38: Statistical Data Representing the Variability of GCL A (FE A5, t_H = 168 hours, t_C = 48 hours, SDR = 0.1 mm/min)..... 136
Table 4.39: Statistical Data Representing the Variability of GCL A (FE A2, t_H = 48 hours, t_C = 0 hours, SDR = 1.0 mm/min)..... 136
Table 4.40: Variability of Direct Shear Tests Results on Dry GCL A Specimens at a Normal Stress of 517.1 kPa..... 137
Table 4.41: Displacement at Peak Shear Strength and Final GCL Water Content Data for GCL A (FE A8: t_H = 0 hours, t_C = 0 hours, SDR = 1.0 mm/min)..... 137
Table 4.42: Displacement at Peak and Large Displacement Shear Strengths and Final GCL Water Content Data for GCL A (FE A5: t_H = 168 hours, t_C = 48 hours, SDR = 0.1 mm/min)..... 138

Table 4.43: Statistical Data for Displacement at Peak Shear Strength and Final GCL Water Content Data for Three GCLs under Identical Test Conditions (FE A5, B4 and C3: t_H = 168 hours, t_C = 48 hours, SDR = 0.1 mm/min) 139
Table 4.44: Displacement at Peak Shear Strength and Final GCL Water Content Data for GCL A; Effect of Variability and Shear Displacement Rate 139
Table 4.45: Displacement at Peak Shear Strength and Final GCL Water Content Data for an Unreinforced GCL (GCL F) 139
Table 5.1: GCL-Geomembrane Interface Sets 269
Table 5.2: Shear Strength Test Results for Interfaces between the Woven Geotextile of GCL A and a THDPE Geomembrane Reported by Pavlik (1997); t_H = 48 hours, t_C = 0 hours, SDR = 1 mm/min 269
Table 5.3: Shear Strength Test Results for Interfaces between the Woven Geotextile of GCL A and Different Geomembranes Reported by Triplett and Fox (2001); t_H = 48 hours, t_C = 0 hours, SDR = 0.1 mm/min 270
Table 5.4: Equivalent Friction Angles for GCL-Geomembrane Sets 270
Table 5.5: Equivalent Friction Angles for GCL-THDPE Geomembrane Sets 271
Table 5.6: Equivalent Friction Angles (Defined for Less than 50 kPa) for Different GCL-Geomembrane Interfaces for *Low* Normal Stresses 271
Table 5.7: Failure Envelopes for Different GCL-Geomembrane Interfaces 272
Table 5.8: Shear Strength Tests on the Interface between a GCL and a Textured HDPE Geomembrane; Failure Envelopes TH 1 and TH 2 (Different Times of Hydration, No Consolidation, SDR = 1.0 mm/min) 273
Table 5.9: Shear Strength Tests on the Interface between GCL C and a Textured HDPE Geomembrane; Failure Envelope TH 3 (Different Times of Hydration, No Consolidation, SDR = 1.0 mm/min) 273
Table 5.10: Shear Strength Tests on the Interface between GCL C and a Textured HDPE Geomembrane; Failure Envelope TH 4 (Same Times of Hydration, No Consolidation, Different Shear Displacement Rates) 274
Table 5.11: Shear Strength Tests on the Interface between GCL C and a Textured HDPE Geomembrane; Failure Envelope TH 5 (t_H = 168 hours, t_C = 48 hours, SDR = 0.1 mm/min) 275
Table 5.12: Shear Strength Tests on the Interface between GCL A and a Textured HDPE Geomembrane; Failure Envelope TH 6 (No Hydration, No Consolidation, SDR = 1.0 mm/min) 275
Table 5.13: Shear Strength Tests on the Interface between GCL A and a Textured HDPE Geomembrane; Failure Envelope TH 7 (t_H = 24 hours, t_C = 0 hours, SDR = 1.0 mm/min 276
Table 5.14: Shear Strength Tests on the Interface between GCL A and a Textured HDPE Geomembrane; Failure Envelope TH 8 (t_H = 48 hours, t_C = 0 hours, SDR = 1.0 mm/min) 277
Table 5.15: Shear Strength Tests on the Interface between GCL A and a Textured HDPE Geomembrane; Failure Envelope TH 9 (Different Times of Hydration, No Consolidation, Different Shear Displacement Rates) 278
Table 5.16: Shear Strength Tests on the Interface between GCL A and a Textured HDPE Geomembrane; Failure Envelope TH 10 (Different Times of Hydration, Different Times of Consolidation, SDR = 1.0 mm/min) 278

Table 5.17: Shear Strength Tests on the Interface between GCL A and a Textured HDPE Geomembrane s; Failure Envelope TH 11 (t_H = 168 hours, t_C = 48 hours, SDR = 0.1 mm/min)..... 279
Table 5.18: Shear Strength Tests on the Interface between GCL B and a Textured HDPE Geomembrane; Failure Envelope TH 12 (No Hydration, No Consolidation, SDR = 1.0 mm/min) 280
Table 5.19: Shear Strength Tests on the Interface between GCL B and a Textured HDPE Geomembrane; Failure Envelope TH 13 (t_H = 24 hours, No Consolidation, SDR = 1.0 mm/min) 281
Table 5.20: Shear Strength Tests on the Interface between GCL B and a Textured HDPE Geomembrane; Failure Envelope TH 14 (t_H = 48 hours, No Consolidation, SDR = 1.0 mm/min) 282
Table 5.21: Shear Strength Tests on the Interface between GCL B and a Textured HDPE Geomembrane; Failure Envelope TH 15 (t_H = 168 hours, t_C = 48 hours, SDR = 0.1 mm/min)..... 282
Table 5.22: Shear Strength Tests on the Interface between a GCL and a Textured VLDPE Geomembrane; Failure Envelopes TV 1, 2 and 3 (Different Times of Hydration, No Consolidation, SDR = 1.0 mm/min) 283
Table 5.23: Shear Strength Tests on the Interface between a GCL and a Textured LLDPE Geomembrane; Failure Envelopes TL 1, 2 and 3 (Different Times of Hydration and Consolidation, SDR = 1.0 mm/min) 284
Table 5.24: Shear Strength Tests on the Interface between a GCL and Smooth Geomembranes; Failure Envelopes SH 1 and 2, SV 1 and 2 and SL 1 and 2 (Different Times of Hydration, No Consolidation, SDR = 1.0 mm/min)..... 285
Table 5.25: Shear Strength Tests on the Interface between GCL A and a Smooth or Faille Finish PVC Geomembrane; Failure Envelopes PVC 1 a, b and c (Different Times of Hydration and Consolidation, SDR = 1.0 mm/min)..... 286
Table 5.26: Linear Best-Fit Line Results for All GCL-Geomembrane Failure Envelopes..... 287
Table 5.27: Comparison of the Average Shear Strengths for Failure Envelopes TH 5, TH 11 and TH 15 (t_H = 168 hours, t_C = 48 hours, SDR = 0.1 mm/min)..... 288
Table 5.28: Effect of the Shear Displacement Rate on the Interface between GCL C and a 60 mil Textured HDPE GM t (t_H = 24 hours, Hydration Normal Stress = 13.8 kPa, Average Final Water Content = 105%, No Consolidation)..... 288
Table 5.29: Effect of the Shear Displacement Rate on the Interface between GCL A and a 60 mil Textured HDPE GM s (t_H = 48 hours, No Consolidation)..... 289
Table 5.30: Effect of the Time of Hydration on the Interface between GCL A and a 60/80 mil Textured HDPE GM s (No Consolidation, SDR = 1.0 mm/min). 289
Table 5.31: Effect of the Time of Hydration on the Interface between GCL B and a 60 mil Textured HDPE GM s (No Consolidation, SDR = 1.0 mm/min)..... 289
Table 5.32: Effect of Different Hydration and Consolidation Times on the Shear Strength of the Interface between GCL B and textured HDPE geomembrane; Constant Normal Stress of 698.5 kPa (SDR = 1.0 mm/min)..... 290
Table 5.33: Statistical Results for the Shear Strength Tests on the Interface between GCL A and a Smooth PVC Geomembrane; Effect of Different Hydration Procedures (SDR = 1.0 mm/min) 290

Table 5.34: Effect of the Time of Consolidation on the Interface between GCL A and a 60 mil Textured HDPE GM v (t_H = 48 hours, No Consolidation) 290
Table 5.35: Variability of the Interface between GCL A and Geomembrane *s*, Listed by Test Series (FE TH 11, t_H = 168 hours, t_C = 48 hours, SDR = 0.1 mm/min) 291
Table 5.36: Comparison of the Displacements at Peak Shear Strength and Final Water Contents for Failure Envelopes TH 5, TH 11 and TH 15 (tH = 168 hours, tC = 48 hours, SDR = 0.1 mm/min) 291
Table 5.37: Displacements at Peak Shear Strength and Final Water Contents for Failure Envelope TH 5 (t_H = 168 hours, t_C = 48 hours, SDR = 0.1 mm/min) 291
Table 5.38: Displacements at Peak Shear Strength and Final Water Contents for Failure Envelope TH 11 (t_H = 168 hours, t_C = 48 hours, SDR = 0.1 mm/min) 292
Table 5.39: Displacements at Peak Shear Strength and Final GCL Water Contents for Failure Envelope TH 15 (t_H = 168 hours, t_C = 48 hours, SDR = 0.1 mm/min) 293
Table 5.40: Comparison of the Average Shear Strengths for Internal GCL Failure Envelopes A5, B4 and C3 and the Average Shear Strengths for GCL-GM Interface Failure Envelopes TH 5, TH 11 and TH 15 (t_H = 168 hours, t_C = 48 hours, SDR = 0.1 mm/min) 293
Table 5.41: Comparison of the Average Displacements at Peak Shear Strength and Average Final Water Contents for Internal and Interface GCL Failure Envelopes A5, B4, C3, TH 5, TH 11 and TH 15 (t_H = 168 hours, t_C = 48 hours, SDR = 0.1 mm/min) 294
Table 6.1: Development of Peak and Large Displacement Failure Envelope Parameters *c* and ϕ for an Internal GCL *A* Interface (t_H = 168 hours, t_C = 48 hours and SDR = 0.1 mm/min) 373
Table 6.2: Development of Peak and Large Displacement Failure Envelope Parameters *c* and ϕ for the Interface between GCL *A* and an 80-mil Geomembrane *s* (t_H = 168 hours, t_C = 48 hours and SDR = 0.1 mm/min) ... 374

Table of Figures

Figure 2.1: Typical Unreinforced GCLs: (a) Sodium Bentonite Mixed with Adhesives, Sandwiched Between Two Geotextiles; (b) Sodium Bentonite Mixed with Adhesives, Adhered to a Geomembrane 26
Figure 2.2: Typical Reinforced GCLs: (a) Sodium Bentonite Sandwiched between Woven and Nonwoven Geotextiles, Needle-Punched; (b) Sodium Bentonite Sandwiched between Two Nonwoven Geotextiles, Needle-Punched; (c) Sodium Bentonite Sandwiched between Woven and Nonwoven Geotextiles, Needle-Punched with Thermal Bonding; (d) Sodium Bentonite Sandwiched between Two Woven Geotextiles, Stitch-Bonded Together..... 26
Figure 2.3: Variation in Shear Stress with Shear Displacement for Different Test Normal Stresses 27
Figure 2.4: Shear Strength at Failure for Different Test Normal Stresses; Assuming a Linear Failure Envelope..... 27
Figure 2.5: GCL Specimen Confinement in the Direct Shear Device (Internal Shear Testing Configuration); Not to Scale..... 28
Figure 2.6: GCL-Geomembrane Specimen Confinement in the Direct Shear Device (Interface Shear Testing Configuration); Not to Scale 28
Figure 2.7: Direct Shear Device for (a) Low, (b) Medium, (c) High Normal Stresses 29
Figure 3.1: Peak Shear Strength Failure Envelopes for Unreinforced Sodium Bentonite Clay (Mesri and Olson, 1970) with Linear Best-Fit Line 30
Figure 3.2: Peak Shear Strength Failure Envelopes for Unreinforced Sodium Bentonite Clay (Mesri and Olson, 1970) with Bilinear Best Fit Lines..... 30
Figure 4.1: Histogram of the GCL Product Types Undergoing Internal Shear Strength Testing, Total of 320 Direct Shear Tests 140
Figure 4.2: Histogram of Normal Stresses Applied During Shearing to All GCLs in the GCLSS Database, Total of 320 Direct Shear Tests 140
Figure 4.3: Histogram of Times of Hydration Used During Testing of All GCLs in the GCLSS Database. Total of 320 Direct Shear Tests (t_H = 0 means Unhydrated) 141
Figure 4.4: Histogram of Hydration Normal Stresses Applied to All GCLs in the GCLSS Database. Total of 320 Direct Shear Tests (Unhydrated Tests Do Not Have a Hydration Normal Stress) 141
Figure 4.5: Histogram of Times of Consolidation Used During Testing of All GCLs in the GCLSS Database. Total of 320 Direct Shear Tests 142
Figure 4.6: Histogram of Consolidation Normal Stresses Applied to All GCLs in the GCLSS Database. Total of 320 Direct Shear Tests 142
Figure 4.7: Histogram of the Final Water Content of Each GCL in the GCLSS Database. Total of 320 Direct Shear Tests..... 143
Figure 4.8: Histogram of the Hydration Procedure for Each GCL in the GCLSS Database. Total of 320 Direct Shear Tests..... 143
Figure 4.9: Histogram of Shear Displacement Rates Used During Testing of All GCLs in the GCLSS Database. Total of 320 Direct Shear Tests..... 144
Figure 4.10: Histogram of Reinforcement Type for All GCLs in the GCLSS Database, Total of 320 Direct Shear Tests (NP = Needle-Punched, SB =

Stitch-Bonded, UN = Unreinforced, W = Woven Backing Geotextile, NW = Nonwoven Backing Geotextile, TB = Thermally Bonded) 144
Figure 4.11: Peak Shear Strength for All GCL Types Included in the GCLSS Database (Total of 320 Tests); (a) Ranges of Equivalent Friction Angles for the Complete Data Set, (b) Detail for Low Normal Stresses 145
Figure 4.12: Peak Shear Strength for All GCL Types Included in the GCLSS Database (Total of 320 Tests); (a) Average Equivalent Friction Angle with Upper and Lower Bounds, (b) Detail for Low Normal Stresses..... 146
Figure 4.13: Large Displacement Shear Strength for All GCL Types Included in the GCLSS Database (Total of 187 Tests); (a) Ranges of Equivalent Friction Angles for the Complete Data Set, (b) Detail for Low Normal Stresses 147
Figure 4.14: Large Displacement Shear Strength for All GCL Types Included in the GCLSS Database (Total of 187 Tests); (a) Average Equivalent Friction Angle with Upper and Lower Bounds, (b) Detail for Low Normal Stresses 148
Figure 4.15: Peak Shear Strengths Test Results for All Reinforced GCLs (Total of 313 Tests); (a) Ranges of Equivalent Friction Angles, (b) Average Equivalent Friction Angle with Upper and Lower Bounds..... 149
Figure 4.16: Large Displacement Shear Strengths Test Results for All Reinforced GCLs (Total of 313 Tests); (a) Ranges of Equivalent Friction Angles, (b) Average Equivalent Friction Angle with Upper and Lower Bounds..... 150
Figure 4.17: Peak Shear Strengths Test Results for All Unreinforced GCLs (Total of 7 Tests); (a) Ranges of Equivalent Friction Angles (with Test Results Reported by Other Studies), (b) Average Equivalent Friction Angle with Upper and Lower Bounds (Results of Other Studies Not Included) 151
Figure 4.18: Large Displacement Shear Strengths Test Results for All Unreinforced GCLs (Total of 7 Tests); (a) Ranges of Equivalent Friction Angles (with Test Results Reported by Other Studies), (b) Average Equivalent Friction Angle with Upper and Lower Bounds (Results of Other Studies Not Included) 152
Figure 4.19: Peak Shear Strength for All Stitch-Bonded GCLs in the GCLSS Database (Total of 48 Tests); (a) Ranges of Equivalent Friction Angles, (b) Average Equivalent Friction Angle with Upper and Lower Bounds..... 153
Figure 4.20: Large Displacement Shear Strength for All Stitch-Bonded GCLs in the GCLSS Database (Total of 5 Tests); (a) Ranges of Equivalent Friction Angles, (b) Average Equivalent Friction Angle with Upper and Lower Bounds 154
Figure 4.21: Peak Shear Strength for All Needle-Punched GCLs in the GCLSS Database (Total of 265 Tests); (a) Ranges of Equivalent Friction Angles, (b) Average Equivalent Friction Angle with Upper and Lower Bounds..... 155
Figure 4.22: Large Displacement Shear Strength for All Needle-Punched GCLs in the GCLSS Database (Total of 175 Tests); (a) Ranges of Equivalent Friction Angles, (b) Average Equivalent Friction Angle with Upper and Lower Bounds 156
Figure 4.23: Peak Shear Strength for All Bentomat GCLs (Total of 211 Tests); (a) Ranges of Equivalent Friction Angles, (b) Average Equivalent Friction Angle with Upper and Lower Bounds 157

Figure 4.24: Large Displacement Shear Strength for All Bentomat GCLs (Total of 124 Tests); (a) Ranges of Equivalent Friction Angles, (b) Average Equivalent Friction Angle with Upper and Lower Bounds..... 158
Figure 4.25: Peak Shear Strength for All Bentofix GCLs (Total of 50 Tests); (a) Ranges of Equivalent Friction Angles, (b) Average Equivalent Friction Angle with Upper and Lower Bounds 159
Figure 4.26: Large Displacement Shear Strength for All Bentofix GCLs (Total of 47 Tests); (a) Ranges of Equivalent Friction Angles, (b) Average Equivalent Friction Angle with Upper and Lower Bounds..... 160
Figure 4.27: Peak Shear Strength for All Woven/Nonwoven Needle-Punched GCLs in the GCLSS Database (Total of 223 Tests); (a) Ranges of Equivalent Friction Angles, (b) Average Equivalent Friction Angles 161
Figure 4.28: Large Displacement Shear Strength for All Woven/Nonwoven Needle Punched GCLs in the GCLSS Database (Total of 148 Tests); (a) Ranges of Equivalent Friction Angles, (b) Average Equivalent Friction Angles..... 162
Figure 4.29: Peak Shear Strength for All Nonwoven/Nonwoven Needle-Punched GCLs in the GCLSS Database (Total of 42 Tests); (a) Ranges of Equivalent Friction Angles, (b) Average Equivalent Friction Angles 163
Figure 4.30: Large Displacement Shear Strength for All Nonwoven/Nonwoven Needle-Punched GCLs in the GCLSS Database (Total of 27 Tests); (a) Ranges of Equivalent Friction Angles, (b) Average Equivalent Friction Angles 164
Figure 4.31: Peak Shear Strengths Test Results for GCL A; (a) Ranges of Equivalent Friction Angles (with Test Results Reported by Other Studies), (b) Average Equivalent Friction Angle with Upper and Lower Bounds (Other Test Results are Not Included) 165
Figure 4.32: Large Displacement Shear Strengths Test Results for GCL A; (a) Ranges of Equivalent Friction Angles (with Test Results Reported by Other Studies), (b) Average Equivalent Friction Angle with Upper and Lower Bounds (Other Test Results are Not Included)..... 166
Figure 4.33: Peak Shear Strength for Four GCL Types – Needle-Punched (GCL A), Stitch-Bonded (GCL B), Needle-Punched with Thermal Bonding (GCL C) GCLs, and Unreinforced (GCL F) ; (a) Ranges of Equivalent Friction Angles, (b) Equivalent Friction Angles..... 167
Figure 4.34: Large Displacement Shear Strength for Four GCL Types – Needle-Punched with no Thermal Bonding (GCL A), Stitch-Bonded (GCL B) , Needle-Punched with Thermal Bonding (GCL C) GCLs, and Unreinforced (GCL F) ; (a) Ranges of Equivalent Friction Angles, (b) Equivalent Friction Angles 168
Figure 4.35: Effect of the Time of Hydration on the Shear Strength of GCL A (a) Peak Shear Strength, (b) Large Displacement Shear Strength 169
Figure 4.36: Effect of the Hydration Normal Stress on the Shear Strength of GCL A (a) Peak Shear Strength, (b) Large Displacement Shear Strength 170
Figure 4.37: Effect of the Time of Consolidation on the Shear Strength of GCL A (a) Peak Shear Strength, (b) Large Displacement Shear Strength 171

Figure 4.38: Effect of the Shear Displacement Rate on the Shear Strength of GCL A (a) Peak Shear Strength, (b) Large Displacement Shear Strength 172
Figure 4.39: Shear Force-Displacement Behavior for Hydrated GCL A, Contact Area is 300 mm by 300 mm, (a) Low Range of Normal Stresses (b) High Range of Normal Stress (t_H = 48 hours, t_C = 0 hours, SDR = 1.0 mm/min) 173
Figure 4.40: Shear Force-Displacement Behavior for GCL A, Contact Area is 300 mm by 300 mm (t_H = 168 hours, t_C = 48 hours, SDR = 0.1 mm/min)..... 173
Figure 4.41: Shear Force-Displacement Behavior for GCL B, Contact Area is 300 mm by 300 mm (t_H = 168 hours, t_C = 48 hours, SDR = 0.1 mm/min)..... 174
Figure 4.42: Shear Force-Displacement Behavior for GCL C, Contact Area is 300 mm by 300 mm (t_H = 168 hours, t_C = 48 hours, SDR = 0.1 mm/min)..... 174
Figure 4.43: Shear Force-Displacement Behavior for GCL F Under Soaked Shear Strength, Contact Area is 300 mm by 300 mm..... 175
Figure 4.44: Shear Force-Displacement Behavior for GCL F Under Unhydrated Conditions, Contact Area is 300 mm by 300 mm..... 175
Figure 4.45: Peak and Large Displacement Shear Strength Failure Envelopes for GCL A (FE A1a and A1b: t_H = 24 hours, t_C = 0 hours, and SDR = 1.0 mm/min); *FE A1a is the Baseline Failure Envelope for GCL A* 176
Figure 4.46: Peak and Large Displacement Shear Strength Failure Envelopes for GCL A (FE A2: t_H = 24 hours, t_C = 0 hours, and SDR = 0.5 mm/min); *Change in SDR from the Baseline* 176
Figure 4.47: Comparison between Failure Envelopes A1 and A2..... 176
Figure 4.48: Peak and Large Displacement Shear Strength Failure Envelopes for GCL A (FE A3a: t_H = 48 hours, t_C = 0 hours, and SDR = 1.0 mm/min); (a) Linear Fit, (b) Bilinear Fit Peak, (c) Bilinear Fit Large Displacement 177
Figure 4.49: Peak and Large Displacement Shear Strength Failure Envelopes for GCL A (FE A3b: t_H = 48 hours, t_C = 0 hours, Hydration Normal Stress = 4.8 kPa, and SDR = 1.0 mm/min); *Change in t_H from the Baseline* 178
Figure 4.50: Peak and Large Displacement Shear Strength Failure Envelopes for GCL A (FE A4: t_H = 72 hours, t_C = 0 hours, and SDR = 1.0 mm/min); *Change in t_H from the Baseline* 178
Figure 4.51: Peak and Large Displacement Shear Strength Failure Envelopes for GCL A (FE A1, A3 and A4: t_H = 24, 48 and 72 hours, respectively, t_C = 0 hours, and SDR = 1.0 mm/min); *Effect of Increasing t_H;* (a) Peak Shear Strength, (b) Large Displacement Shear Strength..... 179
Figure 4.52: Peak and Large Displacement Shear Strength Failure Envelopes for GCL A (FE A5: t_H = 168 hours, t_C = 48 hours, and SDR = 0.1 mm/min); *Change in t_H, t_C and SDR from the Baseline* 180
Figure 4.53: Ratios between Peak or Large Displacement Shear Strength and Normal Stress Plotted Against Normal Stress for GCL A (FE A5: t_H = 168 hours, t_C = 48hours, and SDR = 0.1 mm/min) 180
Figure 4.54: Ratio between the Large Displacement Shear Strength and Peak Shear Strengths Plotted Against Normal Stress for GCL A (FE A5: t_H = 168 hours, t_C = 48 hours, and SDR = 0.1 mm/min)..... 181

Figure 4.55: Peak and Large Displacement Shear Strength Failure Envelopes for GCL A (FE A6: Staged Hydration and Consolidation and SDR = 0.0015 mm/min); *Change in t_H, t_C and SDR from the Baseline*..... 181
Figure 4.56: Peak and Large Displacement Shear Strength Failure Envelopes for GCL A (FE A7a and A7b: SDR = 1.0 mm/min); *Change in t_H and t_C from the Baseline*..... 182
Figure 4.57: Peak Shear Strength Failure Envelope for GCL A (FE A8: Unhydrated and Unconsolidated, and SDR = 1.0 mm/min); *Change in t_H from the Baseline* 182
Figure 4.58: Peak and Large Displacement Shear Strength Failure Envelopes for GCL A (FE A1, A8: t_H = 24 and 0 hours, respectively, t_C = 0 hours, and SDR = 1.0 mm/min); *Effect of Decreasing t_H*..... 183
Figure 4.59: Peak and Large Displacement Shear Strength Failure Envelopes for GCL B (FE B1: t_H = 24 hours, t_C = 0 hours, and SDR = 1.0 mm/min); *Baseline Failure Envelope for GCL B*..... 183
Figure 4.60: Peak Shear Strength Failure Envelopes for GCL B (FE B2: t_H = 48 hours, t_C = 0 hours, and SDR = 1.0 mm/min); *Change in t_H from the Baseline* 184
Figure 4.61: Peak Shear Strength Failure Envelopes for GCL B (FE B3: t_H = 96 hours, t_C = 0 hours, and SDR = 1.0 /min); *Change in t_H from the Baseline* . 184
Figure 4.62: Peak Shear Strength Failure Envelope for GCL B (FE B1, B2 and B3); *Effect of Increasing t_H*..... 184
Figure 4.63: Peak Shear Strength Failure Envelope for GCL B (FE B4: t_H = 168 hrs, t_C = 48 hrs, and SDR = 0.1 mm/min); *Change in t_H, t_C and SDR from the Baseline*..... 184
Figure 4.64: Peak and Large Displacement Shear Strength Failure Envelopes (FE C1: t_H = 24 hrs, t_C = 0 hrs, and SDR = 0.5 mm/min); (a) Linear Fit, (b) Bilinear Fit; *Baseline Failure Envelope for GCL C* 185
Figure 4.65: Peak and Large Displacement Shear Strength Failure Envelopes (FE C2: t_H = 24 hrs, t_C = 0 hrs, and SDR = 0.2 mm/min); *Change in SDR from the Baseline*..... 186
Figure 4.66: Comparison of Failure Envelopes for GCL C (FE C1, C2: t_H = 24, t_C = 0 hrs, and SDR = 0.5 and 0.2 mm/min, respectively); *Effect of Decreasing SDR* 186
Figure 4.67: Peak and Large Displacement Shear Strength Failure Envelopes (FE C3: t_H = 168 hrs, t_C = 48 hrs, and SDR = 0.1 mm/min); *Change in t_H, t_C and SDR from the Baseline* 187
Figure 4.68: Shear Strength Failure Envelopes for GCL D (FE D1, D2 and D3: Different t_H, t_C and SDR) 187
Figure 4.69: Bilinear Peak and Large Displacement Failure Envelopes for GCL D (FE D3: t_H = 24 hours, t_C = 24 hours, SDR = 1.0 mm/min) 188
Figure 4.70: Shear Strength Failure Envelopes for GCL E (FE E1 and E2: Different t_H, No Consolidation, SDR = 1.0 mm/min); (a) Peak, (b) Large Displacement 188

Figure 4.71: Shear Strength Failure Envelopes for GCL F (FE F1 and F2: Hydrated and Unhydrated GCLs, respectively, and SDR = 1.0 mm/min); (a) Peak Shear Strength, (b) Large Displacement Shear Strength 189
Figure 4.72: Comparison Plot Between Failure Envelope F2 and Total Stress Results of Triaxial Cell Tests on Sodium Montmorillonite Reported By Mesri and Olson (1970) 189
Figure 4.73: Peak and Large Displacement Shear Strength Failure Envelope for GCL G (FE G1: t_H = 24 hours, t_C = 0 hours, SDR = 1.0 mm/min) 190
Figure 4.74: Peak Shear Strength Failure Envelopes for GCL H (FE H1, H2 and H3); (a) Full Normal Stress Range, (b) Detail of Low Normal Stresses 190
Figure 4.75: Large Displacement Shear Strength Failure Envelopes for GCL H (FE H1, H2 and H3)..... 191
Figure 4.76: Comparison of Failure Envelopes D1, D2, D3, E1, E2, H1, H2 and H3; Effect of Thermal Bonding on Needle-Punched GCLs with Nonwoven Carrier Geotextiles; (a) Peak, (b) Large Displacement..... 191
Figure 4.77: Peak Shear Strength Failure Envelopes for GCL I (FE I1 and I2, tH = 0 hours and 72 hours, Respectively, No Consolidation, SDR = 1.0 mm/min), with Failure Envelope A1a for Comparison..... 192
Figure 4.78: Peak and Large Displacement Shear Strength Failure Envelopes for GCL J (FE J1: t_C = 24 hours, t_C = 0 hours, SDR = 1.0 mm/min) 192
Figure 4.79: Comparison of the Peak and Large Displacement Failure Envelopes A1 and B1 (SDR = 1.0 mm/min, t_H = 24 hours, t_C = 0 hours)..... 193
Figure 4.80: Comparison of the Peak and Large Displacement Failure Envelopes A2 and C1 (SDR = 0.5 mm/min, t_H = 24 hours, t_C = 0 hours)..... 193
Figure 4.81: Comparison of the Peak and Large Displacement Failure Envelopes A5, B4 and C3 (SDR = 0.1 mm/min, t_H = 168 hours, t_C = 48 hours)..... 194
Figure 4.82: Comparison of the Peak and Large Displacement Shear Strength Ratios for Failure Envelopes A5, B4 and C3 (SDR = 0.1 mm/min, t_H = 168 hours, t_C = 48 hours)..... 194
Figure 4.83: Comparison of Peak Failure Envelopes for GCLs A, B, C and F..... 195
Figure 4.84: Comparison of Large Displacement Failure Envelopes for GCLs A, B, C and F..... 195
Figure 4.85: Comparison of Peak Shear Strength Failure Envelopes for GCLs A .. 195
Figure 4.86: Comparison of Large Displacement Failure Envelopes for GCLs A... 196
Figure 4.87: Comparison of Peak Shear Strength Failure Envelopes for GCLs B... 196
Figure 4.88: Comparison of Peak Shear Strength Failure Envelopes for GCLs C... 196
Figure 4.89: Comparison of Large Displacement Failure Envelopes for GCLs C... 196
Figure 4.90: Effect of Shear Displacement Rate on the Shear Strength of GCL A for Low Normal Stress (50 kPa) and High Normal Stress (520 kPa); (a) Peak, (b) Large Displacement 197
Figure 4.91: Effect of Shear Displacement Rate on the Shear Strength of GCL C; Normal Stress of 50 kPa 198
Figure 4.93: Effect of Time of Hydration on Peak Failure Envelopes for GCL A (Note: Hydration Normal Stress Equals Normal Stress During Shearing)... 199
Figure 4.94: Effect of Hydration Procedure on GCL A..... 199

Figure 4.95: Effect of Consolidation on GCL H (a) Peak Shear Strength with High and Low Normal Stress Distributions, (b) Large Displacement Shear Strength 200
Figure 4.96: Effect of Consolidation on the Peak Shear Strength of GCL A 201
Figure 4.97: Comparison of the Effect of Consolidation on the Peak Shear Strengths of GCL A and GCL H (Low Ranges of Normal Stresses) 201
Figure 4.98: Variation in Standard Deviation of the Peak and Large Displacement Shear with Normal Stress for FE A5 202
Figure 4.99: Variation in the Coefficient of Variation (COV) of the Peak and Large Displacement Shear with Normal Stress for FE A5 202
Figure 4.100: Variation in Peak Shear Strength of GCL A for a Constant Normal Stress of 34.5 kPa, t_H = 168 hrs, t_C = 48 hrs, and SDR = 0.1 mm/min (Failure Envelope A5); (a) Cumulative Distribution Function (CDF), (b) Probability Density Function (PDF) with an Equivalent Normal Distribution 203
Figure 4.101: Variation in Large Displacement Shear Strength of GCL A for a Constant Normal Stress of 34.5 kPa, t_H = 168 hrs, t_C = 48 hrs, and SDR = 0.1 mm/min (Failure Envelope A5) ; (a) Cumulative Distribution Function (CDF), (b) Probability Density Function (PDF) with an Equivalent Normal Distribution 204
Figure 4.102: Variation in Peak Shear Strength of GCL A for a Constant Normal Stress of 137.9 kPa, t_H = 168 hrs, t_C = 48 hrs, and SDR = 0.1 mm/min (Failure Envelope A5) ; (a) Cumulative Distribution Function (CDF), (b) Probability Density Function (PDF) with an Equivalent Normal Distribution 205
Figure 4.103: Variation in Large Displacement Shear Strength of GCL A for a Constant Normal Stress of 137.9 kPa, t_H = 168 hrs, t_C = 48 hrs, and SDR = 0.1 mm/min (Failure Envelope A5) ; (a) Cumulative Distribution Function (CDF), (b) Probability Density Function (PDF) with an Equivalent Normal Distribution 206
Figure 4.104: Variation in Peak Shear Strength of GCL A for a Constant Normal Stress of 310.3 kPa, t_H = 168 hrs, t_C = 48 hrs, and SDR = 0.1 mm/min (Failure Envelope A5) ; (a) Cumulative Distribution Function (CDF), (b) Probability Density Function (PDF) with an Equivalent Normal Distribution 207
Figure 4.105: Variation in Large Displacement Shear Strength of GCL A for a Constant Normal Stress of 310.3 kPa, t_H = 168 hrs, t_C = 48 hrs, and SDR = 0.1 mm/min (Failure Envelope A5) ; (a) Cumulative Distribution Function (CDF), (b) Probability Density Function (PDF) with an Equivalent Normal Distribution 208
Figure 4.106: Probability Density Functions for Failure Envelope A5; (a) Peak Shear Strength Distributions, (b) Large Displacement Shear Strength Distributions 209
Figure 4.107: Variation in Peak Shear Strength of GCL A for a Constant Normal Stress of 9.6 kPa, (FE A3: t_H = 48 hrs, t_C = 0 hrs, and SDR = 1.0 mm/min); (a) Cumulative Distribution Function (CDF), (b) Probability Density Function (PDF) with an Equivalent Normal Distribution 210

Figure 4.108: Variability in Peak and Large Displacement Shear Strength of GCL A Sheared at a Normal Stress of 517.1 kPa (No Hydration, No Consolidation, SDR = 1.0 mm/min)..... 210
Figure 4.109: Final GCL Water Content as a Function of Shear Strength for All GCLs in the GCLSS Database, Outliers are Marked in Gray; (a) Peak, (b) Large Displacement..... 211
Figure 4.110: Final GCL Water Content as a Function of Shear Strength for GCL A, Effect of Time of Hydration, Outliers are Marked in Gray; (a) Peak, (b) Large Displacement..... 212
Figure 4.111: Final GCL Water Content as a Function of Shear Strength for GCL A, Effect of Time of Consolidation, Outliers are Marked in Gray; (a) Peak, (b) Large Displacement 213
Figure 4.112: Final GCL Water Content as a Function of Shear Strength for GCL A, Effect of Shear Displacement Rate, Outliers are Marked in Gray; (a) Peak, (b) Large Displacement 214
Figure 4.113: Final GCL Water Content as a Function of Large Displacement Shear Strength for GCL A, Effect of Order of Normal Stress Application, Outliers are Marked in Gray 215
Figure 4.114: Variation in Peak Shear Strength with the Final GCL Water Content for Failure Envelope A8 (t_H = 0 hours, t_C = 0 hours, SDR = 1.0 mm/min)..... 216
Figure 4.115: Variation in Shear Strength with the Final GCL Water Content for Failure Envelope A5 (t_H = 168 hours, t_C = 48 hours, SDR = 0.1 mm/min).. 216
Figure 4.116: Variation in Average Shear Strength with the Final GCL Water Content for Three GCLs: (Failure Envelopes A5, B4 and C3: t_H = 168 hours, t_C = 48 hours, SDR = 0.1 mm/min); (a) Peak, (b) Large Displacement 217
Figure 4.117: Variation in Displacement at Peak Shear Strength with Normal Stress for Failure Envelope A8 (t_H = 0 hours, t_C = 0 hours, SDR = 1.0 mm/min) .. 218
Figure 4.118: Variation in Displacement at Peak Shear Strength with Normal Stress for Failure Envelope A5 (t_H = 168 hours, t_C = 48 hours, SDR = 0.1 mm/min) 218
Figure 4.119: Movement from Displacement from Peak to Large Displacement Shear Strengths for Failure Envelope A5 (t_H = 168 hours, t_C = 48 hours, SDR = 0.1 mm/min); Normal Stress of (a) 34.5 kPa, (b) 137.9 kPa, (c) 310.3 kPa..... 219
Figure 4.120: Variation in Displacement at Peak Shear Strength with Normal Stress for Failure Envelopes A5, B4 and C3 (t_H = 168 hours, t_C = 48 hours, SDR = 0.1 mm/min)..... 220
Figure 4.121: Variability in Displacement at Peak Shear Strength for GCL A Sheared at a Normal Stress of 517.1 kPa (No Hydration, No Consolidation, SDR = 1.0 mm/min)..... 220
Figure 4.122: Displacement at Peak Shear Strength with Shear Displacement Rate for GCL A (Normal Stress of 517.1 kPa, t_H = 312 hours, t_C = 48 hours)..... 221
Figure 5.1: Histogram of the Number of GCL-Geomembrane Interface Tests on Each Type of Geomembrane 295
Figure 5.2: Histogram of the Number of GCL-Geomembrane Interface Tests on Each Type of Geomembrane, Identifying Geomembrane Manufacturer 295

Figure 5.3: Histogram of the Number of GCL-Geomembrane Interface Tests on Each Type of Geomembrane, Identifying GCL Types 296
Figure 5.4: Histogram of the Number of GCL-Geomembrane Interface Tests on Each Type of Geomembrane, Identifying Geomembrane Thickness 296
Figure 5.5: Shear Strength of All GCL-Geomembrane Interfaces; (a) Peak, (b) Large-Displacement 297
Figure 5.6: Peak Shear Strengths of All GCL-Geomembrane Interfaces (with Average Equivalent Friction Angles); (a) Full Data Set, (b) Detail of Low Normal Stresses 298
Figure 5.7: Large Displacement Shear Strengths of All GCL-Geomembrane Interfaces (with Average Equivalent Friction Angles); (a) Full Data Set, (b) Detail of Low Normal Stresses 299
Figure 5.8: Shear Strength of all Textured Geomembrane Interfaces with the Equivalent, Upper Bound and Lower Bound Equivalent Friction Angles; (a) Peak Shear Strength, (b) Large Displacement Shear Strength 300
Figure 5.9: Shear Strength of all Smooth Geomembrane Interfaces with the Equivalent, Upper Bound and Lower Bound Equivalent Friction Angles; (a) Peak Shear Strength; (b) Large Displacement Shear Strength 301
Figure 5.10: Shear Strength of all Textured HDPE Geomembrane Interfaces with the Equivalent, Upper Bound and Lower Bound Equivalent Friction Angles, with Test Results from Other Studies; (a) Peak Shear Strength, (b) Large Displacement Shear Strength 302
Figure 5.11: Shear Strength of all PVC Geomembrane Interface with the Equivalent, Upper Bound and Lower Bound Equivalent Friction Angles; (a) Peak Shear Strength; (a) Peak Shear Strength, (b) Large Displacement Shear Strength 303
Figure 5.12: Shear Strength of all Textured VLDPE Geomembrane Interface with the Equivalent, Upper Bound and Lower Bound Equivalent Friction Angles; (a) Peak Shear Strength; (a) Peak Shear Strength, (b) Large Displacement Shear Strength 304
Figure 5.13: Shear Strength of all Textured LLDPE Geomembrane Interface with the Equivalent, Upper Bound and Lower Bound Equivalent Friction Angles; (a) Peak Shear Strength; (a) Peak Shear Strength, (b) Large Displacement Shear Strength 305
Figure 5.14: Shear Strength of all Textured HDPE Geomembrane Interfaces (Separated by GCL Interface) with the Equivalent, Upper Bound and Lower Bound Equivalent Friction Angles; (a) Peak Shear Strength; (a) Peak Shear Strength, (b) Large Displacement Shear Strength 306
Figure 5.15: Shear Strength of all GCL A Interfaces with a Textured HDPE Geomembrane with the Equivalent, Upper Bound and Lower Bound Equivalent Friction Angles; (a) Peak Shear Strength; (a) Peak Shear Strength, (b) Large Displacement Shear Strength 307
Figure 5.16: Shear Strength of all GCL B Interfaces with a Textured HDPE Geomembrane with the Equivalent, Upper Bound and Lower Bound Equivalent Friction Angles; (a) Peak Shear Strength; (a) Peak Shear Strength, (b) Large Displacement Shear Strength 308

Figure 5.17: Shear Strength of all GCL C Interfaces with a Textured HDPE Geomembrane with the Equivalent, Upper Bound and Lower Bound Equivalent Friction Angles; (a) Peak Shear Strength; (a) Peak Shear Strength, (b) Large Displacement Shear Strength 309
Figure 5.18: Shear Strength of all GCL K Interfaces with a Textured HDPE Geomembrane with the Equivalent, Upper Bound and Lower Bound Equivalent Friction Angles; (a) Peak Shear Strength; (a) Peak Shear Strength, (b) Large Displacement Shear Strength 310
Figure 5.19: Shear Strength of all Textured HDPE Geomembrane Interfaces (Separated by Geomembrane Manufacturer) with the Equivalent, Upper Bound and Lower Bound Equivalent Friction Angles; (a) Peak Shear Strength; (a) Peak Shear Strength, (b) Large Displacement Shear Strength 311
Figure 5.20: Shear Strength of all Textured HDPE Geomembrane Interfaces (Separated by Geomembrane Thickness) with the Equivalent, Upper Bound and Lower Bound Equivalent Friction Angles; (a) Peak Shear Strength; (a) Peak Shear Strength, (b) Large Displacement Shear Strength 312
Figure 5.21: Shear Strength of all GCL-Geomembrane Interfaces at Low Normal Stress; *with the Equivalent Friction Angles for Normal Stresses Less than 50 kPa*; (a) Peak Shear Strength, (b) Large Displacement Shear Strength..... 313
Figure 5.22: Shear Force-Displacement Curves for the Interface between a Hydrated GCL A and an 80-mil Textured HDPE Geomembrane s (t_H = 168 hours, t_C = 48 hours, SDR = 0.1 mm/min)..... 314
Figure 5.23: Shear Force-Displacement Curves for the Interface between a Hydrated GCL B and an 80-mil Textured HDPE Geomembrane s (t_H = 168 hours, t_C = 48 hours, SDR = 0.1 mm/min)..... 314
Figure 5.24: Shear Force-Displacement Curves for the Interface between a Hydrated GCL C and an 80-mil Textured HDPE Geomembrane s (t_H = 168 hours, t_C = 48 hours, SDR = 0.1 mm/min)..... 315
Figure 5.25: Shear Force-Displacement Curves for the Interface between a Hydrated Needle-Punched GCL and a Textured VLDPE Geomembrane..... 315
Figure 5.26: Shear Force-Displacement Curves for the Interface between a Hydrated Needle-Punched GCL and a Textured LLDPE Geomembrane 316
Figure 5.27: Shear Force-Displacement Curves for the Interface between a Hydrated Needle-Punched GCL and a Faille Finish PVC Geomembrane 316
Figure 5.28: Shear Force-Displacement Curves for the Interface between a Hydrated Needle-Punched GCL and a Smooth HDPE Geomembrane 317
Figure 5.29: Shear Force-Displacement Curves for the Interface between a GCL and a Smooth VLDPE Geomembrane..... 317
Figure 5.30: Shear Force-Displacement Curves for the Interface between a Hydrated GCL and a Smooth LLDPE Geomembrane..... 318
Figure 5.31: Shear Force-Displacement Curves for the Interface between a Hydrated GCL and a Smooth PVC Geomembrane 318
Figure 5.32: Shear Force-Displacement Curves for the Interface between an Unhydrated, Unreinforced Geomembrane-Backed GCL and a Textured HDPE Geomembrane 319

Figure 5.33: Shear Force-Displacement Curves for the Interface between a Hydrated, Unreinforced Geomembrane-Backed GCL and a Textured HDPE Geomembrane 319
Figure 5.34: Failure Envelopes for an Unreinforced Geomembrane-Backed GCL and a Textured HDPE Geomembrane (FE TH 1 and 2: GCL K and GM u, t_H = 0 and 48 hours, respectively, t_C = 0 hours and SDR = 1.0 mm/min); (a) Peak, (b) Large Displacement 320
Figure 5.35: Failure Envelopes for the Interface between GCL C and a Textured HDPE Geomembrane (FE TH 3a and 3b: GCL C and GM t, t_H = 0 and 1 hours, respectively, No Consolidation and SDR = 1.0 mm/min) ; (a) Peak, (b) Large Displacement 321
Figure 5.36: Failure Envelopes for the Interface between GCL C and a Textured HDPE Geomembrane (FE TH 4a, 4b and 4c: GCL C and GM t, t_H = 24 hours, No Consolidation and SDR = 1.0, 0.2 and 0.025 mm/min, respectively); (a) Peak, (b) Large Displacement 322
Figure 5.37: Failure Envelopes for the Interface between GCL C and a Textured HDPE Geomembrane (FE TH 5: GCL C and GM s, t_H = 168 hours, t_C = 48 hours and SDR = 0.1 mm/min) 323
Figure 5.38: Failure Envelopes for the Interface between GCL A and a Textured HDPE Geomembrane (FE TH 6: GCL A and GM s, t_H = 0 hours, t_C = 0 hours and SDR = 1.0 mm/min) 323
Figure 5.39: Failure Envelopes for the Interface between GCL A and a Textured HDPE Geomembrane (FE TH 7a, 7b, and 7c: GCL A and Different Geomembranes, t_H = 24 hours, t_C = 0 hours and SDR = 1.0 mm/min); (a) Peak, (b) Large Displacement 324
Figure 5.40: Failure Envelopes for the Interface between GCL A and a Textured HDPE Geomembrane (FE TH 8a, 8b and 8c: GCL A and Different Geomembranes, t_H = 48 hours, t_C = 0 hours and SDR = 1.0 mm/min); (a) Peak, (b) Large Displacement 325
Figure 5.41: Failure Envelopes for the Interface between GCL A and a Textured HDPE Geomembrane (FE TH 9a and 9b: GCL A and Different Geomembranes, t_H = 24 and 48 hours, respectively, No Consolidation and SDR = 0.2 and 0.1 mm/min, respectively); (a) Peak, (b) Large Displacement 326
Figure 5.42: Failure Envelopes for the Interface between GCL A and a Textured HDPE Geomembrane (FE TH 10a and 10b: GCL A and Different Geomembranes, t_H = 72 and 24 hours, respectively, t_C = 24 and 12 hours, respectively, and SDR = 1.0 mm/min); (a) Peak, (b) Large Displacement .. 327
Figure 5.43: Failure Envelopes for the Interface between GCL A and a Textured HDPE Geomembrane (FE TH 11: GCL A and GM s, t_H = 168 hours, t_C = 48 hours and SDR = 0.1 mm/min) 328
Figure 5.44: Shear Strength Ratios for Failure Envelope TH 11 (GCL A and GM s, t_H = 168 hours, t_C = 48 hours and SDR = 0.1 mm/min); (a) Ratios of Peak and Large Displacement Shear Strengths to Normal Stress, (b) Ratio of Large Displacement Shear Strength to Peak Shear Strength 328

Figure 5.45: Failure Envelopes for the Interface between GCL B and a Textured HDPE Geomembrane (FE TH 12a and 12b: GCL B and GM s or t, respectively, t_H = 0 hours, t_C = 0 hours and SDR = 1.0 mm/min); (a) Peak, (b) Large Displacement 329
Figure 5.46: Failure Envelopes for the Interface between GCL B and a Textured HDPE Geomembrane (FE TH 13a and 13b: GCL B and Different Geomembranes, t_H = 24 hours, t_C = 0 hours and SDR = 1.0 mm/min); (a) Peak, (b) Large Displacement 330
Figure 5.47: Failure Envelopes for the Interface between GCL B and a Textured HDPE Geomembrane (FE TH 14: GCL B and GM s, t_H = 48 hours, t_C = 0 hours and SDR = 1.0 mm/min) 330
Figure 5.48: Shear Failure Envelopes for the Interface between GCL B and a Textured HDPE Geomembrane (FE TH 15: GCL B and GM s, t_H = 168 hours, t_C = 48 hours and SDR = 0.1 mm/min) 331
Figure 5.49: Failure Envelopes for the Interface between a GCL and a Textured VLDPE Geomembrane (FE TV 1a and 1b: GCLs G or B and GM t, t_H = 24 hours, t_C = 0 hours and SDR = 1.0 mm/min); (a) Peak, (b) Large Displacement 331
Figure 5.51: Failure Envelopes for the Interface between a GCL and a Textured VLDPE Geomembrane (FE TV 3a and 3b: GCL B and GM u with Amoco or Clem Geotextiles, respectively, t_H = 0 hours, t_C = 0 hours and SDR = 1.0 mm/min); (a) Peak, (b) Large Displacement 332
Figure 5.52: Failure Envelopes for the Interface between a GCL and a Textured LLDPE Geomembrane (FE TL 1a and 1b: GCLs C and A and GM u, t_H = 72 hours, t_C = 0 hours and SDR = 1.0 mm/min); (a) Peak, (b) Large Displacement 333
Figure 5.53: Failure Envelopes for the Interface between a GCL and a Textured LLDPE Geomembrane (FE TL 2a and 2b: GCLs C and A and GM t, t_H = 72 hours, t_C = 0 hours and SDR = 1.0 mm/min) ; (a) Peak, (b) Large Displacement 334
Figure 5.54: Failure Envelopes for the Interface between a GCL and a Textured LLDPE Geomembrane (FE TL 3: GCL A and GM s, t_H = 72 hours, t_C = 48 hours and SDR = 1.0 mm/min) 335
Figure 5.55: Failure Envelopes for the Interface between a GCL and a Smooth HDPE Geomembrane (FE SH 1a and 1b: GCL B and C and GM t, t_H = 24 and 48 hours, respectively, No Consolidation, and SDR = 1.0 mm/min) 335
Figure 5.56: Failure Envelopes for the Interface between a GCL and a Smooth HDPE Geomembrane (FE SH 2a: GCL B and GM u, t_H = 24 hours, t_C = 0 hours and SDR = 0.2 mm/min; 2b: GCL C and GM t, t_H = 24 hours, t_C = 0 hours and SDR = 0.2 mm/min) 336
Figure 5.57: Failure Envelopes for the Interface between a GCL and a Smooth VLDPE Geomembrane (FE SV 1 and SV 2: t_H = 24 hours, No Consolidation and SDR = 1.0 mm/min) 337
Figure 5.58: Failure Envelopes for the Interface between a GCL and a Smooth LLDPE Geomembrane (FE SL 1 and 2, t_H = 24 and 168 hours, respectively, No Consolidation and SDR = 1.0 mm/min) 337

Figure 5.59: Peak Failure Envelopes for the Interface between a GCL and a PVC Geomembrane (FE PVC 1a, 1b and 1c: t_H = 48, 24 and 24 hours, respectively, No Consolidation, SDR = 1.0, 1.0 and 0.05 mm/min, respectively) 337
Figure 5.60: Failure Envelopes Reported by Pavlik (1997) for the Interface between GCL A and a 60 mil Textured HDPE Geomembrane (t_H = 48 hours, t_C = 0 hours, SDR = 1.0 mm/min)..... 338
Figure 5.62: Comparison of Peak Failure Envelopes for Interfaces between GCL K and a Textured HDPE Geomembrane with Those for Other GCL-Textured HDPE Geomembrane Interfaces (No Consolidation, SDR = 1.0 mm/min); (a) t_H = 0 hours, (b) t_H = 48 hours 339
Figure 5.63: Comparison of Failure Envelopes TH 5, 11 and 15 (t_H = 168 hours, t_C = 48 hours and SDR = 0.1 mm/min); (a) Peak, (b) Large Displacement..... 340
Figure 5.64: Variation in Shear Strength Ratios with Normal Stress for Failure Envelopes 5, 11 and 15 (t_H = 168 hours, t_C = 48 hours and SDR = 0.1 mm/min); (a) Peak Shear Strength Ratio, (b) Large Displacement Shear Strength Ratio, (c) Displacement Shear Strength to Peak Shear Strength Ratio 341
Figure 5.65: All Failure Envelopes for Textured Geomembrane Interfaces; (a) Peaks, (b) Large Displacement..... 342
Figure 5.66: All Failure Envelopes for Textured HDPE Geomembrane Interfaces; (a) Peaks, (b) Large Displacement 343
Figure 5.67: All Failure Envelopes for All Textured VLDPE, LLDPE and PVC Geomembrane Interfaces; (a) Peaks, (b) Large Displacement 344
Figure 5.68: All Failure Envelopes for Smooth Geomembrane Interfaces; (a) Peaks, (b) Large Displacement..... 345
Figure 5.69: Effect of the Shear Displacement Rate on the Shear Strength of the Interface between GCL A and a 60 mil Textured HDPE GM u (t_H = 24 hours, No Consolidation); (a) Peak, (b) Large Displacement..... 346
Figure 5.70: Effect of the Shear Displacement Rate on the Shear Strength of the Interface between GCL C and a 60 mil Textured HDPE GM t (t_H = 24 hours, No Consolidation); (a) Peak, (b) Large Displacement..... 347
Figure 5.71: Effect of the Shear Displacement Rate on the Shear Strength of Interface between GCL A and a 60 mil Textured HDPE GM s (t_H = 48 hours, No Consolidation); (a) Peak, (b) Large Displacement 348
Figure 5.72: Effect of the Time of Hydration on the Shear Strength of the Interface between GCL C and a 40/60 mil Textured HDPE GM t (No Consolidation, SDR = 1.0 mm/min); (a) Peak, (b) Large Displacement 349
Figure 5.73: Effect of the Time of Hydration on the Shear Strength of the Interface between GCL A and a 60/80 mil Textured HDPE GM s (No Consolidation, SDR = 1.0 mm/min); (a) Peak, (b) Large Displacement 350
Figure 5.74: Effect of the Time of Hydration on the Shear Strength of the Interface between GCL A and a 60/80 mil Textured HDPE GM s (No Consolidation, SDR = 1.0 mm/min); (a) Peak, (b) Large Displacement 351
Figure 5.75: Effect of the Time of Hydration on the Shear Strength of the Interface between GCL B and a 60 mil Textured HDPE GM s (No Consolidation, SDR = 1.0 mm/min); (a) Peak, (b) Large Displacement 352

Figure 5.76: Effect of Different Hydration Procedures on the Shear Strength of the Interface between GCL B and a Textured HDPE geomembrane (Constant Normal Stress Level of 689.5 kPa for all Interfaces, Consolidated Interface has a Hydration Normal Stress of 68.9 kPa)..... 353
Figure 5.77: Shear Strength of the Interface between GCL A and a Smooth 40-mil PVC Geomembrane x; Different Hydration Procedures for Different Normal Stress Levels 353
Figure 5.78: Effect of the Time of Consolidation on the Failure Envelopes for the Interface between GCL A and a 80 mil Textured HDPE GM v (Consolidated Interface has a Hydration Normal Stress of 68.9 kPa, SDR = 1.0 mm/min); (a) Peak, (b) Large Displacement..... 354
Figure 5.79: Effect of the Time of Consolidation on the Shear Strength of the Interface between GCL A and a 80 mil Textured HDPE GM v (Consolidated Interface has a Hydration Normal Stress of 68.9 kPa, SDR = 1.0 mm/min) 354
Figure 5.80: Standard Deviation of Peak and Large Displacement Shear Strengths for Failure Envelope TH 11 (t_H = 168 hours, t_C = 48 hours and SDR = 0.1 mm/min)..... 355
Figure 5.81: Coefficients of Variation for the Peak and Large displacement Shear Strengths for Failure Envelope TH 11 (t_H = 168 hours, t_C = 48 hours and SDR = 0.1 mm/min) 355
Figure 5.82: Equivalent Normal Probability Density Functions for the Shear Strength of the Interface between GCL A and an 80 mil Textured HDPE GM s (t_H = 168 hours, t_C = 48 hours and SDR = 0.1 mm/min); (a) Peak, (b) Large Displacement..... 356
Figure 5.83: Standard Deviation of Peak and Large Displacement Shear Strengths for Failure Envelopes TH 5, 11 and 15 (t_H = 168 hours, t_C = 48 hours and SDR = 0.1 mm/min)..... 357
Figure 5.84: Variation in the Average Final GCL Water Content with Normal Stress for Three GCL-Textured HDPE Geomembrane Interfaces; Constant Test Condition with t_H = 168 hours, t_C = 48 hours, SDR = 0.1 mm/min..... 357
Figure 5.85: Relationships between the Average Shear Strength and the Average Final GCL Water Content for Failure Envelopes TH 5, 11 and 15 (t_H = 168 hours, t_C = 48 hours, SDR = 0.1 mm/min); (a) Peak, (b) Large Displacement 358
Figure 5.86: Relationship between the Shear Strength and the Final GCL Water Content for Failure Envelope TH 11 (t_H = 168 hours, t_C = 48 hours, SDR = 0.1 mm/min); (a) Peak, (b) Large Displacement 359
Figure 5.87: Displacement at Peak Shear Strength for Failure Envelopes TH 5, 11, and 15 (t_H = 168 hours, t_C = 48 hours, SDR = 0.1 mm/min) 360
Figure 5.88: Displacement at Peak Shear Strength for Failure Envelope TH 11 (t_H = 168 hours, t_C = 48 hours, SDR = 0.1 mm/min)..... 360
Figure 5.89: Displacement from Peak to Large Displacement Shear Strengths for the Interface between GCL A and a 80 mil Textured HDPE GM (t_H = 168 hours, t_C = 48 hours, SDR = 0.1 mm/min), Normal Stresses of (a) 34.5 kPa, (b) 137.9 kPa, (c) 310.3 kPa 361

Figure 5.90: Comparison between Average Behavior for Internal GCL Failure envelopes A5, B4, C3, and GCL-GM Interface Failure Envelopes TH 5, TH 11 and TH 15 (a) Peak Shear Strength, (b) Large Displacement Shear Strength; (c) Displacements at Peak Shear Strength..... 362
Figure 6.1: Definition of Variables for an Infinite Slope Situation; (a) Names of Different Layers, (b) Free-Body Diagram 375
Figure 6.2: Reliability Based Design Chart for Internal GCL Shear Strength; Peak 376
Figure 6.3: Reliability Based Design Chart for Internal GCL Shear Strength; Large Displacement..... 376
Figure 6.4: Reliability Based Design Chart for Shear Strength of the GCL-Geomembrane Interface; Peak..... 377
Figure 6.5: Reliability Based Design Chart for Shear Strength of the GCL-Geomembrane Interface; Large Displacement 377
Figure 6.6: Reliability Based Chart for Peak GCL-Geomembrane Interface Shear Strength; Arrows for Reliability Based *Design* of a Slope with Height of 1 meters and Required Probability of Failure of 0.01..... 378
Figure 6.7: Reliability Based Chart for Large Displacement Internal GCL Shear Strength; Arrows for Reliability Based *Analysis* of a Slope with a Height of 3 meters and a Slope Angle of 20^0..... 378

1 Introduction

1.1 Motivation of this Study

Landfills for municipal and hazardous waste are constructed for the purpose of containing the waste in a concentrated unit with low mobility. To accomplish this, it is necessary to restrict the flow of water through the upper and lower boundaries of the landfill, referred to as the cover and the base liner of the landfill. In the USA, cover and liner systems for municipal and hazardous waste should be constructed with a compacted clay layer having a hydraulic conductivity below 1×10^{-7} cm/s (40 CFR 264 and 265). However, compacted clay layers may not be the proper solution in many situations because of material availability, susceptibility to cracking, construction difficulties, and slope stability problems. Geosynthetic Clay Liners (GCLs) are a prefabricated alternative to compacted clay liners that may be used for cover and base liner systems at lower costs and equivalent hydraulic performance.

GCLs typically consist of a layer of powdered or granular bentonite clay attached to carrier geosynthetic. A unique characteristic of sodium bentonite is that it can draw water from adjacent soils, possibly reaching water contents in excess of 100 percent (Daniel and Shan, 1993). As the sodium bentonite in a GCL swells, it creates a barrier with hydraulic conductivity values as low as 1×10^{-11} m/s (Gilbert *et. al.,* 1997). Despite the low hydraulic conductivity of sodium bentonite, hydrated sodium bentonite is one of the soils with lowest shear strength (Mesri and Olson, 1970). Internal and interface direct shear testing of GCLs has shown that GCLs also have very low internal and interface shear strengths and, in addition, they display a marked post-peak shear strength reduction (Gilbert *et. al.*, 1997, Fox *et. al.*, 1998). Because of this, Frobel (1996) recommends that GCLs containing unreinforced sodium bentonite should not be used on slopes steeper than 10:1 (H:V) because of significant stability concerns.

The low internal and interface shear strengths of GCLs in layered systems bas also been demonstrated by field tests (Daniel *et. al.*, 1998). Also, variability of the shear strength test results for GCLs has been found to be another significant factor to be addressed (Snow *et. al.*, 1998). Hence, product-specific laboratory shear strength testing is necessary to quantify the strength of GCLs under site-specific conditions.

However, because of the significant time and effort involved in GCL shear strength testing, extrapolation of limited results obtained from laboratory testing to GCL shear strength is generally necessary.

1.2 GCL Internal and Interface Shear Strength Database

The former Soil-Geosynthetics Interactions (SGI®) laboratory of GeoSyntec Consultants, which is currently owned by SGI® Testing Services, has performed several hundred individual direct shear tests focusing on the internal and interface shear strength of GCLs since 1992. The SGI® laboratory is a high quality testing facility that is characterized by the significant consistency of its testing procedures and by its state-of-the-art equipment. The data obtained from these tests was used for individual projects but has not been compiled for a global analysis. It should be noted that specimen preparation and shearing of GCLs may require times from several days to several months to obtain a single test result. Consequently, such a large amount of consistent direct shear test results may provide significant insight into the design of landfill cover and liner systems involving GCLs.

Reports generated by the SGI® laboratory include 320 direct shear tests on the internal shear strength of several GCLs and 332 direct shear tests on the shear strength of different combinations of GCL-geomembrane interfaces. Prior to analysis of the individual shear strength test results, the individual reports were carefully interpreted, the data pertinent to a shear strength analysis were identified, and the data were synthesized into a coherent database in Microsoft ACCESS®. This database is referred to as the "GCL Shear Strength database," or the "GCLSS database".

This database is analyzed in this study in order to validate and extend conclusions of past studies, develop bounds on shear strength parameters, quantify statistical relationships between variables, and develop an understanding of the variability of GCL internal and interface shear strength test results.

1.3 Important Issues on GCL Shear Strength Addressed in this Report

Several issues have risen from recent investigations of GCL shear strength. These may be divided for easier comprehension into categories of GCL material

issues, GCL conditioning issues, laboratory testing procedures, test result issues and design issues.

GCL material issues include the variability in the internal and interface GCL shear strength test results due to different reinforcement characteristics and changes in the GCL associated with the swelling of sodium bentonite during hydration. Although quantification of the amount of the fiber reinforcements per unit area (*i.e.* peel strength test results) or the amount of GCL swell during hydration were not reported by the SGI® laboratory, available shear strength data under different test conditions allows inference of the effects of these phenomena on the variability of the shear strength. Also, the wide range of products tested in the GCLSS database allows comparison between GCLs with different material characteristics.

GCL internal and interface shear strength may be affected by GCL conditioning (*i.e.* GCL hydration and consolidation procedures) due to their influence on the sodium bentonite in the GCL. Comparison of the shear strengths of GCLs with different conditioning procedures permits quantification of these effects.

There are several issues related to direct shear testing and specimen confinement of GCLs. The testing and confinement procedures used by the SGI® laboratory will be discussed in detail, and other approaches will be compared. A major unresolved issue is the effect of the shear displacement rate on the internal shear strength of GCLs. Gilbert *et. al.* (1997) and Eid and Stark (1999) observed that unreinforced and reinforced GCLs show inconsistent shear strength behavior with changing shear displacement rate with that observed for most soils. Evaluation of the swelling behavior of sodium bentonite and the test results in the GCLSS database provides insight into this phenomenon.

An important issue regarding GCL test results is the change in shear strength behavior with normal stress. Mesri and Olson (1970) found that the shear behavior of sodium bentonite clay is non-linear, and this effect has been observed also for GCLs by Gilbert *et. al.* (1996) and Fox *et. al.* (1998). The GCLSS database contains shear strength test results for a wide range of normal stresses and test conditions. In addition, the selection of peak or large-displacement shear strengths for design has been debated. The variability of peak and large displacement shear strengths as well

as the relationship between post-peak shear strength reduction and normal stress may provide insight into this issue.

A design issue addressed in this study is the effect of variability in test results on instability design problems, which can be evaluated using reliability based design methods for.

1.4 Report Organization

The objectives of this report will be addressed by: (*i*) developing an understanding of the materials and testing procedures, (*ii*) discussing the results of past experimental studies of the internal and interface GCL shear strength as well as past studies on the shear strength of sodium bentonite clay, (*iii*) discussing and analyzing the internal and interface GCL shear strength test results in the GCLSS database, and (*iv*) presenting a reliability based design application using the trends found in the internal and interface GCL shear strength test results.

This report is organized in five main chapters, and is meant to provide understanding of GCL shear strength through investigation of theory, presentation of experimental procedures and results, and introduction to possible design applications.

Chapter 2 provides an understanding of sodium bentonite clay, GCLs and geomembranes, which are the materials tested as part of the GCLSS database. This chapter also reviews the basic concepts of shear strength testing for these materials.

Chapter 3 provides a review of the state-of-the-art on issues affecting GCL internal and interface shear strength. This chapter evaluates reported responses of GCLs to different testing parameters such as the time of hydration, time of consolidation, shear displacement rate, and normal stress (during hydration and shearing). Chapter 3 also discusses mechanisms that have been suggested to explain the internal and interface shear strength behavior of GCLs as well as the shear strength behavior of sodium bentonite clay.

Chapters 4 and 5 provide analyses and discussions of a database of internal and interface GCL shear strength test results, respectively. These chapters discuss experimental results from the database by (*i*) analyzing the ranges of different GCL shear strength test results using statistical methods; (*ii*) analyzing the correlation

between different variables associated with shear strength testing of GCLs; (*iii*) analyzing the failure envelopes for GCLs grouped by different product types and test conditions; and (iv) using the results of these analyses to investigate the effects of the shear displacement rate, time of hydration, time of consolidation, GCL material variability, final water content and displacement at peak shear strength on GCL shear strength behavior.

After analysis of the internal and interface GCL shear strength test results in Chapters 4 and 5, Chapter 6 provides a possible use of the data in design, which considers the variability in GCL shear strength. This chapter introduces basic concepts of reliability based design and analysis for infinite slopes involving a GCL and a geomembrane, as well as an example of reliability based design.

Chapter 7 provides a concise summary and a list of the major conclusions for GCL internal and interface shear strength.

In addition, four appendices are included in this report. Appendix A includes the database of experimental test results for the internal and interface shear strength tests on GCLs analyzed in Chapters 4 and 5, Appendix B provides a glossary of terms used in this report, Appendix C includes manufacturer specifications for the different GCLs and geomembranes present in the GCLSS database, and Appendix D includes the details of the reliability-based design charts presented in Chapter 6.

2 Materials and Test Methods

2.1 Introduction

An understanding of the material characteristics, testing methods and equipment is necessary before investigation of the internal and interface shear strength behavior of GCLs. As GCLs are layered composite materials, the shear strength depends on the characteristics of the different materials and of the reinforcements. The materials that constitute a GCL vary from product to product, but are typically sodium bentonite clay, woven or nonwoven carrier geotextiles, geomembranes, and synthetic fiber reinforcements. This chapter provides a concise introduction to each of these materials, and addresses effects that the materials may have on the overall GCL shear strength.

Due to the layered nature of GCLs, shear strength testing methods that facilitate the analysis along predefined shear planes are required. Two such test methods, the direct shear test and the ring shear test, have been employed in the past to investigate the internal and interface shear strength of GCLs (Gilbert *et. al.*, 1996, Stark and Eid, 1996). The triaxial cell device has been used to investigate the shear strength behavior of sodium bentonite clay (Mesri and Olson, 1970), which may have a significant role in the overall GCL shear strength. Although the test results presented in the GCLSS database were obtained using a direct shear device, an overview of the different devices facilitates proper comparison of test results from past studies with those of the GCLSS database.

The test device must provide adequate confinement for any soils or geosynthetics tested, yet must still allow drainage representative of the conditions foreseen in the field. The test device must also be capable of controlling the stress state within the GCL (*i.e.* normal stress and shear stress), as well as controlling the test conditions involved in the hydration, consolidation and shearing of the GCL. This chapter presents the methods of GCL confinement as well as the test conditions for each of the previously mentioned test devices.

This chapter has two purposes: (i) to develop an understanding of the geomaterials discussed in this report, (ii) to review the information relevant to shear strength testing of GCLs and their constituents.

2.2 Materials

2.2.1 Sodium Bentonite Clay

Sodium bentonite is a naturally occurring, mined clay mineral that is extremely hydrophilic because of the small size of the clay particles and the electrical imbalance on the surface on the clay particles. That is, when placed in the vicinity of water or water vapor, the matric suction of dry sodium bentonite clay attracts water molecules into a well developed diffuse double layer leaving little free-water in the voids and resulting in a low saturated hydraulic conductivity (Mitchell, 1994). In addition, sodium bentonite is capable of self-healing. That is, if the soil is punctured or dried to the point of desiccation, the soil is able to swell when it comes into contact with water to regain its previous hydraulic properties. For these reasons, sodium bentonite is used in many engineering applications as a hydraulic barrier, such as in GCLs used as a part of a landfill cover or liner system. However, the sodium bentonite component of a GCL has comparatively low shear strength. Section 3.4 includes further discussion on the mineralogy and shear strength of sodium bentonite.

2.2.2 Geosynthetic Clay Liners (GCLs)

Over the past several years, different geosynthetics manufacturers have proposed several unique GCL products that attempt to minimize hydraulic conductivity while maximizing shear strength (Bouazza, 2002). There are two main categories of GCLs, unreinforced and reinforced. Two unreinforced GCLs are presented in Figure 2.1, and four reinforced GCLs are presented in Figure 2.2.

Unreinforced GCLs typically consist of a layer of sodium bentonite that may be mixed with an adhesive then affixed to geotextile or geomembrane backing components with additional adhesives (Bouazza, 2002). The geotextile or geomembrane backing components of a GCL are typically referred to as the "carrier" geosynthetics. If hydrated, unreinforced GCLs have very low shear strength, but are still used in applications where slope stability is not a serious concern. In arid climates, it may be suitable to use a GCL with a carrier geomembrane next to another geomembrane so as to sandwich the sodium bentonite layer between two impermeable layers. It is expected that the geomembranes limit the passage of water

into the sodium bentonite layer, preventing hydration and an associated loss of shear strength. In this case, the unhydrated sodium bentonite would have sufficient shear strength to be used on steep slopes.

For applications that require higher shear strength, designers and manufacturers have proposed GCLs with internal fiber reinforcement. It is assumed that the shear stresses in the GCL are transmitted as tensile forces through these fiber reinforcements. The two predominant methods of GCL reinforcement are stitch-bonding and needle-punching (Bouazza, 2002). Stitch-bonded GCLs consist of a layer of bentonite between two carrier geotextiles that are sewn together with continuous synthetic fibers in parallel rows pattern.

Needle-punched GCLs consist of a layer of bentonite between two carrier geotextiles (woven or nonwoven), which are bonded together by a random assortment of fibers, punched through the GCL by threaded needles. The fiber reinforcements are punched first through the top carrier geotextile, through the sodium bentonite and the lower carrier geotextile, and then back through the top carrier geotextile. The fiber reinforcements are typically left entangled on the surface of the top carrier geotextile (Bouazza, 2002), which may have implications on the internal and interface shear strength of the GCL. For instance, Gilbert *et. al.* (1996) observed that as a needle-punched GCL is sheared, pullout of the needle-punched fibers from woven carrier geotextile may occur before the fibers rupture. This is especially the case for low normal stresses, as the fiber reinforcement connection with the carrier geotextiles is frictional in nature. To limit fiber pullout, some needle-punched GCL products have been thermally treated. This process, called "thermal bonding" or "thermal locking", heats each side of the GCL to induce bonding between individual fibers on the surface of the carrier geotextiles as well as between the fibers and the carrier geotextiles (Lake and Rowe, 2000). Thermal bonding may affect the shear strength of a needle-punched GCL significantly.

Throughout this study, the different reinforcing techniques for GCL are characterized as having a "rigid" or "flexible" connection between the fiber reinforcements and the carrier geotextiles. A rigid connection implies that the fiber reinforcements may not pullout from the carrier geotextiles during sodium bentonite

swell or during shearing. A flexible connection allows both of these phenomena. Stitch-bonded GCLs and thermal bonded needle-punched GCLs both have rigid connections, while needle-punched GCLs without thermal bonding have flexible connections. A flexible or rigid connection will lead to significant differences in shear strength and shear force-displacement behavior. In addition, Hewitt *et. al.* (1997) found that due to the larger amounts of fiber reinforcement in needle-punched GCLs than in stitch-bonded GCLs, needle-punched GCLs tend to act in a more brittle manner than the stitch-bonded GCLs when sheared (Hewitt *et. al.*, 1997).

Nonwoven or woven carrier geotextiles are used in fiber reinforced GCLs to achieve different purposes. Nonwoven carrier geotextiles provide puncture protection to the bentonite layer of the GCL, allow in-plane drainage and filtration, provide good connection for fiber reinforcements and provide interlocking capabilities with the sodium bentonite clay and other exterior interfaces. Woven carrier geotextiles provide tensile resistance to the GCL, allow filtration, and have limited interlocking capabilities. However, woven carrier geotextiles have the disadvantage of allowing easier bentonite migration (referred to as extrusion) than nonwoven carrier geotextiles (Stark and Eid, 1996).

A total of 11 different GCL product types have been tested by the SGI® laboratory between the period 1992 to 2001: Bentomat® ST (GCL *A*), Claymax® 500SP (GCL *B*), Bentofix® NS (GCL *C*), Bentofix® NW (GCL *D*), Bentofix® NWL (GCL *E*), Claymax® 200R (GCL *F*), Bentomat® DN (GCL *G*), Bentomat® CS (GCL *H*), Bentomat® HS (GCL *I*), Geobent® (GCL *J*), and Gundseal® (GCL *K*) GCLs. All GCLs except for GCL *K* were tested for internal shear strength, and all were tested for geomembrane interface shear strength except GCLs *D, E, G, I* and *J*. Table 2.1 shows the labels of the GCLs tested for internal shear strength, and Table 2.2 shows the labels of the GCLs tested for GCL-geomembrane interface shear strength. These tables also include a short description of the carrier geosynthetics and the reinforcement characteristics. The Bentofix® product line is manufactured by Serrot Inc., both the Bentomat® and Claymax® product lines are manufactured by CETCO® Inc., the Geobent® GCL is manufactured by Alberie Nau Inc., and the Gundseal GCL is manufactured by GSE®. From the above mentioned GCLs, only the Bentofix®

GCLs, the Bentomat® ST GCL and the Claymax® 200R GCL are still commercially available. However, all GCLs tested as part of the GCLSS Database have been used in several completed projects throughout the world. Product specifications for the GCLs still commercially available are provided in Appendix C.

2.2.3 Geomembranes

Geomembranes are flexible, polymeric sheets that have extremely low hydraulic conductivity and are typically used as water or vapor barriers (Sharma and Lewis, 1994). The geomembranes investigated in this study are thermoplastic geomembranes, which means that they have been reworked during manufacturing into their desired shape by heating and cooling. Geomembranes come in a variety of polymer types, interface characteristics and thicknesses, all of which may affect the shear strength of a GCL-geomembrane interface.

Different geomembrane polymer types may have significantly different shear strength behavior. Polyethylene (PE) geomembranes is the polymer predominantly used in geomembranes used in landfill applications. This polymer has a high chemical resistance and is durable for use in long-term applications. As the density of the polyethylene polymer changes, the flexibility of the geomembrane also changes. The flexibility of the geomembrane is related to the "plowing" of soil particles over the surface of the geomembrane (Dove and Frost, 1999). Plowing implies that as the geomembrane is sheared, it deforms in such a way that ridges are formed in the direction of shearing, which increases the shear strength of the interface.

High Density Polyethylene (HDPE) is the most common form of polyethylene because of its high chemical resistance, although its rigidity is a disadvantage in high stress applications. Low-Linear Density Polyethylene (LLDPE) and Very-Low Density Polyethylene (VLDPE) are more flexible forms of polyethylene used in landfill cover applications, where differential settlement is a concern. Polyvinyl Chloride (PVC) is another comparatively flexible polymer, although it has lower long-term durability than HDPE. PVC has other advantages over HDPE, such as lower cost, greater flexibility, easier seaming and larger panel sizes. It should be

noted that similar geomembrane polymers manufactured by different companies may not have similar interface shear strength behavior.

Geomembranes may be textured or smooth, and textured geomembranes may have different types of texturing. For instance, geomembranes may have a roughened surface by passing nitrogen gas through the polymer during formation (coextrusion), or may have a collection of asperities applied to the surface (impingement). These asperities are meant to allow greater connection between the geomembrane and the soil or other geosynthetics. With respect to GCL-geomembrane shear strength, the type of geomembrane texturing will affect the interlocking connections between the geomembrane asperities and the carrier geotextiles of the GCL. In addition, the fiber reinforcements present on the surface of the GCL (mainly in the case of needle-punched GCLs) may provide further interlocking. The strength of the interlocking connections between the textured geomembrane asperities and the carrier geotextiles of the GCL is related to the flexibility of the geomembrane polymer (Dove and Frost, 1999; Triplett and Fox, 2001).

The effect of thickness of the geomembrane on the shear strength of a GCL interface has not been investigated in past studies, although it is not likely to be a major factor. However, the thicknesses of the geomembranes are reported along with the interface shear strength in this study.

Four different geomembrane polymer types were tested in the GCLSS database, each with different surface characteristics. Table 2.3 summarizes the labels for the different polymer types. For each polymer type, a prefix has been added to the polymer label to indicate its texture: a prefix *T* stands for textured surface, and a prefix *S* stands for smooth surface. Geomembranes manufactured by 8 different companies are included in the GCLSS database: GSE® (GM *s*), NSC® (GM *t*), Polyflex® (GM *u*), Serrot® (GM *v*), SLT® (GM *w*), Watersaver® (GM *x*), EL® (GM *y*), and EPI® (GM *z*) geomembranes. Table 2.4 lists the geomembrane manufacturers along with their label, and the different polymer types produced by each manufacturer. Lower-case letters are used for the geomembrane labels to differentiate them from the GCL labels.

2.3 Overview of Shear Strength Testing on GCLs

The main objective of an internal GCL shear strength testing program is to determine the peak and residual (or large-displacement) shear strength values of a failure plane located at the center of the GCL. On the other hand, the main objective of an interface GCL shear strength testing program is to determine the peak and large-displacement shear strength values at the boundary between the carrier geosynthetic of the GCL and another geosynthetic or soil. These shear strength values should be obtained for different conditions that may exist in the field. The peak shear strength is the largest shear stress that can be resisted along the failure plane (Sharma *et. al.*, 1997). The residual shear strength of a GCL is the shear stress that remains at large shear displacements, and is usually reached after all fiber reinforcements (if any) in the failure plane have ruptured and the soil particles in the shear zone have aligned in the direction of shearing. Large-displacement shear strength is typically reported (as opposed to the residual shear strength) because the shear displacement capability of some test devices (50 mm for the standard direct shear box) is often not sufficient to mobilize GCL residual strength conditions. The residual shear strength of a GCL may not be reached until displacements as large as 700 mm (Fox *et. al.*, 1998).

Gilbert *et. al.* (1996) reports that because of the staged construction of landfills, drained conditions are typically present in GCL during shear in the field. This implies that there is no generation of excess pore water pressures due to the shear displacement. Therefore, the peak and large-displacement shear strength values reported should be defined for a sufficiently slow shear displacement rate. This ensures that the effective stress path is similar to the total stress path.

For a displacement controlled direct shear test, Figure 2.3 shows the typical variation of the internal or interface GCL shear stress with displacement. Higher normal stresses applied to the interface result in higher peak and residual shear strength values. The ratios between the peak and residual strength for each normal stress level are not necessarily the same. Also, the ratio between shear strength and the normal stress (the normalized shear strength = τ_f / σ) is not necessarily constant for increasing levels of normal stress.

The test conditions affecting the internal and interface shear strength of GCLs are the times of hydration and consolidation, the normal stress applied to the interface during testing, the normal stress during hydration or consolidation, the amount of swell during hydration, and the shear displacement rate (Gilbert *et. al.*, 1997). Also affecting the internal and interface shear strength are the amount of sodium bentonite extrusion during hydration and consolidation, reinforcement type, the consistency of reinforcement throughout the specimen (needle-punching may vary spatially), the rigidity of the reinforcement connections with the carrier geosynthetics and the amount of interlocking between a textured geomembrane (if present) and the carrier geotextile of the GCL.

2.4 Characterization of Shear Strength Envelopes of GCLs

A failure envelope is the relationship between the shear stress at failure and the normal stress applied to the interface. According to ASTM D6243, the standard for shear strength testing of GCLs, the Mohr-Coulomb failure criterion is used for defining the shear strength envelope for a given internal or external GCL interface. This failure criterion assumes that the peak and residual shear strengths vary linearly with normal stress. A generic interface shear strength envelope is described by the general expression:

$$\tau_f = f(\sigma) = c_A + \sigma\tan\delta \qquad \text{Eq. 2.1}$$

where τ_f is the shear stress at failure, c_A is the adhesion of the interface (or shear strength at zero normal stress), σ is the applied normal stress and δ is the interface friction angle. The term adhesion is used instead of the conventional term cohesion, which is reserved for soil shear strength characterization. Instead, adhesion is used for interface shear strength characterization soil and geosynthetics (Koerner, 1999).

Graphical representation of a generic failure envelope is shown in Figure 2.4. ASTM D6243 requires that a minimum of three points [(τ_{f1}, σ_1), (τ_{f2}, σ_2), (τ_{f3}, σ_3)] be used to define the peak or residual failure envelope for the given interface. The standard allows that the adhesion and friction angle of the failure envelope may be reported as test results, but the variation in shear strength with displacement plot (Figure 2.3) with a minimum of 20 points must also be provided. The standard also

requires that test conditions be reported, as the factors discussed in the previous section affect the shear strength behavior of the interface.

Sharma *et. al.* (1997) discourages dependence on a linear criterion for interface shear strength characterization when data shows a curvilinear trend. They mention that best-fit lines tend to be misleading, especially under low normal stresses where the use of a linear envelope may over-predict shear strengths. They also suggest that the adhesion of an interface should be ignored to provide a conservative shear strength estimate. However, a best-fit line through the origin may also overestimate strengths at higher normal stresses if the failure envelope is curvilinear. Fox *et. al.* (1998) and Gilbert *et. al.* (1996) used the nonlinear criteria proposed by Giroud (1993) and Duncan (1979), respectively, in analyzing the failure envelopes for internal failure of reinforced GCLs and obtained non-linear envelopes that fit their data acceptably. Sharma *et. al.* (1997) proposed that a bilinear failure envelope with best-fit lines for different ranges of normal stress may also be acceptable in representing non-linear behavior.

Yet another approach to describe the shear strength behavior of an internal GCL interface is the concept of an equivalent friction angle, (*e.g.* Giroud *et. al.*, 1990), which combines the effect of the friction angle and adhesion into a single parameter. The strength envelope is represented as a best fit line with a slope equal to the tangent of the apparent friction angle, passing through the origin. Although this approach is not typically used for design, it is useful for comparison of the shear strength behavior of several different GCLs or interfaces.

Also, it is important to assess the variability associated with GCL shear strength testing. Different shear strength values may be obtained at the same normal stress in multiple tests due to manufactured differences between GCL rolls, variations in natural sodium bentonite materials and errors inherent in the testing process (Snow *et. al.*, 1998). In addition, observed non-linear trends may also be a result of variability. Evaluation of variability is a significant aspect to be assessed in the analysis of the GCLSS database.

2.5 Laboratory Test Methods

2.5.1 Background

A shear strength test device for GCLs should mirror conditions in the field by controlling specimen confinement, normal stress during hydration, consolidation and shearing (all of which may be different depending on project-specific loading procedures), specimen hydration, consolidation, and shear displacement rate used during shearing. Although many devices have been built to test the internal shear strength of GCLs under different conditions, two approaches of applying a shear stress to a GCL specimen are predominant. They are the direct shear test, which places a translational shear force on the GCL specimen, and the ring shear (or torsional) test, which places a rotational shear force (about an axis normal to the plane of the specimen) on the GCL specimen. The current standard for shear strength testing of internal GCL or GCL interfaces, ASTM D6243, prescribes the use of the direct shear equipment for testing GCLs, although past testing has been done using both sets of equipment. A brief overview of the direct shear test and ring shear test are given below.

In addition to these two test types, testing of sodium bentonite clay using a conventional triaxial shear device and a simple shear device may provide additional insight into the shear strength behavior of GCLs. Test apparatuses using triaxial or simple shear concepts have not been developed for GCL shear strength testing due to the planar nature of the geosynthetics and specimen confinement difficulties.

2.5.2 Direct Shear Testing

As mentioned, ASTM D6243 prescribes the use of a direct shear device to investigate the internal or interface GCL shear strength. The prescribed direct shear device for GCLs is similar to that used to test geosynthetic-geosynthetic or geosynthetic-soil interfaces, ASTM D5321, yet it differs in specimen confinement, specimen sampling procedures, shear displacement rates and specimen conditioning. The device configurations and test procedures for internal GCL and GCL interfaces are similar, differing only in specimen confinement. In addition to the details in ASTM D6243 and D5231, Marr (2001) and Swan *et. al.* (1999) provide

comprehensive reviews of issues pertinent to internal and interface shear strength testing using a direct shear device. The discussion below applies to a GCL with a layer of sodium bentonite sandwiched between two carrier geosynthetics, although test procedures will not differ greatly for other GCL configurations.

The standard direct shear device for GCLs consists of separate upper and lower boxes which have dimensions of 300 mm by 300 mm. It is customary to use a bottom shear box that is slightly longer (50 to 75 mm) than the top box so that the contact area, and thus the normal and shear stresses, remain constant during shearing. This leads to some difficulties in test interpretation, as "virgin" soil in the bottom box comes into contact with "sheared" soil in the top box. This implies that residual shear strength effects such as particle reorientation may not be investigated adequately using a direct shear device. As peak shear strengths are typically reached within 10 mm of displacement for most reinforced and unreinforced GCLs (Fox *et. al.*, 1998), this issue is mainly of interest for residual shear strength measurements.

For internal GCL shear strength testing, as shown in Figure 2.5, the GCL is positioned in the direct shear device so that the top box is attached to the top carrier geosynthetic of the GCL, and the bottom box is attached to the bottom carrier geosynthetic of the GCL. As the upper and lower boxes are placed together, the width of the gap between the boxes is set so that the mid-plane of the GCL is at the middle of the gap. For GCL-geosynthetic interfaces, as shown in Figure 2.6, the geosynthetic (*e.g.* a geomembrane) is attached to the bottom box, and the GCL is attached to in the top box. The gap between the two boxes must be centered at the interface between the GCL and the external geosynthetic. A guiding system of low friction bearings must be used to ensure that the movement between the boxes is in a single direction.

According to ASTM D6243, for testing internal interface, the GCL specimen should be confined between two porous rigid substrates (usually plywood, porous stone or porous metal) with steel gripping teeth, which are placed between the upper and lower boxes. The gripping teeth allow the applied shear stress to be transferred completely to the inner GCL interface. No slippage should be allowed during testing, as this may allow tensile rupture of the top or bottom geosynthetics, which is not

representative of field failure conditions. The top or bottom carrier geosynthetics may be clamped in this position, but gluing should never be used as it may affect the behavior of the fiber reinforcements.

The GCL is typically conditioned according to project specifications, and ASTM D6243 does not provide specific guidance as to hydration or consolidation times, hydration liquids, and normal stresses applied during hydration and consolidation. The guidelines require, though, that the test conditions be reported. GCL specimen sampling from different sections of the roll is not specifically addressed by ASTM D6243, although it is stated that specimens should not be chosen from near the edge of the GCL roll (a minimum distance of 1/10 the total width of the GCL roll).

It is important to note that in needle-punched GCLs, the strength of the GCL depends on the degree of needle-punching. It has been reported that, as the needle-punching boards wear over time, the amount of needle-punching decreases leading to varying internal shear strength within the roll length (Bouazza, 2002; von Maubenge and Ehrenberg, 2000). ASTM D6243 does not specify the position in the roll from which the GCL specimen should be chosen, but the lot number of the roll should be provided in the results.

A constant normal stress (within 2% accuracy) is applied to the specimen during testing to reach a specified loading state, and once vertical displacements within the GCL specimen have ceased, the top box is translated with respect to the bottom box. It is important to ensure that the normal stress translates with the top box in order to simulate field loading conditions. The normal pressure may be applied in different ways, depending on the ranges of normal pressures of interest, as shown in Figures 2.7(a), 2.7(b) and 2.7(c). Variations on the direct shear box design include the pullout box arrangement used by Fox *et. al.* (1998). This pullout box design was reported to minimize several of the boundary effects present in traditional direct shear testing, allow greater displacements, and prevent the normal load from translating across the GCL specimen during shear.

Shear strength tests can be conducted at a constant shear displacement rate (displacement-controlled test), which means that the magnitude of the shear force

varies in order to move the top box at a constant rate. Alternatively, a constant shear force may be applied (stress-controlled test), which is useful to investigate creep phenomena. Stress-controlled tests are not discussed in this study as all experimental data discussed herein were obtained from displacement-controlled tests. It is important to calibrate the direct shear device to investigate the internal shear resistance of the device. For the displacement-controlled test, the shear force is recorded as a function of the horizontal displacement of the moving box.

ASTM D6243 does not prescribe a shear displacement rate to be used for GCL testing as the earlier standard ASTM D5321 does (1.0 mm/min). The standard states that excess pore water pressures may be generated in the sodium bentonite clay component of the GCLs as the shear force is mobilized, so the shear displacement rate must be significantly slow to allow drainage. As it is not likely for pore pressures to be generated in the field (Gilbert et. al., 1997; Marr, 2001), it is important to control the shear displacement rate in order to correctly simulate field conditions. The generation of excess pore water pressures leads to changes in effective stress throughout the test, which is unrealistic in a field loading situation. However, too slow shear displacement rates will lead to long testing times and increased costs.

If the actual pore pressures during testing were known, a shear displacement rate may be found experimentally that permits sufficient time for excess pore pressure dissipation. As this is not possible with the current level of technology, an estimate of the shear displacement rate that allows adequate pore pressure dissipation is necessary. According to the standard, the shear displacement rate (SDR) should be defined by:

$$SDR = \frac{d_f}{50 \times t_{50} \times \eta} \qquad \text{Eq. 2.2}$$

where d_f is the estimated horizontal displacement, t_{50} is the time required to reach 50% consolidation under the current normal stress assuming drainage from the top and bottom of the specimen, and η is a factor used to account for the actual drainage conditions. For d_f, ASTM D6243 requires a minimum of 2 inches of displacement be allowed when reporting the residual shear strength conditions of the GCL. ASTM D6243 defines the possible values of η to be 1 for drainage from both boundaries, 4

for shearing between the GCL and an impermeable external interface and 0.002 for shearing between the GCL and a permeable external interface. The value of t_{50} will vary for different mixtures of clay used for particular GCLs.

Frobel (1996) and Marr (2001) identify the practical nature of using direct shear tests because of their short duration, quick specimen preparation time and ready availability. These are important advantages of the direct shear device, especially if several tests are necessary. Frobel (1996) identifies the fact that the stress conditions in a sufficiently large (*i.e.* 300 mm by 300 mm) direct shear device are representative of the stresses experienced by a GCL in the field when failure occurs, and that boundary effects are minimized.

2.5.3 Ring Shear Testing

The shear displacement at failure and shear displacement rate may have significant effect on the internal shear strength of a GCL. As it is often difficult to investigate the effect of these aspects using a standard direct shear device due to its finite shear displacement, a ring (or rotational) shear device may be more suitable. This device is capable of achieving large displacement as the ring shaped specimen is rotated about a central axis, with a constant contact area during shearing (Eid *et. al.*, 1999). The top and bottom carrier geosynthetics of the GCL are typically wrapped around the upper and lower rigid substrates and confined with clamps. Because hydrated sodium bentonite is very plastic, it may migrate throughout the specimen. To prevent this, the device machinery that fits through the ring in the specimen ensures that the rigid substrates remain at a constant separation throughout the ring. The normal load moves with the top rotating rigid substrate, which is similar to the loading conditions in the field. Despite their ability to accurately measure residual shear strengths (Skempton, 1985, Lupini *et. al.*, 1981), ring shear tests are more difficult to conduct and may have significant boundary errors.

2.5.4 Verification of Direct Shear and Ring Shear Device Test Results

Direct shear and ring shear test results on soils in general have been found to correlate well with back-calculations of landslides and skin-friction of piles due to

similar laboratory and field loading conditions (Arthur *et. al.*, 1988). Although analyses of slope failures involving GCLs are not widely published, the slope failures at the Mahong Landfill site (Stark *et. al.*, 1998) and the US Environmental Protection Agency (EPA) GCL test section in Cincinnati, Ohio (Stark and Eid, 1996) provide excellent opportunities to verify the results of different test devices for GCLs.

Stark *et. al.* (1998) investigated the Mahong Landfill failure in Youngstown, Ohio. It was found from field forensic investigations that failure occurred along the plane of an unreinforced, geomembrane-backed GCL located in the landfill base liner. In order to correctly simulate the conditions that occurred in the field, the investigation included a study of the loading procedures and the assumed hydration process for the GCL. The field conditions were simulated using a ring shear device. The results of the tests on internal GCL and GCL-geomembrane interfaces were consistent with the back-calculated shear strength of the soil using two dimensional limit equilibrium analyses. In forensic studies, it was found that the settlement of the overlying waste allowed very large shear displacements to occur in the GCL. The GCL had reached residual conditions while the overlying waste had not yet reached peak conditions. Because of this, ring shear tests used by Stark *et. al.* (1998) were more suitable than other testing methods.

Stark and Eid (1996) present the results of a three dimensional back-analysis of the EPA GCL test sections along with test results on the GCLs using a direct shear device and a ring shear device. For the failure interface between a GCL and a geomembrane, the mobilized interface friction angle was approximately 21.5 degrees. Ring and direct shear tests were conducted on the same GCL under fully hydrated conditions, and it was found that the ring shear test obtained a peak friction angle of 22.5 degrees, and the direct shear test obtained a peak friction angle of 23.8 degrees. Both test methods obtained friction angles slightly above the actual back-calculated three dimensional friction angles, so the difference in actual and experimental friction angles may be attributed to three dimensional effects, such as the vertical failure surfaces at the edges of the GCL test pad.

In summary, the shear strength test results from direct shear or ring shear devices may differ from back-calculations of shear strength due to three dimensional

effects or differences in scale. In addition, further differences in the shear strength measured in the laboratory and the shear strength back-calculated from forensic studies may arise from the tensile forces that may develop in the carrier geotextiles of the GCL. This phenomenon may increase the back-calculated shear strength of the GCL as the tensile forces provide additional resistance to down-slope deformations. The tensile forces that develop in the GCL may not be measured using a direct shear or ring shear test, so caution should be used when comparing field-calculated and laboratory-measured shear strengths.

2.5.5 Other Test Methods

Other equipment configurations been developed for testing internal and interface GCL shear strength as well as the shear strength of the individual components of the GCLs (*e.g.* sodium bentonite) under various loading conditions.

The tilt table is a device that has been employed by some laboratories to test large specimens under field loading conditions (Marr, 2001). In this test, the GCL under a constant normal stress is tilted slowly on one side in order to induce a shear force. The angle of tilt and the displacements are measured, and the angle of tilt at which the top box begins to slide indicates the peak friction angle. As this is a stress controlled test (*i.e.* a constant shear force is applied throughout the specimen), it is unable to measure residual shear strengths due to the rapid failure which occurs after peak conditions are reached.

An adaptation of the direct shear box is the cylinder direct shear test, which was used by Moss (1999) to test geosynthetic interface shear strength. In this test, one geosynthetic is affixed to the inside of a hollow cylinder, and another geosynthetic is affixed to the outside of a slightly smaller cylinder. The smaller cylinder has the characteristic of being able to expand to confine the interface under a constant normal stress (equal to the radial stress). For shearing, the outer cylinder is rotated about the stationary inner cylinder. This device may potentially test large specimens to displacements characteristic of residual conditions (Marr, 2001), although there may be issues related to specimen confinement and lateral sodium bentonite migration.

Although GCLs cannot be tested using a conventional triaxial cell because of their planar configuration, this test may provide insight about the shear strength behavior of sodium bentonite. Mesri and Olson (1970) investigated the drained and undrained shear strength of sodium montmorillonite clay, the results of which are discussed in section 3.4. The use of a triaxial cell allows control of the stress state in the specimen with higher precision than direct or ring shear devices. In addition, pore water pressures generated during shearing may be measured. This permits an effective stress analysis, which allows better insight into the shear strength behavior of the sodium bentonite. Table 2.5 summarizes the different characteristics of the direct shear device and the ring shear device with comparison to the characteristics of conventional triaxial compression testing on sodium bentonite clay.

It has been reported that shear strengths measured by triaxial cell tests are lower than those measured by direct shear tests (Lupini *et. al.*, 1981, Kulhawy, 1990). Triaxial cell tests also provide the ability to test soils under different loading conditions, such as compression, extension and pure shear. However, triaxial cells can only control two degrees of freedom, axial and radial, which limits the states of stress that may be applied to the soil sample. There is also an incompatibility in the boundary conditions of the triaxial cell, with rigid platens on the top and bottom of the specimen and a flexible membrane on the sides.

A simple shear test may also provide additional insight into the shear strength of sodium bentonite clay (Wroth, 1987), although there has not been a study focusing on sodium bentonite. The simple shear device was initially developed so that an element of soil could be distorted in pure shear (*i.e.* the change in vertical angle can be measured directly as the shear strain). In this test device, backpressure may be applied, which permits the pore pressures to be measured and allows an understanding of the effective stress state in the soil. Also, the stress-strain relations for the soil may be developed as the shear and normal strains measured by the simple shear device are consistent with the definitions developed in mechanics theory.

Table 2.1: GCLs in the GCLSS Database Tested for Internal Shear Strength Listed by Product Name; with Labels and Reinforcement Description

GCL Product Type	Description	GCLSS Label
Bentomat® ST	Needle-Punched W-NW	A
Claymax® 500SP	Stitch-Bonded W-W	B
Bentofix® NS	Needle-Punched W-NW, Thermally Bonded	C
Bentofix® NW	Needle-Punched NW-NW, Thermally Bonded	D
Bentofix® NWL	Lightly Needle-Punched NW-NW, Thermally Bonded	E
Claymax® 200R	Unreinforced W-W	F
Bentomat® CS	GCL A with Hydraulic Improvement Additives to the Sodium Bentonite	G
Bentomat® DN	Needle-Punched NW-NW	H
Bentomat® HS	Needle-Punched W-NW, Adhesive Strengthened Reinforcements	I
Geobent®	Needle-Punched W-NW	J

Note: W = Woven Carrier Geotextile
NW = Nonwoven Carrier Geotextile

Table 2.2: GCLs Tested for GCL-Geomembrane Interface Shear Strength Listed By Product Name; with Labels and Reinforcement Description

GCL Product Type	Description	GCLSS Label
Bentomat® ST	Needle-Punched W-NW	A
Claymax® 500SP	Stitch-Bonded W-W	B
Bentofix® NS	Needle-Punched W-NW, Thermally Bonded	C
Claymax® 200R	Unreinforced W-W	F
Bentomat® CS	GCL A with Hydraulic Improvement Additives to the Sodium Bentonite	G
GSE® Gundseal®	Unreinforced Sodium Bentonite with a Geomembrane Backing	K

Note: W = Woven Carrier Geotextile
NW = Nonwoven Carrier Geotextile

Table 2.3: Definitions of the Different Geomembrane Polymer and Surface Characteristics

Name Designations	Surface Characteristics	Polymer Type
THDPE	Textured	High Density Polyethylene
SHDPE	Smooth	High Density Polyethylene
TVLDPE	Textured	Very Low Density Polyethylene
SVLDPE	Smooth	Very Low Density Polyethylene
TLLDPE	Textured	Low-Linear Density Polyethylene
SLLDPE	Smooth	Low-Linear Density Polyethylene
PVC	Smooth	Polyvinlychloride

Table 2.4: Geomembranes Tested for GCL-Geomembrane Interface Shear Strength Listed by Manufacturer; with Labels and Polymer Types Manufactured

Geomembrane Manufacturer Name	Polymer Types Manufactured	GCLSS Label
GSE®	THDPE, TLLDPE, SVLDPE	s
NSC®	THDPE, TVLDPE, TLLDPE, SHDPE	t
Polyflex®	THDPE, TVLDPE, TLLDPE, SVLDPE, SLLDPE, SHDPE	u
Serrot®	THDPE	v
SLT®	THDPE	w
Watersaver®	Smooth PVC	x
EL®	Faille Finish PVC	y
EPI®	Smooth PVC	z

Table 2.5: Comparison between Different Test Procedures for Sodium Bentonite Clay and GCLs

Category for Comparison		Direct Shear Testing on GCL Internal and Internface Shear Strength	Ring Shear Testing on GCL Internal and Internface Shear Strength	Conventional Undrained Triaxial Shear Testing on Sodium Montmorillonite
Technicalities	Supporting Papers/Users	SGI Laboratory (1992-Present), Gilbert *et. al.*, (1996), Fox *et. al.* (1998), Triplett and Fox (2001)	Stark and Eid, (1996), Eid and Stark (1997, 1999)	Mesri and Olson (1970)
	Availability and Familiarity of the Device to Researchers	Not widely available, but familiar	Neither (Modified Device)	Available and Familiar
Normal Stress Concerns	Range of Normal Stresses	2.4 kPa - 2880 kPa	80-340 kPa	70-414 kPa
	Normal Stress Translates Across Specimen During Shear?	Yes	No	No
Specimen Preparation	Duration of Sample Preparation (Cutting of GCL, Placement in Device, *etc.*)	Fast	Lengthy	Lengthy
	Specimen Fixity	Clamp edges	Glue or clamp edges	Not Applicable
	Loss of Bentonite an Issue?	No	Yes	Not Applicable
	Specimen Hydration Time	24 hours to several weeks	2 weeks	Lengthy
	Specimen Hydrated within the Assembled Device?	Yes	No	Not Applicable
Testing Aspects	Typical Specimen Size	300-mm by 300-mm top box	100-mm outside diameter, 40-mm inside diameter	1.5 in diameter, 3.0 in height
	Shear Displacement Rates Used in Tests	Less than or equal to 1 mm/min	0.015 - 36.5 mm/min	0.000381 - 0.423 mm/min
	Maximum Displacement	75 mm	Infinite	Limited by definition of a failure plane
	Forced Failure Plane?	Yes	No	No
	Accurate and Consistent Measurement of Pore Water Pressures?	No	No	Yes

Figure 2.1: Typical Unreinforced GCLs: (a) Sodium Bentonite Mixed with Adhesives, Sandwiched Between Two Geotextiles; (b) Sodium Bentonite Mixed with Adhesives, Adhered to a Geomembrane

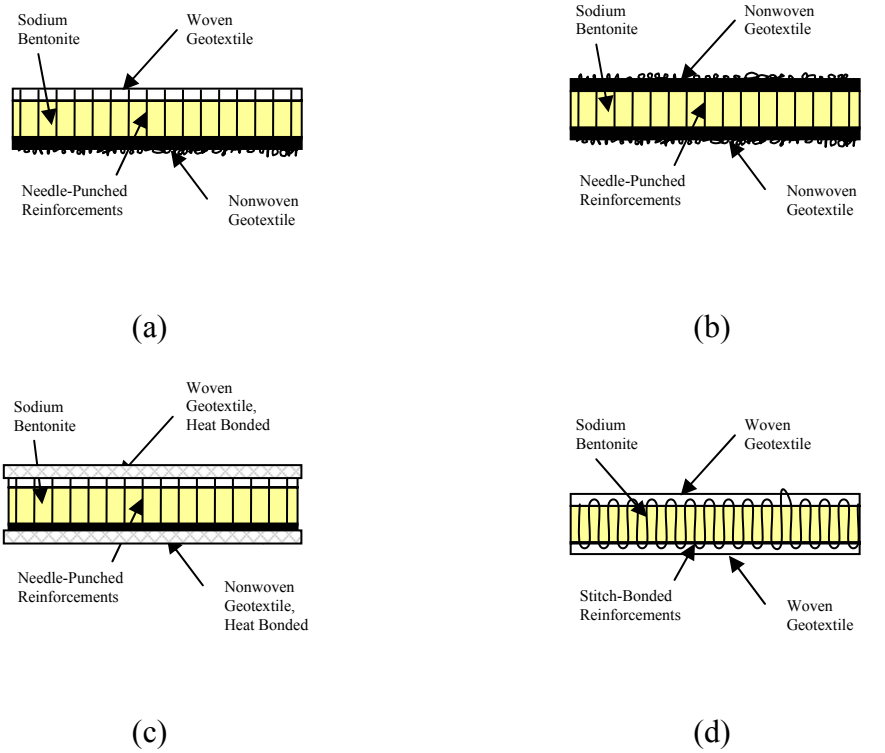

Figure 2.2: Typical Reinforced GCLs: (a) Sodium Bentonite Sandwiched between Woven and Nonwoven Geotextiles, Needle-Punched; (b) Sodium Bentonite Sandwiched between Two Nonwoven Geotextiles, Needle-Punched; (c) Sodium Bentonite Sandwiched between Woven and Nonwoven Geotextiles, Needle-Punched with Thermal Bonding; (d) Sodium Bentonite Sandwiched between Two Woven Geotextiles, Stitch-Bonded Together

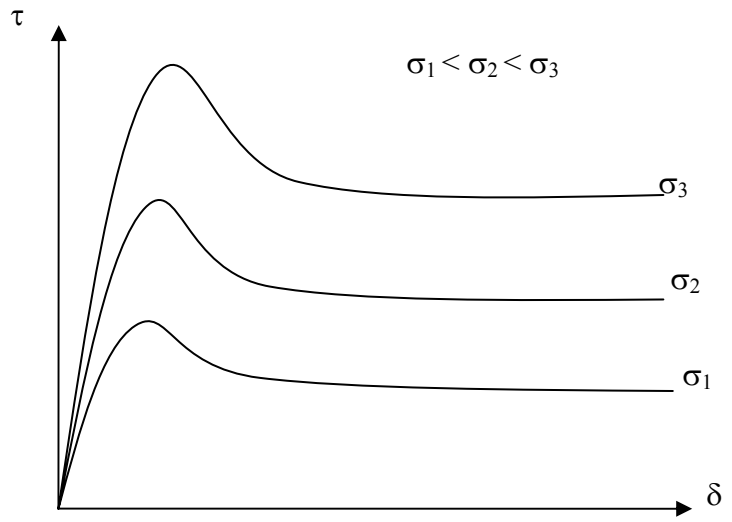

Figure 2.3: Variation in Shear Stress with Shear Displacement for Different Test Normal Stresses

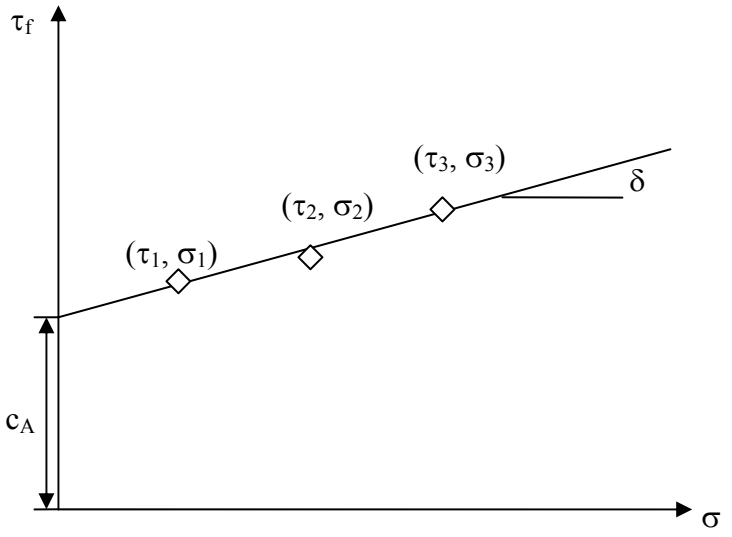

Figure 2.4: Shear Strength at Failure for Different Test Normal Stresses; Assuming a Linear Failure Envelope

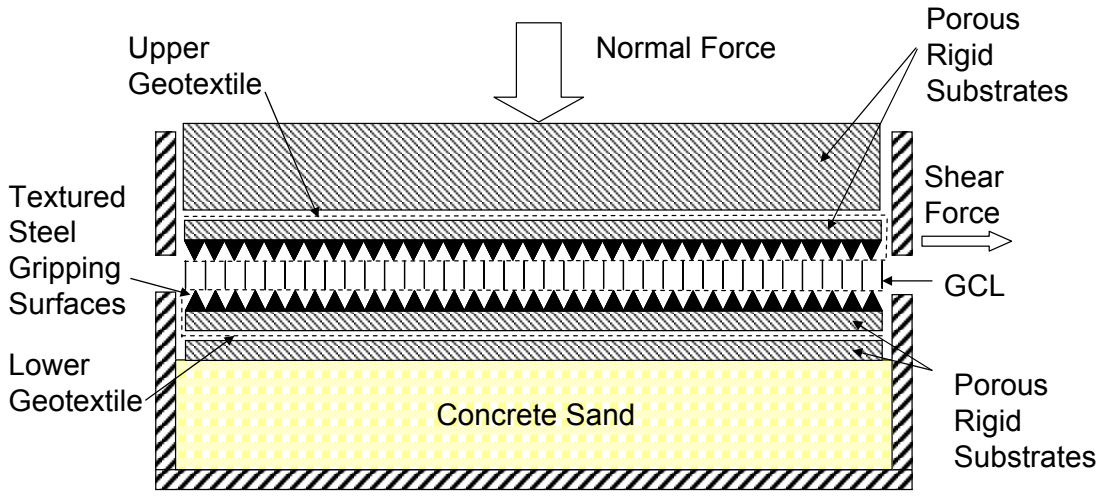

Figure 2.5: GCL Specimen Confinement in the Direct Shear Device (Internal Shear Testing Configuration); Not to Scale

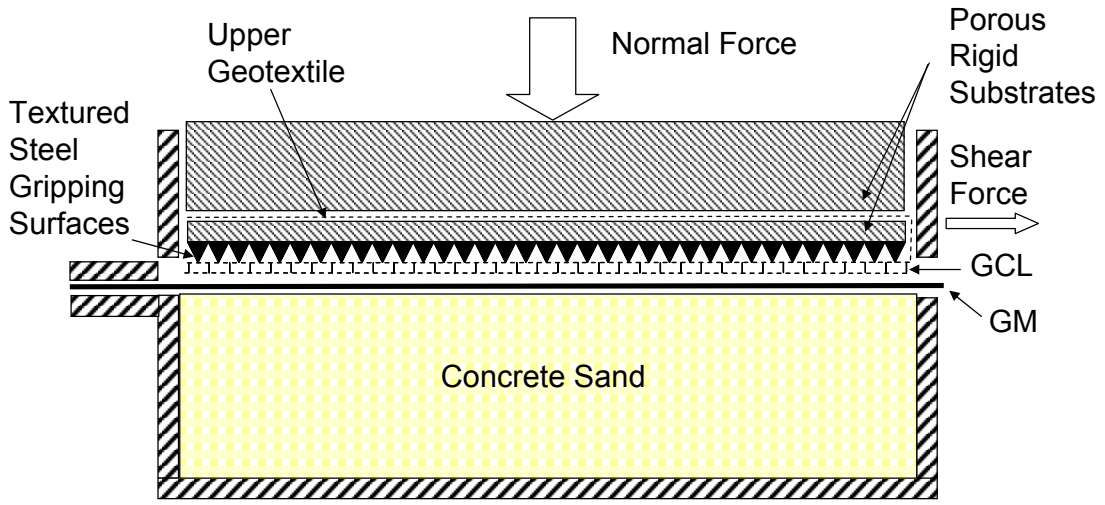

Figure 2.6: GCL-Geomembrane Specimen Confinement in the Direct Shear Device (Interface Shear Testing Configuration); Not to Scale

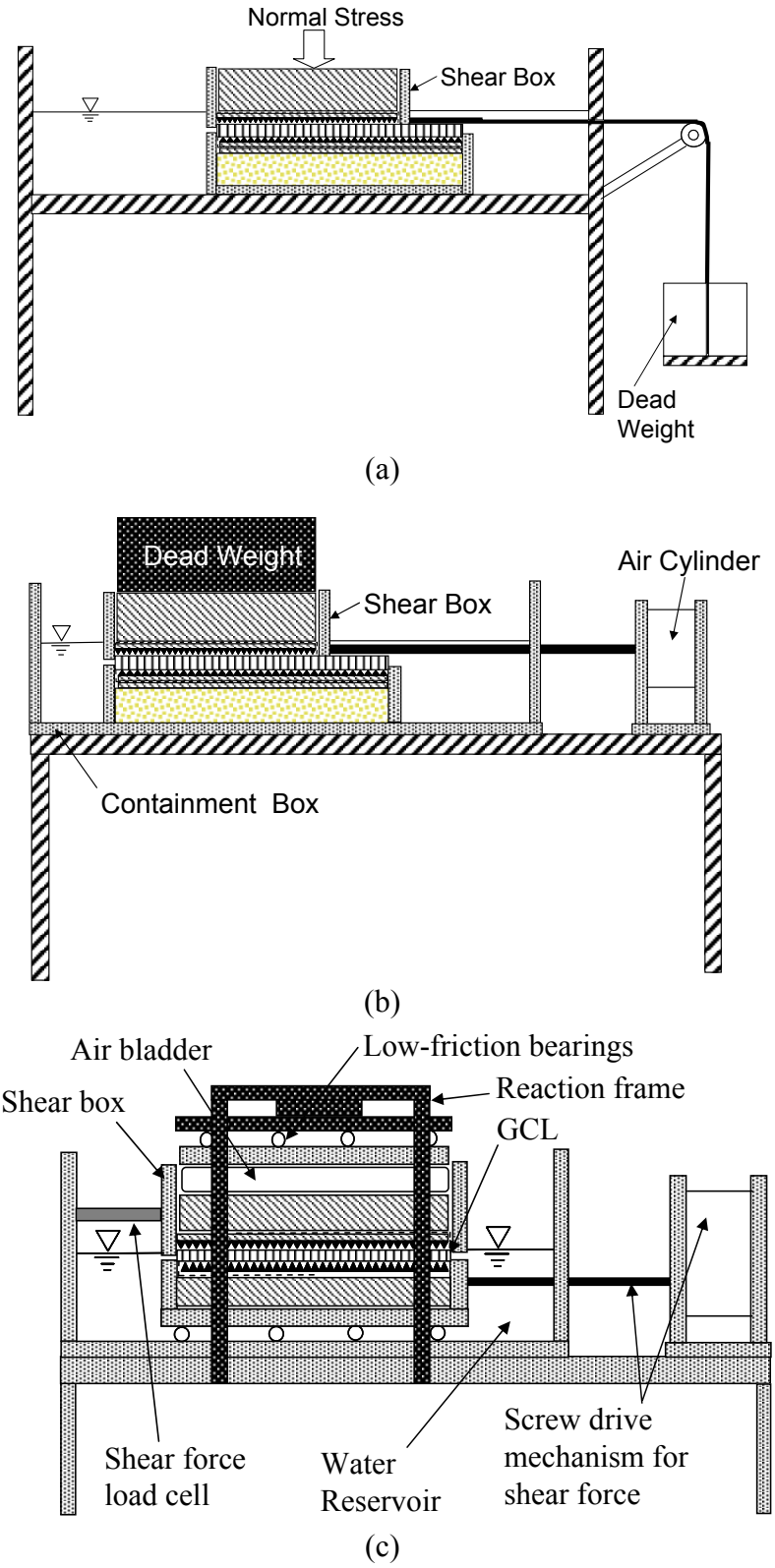

Figure 2.7: Direct Shear Device for (a) Low, (b) Medium, (c) High Normal Stresses

3 State-of-the-Art Review of Shear Strength Testing of GCLs

3.1 Introduction

Several studies in the past decade have investigated internal and interface GCL shear strength. Of particular interest was the assessment of the effects of field conditions (*e.g.* hydration time, consolidation time, shear displacement rate) on the internal and interface shear behavior of GCLs (Gilbert *et. al.*, 1996; Gilbert *et. al.*, 1997; Eid and Stark, 1997; Eid *et. al.*, 1999; Fox *et. al.*, 1998; Triplett and Fox, 2001). These studies have addressed important practical design considerations, but full understanding of GCL shear strength behavior is, at best, incomplete. Since these studies are based on a limited number of test results, a significant database of shear strength tests on GCLs is required to provide further conclusions concerning GCL shear strength under a wide range of conditions. As mentioned in Chapter 1, a database of internal and interface GCL shear strength test results has been compiled (the GCLSS database) with 320 internal GCL direct shear test results 325 direct shear test results for the interface between a GCL and a geomembrane. In order to provide a sound basis in the analysis of such significant database, it is necessary to conduct a state-of-the-art review on the available information. The information gathered through this review aids in the interpretation of the results of the database analysis, and provides a perspective on current GCL shear strength testing aspects.

Although available studies explaining the physical mechanisms related to the shear behavior of GCLs are somehow limited, numerous studies have been reported on the behavior of sodium bentonite clay, the main component of manufactured GCL products. It is useful then to also evaluate the results of these studies on sodium bentonite, as it is relevant for better understanding of the shear behavior of different GCL products.

This chapter has three purposes: to (*i*) review findings from past studies on the shear strength behavior of sodium bentonite clay, (*ii*) review findings from past studies on the internal shear strength of GCLs, (*iii*) review findings from past studies on the interface shear strength between the woven carrier geotextile of a GCL and a geomembrane.

3.2 Shear Strength of Sodium Bentonite Clay

3.2.1 Introduction

Despite its low hydraulic conductivity, sodium bentonite has very low shear strength when hydrated. Due to different factors, the shear strength is also highly variable and often difficult to predict. This section addresses several of the factors affecting the shear strength of sodium bentonite, but does not dwell on those factors affecting hydraulic conductivity or other geotechnical aspects.

As many of the shear strength characteristics of sodium bentonite depend on clay mineralogy, a brief discussion of the structure of sodium bentonite is appropriate. Sodium bentonite is form of montmorillonite, which is a smectite mineral (Mitchell, 1994). Smectite minerals have a unit cell consisting of a 2:1 structural unit with one silica tetrahedron unit combined with two aluminum octahedral units. In smectite, every sixth Al^{3+} ion in the aluminum octahedron is replaced by an Mg^{2+} ion, resulting in a net negative charge on the surface of the smectite particle. The net negative charge is balanced by cations in the pore water between the clay particles. The water and dissolved cations are closely attracted to the clay particles, and form a composite layer known as a "diffuse double layer" (Mitchell, 1994). The size of the diffuse double layer determines the balance between attractive and repulsive forces between the clay particles, which are a significant factor in the shear strength of the clay as a whole. Sodium bentonite is a montmorillonite with sodium (Na^{+}) as exchangeable cations.

The geometry and structure of sodium bentonite particles are other factors that affect the shear strength behavior of sodium bentonite clay. Sodium bentonite crystals are platy in nature with a diameter to thickness ratio of 150-500 and a thickness of about 10 Angstroms, implying a very large specific surface (Mitchell, 1994). This large surface area implies that there is more surface area to attract oppositely charged ions to the negatively charged clay particle surfaces. The more cations attracted to the surface of each particle, the greater the repulsion forces between particles. As the faces have the largest charge concentration, they repel each other, tending the structure to a face-to-face orientation. Sodium bentonite particles

have also been found to have great flexibility, implying that the particles may warp or bend similar to a beam. This facilitates reorientation of the particles into the direction of shear as shear displacement increases with only a small amount of dilation (Mesri and Olson, 1970). Because of these facts, Mesri and Olson (1970) postulated that that the planar arrangement related to a dispersed structure prevents significant dilatancy effects during shearing. Also, although the in-situ dispersed structure implies that the sodium bentonite crystals are face-to-face, they are not necessarily aligned with the direction of shearing, so reorientation may still be necessary.

The chemistry of the pore water is another factor that affects the shear strength of smectite clays, as it affects the thickness of the diffuse double layer and thus the interaction between clay particles. Sodium bentonite is the result of a large concentration of sodium ions present in the diffuse-double layers of the clay particles. Mesri and Olson (1970) found that as the sodium concentration in the diffuse double layer of smectite varies, there are negligible changes in the friction angle of the clay.

Sodium bentonite also has a very high cation exchange capacity (80 to 150 meq/100 g Clay) due to the free sodium cations present in the diffuse double layer. Significant changes in shear strength behavior can be expected if cation exchange occurs, substituting monovalent sodium with multivalent cations, like calcium or magnesium. The change in charge of the cations decreases the size of the diffuse double layer, thus changing the interaction forces between particles, and thus volume changes during wetting or drying.

3.2.2 Effect of Sodium Bentonite Swell

The swelling behavior of sodium bentonite as it hydrates can influence its shear strength behavior by changing both the structure of the soil and the effective stress between the particles. In other words, swelling affects the material properties of a soil and the fluid pore pressure (which in turn affects the effective stress between particles). When confined sodium bentonite swells, it exerts an outward pressure as it changes in volume. The "*swell pressure*" is defined as the level of normal stress at which the sodium bentonite does not swell beyond its initial height, although the soil reaches saturation (Petrov *et. al.*, 1997).

In an unhydrated state, there is little particle interaction and the particles are initially randomly oriented. If hydration occurs under unconfined conditions, the sodium bentonite particles absorb water into their diffuse double layers and begin to repel each other, leading to swelling of the soil matrix. As this occurs, Madsen and Muller-Vonmoos (1989) report that the particles become arranges into a dispersed structure with high void ratio. However, if the sodium bentonite is confined, the soil may not freely expand as it hydrates, and the particles may or may not be able to change orientation thus remaining in a flocculated structure with low void ratio. For high confining pressures (*i.e.* above the swell pressure), the sodium bentonite particles remain in their initial orientation with a low void ratio. In contrast, for low pressures, the particles arrange themselves in a dispersed, parallel-oriented structure with a high void ratio similar to unconfined sodium bentonite.

The suction within the sodium bentonite is due both the capillarity between soil particles and an electrical imbalance on the surface of the clay particles. The suction corresponding to the latter phenomenon is referred to as the "osmotic" suction. The suction related to capillarity depends on the meniscus effect in a partially saturated soil in which there is both an air and water phase. The capillary suction is thus be equal to zero when the soil reaches saturation (w = 100%) and all of the soil voids are filled with water. However, at saturation, osmotic suctions still may be present, implying that the soil is able to have a greater percentage by weight of confined water than soil particles. Osmotic suction is related to the imbalance between the cation concentrations near the soil particles and in the free pore water, so until the soil has reached electrostatic equilibrium, the osmotic suction continues to draw water into the soil. In non-swelling soils, the effect of the osmotic suction on the effective stress in the soil is typically not considered, yet it is potentially quite important to the shear strength behavior of sodium bentonite clays.

When the sodium bentonite reaches a steady state swell level, any disturbance, such as shearing tends to disrupt the structure and realign the orientation of the clay particles. This will lead to the mobilization of excess pore pressures during shearing. For high confining pressures (*i.e.* above the swell pressure) the excess pore pressures generated during shearing will be positive (as expected for a normally consolidated

soil). However, for low confining pressures, the excess pore pressures may be related to the osmotic suction in the soil. If the soil is not fully hydrated (i.e. osmotic suction still exists), then any disturbance will result in negative excess pore water pressures being generated.

3.2.3 Non-Linear Failure Envelope

Mesri and Olson (1970) reported that sodium montmorillonite specimens tested in undrained triaxial compression tests exhibited a pronounced curvature, and the friction angle of the failure envelope decreased from 4 degrees to zero degrees as the consolidation pressure varied from 68.9 to 552 kPa. The shear strength of sodium montmorillonite with a sodium concentration of 0.1 N is shown in Figure 3.1, with a linear best-fit line shown to emphasize the non-linearity. The test results are shown in Table 3.1. As the tests were conducted in a drained triaxial compression test, only the peak shear strength test results were reported due to time constraints. This figure shows a slightly different behavior for tests conducted at low and high confining pressures. To account for these differences in behavior, a bilinear failure envelope is proposed in Figure 3.2. It is clear that different trends are apparent for both of the failure envelopes. Linear failure envelope data for Figures 3.1 and 3.2 are presented in Table 3.2. This table shows that for the bilinear failure envelope, the failure envelope for low confining pressures has a greater friction angle and a lower intercept value than the failure envelope for high confining pressures. The non-linear failure envelope may be due to variability in the shear strength data, or to the excess pore pressure generated during shearing at different levels of confining pressure.

The test conditions used by Mesri and Olson (1970) have been reported to place a lower bound on the peak shear strength of sodium montmorillonite clay (Eid and Stark, 1997). Because of this, these test results are very useful in investigating the internal shear strength of unreinforced GCLs.

3.2.4 Residual Shear Strength of Sodium Bentonite Clay

Lupini *et. al.* (1981) reported that at large displacements, the shear strength of clays may decrease to a level below the critical state shear strength (*i.e.* where zero volume change occurs with continued shear displacement). The residual shear

strength is the minimum constant shear strength value attained at large displacements for slow shear displacement rates (Skempton, 1985). At critical state, the particles (or groups of particles) are randomly oriented due to churning and remolding (Lupini *et. al.*, 1981). After reaching critical state conditions, the individual clay particles begin to reorient into the direction of shear and the shear strength stabilizes as particles slide past each other in a frictional nature. The reorientation of the clay particles into the direction of shearing is a function of the flexibility of the particles and the shear displacement rate. Skempton (1985) found that faster shear displacement rates result in higher residual shear strength, as this is related to the amount of remolding at critical state levels. At higher normal stresses, particle reorientation into the direction of shear occurs at smaller displacements (Skempton, 1985).

3.3 Internal Shear Strength of GCLs

3.3.1 Background and Significance

Several studies have been conducted in the past ten years during the development period of the current standard ASTM D6243 using different test devices, procedures and conditions to develop the testing aspects representative of the key field conditions. An understanding of these testing aspects is necessary in order to focus the analysis of the GCLSS database on any conflicts seen in the shear strength behavior of GCLs.

It should be noted that the range of test conditions (normal stress, shear displacement rate, *etc.*) currently reported in literature is not broad enough to draw conclusions concerning the full range of conditions in the field. That is, the conclusions from past studies only apply to specific test conditions. This is important, as the results of the past studies may contradict the results of the analysis of the GCLSS database when test conditions differ.

3.3.2 Hydration History of Sodium Bentonite Clay in GCLs

The sodium bentonite clay in unreinforced GCLs is initially in a powdered, dry form and is typically mixed with an adhesive to provide cohesion between particles while in dry conditions. At this point, negative pore water pressures are present in the GCL. This implies that the dry sodium bentonite is similar to an

overconsolidated clay with a preconsolidation pressure equal to the swell pressure of the sodium bentonite. Loading of a partially hydrated GCL in an oedometer test will follow the unloading-reloading curve in a normal effective stress vs. void ratio plane until the swell pressure (the preconsolidation pressure) is reached. On the other hand, loading of a fully hydrated GCL (static pore water pressures) will follow the normally consolidated line in a normal effective stress vs. void ratio plane. The shear-force displacement curves of most GCLs are similar to an overconsolidated soil (Gilbert *et. al.*, 1996; Fox *et. al.*, 1998).

It is also assumed that the structure of sodium bentonite (when uniformly hydrated) is equivalent in to that of remolded natural sodium bentonite clay with the same water content. There should be no preferred orientation of the particles. However, bonding may exist between the particles due to the admixed adhesives. The effect of these adhesives on the shear strength of the sodium bentonite clay has not been investigated. It is expected that they have some effect on the shear strength of dry sodium bentonite and a negligible effect on the shear strength of hydrated sodium bentonite (Eid and Stark, 1997).

3.3.3 Effect of GCL Hydration

Among the many factors that affect GCL shear strength, hydration of the sodium bentonite layer has been reported to result in the greatest decrease in shear strength (Gilbert *et. al.*, 1997). Hydration increases the initially negative matric suction in the dry sodium bentonite to static pore water pressure conditions through the contact with water. Contact with water will also result in significant swelling of the sodium bentonite. Full hydration can be defined as the equilibration of pore pressures and a cease in further swelling. A percentage change in vertical swell of less than 5% can be obtained for unconfined GCLs in a period of 10 to 20 days, typically indicating full hydration (Gilbert *et. al.*, 1997).

As pore pressures or changes in vertical swell were not measured during the hydration of the GCL specimens in the GCLSS database, the level of hydration of the sodium bentonite may be estimated by the time of hydration (t_H) allowed, which has been correlated well with the level of hydration (Gilbert *et. al.*, 1997). Frobel (1996)

recommends a time of hydration greater than 72 hours to ensure that the sodium bentonite has adequate time to reach approximate pore pressure equilibrium. However, Stark and Eid (1996) found that a time of hydration of 250 hours may be required to reach full hydration. Still, additional hydration time beyond 72 hours does not significantly increase the water content of the GCL, especially under high normal stresses. ASTM D6243 does not recommend a specific time of hydration, but requires the hydration conditions to be reported with the results.

The water content of the sodium bentonite is not used extensively to estimate the level of hydration because the water content at full hydration may vary depending on the normal stress applied during hydration. This normal stress will be referred to as the "hydration normal stress (σ_H)". For example, at high hydration normal stresses, the sodium bentonite cannot swell, so less water is drawn into the soil to reach pore pressure equilibrium. This implies that a lower water content would be measured in this case than for a GCL hydrated under a low hydration normal stress. Instead, the water content of the sodium bentonite may better infer the void ratio of the sodium bentonite clay.

Stark and Eid (1996) found that hydration of GCLs from unhydrated moisture conditions (w = 10-20%, t_H = 0 hours) to fully hydrated conditions (w = 150-200%, t_H = 250 hours) reduced the peak and residual friction angles by about 40%. However, GCLs do not lose shear strength at a rate proportional to the increase in specimen water content. Daniel and Shan (1993) found that partially hydrated GCL specimens have similar shear strength as fully hydrated GCL specimens for low levels of normal stress (*i.e.* below 100 kPa). Their analysis showed that GCLs with a water contents between 50 and 80% (t_H < 24 hours) performed similarly in shear to GCLs with water contents between 180 and 200% (t_H > 24 hours). This may not be true of GCLs sheared at higher normal stress levels.

The liquid used in hydrating GCL test specimens may also yield varying shear strength results. Cation exchange may occur in the sodium bentonite if the liquid contains high levels of calcium or magnesium ions, which may lead to a change in GCL shear strength (Bouazza, 2002). Calcium bentonite has significantly higher shear strength than sodium bentonite, but calcium bentonite has higher hydraulic

conductivity and less ability to swell. For this reason, GCLs are not recommended to be used in conjunction with cover soils that contain large amounts of multivalent cations (Bouazza, 2002).

GCLs should be hydrated with a liquid that is representative of liquids found in the field, or more conservatively, one that results in the lowest shear strength. GCLs in landfill liners systems become hydrated with the waste liquids (leachate) they are meant to contain, while landfill covers become hydrated from percolation through the vegetated cover or moisture in landfill gases (Gilbert *et. al.*, 1997). Daniel and Shan (1993) tested the shear strength of GCLs with several different hydration liquids, including simulated leachate, and found that the use of distilled water leads to the lowest shear strength. Gilbert *et. al.* (1997) reported that the magnitude of sodium bentonite swell also depends on the hydration fluid, where distilled water induces the largest amount of swell, and inorganic and organic fluids cause the least. The SGI® laboratory uses tap water for all GCL shear strength testing, as it has similar cation content to groundwater and provides a compromise between the effects of leachate and distilled water (GeoSyntec, 1995).

3.3.4 Effect of Sodium Bentonite Swelling

The swelling behavior of GCLs is similar to that of sodium bentonite, in that it depends on the hydration normal stress. Petrov *et. al.* (1997) reported that reinforced GCLs are unable to swell beyond their initial thickness for hydration normal stresses greater than 160 kPa, while the unreinforced sodium bentonite found in GCLs is unable to swell beyond it original thickness for hydration normal stresses greater than 200 kPa. These normal stresses may be referred to as the "swell pressures" of reinforced and unreinforced GCLs, respectively. The swell pressure for unreinforced GCLs (essentially unreinforced sodium bentonite) is higher than that for reinforced GCLs as the fiber reinforcements in reinforced GCLs provide addition confinement to the sodium bentonite. The effect the swell pressure on the shear strength of GCLs at different levels of normal stress has not been discussed in the literature.

Swelling of the sodium bentonite in a GCL during hydration may have significant effects on internal GCL shear strength. As the sodium bentonite swells,

the soil structure of the clay changes markedly, with the void ratio increasing as water enters into the pore spaces (Lake and Rowe, 2000). As the void ratio increases, the shear strength of the sodium bentonite decreases. Further effects of swelling on the sodium bentonite soil structure are discussed in detail in section 3.4.2.

An important effect of sodium bentonite swelling on internal GCL shear strength is on the fiber reinforcements. The effect of swelling on the fiber reinforcements is especially an issue at hydration normal stresses below the swell pressure, when the GCL is able to swell beyond its original height. As the sodium bentonite swells, the fiber reinforcements may be stretched or they may be pulled out of the carrier geotextiles, depending on if the connection is rigid or flexible (see section 2.2.2). Stretching of the fiber reinforcements may cause yielding of the fiber reinforcements, which may lead to lower peak GCL shear strength. Pullout of the fiber reinforcements leads to nullification of the effect of the fiber reinforcements. However, pullout of the entire fiber reinforcement is unlikely as the change in vertical swell of the GCL is typically less than the length of fiber reinforcement entangled on the surface of the woven carrier geotextile. Both stretching and pullout of fiber reinforcements have been reported to decrease the shear strength of a reinforced GCL (Gilbert *et. al.*, 1997, Eid and Stark, 1999).

Uneven swell may occur if hydration is not uniform or if the GCL is unconfined. This may lead to different shear resistance properties throughout the specimen, which is not representative of field conditions. In direct shear testing, sodium bentonite may extrude through the top or bottom carrier geotextiles into the interface with the rigid substrates which confine the GCL specimen in the shear boxes (see Figure 2.5). This may result in slipping and stress concentrations in the GCL. Past testing has not indicated if the amount of sodium bentonite extruded from the GCL impacts internal shear strength of the GCL.

3.3.5 Effect of GCL Consolidation

To simulate field loading conditions, a GCL may be consolidated after hydration. Consolidation in direct shear testing implies an increase in normal stress from the hydration normal stress to the normal stress to be used in shearing, and

allowing a sufficient time for excess pore water pressures to dissipate. The time for dissipation should be consistent with Terzaghi's one dimensional consolidation theory, and is often in the range of several days to several weeks for sodium bentonite (Gilbert *et. al.*, 1997). The effective stress and the density of the sodium bentonite increase due to consolidation, which lead to higher shear strength.

It is important to note that GCLs that are *not* consolidated are not necessarily sheared in an "undrained" state. Often, when the GCL is not consolidated, the hydration normal stress is equal to the normal stress used during shearing. This implies that after hydration, the pore pressures are static. GCLs are very seldom hydrated under a low hydration normal stress and then sheared under a greater normal stress without adequate consolidation time.

If, during hydration, pullout or stretching of the fiber reinforcements occurs, subsequent consolidation will not regain the lost reinforcement characteristics. The tension in the fiber reinforcements due to the swelling process will be relaxed during consolidation, implying that they will not become "taut" again until the GCL is sheared by a displacement equal to the change in height during consolidation (Eid and Stark, 1996). This implies that the displacement at peak shear strength will be slightly greater for consolidated GCLs than for unconsolidated GCLs. The main effect of consolidation on the internal GCL shear strength is the decrease in the void ratio of the sodium bentonite. Despite the lower void ratio after consolidation, the sodium bentonite may still be in a dispersed structure, if the GCL was allowed to swell under a low confining pressure (*i.e.* below the swell pressure).

Drainage conditions during consolidation are very important if to ensure in laboratory testing. Drainage throughout the GCL specimen may be provided by the carrier geotextiles or through the porous rigid substrates which confine the GCL specimen. However, at normal stresses typically applied to GCLs in landfill applications, the GCL carrier geotextiles may compress excessively so that flow is restricted. The rigid substrates which confine the GCL specimen should be designed to allow filtration through pores in the substrate (without being clogged by extruded bentonite) and to allow lateral drainage through a network of grooves (Pavlik, 1997).

Longer times of consolidation may be appropriate to account for the limited drainage paths.

3.3.6 Effect of Normal Stress

As represented by the Mohr-Coulomb failure criterion, the effective normal stress applied to an interface determines the magnitude of the shear strength. According to this criterion, the friction angle defines a linear increase in the shear strength with increasing effective normal stress. However, due to the effect of swelling on the shear strength of the GCL, the time of application of the normal stress (*i.e.* before hydration to prevent swelling or after hydration for consolidation) to be used during shearing leads to different internal GCL shear strengths. This section investigates the effect of the normal stress on internal GCL shear strength.

3.3.6.1 Effect of Hydration Normal Stress

A GCL in the field may become hydrated before or after the confining fill or waste has been placed. During laboratory testing, a hydration normal stress is applied to prevent uneven swell of the GCL (Eid and Stark, 1999). Gilbert *et. al.* (1997) report that in a laboratory situation, the level of hydration normal stress was found to have little effect on unreinforced GCLs, but had significant impact on the shear strength of reinforced GCLs. Low hydration normal stresses lead to swelling of the sodium bentonite in GCLs, which for unreinforced GCLs implies only a change in the sodium bentonite void ratio. As the shear strength of unreinforced GCLs is comparatively low, this change does not lead to an appreciable difference in shear strength. Reinforced GCLs subjected to sodium bentonite swelling experience stretching or pullout of the fiber reinforcements. High hydration normal stresses do not allow excessive sodium bentonite swelling, which leads to little material changes for unreinforced or reinforced GCLs.

For unreinforced GCLs, Gilbert *et. al.* (1997) recommends that the normal stress to be used during shearing be applied before GCL hydration (to avoid the time needed to consolidate a fully hydrated GCL, placed under no confining pressure, to the normal stress level to be used during shear strength testing). Shear strength

testing of reinforced GCLs should model the order of hydration and fill placement found in the field. For reinforced GCLs, a hydration normal stress equal to the normal stress used during shearing results in less vertical swell than with a lower hydration normal stress (Lake and Rowe, 2000). This implies that less sodium bentonite extrusion occurs than in unconfined swell, and the stretching of fiber reinforcements is minimized. In general, as the hydration normal stress increases, the water content of the GCL after hydration decreases (Daniel and Shan, 1993, Lake and Rowe, 2000).

3.3.6.2 Effect of Normal Stress Used During Shearing

The normal stress applied to an interface during shearing has several impacts on the internal shear strength of a GCL. As mentioned, the shear strength of the GCL increases with increasing normal stress. This may be used to extrapolate information about the shear strength of a GCL interface at different loading condition from a limited amount laboratory tests. However, the use of a Mohr-Coulomb linear failure envelope may not be sufficient as the shear strength may be non-linear, similar to the findings of Mesri and Olson (1970) for sodium montmorillonite. Fox *et. al.* (1998) and Gilbert *et. al.* (1996) both found slight non-linear behavior in the internal shear strength of GCLs with increasing normal stress. Sharma *et. al.* (1997) suggested that the internal GCL shear strength should be tested over a wide range of normal stresses if the shear strength test results are to be used for both landfill cover (low normal stress) and base liner (high normal stress) system design.

The normal stress may also impact the material properties of the GCL. The uniformity of the normal stress over the area of the GCL is an important issue, as lateral bentonite migration from the edges of the GCL may occur. Stark (1998) identified this as a significant problem in the field because the lateral migration results in zones of differing amounts sodium bentonite throughout the extent of the GCL, yielding a lower long-term hydraulic performance. Also, the normal stress applied to the interface may affect the lateral transmissivity of the carrier geotextiles. High normal stresses decrease the thickness of the carrier geotextiles (depending on their compressibility, and if they are woven or nonwoven), which results in decreased

later drainage from the sodium bentonite. As shearing occurs, excess pore water pressures may be generated, and if the level of normal stress is high enough to affect the lateral transmissivity, undrained conditions may occur. The shear strength of undrained sodium bentonite is lower than drained sodium bentonite (Lambe and Whitman, 1979). The normal stress may also affect the strength of GCL reinforcements; Gilbert *et. al.* (1996) reported that the resistance of fiber reinforcements to pullout from the carrier geotextiles increased with normal stress because of the frictional nature of the connections.

It should be noted that the most of the shear strength testing conducted by Gilbert *et. al.* (1998), Daniel and Shan (1993), Stark and Eid (1996), and Eid and Stark (1997, 1999) were under low levels of normal stresses (typically below 200 kPa). It cannot be assumed that the trends observed in these studies are representative of higher ranges of normal stress

3.3.7 Effect of Shear Displacement Rate

GCLs are subjected in the field to shear loads when placed on a slope or the base of a slope. The GCL is most likely overlain by fill soil or waste, which impart normal and shear forces to the GCL. It is expected that, throughout the lifetime of the GCL, normal and shear forces are static except possibly during construction or seismic events. During construction, the rate of soil or waste placement on the GCL will determine if the sodium bentonite is initially under drained or undrained conditions. Gilbert *et. al.* (1997) estimated the time required for the sodium bentonite to reach 95% consolidation, assuming a linear increase in time with the applied normal load. It was found that the excess pore pressures related to fill placement dissipate over a period of one to two weeks by consolidating under the increased load. By comparing these times, this study found that it is not probable that construction loads increase rapidly enough for undrained conditions to exist because of the staged construction associated with soil or waste placement. Gilbert *et. al.* (1997) suggest that excess pore pressures related to construction are fully dissipated during shearing because of staged loading. This implies that a shear displacement rate should be slow enough to allow dissipation of all excess pore pressures during shearing.

In addition to construction loading, waste degradation may lead to a "down dragging" force acting on a GCL in a landfill base liner system or shear forces transmitted from the differential settlement of waste acting on a GCL in a landfill cover system. Shearing due to waste degradation is a long-term process that should be modeled with a slow shear displacement rate.

The shear displacement rate has been reported to affect the shear strength of GCLs (Gilbert *et. al*. 1997; Eid *et. al.*, 1999; Daniel and Shan, 1991; Gilbert *et. al*. 1996; Stark and Eid, 1996). Gilbert *et. al.* (1997) conducted direct shear tests at shear displacement rates ranging between 0.0005 and 1.0 mm/min on unreinforced GCLs with normal stresses of 17 kPa and 170 kPa. Eid *et. al.* (1999) conducted ring shear tests at shear displacement rates ranging between 0.015 mm/min and 36.5 mm/min for reinforced GCLs sheared at normal stresses of 17, 100, 200 and 400 kPa.

The conclusions of these studies were similar for shear displacement rates *below* 1.0 mm/min: (*i*) an increase in peak shear strength was reported for increasing shear displacement rates for unreinforced and reinforced GCLs sheared at normal stresses below 170 kPa, and (*ii*) an decrease in peak shear strength was observed for increasing shear displacement rates (*up to 1.0 mm/min*) for reinforced GCLs sheared at normal stresses greater than 200 kPa. Stark and Eid (1996) proposed a mechanism which may explain the first finding for reinforced GCLs, by which slow shear displacement rates would result in slow pullout of the fiber reinforcements from the woven carrier geotextile component of the GCL, while rapid shear displacement rates would result in tensile rupture of the fiber reinforcements. At low normal stresses, the tensile strength of the fiber reinforcements is greater than their pullout resistance. For low normal stresses on unreinforced GCLs, the peak shear strength at a shear displacement rate of 0.0005 mm/min is about 60 percent of the strength at a rate of 1.0 mm/min (Gilbert *et. al.*, 1997). Conclusion (2) was not addressed by Eid *et. al.* (1999); instead the trend discussed in that study was representative of shear displacement rates greater than 1.0 mm/min. Eid *et. al.* (1999) observed an increase in peak shear strength for increasing shear displacement rates greater than 1.0 mm/min (Eid *et. al.*, 1999). In addition, these studies also reported that the large-displacement shear strength was not sensitive to the shear displacement rate.

Gilbert *et. al.* (1997) reported a pore water pressure dissipation time analysis using a model proposed by Gibson and Henkel (1954), which predicted that shear displacement rates less than 0.001 mm/min result in constant peak shear strength for unreinforced GCLs. Gilbert *et. al.* (1997) suggested that slow shear displacement rates could result in creep, as it is a rate-dependent mechanism. This may explain the decreasing trend of shear strength with decreasing shear displacement rate.

Kovacevic Zelic *et. al.* (2002) reported that the peak and large-displacement shear strength of an unreinforced GCLs increase with increasing shear displacement rates for normal stresses of 50, 100 and 200 kPa. This was postulated to be a result of changing effective stress (*i.e.* excess pore water pressure generation) on the failure plane or rate effects such as creep. However, when the vertical displacement during shearing was measured, inconsistent findings were apparent. Swelling occurred during shearing for slow shear displacement rates, and settlement occurred during shearing for fast shear displacement rates. Swelling is associated to negative pore water pressure generation, which should yield higher shear strength, which was the opposite observed. Because of this, no conclusions were made as the effect of the shear displacement rate on pore water pressure generation.

Stark and Eid (1996) observed that the peak shear strength increased with increasing shear displacement rates for GCLs with the sodium bentonite component removed (*i.e.* the interface between two geotextiles, needle-punched together). It was suggested that this phenomenon is due to tensile rupture of the fiber reinforcements at high shear displacement rates, and gradual pullout of the fiber reinforcements at slow shear displacement rates. For filled GCLs, the peak shear strength was constant below 0.4 mm/min, then increased with increasing shear rate up to about 1.5 mm/min, and then decreased for greater shear displacement rates. Stark and Eid (1996) hypothesized several mechanisms that explained these phenomena. Although pore water pressures may have been generated in the GCL at shear displacement rates between 0.4 mm/min and 1.5 mm/min, the increased shear strength was associated with rapid rupture of the fiber reinforcements. The decrease in strength associated with excess pore water pressures in the sodium bentonite dominated at shear displacement rates above 1.5 mm/min. At shear displacement rates below 0.4

mm/min, no excess pore water pressures generated, and gradual pullout failure of the fiber reinforcements may have led to the minimum peak shear strength. Stark and Eid (1996) recommended that shear displacement rates of less that 0.4 mm/min be used for shear strength testing of needle-punched GCLs.

In contrast to the trend of peak shear strength with shear displacement rate, Stark and Eid (1996) found that the residual shear strength of reinforced GCLs remains constant with decreasing shear rate. It was suggested that this is due to the orientation of the sodium bentonite particles and fiber reinforcements in the direction of shear in residual conditions. Trends in large-displacement (i.e. post-peak but not residual) shear strengths with shear displacement rate have not been reported.

Eid and Stark (1999) reported a decrease in final water content at high normal stresses as a result of consolidation during shear. This implies that drainage, and thus consolidation, occurs as the excess pore water pressures in the sodium bentonite dissipate. Because of this, adequate drainage must be provided during GCL shearing. Gilbert *et. al.* (1997) suggests that if only one side of the GCL has free drainage, then the shear displacement rate associated with full pore water dissipation in GCLs with free drainage on both sides should be divided by four as a factor of safety.

3.3.8 Peak Shear Displacement Magnitude

The shear displacement at peak shear strength of a GCL is typically reported. It has been reported that the peak strength is typically developed between 2 and 10 mm due to bentonite particle orientation in the direction of shear or adhesive failure for unreinforced GCLs, or due to reinforcement orientation in the direction of shear and tensile rupture or pullout for reinforced GCLs (Gilbert *et. al.*, 1997; Fox *et. al*., 1998; Eid *et. al.*, 1999). The relatively short displacement required to reach peak conditions, combined with the comparatively large post-peak shear strength loss are important factors to consider when selecting shear strength values for design. Eid *et. al.* (1999) found that the shear displacement required to reach peak strength conditions does not vary with shear displacement rate.

As mentioned, the fiber reinforcements may stretch (plastically) as the sodium bentonite swells during hydration, especially in thermally bonded GCLs where the

fiber reinforcements are rigidly attached to the upper and lower carrier geotextiles. If the GCL is consolidated at this point, the permanently stretched fiber reinforcements are no longer under tension, and the fiber reinforcements are longer than the initial reinforcement length. As the fiber reinforcements become oriented in the direction of shear and become taut during shearing, higher displacements are required to reach peak shear conditions for fully hydrated reinforced GCLs (Stark and Eid, 1996).

3.3.9 Failure Plane Location

If the gap between the upper and lower shear boxes in a direct shear apparatus is wide enough, failure occurs along the weakest horizontal plane in the GCL. There are three possibilities for internal failure of reinforced GCLs: (1) failure through the bentonite layer combined with tensile rupturing of fiber reinforcements, (2) failure at the interface between the bentonite layer and the carrier geosynthetic combined with tensile rupturing of fiber reinforcements, and (3) failure between the bentonite layer and the carrier geosynthetic combined with pullout of fiber reinforcements from the carrier geosynthetic (Gilbert *et. al.*, 1997). It is uncertain why failure would occur at any of these interfaces, but possible causes are product variability, normal stress during shearing, amount of swell during hydration or shear displacement rate. Gilbert *et. al.* (1996), Fox *et. al.* (1998) and Stark and Eid (1996) tested similar non-thermally treated need-punched GCLs and found that shear failure occurred at the interface between the woven carrier geotextile of the GCL and the sodium bentonite component because of pullout of the fiber reinforcements. The use of thermally bonded needle-punched GCL may decrease the likelihood of fiber reinforcement pullout resulting in tensile rupture of the fiber reinforcements at failure.

3.3.10 Effect of GCL Reinforcement

The peak internal shear strength of reinforced GCLs is significantly higher than that of unreinforced GCLs (Gilbert *et. al.*, 1996). Still, the peak shear strength of different reinforced GCLs (*i.e.* non-thermally bonded needle-punched GCL, thermally-bonded GCLs, stitch-bonded GCLs) are not necessarily the same (von Maubeuge and Ehrenberg, 2000). Needle-punched GCLs typically have the largest amount of fiber reinforcement per unit area, but their short length allows pullout if

not thermally bonded to the carrier geotextiles. On the other hand, stitch-bonded GCLs have less fiber reinforcement per unit area (stitches are typically at a 3-inch spacing), but the fiber reinforcements are continuous throughout the length of the GCL. Fox *et. al.* (1998) found that the type of fiber reinforcement used in GCLs (needle-punched or stitch-bonded) has minor effect on the residual shear strength of a GCL as all fiber reinforcements are ruptured or pulled out. The change in residual shear strength with different reinforcement types is discussed in Chapters 4 and 5 of this study.

Stark and Eid (1996) performed shear strength tests on reinforced GCLs with and without a sodium bentonite component (filled and unfilled, respectively) to find the effect of the reinforcement of the shear strength of reinforced GCLs. They found that the peak shear strength of unfilled GCLs was higher than that of filled GCLs. It was expected that the opposite would have occurred because it was anticipated that the shear resistances of the sodium bentonite and the reinforcements would be additive. It is speculated that this trend was due to the fact that the swell of the sodium bentonite during hydration of the filled GCL could have plastically deformed the fiber reinforcements and decreased their tensile resistance, that extruded bentonite lubricated the fiber reinforcements and induced pullout in the filled GCL, that there was contact between the two carrier geotextiles in the unfilled GCL, and that excess pore water pressures were generated in the filled GCL. The unfilled GCL still exhibited a large post-peak shear loss because of the reinforcement failure, but had a residual strength greater than the filled GCL due to contact between the two carrier geotextiles.

The presence of reinforcement may cause an adhesive component in the shear strength failure envelope of the GCL, because the fiber reinforcements provide tensile resistance to the sodium bentonite clay. The tensile strength of the fiber reinforcements provides confinement of the sodium bentonite portion of the GCL. Lake and Rowe (2000) found that thermally bonded fiber reinforcements provide better confinement to the sodium bentonite than typical needle-punched fiber reinforcements, implying that the normal stress confining the sodium bentonite is greater than the externally applied normal stress. This behavior is different from

sodium bentonite clay, which is assumed to have little or no adhesive strength (Mesri and Olson, 1970). No studies have been conducted on reinforced GCLs at very low values of normal stress (below 10 kPa).

The shear strength of a needle-punched GCL varies proportionally with the amount of needle punching per unit area of the GCL (von Maubeuge and Ehrenberg, 2000). In other words, a larger amount of needle-punched fiber reinforcements per unit area results in larger shear strength. According to conversations with SGI® representatives, variability in peak internal GCL shear strength is mostly due to the GCL manufacturing process. Needle-punched GCLs are manufactured using a production line assembly which employs several threaded needles connected to a board (von Maubeuge and Ehrenberg, 2000). As the lifetime of the needle-punching boards increases, more needles break, and a lower amount of needle-punching may be apparent throughout the lifetime of the needle-punching board.

Before performing laboratory tests on a needle-punched GCL, it is important to know if the level of needle punching is representative of the actual level of needle punching in GCLs used in field applications. A design based on tests results from over-punched samples of GCL may result in an overestimate of the strength of GCLs used in the field. For this reason, peel strength tests should be performed on needle-punched specimens to determine the level of needle punching, according to the specifications for the grab strength of geotextiles explained in ASTM D4632 (von Maubeuge and Ehrenberg, 2000). Peel strength tests are conducted by confining the carrier geotextile of a needle-punched GCL in a wide width tensile testing machine after which they are pulled apart. The amount of force required to separate a 100 mm wide section of the specimen is referred to as the peel strength of the needle-punched GCL. Typical material specifications for needle-punched GCLs recommend peel strengths above 65 N/100 mm (Eid *et. al.*, 1999).

3.3.11 Effect of Specimen Size and Confinement Procedures

The size of the GCL specimen may affect the results of a shear strength test due to scale effects such as the density of fiber reinforcements or stress

concentrations related to specimen confinement (Gilbert *et. al.*, 1997). The size of the GCL specimen being tested may affect the ability to replicate field conditions.

The small direct shear boxes used in soil specimen testing (50 mm by 50 mm) are not recommended for GCL shear strength testing, as maximum displacement are typically 5 to 10 mm, which is not enough to reach residual conditions. To continue shear displacements after maximum displacement have been reached, it is possible to reseat the top shearing box, or to shear in the opposite direction. However, none of these test methods reproduce field conditions. In a small direct shear box, the gap between the upper and lower direct shear boxes cannot be adjusted wide enough to allow shear failure along the weakest plane within a GCL (a GCL is several centimeters thick after hydration) without adjustment of the shear box. Confinement of the GCL in a small direct shear box may result in stress concentrations, which are not representative of lateral confinement in the field. Shear strength specimens for small shear boxes typically can be hydrated rapidly because of lateral drainage through the carrier geotextiles. Direct shear boxes used for soil shear strength testing are also more readily available than those used for GCL shear strength testing alone.

The larger ASTM D5321 standard direct shear box (300 mm by 300 mm) typically allows displacements of 50 to 75 mm. Larger shear boxes have less boundary effects from specimen confinement and have a larger gap between the upper and lower boxes, which allows failure at the weakest internal interface. However, it is more difficult to obtain uniform degree of saturation throughout the specimen during hydration, and lateral drainage may be an issue during consolidation. Pavlik (1997) found that while large size GCL specimens are confined between rigid substrates with an applied load, there is little lateral movement of water through the sodium bentonite and carrier geotextiles. This study stressed the importance of using rigid substrates to confine the GCL specimen that are porous or have grooves to channel water during testing. In addition to allowing improved hydration, the grooves allow better drainage during shear, which may facilitate the dissipation of pore water pressures. Although standard direct shear boxes for GCLs are larger than direct shear boxes for soil testing, they are still not able to adequately account for the reinforcement effect of stitch-bonded GCLs, which typically have a stitch spacing of

100 mm. Also, only three rows of stitching may be tested in a 300 mm by 300 mm specimen, so the effect of the reinforcements may not correctly investigated.

Although larger specimen sizes (i.e. 600 mm by 600 mm) such as those used by Fox *et. al.* (1998) may reduce effects related to specimen confinement and boundary effects, specimen conditioning may be complicated. The GCL specimens tested in this study were not confined by clamping the upper and lower geotextiles to the upper and lower shear boxes, respectively, but instead were placed between two roughly textured plates. The top textured plate was translated across the bottom textured plate, and shear forces were imparted to the GCL via the frictional connections between the carrier geotextiles and the textured plates. This minimizes stress concentrations typically found in direct shear testing involving clamped connections. Slippage between the carrier geosynthetics and the rough surface of the rigid substrates may still occur at low normal stresses. Concurring with the results of Pavlik (1997), Fox *et. al.* (1998) found that increased specimen size resulted in incomplete specimen hydration, especially at the center of the GCL specimen, unless the time of hydration was at least 48 hours.

Ring shear specimen sizes are small, but the testing method allows for unlimited displacement, so the advantages of the large and small direct shear boxes are combined. Ring shear test specimens still have limitations with respect to specimen confinement and edge effects, as well as possible lateral bentonite migration during loading (Eid *et. al.*, 1997).

3.4 Interface Shear Strength between GCLs and Geomembranes

3.4.1 Background and Significance

The woven or nonwoven carrier geotextiles of a GCL may be placed in contact with a soil or many different geosynthetics. These interfaces most likely have different peak and residual shear strengths. However, the interface between the woven carrier geotextile of a GCL and a geomembrane has comparatively low shear strength (Gilbert *et. al.*, 1996; Daniel *et. al.*, 1998). This is a result of the ease of sodium bentonite movement through the woven geotextile of the GCL as well as the comparatively low interlocking capabilities of geomembranes. The importance of the

GCL-geomembrane interface can be inferred from actual field failures along this interface. One significant example is the EPA GCL test slopes in Cincinnati, Ohio (Daniel *et. al.*, 1998). These slopes were designed to investigate the shear strength of the internal GCL shear strength. However, failure occurred at the interfaces between the woven geotextiles of a Bentomat ST and a Claymax 500SP GCL and a textured HDPE geomembrane, lying on a slope of about 23.5 degrees (Daniel *et. al.*, 1998). The failures occurred only 20 and 50 days after construction, respectively. This implies that the interface between a textured geomembrane and a GCL may have significantly lower peak shear strength than the internal GCL.

Many issues that were discussed for internal GCL shear strength, such as GCL hydration and consolidation, also apply to GCL-geomembrane interface shear strength. Issues unique to GCL-geomembrane interfaces are discussed in this section.

3.4.2 Effect of GCL Swell

As mentioned in Section 3.2.3, the sodium bentonite component of GCLs swells during hydration. The swell of sodium bentonite has three important effects on the interface shear strength: (1) the sodium bentonite may flow out of the woven carrier geotextile (a process called "extrusion"), (2) the sodium bentonite may impregnate the woven geotextile (and thus lubricate the connections between the fiber reinforcements and the carrier geotextile), or (3) the swelling of the sodium bentonite causes pullout of the fiber reinforcements (Triplett and Fox, 2001). The occurrence of mechanism (2) may lead to an increased likelihood of mechanism (3) occurring. In the case of mechanism (3), pullout of the fiber reinforcements will lead to less material on the surface of the woven carrier geotextile, which has been reported to decrease the GCL-textured geomembrane interface shear strength (Triplett and Fox, 2001). The amount of swell allowed for the sodium bentonite clay is a function of the normal stress used during hydration (Hewitt *et. al.*, 1997). For high levels of normal stress, little swell occurs, implying that little sodium bentonite extrudes and that the fiber reinforcements are unaffected during hydration.

Extrusion of sodium bentonite through the carrier geotextiles leads to an unreinforced layer of sodium bentonite between the GCL and the geomembrane,

which is a significant plane of weakness in a landfill cover or liner system (Eid and Stark, 1997; Lake and Rowe, 2000). Extruded sodium bentonite affects the shear strength of a GCL-geomembrane interface more than other GCL interfaces because the geomembrane has very little interlocking capabilities with the sodium bentonite clay. Triplett and Fox (2001) collected the extruded sodium bentonite for different GCL-geomembrane interfaces after failure, and found that the amount of sodium bentonite extruded from the GCL increases with normal stress. The normal stress was applied after hydration, so as the GCL consolidated to equilibrium pore pressure levels, bentonite extruded from through the geotextiles. This phenomenon must be distinguished from the phenomenon observed by Gilbert *et. al.* (1997), who reported that the amount of extruded sodium bentonite decreases with increasing normal stress, but only when the normal stress is applied to the GCL before hydration to prevent swelling. The amount of sodium bentonite that extrudes through GCLs with different reinforcement types (*e.g.* needle-punched, stitch-bonded, *etc.*) has not been discussed.

As the sodium bentonite swells, it may move into the woven geotextile without extruding into the interface. This phenomenon is referred to as sodium bentonite impregnation. The impregnation of the woven geotextile with sodium bentonite has been shown to lead to lower shear strength than clean woven geotextile-geomembrane interfaces (Lake and Rowe, 2000). The hydrated sodium bentonite lubricates any interlocking connections between the GCL and the geomembrane.

As the sodium bentonite in a reinforced GCL swells, it exerts an outward pressure on the carrier geotextiles, tending to separate them. As the carrier geotextiles separate, the fiber reinforcements must either stretch or pull out of the carrier geotextiles. If the fiber reinforcements pull out of the (woven) carrier geotextile, the length of fiber reinforcements present at the interface is decreased (Lake and Rowe, 2000). With less fiber reinforcements present in the GCL-geomembrane interface during testing, less interlocking occurs between the GCL and the geomembrane. Issues related to the interlocking of GCL fiber reinforcements and geomembrane asperities are discussed further in Section 3.4.6.

3.4.3 Effect of Normal Stress

Eid and Stark (1997) found that for interface tests between a geomembrane and an unreinforced GCL involving a layer of sodium bentonite adhered to a geomembrane, an adhesive failure occurs between the two components at high normal stresses. At lower normal stresses, the GCL failed at the expected sodium bentonite-geomembrane interface. Eid and Stark (1997) also found that the peak shear strength failure envelope for this interface is slightly non-linear.

The critical interface in a layered system may change with normal stress due to the difference in the friction angles of the internal and interface GCL failure envelopes (Stark and Eid, 1996). It is possible that the failure envelopes may cross at a certain normal stress, above and below which the internal or interface shear strength may be the critical interface (Gilbert *et. al.*, 1996). The normal stress may also vary along the length of a slope (*i.e.* a veneer cover or a mounded layer of waste), implying that the critical interface may change along the length of the slope if the failure envelopes cross at a level of normal stress present somewhere along the length of the slope. This phenomenon may lead to localized zones under peak or residual conditions, leading to progressive slope failure.

3.4.4 Effect of Shear Displacement Rate

Triplett and Fox (2001) found that the peak and large-displacement shear strength of the GCL-geomembrane interface do not vary significantly with the shear displacement rate. This is in aggreement with the findings of Eid *et. al.* (1999), who found that the shear displacement required to reach peak strength conditions does not vary with shear displacement rate. Because of these findings, Triplett and Fox (2001) suggest that longer periods of hydration than 24 hours and slower shear displacement rates than 1.0 mm/min are not necessary for shear strength testing of GCL-geomembrane interfaces.

3.4.5 Peak Shear Displacement Magnitude

The relatively short displacement required to reach peak conditions, combined with the large post-peak shear strength loss are important factors to consider when designing for static and dynamic design loads. The displacement at peak shear

strength for the GCL-textured geomembrane interface has been reported to be similar to that measured for internal GCLs (Triplett and Fox, 2001). The peak strength of textured geomembrane interfaces is usually developed at 7 to 20 mm when the interlocking connections between the GCL and the textured geomembrane rupture. However, the peak shear strength of smooth geomembranes is typically developed at shear displacements below 3 mm (Triplett and Fox, 2001). Triplett and Fox (2001) found that most GCL-textured geomembrane interfaces showed a marked post-peak shear strength loss.

Hewitt *et. al.* (1997) found that the shear displacement behavior of the interface between a stitch-bonded GCL and a textured geomembrane was quite ductile in nature for high normal stresses, although it was much lower than the interface between a needle-punched GCL and a textured geomembrane. This implies that after an initial yielding point, increased shear displacements initially result in a decrease in shear strength for the stitch-bonded GCL interface. However, after a certain amount of shear displacement, this interface increases in shear strength until reaching a peak level. This is similar to the internal stitch-bonded GCL shear strength. The stitch-bonded GCL interfaces also reach peak shear strengths at larger displacements than the needle-punched GCL interfaces. Hewitt *et. al.* (1997) postulated that the large amount of reinforcement in needle-punched GCLs led to a sudden, brittle failure of the interface with a textured geomembrane because of the rupture or plowing of the interlocking connections at a peak level. The failure of a stitch-bonded GCL interface, with a lower density of reinforcements, undergoes a more gradual slip-like failure.

3.4.6 Effect of Internal GCL Reinforcement

The interface between needle-punched GCLs and geomembranes has been studied by Triplett and Fox (2001), Stark and Eid (1998), Gilbert *et. al.* (1996) and Hewitt *et. al.* (1997), to name a few. These studies identified three mechanisms which represent the shear strength of GCL-textured geomembrane interfaces: (*i*) frictional resistance to shearing between the untextured portions of the geomembrane and the woven carrier geotextile of the GCL, (*ii*) interlocking between the woven

carrier geotextile and the textured geomembrane asperities and (*iii*) interlocking between the protruding fiber reinforcements of the GCL on the surface of the woven carrier geotextile and the geomembrane asperities. Mechanism (*iii*) implies that the internal fiber reinforcements of the GCL may affect the GCL-geomembrane interface shear strength. In needle-punched GCLs, the protruding fiber reinforcements formed small bundles (not thermally bonded) or asperities (thermally bonded) on the surface of the woven geotextile, creating a layer of reinforcements on the GCL which were flattened during shearing (Gilbert *et. al.*, 1996). Triplett and Fox (2001) postulate that there may be a link between the peel shear strength of a GCL and the interface shear strength with a geomembrane because of these interlocking effects.

Lake and Rowe (2000) found that during swelling of the sodium bentonite in needle-punched GCL, the fiber reinforcements either stretch to permit the increase in volume between the upper and lower carrier geotextiles, or pull out of the woven carrier geotextile of the GCL. If the fiber reinforcements do not stretch or pull out, then the sodium bentonite has been observed to extrude from the woven carrier geotextiles. This implies that both the stiffness of the fiber reinforcements and the rigidity of the connections between the fiber reinforcements and the carrier geotextiles determine the amount of sodium bentonite extruded from the GCL. Needle-punched GCLs without thermal bonding allow the pullout of the fiber reinforcements from the woven carrier geotextile, while GCLs with thermally bonded needle-punched or stitch-bonded fiber reinforcements have more rigid connections between the fiber reinforcements and do not allow pullout from the carrier geotextiles. This implies that thermally bonded needle-punched and stitch-bonded GCLs may allow more sodium bentonite to extrude through the woven carrier geotextile because the fiber reinforcements are not allowed to pull out as the sodium bentonite swells. Hewitt *et. al.* (1997) confirmed that the least amount of sodium bentonite extrusion occurs in needle-punched GCLs without thermal bonding.

3.4.7 Effect of Geomembrane Texturing

Triplett and Fox (2001) reported that textured HDPE geomembrane interfaces experience a greater reduction in shear strength after peak conditions were reached

than smooth HDPE geomembranes. In other words, for the textured HDPE geomembrane interfaces, the difference between the peak and residual shear strengths was greater. In fact, smooth HDPE geomembrane interface rarely experienced any post-peak shear strength reduction. This is most likely due to the fact that at the peak shear strength, the interlocking capabilities of the geotextile and fiber reinforcements with the geomembrane asperities break, resulting in a large loss of strength. This means that smooth geomembranes have little or no interlocking capabilities, and thus the shear displacement behavior is similar to that of unreinforced sodium bentonite clay. Sodium bentonite clay still shows post-peak shear strength reduction, but it is not as marked as the GCL-textured geomembrane interface. Triplett and Fox (2001) found that less bentonite was extruded from the GCLs when a smooth geomembrane was used, which may also be a cause of the decreased amount of post-peak softening.

Triplett and Fox (2001) reported that pore pressures are higher for smooth HDPE geomembrane interfaces. However, pore pressure measurements were conducted without back-pressure and were often affected by clogged needles. Still, pore water measurements were useful in developing qualitative trends.

Due to manufacturing differences for PVC geomembranes, the surface texturing for these geomembranes is different than those for polyethylene geomembranes (EPI, 1999). According to EPI (1999), PVC geomembranes are usually manufactured with one side being smooth and the other side being embossed with a “faille” or file finish. EPI (1999) presented shear strength test results for PVC geomembranes with soils and nonwoven geotextiles. The shear strength behavior reported in this study may be of relevance for interfaces between GCLs and PVC geomembranes. It was found that the interface between a nonwoven geotextile and the smooth PVC geomembrane yields a higher interface shear resistance than the faille PVC geomembrane (friction angles of 30 and 23 degrees, respectively). The smooth PVC geomembrane also exhibited little post-peak strength reduction while the faille side exhibited a drop in friction angle of 3 degrees. The higher frictional strength of smooth PVC geomembranes is attributed to the greater interface contact area during shear and the more "sticky" and flexible nature of the smooth side versus

the faille side (EPI, 1999). However, the post-peak shear strength loss for the faille PVC geomembrane is much less than for textured HDPE geomembranes.

3.4.8 Effect of Geomembrane Polymers

There have been no studies to date which investigate the effect of different geomembrane polymer types on the GCL-geomembrane interface shear strength. This may be an issue in interfaces involving textured geomembranes with different polymer types, where removal or deformation of geomembrane asperities leads to differences in GCL-geomembrane interface peak shear strength. It is anticipated that the GCL-geomembrane interface residual shear strength is not affected by polymer type, as all asperities are expected to have been removed or lubricated with sodium bentonite. Still, the removed asperities may align into the direction of shear along with the sodium bentonite particles, leading to different residual shear strengths. In addition, it is anticipated that the polymer type has little effect on the GCL-geomembrane interface shear strength for smooth geomembranes.

3.5 Conclusions

Despite numerous studies focusing on the shear strength of GCLs in the past decade, there are still many unresolved issues. It has been reported that the internal shear strength of most GCLs increased with increasing normal stress, increased with increasing time of hydration, increased with increasing time of consolidation, and decreased with decreasing shear displacement rates (for low levels of normal stress). The same results were reported for the GCL-geomembrane interface, except the shear displacement rate had less effect on the shear strength of the interface. It was found that past studies on GCLs have not explained the non-linear behavior of GCL failure envelopes, the decrease in shear strength from peak to residual levels, the effects of different fiber reinforcement types on internal and interface GCL shear strength, and the effects of different geomembrane polymers on the GCL-geomembrane interface shear strength. These issues will be addressed through the analysis of the GCLSS database.

Table 3.1: Triaxial Cell Shear Strength Test Results for a Sodium Montmorillonite Clay reported by Mesri and Olson (1970)

Sodium Concentration (N)	$w_{initial} = w_{failure}$	$\sigma_c = \sigma_3$ (kPa)	$(\sigma_1-\sigma_3)$ (kPa)	u_f (kPa)	$\tau_{peak} = (\sigma_1-\sigma_3)_f/2$ (kPa)	$\sigma_1 = \sigma_c + (\sigma_1-\sigma_3)_f$ (kPa)	Degree of Consolidation Before Shearing
0.1	305	68.9	31.7	24.8	15.9	4.8	95
0.1	212	137.9	36.5	43.4	18.3	8.4	100
0.1	155	275.8	58.6	63.4	29.3	16.0	100
0.1	134	344.7	67.6	64.1	33.8	19.7	98
0.1	121	413.7	67.6	71.0	33.8	23.0	100

Table 3.2: Failure Envelope Data for Different Levels of Confining Pressure for Sodium Montmorillonite Clay

Failure Envelopes	Friction Angles (degrees)	Intercept Values (kPa)
Confining Pressures 0-150 kPa	2.0	13.4
Confining Pressures >150 kPa	1.9	21.1
All Confining Pressures	3.4	11.6

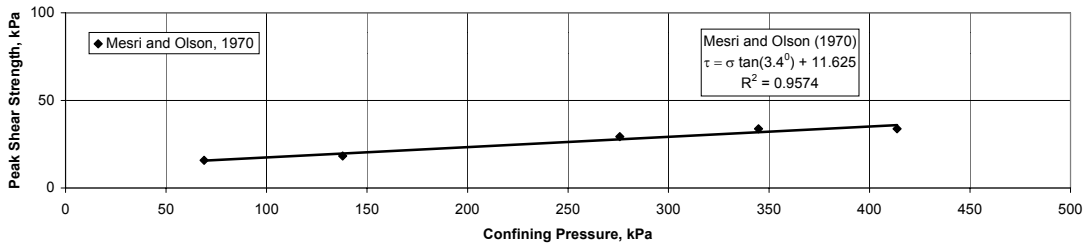

Figure 3.1: Peak Shear Strength Failure Envelopes for Unreinforced Sodium Bentonite Clay (Mesri and Olson, 1970) with Linear Best-Fit Line

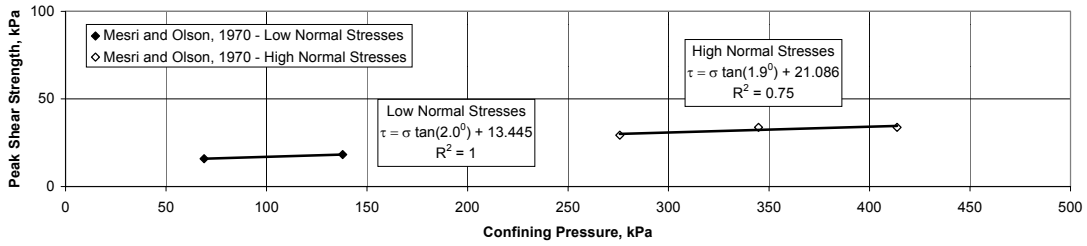

Figure 3.2: Peak Shear Strength Failure Envelopes for Unreinforced Sodium Bentonite Clay (Mesri and Olson, 1970) with Bilinear Best Fit Lines

4 Internal Shear Strength of GCLs

4.1 Overview of the Database of Internal Shear Strength of GCLs

4.1.1 The GCLSS Database

The Soil-Geosynthetics Interactions (SGI®) laboratory, formerly of GeoSyntec Consultants, performed 320 direct shear tests focusing on the internal shear strength of GCLs of several GCLs since 1992. The data obtained from these tests was used for individual projects but has not been compiled for global analysis.

4.1.2 Information Included in the GCLSS Database

Test conditions and reporting of results for GCL direct shear tests conducted by the SGI® laboratory over the period 1992 to 2001 are consistent with the requirements of the standard, ASTM D6243, although this was not instituted until 1998. Stoewahse *et. al.* (2002) discusses the significance of using consistent procedures and equipment to prevent undue variability. For each shear strength test series on a GCL in the GCLSS database, reported test conditions include the specimen preparation and confinement procedures, hydration procedure, times of hydration and consolidation, normal stresses applied during hydration, consolidation and shearing, and shear displacement rate. For each individual test (under a single test normal stress) the SGI® laboratory reported the applied shear stress as a function of shear displacement, the corresponding peak and large-displacement shear strength values, and the final GCL water content at the completion of shearing. Table 4.1 lists the variables used in the GCLSS database.

4.1.3 Shear Strength Test Procedures

The SGI® laboratory used different test configurations of the direct shear device in order to apply different ranges of confining normal stresses to the GCL during shearing. The schematics for three direct shear device test configurations were discussed in chapter 2, and are shown in Figures 2.7(a), 2.7(b) and 2.7(c). For all three of these test configurations, the direct shear device was constructed by inserting a 300 mm by 300 mm direct shear box into a pull-out box. The bottom box is slightly longer than the top box to ensure a constant cross sectional area. Normal stresses were applied using dead weights as shown in Figures 2.7 and 2.8 or using an air

bladder combined with a reaction frame as seen in Figure 2.9. Shear forces are typically applied to the top box by a pullout "tongue", which is connected to a hydraulic ram or a dead weight.

Test specimens are prepared by cutting sections of GCL with dimensions larger than the direct shear box, trimming the sections so that a flap of the upper carrier geotextile extends slightly in the direction of displacement and a flap of the lower carrier geotextile extends in the direction opposite to displacement. The GCL specimen is placed between two rigid wooden substrates with textured steel gripping surfaces, used to minimize slippage between the carrier geotextiles and the substrate. To confine the specimen, the upper and lower carrier geotextile flaps (extending in opposite directions) are folded over the rigid substrates and held in place with another set of rigid substrates. A detail of this test setup is shown in Figure 2.5. Olsta *et. al.* (2001) provides further details concerning equipment and specimen confinement.

As mentioned, the GCL conditioning procedures used by the SGI® laboratory are consistent with ASTM D6243, but the times of hydration and consolidation are specified for each project. The procedure at the SGI® laboratory is to hydrate the specimen simultaneously with the application of the hydration normal stress for a minimum of 24 hours. The specimen and its backing plates are typically soaked together in tap water, outside of the direct shear device. Depending project specifications, the specimen may then be consolidated (to the normal stress to be used during shearing) before shearing.

The shear displacement rate for direct shear testing used by the SGI® laboratory is also specified for each project. The maximum shear displacement rate employed by the SGI® laboratory is consistent with ASTM D6243, which suggests a maximum shear displacement rate of 1.0 mm/min (or sufficiently slow to allow dissipation of excess pore water pressures). Equipment in the SGI® laboratory is capable of shear displacement rates as slow as 0.0015 mm/min.

Peak shear strength is reported as the maximum shear stress experienced by the interface. The large-displacement shear strength is reported as the shear stress when there is constant deformation with no further change in shear stress, or at a displacement of typically 50 to 70 mm.

It is important to note that the reported large-displacement shear strength of a GCL tested by the SGI® laboratory is not necessarily the residual shear strength because the shear stress may still decrease at displacements beyond the maximum displacement of the device. In addition, when projects only required the reporting of peak shear strength values, shearing was stopped after reaching peak conditions. The SGI® laboratory only reported large-displacement shear strengths when the shear stress appeared to be stable at the maximum shear displacement of the test.

Occasionally, during direct shear strength testing of stitch-bonded and unhydrated GCLs at low normal stresses, the specimen did not fail along the predefined failure plane (*i.e.* through the center of the GCL). Instead, the carrier geotextiles were observed to rupture in tension *after* peak conditions were reached, but before the maximum displacement of the test device. This tensile rupture may be due to the particular method of GCL confinement. As the GCL is confined in the direct shear box by the carrier geotextiles, slipping between the carrier geotextiles and the rigid plates results in stress concentrations that lead to tensile rupture of the carrier geotextiles. In other words, the externally applied shearing force leads to a tensile force in the carrier geotextiles rather than being transmitted to the sodium bentonite component of the GCL. This typically occurs at low levels of normal stress. When a GCL fails by rupture, only the peak shear strength is reported.

The amount of needle-punching was found to be an important factor in the shear strength of needle-punched GCLs by several studies (Gilbert *et. al.*, 1996; Berard, 1997; Gilbert *et. al.*, 1997; Eid *et. al.*, 1999; Fox *et. al.*, 1998). However, the amount of needle-punching of the different GCLs in the GCLSS database was not directly quantified by peel strength tests. Because of this, caution should be used when comparing the peak shear strength values reported for needle-punched GCLs in the GCLSS database with those of other studies. If a GCL roll (as opposed to pre-cut samples) was provided to the SGI® laboratory for a project, the SGI® laboratory typically selects specimens from the middle of the roll in order to provide representative shear strength characteristics for the roll.

4.2 Shear Strength Test Results and Preliminary Analysis

The internal shear strength values of 10 GCLs were tested by the SGI® laboratory over the period 1992-2001. These GCLs are listed below, as well as in Table 2.1:

- Bentomat® ST (GCL A)
- Claymax® 500SP (GCL B)
- Bentofix® NS (GCL C)
- Bentofix® NW (GCL D)
- Bentofix® NWL (GCL E)
- Claymax® 200R (GCL F)
- Bentomat® CS (GCL G)
- Bentomat® DN (GCL H)
- Bentomat® HS (GCL I)
- Geobent® (GCL J)

4.2.1 Histogram Analysis

Figure 4.1 shows a histogram of the internal direct shear strength tests on different GCL products conducted by the SGI® laboratory. As the majority of the tests were conducted on GCL *A*, a needle-punched GCL, primary focus of this study is on this GCL. Several tests are also conducted on GCLs *B* and *C*, a stitch-bonded GCL and a needle-punched GCL with thermal bonding, respectively, so they are also analyzed in detail. Although the number of direct shear tests conducted on GCLs *D, E, F, G, H, I* and *J* are not as significant as GCLs *A, B* and *C*, preliminary evaluations will still be made using these test results. In addition, this histogram shows the number of GCLs sheared to stable large-displacement shear strength values. As mentioned, several projects only required the peak shear strength values, so large-displacement shear strength values were not reported. In addition, only 5 GCL *B* specimens were sheared to large-displacement conditions without rupturing.

To summarize the different test conditions, histograms were also compiled considering the normal stress, time of hydration, hydration normal stress, time of consolidation, consolidation normal stress, hydration procedure, final GCL water

content, shear displacement rate and reinforcement type for each GCL test. Only the final GCL water content is considered as only the initial GCL water content *before* hydration was reported, which is typically the same for all GCLs (w = 10-20 %).

Figure 4.2 shows a histogram of the normal stresses used during shearing of the GCLs. This histogram shows that the majority of the tests were conducted at normal stresses less than 100 kPa (representative of landfill cover conditions), although there are many tests conducted at normal stresses between 100 and 3000 kPa (representative of landfill base liner conditions).

Figure 4.3 shows the times of hydration used for GCL conditioning. The majority of the tests were hydrated for 24 hours, although there were several tests hydrated for longer periods of time. It was not reported if the GCLs reached pore pressure equilibrium at the end of hydration. 20 tests were conducted on unhydrated GCLs (t_H = 0 hrs), which have a gravimetric water contents between 10 and 20%. Figure 4.4 shows the variation in hydration normal stress. The majority of the tests had hydration normal stresses less than 100 kPa. It should be noted that the majority of the hydration normal stresses were *below* the swell pressure of reinforced GCLs (*i.e.* 100-200 kPa). Note also that a hydration normal stress of zero indicates that the test was conducted under unhydrated conditions (no GCLs were allowed to hydrate without confining pressure).

Figure 4.5 shows the different times of consolidation. Most of the GCLs were not consolidated. It should be noted that if the time of consolidation is zero, the hydration normal stress was equal to the normal stress used during shearing. When a GCL was consolidated, the hydration normal stress was below the swell pressure of reinforced and unreinforced GCLs. Figure 4.6 shows the consolidation normal stresses. It should be noted that when the consolidation normal stress is not equal to zero, it is equal to the normal stress used during shearing. Typical testing procedure was to leave the GCL submerged after hydration, and to increase the normal stress to the level of normal stress used during shearing. In other words, the consolidation normal stress equals the normal stress used during shearing when a consolidation phase is employed.

Figure 4.7 shows a histogram of the final GCL water content. The final GCL water content is the water content of the GCL after shearing. From this figure, it can be seen that many tests had final water contents well above 100%. This is consistent with the fact that most specimens were hydrated under low levels of normal stress during hydration, and that full hydration was possible.

Figure 4.8 shows a histogram of the hydration procedure used for conditioning of the GCLs. Most of the GCLs were soaked in tap water for the specified time of hydration and then removed from the water for shearing. Three tests were conducted under submerged condition. That is, the GCL was sheared while submerged. Three tests were hydrated and consolidated under a staged loading procedure. This means that the normal stress was slowly increased while the GCL was soaked in tap water. For the other tests, the hydration normal stress was immediately applied (in one stage) when the specimen was placed in the water.

Figure 4.9 shows the shear displacement rate used during shearing of the GCLs. The majority of the tests were conducted at the shear displacement rate prescribed by ASTM D6243 (1.0 mm/min), although there are several tests with slower shear displacement rates. Figure 4.10 shows a histogram of the reinforcement type of the GCLs. Most of the GCLs tested were needle-punched, although some of these needle-punched GCLs were thermal bonded. There were nearly 50 tests on stitch-bonded GCLs as well. Only 7 unreinforced GCLs were tested.

These histograms show the wide range of GCL types and test conditions that were used in the available database. These histograms illustrate that the shear strength behavior of GCLs has been investigated under a very wide range of test conditions representative of the wide range of field conditions. As can be observed from the histograms, most GCLs had a time of hydration of 24 hours, were soaked in tap water, were not consolidation, were sheared at a displacement rate of 1.0 mm/min, and had needle-punched reinforcement between woven and a nonwoven carrier geotextiles. Also, the majority of the GCLs were sheared under low normal stress, the hydration normal stresses were typically less than the normal stress used during shearing, and they were not consolidated (t_C = 0 hrs and σ_C = 0 kPa).

4.2.2 Equivalent Friction Angle Analysis

4.2.2.1 Background

Internal GCL direct shear test results have been shown to depend on many variables such as product type, reinforcement type (if any), location of the specimen in the GCL roll, and specimen conditioning procedures (Gilbert *et. al.*, 1997). It is useful to first examine the test results globally before accounting for the effects of these variables. The GCLs may be grouped into sets based on reinforcement types and specimen conditioning procedures. Average shear strength values as well as upper and lower shear strength bounds may be developed for the data sets. This global, preliminary analysis will help tailoring the variable-specific analysis to be conducted subsequently.

A useful comparative approach to investigate GCL shear strength is to define equivalent friction angles. The equivalent friction angle is defined by forcing the intercept value of a failure envelope to zero. That is, the data trend is represented by a straight line through the origin with a slope equal to the tangent of the equivalent friction angle. An equivalent friction angle facilitates comparison between the behaviors of different GCLs because there is only one shear strength parameter for comparison.

The limitations of an equivalent friction angle analysis must be emphasized. This approach may lead to significant underestimation of the shear strength at low confining pressures and overestimation of the shear strength at high confining pressures. Nonetheless, the statistical data reported in this section may assist in the comparison of the shear strength values of different GCLs, but this should not be used for design purposes.

The equivalent friction angle is defined using conventional linear-regression techniques. An "average" linear regression equivalent friction angle based on the least-squares method can be defined as (Neter and Wasserman, 1974):

$$\phi_{EQ} = \tan^{-1}\left(\frac{\sum \tau_i \sigma_i}{\sum \sigma_i^2}\right) \qquad \text{Eq. 4.1}$$

where ϕ_{EQ} is the average equivalent friction angle and σ_i and τ_i are the normal stress and corresponding shear strength, respectively. The term "average" does not indicate probabilistic significance, but instead differentiates this equivalent friction angle from the upper and lower equivalent friction angle bounds, which will be developed later.

The coefficient of determination, R^2, compares estimated and actual ordinate values (*i.e.* τ) to assess the quality of the representation, and ranges in value from 0 to 1. In regression analysis, the squared difference between the estimated shear strength for that point ($\tau_e = \sigma\phi_{EQ}$) and the actual shear strength value (τ_a) is calculated at each normal stress value (σ):

$$ss_{res} = \Sigma(\tau_e - \tau_a)^2 \qquad \text{Eq. 4.2}$$

where ss_{res} is the sum of the squared differences, and is called the residual sum of squares. The sum of the squared differences between the actual ordinate values and the average of the shear strength values ($\tau_{average}$) is called the total sum of squares (ss_{total}):

$$ss_{total} = \Sigma(\tau_a - \tau_{average})^2 \qquad \text{Eq. 4.3}$$

The coefficient of determination (R^2) may thus be developed:

$$R^2 = \frac{ss_{total} - ss_{res}}{ss_{total}} \qquad \text{Eq. 4.4}$$

The smaller the residual sum of squares is compared with the total sum of squares, the larger the value of R^2. If the R^2 value is 1, there is a perfect correlation in the sample (*i.e.* there is no difference between the estimated shear strength value and the actual shear strength value). If the coefficient of determination is 0, the regression equation is not helpful in predicting a shear strength value.

The upper and lower equivalent friction angle bounds may also be developed from the data. These bounds were defined in this study using an estimate of the standard deviation of the data about the average equivalent friction angle. Preliminary observation of the data indicated that the spread of the data above and below the average equivalent friction angle was found to increase with normal stress. This implies that the variability, and thus the standard deviation of the data, increases with normal stress. This complicates the development of upper and lower equivalent

friction angle bounds on the data. The change in the standard deviation may be quantified through the use of a "weighting parameter", which represents the contribution of each data point to the trend in the data. The definition of the weighting factor is not standard, so a weighting factor was selected so that the upper and lower bounds fit the data in an acceptable manner. The weighting factor is defined for this study as:

$$w_i = \frac{1}{\sigma_i} \qquad \text{Eq. 4.5}$$

where w_i is the weighting factor, σ_i is the normal stress, and i signifies each data point.

The definition of the standard deviation requires the summation of the squared difference between the equivalent friction angle for each data point and the average equivalent friction angle (Ang and Tang, 1975). The equivalent friction angle for each point is equal to the arctangent of the ratio between the shear strength and the normal stress:

$$\phi_{EQ,i} = \tan^{-1}\left(\frac{\tau_i}{\sigma_i}\right) \qquad \text{Eq. 4.6}$$

where $\phi_{EQ,i}$ is the equivalent friction angle at each point, and τ_i and σ_i are the shear strength and normal stress at each particular point, respectively. The standard deviation of the data may then be calculated as:

$$s(\phi_{EQ}) = \sqrt{\frac{\sum w_i\left(\phi_{EQ,i} - \phi_{EQ,Average}\right)^2}{n-2}} \qquad \text{Eq. 4.7}$$

where $s(\phi_{EQ})$ is the standard deviation of the equivalent friction angle, $\phi_{EQ,i}$ is the equivalent friction angle at each point, $\phi_{EQ,Average}$ is the average equivalent friction angle calculated using Equation 4.1, w_i is the weighing factor, and n is the number of data points used to define the average equivalent friction angle (Neter and Wasserman, 1974).

The estimated standard deviation was then used to define upper and lower equivalent friction angle bounds for the data. Specifically, the equivalent friction angle bounds are calculated as:

$$\phi_{EQ,\text{ Lower}} = \phi_{EQ} - 2s(\phi_{EQ}) \quad \text{Eq. 4.8}$$

$$\phi_{EQ,\text{ Upper}} = \phi_{EQ} + 2s(\phi_{EQ}) \quad \text{Eq. 4.9}$$

where $\phi_{EQ,Lower}$ is the lower bound of the equivalent friction angle, and $\phi_{EQ,\ Upper}$ is the upper bound of the equivalent friction angle. The factor of 2 multiplied by the estimated standard deviation may be explained by the fact that for a normally distributed variable, 95% of the data points fall within the range of 2 standard deviations on each side of the average value. However, if the R^2 value for the data indicates that the average trend does not represent the data, then it is likely that the upper and lower bounds will not represent the data either.

Further investigation of the data indicated that the data displays a significantly different trend at very high normal stresses (*i.e.* greater than 550 kPa). However, the majority of the data lies at lower normal stresses. The outlier data points at normal stresses greater than 550 kPa were found to skew the definition of the standard deviation, despite their very low weighting factors. Because of this, data points at normal stresses greater than 550 kPa were not considered the determination of equivalent friction angles, although they are still considered in later analyses in this chapter.

In summary, the equivalent friction angle analysis was performed as follows:

- The "average" equivalent friction angle was developed using linear regression techniques (Equation 4.1)
- The weighting factor for the standard deviation was defined as the inverse of the normal stress (Equation 4.5), and the standard deviation was defined using standard linear regression techniques (Equation 4.7)
- The upper and lower equivalent friction angle bounds (Equations 4.8 and 4.9) on the data were defined using 2 standard deviations away from the average equivalent friction angle
- Data points with normal stresses greater than 550 kPa were not considered in the equivalent friction angle analysis

4.2.2.2 Effect of GCL Reinforcement

A list of 12 sets of GCLs grouped by different reinforcement types is presented in Table 4.2. The GCL sets investigated are:

- All GCLs
- Reinforced GCLs
- Unreinforced GCLs
- Stitch-bonded GCLs
- Needle-punched GCLs
- Bentomat® needle-punched GCLs
- Bentofix® needle-punched GCLs
- Needle-punched GCLs with woven-nonwoven carrier geotextiles, not thermal bonded
- Needle-punched GCLs with woven-nonwoven carrier geotextiles, thermal bonded
- Needle-punched GCLs with nonwoven-nonwoven carrier geotextiles, not thermal bonded
- Needle-punched GCLs with nonwoven-nonwoven carrier geotextiles, thermal bonded
- GCL *A*

The latter eight sets consist of different groups of needle-punched GCLs. This is due to the large amount of different manufactured configurations of needle-punched GCLs. Different carrier geotextile types as well as the presence of thermal bonding may have significant effects on the internal GCL shear strength.

Figure 4.11(a) shows the peak shear strength values for all GCLs in the database (analysis set 1). As there is a large concentration of data points at low normal stresses, Figure 4.11(b) shows a detail of this data at normal stresses less than 100 kPa. In these figures, ranges equivalent friction angles are presented to facilitate interpretation of the data. Figure 4.11(a) shows that the majority of the test results for normal stresses above 100 kPa lie between the equivalent friction angles of 5 and 40^0. However, Figure 4.11(b) shows that a cluster of data points at low normal stresses does not fit into this range. The range of equivalent friction angles for low confining pressures is between 10 and 80^0, which is unreasonably high (*i.e.* a GCL in the field

would not be able to remain stable on a slope with such an angle). This is due to adhesion or a highly non-linear failure envelope (*i.e.* a very high friction angle at low normal stresses and a lower friction angle at higher normal stresses).

Figures 4.12(a) and 4.12(b) show the same data as Figures 4.11(a) and 4.11(b), respectively, although only data points for normal stresses lower than 550 kPa are presented. Linear regression best fit lines for all GCLs are presented. Upper and lower bounds for all GCLs are also presented. The peak equivalent friction angle of 30.4^0 for the set of all GCLs represents the data well. Figure 4.12(a) shows that the statistical bounds include over 95% of the data points at normal stresses greater than 100 kPa. However, Figure 4.12(b) shows that many data points fall outside of these bounds at low normal stresses (*i.e.* less than 100 kPa).

Figures 4.13(a) and 4.13(b) show the large-displacement shear strength results for all GCLs in the database, for the full range of normal stresses and a detail for low normal stresses, respectively. Figure 4.13(a) shows that the large-displacement data points fall within a narrower range of equivalent friction angles than the peak data points (5 to 18^0). Figure 4.13(b) shows that this is also true for low normal stresses, although there is still significant scatter. This may imply that there is a negligible intercept value for large-displacement shear strength. Figures 4.14(a) and 4.14(b) show the same data as in Figure 4.13(a) and 4.13(b), respectively, for normal stresses less than 550 kPa. Linear regression best fit lines for all GCLs are presented. Upper and lower bounds for all GCLs are also presented. Figure 4.14(a) shows that the upper and lower bounds for the large-displacement data are closer than for the peak data. However, Figure 4.14(b) shows that most data points at low normal stresses are still well above the average equivalent friction angle.

For the rest of the GCL sets, the data is presented with two figures: (a) all data points plotted along with ranges of equivalent friction angles and (b) data points with a normal stress less than 550 kPa along with the results of a linear regression analysis.

Figure 4.15 shows the peak shear strength data for all reinforced GCLs (analysis set 2). As there are only seven unreinforced GCL test results in the GCLSS database, the results shown in Figure 4.15 have relatively the same trend as those shown in Figures 4.11(a) and 4.12(a). In other words, the peak equivalent friction

angle is only 0.8^0 greater for the reinforced GCL set than for the full GCL set (31.2^0 as opposed to 30.4^0). The spread in the peak shear strength data is high, with a standard deviation equivalent friction angle of 19.8^0. Figure 4.16 shows the large-displacement shear strength data for all reinforced GCLs. The average large-displacement friction angle for the reinforced GCL set is only 0.3^0 that that for the full GCL set (13.0^0 as opposed to 12.7^0). The peak equivalent friction angle for the reinforced GCL set is much greater than the large-displacement equivalent friction angle (18.2 degree difference). This indicates that the post-peak shear strength loss is quite marked for the reinforced GCLs. Similar to the full GCL set, the spread in the large-displacement data for the reinforced GCL set is much less than that for the peak data.

Figure 4.17 shows the peak shear strength data for all unreinforced GCLs (analysis Set 3: GCL *F*). Figure 4.17(a) also includes the shear strength test results for GCL *F* reported by Fox *et. al.* (1998). These test results align well with those reported in the GCLSS database. Figure 4.17(b) shows that the upper and lower bounds for this GCL set are represented by an average equivalent friction angle of 6.6^0, with a standard deviation equivalent friction angle of about 3.0^0. The average peak equivalent friction angle as well as the spread in the data for the unreinforced GCL set is much lower than those for the reinforced GCL set (an average of 31.2^0 and a standard deviation of 19.8^0). This shows the significant effect of reinforcements on the peak shear strength of GCLs.

Figure 4.18 shows the large-displacement shear strength for all unreinforced GCLs. The large displacement data reported in this study aligns well with the values reported by Fox *et. al.* (1998). This figure shows a small post-peak shear strength loss for unreinforced GCLs, as there is only a 0.7 degree difference between the peak and large-displacement equivalent friction angles. This implies that the contribution of GCL reinforcements is the primary cause of the significant post-peak shear strength loss of reinforced GCLs. Based on equivalent friction angles, the post-peak shear strength loss for reinforced GCLs is 18.2^0, while it is only 0.7^0 for unreinforced GCLs.

The peak shear strength values for all stitch-bonded GCLs are presented in Figure 4.19 (analysis set 4: GCL *B*). The behavior of this GCL is not well represented by an equivalent friction angle approach. This GCL has a distinct intercept value (characteristic of reinforced GCLs) and a low friction angle (characteristic of unreinforced GCLs). Figure 4.19(a) shows that the peak shear strength test results normal stresses above 100 kPa lie between equivalent friction angles of 5 and 20^0, which is a low range for a reinforced GCL. The average peak equivalent friction angle is 12.2^0, which fits the data at high normal stresses. This equivalent friction angle is much lower than that for all reinforced GCLs (31.2^0) yet is only slightly greater than that for unreinforced GCLs (6.6^0). However, the R^2 value representing the quality of the linear regression fit is very small, implying a poor fit for the data as a whole. Because of this, the upper and lower bounds do not fit the data well.

The large-displacement shear strength values for all stitch-bonded GCLs are presented in Figure 4.20. The large-displacement equivalent friction angle of 6.7^0 for this GCL set is almost as low as that of unreinforced GCLs (5.9^0). This may be due to the fact that the shear reinforcement does not cover the entire area of the GCL, but only along the lines of stitching. As the lines of stitching are three inches on center, the majority of the sodium bentonite in this GCL is unreinforced. Thus when the GCL reaches large-displacement conditions, its behavior should be closer to unreinforced GCLs than to needle-punched GCLs.

Figure 4.21 shows the peak shear strength for all needle-punched GCLs (analysis set 5: GCLs *A, C, D, E, G, H, I* and *J*). This figure shows the behavior of needle-punched GCLs in general, and does not show the effects of different manufacturing techniques, carrier geotextiles or thermal bonding. The average peak equivalent friction angle for this GCL set is 32.9^0, which is greater than that for all reinforced GCLs as the low shear strength values of the stitch-bonded GCLs are not included. This figure shows that the range of equivalent friction angles is between 20 and 40^0, which is a much wider range than that observed for stitch-bonded GCLs in Figure 4.19(a). The upper and lower bounds do not represent the variability of the data well. At normal stresses below 100 kPa, several data points fall outside of the

upper bound while at normal stresses between 100 and 550 kPa, the upper and lower bounds are too wide. This indicates that the data could be better represented by a non-linear failure envelope.

Figure 4.22 shows the large-displacement failure envelope for all needle-punched GCLs. Although the average large-displacement equivalent friction angle is quite high compared to other GCL groupings (13.2^0), the statistical upper and lower bounds again do not represent the variability of the data well. This is especially true at normal stresses below 50 kPa, although there are also several outliers at normal stresses between 50 and 550 kPa. Still, Figure 4.22(a) shows that most of the data lies between 5 and 20^0, indicating that the upper and lower bounds in Figure 4.22(b) are acceptable.

Figure 4.23 shows the peak shear strength of all Bentomat® needle-punched GCLs manufactured by CETCO Inc. (analysis set 6: GCLs *A, G, H* and *I*). These GCLs do not necessarily have the same carrier geotextile configurations, but the manufacturing processes are similar. The average peak equivalent friction angle for this GCL set is 33.7^0, which is greater than that for the needle-punched GCL set, indicating that the Bentomat® needle-punched GCLs have slightly higher shear strength values than the other needle-punched GCLs. However, the spread in the data is quite significant compared to the other groups of GCLs. Most data points appear to lie between 20 and 40^0, although the statistical bounds on the shear strength are slightly wider (14^0 to 53^0). It can be seen from Figure 4.23(b) that the statistical upper and lower bounds do not represent the variability in the data well between normal stresses of 100 and 550 kPa.

Figure 4.24 shows the large-displacement shear strength for all Bentomat® needle-punched GCLs manufactured by CETCO Inc. This GCL set has an average large-displacement equivalent friction angle of 13.5^0, which is only slightly larger than that for all needle-punched GCLs (13.2^0). The bounds on the data shown in Figure 4.20(b) indicate that the scatter is small (10^0 to 17^0), while the data appears to be spread between 5 and 20^0, with several outliers.

Figure 4.25 shows the peak shear strength of all Bentofix® needle-punched GCLs manufactured by Serrot, Inc. (Analysis set 7: GCLs *C, D* and *E*). These GCLs

do not necessarily have the same carrier geotextile configurations, but the manufacturing processes are similar. The average peak equivalent friction angle for this group of GCLs is 4.2^0 less than that for the group of needle-punched GCLs manufactured by CETCO Inc (29.5^0), and is lower than the average for all needle-punched GCLs (32.9^0). This difference in equivalent friction angle is most likely due to the GCL manufacturing differences between Serrot, Inc. and CETCO, Inc. GCLs manufactured by Serrot, Inc. are thermal bonded to prevent the pullout of the reinforcements from the carrier geotextiles during shear, while those of CETCO, Inc. are not. However, thermal bonding appears to have lead to lower peak shear strength than similarly reinforced GCLs without thermal bonding. The statistical bounds on the data for this GCL group capture the behavior of most data points at high normal stresses, but a large amount of data points at low normal stress fall outside of this range.

Figure 4.26 shows the large-displacement shear strength of all Bentofix® needle-punched GCLs manufactured by Serrot, Inc. The average large-displacement friction angle for this GCL set is 12.0^0, which is less than that for those manufactured by CETCO, Inc. (13.5^0), all needle-punched GCLs (13.2^0), and reinforced GCLs (13.0^0). The shear strength results appear to fall within the range of 5 to 18^0, yet the statistical bounds are slightly wider (3.2^0 to 20.8^0). This is most likely due to the influence of the data points at low normal stresses that widen the bounds for data points at higher normal stresses. GCLs with thermal bonding have lower peak and large-displacement equivalent friction angles than do GCLs do not have thermal bonding. However, thermal bonded GCLs still have greater peak and large-displacement equivalent friction angles than stitch-bonded and unreinforced GCLs.

The needle-punched GCLs may be grouped into smaller sets that differentiate behavior based on the carrier geotextile configuration as well as the presence of thermal bonding. Figure 4.27 shows the peak shear strength of all needle-punched GCLs with a woven-nonwoven carrier geotextile configuration, and groups the GCLs by the presence of thermal bonding (analysis set 8: GCLs *A, G,* and *I*; analysis set 9: GCL *C*). GCLs *A, G* and *I* do not have thermal bonding, while GCL *C* does. This figure shows that the needle-punched GCLs without thermal bonding have a higher

peak equivalent friction angle (33.5^0) than those with thermal bonding (28.9^0). However, the spread of the data for needle-punched GCLs without thermal bonding is much wider. This implies that thermal bonding may decrease the variability of shear strength results.

Figure 4.28 shows the large-displacement shear strength values for all needle-punched GCLs with a woven-nonwoven carrier geotextile configuration. The needle-punched GCLs with no thermal bonding have a large-displacement equivalent friction angle of 13.7^0, which is the highest of all the GCL sets. There is a slight difference (less than 1^0) between the large-displacement equivalent friction angles for needle-punched GCLs without thermal bonding (13.7^0) and those with thermal bonding (12.9^0). It is important to note that the needle-punched GCLs without thermal bonding have a greater amount of post-peak shear strength loss (19.8^0) than those with thermal bonding (16^0). The needle-punched GCLs with thermal bonding have a greater amount of variability for large-displacement conditions than for peak conditions.

Figure 4.29 shows the peak shear strength values for all needle-punched GCLs with a nonwoven-nonwoven carrier geotextile configuration grouped by the presence of thermal bonding (analysis set 10: GCL *H,* analysis set 11: GCLs *D* and *E*). GCL *H* is not thermal bonded, while GCLs *D* and *E* are thermal bonded. GCLs *D* and *E* differ in the amount of needle-punching, with GCL *E* having a lower amount of needle-punching. Again, the needle-punched GCLs without thermal bonding have a higher equivalent friction angle than those with thermal bonding. In fact, the needle-punched GCLs with no thermal bonding have the highest average equivalent friction angle of all GCLs (37.1^0). This is most likely due to the fact that most tests on GCL *H* were under unhydrated moisture conditions. The peak equivalent friction angle for the analysis set 11 corresponds with other needle-punched GCLs (30.3^0), although the data is quite dispersed. The data points are clustered between 20^0 and 40^0, but there are few data points for intermediate equivalent friction angles. The lower bounds are similar for both GCLs with and without thermal bonding, but the needle-punched GCLs without thermal bonding have a higher upper bound. This is the same trend

observed for needle-punched GCLs with a woven-nonwoven carrier geotextile configuration.

Figure 4.30 shows the large-displacement shear strength for all needle-punched GCLs with a nonwoven-nonwoven carrier geotextile configuration grouped by thermal bonding. The average equivalent friction angles for both of the GCL groups are nearly the same. This implies that thermal bonding has less of an effect on the shear strength of GCLs with nonwoven-nonwoven carrier geotextile configurations. The variability of the needle-punched GCLs with thermal bonding is greater than for those without thermal bonding. This is the same trend observed for needle-punched GCLs with a woven-nonwoven carrier geotextile configuration.

The GCLSS database includes results for 182 direct shear tests on the GCL *A*, so it is expected that the range of the test results reported in this study should encompass other shear strength test results found in other studies. Fox *et. al.* (1998), Eid *et. al.* (1999), Berard *et. al.* (1997), and Gilbert *et. al.* (1996) conducted shear strength tests on needle-punched GCLs similar to GCL *A*. The shear strength test results reported by each of these four studies are shown in Tables 4.3, 4.4, 4.5 and 4.6, respectively. Figures 4.31(a) and 4.31(b) show the peak shear strength of GCL *A* (analysis set 12) reported in the GCLSS database as well as those reported by other studies on GCL *A*. Similarly, Figures 4.32(a) and 4.32(b) show the large-displacement shear strength values of GCL A reported in the GCLSS database and by other studies. Despite the differences in test procedures and conditions, the trends of the data reported by the other studies are consistent with those in the database, with the exception of the results reported by Eid *et. al.* (1999). The needle-punched GCL specimens tested by Eid *et. al.* (1999) have an average peel strength of 27 N/100 mm, which is significantly below the value of 60 N/100 mm prescribed by the material specifications of most GCL manufacturers. This would explain the lower shear strength results. The GCLs in the GCLSS database cover a wide range of needle-punching characteristics which may be encountered in the field.

Figure 4.33 presents the peak shear strength test results for four GCLs with different reinforcement types in the GCLSS database (GCLs *A, B, C* and *F*). These GCLs are most representative of the needle-punched, stitch-bonded, thermal bonded

and unreinforced GCLs in the GCLSS database. Although Figure 4.33(b) does not present statistical bounds on the data, the average peak equivalent friction angles may be compared. The order of peak equivalent friction angles in decreasing order is GCL *A, C, B* and *F* (33.5, 28.9, 12.2 and 6.6^0, respectively). Figure 4.34 presents the large-displacement shear strength test results for the same four GCLs. The order of GCL shear strength is the same (13.7, 12.9, 6.7 and 5.9^0, respectively), although GCLs *A* and *C* and GCLs *B* and *F* have very similar large-displacement friction angles, respectively. GCL *A* is highly variable at high normal stresses, and GCL *B* is highly variable at low normal stresses.

Table 4.7 presents the results of the linear regression analysis for each of the GCL groups in Table 4.2. The upper and lower bounds developed using statistical techniques correspond well to the trends observed in the data.

The highest peak equivalent friction angle obtained from best fit lines is the needle-punched GCL with nonwoven carrier geotextile backings (analysis set 10: GCL *H*) with a peak equivalent friction angle of 37.1^0. The lowest peak equivalent friction angle of the reinforced GCLs is the stitch-bonded GCL (analysis set 4: GCL *B*) with a peak equivalent friction angle of 12.2^0. For peak conditions, most of the reinforced GCL sets (*i.e.* all except analysis set number 3) had upper and lower bounds between equivalent friction angles roughly between 15 and 45^0.

The similarity between the large-displacement equivalent friction angles should be noted. The results of this analysis show that the reinforcement type has only a minor effect on the large-displacement shear strength. Needle-punched GCLs tend to have higher large-displacement shear strength values than do stitch-bonded and unreinforced GCLs. Thermal bonded and non-thermal bonded needle-punched GCLs have roughly the same large-displacement shear strength, although the non-thermal bonded needle-punched GCLs tend to have slightly higher peak and large-displacement shear strength values. In general, the differences in large-displacement shear strength values for all of the GCL groupings were relatively small compared to those between the peak shear strength values.

With respect to variability, the unreinforced GCLs had the lowest standard deviation, although only 7 tests were performed on GCL *F*. The stitch-bonded GCL

set had the highest peak standard deviation value of 34.6^0, but this is due to the fact that the equivalent friction angle did not represent the trend observed in the data well. The peak standard deviation for each of the needle-punched GCL sets varied between 10 and 20^0, and the GCLs without thermal bonding tended to have higher peak standard deviation values than those with thermal bonding. Most of the GCL sets had similar standard deviation values for large-displacement conditions. The needle-punched GCLs with thermal bonding tended to have higher large-displacement standard deviation values than the other GCL sets.

4.2.2.3 Effect of GCL Test Conditions

As GCL *A* has the largest number of shear strength test results, the test results for this GCL were divided into categories corresponding to different test conditions. In this sense, different clusters of data may be identified, which may define the importance of each of the test conditions. Table 4.8 shows several sets of the same test results for GCL *A*, each characterized by different hydration times, consolidation times, shear displacement rates, and hydration normal stress application procedures.

Figures 4.35(a) and 4.35(b) show the effect of the time of hydration on the peak and large-displacement shear strength values, respectively. This analysis does not include consolidated GCL *A* results. As expected, figure 4.35(a) shows that GCL *A* specimens with a time of hydration of zero hours (*i.e.* unhydrated) have high peak equivalent friction angles (38.1^0), while hydrated GCL *A* specimens (*e.g.* t_H = 24 and 48 hours) have lower peak equivalent friction angles (30.8^0 and 27.1^0, respectively). The large-displacement shear strength shown in Figure 4.35(b) shows a similar phenomenon. The unhydrated GCL *A* has the greatest equivalent friction angle of 24.2^0, while the hydrated GCLs have lower equivalent friction angles. This implies that the large-displacement shear strength slightly sensitive to the time of hydration beyond 24 hours.

Figure 4.36(a) shows the effect of the hydration normal stress application procedure on the peak shear strength of GCL *A*. When the hydration normal stress is less than the normal stress used during shearing, the GCL must be subsequently consolidated to the normal stress to be used during shearing. In other words, if the

hydration normal stress is less than the normal stress during shearing, the specimen will be consolidated. In general, GCL specimens that are consolidated have higher shear strength than those without consolidation. Due to the variability, final conclusions may not be drawn from this figure. Table 4.8 confirms that comparison is difficult due to the close proximity of the peak equivalent friction angles (32.5^0 opposed to 30.3^0). Figure 4.36(b) and Table 4.8 show that the large-displacement equivalent friction angles are roughly the same for both groups of data (11.0^0 and 10.5^0).

Figure 4.37(a) shows the effect of the time of consolidation on the peak shear strength of GCL *A*. In this figure, GCLs consolidated for 48 hours are compared to GCLs without consolidation. Unhydrated GCLs were not included in this particular analysis even though they were not consolidated. Due to variability in the data, this figure does not show conclusively that GCLs with higher times of consolidation have higher peak equivalent friction angles. Still, Table 4.8 shows that the peak equivalent friction angle for GCLs with a time of consolidation of 48 hours (33.5^0) is greater than that for GCLs with no consolidation (30.0^0). Figure 4.37(b) shows the effect of the time of consolidation on the large-displacement shear strength for this GCL. This figure shows that there is no clear relationship between the shear strength and the time of consolidation. This is verified by the large-displacement equivalent friction angles shown in Table 4.8 (9.6^0 and 8.3^0).

Figure 4.38(a) shows the effect of the shear displacement rate on the peak shear strength of GCL *A*. GCLs tested at slower shear displacement rates tend to have lower equivalent friction angles than the rest of the data points (except those tested at 0.1 mm/min). Figure 4.38(b) shows similar results for large-displacement shear strength. Table 4.8 shows that the peak equivalent friction angle is not particularly sensitive to changes in the shear displacement rate. The large-displacement equivalent friction angle is relatively constant for shear displacement rates less than 0.5 mm/min. As there are a large amount of test results for shear displacement rates of 1.0 mm/min and much less for other shear displacement rates, final conclusions may not be drawn.

In summary, different combinations of test conditions determine the shear strength behavior of a GCL. Final conclusions could not be drawn from the equivalent friction angle analysis in this section due to the variability in the data. Nonetheless, this analysis was useful in determining the sensitivity of the peak and large-displacement shear strength values to the different test conditions. Sections 4.3.3 through 4.3.5 will further investigate the effects of test conditions on the peak and large-displacement shear strength values of different GCLs.

4.3 Internal GCL Shear Strength Analysis

This section will group each of the different GCLs by different test conditions to form relationships between the shear strength and normal stress (failure envelopes). In contrast to the previous section, the effects of the test conditions on the shear strength may be investigated directly. The effects of the shear displacement rate, the time of hydration and the time of consolidation will be investigated individually when all other testing conditions are held constant. The variability of peak and large displacement shear strength is also investigated in this section using probabilistic methods. Testing observations such as the final GCL water content and the displacement at peak shear strength are also discussed in detail.

4.3.1 Typical Shear Force-Displacement Curves

During shearing, a constant displacement rate is applied to the direct shear box, and the required shear force to maintain this displacement rate is recorded with displacement. The maximum shear strength recorded during shearing is identified as the peak shear strength, and the stable level of shear stress obtained at the end of shearing is the large displacement shear strength.

Figure 4.39(a) and 4.39(b) show shear force-displacement curves for GCL *A* obtained at various normal stresses. As the area of the specimen is constant at 1 square foot (i.e. 300 mm by 300 mm) due to the slightly longer bottom box, the magnitude of the shear force is equal to the shear stress. The curves in Figure 4.39(a) illustrate that the peak shear strength is well defined and there is a clear decrease to stable large-displacement shear strength values. The post-peak shear strength loss is significant for the GCLs tested at high normal stresses. The curves in Figure 4.39(b)

illustrate that stable large displacement shear strength values were often not obtained at the end of a test (in this case as the project required only the peak shear strength). In this situation, only the peak shear strength was reported.

Figures 4.40, 4.41 and 4.42 show the shear force-displacement curves for GCLs *A, B* and *C*, respectively, tested under similar test conditions (t_H = 168 hours, t_C = 48 hours and SDR = 0.1 mm/min) and normal stress levels. Figure 4.40 shows that GCL *A* has different behavior for different normal stress levels. Results show an increasing amount of post-peak shear strength loss with increasing normal stress. Figure 4.41 shows that the behavior for GCL *B* is significantly different that that of GCL *A* tested under the same conditions. After an initially steep increase in shear strength, the shear force reaches a plateau level before hardening up to the peak shear strength. There is no significant post-peak shear strength loss related to the rupture of the carrier geotextiles after the peak shear strength was reached. This may imply that the continuous reinforcements in GCL *B* lend it a ductile shear failure behavior. Figure 4.42 shows the behavior for GCL *C*, which is similar to that of GCL *A*, although the peak and large-displacement shear strength levels are generally lower than those obtained for GCL *A*.

Figures 4.43 and 4.44 show the shear force-displacement curves for GCL *F* tested under hydrated and unhydrated conditions, respectively. Figure 4.43 shows a large amount of post-peak shear strength loss for the hydrated unreinforced GCL. Also, the hydrated unreinforced GCLs show a similar initial modulus under various normal stresses. Figure 4.44 shows that the unhydrated GCL instead has a high initial modulus leading to a peak level, after which the shear force decreases slightly until large-displacement conditions were reached.

4.3.2 Effect of Test Conditions on Failure Envelopes

This section presents an analysis of the GCL shear strength test results by grouping the test results for each GCL according to the test conditions. Peak and large-displacement internal shear strength failure envelopes were developed for 10 GCL products listed in section 4.2, each with a constant set of test conditions. In addition, the variability of the shear strength of the GCLs is investigated by

examining test results conducted under identical test conditions and the same normal stress.

Table 4.9 lists 38 different failure envelopes with their respective test conditions (i.e. shear displacement rate, time of hydration and time of consolidation. Three failure envelopes are identified as the "baseline" failure envelopes for GCLs *A, B* and *C*. The baseline failure envelopes serve as a reference for discussion and comparison of other failure envelopes. Other GCLs did not have sufficient tests to justify comparison to a baseline failure envelope. Table 4.9 also identifies three "bilinear" failure envelopes. Linear failure envelopes in these situations did not represent the data well for the full range of normal stresses because of non-linearity. Significantly different trends were observed at normal stresses approximately below 100 kPa and above 200 kPa.

4.3.2.1 Analysis of GCL A

Eight different combinations of test conditions were defined for GCL A. Peak and large-displacement failure envelopes were obtained for each of these combinations. Also, multiple tests were performed in some cases for the same normal stress and test conditions. In these cases, the average and standard deviation of the peak and large-displacement shear strength values were determined for each normal stress level and are reported in the tables. The specific failure envelopes for GCL *A* are listed below (see also Table 4.9):

- Failure envelope A1a and A1b consist of GCLs with a time of hydration of 24 hours and no consolidation, and a shear displacement rate of 1.0 mm/min;
- Failure envelope A2 consists of GCLs with a time of hydration of 24 hours and no consolidation, and a shear displacement rate of 0.5 mm/min;
- Failure envelope A3a and A3b consist of GCLs with a time of hydration of 48 hours and no consolidation, and a shear displacement rate of 1.0 mm/min;
- Failure envelope A4 consists of GCLs with a time of hydration of 72 hours and no consolidation, and a shear displacement rate of 1.0 mm/min;
- Failure Envelope A5 consists of GCLs with a time of hydration of 168 hours, a time of consolidation of 48 hours, and a shear displacement rate of 0.1 mm/min;

- Failure envelope A6 consists of GCLs with a staged hydration and consolidation procedure, and a shear displacement rate of 0.0015 mm/min;
- Failure envelopes A7a and A7b consist of GCLs with different times of hydration and consolidation, and a shear displacement rate of 1.0 mm/min; and
- Failure envelope A8 consists of GCLs sheared under unhydrated moisture conditions, and a shear displacement rate of 1.0 mm/min

Figure 4.45 shows the peak and large-displacement failure envelopes A1a and A1b. The data for each test in these failure envelopes is shown in Table 4.10. Failure envelope A1a serves as the baseline failure envelope for the analysis of GCL A. These failure envelope envelopes have similar test conditions, but differ in the fact that failure envelope A1a has a hydration normal stress equal to the normal stress used during shearing, while failure envelope A1b has a constant hydration normal stress of 4.8 kPa. Failure envelope A1a is higher than A1b because the lower hydration normal stress for failure envelope A1b allows a greater amount of swelling. A slight variability in the data should be noted, but the trend is quite linear over the range of normal stresses tested for this failure envelope. The large-displacement failure envelope is approximately linear. The friction angles of the large-displacement failure envelopes are much lower than the peak failure envelopes (on the order of 40^0), and the data follows clear linear trends. Failure envelopes A1a and A1b predict roughly the same large-displacement shear strength values, so the hydration normal stress does not have a significant effect on the large-displacement shear strength.

Failure envelope A2 is shown in Figure 4.46, and the data for this failure envelope is shown in Table 4.11. This failure envelope is different from the baseline failure envelope in that the shear displacement rate is 0.5 mm/min instead of 1.0 mm/min. Another important difference between failure envelopes A1a and A2 is the different range of normal stresses. Failure envelope A1a is representative of low normal stresses, which is not the case for failure envelope A2. As the majority of the points in each failure envelope are on different sides of the swell pressure of reinforced GCLs (about 160 kPa), differences in behavior are expected which that may not be necessarily associated with the difference in shear displacement rate.

While failure envelopes A1a and A2 show very different shear strength values, it is difficult to determine if the difference in shear displacement rate leads to the difference in behavior.

Figure 4.47 shows a comparison plot for failure envelopes A1a and A2, and it can be seen that the two peak failure envelopes align well into a slightly non-linear trend. At the point of intersection of the two failure envelopes (50 kPa), the shear strength values predicted by both failure envelopes are similar. Still, the GCL with a slower shear displacement rate of 0.5 mm/min (A2) has slightly lower shear strength. Beyond this point, failure envelope A2 has a slightly lower peak friction angle than failure envelope A1a. The difference in trends observed for the peak shear strength values is not apparent for large-displacement failure envelopes.

Failure envelope A3a is shown in Figure 4.48, and the data is presented in Table 4.12. A time of hydration of 48 hours was used in this series instead of 24 hours (baseline). A longer time of hydration is expected to result in a lower failure envelope. Figure 4.48(a) shows a single best-fit linear regression for the whole range of normal stresses. This failure envelope tends to overestimate the shear strength at low and high normal stresses. Still, when comparing the two failure envelopes at the full ranges of normal stresses, failure envelope A3a has lower peak and large-displacement shear strength values than failure envelope A1a. However, it should be noted that the normal stress range for this failure envelope is wider than in failure envelope A1a. For this reason, Figure 4.48(b) presents best fit linear regressions for the peak data at normal stresses below 100 kPa and above 200 kPa. Similarly, Figure 4.48(c) presents best fit linear regressions for the large-displacement data at normal stresses below 100 kPa and above 200 kPa. Figure 4.48(b) shows a distinct difference in behavior for the peak failure envelopes at different ranges of normal stress, but only a slight difference between the large-displacement failure envelopes. Figure 4.48(b) shows that the peak friction angle for failure envelope A3a at low normal stresses is similar to that of failure envelope A1a. Figure 4.48(c) shows that the large-displacement failure envelope is well represented by a linear trend.

Failure envelope A3b is shown in Figure 4.49, and the data is presented in Table 4.12. This failure envelope includes tests with the same test conditions as

failure envelope A3a, but the hydration normal stress for failure envelope A3b is constant at 4.8 kPa. The peak and large-displacement shear strength values represented by this failure envelope are lower than those for failure envelope A3a. There is significant scatter in the peak failure envelope, but the large-displacement failure envelope follows a more linear trend.

Failure envelope A4 is shown in Figure 4.50, and the data for this failure envelope is presented in Table 4.13. The time of hydration in this failure envelope is 72 hours, a large increase in the time of hydration from the baseline failure envelope (24 hours). The peak shear strength values at low normal stresses show a significant scatter. This scatter may be explained as by changes in the manufacturing specifications for GCL *A* over time. For instance, inspection of the SGI® laboratory reports indicates that the shear strength values reported for the tests conducted at normal stresses of 2.4, 7.2, 14.4 and 23.9 kPa were all conducted in 1993, while the other tests were conducted in 1995. This was a period of product development for GCL *A*. The large-displacement shear strength values are more consistent, and have a more distinct linear trend. The large-displacement friction angle for failure envelope A4 is slightly less than that of the baseline failure envelope

Failure envelopes A1a, A3a and A4, which differ in the time of hydration, are plotted together in Figures 4.51(a) and 4.51(b) for peak and large-displacement shear strength values, respectively, corresponding to normal stresses below 110 kPa. As expected, these plots show that the peak failure envelopes decrease with increasing time of hydration, as would be expected. The decrease in peak friction angle for GCLs with increasing time of hydration beyond 48 hours is not significant. This confirms the study by Daniel and Shan (1993) that found that a partially saturated GCL (w = 80%) performs similar in shear to a fully hydrated specimen (w = 200%). The difference in the large-displacement failure envelopes is not significant. This indicates that the large-displacement failure envelope is not sensitive to the time of hydration.

Failure envelope A5 is presented in Figure 4.52, and the data is presented in Table 4.14. Table 4.14 shows 19 series, each including peak and large-displacement shear strength values for three normal stresses (34.5, 137.9 and 320.3 kPa). This

failure envelope differs in the time of hydration, time of consolidation and shear displacement rate from the baseline condition, which makes comparison between failure envelopes A1a and A5 difficult. Nonetheless, this failure envelope is very useful in understanding the variability of GCL shear strength. The wide range of peak and large-displacement shear strength values that are obtained for a constant normal stress level and constant test conditions is relevant. It should also be noted that the variability increases with normal stress. This failure envelope is discussed in detail in section 4.6 of this chapter. Figure 4.52 indicates that the peak friction angle for this failure envelope (28.8^0) is lower than that of the baseline failure envelope (46.5^0), yet the ranges of normal stress are different. The large-displacement friction angle (9.0^0) is greater than that of the baseline failure envelope (8.6^0).

Figure 4.53 shows the ratios of peak shear strength to the normal stress and large-displacement shear strength to the normal stress for failure envelope A5. This is another approach to characterize the shear strength as a function of normal stress. A highly non-linear decreasing trend is apparent from the power law fitting for the data. The peak shear strength is often greater than the normal stress for low levels of normal stresses. Figure 4.54 shows the ratio of peak shear strength to the large-displacement shear strength. This ratio reflects the amount of post-peak shear strength loss with increasing normal stress (i.e. the difference between peak and large-displacement shear strength values). Again, a non-linear trend is apparent, but the power law fitting appears to reach an asymptote. Because of this, it may be concluded that for normal stresses beyond a certain point (about 250 kPa), the amount of post-peak shear strength loss becomes constant.

Failure envelope A6 is shown in Figure 4.55, and the test results are presented in Table 4.15. This failure envelope includes test results with a staged hydration and consolidation procedure, and the very slow shear displacement rate of 0.0015 mm/min, which are all significantly different than the baseline failure envelope. The range of normal stresses is also quite different from the baseline failure envelope. The staged hydration and consolidation procedure is similar to field loading conditions, as fill or waste is typically placed above the GCL in lifts. These lifts allow dissipation of the pore water pressures during each stage of construction.

However, the initial hydration of the GCL is under a low hydration normal stress (below 100 kPa), so the fiber reinforcements may be affected before shearing begins. The slow displacement rate is also similar to the shear displacement rates present in the field (Gilbert *et. al.*, 1996). This failure envelope has similar behavior to that of failure envelope A3a for *high* normal stresses in Figure 4.48(b). Both failure envelopes have low friction angles but significant intercept values. It should be noted that peak failure envelope A3a for high normal stresses has a lower friction angle (14.8^0) than that for failure envelope A6 (21.9^0).

Failure envelopes A7a and A7b are shown in Figure 4.56, and the test results are presented in Table 4.16. This failure envelope shows tests that differ from the baseline failure envelope because failure envelope A7a has an increased time of consolidation of 12 hours and a higher normal stress range, and failure envelope A7b has an increased time of hydration (60 hours) and an increased time of consolidation (24 hours). As the two series have slightly different test conditions and were sheared at differing ranges of normal stress, it is difficult to directly compare the results of the two failure envelopes. However, similar to failure envelope A3a in Figure 4.48(b) there are two distinct behaviors at low and high normal stresses. The two peak shear strength envelopes define roughly a non-linear failure envelope. Peak failure envelope A7b has the highest friction angle (50.1^0) of all failure envelopes for GCL A, while peak failure envelope A7a had a friction angle (22.7^0) greater than that for failure envelope A3a at high normal stresses (12.0^0), and similar to that of failure envelope A6 (21.9^0).

Failure envelope A8 is shown in Figure 4.57, and the test results are shown in Table 4.17. This failure envelope differs from the baseline failure envelope as GCL *A* is unhydrated. The shear strength of an unhydrated GCL is expected to be significantly greater than the baseline failure envelope (Gilbert *et. al.*, 1997). The peak friction angle for this failure envelope is less than that of the baseline failure envelope, but the intercept for failure envelope A8 is significantly larger. The shear strength for GCL *A* in unhydrated conditions is quite variable. All unhydrated GCL specimens experienced a rupture of the carrier geotextiles after reaching peak shear strength, so the large-displacement conditions were not reported. Figure 4.58 shows a

comparison plot of the peak failure envelopes A1a and A8. The shear strength represented by failure envelope A8 is greater for the range of normal stresses tested. A large variability in shear strength is apparent in both failure envelopes.

4.3.2.2 Analysis of GCL B

The analysis of test results for GCL *B* from the GCLSS database is based on 48 direct shear tests. These test results may be grouped into four separate sets of different conditions, from which failure envelopes may be developed for GCL *B* (see also Table 4.9):

- Failure envelope B1 consists of a time of hydration of 24 hours, no consolidation and a shear displacement rate of 1.0 mm/min,
- Failure envelope B2 consists of a time of hydration of 48 hours, no consolidation and a shear displacement rate of 1.0 mm/min;
- Failure envelope B3 consists of a time of hydration of 96 hours, no consolidation and a shear displacement rate of 1.0 mm/min; and
- Failure envelope B4 consists of a time of hydration of 168 hours, a time of consolidation of 48 hours and a shear displacement rate of 0.1 mm/min

Failure envelope B1 is shown in Figure 4.59, and the test results are presented in Table 4.18. Failure envelope B1 is taken as the baseline failure envelope for GCL *B*. The peak failure envelope for GCL *B* has a significantly lower friction angle (7.3^0) than any failure envelopes for GCL *A*. However, the intercept value for this failure envelope is comparatively high (53 kPa). The peak shear strength of GCL *B* is characterized by a large intercept value. The large-displacement values also follow a distinct linear trend with a friction angle of 4.6^0. The large-displacement failure envelope also has a comparatively high intercept value of 12.7 kPa. Many of the tests on GCL B at low normal stresses did not reach large-displacement conditions because of tensile rupture of the carrier geotextile components.

Failure envelope B2 is shown in Figure 4.60, and the test results are presented in Table 4.19. This failure envelope differs from the baseline failure envelope by an increased time of hydration of 48 hours. The peak friction angle and intercept value (4.4^0 and 24.1 kPa) are approximately half of those of the baseline failure envelope.

This implies that the time of hydration affects the friction angle and the intercept value.

Failure envelope B3 is shown in Figure 4.61, and the test results are presented in Table 4.20. This failure envelope differs from the baseline failure envelope by an increased time of hydration of 96 hours. This failure envelope is similar to failure envelope B2.

Figure 4.62 shows a comparison plot of peak failure envelopes B1, B2 and B3. This figure shows the affect of increasing times of hydration on the shear strength of GCL *B*. There is a large decrease in shear strength corresponding to a decrease in intercept value when the time of hydration increased from 24 hours to 48 hours, but there was comparatively no change with an increase in time of hydration from 48 hours to 96 hours.

Failure envelope B4 is shown in Figure 4.63, and the test results for this failure envelope are presented in Table 4.21. This failure envelope differs from the baseline failure envelope in terms of the times of hydration and consolidation as well as the shear displacement rate. This failure envelope shows lower peak shear strength values for these test conditions than for the baseline failure envelope. It can be postulated that the large time of hydration decreased the friction angle and intercept value as observed in failure envelopes B2 and B3, but consolidation led to a subsequent increase in the friction angle and intercept value. The friction angle regained the same value as in the baseline failure envelope, but the intercept value was not increased to the same level as the baseline failure envelope.

Overall, it is observed that GCL *B* has lower shear strength than GCL *A*, and that the scatter in peak shear strength at low normal stresses is very high for GCL *B*. This may be due to the effect of the stitched reinforcements. No internal failures of GCL B in the field have been reported, which may indicate that the low observed shear strength in laboratory testing may be the result of limitations of the direct shear device. The small size of the direct shear device may not fully capture the behavior of the stitch-bonding reinforcements, as they are placed at 3-inch intervals. This allows only three lines of stitching to be tested in a 12-inch wide direct shear device.

4.3.2.3 Analysis of GCL C, D and E

GCLs *C, D* and *E* are needle-punched GCLs with thermal bonding. Thermal bonding involves the use of heat to affix the needle-punched threads protruding from the GCL to the carrier geotextiles of the GCL. This prevents pullout of the fiber reinforcements from the woven carrier geotextile during swelling of the sodium bentonite or during shear. This creates a "rigidly" reinforced GCL, in which the GCL typically fails internally when the needle-punched fibers fail in tension.

The analysis of test results for GCL *C* from the GCLSS database is based on 26 direct shear tests, which included three failure envelopes. For each of the failure envelopes, the average and standard deviation of the peak and large-displacement shear strength values were determined for each normal stress level. The specific failure envelopes are listed below (see also Table 4.9):

- Failure envelope C1 consists of a time of hydration of 24 hours, no consolidation and a shear displacement rate of 0.5 mm/min;
- Failure envelope C2 consists of a time of hydration of 24 hours, no consolidation and a shear displacement rate of 0.2 mm/min; and
- Failure envelope C3 consists of a time of hydration of 168 hours, a time of consolidation of 48 hours, and a shear displacement rate of 0.1 mm/min

Failure envelope C1 was chosen as the baseline failure envelope for GCL *C*. This failure envelope is shown in Figure 4.64, with the test results in Table 4.22. Figure 4.64(a) shows peak and large-displacement shear strength data for the full range of test results. This failure envelope tends to overestimate stresses at low and high levels of normal stress. Figure 4.64(b) shows bilinear failure envelopes for the same test results with different trends for normal stresses below and above 100 kPa. The behavior shown in Figure 4.64(b) is similar to that of failure envelope A3a, with a higher friction angle and lower intercept for low normal stresses, and the opposite for high normal stresses. There is slight scatter in the peak and large-displacement failure envelopes, but the data follows a linear trend.

Failure envelope C2 is shown in Figure 4.65, and the test results are presented in Table 4.23. This failure envelope differs from the baseline by a slower shear displacement rate of 0.2 mm/min. There appears to be a break in the failure envelope

at 100 kPa, but there are too few data points to define a bilinear failure envelope. The data still follows a more linear trend than the baseline failure envelope. Figure 4.66 shows a plot of failure envelopes C1 and C2 to view the effect of the shear displacement rate. This figure confirms that the slower shear displacement rate results in a higher peak shear strength. Specifically, failure envelope C2 has a higher intercept value (22.0 kPa for C2 and 2.4 kPa for C1) and a slightly higher peak friction angle (29.3^0 for C2 and 23.7^0 for C1). The large-displacement failure envelope appears to be unaffected by the decrease in shear displacement rate.

Failure envelope C3 is shown in Figure 4.67, and the test results are presented in Table 4.24. This failure envelope differs from the baseline by different times of hydration and consolidation as well as shear displacement rate. This failure envelope has similar test conditions to failure envelopes A5 and B4. The similarities and differences will be discussed later. The peak and large-displacement shear strength values for this failure envelope are lower than those for both failure envelopes C1 and C2. However, the trend for higher normal stresses for failure envelope C1 shown in Figure 4.55(b) has a similar trend to peak failure envelope C3.

GCL D is similar to GCL C, but two nonwoven carrier geotextiles are used instead of the woven-nonwoven configuration of GCL C. From a total of 15 test results, three failure envelopes were developed for GCL D (see also Table 4.9):

- Failure envelope D1 has a time of hydration of 72 hours, no consolidation and a shear displacement rate of 1.0 mm/min,
- Failure envelope D2 has a time of hydration of 24 hours, no consolidation and a shear displacement rate of 0.5 mm/min, and
- Failure envelope D3 has a time of hydration of 24 hours, a time of consolidation of 24 hours, and a shear displacement rate of 1.0 mm/min.

All three failure envelopes for GCL D are shown in Figure 4.68 and the data is presented in Table 4.25. It is difficult to compare the effect of the test conditions on the behavior of the GCL, as the failure envelopes differ in more than one test condition. For this reason, no baseline failure envelope was defined. Figure 4.68(a) shows the peak failure envelopes. Failure envelope D1 has the fastest shear displacement rate and the longest time of hydration, so it is expected to have the

lowest peak shear strength (a friction angle of 18.6^0 and an intercept value of 5.65 kPa). Failure envelope D2 has the highest peak shear strength (a friction angle of 25.1^0 and an intercept value of 75.3 kPa). Failure envelope D3 has intermediate peak shear strength values (a friction angle of 27.1^0 and an intercept value of 40.9 kPa). Figure 4.68(b) shows the large-displacement failure envelopes for failure envelopes D1, D2 and D3. All three failure envelopes are clearly linear. Failure envelope D2 has the highest large-displacement shear strength, while failure envelope D1 has the lowest large-displacement shear strength. All three failure envelopes have similar large-displacement friction angles, but differ in terms of intercept values.

Failure envelope D3 is highly non-linear, so a linear best fit line did not represent the data well at low and high normal stresses. For this reason, a bilinear fit was chosen for the data, which is shown in Figure 4.69. The bilinear failure envelope for failure envelope D3 is similar to those for failure envelopes A3a and C1, with a high friction angle and low intercept for low normal stresses (38.9^0, 22.4 kPa) and a low friction angle and high intercept for high normal stresses (21.6^0, 101 kPa). The trends for data at low and high normal stress ranges fit the data well.

GCL *E* is similar to GCL *D*, but GCL *E* is manufactured with a lower amount of needle-punching for low normal stress applications. From a total of 8 test results on GCL E, two failure envelopes were developed (see also Table 4.9):

- Failure envelope E1 consisting of a time of hydration of 336 hours, no consolidation and a shear displacement rate of 1.0 mm/min; and
- Failure envelope E2 consisting of a time of hydration of 48 hours, no consolidation and a shear displacement rate of 1.0 mm/min

Failure envelopes E1 and E2 are shown in Figure 4.70, and the data is presented in Table 4.26. Failure envelope E2 shows slightly higher shear strength than failure envelope E1, although the time of hydration is very different for the two failure envelopes (48 hours for failure envelope E2 and 336 hours for failure envelope E1). However, there is only a difference of 7^0 between the friction angles for the two failure envelopes, corresponding to the increase in the time of hydration from 48 hours to 336 hours. Both failure envelopes have a similar intercept value. This may indicate that the time of hydration beyond 48 hours does not result in a significant

decrease in peak shear strength. The large-displacement conditions for failure envelopes E1 and E2 are shown in Figure 4.63. This figure shows the same trend for large-displacement shear strength as for peak shear strength. There is only a difference of 2.4^0 between the two friction angles. Therefore, the large-displacement shear strength is less sensitive to an increase in time of hydration.

4.3.2.4 Analysis of an Unreinforced GCL (GCL F)

GCL *F* is the sole GCL in the database that is not reinforced. This GCL consists of a layer of sodium bentonite with a woven carrier geotextile and a nonwoven carrier geotextile adhered to the top and bottom surfaces of the sodium bentonite, respectively. Seven tests were conducted on this GCL, and two failure envelopes were developed:

- Failure envelope F1 consisting of a time of hydration of 168 hours, no consolidation and a shear displacement rate of 1.0 mm/min; and
- Failure envelope F2 consists of times of hydration or consolidation of zero hours (unhydrated) and a shear displacement rate of 1.0 mm/min

The peak and large-displacement failure envelopes F1 and F2 are shown in Figures 4.71(a) and 4.71(b), respectively, and the test results are presented in Table 4.27. This figure shows that the two failure envelopes include data points at different ranges of normal stress, so the two failure envelopes may not be compared directly. However, the two failure envelopes show representative behavior for low and high levels of normal stress for their respective test conditions, with a high friction angle and low intercept value for low normal stresses and a low friction angle and high intercept value for high normal stresses. The peak and large-displacement shear strength values for both failure envelopes are much less than those for the failure envelopes for reinforced GCLs at the same ranges of normal stress (*e.g.* FE A1a compared with FE F1, and FE A3a compared with FE F2).

As GCL *F* is essentially a layer of unreinforced sodium bentonite, triaxial cell tests on sodium bentonite clay may be compared with the direct shear test results found in the GCLSS database. Total stress data for triaxial tests on sodium montmorillonite reported by Mesri and Olson (1970) are presented in Figure 4.72

along with the peak shear strength values of failure envelope F2. This figure shows that the triaxial test results represent a lower bound on the peak shear strength, possibly due to the differences of boundary conditions between direct shear and triaxial tests. Still, as the GCLs in failure envelope F2 are unhydrated, it is expected that the shear strength for this interface is greater than fully hydrated sodium bentonite clay. Mesri and Olson (1970) did not report large-displacement shear strength values for the unreinforced sodium montmorillonite clay.

4.3.2.5 Analysis of Other GCLs

The GCLSS database also includes several other GCLs that either do not have enough tests to justify a full analysis or too few tests conducted under similar test conditions to develop strength envelopes. These are GCLs *G, H, I* and *J*, which are all needle-punched GCLs.

GCL *G* is a needle punched GCL similar to GCL *A*, but includes additives to improve the hydraulic properties of the GCL. This GCL has one failure envelope consisting of a time of hydration of 24 hours, no consolidation and a shear displacement rate of 1.0 mm/min. Failure envelope G1 is shown in Figure 4.73, and the test results are presented in Table 4.28. Also included in Figure 4.73 are the test results for failure envelope A1a, which shows that failure envelope A1a has significantly higher peak shear strength values. This implies that the hydraulic additives result in a significant decrease in shear strength.

GCL *H* is a needle-punched similar to GCLs *D* and *E*, although it is not thermal bonded. The 18 test results for this GCL can be divided into three failure envelopes:

- Failure envelope H1 consists of a time of hydration of 24 hours, no consolidation and a shear displacement rate of 1.0 mm/min;
- Failure envelope H2 consists of a time of hydration of 24 hours, a time of consolidation of 24 hours and a shear displacement rate of 1.0 mm/min;
- Failure envelope H3 consists of a time of hydration of 96 hours, time of consolidation of 24 hours and a shear displacement rate of 0.25 mm/min

Peak failure envelopes H1, H2 and H3 are shown in Figure 4.74, and the test results are presented in Table 4.29. Figure 4.74(a) shows the full range of normal stresses, while Figure 4.74(b) shows a detail of the low normal stresses so that the behavior of failure envelope H3 may be better seen. Failure envelopes H1 and H2 are similar despite the longer time of consolidation for failure envelope H1. Failure envelope H2 has a slightly greater intercept value and a lower friction angle. Failure envelope H3 has lower shear strength than the other two failure envelopes, despite its higher friction angle. Although the trend of failure envelope H3 falls below that of the other two failure envelopes, it can be seen from Figure 4.74(b) that the shear strength values of the other failure envelopes at the same normal stress are comparatively the same. Figure 4.75 shows large-displacement failure envelopes H1 and H2. Failure envelope H1 has lower large-displacement shear strength than failure envelope H2. This is expected as failure envelope H2 had a longer time of consolidation. Failure envelope H1 has the lowest large-displacement friction angle of all needle-punched GCLs.

Failure envelopes H1, H2 and H3 for GCL *H* may be compared to failure envelopes D1, D2, D3, E1 and E2 for GCLs *D* and *E*, as all three GCLs are needle-punched with nonwoven carrier geotextiles on each side of the sodium bentonite layer. GCL *H* differs from GCLs *D* and *E* in that the latter two GCLs are thermal bonded while GCL *H* is not. Figure 4.76(a) shows that the peak shear strength of GCL *H* is generally greater than that of GCLs *D* and *E*, although there is not a significant difference in the behavior of the three GCLs. Failure envelope D1 is weaker than all other failure envelopes. Figure 4.76(b) shows that the large-displacement shear strength values of all three GCLs are comparatively the same, with small differences in intercept values between the different failure envelopes.

GCL *I* is a needle-punched GCL similar to GCL *A*, but an adhesive is added to the sodium bentonite to prevent the fiber reinforcements from pulling out of the confining carrier geotextiles during hydration. From the eight test results for GCL *I*, two failure envelopes were developed:

- Failure envelope I1, which consists of no hydration or consolidation and a shear displacement rate of 1.0 mm/min; and

- Failure envelope I2, which consists of a time of hydration of 72 hours, no consolidation and a shear displacement rate of 1.0 mm/min

Peak failure envelopes I1 and I2 are shown in Figure 4.77, and the test results are presented in Table 4.30. The failure envelope for the unhydrated GCL shows slightly greater peak shear strength than the failure envelope for the hydrated GCL. Similar to failure envelope A8, which also involves GCLs tested under unhydrated conditions, failure envelope I1 shows a non-linear trend for low normal stresses. It should be noted that the peak shear strength values for these failure envelopes are much greater than for failure envelope A1a, despite the longer time of hydration for failure envelope I2 (72 hours).

GCL *J* is a needle-punched GCL that is commonly used in European applications, as it was manufactured in Germany. The test conditions for the single failure envelope are a time of hydration of 24 hours, no consolidation and a shear displacement rate of 1.0 mm/min. Peak and large-displacement failure envelopes J1 are shown in Figure 4.78, and the test results are presented in Table 4.31. This GCL has a linear trend across a wide range of normal stresses, and the peak and large-displacement friction angles are relatively parallel. The peak and large-displacement shear strength values of this GCL are relatively low compared to other needle-punched GCLs. In fact, peak failure envelope A1a, which includes GCL specimens tested under the same hydration conditions, shows that the shear strength of GCL *A* is much greater (a friction angle of 46.5^0 and an intercept value of 13.20 kPa) than GCL *J* (a friction angle of 9.6^0 and an intercept value of 5.52 kPa). This difference may be in lower amounts of needle-punching required in European manufacturing specifications, or different sodium bentonite clay (*i.e.* different sodium ion concentration, different additives, *etc.*).

4.3.2.6 Comparisons between Failure Envelopes

Table 4.32 shows the linear regression results (the friction angle and intercept values) for each of the peak and large-displacement failure envelopes discussed in this section. The baseline failure envelopes (A1a, B1 and C1) are highlighted in light gray. This table includes the test conditions for each failure envelopes, as well as the

ranges of normal stresses over which the best-fit lines are applicable. The friction angles and intercept values are reported for the full range of normal stresses for each of the GCLs, but the bilinear trend is still reported in this table for failure envelopes A3a, C1 and D3, which are highlighted in dark gray.

Figure 4.79 shows a comparison plot of failure envelopes A1 and B1, as both of these failure envelopes have the same test conditions. The peak failure envelopes are quite different and may reflect the difference between needle-punched and stitch-bonded GCLs. Failure envelope A1 has a very high friction angle and a very low intercept value. The opposite is true for failure envelope B1, which implies that that GCL B may be more suitable for low levels of normal stress (*i.e.* less than 50 kPa). The large-displacement failure envelopes are similar compared to the difference in behavior for the peak failure envelopes.

Figure 4.80 shows a comparison plot of failure envelopes A2 and C1, both of which have the same test conditions. This figure shows the effect of thermal bonding on the shear strength of needle-punched GCLs. The two failure envelopes have roughly the same peak friction angle, but GCL *A* (which is not thermal bonded) has a slightly higher intercept value. The large-displacement failure envelopes for both GCLs are relatively the same.

Figure 4.81 shows a plot of the average peak and large-displacement failure envelopes for GCLs *A, B* and *C* for constant test conditions (failure envelopes A5, B4 and C3: a time of hydration of 168 hours, a time of consolidation of 48 hours and a shear displacement rate of 0.1 mm/min). GCL *A* has a higher peak and large-displacement shear strength than the other two GCLs, while GCL *B* consistently has the lowest shear strength except at low normal stresses. It should be noted that GCL *C* has lower peak and large-displacement shear strength values that GCL *A* although they are both needle-punched. It may be postulated that GCL *C*, which is thermal bonded, experiences little pullout of the fiber reinforcements from the carrier geotextiles during hydration, thus leading to plastic deformation of the reinforcements before shearing begins. This may lead to premature shear failure of GCL *C*. The large-displacement shear strength values for the thermal bonded, needle-punched GCL are also lower than non-thermal bonded needle-punched GCLs.

Figure 4.82 shows the ratio of peak to large-displacement shear strength for all three of the GCLs mentioned in the previous paragraph. GCL *B* has negligible post-peak shear strength loss, while GCLs *A* and *C* have similar post-peak shear strength loss. GCL *A* tends to decrease in the amount of post-peak softening with increasing normal stress, and GCL *C* tends to increase in the amount of post-peak shear strength loss with increasing normal stress.

Figure 4.83 shows a comparison plot of all of the peak failure envelopes for GCLs *A, B, C* and *F*. GCLs *A* and *C* are grouped in the upper range of peak shear strength values, while GCLs *B* and *F* are grouped in the lower range of peak shear strength values. Figure 4.84 shows a comparison plot of all of the large-displacement failure envelopes for GCLs *A, B, C* and *F*. When viewed at this scale, it appears that the large-displacement behavior for all GCLs is relatively the same. The maximum difference in large-displacement friction angle for all GCLs is about 7^0.

Figure 4.85 shows a comparison plot of all peak failure envelopes for GCL *A*. This figure shows that all of the failure envelopes are closely grouped together except failure envelope A3. However, failure envelope A3a was shown to have different behavior for low and high ranges of normal stress, which make comparison of this failure envelope with the others difficult. Figure 4.86 shows a comparison plot of all large-displacement failure envelopes for GCL *A*. This figure shows that all of the failure envelopes tend to align linearly.

Figure 4.87 shows a comparison plot of all peak failure envelopes for GCL *B*. This figure suggests that this GCL has similar friction angles for all test conditions, but different intercept values. The magnitude of the intercept value depends on the time of hydration.

Figure 4.88 shows a comparison plot of all peak failure envelopes for GCL *C*. This figure shows that all of the GCLs have similar intercept values, but different friction angles. The same trend is apparent in Figure 4.89, which shows a plot of all large-displacement failure envelopes for GCL *C*, although the failure envelopes are nearly parallel.

4.3.3 Shear Displacement Rate Analysis

Figure 4.90 presents the effect of shear displacement rate on GCL *A* specimens tested at a comparatively low normal stress (50 kPa) and a comparatively high normal stress (517.1 kPa), with the test results presented in Table 4.33. For a normal stress of 50 kPa, the average peak shear strength values increase with increasing shear displacement rate. This confirms the findings of Eid *et. al.* (1999) for specimens tested at normal stresses below 170 kPa. This implies that there is a greater amount of post-peak shear strength loss for tests conducted at faster shear displacement rates. Contrary to the trends observed for GCLs sheared at a normal stress of 50 kPa, GCLs sheared at a normal stress of 517.1 kPa show a decrease in peak shear strength with increasing shear displacement rates. GCL shear strength behavior is significantly different for low and high normal stresses.

Figure 4.90(b) shows that the large-displacement shear strength for GCL *A* specimens tested at a comparatively low normal stress (50 kPa) and a comparatively high normal stress (517.1 kPa). This figure shows that for both levels of normal stress, the large-displacement shear strength decreases with increasing shear displacement rate.

The trends observed in Figures 4.90(a) and 4.90(b) can be explained by the reinforcement behavior during shear and by the swelling behavior of sodium bentonite. For low normal stresses, it is expected that the fiber reinforcements in GCL A tend to pull out of the woven carrier geotextile, as the frictional connection between the fibers and the woven carrier geotextile is not high. Pullout is expected to be facilitated with decreasing shear displacement rates. For high normal stresses, the higher pullout resistance makes the governing mechanism of failure the tensile breakage of the fiber reinforcements. Still, this is expected to be independent of the shear displacement rate. Therefore, the sodium bentonite clay must have an additional effect on the shear strength of the GCL as a whole.

The behavior of sodium bentonite under low and high confinement may explain the observed difference in behavior. For normal stresses below the swell pressure of reinforced GCLs (*i.e.* 160 kPa), the sodium bentonite tends to swell. Negative pore pressures in the sodium bentonite due to the matric and osmotic

suctions decrease during the swelling process until the sodium bentonite reaches hydrostatic levels. For high normal stresses, the sodium bentonite is not allowed to swell beyond its original thickness. Instead, positive pore pressures in the sodium bentonite due to rapid loading decrease during a consolidation process until reaching hydrostatic levels.

For needle-punched GCLs tested at low normal stresses, the pore pressure in the sodium bentonite is negative if the swelling process is incomplete. Rapid shear displacement rates (*e.g.* at 1.0 mm/min) generate additional negative excess pore water pressures. In other words, an increasing shear displacement rate will lead to increased effective stresses, and thus increased peak shear strength in the GCL.

On the other hand, for needle-punched GCLs tested at high normal stresses, pore pressure in the sodium bentonite is positive if the consolidation process is incomplete. In addition, rapid shear displacement rates (*e.g.* 1.0 mm/min) will generate positive excess pore water pressures. In other words, an increasing shear displacement rate will lead to decreased effective stresses, and thus decreased peak shear strength in the GCL.

With respect to large-displacement shear strength, a conventional behavior is expected for large-displacement shear strength is expected (*i.e.* decreasing shear strength with increasing shear displacement rates) for both high and low levels of normal stress. Indeed, positive pore water pressures are feasible at large shear displacement rates. However, for *actual* residual shear strengths, the shear displacement rate should have no effect, as the soil is at constant volume/pore water pressure conditions.

Figure 4.91 shows the effect of shear displacement rate on the peak shear strength values of GCL *C* tested at a normal stress of 50 kPa, with the specific test results presented in Table 4.34. This figure indicates that for low normal stresses, the peak shear strength of GCL *C* decreases slightly with increasing shear displacement rate. This behavior may be the result of the thermal bonding of the GCL, which prevents pullout of the needle-punched fibers and provides additional normal confinement to the sodium bentonite in the GCL. The additional confinement may imply that GCL *C* behaves similar to GCL *A* tested at high normal stresses.

4.3.4 Time of Hydration Analysis

The analysis of different failure envelopes that were tested under similar test conditions but different times of hydration were investigated in section 4.2.4. Comparison of failure envelopes A1a, A3a and A4 as well as B1, B2 and B3 shows a decrease in peak shear strength with increasing times of hydration. However, observations of these failure envelopes indicates that the peak shear strength does not decrease linearly with increasing time of hydration, but reaches a limiting value, at which further increase in the time of hydration does not result in significant shear strength reduction.

Figure 4.92(a) presents the effect of the time of hydration on the peak shear strength of GCL *A* when tested at two different normal stresses. The specific test results for this figure are presented in Table 4.36(a). It should be noted that these tests had a normal stress used during hydration equal to the hydration stress used during shearing. Results from tests conducted at a normal stress of 6.9 kPa indicate that there is no further decrease in shear strength beyond a time of hydration of 48 hours. Both normal stress levels show a decrease in shear strength from unhydrated tests to times of hydration of 48 hours. Figure 4.92(b) shows a similar plot of the effect of hydration on the peak shear strength of GCL A, but the tests conducted in this figure had different hydration normal stresses than those used during shearing. A similar trend to Figure 4.92(a) is observed, although there is a slight increase in shear strength for the tests with a time of hydration of 48 hours, which can be explained by the fact that the hydration normal stress was greater for this set of tests than the hydration normal stresses for the tests with a time of hydration of 24 hours. The data for this figure is also presented in Table 4.36(a).

Figure 4.93 shows the same data as presented in Figures 4.92(a) and 4.92(b), but the failure envelopes with different times of hydration are shown. The rearranged data for this figure is presented in Table 4.36(b). Although the normal stress values for each of the failure envelopes do not coincide, there is a decrease in shear strength from those tests conducted with no hydration, to those conducted at a time of

hydration of 24 hours and then to those conducted at times of hydration of 48 and 72 hours, which roughly coincide.

Figure 4.94 shows the effect of a staged hydration and consolidation procedure for very slow shear displacement rates on the shear strength of GCL *A* (0.0015 mm/min). The data for this figure is shown in Table 4.37. Figure 4.94 shows that a staged hydration and consolidation procedure results in a lower peak and large-displacement shear strength. This difference is most likely because the first stage of GCL hydration involves free swelling under a normal stress of about 10 kPa, in which the fiber reinforcements are most likely pulled out of the woven carrier geotextile. The subsequent consolidation phases are not capable of regaining the loss of reinforcements, so the shear strength values of these GCLs are lower. This finding implies that designers should employ a high hydration normal stress in the field.

4.3.5 Time of Consolidation Analysis

As previously discussed, increasing the time of consolidation led to significantly increased peak shear strength values, while the large-displacement shear strength was only slightly increased. Figure 4.95(a) shows the effect of increasing times of consolidation on the peak shear strength of GCL *H*, for low and high normal stresses. This figure indicates that when GCL *H* is consolidated, the peak shear strength does not change appreciably, although the consolidated GCL still has slightly greater peak shear strength. Figure 4.95(b) shows the effect of increasing times of consolidation on the large-displacement shear strength of GCL *H* at high normal stresses. This figure shows that the large-displacement shear strength values for the consolidated GCL are larger than for unconsolidated GCL.

Figure 4.96 shows the effect of consolidation on GCL *A* through the comparison of the data in failure envelopes A1a and A7a. Test results for GCLs with a time of hydration of 24 hours and no consolidation and others with a time of hydration of 60 hours and a time of consolidation of 24 hours are compared in this figure. Due to the discussion in section 4.4, it can be assumed that the peak shear strength of GCL *A* when hydrated for 24 and 60 hours is not significantly different.

Despite the greater time of hydration, failure envelope A7b has higher peak shear strength.

As GCLs *A* and *H* are relatively the same except for the difference in carrier geotextiles, so their shear strength test results may be compared with caution to investigate the effect of the time of consolidation. Shear strength results for these GCLs are presented together in Figure 4.97. This figure shows that both GCLs have similar behavior when tested under similar hydration conditions with no consolidation. In addition, the intercept value of GCL A increases if the time of consolidation is increased.

4.3.6 Variability Analysis

The variability of the peak and large-displacement shear strength results obtained from specimens tested at the same normal stress and under the same test conditions is an important issue in shear strength testing of GCLs. The variability in the shear strength is a function of the natural variability of sodium bentonite clay (Mesri and Olson, 1970), as well as the variability of GCL manufacturing procedures (*i.e.* needle-punching variability, thermal bonding variability). This variability may be understood and quantified through the use of probabilistic techniques. Of particular relevance is failure envelope A5, which includes of 19 series of three tests conducted at different normal stresses (34.5, 137.9, and 310.3 kPa).

Figure 4.98 shows the standard deviation of the peak and large-displacement shear strength with increasing normal stress for GCL *A* under constant test conditions (FE A5: t_H = 24 hours, t_C = 48 hours and SDR = 0.1 mm/min). These test conditions are representative of conditions in the field. There were 19 tests conducted at each normal stress, so 57 peak and 54 large-displacement shear strength values were obtained (three tests did not reach large-displacement conditions). The data for this failure envelope is presented in Table 4.38. Note that the axis scales in this figure are not the same in order to magnify the differences in standard deviation for each normal stress level. There is an increasing trend in the standard deviation with increasing normal stress for both the peak and large-displacement shear strength values. Figure

4.99 presents the variation in coefficient of variation (COV) for the same test results. The COV is defined as:

$$COV = \frac{\sigma}{\mu} \qquad \text{Eq. 4.6}$$

where σ is the standard deviation of a data set and μ is the mean (average) of a data set. A high COV implies that the variability of the data is very high.

Assuming that any of the observed values of peak and large-displacement shear strength are equally probable, a probability distribution may be developed. A probability distribution quantifies the spread of the data about a central value, and is characterized by a relationship between the values of a certain variable and the probability of occurrence for each value. A probability density function (PDF) may be developed as follows:

$$f_X(x) = P(X = x) = p_x \times x \qquad \text{Eq. 4.7}$$

where x is a random variable, $f_x(x)$ is the PDF function, $P(X=x)$ is the probability function at which *any* value X in the function equals a *present* value of x, and p_x is the individual probability of each value of x. The area under the PDF function is equal to unity, and may be developed discretely (as is the case with the data from the GCLSS database) or continuously.

As it is difficult to interpret the results of a PDF, a PDF may be integrated to develop a cumulative distribution function (CDF), which is a simpler interpretation of the probability distribution. In essence, a CDF presents the probability that the present value is less than a given value. For instance, the probability that a value is less than infinity is one. The CDF can be formulated from the PDF as follows:

$$F_X(x) = P(X \le x) = \sum p_{x,i} x_i = \int f_X(x) dx \qquad \text{Eq. 4.8}$$

where x is a random variable, $F_x(x)$ is the CDF function, and $P(X<x)$ is the probability that *any* value X in the function is less than a *specific* value x.

If a probability distribution is defined as a continuous function, the random variable must have two or more descriptors, such as the mean and the standard deviation. Therefore, it is possible to create a discrete CDF and PDF then use the

mean and standard deviation of the data to develop an "equivalent" continuous distribution to be used in probabilistic analyses.

Figure 4.100(a) shows the peak CDF and Figure 4.100(b) shows the peak PDF tests from failure envelope A5 conducted using a normal stress of 34.5 kPa. Figure 4.100(b) also shows the equivalent normal distribution. The descriptors of the equivalent normal distribution are the mean and standard deviation of the peak shear strength. Although the discrete and continuous PDF functions are not plotted to the same ordinate scale, the areas under the discrete and continuous functions are equal to unity. A probability may be represented as the "percent chance" that the peak shear strength outcome is less than a certain value. For instance, it could be observed from Figure 100(a) that, "90 tests out of 100 have peak shear strength values less than 53.1 kPa". Figure 4.101(a) and 4.101(b) show the large-displacement CDF and PDF for tests from failure envelope A5 conducted using a normal stress of 34.5 kPa. The data in this figure shows that the data is skewed to a lower shear strength range, although there are several outliers at higher shear strength.

Figure 4.102(a) and 4.102(b) show the peak CDF and PDF for tests from failure envelope A5 conducted using a normal stress of 137.9 kPa. As with the peak shear strength distribution for 34.5 kPa, most of the data is grouped close to the mean (~111 kPa). Figure 4.103(a) and 4.103(b) show the large-displacement CDF and PDF for tests from failure envelope A5 conducted using a normal stress of 137.9 kPa. The data in this figure is grouped to the high side of the mean, which is different from the behavior for a normal stress of 34.5 kPa.

Figure 4.104(a) and 4.104(b) show the peak CDF and PDF for tests from failure envelope A5 conducted using a normal stress of 310.3 kPa. The data for this normal stress level is quite dispersed, but there is still a large concentration of data at the mean peak shear strength of 203 kPa. Figure 4.105(a) and 4.105(b) show the large-displacement CDF and PDF for tests from failure envelope A5 conducted using a normal stress of 310.3 kPa. Unlike the two lower normal stress levels, the large-displacement shear strength is grouped closely around the mean except for a few outliers.

Figure 4.106(a) and 4.106(b) show the "equivalent" peak and large-displacement normal distribution functions for each of the normal stress levels, respectively. There are significant differences in variability for the peak shear strength. The lowest peak shear strength has a low standard deviation, so the data is grouped closely about the mean value. A similar trend is shown in the plot for the large-displacement shear strength probability functions, although the differences in the probability distributions are not as significant as the peak conditions. These equivalent peak and large-displacement normal distribution functions may be used for a wide variety of probabilistic and reliability analyses.

Figure 4.107 shows the peak CDF and PDF distributions for tests from failure envelope A3a conducted using a normal stress of 9.6 kPa (t_H = 48 hours, t_C = 0 hours and SDR = 1.0 mm/min). The CDF and PDF were developed from 19 tests at these conditions. The actual data used to develop this probability distribution is presented in Table 4.39. The trends are similar to those discussed above.

The variability GCL *A* under unhydrated conditions is shown in Figure 4.108. This figure shows a bar chart with five tests on the peak and large-displacement shear strength values for GCL A under identical test conditions and confining pressure. The data for this figure is shown in Table 4.40. There was not enough data to build a probability density function, but these tests are useful in developing a mean and standard deviation shear strength for this set of test conditions. The peak shear strength varies more than the large-displacement shear strength.

4.3.7 Final GCL Water Content Analysis

The final GCL water content (at failure) is another variable that can be investigated in this study. It has been shown earlier in this study that longer times of hydration or shorter times of consolidation result in a GCL with a lower peak and large-displacement shear strength. Greater times of hydration and lower times of consolidation correspond to higher GCL water contents. Before hydration, GCLs are under unhydrated moisture conditions (w = 10 to 15%). After being soaked in water, GCLs reach water contents in excess of 100%. Potential correlation may exist between the GCL water content (*i.e.* the void ratio) at failure and the shear strength.

Figure 4.109(a) and 4.109(b) show the peak and large-displacement shear strength, respectively, as a function of final water content for all GCLs in the database, respectively. As expected, increasing the final water content leads to a decrease in shear strength due to the low shear strength of the sodium bentonite. This confirms that a higher void ratio results in lower shear strength. Despite the clear downward trend, there is significant scatter in the data. It should be noted that a cluster of unhydrated GCLs (w ~ 25%), which have a comparatively low shear strength and do not fit the overall trend of saturated GCL specimens. There are also several data points at high shear strength and high water contents. These "outlier" data points are highlighted in gray. The remaining points show that there is a steep decrease in shear strength at water contents between 75 and 150%. Figure 4.109(a) shows that most of the needle-punched GCLs (GCLs *A* and *C*) failed at lower water contents than the stitch-bonded GCLs (GCL *B*). The decreasing trend is also apparent for the large-displacement shear strength shown in Figure 4.109(b). In general, there is a wide range of peak and large-displacement shear strength values for water contents below 100%. Low shear strength should be expected when the final water content is greater than 100%.

The peak and large-displacement shear strength values may be plotted against the final water content for GCL *A* for different test conditions. Figures 4.110(a) and 4.110(b) group the peak and large-displacement shear strength values, respectively, by different times of hydration for GCL *A*. Similar to Figure 4.109, the outlying data points are highlighted in gray. It should be noted that times of hydration of 24 and 48 hours are adequate enough to allow the GCL to reach water contents near 175%. Most GCLs fail at water contents from 75 to 100%. Still, some specimens with long times of hydration (*e.g.* 168 hours) show lower final GCL water contents, most likely as a result of subsequent consolidation.

Figures 4.111(a) and 4.111(b) group the peak and large-displacement shear strength values, respectively, by the time of consolidation for GCL *A*. These figures show clear groupings of test results. In general, GCLs with a time of consolidation of 48 hours have lower final GCL water contents and higher peak shear strength values. Unconsolidated GCL specimens ($t_C = 0$) tend to have large final water contents.

Figures 4.112(a) and 4.112(b) group peak and large-displacement shear strength values, respectively, by shear displacement rate for GCL *A*. The peak shear strength values for tests with faster shear displacement rates are lower than other tests, and also correspond to the highest final GCL water contents. Tests at high GCL water contents and fast shear displacement rate have low peak shear strength values possibly because pore water pressures were not dissipated during shearing.

Figures 4.113(a) and 4.113(b) group the peak and large-displacement shear strength values, respectively, by the order of normal stress application for GCL *A*. When the normal stress is held at the same level throughout the tests, the GCLs have a wide range of final water contents and generally have lower peak shear strength values. Still, these findings are in contradiction to the results of Gilbert *et. al.* (1996), who found that GCLs hydrated at a high normal stresses did not reach as high of water contents as GCLs hydrated at low normal stresses.

In summary, the effect of the test conditions on the final water content are difficult to grasp as the final water depends on more than one variable (the times of hydration and consolidation as well as the normal stress during hydration). In addition, the large variation in peak and large-displacement shear strength for water contents between 75 and 150% may indicate that the final void ratio of the sodium bentonite is not the only factor that affects the shear strength of the GCL.

Next, the some of the different failure envelopes explained in section 4.3.2 of this study were investigated to find trends between shear strength, normal stress and the final GCL water content.

Figure 4.114 shows the variation in peak shear strength with the final GCL water content for failure envelope A8. The test results for this failure envelope are presented in Table 4.41. This failure envelope includes GCL *A* specimens tested under unhydrated conditions. A slight upward trend is apparent, although there is significant scatter in the data. For these unhydrated tests, the initial water content is higher than the final water content, implying that consolidation of the GCL may have occurred during shearing of the GCL.

Figure 4.115 shows the variation in peak and large-displacement shear strength values with final water content for failure envelope A5. The test results for

this failure envelope are presented in Table 4.42. It is apparent that there is a decrease in the average peak and large-displacement shear strength values with increasing final GCL water content. The best fit lines do not represent the data well, as there is a large amount of variability in the shear strength at final water contents around 80%. Although there are insufficient data points to reach specific conclusions, it is possible that the peak shear strength of GCL *A* may be high (approximately 250 kPa) until reaching a final water content of 80%, at which point the shear strength is highly variable. At water contents higher than 80%, the peak shear strength may be very low (approximately 50 kPa). It appears that all of the tests fall within a relatively narrow band of final GCL water contents. The large amount of variability at final water contents near 80% may indicate failure of fiber reinforcements due to swelling of the sodium bentonite.

Finally, Figures 4.116(a) and 4.116(b) show the relationships between the peak and large-displacement shear strength values, respectively, and the final water content for GCLs *A, B* and *C* tested under identical conditions (t_H = 168 hours, t_C = 48 hours, SDR = 0.1 mm/min). The test results for these failure envelopes are presented in Table 4.43. GCL *C* (a thermal bonded needle-punched GCL) reaches higher final water contents for both peak and large-displacement conditions. The test results for GCL *A* (a non-thermal bonded needle-punched GCL) fall within a much narrower range of final water contents than the other GCLs. GCL *B* (a stitch-bonded GCL) behaves similarly to GCL *C* with respect to final water contents, although the peak and large-displacement shear strength values for this GCL are lower.

4.3.8 Analysis of Displacement at Peak Shear Strength

The shear displacement of the GCL should be evaluated as past studies have reported that small slope movements (*e.g.* 10 mm) may mobilize the peak internal shear strength of the GCL (Eid and Stark, 1997). Strain localization in a slope liner is an aspect of concern as a GCL may reach higher shear displacements for a given applied load than overlying layers (Stark *et. al.*, 1998). A small shear displacement at peak shear strength leads to little warning of failure of liner systems. The

displacements at peak shear strength values were noted for several failure envelopes reported in the GCLSS database.

The displacement at peak shear strength for failure envelope A8 is shown in Figure 4.117, and the test results for this failure envelope are presented in Table 4.41. The results show a decreasing trend in shear displacement with normal stress. As the peak shear strength of GCL under unhydrated conditions increases with normal stress, this finding implies that larger displacements are required to reach larger peak shear strength values.

The displacement at peak shear strength for failure envelope A5 is shown in Figure 4.118. The test results for this failure envelope are presented in Table 4.42. There is little sensitivity of the displacement at peak shear strength with normal stress. Consistent with the significant variability in the shear strength of GCL A, there is significant variability in the amount of displacement required to reach peak shear strength.

Figures 4.119(a), 4.119(b) and 4.119(c) show shear strength loss with displacement for tests taken from failure envelope A5 at normal stresses of 34.5, 137.9 and 310.3 kPa, respectively. Most of the lines in this figure have similar slopes, although the peak and large-displacement values themselves vary widely. For a normal stress of 34.5 kPa, the shear strength drops at a rate of 1.0 kPa/mm, for a normal stress of 137.9 kPa the shear strength drops at a rate of 2.0 kPa/mm, and for a normal stress of 310.3 kPa, the shear strength drops at a rate of 3.0 kPa/mm. This may have implications on stability analyses that need to quantify the shear strength loss with displacement. For example, this is necessary in seismic displacement-based analyses such as Newmark-type stability analyses. In general, it appears that the rate of post-peak shear strength loss is constant for a given normal stress, in spite of the variability of both the peak shear strength and the displacement at failure.

Figure 4.120 shows the variation in the *average* displacement at peak shear strength for GCLs *A, B* and *C* tested under identical conditions. The test results for these GCLs are presented in Table 4.43. The results for GCLs *A* and *C* show that the displacement at peak shear strength is relatively insensitive to normal stress.

However, GCL *B* shows a comparatively large increase in displacement at peak shear strength with increasing normal stress.

Figure 4.121 shows the variation in displacement at peak shear strength for unhydrated tests on GCL *A* tested at a normal stress of 517.1 kPa. The shear strength values are shown in Table 4.44. It can be seen that the peak shear strength values generally are reached at a relatively constant displacement. Figure 4.122 shows the displacement required to reach peak shear strength conditions with changing shear displacement rates. The shear strength values are also shown in Table 4.44. This figure shows a decreasing trend in displacement at peak shear strength with increasing shear displacement rate.

Figures 4.123(a) and 4.123(b) show the variation in displacement at peak and large-displacement shear strength for hydrated and unhydrated GCL *F* specimens, respectively. The test results for this GCL are presented in Table 4.45. It should be noted that stable large-displacement shear strength values were reached in displacements less than 25 mm, which is less than the maximum displacement of the direct shear device. This indicates that the displacements at large-displacement shear strength may be investigated. Both figures show that the amount of displacement required to reach peak shear strength conditions is constant with increasing normal stress. The displacement at large-displacement shear strength increases with increasing normal stress for the hydrated GCL, while the opposite is true of the unhydrated GCL.

4.4 Summary and Conclusions

4.4.1 Summary

The database for internal GCL shear strength evaluated in this study is probably the largest compilation such tests available, with a total of 320 tests on different GCLs, conducted at different normal stresses and test conditions. This database was compiled from a single laboratory, which eliminates a significant source of variability in testing procedures. This database extends the scarce information currently available for internal GCL shear strength.

Analysis of the database was performed using different approaches. Equivalent friction angles were developed for different sets of GCLs or test conditions to identify the sensitivity of the peak and large-displacement shear strength to different material characteristics or test conditions. A failure envelope analysis for GCLs with similar test conditions was conducted to investigate the changes in shear strength for different GCLs with normal stress. Based on the conclusions of the failure envelope analysis, the effects of the time of hydration, the time of consolidation, the shear displacement rate on the peak and large-displacement shear strength values were investigated. In addition, the variability in shear strength under constant test conditions, the relationship between the shear strength and the final water content, and the variation in the displacement at peak shear strength were also investigated. The findings of these analyses generally confirm and expand the findings of previous studies investigated as part of the state-of-the-art review in Chapter 3, as well as identify new trends particularly for high normal stresses.

4.4.2 Conclusions

The following conclusions regarding internal shear strength of GCLs may be drawn from the analysis of the GCLSS database:

a) Peak equivalent friction angles: $\phi_{GCL\ A} = 33.5^0$ (needle-punched), $\phi_{GCL\ C} = 28.9^0$ (needle-punched, thermal bonded), $\phi_{GCL\ B} = 12.2^0$ (stitch-bonded), $\phi_{GCL\ F} = 6.6^0$ (unreinforced)
b) Large-displacement equivalent friction angles: $\phi_{GCL\ A} = 13.7^0$ (needle-punched), $\phi_{GCL\ C} = 12.9^0$ (needle-punched, thermal bonded), $\phi_{GCL\ B} = 6.7^0$ (stitch-bonded), $\phi_{GCL\ F} = 5.9^0$ (unreinforced)
c) Reinforced GCLs had higher peak and large-displacement shear strength values than did unreinforced GCLs.
d) Needle-punched GCLs had higher peak and large-displacement shear strength values than stitch-bonded GCLs.
e) Non-thermal bonded Needle-punched GCLs were found to have higher peak and large-displacement shear strength values than thermal bonded needle-punched GCLs.

f) The shear strength of stitch-bonded GCL at low normal stresses is quite prominent, implying that is may be useful for low normal stress applications.

g) There was significant scatter in the peak shear strength values, but less scatter in the large-displacement shear strength values

h) Test results on GCL *A* obtained in this study compare well with the results from past studies. This is the case in spite of the variability in shear strength values for needle-punched GCLs with different peel strength values.

i) Shear strength envelopes evaluated in the analysis of the GCLSS database typically show non-linear trends for a wide range of normal stresses. A bilinear failure envelope for high and low normal stresses was employed. For low normal stresses, the friction angle was comparatively high while the intercept value was low, and for high normal stresses, the friction angle was low while the intercept was high. The intersection between the high and low normal stress failure envelopes fell within the range of the swell pressure of reinforced GCLs.

j) The peak shear strength was found to decrease with increasing time of hydration. This is in agreement with Gilbert *et. al.* (1996). However, the peak shear strength appears to be insensitive to times of hydration above approximately 48 hours. The large-displacement shear strength was found to not be sensitive to the time of hydration.

k) Lower hydration normal stresses lead to lower peak shear strength for reinforced GCLs. The large-displacement shear strength was found to not be sensitive to the hydration normal stress.

l) The peak and large-displacement failure envelopes were found to be sensitive to the time of consolidation. The peak shear strength of consolidated GCLs is almost always greater than unconsolidated GCLs.

m) For increasing shear displacement rates, the peak shear strength increases for low normal stresses and decreases for high normal stresses

n) For increasing shear displacement rates, the large-displacement shear strength was found to decrease for both low and high normal stresses.

o) This can be explained as follows:

- The effect of the shear displacement rate on needle-punched GCLs is most likely a combination of the effects of the fiber reinforcements and the swell behavior of the sodium bentonite in the GCL. This implies that exact definition of the mechanisms affecting the shear strength with different shear displacement rates is difficult.
- For needle-punched GCLs tested at low normal stresses an increasing shear displacement rate will lead to increased effective stresses due to the generation of negative pore water pressures during shearing and thus increased peak shear strength in the GCL. This is in agreement with the findings of Gilbert *et. al.* (1997) and Eid *et. al.* (1999).
- For needle-punched GCLs tested at high normal stresses an increasing shear displacement rate will lead to decreased effective stresses as rapid shear displacement rates will generate positive excess pore water pressures, and thus decreased peak shear strength in the GCL.
- For needle-punched GCLs with thermal bonding, it was found that the peak shear strength is not sensitive to the shear displacement rate. This is most likely due the increased confinement of the sodium bentonite provided by the thermal bonded fiber reinforcements.

p) Higher normal stresses lead to higher variability in peak and large-displacement shear strength. This variability is a result of manufactured differences in GCLs, changes in manufacturer specifications over time, test equipment, human errors, improper hydration, uneven normal stress application, or other testing errors.

q) The final water content, which is related to the void ratio for saturated soils, decreases with increasing normal stress. Lower final water contents were found to be related to lower peak and large-displacement shear strength values, which were often linearly related. The final water content was not sensitive to the time of hydration if the GCL was saturated, most likely because other test conditions affect the final water content. Increasing times of consolidation led to lower final water contents. The final water content was not sensitive to the shear displacement rate.

r) There is a significant variability in shear strength at water contents between 75 and 150%. For water contents above 100%, it is likely that the peak and large-displacement shear strength values will be relatively low. It is likely that there are other variables that affect the shear strength of GCLs than the final water content of the sodium bentonite.

s) The displacement at peak shear strength was not sensitive to the normal stress for needle-punched GCLs. Still, a slight decrease in displacements at peak shear strength with increasing stress was observed. For unreinforced GCLs, it was found that the displacement at peak shear strength remained constant for increasing levels of normal stress.

t) The rate of shear strength loss with increasing displacement beyond peak shear strength was found to be relatively constant. In fact, the rate of shear strength loss was found to increase non-linearly with increasing normal stresses.

Table 4.1: Definition of Variables used in the GCLSS Database

Variable	Definition
σ_N	Shearing Normal Stress
τ_p	Peak Shear Strength
τ_{LD}	Large Displacement Shear Strength
t_H	Time of Hydration
t_C	Time of Consolidation
σ_H	Hydration Normal Stress
σ_C	Consolidation Normal Stress
w_f	Final GCL Water Content
SDR	Shear Displacement Rate
Θ	Displacement at Peak Shear Strength

Table 4.2: Sets of GCLs in the GCLSS Database

Set Number	Description of Each Set	GCLs in Each Set
1	All GCLs	A-J
2	All Reinforced GCLs	A, B, C, D, E, G, H, I and J
3	All Unreinforced GCLs	F
4	All Stitch-Bonded GCLs	B
5	All Needle-Punched GCLs	A, C, D, E, G, H, I and J
6	All Bentomat GCLs	A, G, H and I
7	All Bentofix GCLs	C, D and E
8	W-NW Needle-Punched, Not Thermally Bonded GCLs	A, G, I
9	W-NW Needle-Punched, Thermally Bonded GCLs	C, D and E
10	NW-NW Needle-Punched, Not Thermally Bonded GCLs	H
11	NW-NW Needle-Punched, Thermally Bonded GCLs	D and E
12	GCL A	A

Table 4.3 Results of Direct Shear Tests on GCLs A and F (Fox *et. al.*, 1998)

GCL Name	Hydration Time (hrs)	Normal Stress (kPa)	Peak Shear Strength (kPa)	Large Displacement Shear Strength (kPa)	Shear Displacement Rate (mm/min)	Final GCL Water Content, (%)
GCL A	96	37.8	122.7	5.0	0.1	198
GCL A	96	72.2	160.3	9.0	0.1	158
GCL A	96	141.0	184.8	13.8	0.1	138
GCL A	96	279.0	276.8	22.0	0.1	101
GCL A	96	17.1	62.4	3.8	0.1	228
GCL A	96	37.8	75.8	5.6	0.1	191
GCL A	96	72.2	114.5	9.3	0.1	137
GCL A	96	141.0	169.3	#N/A	0.1	121
GCL A	96	37.8	93.3	5.8	0.1	181
GCL A	96	37.8	88.2	5.2	0.1	184
GCL A	96	72.2	139.3	9.6	0.01	162
GCL A	96	72.2	147.9	9.5	1	160
GCL A	96	72.2	156.1	9.7	10	161
GCL F	96	6.9	3.6	1.7	0.1	273
GCL F	96	24.0	8.5	3.8	0.1	194
GCL F	96	37.8	12.0	5.0	0.1	189
GCL F	96	72.2	18.3	7.3	0.1	148
GCL F	96	141.0	28.7	13.3	0.1	149
GCL F	96	279.0	52.7	22.2	0.1	105

Note: GCL A tested in this study had an average Peel Strength of 160 N/mm

Table 4.4: Results of Ring Shear Tests on GCL A (Eid and Stark, 1999)

Normal Stress (kPa)	Peak Shear Strength (kPa)	Large Displacement Shear Strength (kPa)	Shear Displacement Rate (mm/min)
17.0	28.0	4.0	0.015
100.0	37.0	20.0	0.015
200.0	55.0	28.0	0.015
400.0	71.0	46.0	0.015

Note: GCL A tested in this study had an average Peel Strength of 27 N/mm

Table 4.5: Results of Direct Shear Tests on a Needle-Punched GCL (Berard, 1997)

Normal Stress (kPa)	Peak Shear Strength (kPa)	Shear Displacement Rate (mm/min)	Final GCL Water Content (%)
25.0	26.3	0.01	109
25.0	29.5	0.1	102
25.0	35.3	1	86
50.0	41.2	0.01	95
50.0	44.7	0.1	90
50.0	59.3	1	81
100.0	66.8	0.01	83
100.0	81.2	0.1	78
100.0	101.8	1	75

Note: GCL A tested in this study had an average Peel Strength of71 N/100mm

Table 4.6: Results of Direct Shear Tests on a Needle-Punched GCL (GCL A) Reported by Gilbert *et. al.* (1996)

Test Number	Normal Stress Corrected for Area Change During Shear (kPa)	Hydration Time (hrs)	Peak Shear Strength (kPa)	Large Displacement Shear Strength (kPa)	Shear Displacement Rate (mm/min)	Final GCL Water Content (%)
1 - Peak	3.52	24.7	3.9	#N/A	0.072	360
2 - Peak	7.20	21.7	7.7	#N/A	0.059	413
3 - Peak	14.30	14	12.3	#N/A	0.059	236
4 - Peak	28.20	12.6	14.2	#N/A	0.072	302
1 - Large Displacement	3.81	24.7	#N/A	1.9	0.072	360
2 - Large Displacement	7.66	21.7	#N/A	5.2	0.059	413
3 - Large Displacement	15.30	14	#N/A	6.2	0.059	236
4 - Large Displacement	30.10	12.6	#N/A	7.8	0.072	302

Note: Average peel strength of GCL A specimens tested was not reported

Table 4.7: Equivalent Friction Angles for Different GCL Sets with Standard Deviation, Upper Bound and Lower Bound

GCL Set Number	GCL Set Description	Peak				Large Displacement			
		Equivalent Friction Angle (Degrees)	Standard Deviation Equivalent Friction Angle (Degrees)	Upper Bound Equivalent Friction Angle (Degrees)	Lower Bound Equivalent Friction Angle (Degrees)	Equivalent Friction Angle (Degrees)	Standard Deviation Equivalent Friction Angle (Degrees)	Upper Bound Equivalent Friction Angle (Degrees)	Lower Bound Equivalent Friction Angle (Degrees)
1	All GCLs	30.4	19.9	50.4	10.5	12.7	5.1	17.8	7.7
2	All Reinforced GCLs	31.2	19.8	51.0	11.4	13.0	5.1	18.2	7.9
3	All Unreinforced GCLs	6.6	3.1	9.7	3.5	5.9	2.5	8.4	3.4
4	Stitch-Bonded GCLs	12.2	34.6	46.8	0.0	6.7	0.4	7.1	6.3
5	All Needle-Punched GCLs	32.9	18.4	51.3	14.5	13.2	5.2	18.4	8.1
6	All Bentomat® GCLs	33.7	19.4	53.2	14.3	13.5	3.2	16.8	10.3
7	All Bentofix® GCLs	29.5	11.8	41.2	17.7	12.0	8.8	20.8	3.2
8	W-NW Needle-Punched, Not Thermally Bonded GCLs	33.5	19.3	52.8	14.2	13.7	3.5	17.2	10.2
9	W-NW Needle-Punched, Thermally Bonded GCLs	28.9	9.8	38.7	19.1	12.9	9.2	22.1	3.6
10	NW-NW Needle-Punched, Not Thermally Bonded GCLs	37.1	20.0	57.1	17.1	10.8	2.5	13.3	8.3
11	NW-NW Needle-Punched, Thermally Bonded GCLs	30.3	13.9	44.1	16.4	10.7	8.1	18.8	2.5
12	GCL A	33.5	17.7	51.2	15.8	13.7	3.5	17.2	10.2

Note: Equivalent friction angles defined for the normal stress range 0-550 kPa for each GCL set

Table 4.8: Effects of Test Conditions on the Shear Strength of GCL A

Test Condition Examined	Selected Test Conditions	Peak Equivalent Friction Angle (Degrees)	Large Displacement Equivalent Friction Angle (Degrees)
Hydration Time[#]	t_H = 0 hours	38.1	24.2
	t_H = 24 hours	30.8	11.7
	t_H = 48 hours	27.1	7.5
Hydration Normal Stress*	Hydration Normal Stress < Normal Stress Used During Shearing	32.5	11.0
	Hydration Normal Stress = Normal Stress Used During Shearing	30.3	10.5
Consolidation Time*	t_C = 0 hours	30.0	9.6
	t_C = 48 hours	33.5	8.3
Shear Displacement Rate	SDR = 0.0015 mm/min	32.1	10.7
	SDR = 0.1 mm/min	33.8	12.1
	SDR = 0.5 mm/min	30.9	11.5
	SDR = 1.0 mm/min	33.5	16.3

[#]Consolidated tests are not included in the calculation of the equivalent friction angles
*Unhydrated tests are not included in the calculation of the equivalent friction angles

Table 4.9: Failure Envelopes for All GCLs in the GCLSS Database

Failure Envelope Number	Failure Envelope Name	Shear Displacement Rate (mm/min)	t_H (hours)	t_C (hours)	Comments
1	A1a	1.0	24	0	Baseline for GCL A
2	A1b	1.0	24	0	Constant Low Hydration Normal Stress
3	A2	0.5	24	0	Decrease in Shear Displacement Rate
4	A3a	1.0	48	0	Increase in Time of Hydration
5	A3a Low	1.0	48	0	Bilinear Failure Envelope
6	A3a High	1.0	48	0	
7	A3b	1.0	48	0	Constant Low Hydration Normal Stress
8	A4	1.0	72	0	Increase in Time of Hydration
9	A5	0.1	168	48	Increase in Time of Hydration and Time of Consolidation; Decrease in Shear Displacement Rate
10	A6*	0.0015	#N/A	#N/A	Staged Hydration Procedure, Decrease in Shear Displacement Rate
11	A7a	1.0	24	12	Increase in Time of Consolidation
12	A7b	1.0	60	24	Increase in Time of Hydration and Time of Consolidation
13	A8	1.0	0	0	Decrease in Time of Hydration
14	B1	1.0	24	0	Baseline for GCL B
15	B2	1.0	48	0	Increase in Time of Hydration
16	B3	1.0	96	0	Increase in Time of Hydration
17	B4	0.1	168	48	Increase in Time of Hydration and Time of Consolidation; Decrease in Shear Displacement Rate
18	C1	0.5	24	0	Baseline for GCL C
19	C1 Low	0.5	24	0	Bilinear Failure Envelope
20	C1 High	0.5	24	0	
21	C2	0.2	24	0	Decrease in Shear Displacement Rate
22	C3	0.1	168	48	Increase in Time of Hydration and Time of Consolidation; Decrease in Shear Displacement Rate
23	D1	1.0	72	0	Different Times of Hydration and Shear Displacement Rates
24	D2	0.5	24	0	
25	D3	0.1	24	24	
26	D3 Low	0.1	24	24	Bilinear Failure Envelope
27	D3 High	0.1	24	24	
28	E1	1.0	336	0	Different Times of Hydration
29	E2	1.0	48	0	
30	F1	1.0	168	0	Hydrated
31	F2	1.0	0	0	Unhydrated
32	G	1.0	24	0	Hydrated
33	H1	1.0	24	0	Different Times of Hydration and Times of Consolidation
34	H2	1.0	24	24	
35	H3	0.25	96	24	
36	I1	1.0	0	0	Unhydrated
37	I2	1.0	72	0	Hydrated
38	J	1.0	24	0	Hydrated

Table 4.10: Failure Envelope for GCL A (FE A1: t_H = 24 hrs, t_C = 0 hrs and SDR = 1.0 mm/min); *Baseline Failure Envelope*

Failure Envelope Name	Normal Stress (kPa)	Peak Shear Strength (kPa)	Mean Peak Shear Strength (kPa)	Standard Deviation of Peak Shear Strength (kPa)	Large Displacement Shear Strength (kPa)	Mean Large Displacement Shear Strength (kPa)	Standard Deviation of Large Displacement Shear Strength (kPa)	τ_{LD}/τ_p	Hydration Normal Stress (kPa)	Final Water Content (%)
FE A1a	3.4	13.8	13.8	0.0	#N/A	#N/A	#N/A	#N/A	3.4	158.3
FE A1a	4.8	12.8			3.1			0.24	4.8	156.4
FE A1a	4.8	19.9			#N/A			#N/A	4.8	120.0
FE A1a	4.8	17.9	17.8	2.7	#N/A	3.1	0.0	#N/A	4.8	127.0
FE A1a	4.8	18.7			#N/A			#N/A	4.8	122.0
FE A1a	4.8	17.2			#N/A			#N/A	4.8	122.0
FE A1a	4.8	20.4			#N/A			#N/A	4.8	127.5
FE A1a	6.9	16.5	16.5	0.0	#N/A	#N/A	#N/A	#N/A	6.9	163.5
FE A1a	9.6	23.8			#N/A			#N/A	9.6	120.0
FE A1a	9.6	24.8			#N/A			#N/A	9.6	127.0
FE A1a	9.6	25.2	25.1	1.1	#N/A	#N/A	#N/A	#N/A	9.6	122.0
FE A1a	9.6	24.7			#N/A			#N/A	9.6	122.0
FE A1a	9.6	26.9			#N/A			#N/A	9.6	127.5
FE A1a	19.2	30.1			#N/A			#N/A	19.2	120.0
FE A1a	19.2	34.1			#N/A			#N/A	19.2	127.0
FE A1a	19.2	36.5	33.9	2.4	#N/A	#N/A	#N/A	#N/A	19.2	122.0
FE A1a	19.2	33.3			#N/A			#N/A	19.2	122.0
FE A1a	19.2	35.3			#N/A			#N/A	19.2	127.5
FE A1a	34.5	36.9	36.9	0.0	#N/A	#N/A	#N/A	#N/A	34.5	175.3
FE A1a	47.9	69.7			7.7			0.11	47.9	70.8
FE A1a	47.9	67.1	68.1	1.4	9.9	9.3	1.4	0.15	47.9	69.1
FE A1a	47.9	67.6			10.4			0.15	47.9	71.8
FE A1a	59.9	81.3			9.8			0.12	59.9	70.8
FE A1a	59.9	74.3	78.0	3.5	10.8	10.8	1.0	0.14	59.9	69.1
FE A1a	59.9	78.3			11.7			0.15	59.9	71.8
FE A1a	71.8	88.5			11.0			0.12	71.8	70.8
FE A1a	71.8	85.3	85.8	2.4	14.6	13.4	2.1	0.17	71.8	69.1
FE A1a	71.8	83.7			14.6			0.17	71.8	71.8
FE A1b	14.4	21.5	21.5	0.0	4.3	4.3	0.0	0.20	4.8	182.8
FE A1b	23.9	28.7	28.7	0.0	4.9	4.9	0.0	0.17	4.8	186.1

Table 4.11: Failure Envelope for GCL A (FE A2: t_H = 24 hrs, t_C = 0 hrs and SDR = 0.5 mm/min)

Failure Envelope Name	Normal Stress (kPa)	Peak Shear Strength (kPa)	Mean Peak Shear Strength (kPa)	Standard Deviation of Peak Shear Strength (kPa)	Large Displacement Shear Strength (kPa)	Mean Large Displacement Shear Strength (kPa)	Standard Deviation Large Displacement Shear Strength (kPa)	τ_{LD}/τ_p	Hydration Normal Stress (kPa)	Final Water Content (%)
FE A2	48.3	62.7	62.6	2.1	22.8	19.8	2.7	0.36	48.3	86.0
FE A2	48.3	65.5			21.4			0.33	48.3	95.0
FE A2	48.3	60.7			17.2			0.28	48.3	87.0
FE A2	48.3	61.4			17.9			0.29	48.3	90.5
FE A2	213.7	155.8	145.3	12.4	45.5	42.2	3.8	0.29	213.7	86.0
FE A2	213.7	153.1			37.2			0.24	213.7	95.0
FE A2	213.7	144.1			44.8			0.31	213.7	87.0
FE A2	213.7	128.2			41.4			0.32	213.7	90.5
FE A2	386.1	237.2	217.4	14.2	74.5	78.1	4.6	0.31	386.1	87.0
FE A2	386.1	205.5			74.5			0.36	386.1	90.5
FE A2	386.1	208.9			79.3			0.38	386.1	86.0
FE A2	386.1	217.9			84.1			0.39	386.1	95.0

Table 4.12: Failure Envelope for GCL A (FE A3: t_H = 48 hrs, t_C = 0 hrs and SDR = 1.0 mm/min)

Failure Envelope Name	Normal Stress (kPa)	Peak Shear Strength (kPa)	Mean Peak Shear Strength (kPa)	Standard Deviation of Peak Shear Strength (kPa)	Large Displacement Shear Strength (kPa)	Mean Large Displacement Shear Strength (kPa)	Standard Deviation of Large Displacement Shear Strength (kPa)	τ_{LD}/τ_p	Hydration Normal Stress (kPa)	Final Water Content (%)
FE A3a	2.4	15.8	15.8	0.0	#N/A	#N/A	#N/A	#N/A	2.4	143.0
FE A3a	3.6	12.6	12.6	0.0	#N/A	#N/A	#N/A	#N/A	3.6	156.0
FE A3a	4.8	14.6	14.1	0.7	#N/A	#N/A	#N/A	#N/A	4.8	58.6
FE A3a	4.8	13.6			#N/A			#N/A	4.8	156.0
FE A3a	7.2	15.2	15.2	0.0	#N/A	#N/A	#N/A	#N/A	7.2	156.0
FE A3a	9.6	25.6	30.5	6.1	#N/A	#N/A	#N/A	#N/A	9.6	129.1
FE A3a	9.6	31.6			#N/A			#N/A	9.6	129.1
FE A3a	9.6	27.6			#N/A			#N/A	9.6	129.0
FE A3a	9.6	27.2			#N/A			#N/A	9.6	129.0
FE A3a	9.6	31.7			#N/A			#N/A	9.6	129.0
FE A3a	9.6	26.9			#N/A			#N/A	9.6	129.1
FE A3a	9.6	34.6			#N/A			#N/A	9.6	110.5
FE A3a	9.6	27.6			#N/A			#N/A	9.6	129.1
FE A3a	9.6	30.8			#N/A			#N/A	9.6	103.7
FE A3a	9.6	30.9			#N/A			#N/A	9.6	103.7
FE A3a	9.6	32.9			#N/A			#N/A	9.6	103.7
FE A3a	9.6	29.7			#N/A			#N/A	9.6	103.7
FE A3a	9.6	34.9			#N/A			#N/A	9.6	110.5
FE A3a	9.6	26.8			#N/A			#N/A	9.6	103.7
FE A3a	9.6	20.3			#N/A			#N/A	9.6	58.6
FE A3a	9.6	20.2			#N/A			#N/A	9.6	143.0
FE A3a	9.6	41.3			#N/A			#N/A	9.6	110.5
FE A3a	9.6	44.9			#N/A			#N/A	9.6	110.5
FE A3a	9.6	34.6			#N/A			#N/A	9.6	110.5
FE A3a	13.8	29.6	29.6	0.0	#N/A	#N/A	#N/A	#N/A	13.8	109.4
FE A3a	14.4	23.5	23.5	0.0	#N/A	#N/A	#N/A	#N/A	14.4	58.6
FE A3a	23.9	30.4	30.4	0.0	#N/A	#N/A	#N/A	#N/A	23.9	143.0
FE A3a	27.6	39.3	39.3	0.0	#N/A	#N/A	#N/A	#N/A	27.6	109.35
FE A3a	41.4	48.3	48.3	0.0	#N/A	#N/A	#N/A	#N/A	41.4	109.4
FE A3a	68.9	57.2	57.2	0.0	13.8	13.8	0.0	0.24	68.9	87.7
FE A3a	95.8	83.3	83.3	0.0	33.8	33.8	0.0	0.41	95.8	124.8
FE A3a	206.8	117.2	117.2	0.0	35.9	35.9	0.0	0.31	206.8	87.7
FE A3a	344.7	185.5	166.5	26.8	55.2	46.2	12.7	0.30	344.7	87.7
FE A3a	344.7	147.5			37.2			0.25	344.7	89.1
FE A3a	478.8	230.8	230.8	0.0	82.4	82.4	0.0	0.36	478.8	111.3
FE A3a	689.5	246.8	246.8	0.0	77.9	77.9	0.0	0.32	689.5	88.3
FE A3a	981.5	471.4	471.4	0.0	136.0	136.0	0.0	0.29	981.5	103.5
FE A3a	1034.2	333.7	333.0	1.0	144.8	140.7	5.9	0.43	1034.2	77.1
FE A3a	1034.2	332.3			136.5			0.41	1034.2	82.4
FE A3a	1723.7	477.8	477.8	0.0	217.2	217.2	0.0	0.45	1723.7	68.2
FE A3a	2760.0	668.1	668.1	0.0	306.1	306.1	0.0	0.46	2757.9	57.5
FE A3b	13.8	35.9	35.9	0.0	2.8	2.8	0.0	0.08	4.8	110.5
FE A3b	48.3	66.9	66.9	0.0	6.2	6.2	0.0	0.09	4.8	110.5
FE A3b	89.6	34.5	34.5	0.0	12.4	12.4	0.0	0.36	4.8	134.1
FE A3b	103.4	100.7	100.7	0.0	10.3	10.3	0.0	0.10	4.8	110.5
FE A3b	172.4	138.6	138.6	0.0	14.5	14.5	0.0	0.10	4.8	110.5
FE A3b	186.2	46.2	46.2	0.0	13.1	13.1	0.0	0.28	4.8	139.3
FE A3b	275.8	66.9	128.2	86.8	13.8	18.6	6.8	0.21	4.8	134.8
FE A3b	275.8	189.6			23.4			0.12	4.8	110.5

Table 4.13: Failure Envelope for GCL A (FE A4: t_H = 72 hrs, t_C = 0 hrs and SDR = 1.0 mm/min)

Failure Envelope Name	Normal Stress (kPa)	Peak Shear Strength (kPa)	Large Displacement Shear Strength (kPa)	τ_{LD}/τ_p	Hydration Normal Stress (kPa)	Final Water Content (%)
FE A4	2.4	16.3	#N/A	#N/A	2.4	169.3
FE A4	6.9	15.2	4.1	0.27	6.9	109.4
FE A4	7.2	24.9	#N/A	#N/A	2.4	160.0
FE A4	14.4	36.6	#N/A	#N/A	2.4	153.2
FE A4	20.7	21.4	4.1	0.19	6.9	103.8
FE A4	23.9	52.0	#N/A	#N/A	2.4	148.1
FE A4	41.4	35.2	11.0	0.31	6.9	101.0
FE A4	103.4	90.3	17.9	0.20	6.9	100.4

Table 4.14: Failure Envelope for GCL A (FE A5: t_H = 168 hrs, t_C = 48 hrs and SDR = 0.1 mm/min)

Failure Envelope Name (With Series Number)	Normal Stress (kPa)	Peak Shear Strength (kPa)	Large Displacement Shear Strength (kPa)	τ_p/σ	τ_{LD}/σ	τ_{LD}/τ_p	Hydration Normal Stress (kPa)	Consolidation Normal Stress (kPa)	Final Water Content (%)
A5 1	34.5	37.9	13.8	1.1	0.4	0.4	20.7	34.5	78.0
	137.9	75.8	24.8	0.6	0.2	0.3	20.7	137.9	78.0
	310.3	169.6	43.4	0.5	0.1	0.3	20.7	310.3	78.0
A5 2	34.5	46.9	18.6	1.4	0.5	0.4	20.7	34.5	78.5
	137.9	107.6	37.2	0.8	0.3	0.3	20.7	137.9	78.5
	310.3	204.8	63.4	0.7	0.2	0.3	20.7	310.3	78.5
A5 3	34.5	42.1	17.9	1.2	0.5	0.4	20.7	34.5	74.0
	137.9	96.5	32.4	0.7	0.2	0.3	20.7	137.9	74.0
	310.3	177.9	65.5	0.6	0.2	0.4	20.7	310.3	74.0
A5 4	34.5	50.3	33.8	1.5	1.0	0.7	20.7	34.5	81.5
	137.9	135.1	47.6	1.0	0.3	0.4	20.7	137.9	81.5
	310.3	217.9	72.4	0.7	0.2	0.3	20.7	310.3	81.5
A5 5	34.5	41.4	31.7	1.2	0.9	0.8	20.7	34.5	73.5
	137.9	113.8	55.8	0.8	0.4	0.5	20.7	137.9	73.5
	310.3	233.0	89.6	0.8	0.3	0.4	20.7	310.3	73.5
A5 6	34.5	46.2	24.1	1.3	0.7	0.5	20.7	34.5	78.0
	137.9	113.8	51.7	0.8	0.4	0.5	20.7	137.9	78.0
	310.3	213.7	86.2	0.7	0.3	0.4	20.7	310.3	78.0
A5 7	34.5	46.2	18.6	1.3	0.5	0.4	20.7	34.5	72.5
	137.9	109.6	37.9	0.8	0.3	0.3	20.7	137.9	72.5
	310.3	199.9	62.7	0.6	0.2	0.3	20.7	310.3	72.5
A5 8	34.5	49.6	14.5	1.4	0.4	0.3	20.7	34.5	72.0
	137.9	126.2	43.4	0.9	0.3	0.3	20.7	137.9	72.0
	310.3	231.0	75.2	0.7	0.2	0.3	20.7	310.3	72.0
A5 9	34.5	46.2	38.6	1.3	1.1	0.8	20.7	34.5	75.5
	137.9	89.6	49.0	0.7	0.4	0.5	20.7	137.9	75.5
	310.3	175.1	62.7	0.6	0.2	0.4	20.7	310.3	75.5
A5 10	34.5	39.3	17.2	1.1	0.5	0.4	20.7	34.5	75.5
	137.9	94.5	39.3	0.7	0.3	0.4	20.7	137.9	75.5
	310.3	194.4	75.8	0.6	0.2	0.4	20.7	310.3	75.5
A5 11	34.5	46.2	15.9	1.3	0.5	0.3	20.7	34.5	71.0
	137.9	111.0	29.6	0.8	0.2	0.3	20.7	137.9	71.0
	310.3	202.0	64.8	0.7	0.2	0.3	20.7	310.3	71.0
A5 12	34.5	55.2	#N/A	1.6	#N/A	#N/A	20.7	34.5	91.9
	137.9	137.2	#N/A	1.0	#N/A	#N/A	20.7	137.9	65.6
	310.3	241.3	#N/A	0.8	#N/A	#N/A	20.7	310.3	58.7
A5 13	34.5	49.0	8.3	1.4	0.2	0.2	20.7	34.5	107.8
	137.9	91.0	13.8	0.7	0.1	0.2	20.7	137.9	94.5
	310.3	156.5	39.3	0.5	0.1	0.3	20.7	310.3	59.0
A5 14	34.5	44.1	15.2	1.3	0.4	0.3	20.7	34.5	73.0
	137.9	108.9	30.3	0.8	0.2	0.3	20.7	137.9	73.0
	310.3	157.2	42.1	0.5	0.1	0.3	20.7	310.3	73.0
A5 15	34.5	53.1	31.0	1.5	0.9	0.6	20.7	34.5	71.5
	137.9	135.8	44.8	1.0	0.3	0.3	20.7	137.9	71.5
	310.3	204.1	68.9	0.7	0.2	0.3	20.7	310.3	71.5
A5 16	34.5	43.4	11.7	1.3	0.3	0.3	20.7	34.5	76.0
	137.9	113.8	29.0	0.8	0.2	0.3	20.7	137.9	76.0
	310.3	222.0	60.0	0.7	0.2	0.3	20.7	310.3	76.0
A5 17	34.5	58.6	32.4	1.7	0.9	0.6	20.7	34.5	79.0
	137.9	117.9	44.8	0.9	0.3	0.4	20.7	137.9	79.0
	310.3	195.8	65.5	0.6	0.2	0.3	20.7	310.3	79.0
A5 18	34.5	51.7	9.7	1.5	0.3	0.2	20.7	34.5	88.5
	137.9	104.8	29.0	0.8	0.2	0.3	20.7	137.9	88.5
	310.3	183.4	46.9	0.6	0.2	0.3	20.7	310.3	88.5
A5 19	34.5	44.1	21.4	1.3	0.6	0.5	20.7	34.5	72.5
	137.9	113.8	40.7	0.8	0.3	0.4	20.7	137.9	72.5
	310.3	216.5	75.8	0.7	0.2	0.4	20.7	310.3	72.5

Table 4.15: Failure Envelope for GCL A (FE A6: Staged Hydration and Consolidation, SDR = 0.0015 mm/min)

Failure Envelope Name	Normal Stress (kPa)	Peak Shear Strength (kPa)	Large Displacement Shear Strength (kPa)	τ_{LD}/τ_p	Initial Hydration Normal Stress (kPa)	Final Water Content (%)
FE A6	250	162.5	63.2	0.39	8.00	66.5
FE A6	520	301.7	83.8	0.28	62.50	66.5
FE A6	1000	468.6	138.4	0.30	8.00	66.5

Note: As these GCLs were hydrated/consolidated in a staged procedure, the hydration normal stress was increased slowly while the GCL was submerged. The hydration normal stress reported here is that for the initial hydration step

Table 4.16: Failure Envelopes for GCL A (FE A7a and A7b: t_H = 24 and 60 hrs, respectively, t_C = 12 and 24 hrs, respectively, and SDR = 1.0 mm/min)

Failure Envelope Name	Normal Stress (kPa)	Peak Shear Strength (kPa)	Large Displacement Shear Strength (kPa)	τ_{LD}/τ_p	Shear Displacement Rate (mm/min)	Hydration Time (hrs)	Hydration Normal Stress (kPa)	Consolidation Time (hrs)	Consolidation Normal Stress (kPa)	Final Water Content (%)
FE A7a	137.9	98.6	20.7	0.21	1.000	24	68.9	12	137.9	163.5
FE A7a	275.8	148.9	71.7	0.48	1.000	24	68.9	12	275.8	163.5
FE A7a	551.6	270.3	107.6	0.40	1.000	24	68.9	12	551.6	163.5
Not Included	344.7	220.6	84.8	0.38	0.025	24	6.9	48	344.7	85.3
FE A7b	4.8	17.1	#N/A	#N/A	1.000	60	6.9	24	4.8	88.45
FE A7b	14.4	31.2	#N/A	#N/A	1.000	60	6.9	24	14.4	88.45
FE A7b	28.7	46.1	#N/A	#N/A	1.000	60	6.9	24	28.7	88.45

Table 4.17: Failure Envelope for GCL A (FE A8: t_H = 0 hrs (Dry), t_C = 0 hrs and SDR = 1.0 mm/min)

Failure Envelope Name	Normal Stress (kPa)	Peak Shear Strength (kPa)	Final Water Content (%)
FE A8	2.4	20.1	16.5
FE A8	3.4	15.4	10.3
FE A8	6.9	19.2	10.7
FE A8	7.2	31.1	16.3
FE A8	14.4	38.3	16.8
FE A8	23.9	54.3	16.5
FE A8	34.5	40.2	10.9

Table 4.18: Failure Envelope for GCL B (FE B1: t_H = 24 hrs, t_C = 0 hrs and SDR = 1.0 mm/min); *Baseline Failure Envelope*

Failure Envelope	Normal Stress (kPa)	Peak Shear Strength (kPa)	Large Displacement Shear Strength (kPa)	τ_{LD}/τ_p	Hydration Normal Stress (kPa)	Final Water Content (%)
FE B1	23.9	71.1	#N/A	#N/A	12.0	141.1
FE B1	47.9	71.6	#N/A	#N/A	12.0	140.0
FE B1	137.9	43.4	21.4	0.49	137.9	151.4
FE B1	275.8	90.3	40.0	0.44	275.8	138.2
FE B1	413.7	91.7	42.1	0.46	413.7	120.9
FE B1	551.6	131.7	57.9	0.44	551.6	108.2
FE B1	689.5	147.5	67.6	0.46	689.5	100.1

Table 4.19: Failure Envelope for GCL B (FE B2: t_H = 48 hrs, t_C = 0 hrs and SDR = 1.0 mm/min)

Failure Envelope Name	Normal Stress (kPa)	Peak Shear Strength (kPa)	Mean Peak Shear Strength (kPa)	Standard Deviation of Peak Shear Strength (kPa)	Hydration Normal Stress (kPa)	Final Water Content (%)
FE B2	2.4	18.7	21.8	2.7	4.8	144.0
FE B2	2.4	23.8			4.8	143.8
FE B2	2.4	23.0			4.8	177.6
FE B2	4.8	24.2	24.6	0.6	4.8	190.1
FE B2	4.8	25.0			4.8	186.5
FE B2	9.6	27.8	26.4	3.3	9.6	185.0
FE B2	9.6	28.0			9.6	185.6
FE B2	9.6	27.6			9.6	143.3
FE B2	9.6	28.1			4.8	140.2
FE B2	9.6	20.6			4.8	156.9
FE B2	14.4	31.3	31.4	0.2	14.4	168.1
FE B2	14.4	31.6			14.4	176.9
FE B2	19.2	27.7	25.4	2.6	4.8	142.7
FE B2	19.2	22.6			4.8	142.1
FE B2	19.2	25.9			4.8	160.6
FE B2	33.5	18.8	26.3	7.2	4.8	143.1
FE B2	33.5	33.1			4.8	141.3
FE B2	33.5	27.1			4.8	171.5
FE B2	47.9	20.7	26.3	4.9	4.8	143.0
FE B2	47.9	28.4			4.8	143.3
FE B2	47.9	29.7			4.8	154.7
FE B2	95.8	28.7	28.7	0.0	4.8	176.6
FE B2	143.6	34.2	34.2	0.0	4.8	178.7
FE B2	478.8	62.2	62.2	0.0	4.8	187.9
FE B2	981.5	100.5	100.5	0.0	4.8	170.9

Table 4.20: Failure Envelope for GCL B (FE B3: t_H = 96 hrs, t_C = 0 hrs and SDR = 1.0 mm/min)

Failure Envelope Name	Normal Stress (kPa)	Peak Shear Strength (kPa)	Mean Peak Shear Strength (kPa)	Standard Deviation of Peak Shear Strength (kPa)	Hydration Normal Stress (kPa)	Final Water Content (%)
FE B3	9.6	19.6	23.5	5.5	7.2	255.8
FE B3	9.6	27.4			7.2	238.5
FE B3	19.2	23.3	25.6	3.3	7.2	214.2
FE B3	19.2	27.9			7.2	229.4
FE B3	68.9	27.2	30.6	4.9	7.2	203.2
FE B3	68.9	34.1			7.2	252.9
FE B3	344.7	47.8	52.4	6.5	7.2	237.5
FE B3	344.7	57.0			7.2	242.5
FE B3	999.7	96.2	103.4	10.2	7.2	267.5
FE B3	999.7	110.6			7.2	213.8

Note: The large displacement shear strength was reported to be the same as the peak shear strength for all levels of normal stress

Table 4.21: Failure Envelope for GCL B (FE B4: t_H = 168 hrs, t_C = 48 hrs and SDR = 0.1 mm/min)

Failure Envelope Name	Normal Stress (kPa)	Peak Shear Strength (kPa)	Hydration Normal Stress (kPa)	Consolidation Normal Stress (kPa)	Final Water Content (%)
FE B4	34.5	35.9	20.7	34.5	109.6
FE B4	137.9	51.7	20.7	137.9	98.2
FE B4	310.3	71.7	20.7	310.3	61.4

Table 4.22: Failure Envelope for GCL C (FE C1: t_H = 24 hrs, t_C = 0 hrs and SDR = 0.5 mm/min); *Baseline Failure Envelope*

Failure Envelope Name	Normal Stress (kPa)	Peak Shear Strength (kPa)	Mean Peak Shear Strength (kPa)	Standard Deviation of Peak Shear Strength (kPa)	Large Displacement Shear Strength (kPa)	Mean Large Displacement Shear Strength (kPa)	Standard Deviation of Large Displacement Shear Strength (kPa)	τ_{LD}/τ_p	Hydration Normal Stress (kPa)	Final Water Content (%)
FE C1	7.2	13.9	13.9	0.0	7.8	7.8	0.0	0.56	7.2	107.0
FE C1	14.4	19.5	19.5	0.0	10.2	10.2	0.0	0.52	14.4	107.0
FE C1	21.5	26.6	26.6	0.0	11.8	11.8	0.0	0.45	21.5	107.0
FE C1	48.3	60.0	56.2	5.4	25.5	31.7	8.8	0.43	48.3	80.0
FE C1	48.3	52.4			37.9			0.72	48.3	83.5
FE C1	95.8	57.4	104.2	0.0	27.6	43.5	0.0	0.48	95.8	112.5
FE C1	191.5	104.2	127.6	8.8	43.5	49.6	10.7	0.42	191.5	112.5
FE C1	213.7	121.3	127.6	8.8	42.1	49.6	10.7	0.35	213.7	80.0
FE C1	213.7	133.8			57.2			0.43	213.7	83.5
FE C1	383.0	187.8	263.0	0.0	119.8	119.8	0.0	0.64	383.0	112.5
FE C1	386.1	183.4	199.3	22.4	57.2	72.1	21.0	0.31	386.1	80.0
FE C1	386.1	215.1			86.9			0.40	386.1	83.5
FE C1	574.6	263.0	263.0	0.0	119.8	119.8	0.0	0.46	574.6	112.5

Table 4.23: Failure Envelope for GCL C (FE C2: t_H = 24 hrs, t_C = 0 hrs and SDR = 0.2 mm/min)

Failure Envelope Name	Normal Stress (kPa)	Peak Shear Strength (kPa)	Mean Peak Shear Strength (kPa)	Standard Deviation of Peak Shear Strength (kPa)	Large Displacement Shear Strength (kPa)	Mean Large Displacement Shear Strength (kPa)	Standard Deviation of Large Displacement Shear Strength (kPa)	τ_{LD}/τ_p	Hydration Normal Stress (kPa)	Final Water Content (%)
FE C2	9.7	20.7	21.7	1.5	10.3	10.7	0.5	0.50	55.2	75.0
FE C2	9.7	22.8			11.0			0.48	55.2	75.0
FE C2	48.3	53.8	56.5	3.9	20.0	20.7	1.0	0.37	55.2	75.0
FE C2	48.3	59.3			21.4			0.36	55.2	75.0
FE C2	117.2	87.6	86.2	2.0	26.2	30.0	5.4	0.30	55.2	75.0
FE C2	117.2	84.8			33.8			0.40	55.2	75.0
FE C2	193.1	132.4	131.0	2.0	48.3	46.5	2.4	0.36	55.2	75.0
FE C2	193.1	129.6			44.8			0.35	55.2	75.0
FE C2	289.6	182.0	183.7	2.4	75.8	72.1	5.4	0.42	55.2	75.0
FE C2	289.6	185.5			68.3			0.37	55.2	75.0

Table 4.24: Failure Envelope for GCL C (FE C3: t_H = 168 hrs, t_C = 48 hrs and SDR = 0.1 mm/min)

Failure Envelope Name	Normal Stress (kPa)	Peak Shear Strength (kPa)	Large Displacement Shear Strength (kPa)	τ_{LD}/τ_p	Hydration Normal Stress (kPa)	Consolidation Normal Stress (kPa)	Final Water Content (%)
FE C3	34.5	32.4	8.3	0.26	20.7	34.5	84.4
FE C3	137.9	63.4	17.2	0.27	20.7	137.9	77.8
FE C3	310.3	114.5	47.6	0.42	20.7	310.3	64.0

Table 4.25: Failure Envelopes for GCL D (FE D1, D2 and D3)

Failure Envelope Name	Normal Stress (kPa)	Peak Shear Strength (kPa)	Large Displacement Shear Strength (kPa)	τ_{LD}/τ_p	t_H (hrs)	t_C (hrs)	Shear Displacement Rate (mm/min)	Hydration Normal Stress (kPa)	Consolidation Normal Stress (kPa)	Final Water Content (%)
FE D1	6.9	11.0	6.2	0.56	72	0	1.0	6.9	0.0	109.5
FE D1	137.9	55.2	20.7	0.38	72	0	1.0	6.9	0.0	109.5
FE D1	275.8	91.0	35.9	0.39	72	0	1.0	6.9	0.0	109.5
FE D1	413.7	144.8	57.2	0.40	72	0	1.0	6.9	0.0	109.5
FE D1	551.6	188.9	80.0	0.42	72	0	1.0	6.9	0.0	109.5
FE D1	689.5	243.4	108.2	0.44	72	0	1.0	6.9	0.0	109.5
FE D2	48.3	97.9	31.7	0.32	24	0	0.5	48.3	0.0	83.5
FE D2	213.7	175.8	53.1	0.30	24	0	0.5	213.7	0.0	83.5
FE D2	386.1	256.5	88.9	0.35	24	0	0.5	386.1	0.0	83.5
FE D3	6.9	26.9	#N/A	#N/A	24	24	1.0	3.4	6.9	86.0
FE D3	13.8	35.2	#N/A	#N/A	24	24	1.0	3.4	13.8	86.0
FE D3	27.6	44.1	#N/A	#N/A	24	24	1.0	3.4	27.6	86.0
FE D3	172.4	168.2	40.0	0.24	24	24	1.0	3.4	172.4	86.0
FE D3	344.7	239.2	64.1	0.27	24	24	1.0	3.4	344.7	86.0
FE D3	689.5	373.7	113.1	0.30	24	24	1.0	3.4	689.5	86.0

Table 4.26: Failure Envelopes for GCL E (FE E1 and E2: No Consolidation, SDR = 1.0 mm/min)

Failure Envelope Name	Normal Stress (kPa)	Peak Shear Strength (kPa)	Large Displacement Shear Strength (kPa)	t_H (hrs)	τ_{LD}/τ_p	Hydration Normal Stress (kPa)	Final Water Content (%)
FE E1	14.4	41.0	10.3	336	0.25	14.4	104.9
FE E1	28.7	50.8	12.6	336	0.25	28.7	104.9
FE E1	43.1	60.7	16.2	336	0.27	43.1	104.9
FE E1	57.5	67.4	18.7	336	0.28	57.5	104.9
FE E2	14.4	41.2	10.7	48	0.26	14.4	104.9
FE E2	28.7	54.6	13.3	48	0.24	28.7	104.9
FE E2	43.1	66.7	17.4	48	0.26	43.1	104.9
FE E2	57.5	75.8	21.0	48	0.28	57.5	104.9

Table 4.27: Failure Envelopes for GCL F (FE F1 and F2)

Failure Envelope Name	Normal Stress (kPa)	Peak Shear Strength (kPa)	Large Displacement Shear Strength (kPa)	τ_{LD}/τ_p	t_H (hrs)	Hydration Normal Stress (kPa)	t_C (hrs)	Consolidation Normal Stress (kPa)	Shear Displacement Rate (mm/min)	Final Water Content (%)
FE F1	13.8	4.8	4.1	0.9	168	13.8	0	0.0	1.0	252.5
FE F1	27.6	7.6	6.2	0.8	168	27.6	0	0.0	1.0	252.5
FE F1	55.2	13.8	10.3	0.8	168	55.2	0	0.0	1.0	252.5
Not Included	275.8	38.6	35.2	0.9	0	0.0	14	275.8	0.1	34.0
FE F2	68.9	20.7	14.5	0.7	0	0.0	0	0.0	1.0	84.0
FE F2	275.8	33.8	30.3	0.9	0	0.0	0	0.0	1.0	84.0
FE F2	482.6	47.6	43.4	0.9	0	0.0	0	0.0	1.0	84.0

Table 4.28: Failure Envelope for GCL G (FE G1: t_H = 24 hrs, t_C = 0 hrs and SDR = 1.0 mm/min)

Failure Envelope Name	Normal Stress (kPa)	Peak Shear Strength (kPa)	Hydration Normal Stress (kPa)	Final Water Content (%)
FE G1	2.4	6.2	2.4	144.6
FE G1	9.6	10.3	9.6	120.0
FE G1	19.2	16.0	19.2	100.2

Table 4.29: Failure Envelopes for GCL H (FE H1, H2 and H3)

Failure Envelope Name	Normal Stress (kPa)	Peak Shear Strength (kPa)	Large Displacement Shear Strength (kPa)	τ_{LD}/τ_p	t_H (hrs)	Hydration Normal Stress (kPa)	t_C (hrs)	Consolidation Normal Stress (kPa)	Shear Displacement Rate (mm/min)	Final Water Content (%)
FE H1	4.8	15.6	#N/A	#N/A	24	4.8	0	0.0	1.00	147.1
FE H1	9.6	22.0	#N/A	#N/A	24	9.6	0	0.0	1.00	147.1
FE H1	19.2	30.0	#N/A	#N/A	24	19.2	0	0.0	1.00	147.1
FE H1	48.3	62.7	27.6	0.4	24	48.3	0	0.0	1.00	72.0
FE H1	241.3	188.9	47.6	0.3	24	241.3	0	0.0	1.00	72.0
FE H1	482.6	337.8	68.3	0.2	24	482.6	0	0.0	1.00	72.0
FE H2	6.9	22.1	#N/A	#N/A	24	3.4	24	6.9	1.00	120.5
FE H2	13.8	32.4	#N/A	#N/A	24	3.4	24	13.8	1.00	120.5
FE H2	27.6	43.4	#N/A	#N/A	24	3.4	24	27.6	1.00	120.5
FE H2	172.4	173.7	53.8	0.3	24	3.4	24	172.4	1.00	85.0
FE H2	344.7	262.7	84.1	0.3	24	3.4	24	344.7	1.00	85.0
FE H2	689.5	452.3	131.9	0.3	24	3.4	24	689.5	1.00	85.0
FE H3	4.8	18.8	#N/A	#N/A	96	0.0	24	4.8	0.25	217.0
FE H3	4.8	15.5	#N/A	#N/A	96	0.0	24	4.8	0.25	217.0
FE H3	7.2	20.8	#N/A	#N/A	96	0.0	24	7.2	0.25	217.0
FE H3	7.2	18.3	#N/A	#N/A	96	0.0	24	7.2	0.25	217.0
FE H3	9.6	23.1	#N/A	#N/A	96	0.0	24	9.6	0.25	217.0
FE H3	9.6	21.2	#N/A	#N/A	96	0.0	24	9.6	0.25	217.0

Table 4.30: Failure Envelopes for GCL I (FE I1 and I2)

Failure Envelope Name	Normal Stress (kPa)	Peak Shear Strength (kPa)	t_H (hrs)	Hydration Normal Stress (kPa)	Final Water Content (%)
FE I1	2.4	19.2	0	0.0	20.9
FE I1	7.2	33.8	0	0.0	20.6
FE I1	14.4	46.7	0	0.0	21.8
FE I1	23.9	55.1	0	0.0	21.6
FE I2	2.4	23.5	72	2.4	168.8
FE I2	7.2	32.3	72	2.4	194.8
FE I2	14.4	40.2	72	2.4	154.8
FE I2	23.9	51.0	72	2.4	162.0

Table 4.31: Failure Envelope for GCL J (FE J1: t_H = 24 hrs, t_C = 0 hrs and SDR = 1.0 mm/min)

Failure Envelope Name	Normal Stress (kPa)	Peak Shear Strength (kPa)	Large Displacement Shear Strength (kPa)	Hydration Normal Stress (kPa)	Final Water Content (%)
FE J1	24.1	9.7	4.8	24.1	103.0
FE J1	48.3	13.1	4.8	48.3	103.0
FE J1	96.5	20.7	11.7	96.5	103.0
FE J1	193.1	36.5	24.1	193.1	103.0

Table 4.32: Best-Fit Friction Angles and Adhesive Values for the Peak and Large-Displacement Shear Strength Failure Envelopes

Failure Envelope Number	Failure Envelope Name	Shear Displacement Rate (mm/min)	t_H (hours)	t_C (hours)	Approximate Normal Stress Range (kPa)		Peak Friction Angle (Degrees)	Peak Intercept (kPa)	Peak R^2 Value	Large Displacement Friction Angle (Degrees)	Large Displacement Intercept (kPa)	Large Displacement R^2 Value
1	A1a	1.0	24	0	3.4	72	46.5	13.2	0.98	8.6	2.1	0.84
2	A1b	1.0	24	0	14	24	37.1	10.7	1.00	4.0	3.3	1.00
3	A2	0.5	24	0	48	386	24.6	42.8	0.98	9.8	9.4	0.97
4	A3a	1.0	48	0	2.4	2759	14.8	36.7	0.94	6.3	17.0	0.98
5	A3a Low	1.0	48	0	48	97	31.8	21.3	0.75	16.7	0.0	0.63
6	A3a High	1.0	48	0	97	2758	12.0	18.1	0.90	6.2	4.2	0.98
7	A3b	1.0	48	0	14	276	17.6	38.8	0.32	3.1	4.2	0.75
8	A4	1.0	72	0	2.4	103	34.7	17.4	0.84	8.5	2.8	0.94
9	A5	0.1	168	48	35	310	28.8	30.4	0.93	9.0	15.6	0.72
10	A6*	0.0015	#N/A	#N/A	248	993	21.9	74.3	0.99	5.8	35.0	0.99
11	A7a	1.0	24	12	138	552	22.7	37.9	1.00	11.2	2.8	0.92
12	A7b	1.0	60	24	4.8	29	50.1	12.4	0.99	#N/A	#N/A	#N/A
13	A8	1.0	0	0	2.4	35	43.0	18.9	0.62	#N/A	#N/A	#N/A
14	B1	1.0	24	0	24	690	7.3	53.4	0.82	4.6	12.7	0.96
15	B2[x]	1.0	48	0	2.4	982	4.4	24.3	0.95	#N/A	#N/A	#N/A
16	B3[x]	1.0	96	0	10	1000	4.6	24.1	0.98	#N/A	#N/A	#N/A
17	B4[x]	0.1	168	48	35	310	7.3	32.4	0.99	#N/A	#N/A	#N/A
18	C1	0.5	24	0	7.2	575	23.7	23.4	0.93	10.9	11.7	0.89
19	C1 Low	0.5	24	0	7.2	103	28.3	17.2	1.00	21.7	38.8	0.95
20	C1 High	0.5	24	0	103	575	14.9	9.7	0.80	11.4	7.3	0.73
21	C2	0.2	24	0	10	290	29.3	22.0	0.99	12.0	8.0	0.97
22	C3	0.1	168	48	35	310	16.6	22.3	1.00	8.3	0.9	0.97
23	D1	1.0	72	0	6.9	552	18.6	5.7	1.00	8.4	0.1	0.99
24	D2	0.5	24	0	98	380	25.1	75.3	1.00	9.6	21.3	0.98
25	D3	0.1	24	24	6.9	690	27.1	40.9	0.97	8.0	15.5	1.00
26	D3 Low	0.1	24	24	6.9	28	38.9	22.4	0.97	#N/A	#N/A	#N/A
27	D3 High	0.1	24	24	172	690	21.6	101.0	1.00	8.0	15.5	1.00
28	E1	1.0	336	0	14	58	31.8	32.7	0.99	11.3	7.3	0.99
29	E2	1.0	48	0	14	58	38.9	30.6	0.99	13.7	6.8	0.99
30	F1	1.0	168	0	14	55	12.3	1.7	1.00	8.5	2.1	1.00
31	F2	1.0	0	0	69	483	3.7	16.1	1.00	4.0	10.1	1.00
32	G	1.0	24	0	2.4	19	30.4	4.8	1.00	#N/A	#N/A	#N/A
33	H1	1.0	24	0	4.8	483	33.8	19.7	1.00	5.3	23.8	1.00
34	H2	1.0	24	24	6.9	690	32.1	33.0	0.99	8.5	29.9	1.00
35	H3	0.25	96	24	4.8	10	46.3	12.1	1.00	#N/A	#N/A	#N/A
36	I1	1.0	0	0	2.4	24	58.2	19.3	0.99	#N/A	#N/A	#N/A
37	I2	1.0	72	0	2.4	24	51.1	21.9	0.93	#N/A	#N/A	#N/A
38	J	1.0	24	0	24	193	9.1	5.5	1.00	6.9	0.4	0.98

* For FE A6, a staged hydration/consolidation procedure was employed, in which the normal stress was slowly incremented while the GCL was submerged

[x] For GCL B, the large displacement shear strength is typically reported to be the same as the peak shear strength

Baseline failure envelope for the particular GCL

Bilinear Failure Envelope

Table 4.33: Effect of Shear Displacement Rate on the Shear Strength of GCL A; Low and High Normal Stresses (50 kPa and 517.1 kPa, respectively)

Normal Stress Level	Test Conditions	Normal Stress (kPa)	Peak Shear Strength (kPa)	Large Displacement Shear Strength (kPa)	Shear Displacement Rate (mm/min)
Low	t_H = 24 hours, t_C = 0 hours	48.3	62.7	22.8	0.5
		48.3	65.5	21.4	0.5
		48.3	60.7	17.2	0.5
		48.3	61.4	17.9	0.5
		47.9	69.7	7.7	1.0
		47.9	67.1	9.9	1.0
		47.9	67.6	10.4	1.0
High	t_H = 312 hrs, t_C = 48 hrs	517.1	344.7	103.4	0.0015
		517.1	338.5	96.5	0.01
		517.1	317.2	80.7	0.1
		517.1	308.9	57.2	1

Table 4.34: Effect of Shear Displacement Rate on the Peak Shear Strength of GCL C; Normal Stress of 50 kPa

Normal Stress Level	Test Conditions	Normal Stress (kPa)	Peak Shear Strength (kPa)	Shear Displacement Rate (mm/min)
Low	t_H = 24 hours, t_C = 0 hours	48.3	59.3	0.2
		48.3	53.8	0.2
		48.3	60.0	0.5
		48.3	52.4	0.5

Table 4.35: Effect of Shear Displacement Rate on the Shear Strength of an Unreinforced, Unhydrated GCL (GCL F); Normal Stress of 275.8 kPa

Test Numberg	Peak Shear Strength (kPa)	Large Displacement Shear Strength (kPa)	Shear Displacement Rate (mm/min)
1*	38.6	35.2	0.1
2	33.8	30.3	1

*The unhydrated GCL in this test was consolidated for 14 hours at the normal stress used during shearing

Table 4.36: Effect of Time of Hydration on the Peak Shear Strength of GCL A (a) Data Grouped by Normal Stress Level, (b) Data Grouped by Time of Hydration

Normal Stress (kPa)	Peak Shear Strength (kPa)	Time of Hydration (hrs)	Hydration Normal Stress (kPa)
2.4	20.1	0	0.0
2.4	15.8	48	2.4
2.4	16.3	72	2.4
3.4	15.4	0	0.0
3.4	13.8	24	3.4
3.6	12.6	48	3.6
6.9	19.2	0	0.0
6.9	16.5	24	6.9
7.2	15.2	48	7.2
6.9	15.2	72	6.9
14.4	38.3	0	0.0
14.4	21.5	24	4.8
14.4	23.5	48	14.4
14.4	36.6	72	2.4
23.9	54.3	0	0.0
23.9	28.7	24	4.8
23.9	30.4	48	23.9
23.9	52.0	72	2.4

(a)

Normal Stress (kPa)	Peak Shear Strength (kPa)	Time of Hydration (hrs)	Hydration Normal Stress (kPa)
tH = 0 hours			
2.4	20.1	0	0.0
3.4	15.4	0	0.0
6.9	19.2	0	0.0
14.4	38.3	0	0.0
23.9	54.3	0	0.0
tH = 24 hours			
3.4	13.8	24	3.4
6.9	16.5	24	6.9
14.4	21.5	24	4.8
23.9	28.7	24	4.8
tH = 48 hours			
2.4	15.8	48	2.4
3.6	12.6	48	3.6
7.2	15.2	48	7.2
14.4	23.5	48	14.4
23.9	30.4	48	23.9
tH = 72 hours			
2.4	16.3	72	2.4
6.9	15.2	72	6.9
14.4	36.6	72	2.4
23.9	52.0	72	2.4

(b)

Table 4.37: Effect of Hydration Procedure on GCL A

Normal Stress (kPa)	Hydration Procedure					Peak Shear Strength (kPa)	Large Displacement Shear Strength (kPa)
	Description	Shear Displacement Rate (mm/min)	t_H (hours)	σ_H (kPa)	t_C (hours)		
517.1	One Step Hydration	0.0015	312	496	48	344.7	103.4
517.1	Staged Hydration/Consolidation	0.0015	48	62.5	132	301.3	83.4

For this Table:

t_H = Time the GCL was Hydrated at a Normal Stress of σ_H

σ_H = Hydration Normal Stress Applied Initially to the GCL

t_C = Total Amount of Time to Reach the Normal Stress During Shearing

Table 4.38: Statistical Data Representing the Variability of GCL A (FE A5, t_H = 168 hours, t_C = 48 hours, SDR = 0.1 mm/min)

Failure Envelope Name	Statistical Values	σ = 34.5 kPa		σ = 137.9 kPa		σ = 310.3 kPa	
		Peak Shear Strength (kPa)	Large Displacement Shear Strength (kPa)	Peak Shear Strength (kPa)	Large Displacement Shear Strength (kPa)	Peak Shear Strength (kPa)	Large Displacement Shear Strength (kPa)
A5	Average	46.92	20.84	110.35	38.69	199.80	67.25
	St. Dev.	5.33	8.80	16.36	11.00	24.88	18.44
	COV	0.11	0.42	0.15	0.28	0.12	0.27

Table 4.39: Statistical Data Representing the Variability of GCL A (FE A2, t_H = 48 hours, t_C = 0 hours, SDR = 1.0 mm/min)

Failure Envelope	Statistical Values	σ = 9.6 kPa
		Peak Shear Strength (kPa)
A2	Average	30.53
	St. Dev.	6.11
	COV	0.20

Table 4.40: Variability of Direct Shear Tests Results on Dry GCL A Specimens at a Normal Stress of 517.1 kPa

Test Number	Peak Shear Strength (kPa)	Large Displacement Shear Strength (kPa)
1	398.5	259.9
2	350.9	202.7
3	382.7	219.3
4	454.4	261.3
5	435.7	217.2
Average	**404.45**	**232.08**
St.Dev.	**41.36**	**26.83**
COV	**0.10**	**0.12**

Table 4.41: Displacement at Peak Shear Strength and Final GCL Water Content Data for GCL A (FE A8: t_H = 0 hours, t_C = 0 hours, SDR = 1.0 mm/min)

Normal Stress (kPa)	Peak Shear Strength (kPa)	Final GCL Water Content (%)	Displacement at Peak Shear Strength (mm)
2.4	20.1	16.5	45.72
3.4	15.4	10.3	30.48
6.9	19.2	10.7	31.75
7.2	31.1	16.3	46.99
14.4	38.3	16.8	46.99
23.9	54.3	16.5	29.21
34.5	40.2	10.9	33.02

Table 4.42: Displacement at Peak and Large Displacement Shear Strengths and Final GCL Water Content Data for GCL A (FE A5: t_H = 168 hours, t_C = 48 hours, SDR = 0.1 mm/min)

Failure Envelope Name (With Series Number)	Normal Stress (kPa)	Peak Shear Strength (kPa)	Large Displacement Shear Strength (kPa)	Final GCL Water Content (%)	Displacement at Peak Shear Strength (mm)	Displacement at Large Displacement Shear Strength (mm)	Large Displacement to Peak Displacement Ratio
A5 1	34.5	37.9	13.8	78	27.94	54.61	1.95
	137.9	75.8	24.8	78	23.50	48.26	2.05
	310.3	169.6	43.4	78	21.59	53.34	2.47
A5 2	34.5	46.9	18.6	78.5	21.59	45.72	2.12
	137.9	107.6	37.2	78.5	19.05	48.26	2.53
	310.3	204.8	63.4	78.5	23.50	60.96	2.59
A5 3	34.5	42.1	17.9	74	20.32	45.72	2.25
	137.9	96.5	32.4	74	19.05	55.88	2.93
	310.3	177.9	65.5	74	17.78	48.26	2.71
A5 4	34.5	50.3	33.8	81.5	55.88	67.31	1.20
	137.9	135.1	47.6	81.5	24.13	53.34	2.21
	310.3	217.9	72.4	81.5	19.05	53.34	2.80
A5 5	34.5	41.4	31.7	73.5	45.72	60.96	1.33
	137.9	113.8	55.8	73.5	19.05	45.72	2.40
	310.3	233.0	89.6	73.5	18.42	53.34	2.90
A5 6	34.5	46.2	24.1	78	20.32	49.53	2.44
	137.9	113.8	51.7	78	19.69	49.53	2.52
	310.3	213.7	86.2	78	25.40	46.99	1.85
A5 7	34.5	46.2	18.6	72.5	24.13	58.42	2.42
	137.9	109.6	37.9	72.5	21.59	53.34	2.47
	310.3	199.9	62.7	72.5	20.32	60.96	3.00
A5 8	34.5	49.6	14.5	72	21.59	54.61	2.53
	137.9	126.2	43.4	72	24.13	53.34	2.21
	310.3	231.0	75.2	72	21.59	52.07	2.41
A5 9	34.5	46.2	38.6	75.5	41.91	58.42	1.39
	137.9	89.6	49.0	75.5	18.42	50.80	2.76
	310.3	175.1	62.7	75.5	16.51	49.53	3.00
A5 10	34.5	39.3	17.2	75.5	20.96	53.34	2.55
	137.9	94.5	39.3	75.5	20.32	52.07	2.56
	310.3	194.4	75.8	75.5	25.40	48.26	1.90
A5 11	34.5	46.2	15.9	71	25.40	57.15	2.25
	137.9	111.0	29.6	71	24.13	66.04	2.74
	310.3	202.0	64.8	71	21.59	71.12	3.29
A5 12	34.5	55.2	8.3	91.9	40.64	46.99	1.16
	137.9	137.2	13.8	65.6	16.51	54.61	3.31
	310.3	241.3	39.3	58.7	29.21	51.44	1.76
A5 13	34.5	49.0	8.3	107.8	14.61	64.77	4.43
	137.9	91.0	13.8	94.5	22.23	59.69	2.69
	310.3	156.5	39.3	59	29.85	59.69	2.00
A5 14	34.5	44.1	15.2	73	17.78	45.09	2.54
	137.9	108.9	30.3	73	12.07	41.91	3.47
	310.3	157.2	42.1	73	11.43	36.83	3.22
A5 15	34.5	53.1	31.0	71.5	31.75	53.34	1.68
	137.9	135.8	44.8	71.5	19.05	55.88	2.93
	310.3	204.1	68.9	71.5	29.85	53.34	1.79
A5 16	34.5	43.4	11.7	76	22.86	55.88	2.44
	137.9	113.8	29.0	76	20.32	53.34	2.63
	310.3	222.0	60.0	76	19.05	50.80	2.67
A5 17	34.5	58.6	32.4	79	22.23	52.71	2.37
	137.9	117.9	44.8	79	22.86	53.34	2.33
	310.3	195.8	65.5	79	26.04	50.80	1.95
A5 18	34.5	51.7	9.7	88.5	22.23	66.04	2.97
	137.9	104.8	29.0	88.5	17.78	49.53	2.79
	310.3	183.4	46.9	88.5	10.80	45.72	4.24
A5 19	34.5	44.1	21.4	72.5	26.67	55.88	2.10
	137.9	113.8	40.7	72.5	24.13	60.96	2.53
	310.3	216.5	75.8	72.5	22.86	60.96	2.67
				Average	**23.21**	**53.69**	**2.48**
				St. Dev.	**7.77**	**6.54**	**0.62**
				COV	**0.33**	**0.12**	**0.25**

Note: Large displacement is reported when the shear strength has reached a constant level, it still should not be used as the residual displacement

Table 4.43: Statistical Data for Displacement at Peak Shear Strength and Final GCL Water Content Data for Three GCLs under Identical Test Conditions (FE A5, B4 and C3: t_H = 168 hours, t_C = 48 hours, SDR = 0.1 mm/min)

Failure Envelope Name	Normal Stress (kPa)	Number of Tests	Mean Peak Shear Strength (kPa)	Mean Large Displacement Shear Strength (kPa)	Mean Displacement at Peak Shear Strength (mm)	Standard Deviation Displacement at Peak Shear Strength (mm)	Mean FinalWater Content (%)	Standard Deviation FinalWater Content (%)
A5	34.5	19	46.9	20.8	20.5	4.4	81.2	5.7
	137.9	19	110.4	38.7	20.2	4.6	81.8	5.7
	310.3	19	199.8	67.2	22.2	6.9	77.2	11.0
B4	34.5	1	35.9	35.9	38.1	0.0	84.4	0.0
	137.9	1	51.7	51.7	43.18	0.0	77.8	0.0
	310.3	1	71.7	71.7	64.77	0.0	64.0	0.0
C3	34.5	1	32.4	8.3	12.700	0.0	109.6	0.0
	137.9	1	63.4	17.2	20.955	0.0	98.2	0.0
	310.3	1	114.5	47.6	12.065	0.0	61.4	0.0

Table 4.44: Displacement at Peak Shear Strength and Final GCL Water Content Data for GCL A; Effect of Variability and Shear Displacement Rate

Normal Stress (kPa)	Peak Shear Strength (kPa)	Large Displacement Shear Strength (kPa)	Hydration Time (hrs)	Hydration Normal Stress (kPa)	Consolidation Time (hrs)	Consolidation Normal Stress (kPa)	Shear Displacement Rate (mm/min)	Displacement at Peak Shear Strength (mm)	Displacement at Large Displacement Shear Strength (mm)
517.1	382.7	219.3	0	0	0	0	1	20.96	50.80
517.1	454.4	261.3	0	0	0	0	1	19.05	63.50
517.1	435.7	217.2	0	0	0	0	1	20.32	44.45
517.1	398.5	259.9	0	0	0	0	1	21.59	53.34
517.1	350.9	202.7	0	0	0	0	1	18.80	46.99
517.1	344.7	103.4	312	496.4	48	517.1	0.0015	21.59	68.58
517.1	338.5	96.5	312	496.4	48	517.1	0.01	22.86	67.31
517.1	317.2	80.7	312	496.4	48	517.1	0.1	13.97	77.47
517.1	308.9	57.2	312	496.4	48	517.1	1	15.24	58.42
517.1	301.3	83.4	Staged	Staged	48	517.1	0.0015	19.05	64.77

Table 4.45: Displacement at Peak Shear Strength and Final GCL Water Content Data for an Unreinforced GCL (GCL F)

Failure Envelope Name	GCL Moisture Condition	Normal Stress (kPa)	Peak Shear Strength (kPa)	Large Displacement Shear Strength (kPa)	Final Water Content (%)	Displacement at Peak Shear Strength (mm)	Displacement at Large Displacement Shear Strength (mm)
F1	Hydrated	13.8	4.8	4.1	252.5	5.08	10.16
F1	Hydrated	27.6	7.6	6.2	252.5	5.08	15.24
F1	Hydrated	55.2	13.8	10.3	252.5	5.08	20.32
Not Included	Unhydrated	275.8	38.6	35.2	34	9.525	45.72
F2	Unhydrated	68.9	20.7	14.5	84	8.89	54.61
F2	Unhydrated	275.8	33.8	30.3	84	8.89	45.72
F2	Unhydrated	482.6	47.6	43.4	84	8.89	40.64

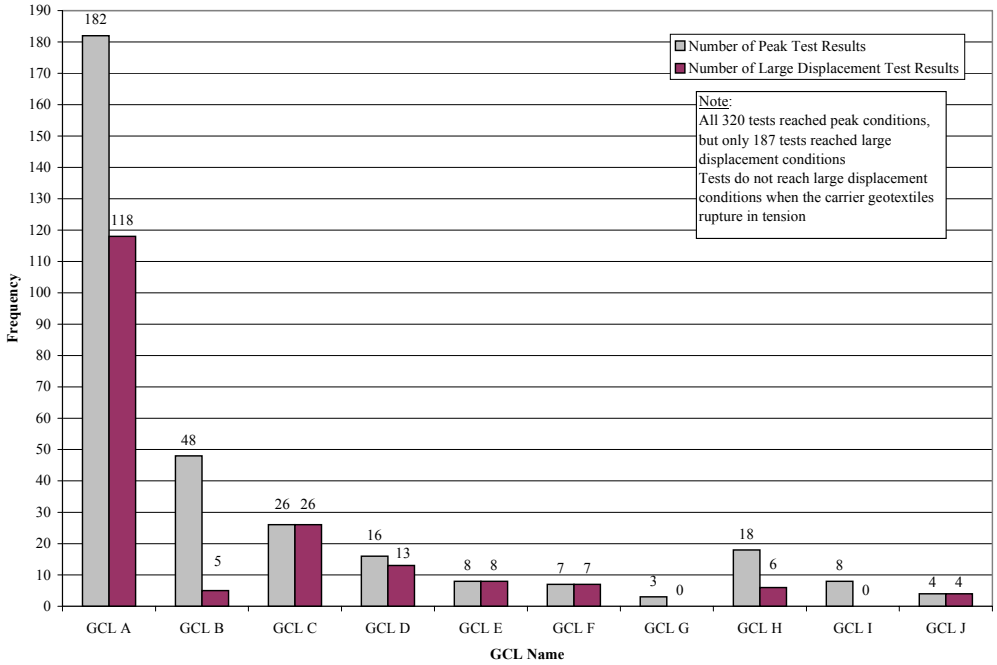

Figure 4.1: Histogram of the GCL Product Types Undergoing Internal Shear Strength Testing, Total of 320 Direct Shear Tests

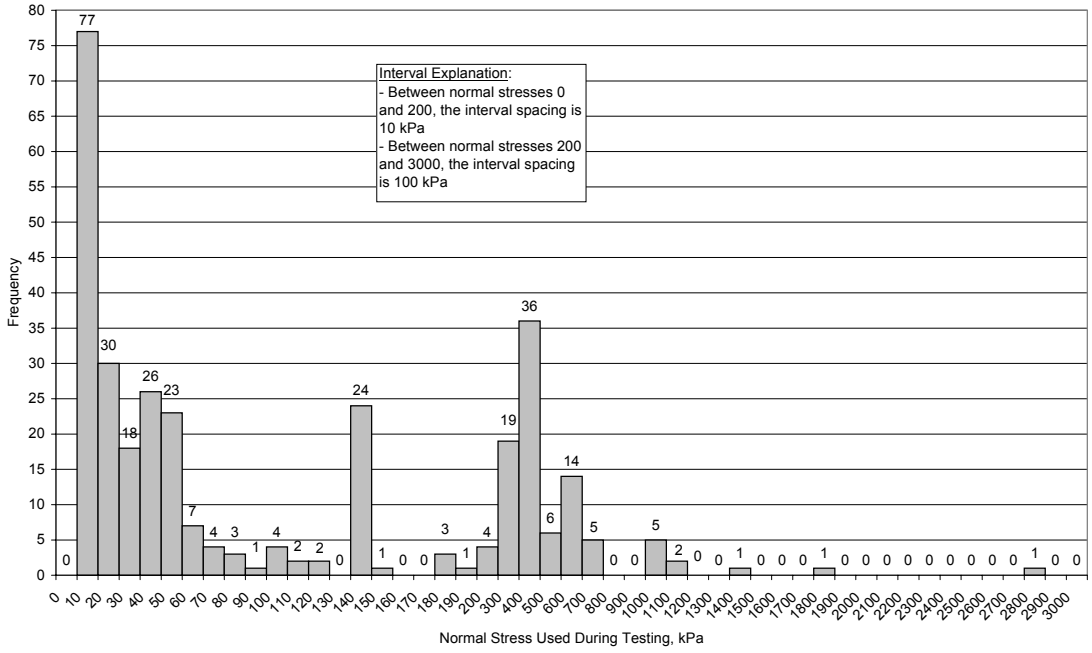

Figure 4.2: Histogram of Normal Stresses Applied During Shearing to All GCLs in the GCLSS Database, Total of 320 Direct Shear Tests

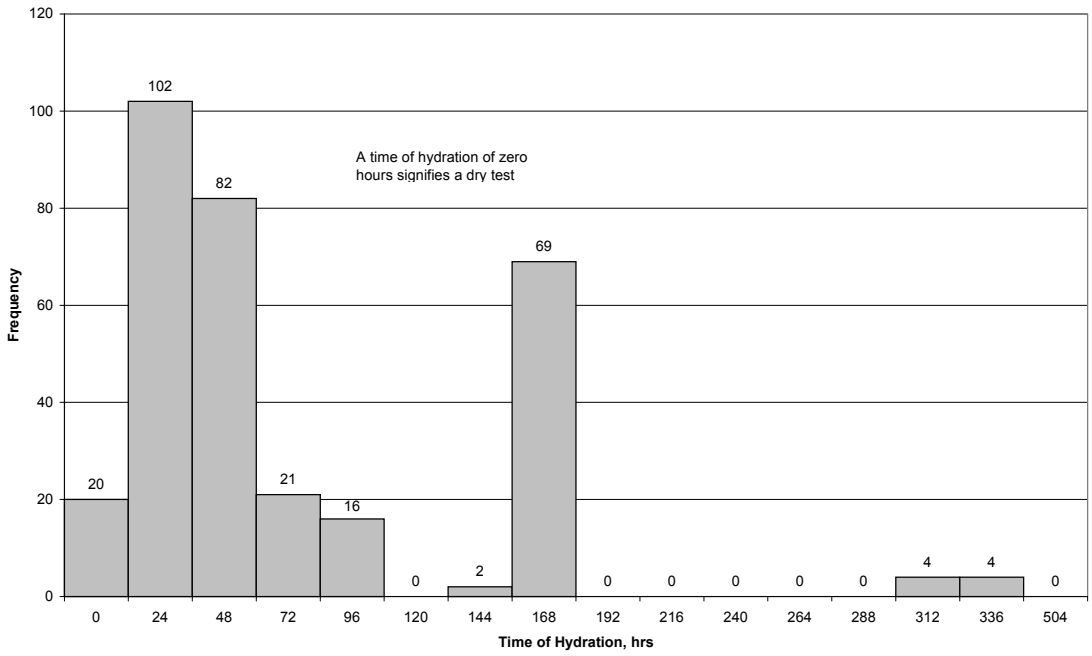

Figure 4.3: Histogram of Times of Hydration Used During Testing of All GCLs in the GCLSS Database. Total of 320 Direct Shear Tests (t_H = 0 means Unhydrated)

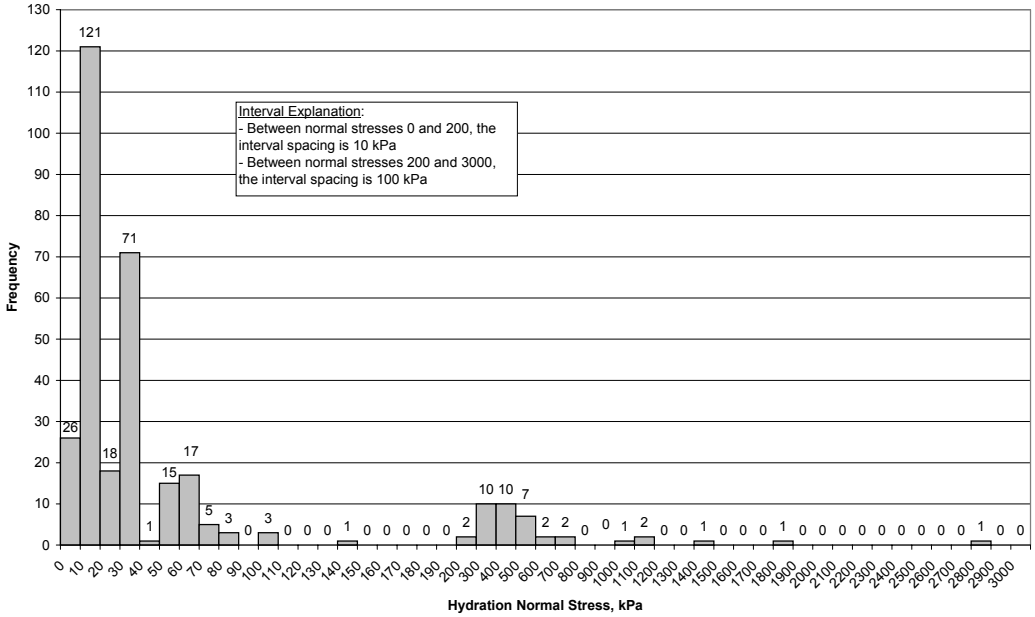

Figure 4.4: Histogram of Hydration Normal Stresses Applied to All GCLs in the GCLSS Database. Total of 320 Direct Shear Tests (Unhydrated Tests Do Not Have a Hydration Normal Stress)

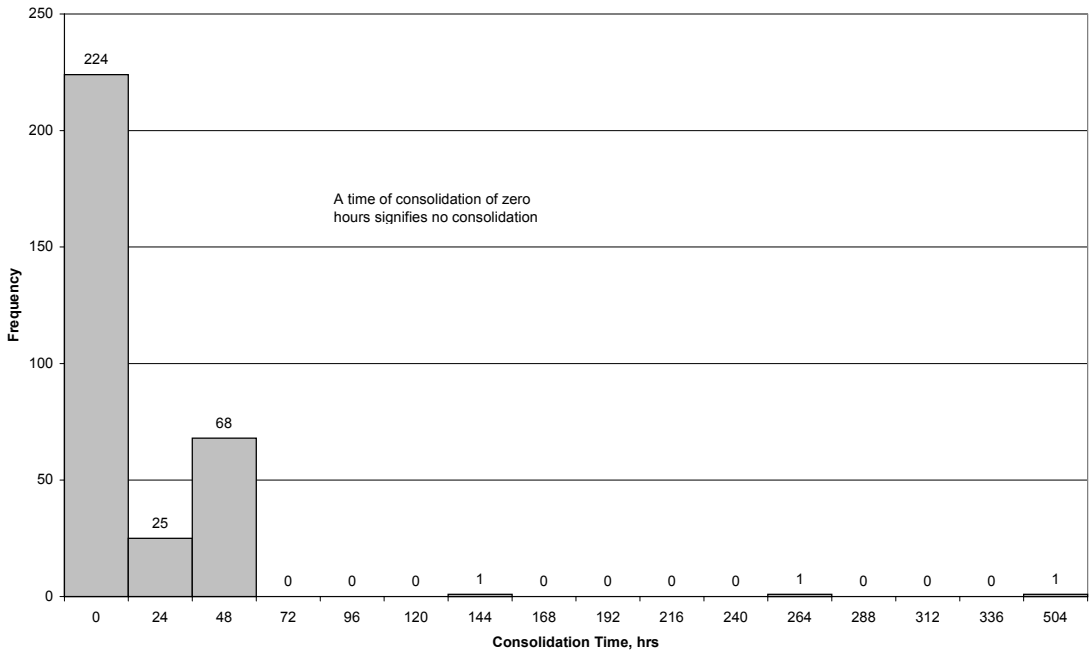

Figure 4.5: Histogram of Times of Consolidation Used During Testing of All GCLs in the GCLSS Database. Total of 320 Direct Shear Tests

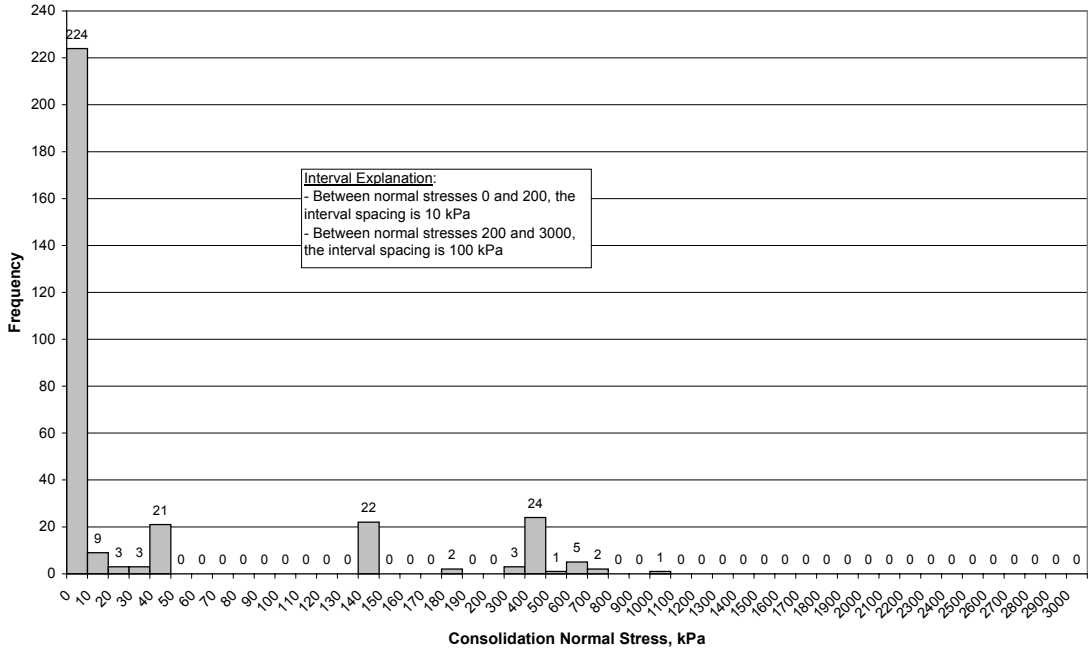

Figure 4.6: Histogram of Consolidation Normal Stresses Applied to All GCLs in the GCLSS Database. Total of 320 Direct Shear Tests

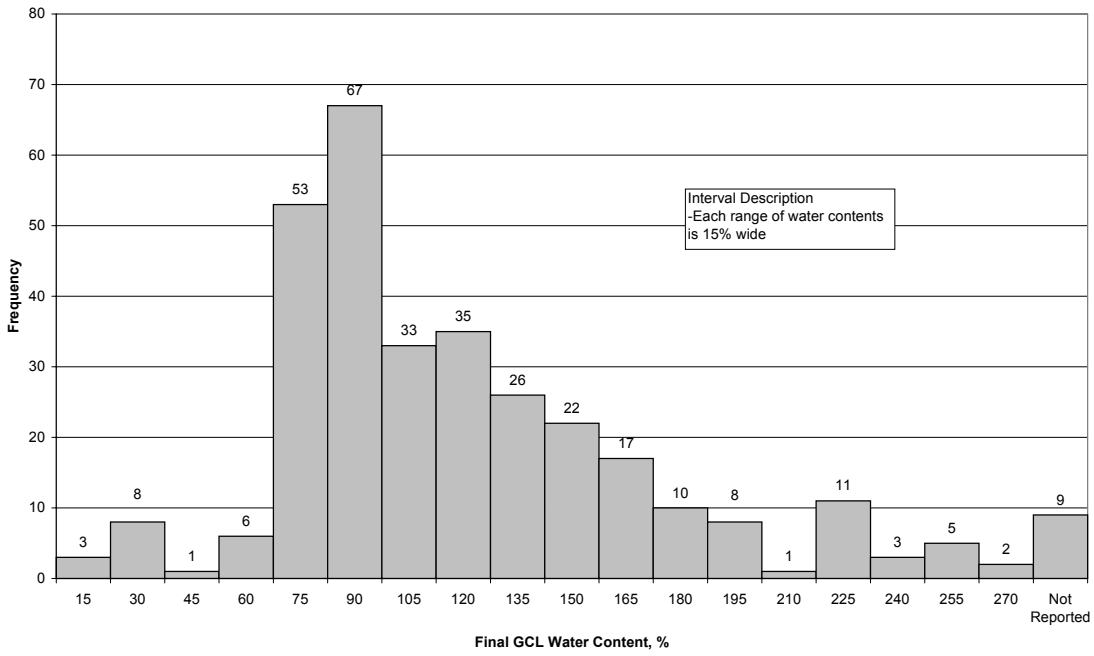

Figure 4.7: Histogram of the Final Water Content of Each GCL in the GCLSS Database. Total of 320 Direct Shear Tests

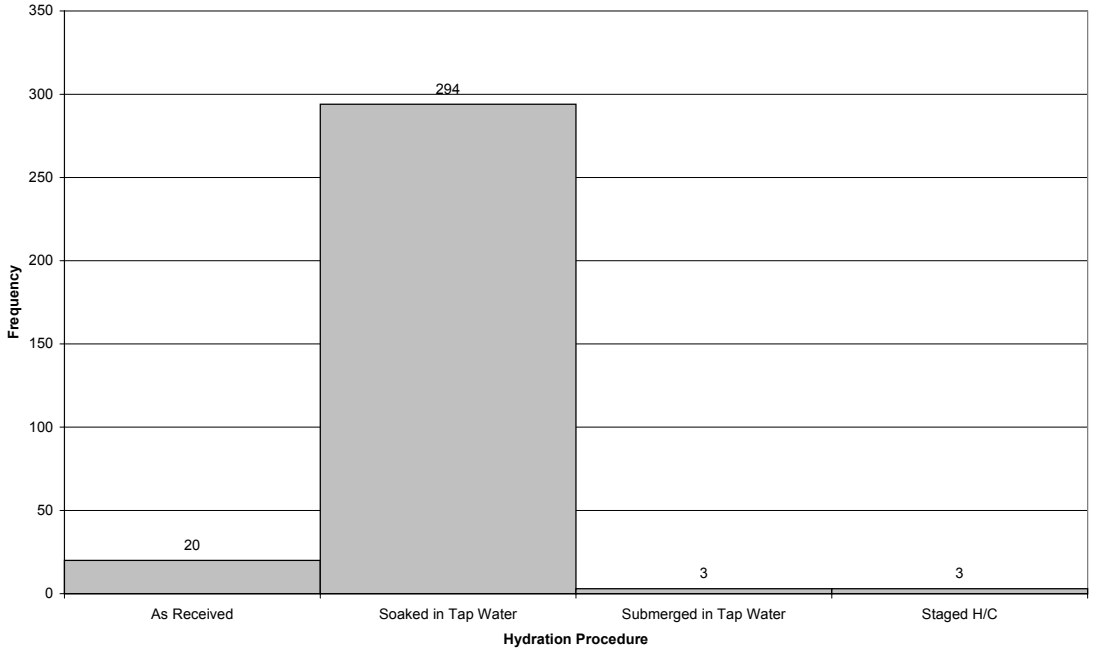

Figure 4.8: Histogram of the Hydration Procedure for Each GCL in the GCLSS Database. Total of 320 Direct Shear Tests

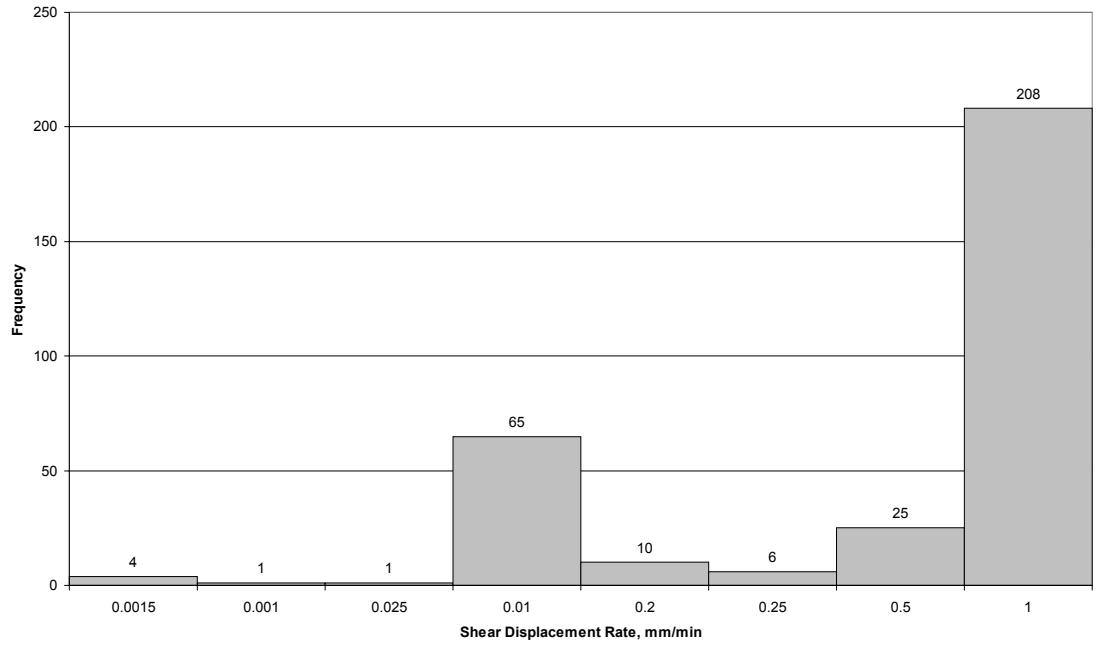

Figure 4.9: Histogram of Shear Displacement Rates Used During Testing of All GCLs in the GCLSS Database. Total of 320 Direct Shear Tests

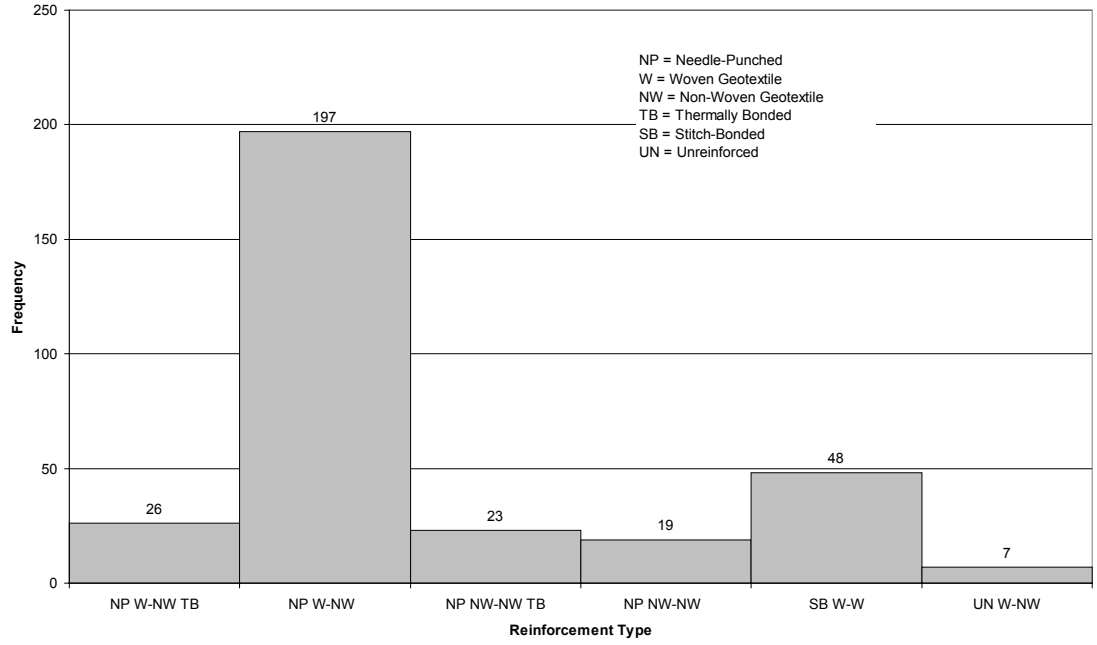

Figure 4.10: Histogram of Reinforcement Type for All GCLs in the GCLSS Database, Total of 320 Direct Shear Tests (NP = Needle-Punched, SB = Stitch-Bonded, UN = Unreinforced, W = Woven Backing Geotextile, NW = Nonwoven Backing Geotextile, TB = Thermally Bonded)

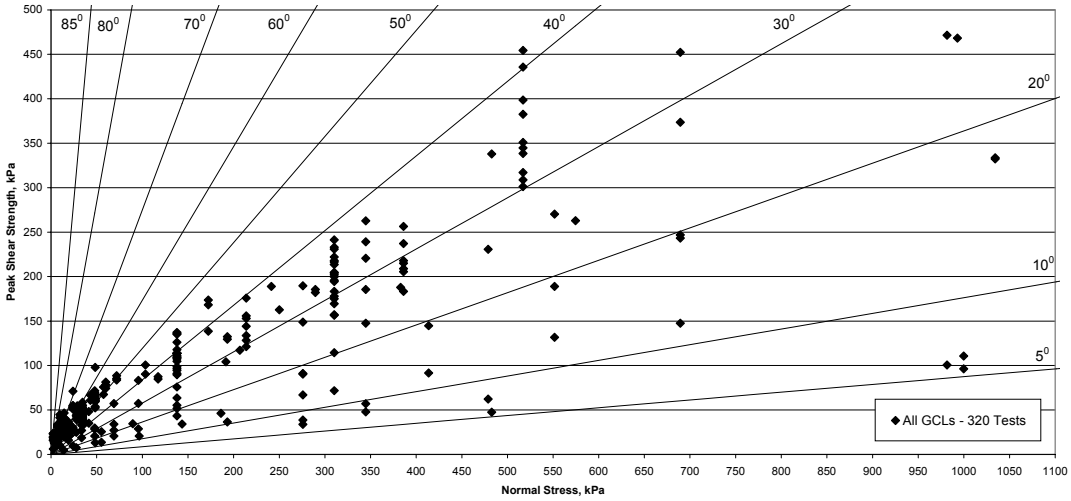

(a)

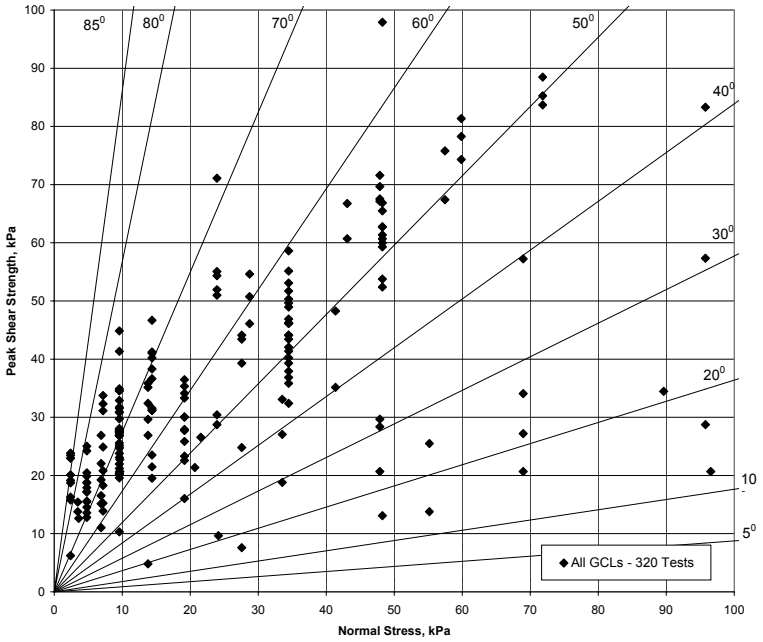

(b)

Figure 4.11: Peak Shear Strength for All GCL Types Included in the GCLSS Database (Total of 320 Tests); (a) Ranges of Equivalent Friction Angles for the Complete Data Set, (b) Detail for Low Normal Stresses

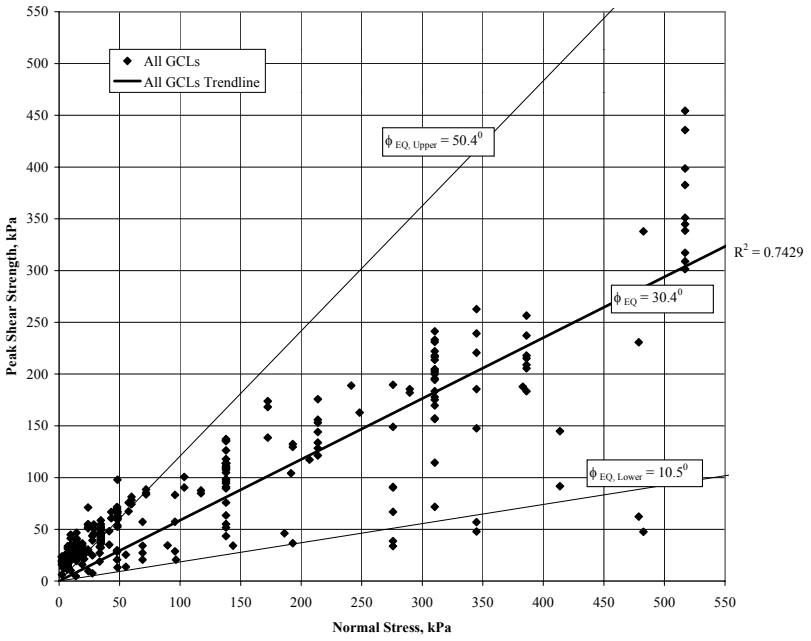

(a)

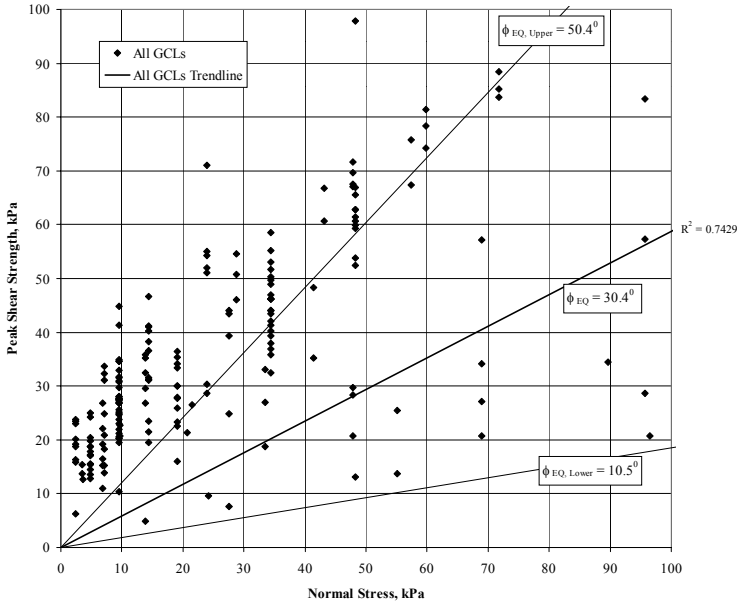

(b)

Figure 4.12: Peak Shear Strength for All GCL Types Included in the GCLSS Database (Total of 320 Tests); (a) Average Equivalent Friction Angle with Upper and Lower Bounds, (b) Detail for Low Normal Stresses

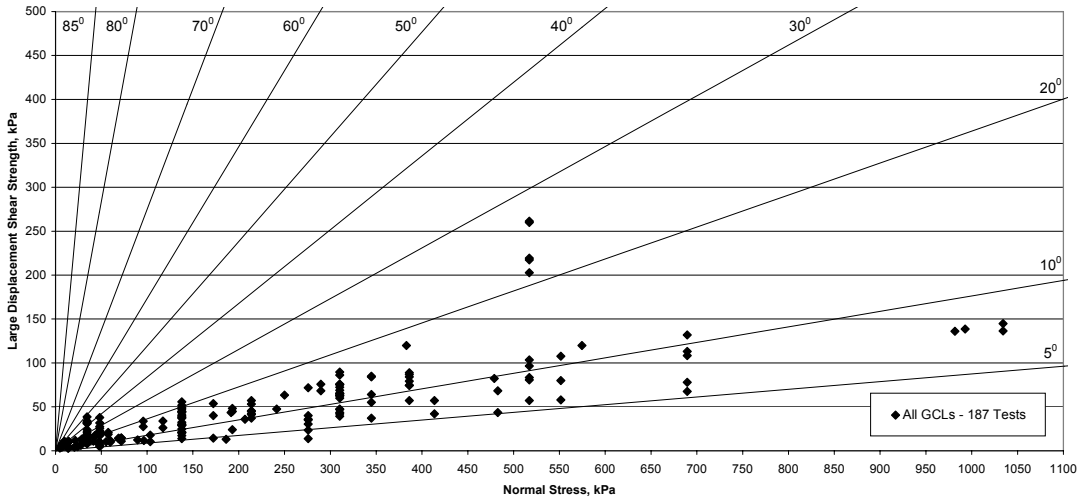

(a)

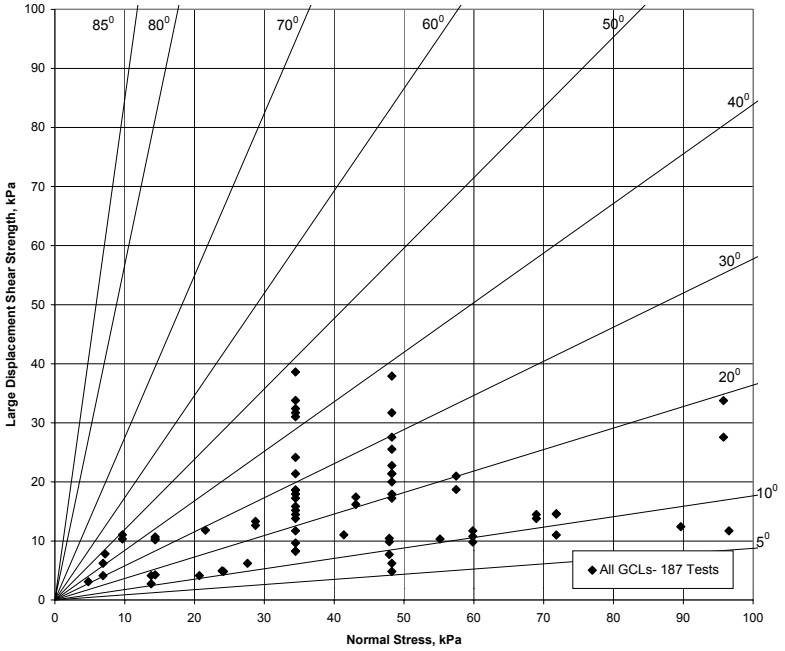

(b)

Figure 4.13: Large Displacement Shear Strength for All GCL Types Included in the GCLSS Database (Total of 187 Tests); (a) Ranges of Equivalent Friction Angles for the Complete Data Set, (b) Detail for Low Normal Stresses

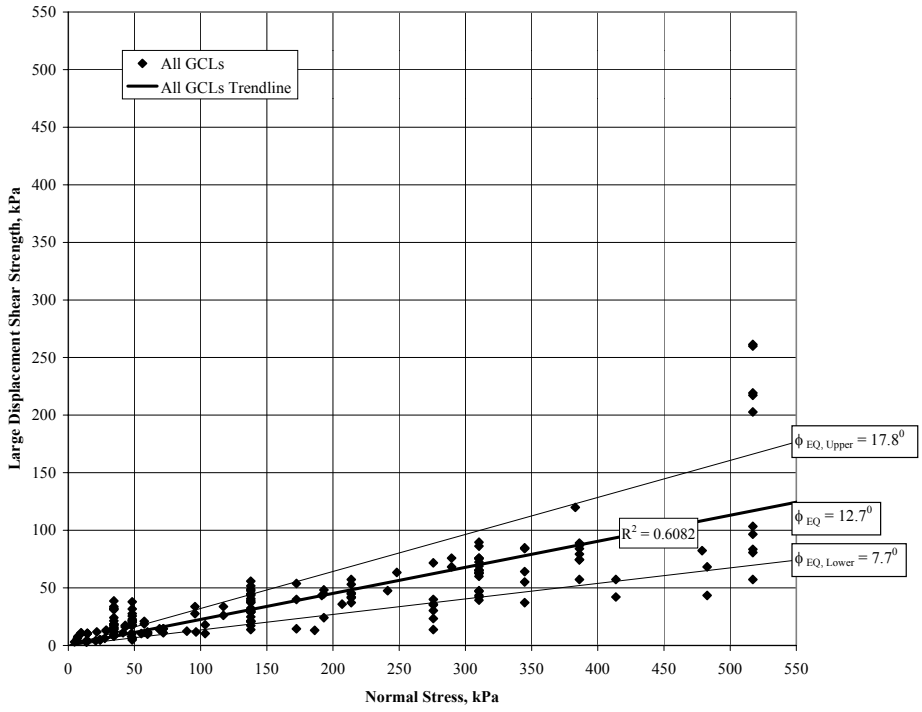

(a)

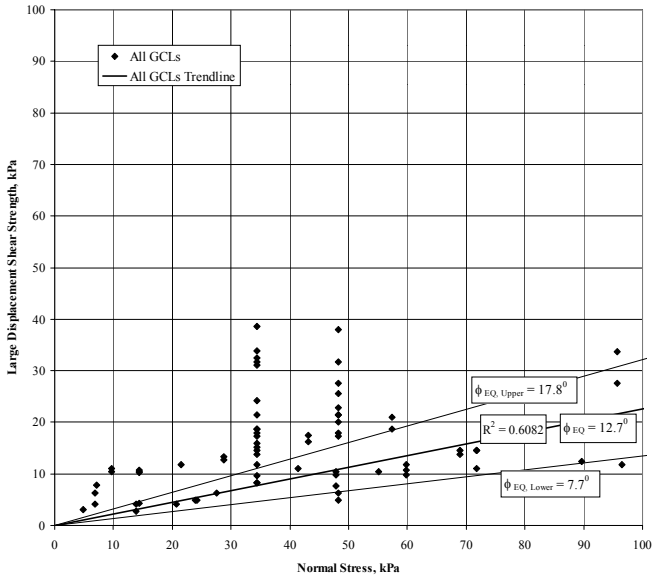

(b)

Figure 4.14: Large Displacement Shear Strength for All GCL Types Included in the GCLSS Database (Total of 187 Tests); (a) Average Equivalent Friction Angle with Upper and Lower Bounds, (b) Detail for Low Normal Stresses

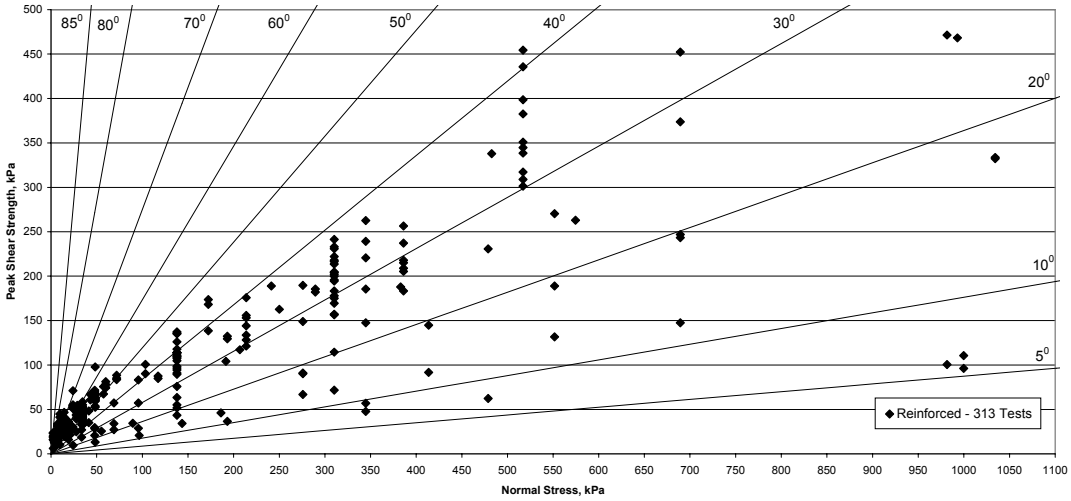

(a)

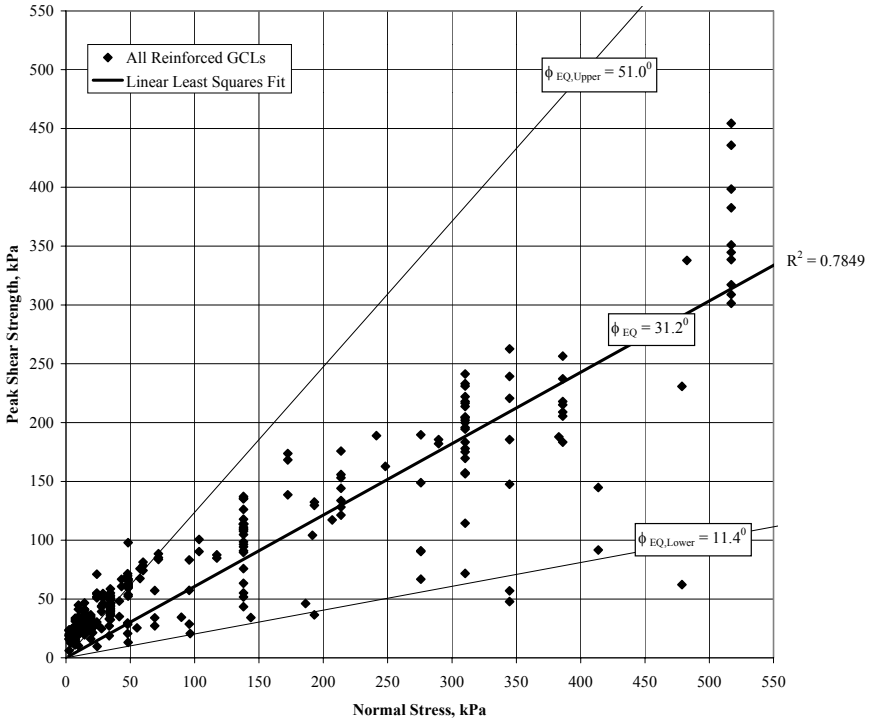

(b)

Figure 4.15: Peak Shear Strengths Test Results for All Reinforced GCLs (Total of 313 Tests); (a) Ranges of Equivalent Friction Angles, (b) Average Equivalent Friction Angle with Upper and Lower Bounds

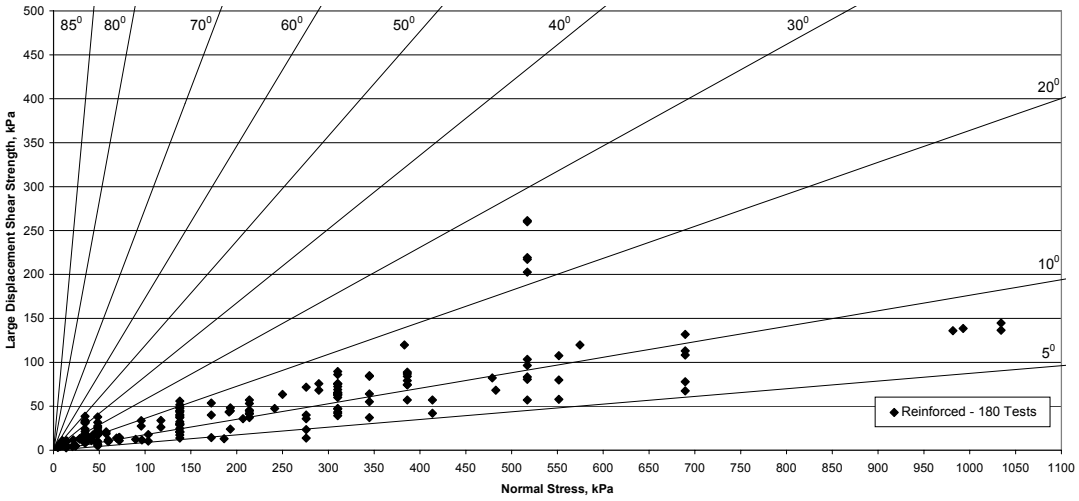

(a)

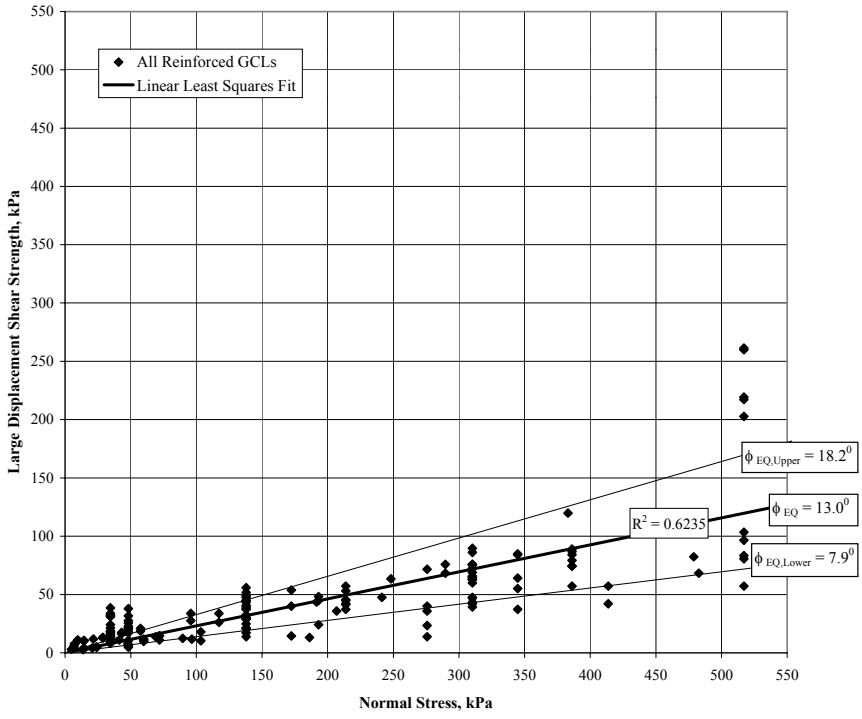

(b)

Figure 4.16: Large Displacement Shear Strengths Test Results for All Reinforced GCLs (Total of 313 Tests); (a) Ranges of Equivalent Friction Angles, (b) Average Equivalent Friction Angle with Upper and Lower Bounds

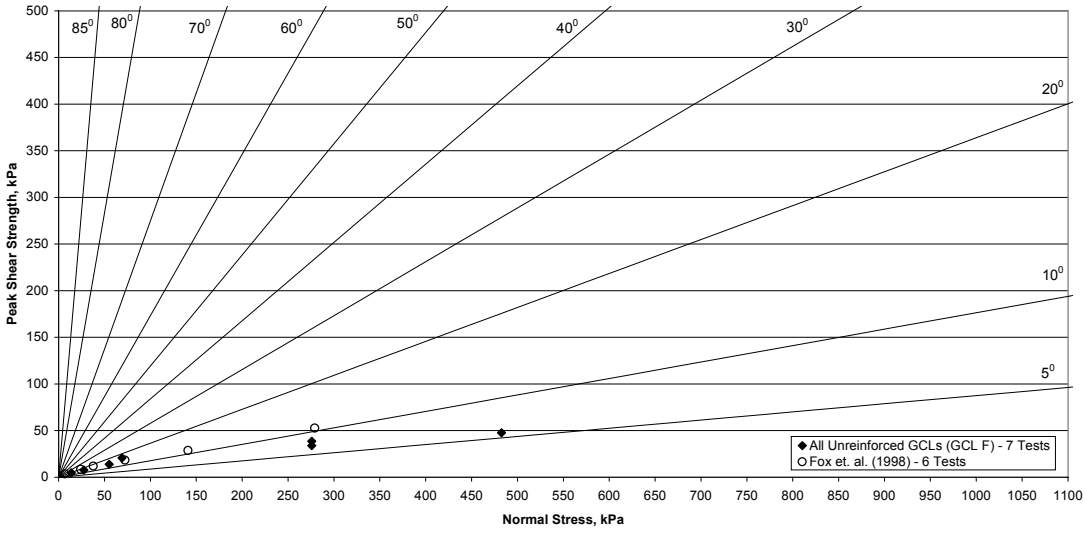

(a)

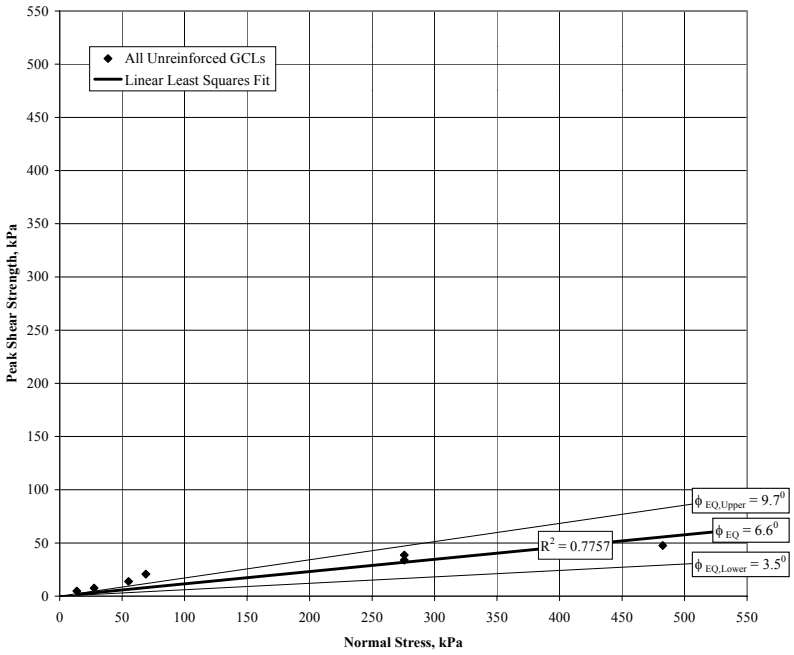

(b)

Figure 4.17: Peak Shear Strengths Test Results for All Unreinforced GCLs (Total of 7 Tests); (a) Ranges of Equivalent Friction Angles (with Test Results Reported by Other Studies), (b) Average Equivalent Friction Angle with Upper and Lower Bounds (Results of Other Studies Not Included)

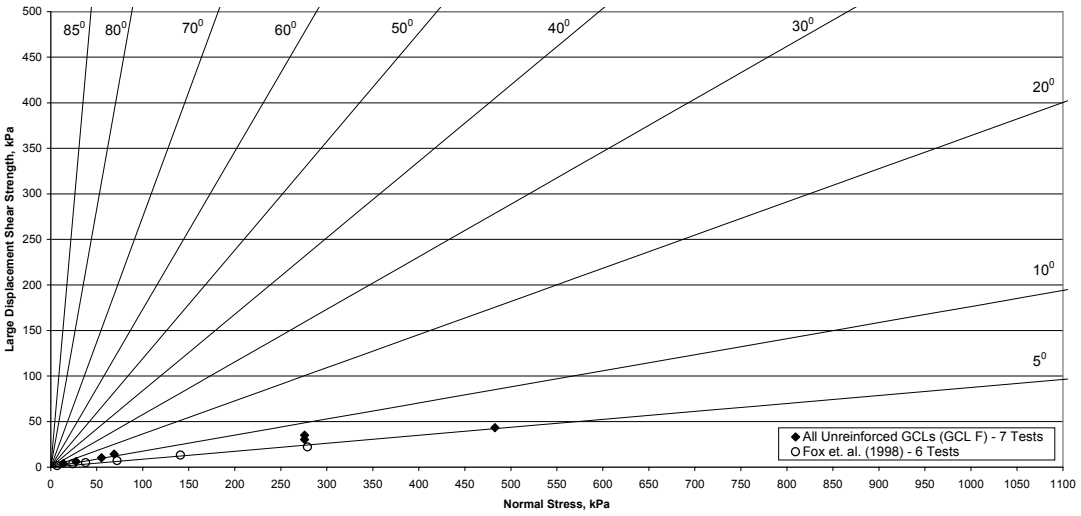

(a)

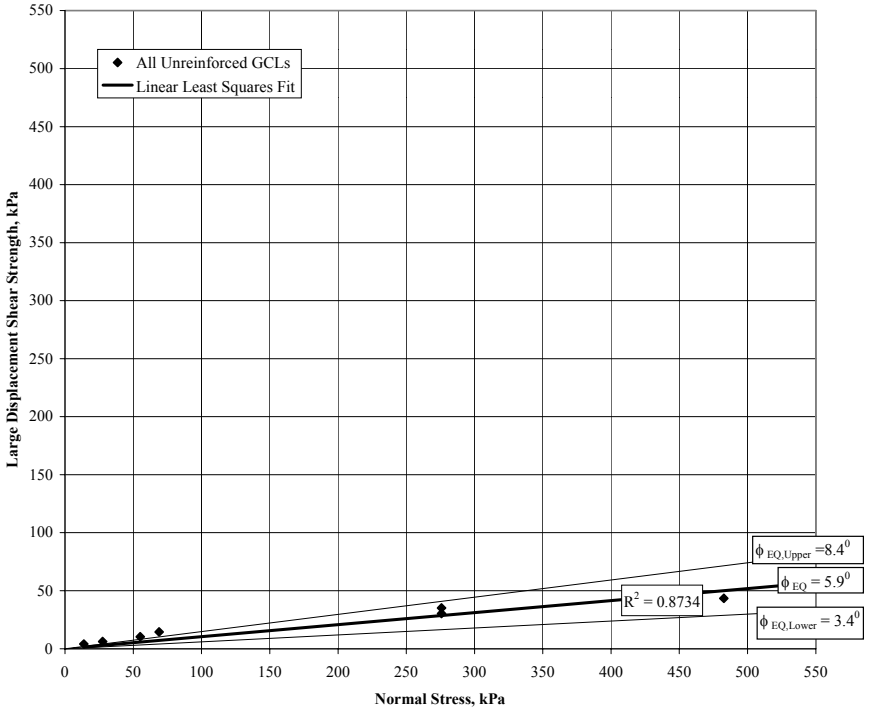

(b)

Figure 4.18: Large Displacement Shear Strengths Test Results for All Unreinforced GCLs (Total of 7 Tests); (a) Ranges of Equivalent Friction Angles (with Test Results Reported by Other Studies), (b) Average Equivalent Friction Angle with Upper and Lower Bounds (Results of Other Studies Not Included)

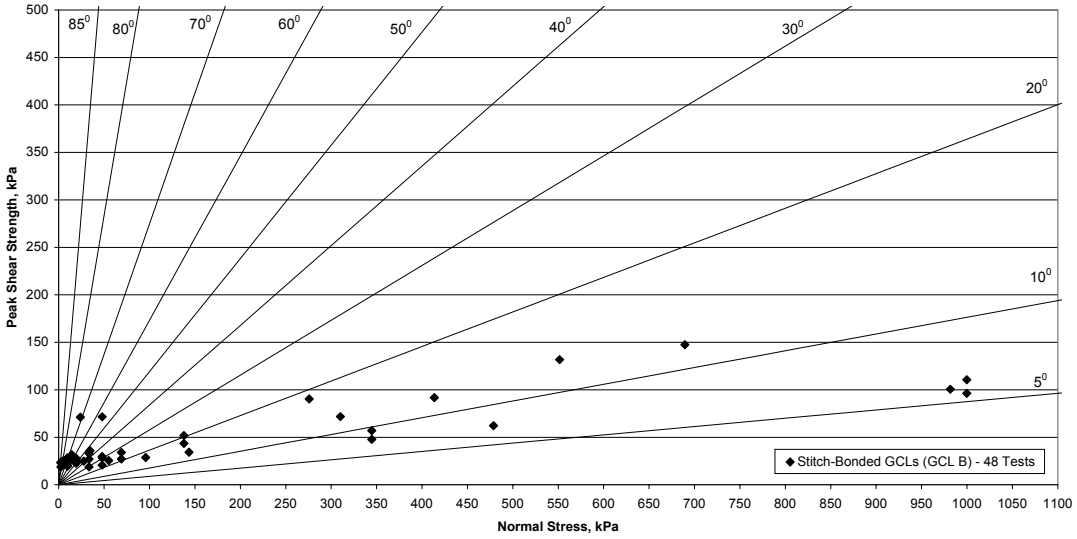

(a)

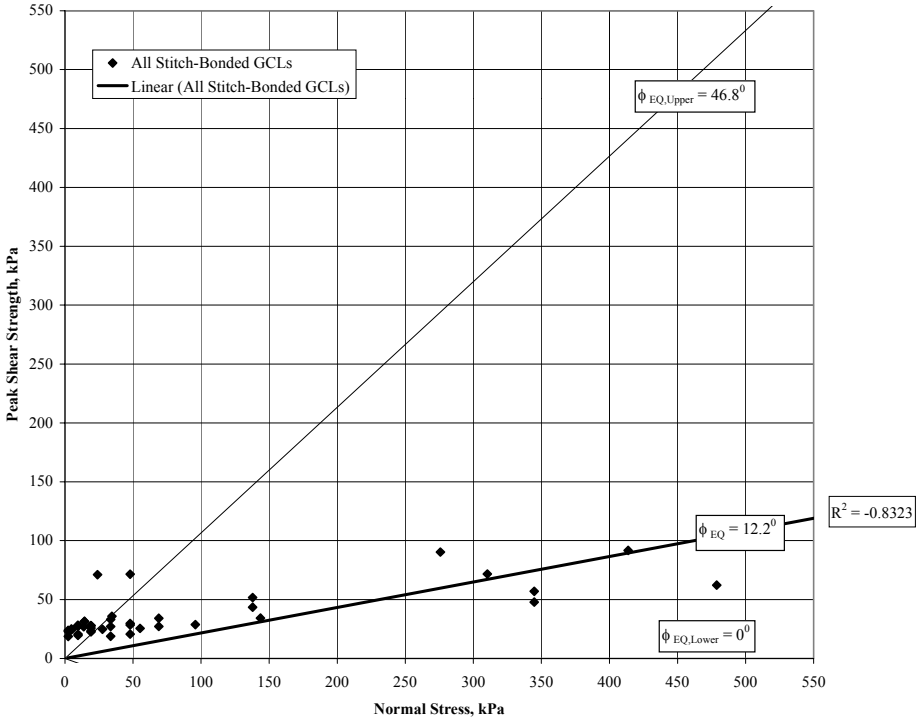

(b)

Figure 4.19: Peak Shear Strength for All Stitch-Bonded GCLs in the GCLSS Database (Total of 48 Tests); (a) Ranges of Equivalent Friction Angles, (b) Average Equivalent Friction Angle with Upper and Lower Bounds

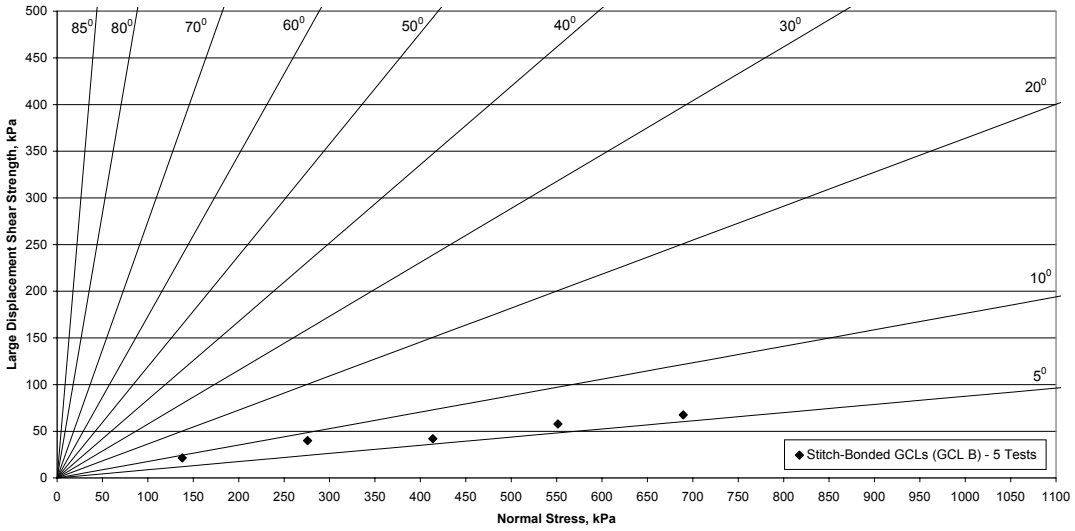

(a)

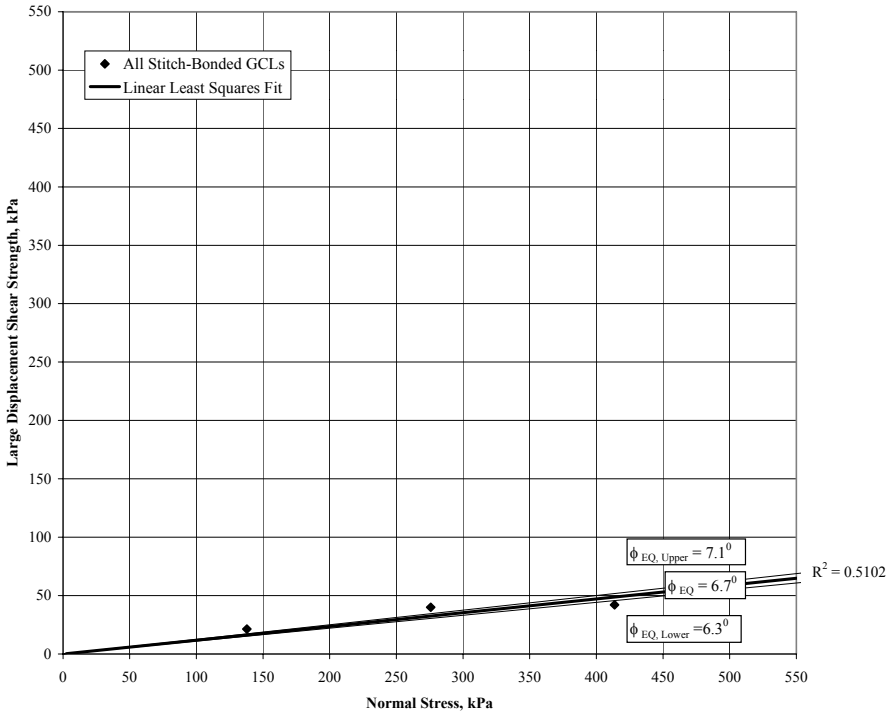

(b)

Figure 4.20: Large Displacement Shear Strength for All Stitch-Bonded GCLs in the GCLSS Database (Total of 5 Tests); (a) Ranges of Equivalent Friction Angles, (b) Average Equivalent Friction Angle with Upper and Lower Bounds

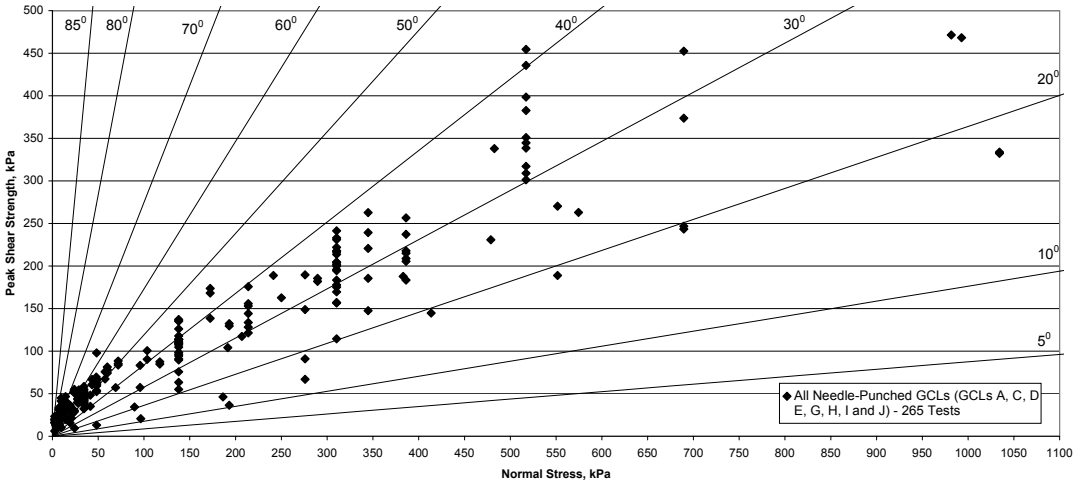

(a)

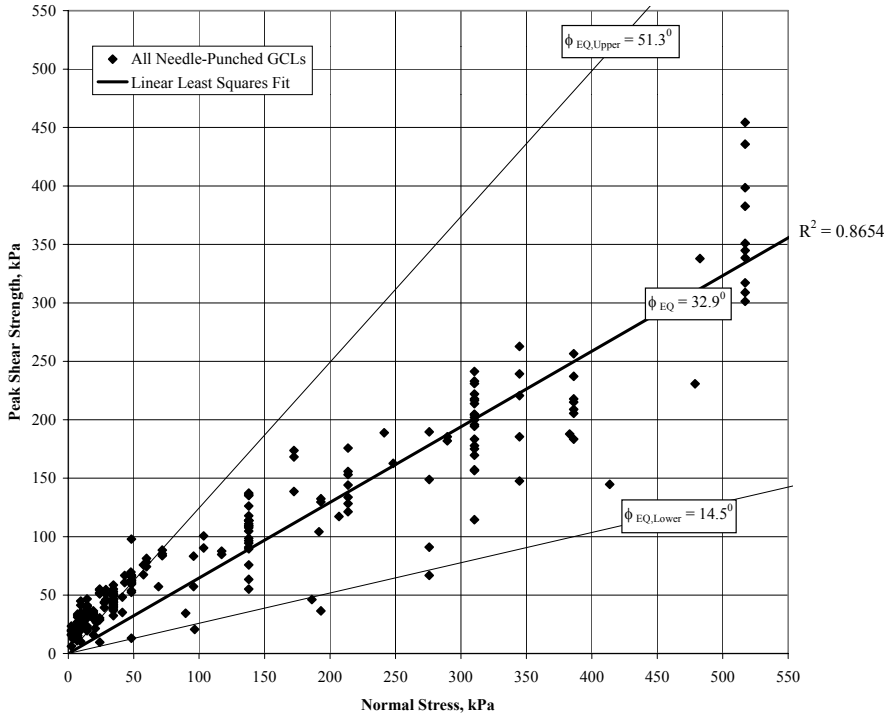

(b)

Figure 4.21: Peak Shear Strength for All Needle-Punched GCLs in the GCLSS Database (Total of 265 Tests); (a) Ranges of Equivalent Friction Angles, (b) Average Equivalent Friction Angle with Upper and Lower Bounds

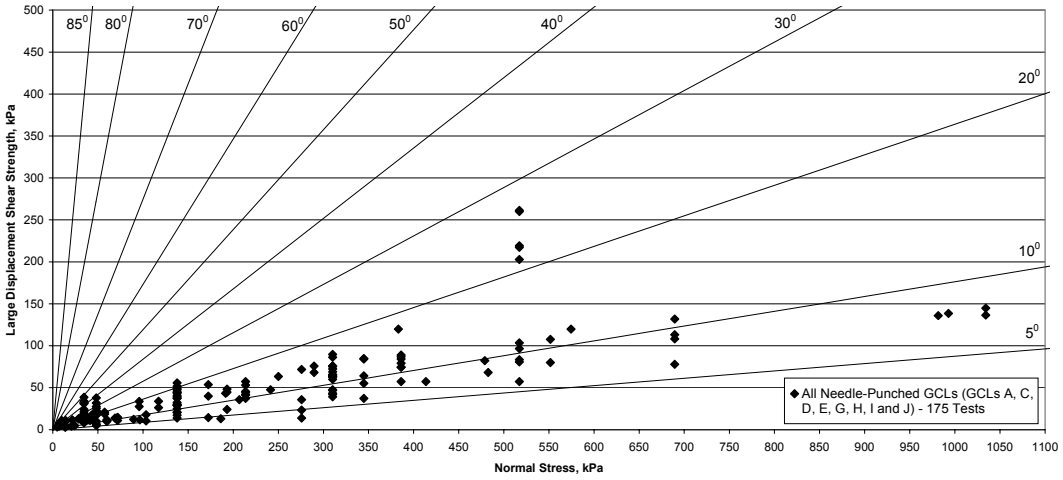

(a)

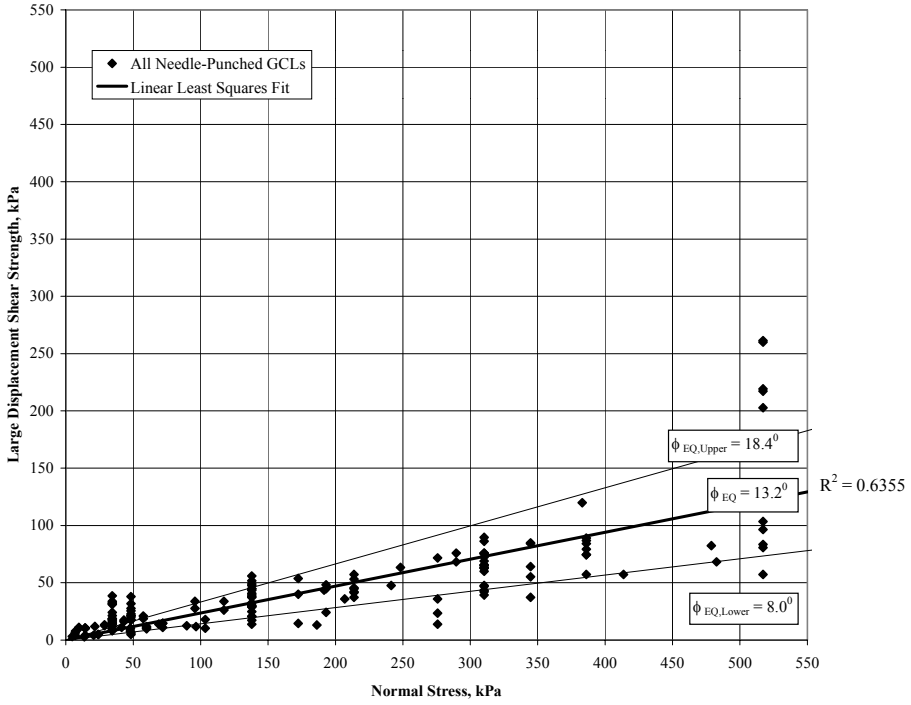

(b)

Figure 4.22: Large Displacement Shear Strength for All Needle-Punched GCLs in the GCLSS Database (Total of 175 Tests); (a) Ranges of Equivalent Friction Angles, (b) Average Equivalent Friction Angle with Upper and Lower Bounds

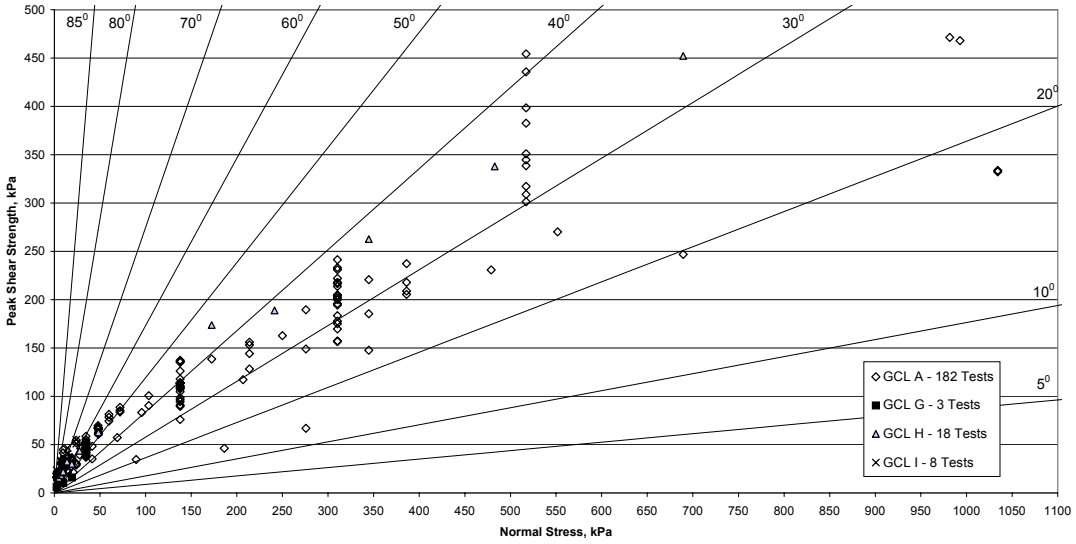

(a)

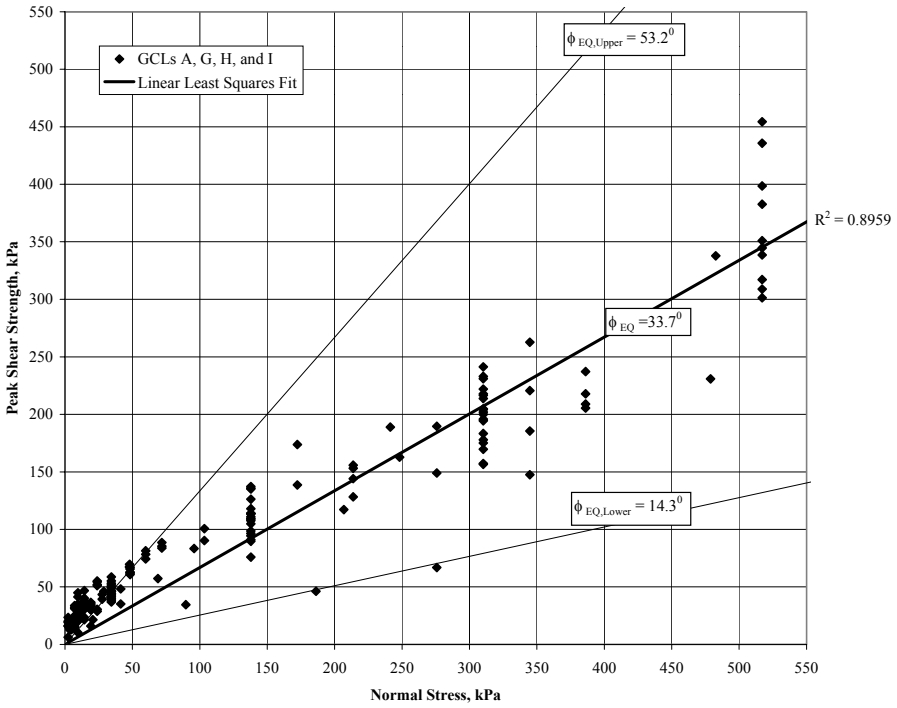

(b)

Figure 4.23: Peak Shear Strength for All Bentomat GCLs (Total of 211 Tests); (a) Ranges of Equivalent Friction Angles, (b) Average Equivalent Friction Angle with Upper and Lower Bounds

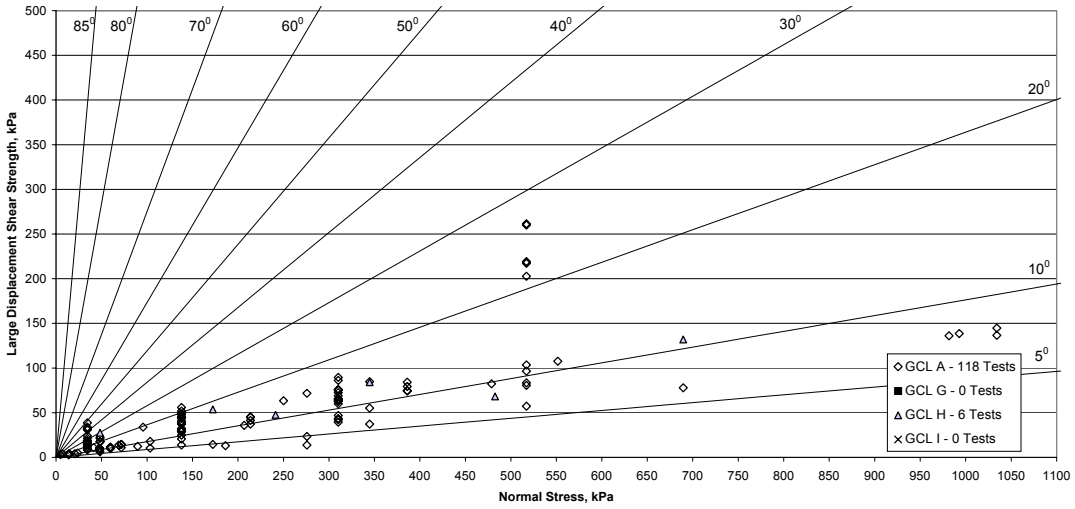

(a)

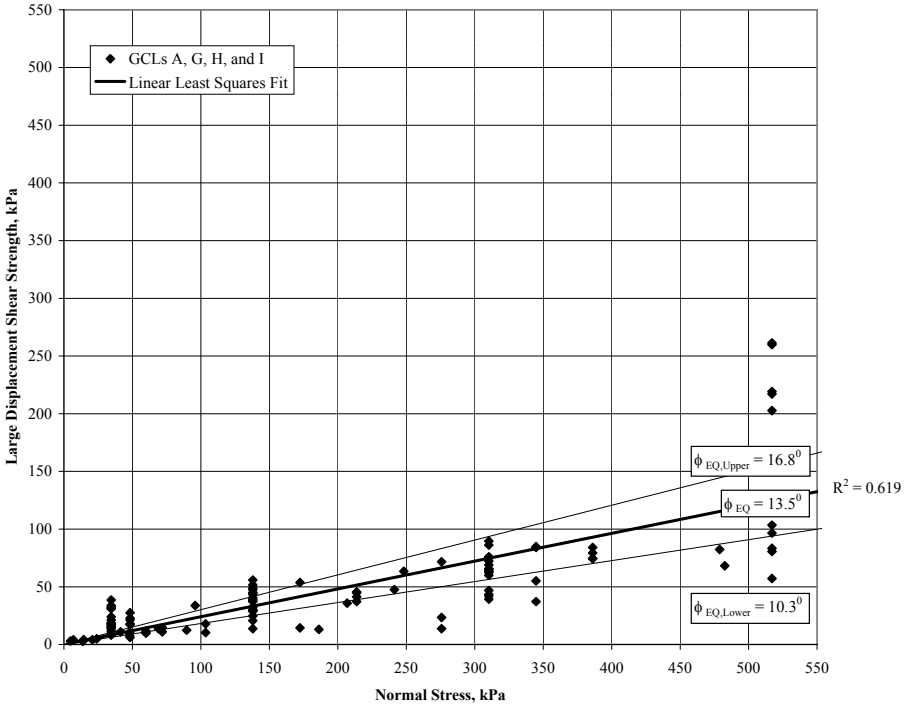

(b)

Figure 4.24: Large Displacement Shear Strength for All Bentomat GCLs (Total of 124 Tests); (a) Ranges of Equivalent Friction Angles, (b) Average Equivalent Friction Angle with Upper and Lower Bounds

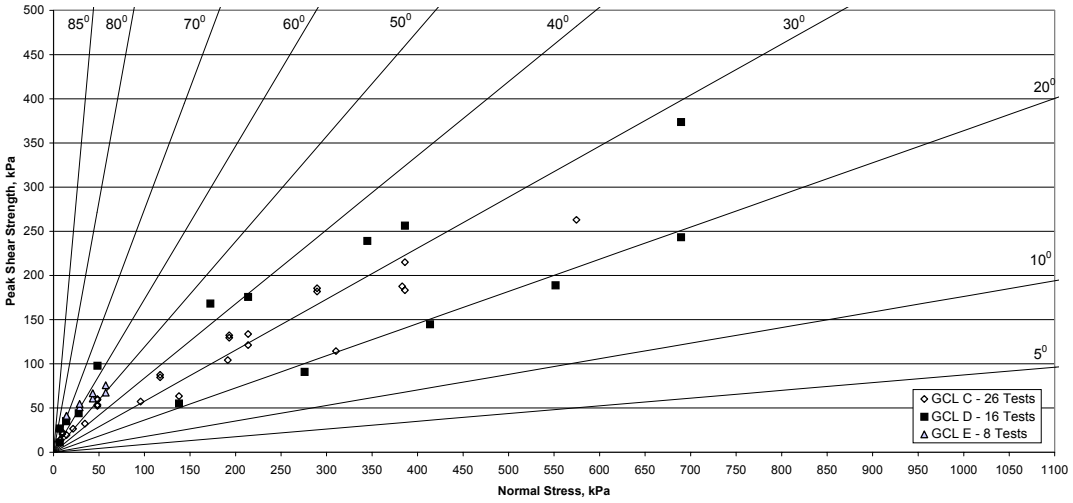

(a)

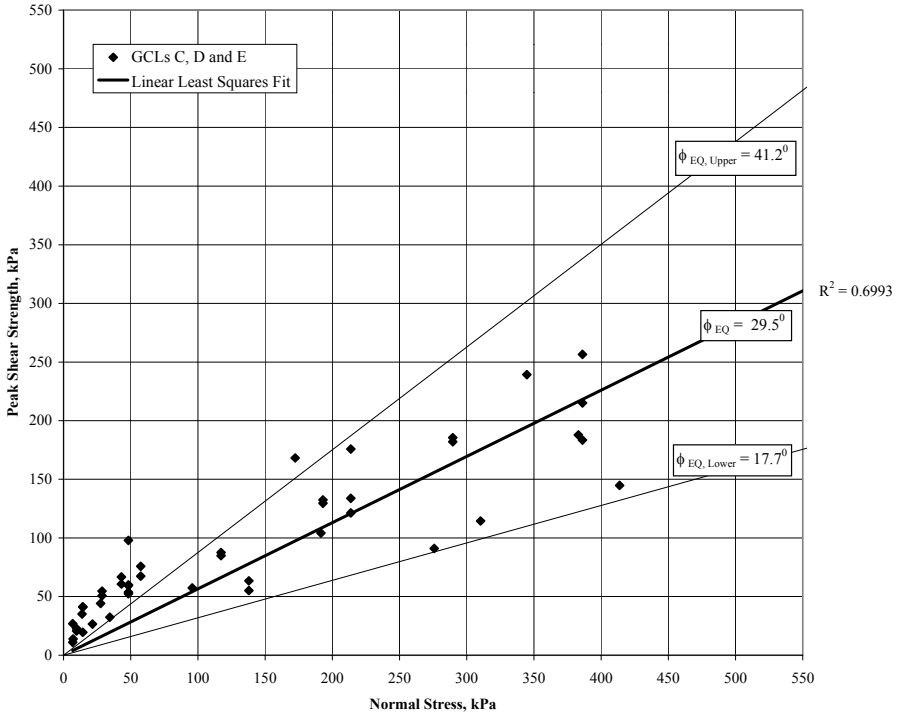

(b)

Figure 4.25: Peak Shear Strength for All Bentofix GCLs (Total of 50 Tests); (a) Ranges of Equivalent Friction Angles, (b) Average Equivalent Friction Angle with Upper and Lower Bounds

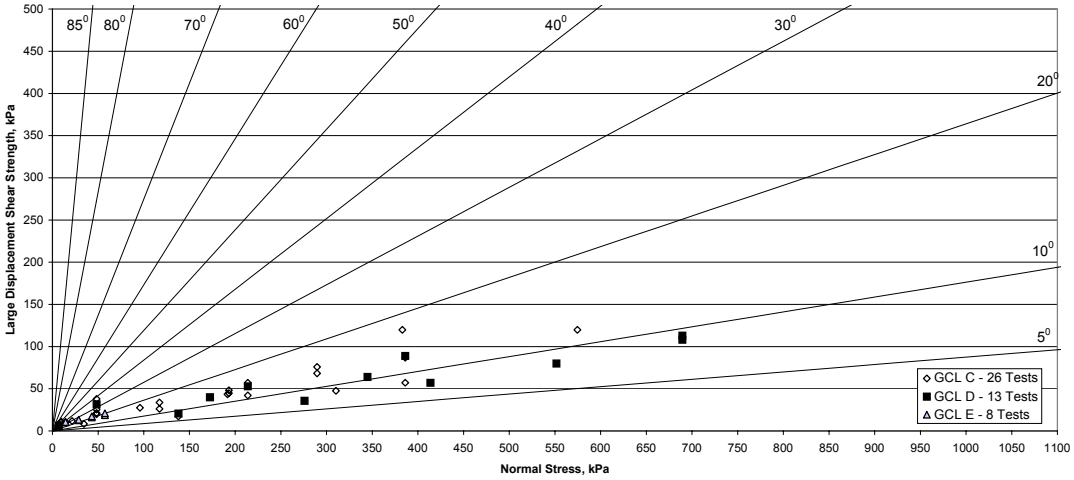

(a)

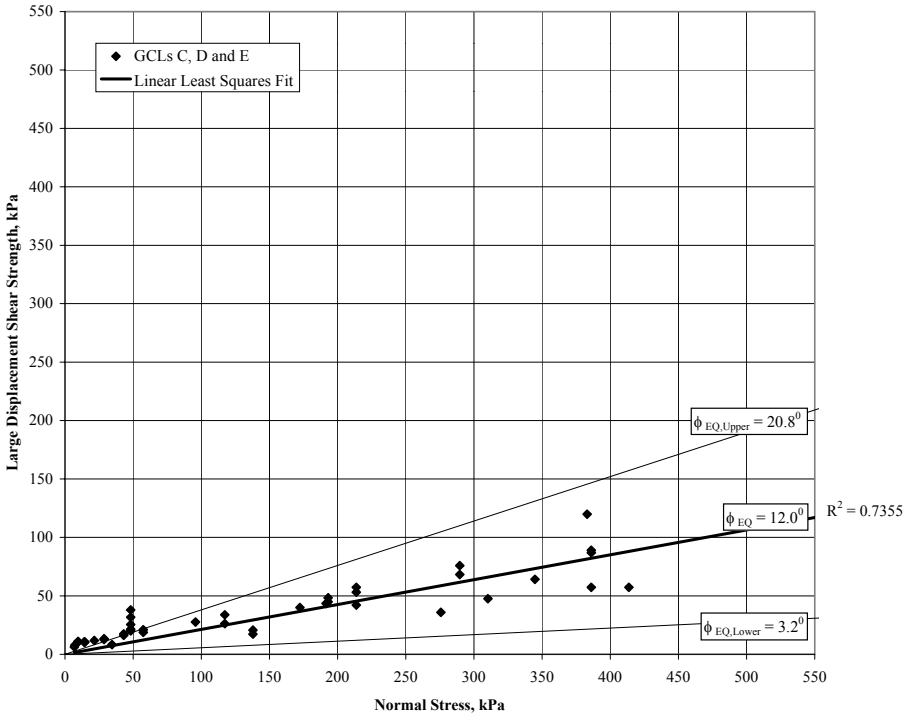

(b)

Figure 4.26: Large Displacement Shear Strength for All Bentofix GCLs (Total of 47 Tests); (a) Ranges of Equivalent Friction Angles, (b) Average Equivalent Friction Angle with Upper and Lower Bounds

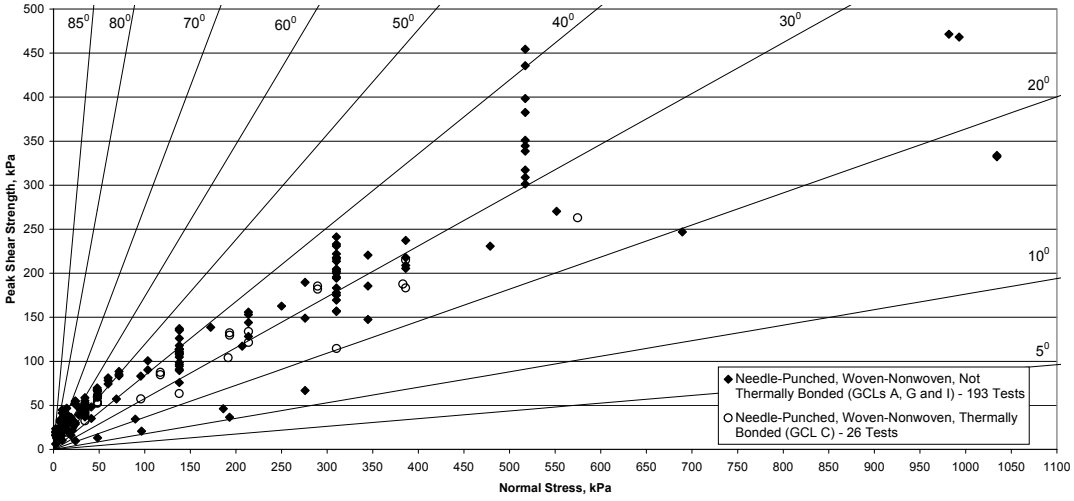

(a)

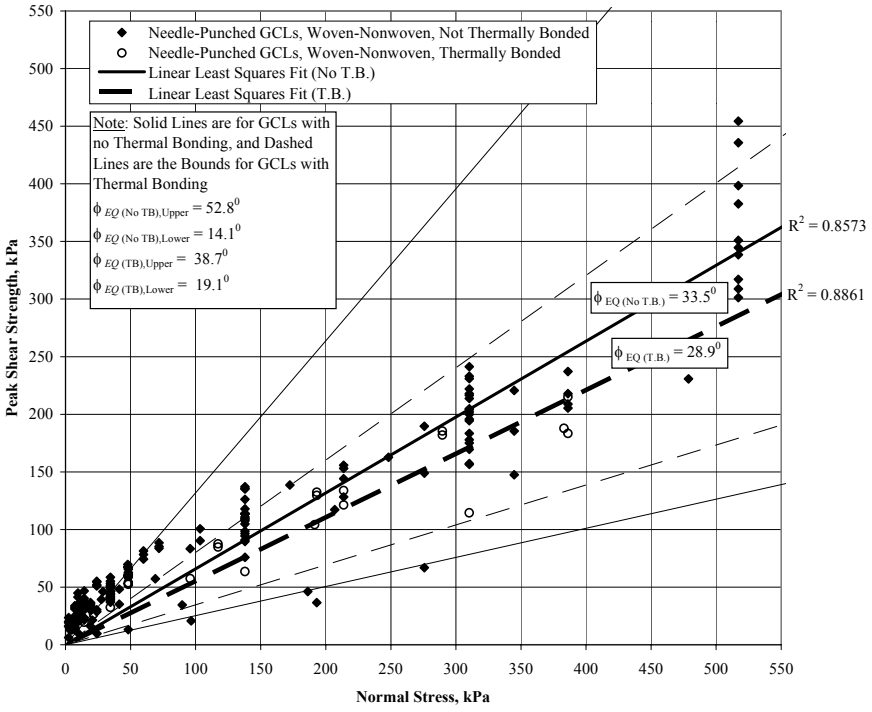

(b)

Figure 4.27: Peak Shear Strength for All Woven/Nonwoven Needle-Punched GCLs in the GCLSS Database (Total of 223 Tests); (a) Ranges of Equivalent Friction Angles, (b) Average Equivalent Friction Angles

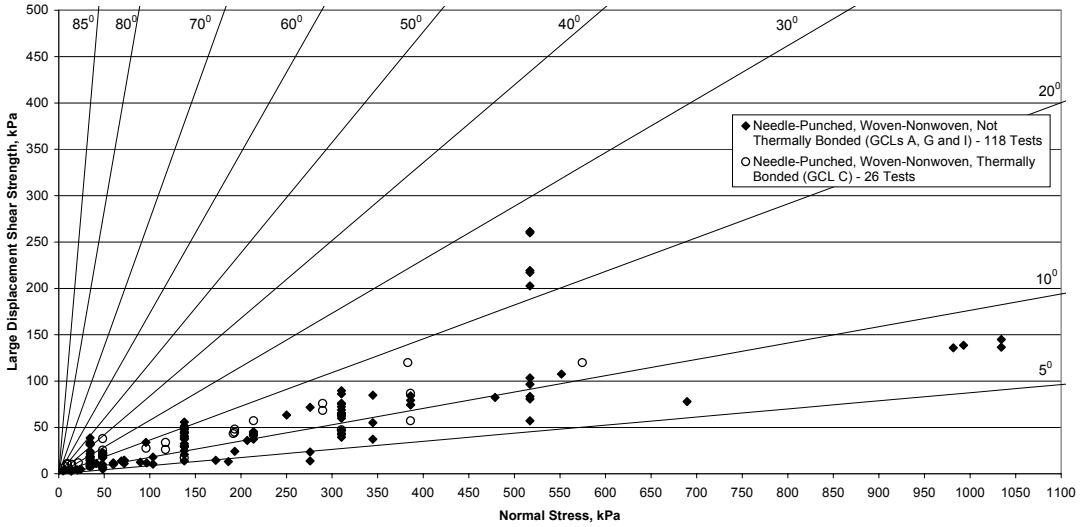

(a)

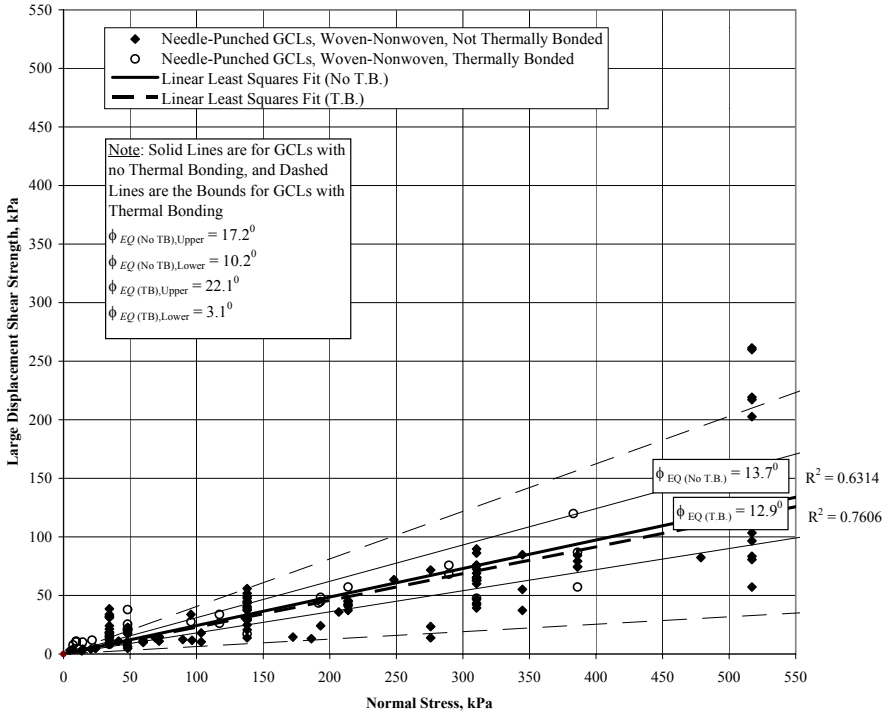

(b)

Figure 4.28: Large Displacement Shear Strength for All Woven/Nonwoven Needle Punched GCLs in the GCLSS Database (Total of 148 Tests); (a) Ranges of Equivalent Friction Angles, (b) Average Equivalent Friction Angles

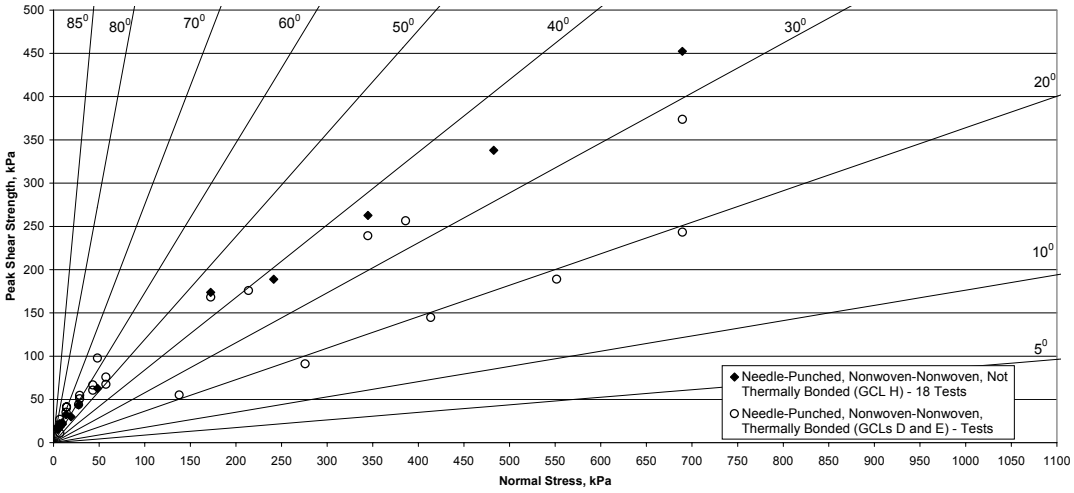

(a)

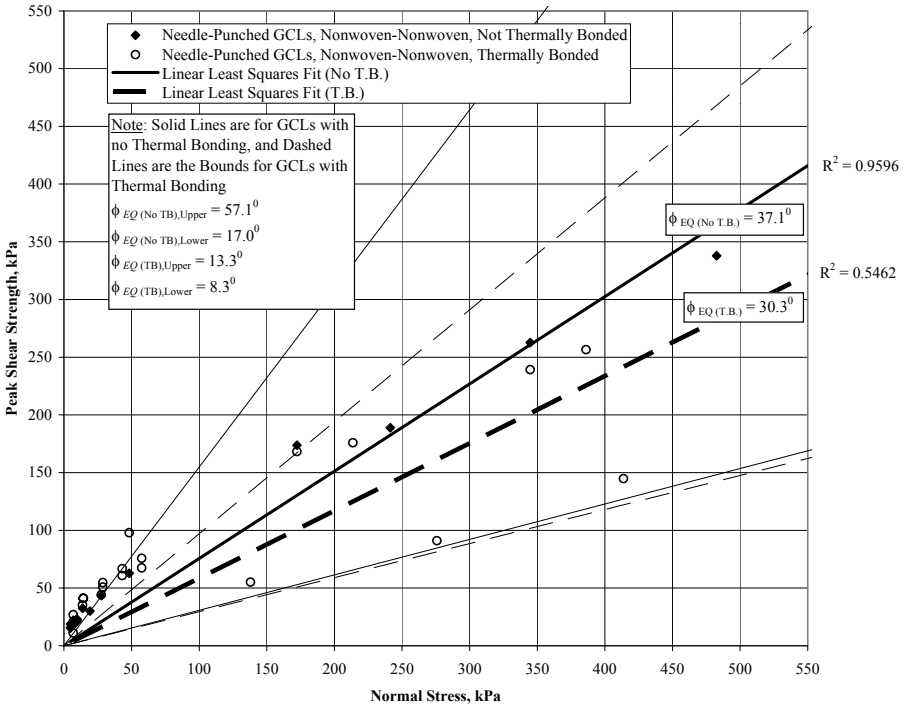

(b)

Figure 4.29: Peak Shear Strength for All Nonwoven/Nonwoven Needle-Punched GCLs in the GCLSS Database (Total of 42 Tests); (a) Ranges of Equivalent Friction Angles, (b) Average Equivalent Friction Angles

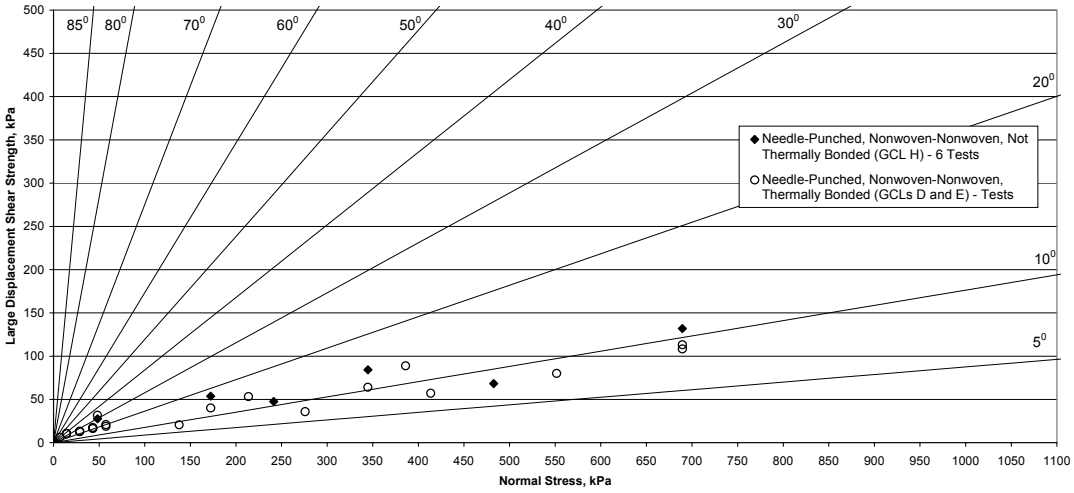

(a)

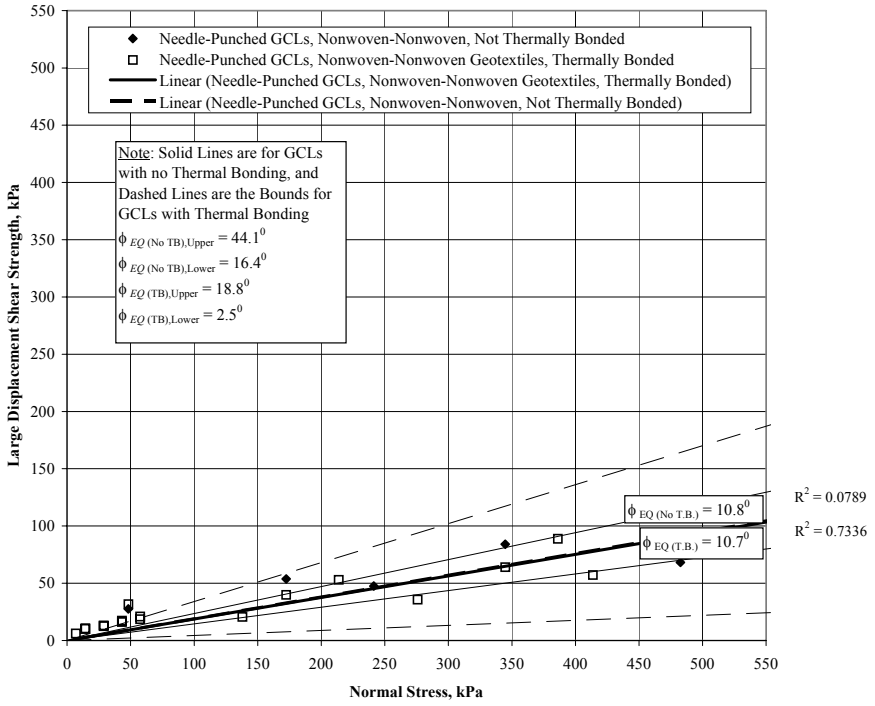

(b)

Figure 4.30: Large Displacement Shear Strength for All Nonwoven/Nonwoven Needle-Punched GCLs in the GCLSS Database (Total of 27 Tests); (a) Ranges of Equivalent Friction Angles, (b) Average Equivalent Friction Angles

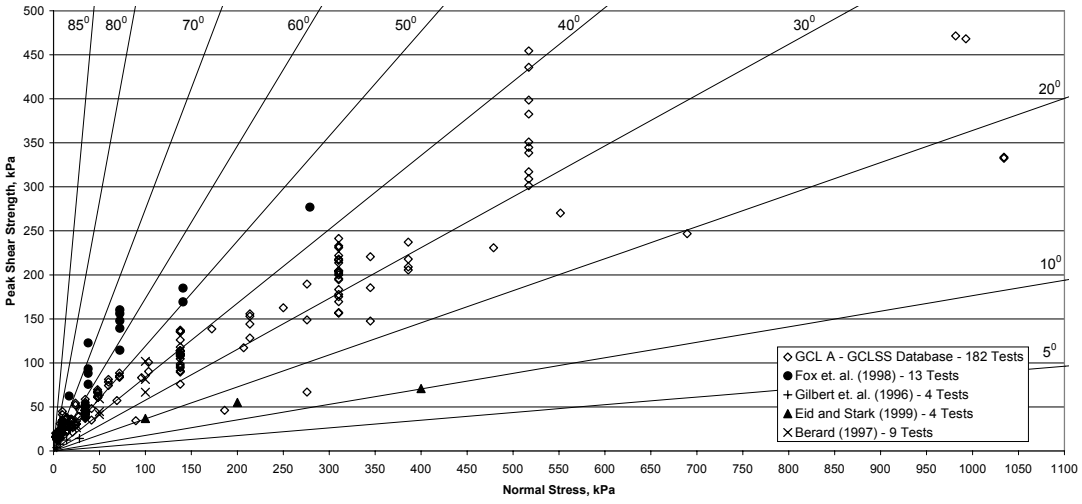

(a)

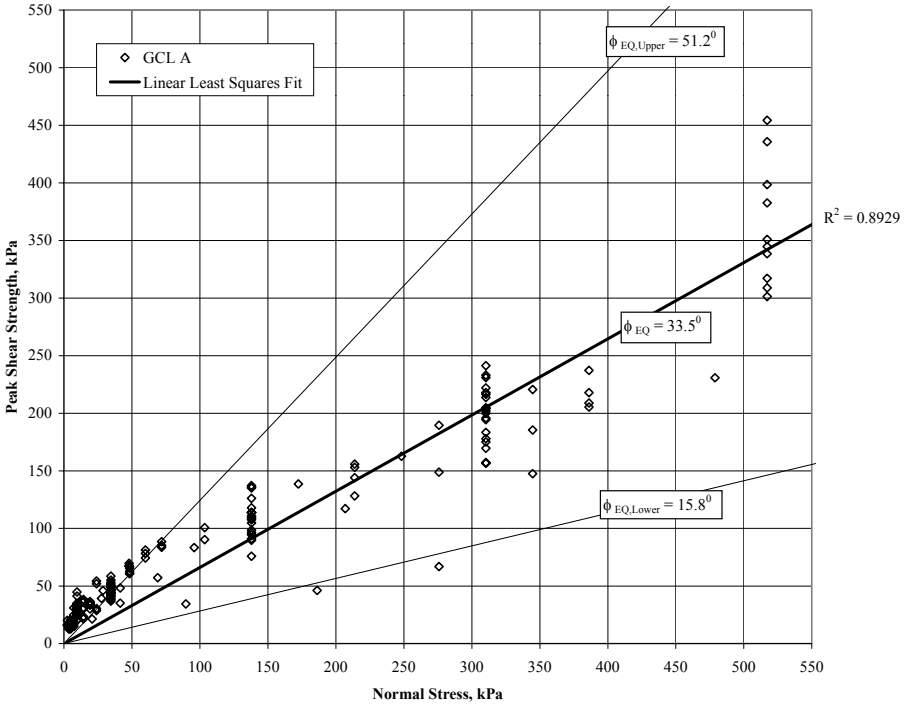

(b)

Figure 4.31: Peak Shear Strengths Test Results for GCL A; (a) Ranges of Equivalent Friction Angles (with Test Results Reported by Other Studies), (b) Average Equivalent Friction Angle with Upper and Lower Bounds (Other Test Results are Not Included)

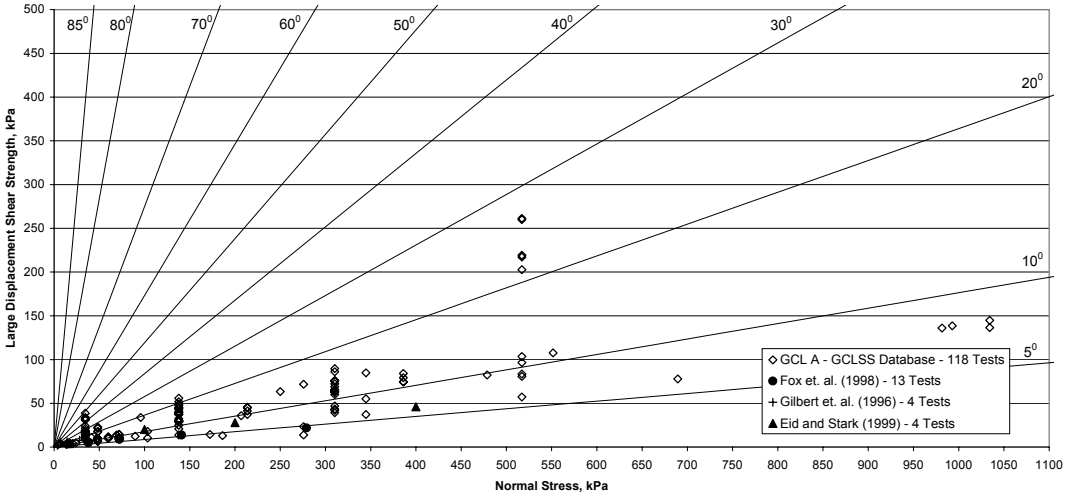

(a)

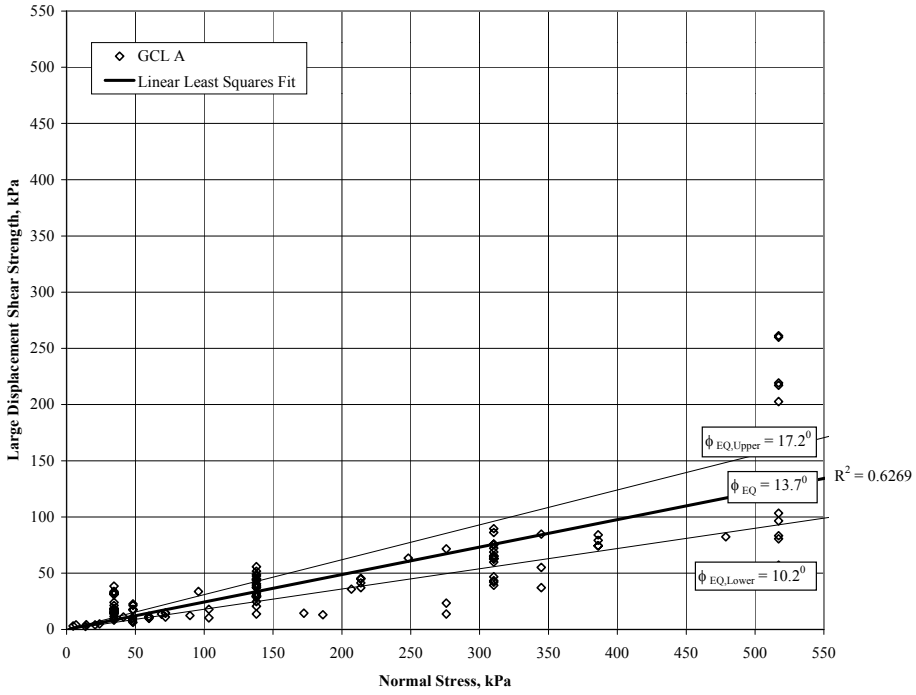

(b)

Figure 4.32: Large Displacement Shear Strengths Test Results for GCL A; (a) Ranges of Equivalent Friction Angles (with Test Results Reported by Other Studies), (b) Average Equivalent Friction Angle with Upper and Lower Bounds (Other Test Results are Not Included)

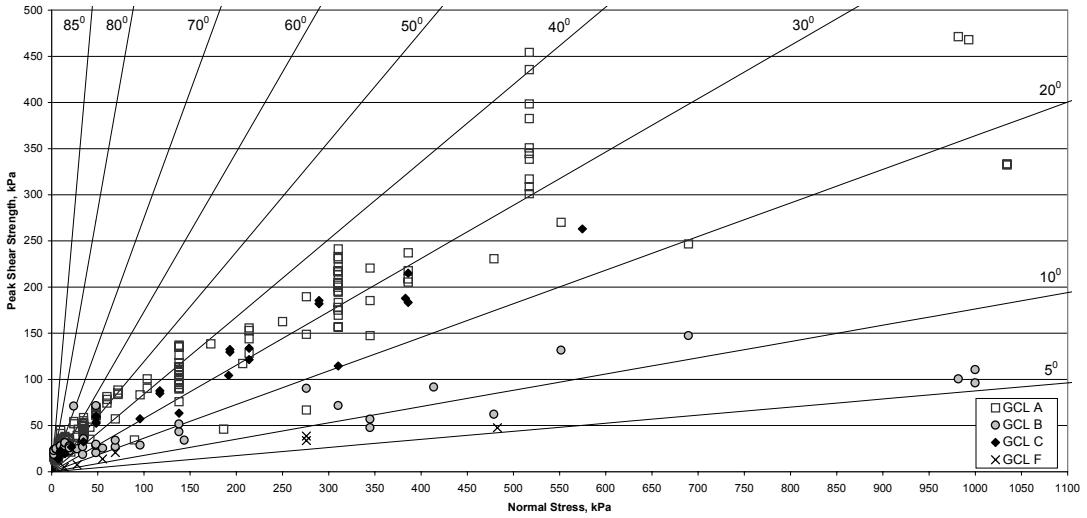

(a)

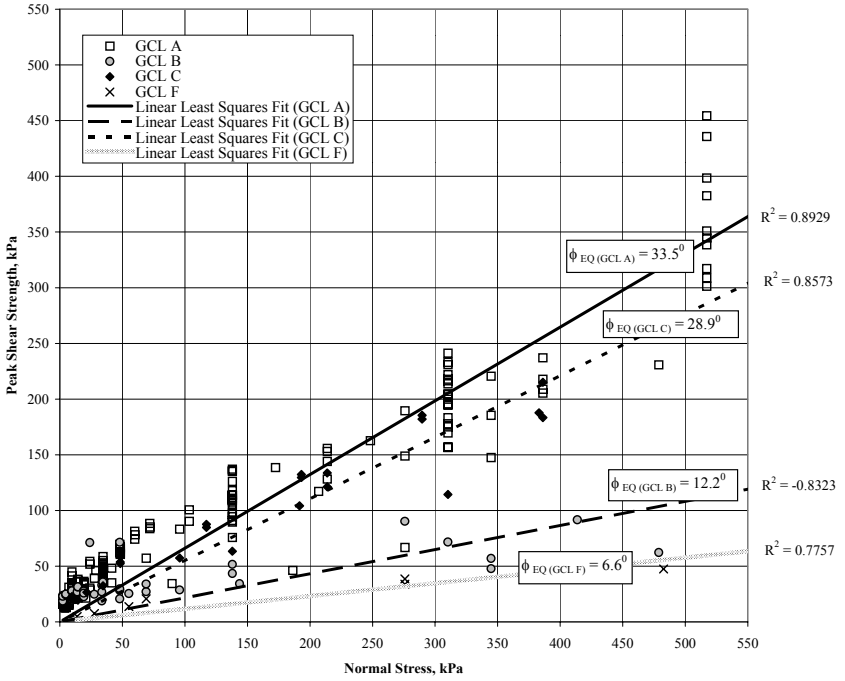

(b)

Figure 4.33: Peak Shear Strength for Four GCL Types – Needle-Punched (GCL A), Stitch-Bonded (GCL B), Needle-Punched with Thermal Bonding (GCL C) GCLs, and Unreinforced (GCL F) ; (a) Ranges of Equivalent Friction Angles, (b) Equivalent Friction Angles

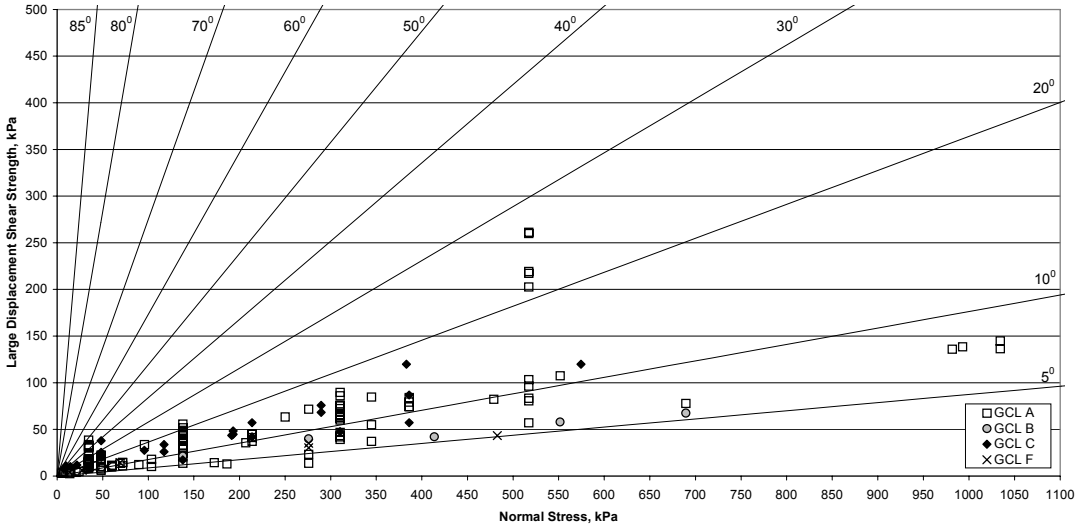

(a)

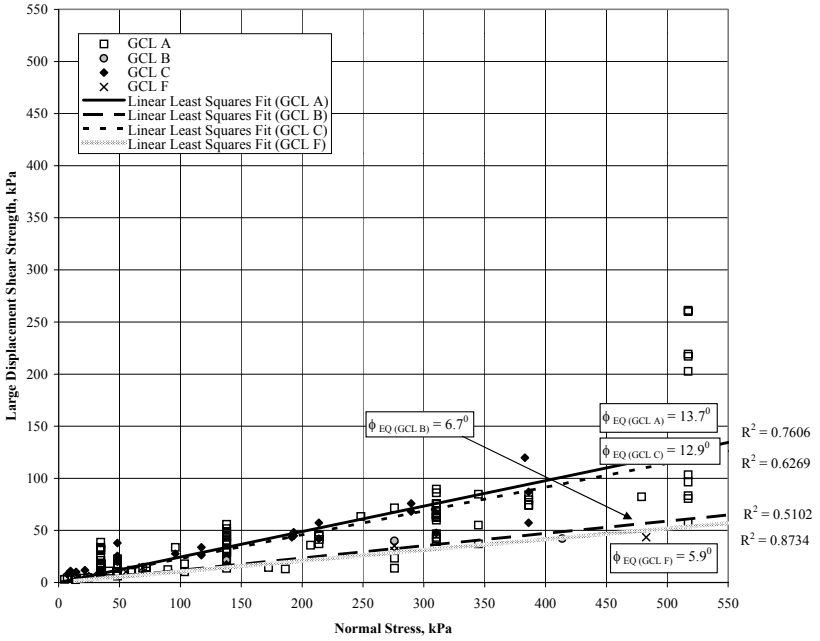

(b)

Figure 4.34: Large Displacement Shear Strength for Four GCL Types – Needle-Punched with no Thermal Bonding (GCL A), Stitch-Bonded (GCL B) , Needle-Punched with Thermal Bonding (GCL C) GCLs, and Unreinforced (GCL F) ; (a) Ranges of Equivalent Friction Angles, (b) Equivalent Friction Angles

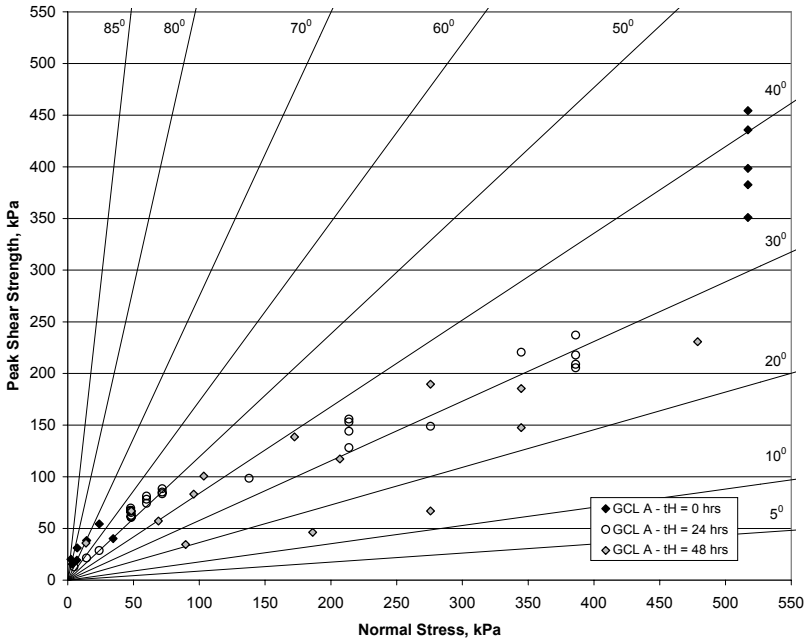

(a)

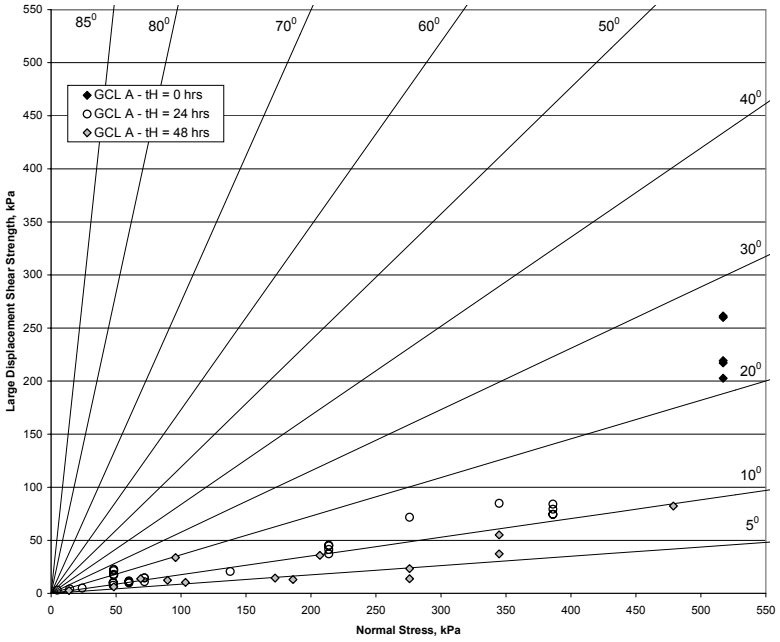

(b)

Figure 4.35: Effect of the Time of Hydration on the Shear Strength of GCL A (a) Peak Shear Strength, (b) Large Displacement Shear Strength

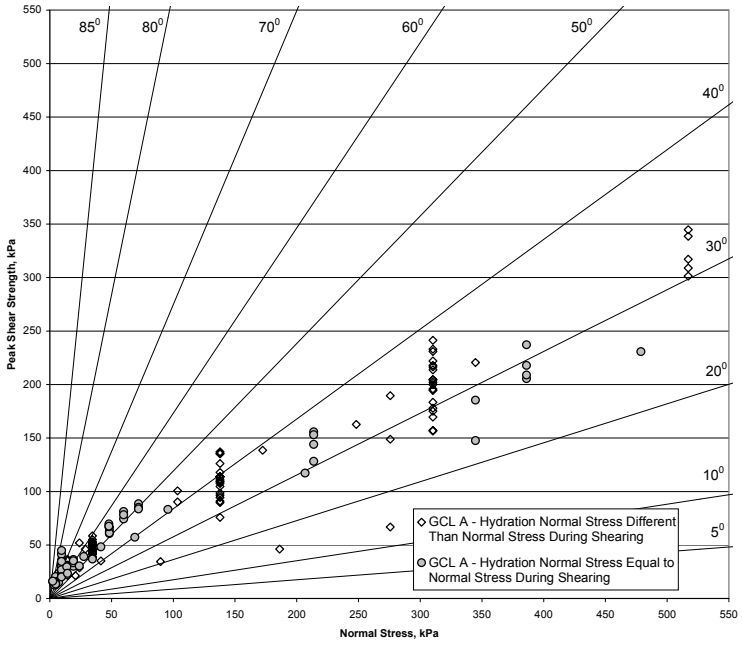

(a)

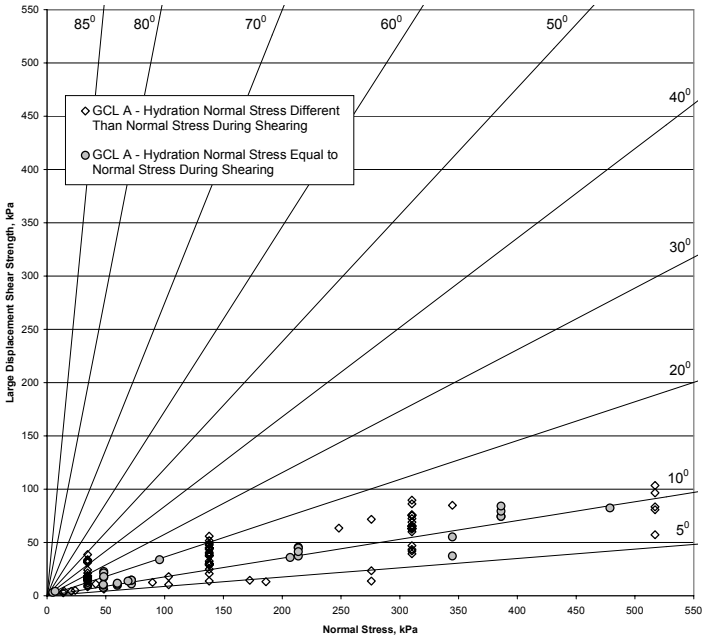

(b)

Figure 4.36: Effect of the Hydration Normal Stress on the Shear Strength of GCL A (a) Peak Shear Strength, (b) Large Displacement Shear Strength

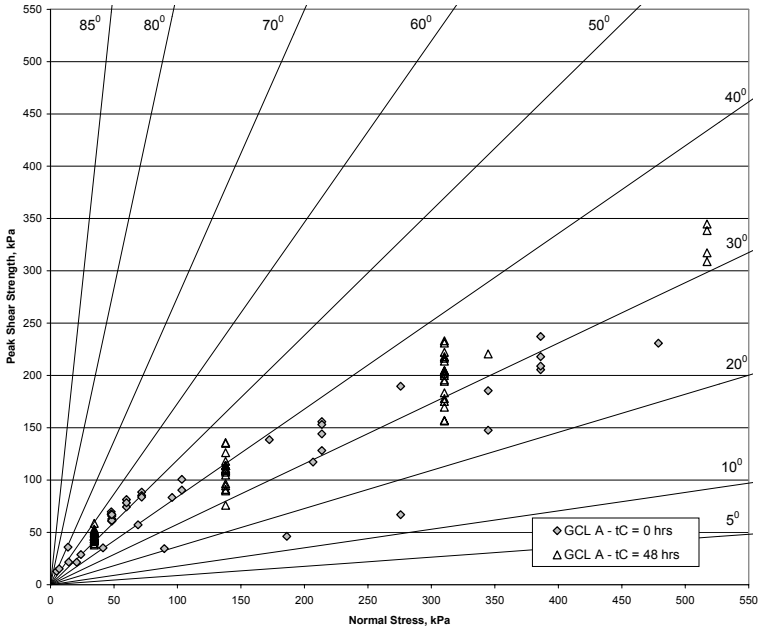

(a)

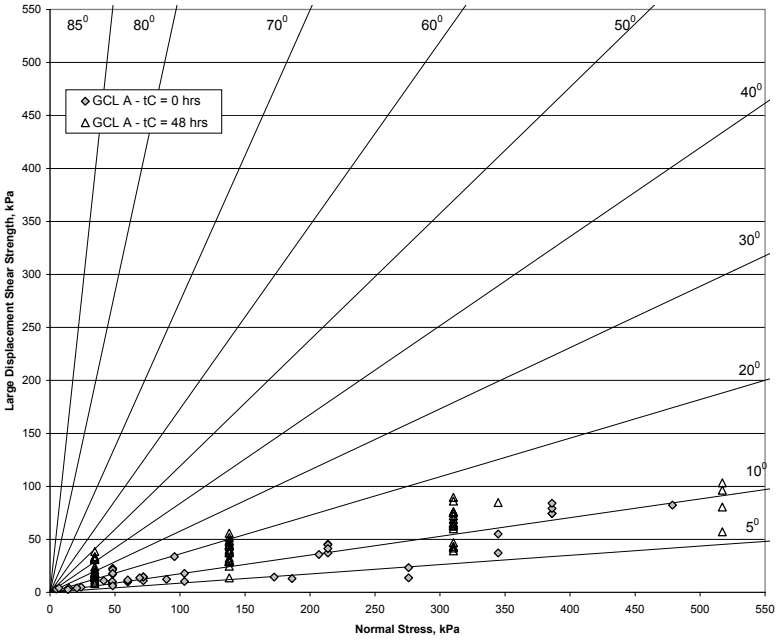

(b)

Figure 4.37: Effect of the Time of Consolidation on the Shear Strength of GCL A (a) Peak Shear Strength, (b) Large Displacement Shear Strength

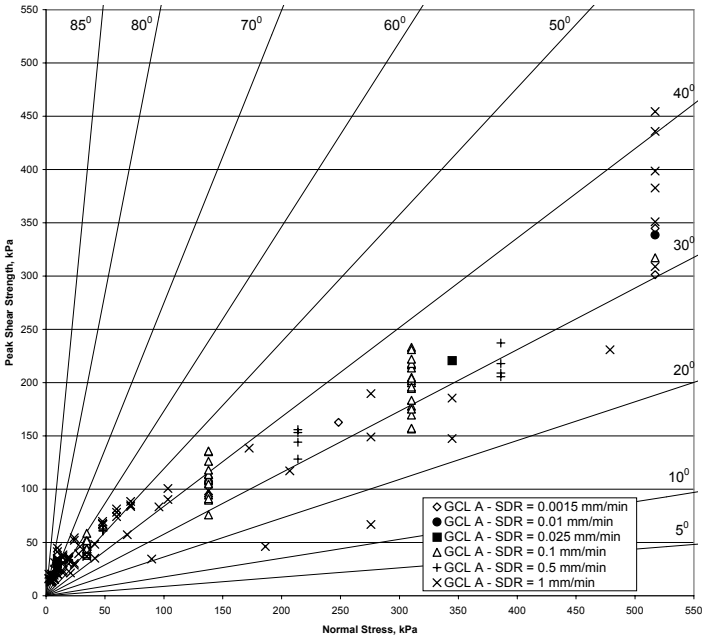

(a)

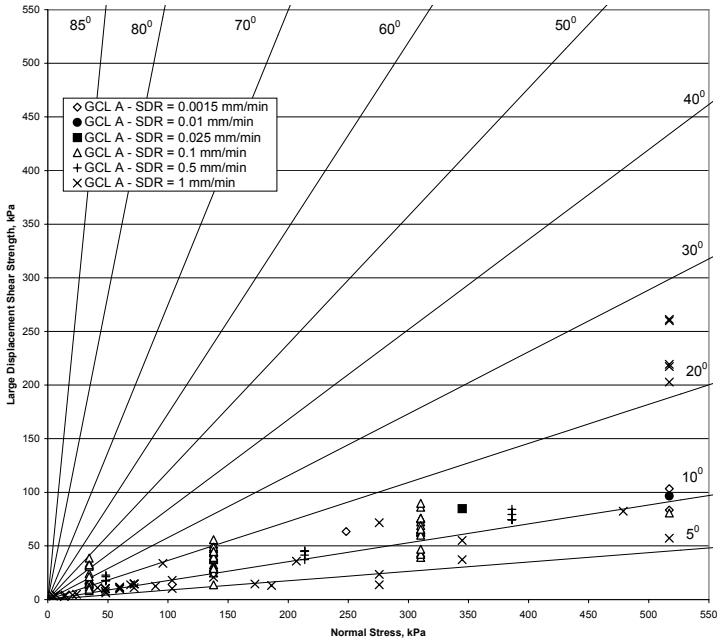

(b)

Figure 4.38: Effect of the Shear Displacement Rate on the Shear Strength of GCL A (a) Peak Shear Strength, (b) Large Displacement Shear Strength

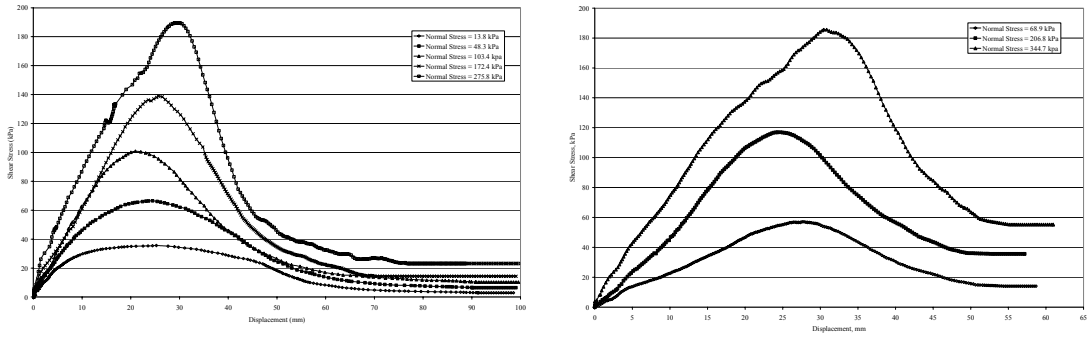

(a) (b)

Figure 4.39: Shear Force-Displacement Behavior for Hydrated GCL A, Contact Area is 300 mm by 300 mm, (a) Low Range of Normal Stresses (b) High Range of Normal Stress (t_H = 48 hours, t_C = 0 hours, SDR = 1.0 mm/min)

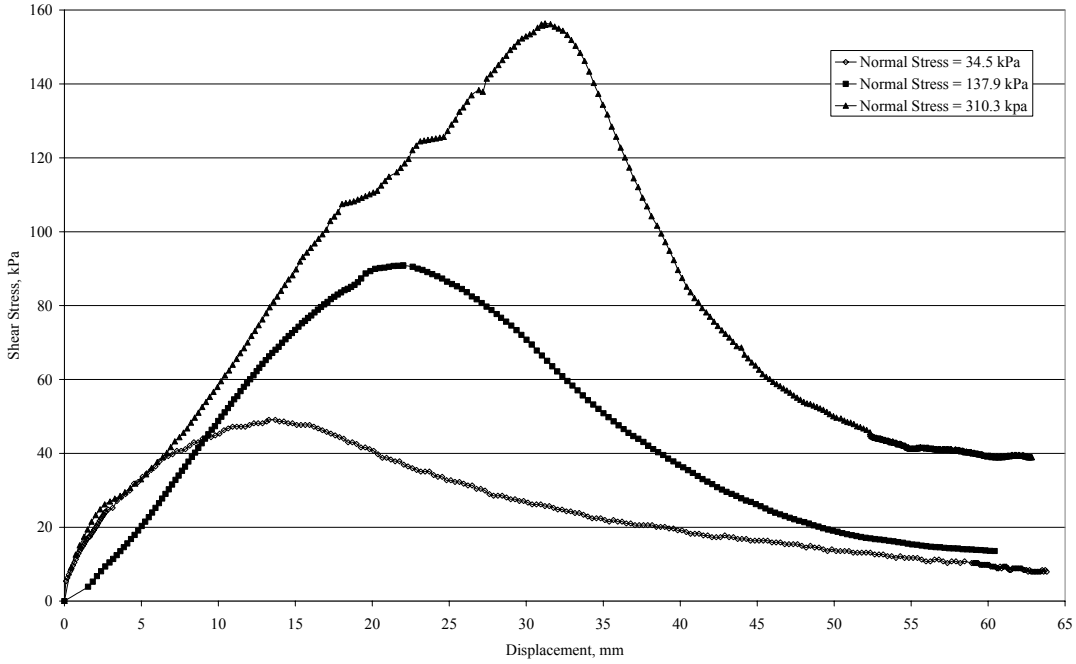

Figure 4.40: Shear Force-Displacement Behavior for GCL A, Contact Area is 300 mm by 300 mm (t_H = 168 hours, t_C = 48 hours, SDR = 0.1 mm/min)

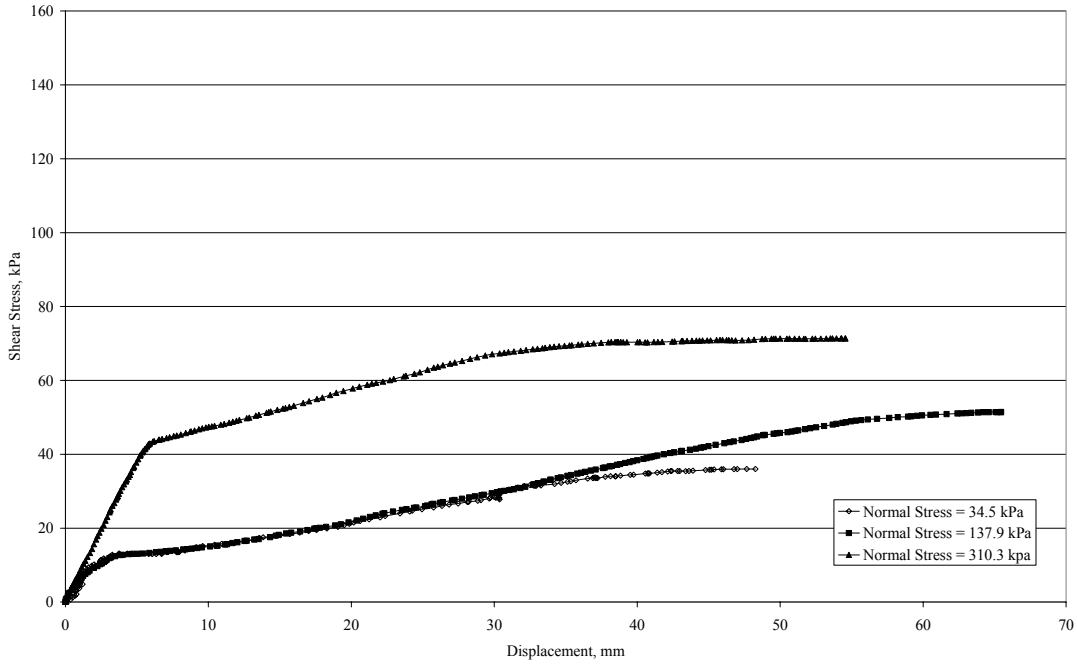

Figure 4.41: Shear Force-Displacement Behavior for GCL B, Contact Area is 300 mm by 300 mm (t_H = 168 hours, t_C = 48 hours, SDR = 0.1 mm/min)

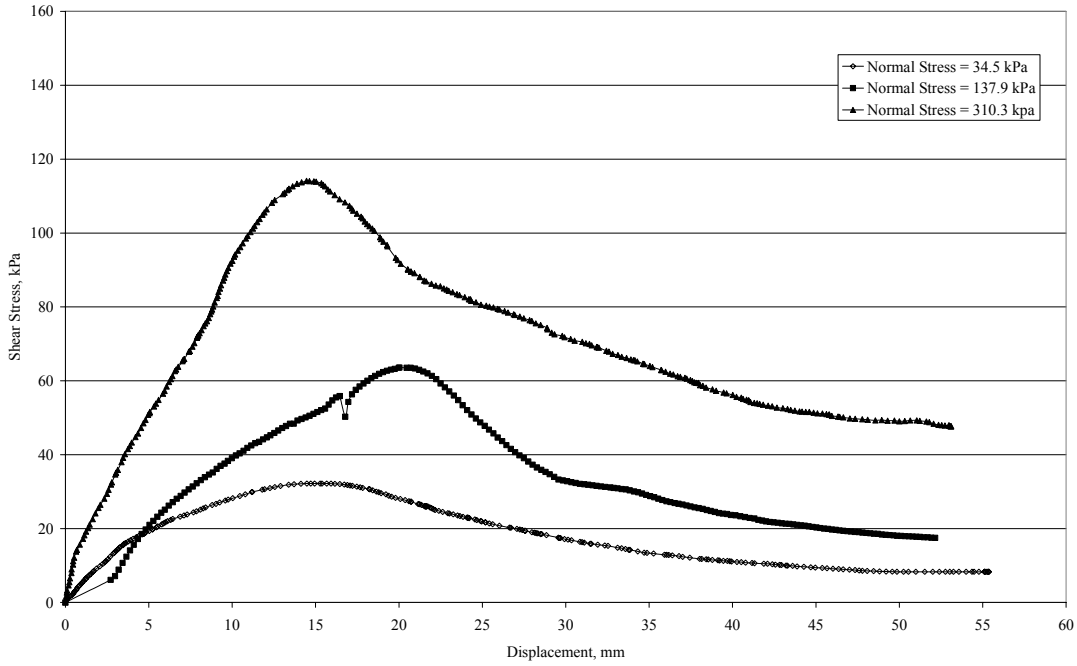

Figure 4.42: Shear Force-Displacement Behavior for GCL C, Contact Area is 300 mm by 300 mm (t_H = 168 hours, t_C = 48 hours, SDR = 0.1 mm/min)

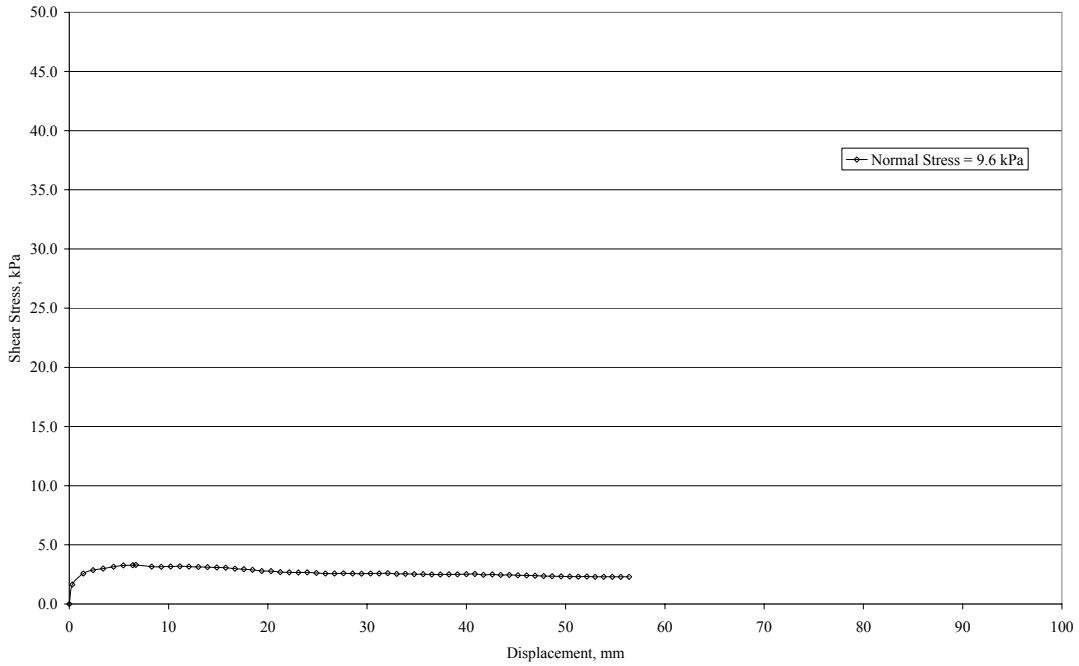

Figure 4.43: Shear Force-Displacement Behavior for GCL F Under Soaked Shear Strength, Contact Area is 300 mm by 300 mm

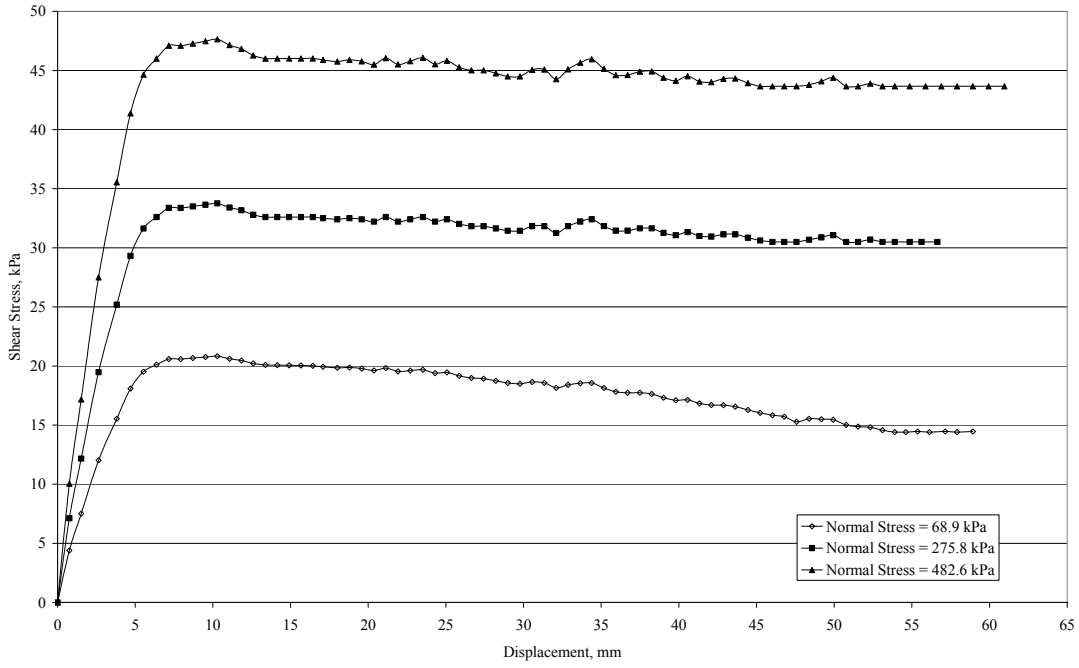

Figure 4.44: Shear Force-Displacement Behavior for GCL F Under Unhydrated Conditions, Contact Area is 300 mm by 300 mm

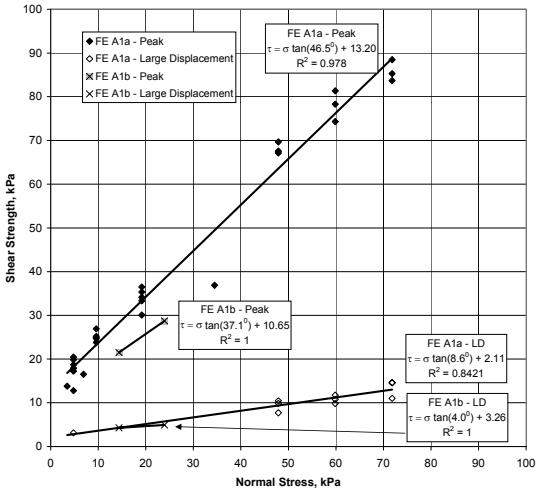

Figure 4.45: Peak and Large Displacement Shear Strength Failure Envelopes for GCL A (FE A1a and A1b: t_H = 24 hours, t_C = 0 hours, and SDR = 1.0 mm/min); *FE A1a is the Baseline Failure Envelope for GCL A*

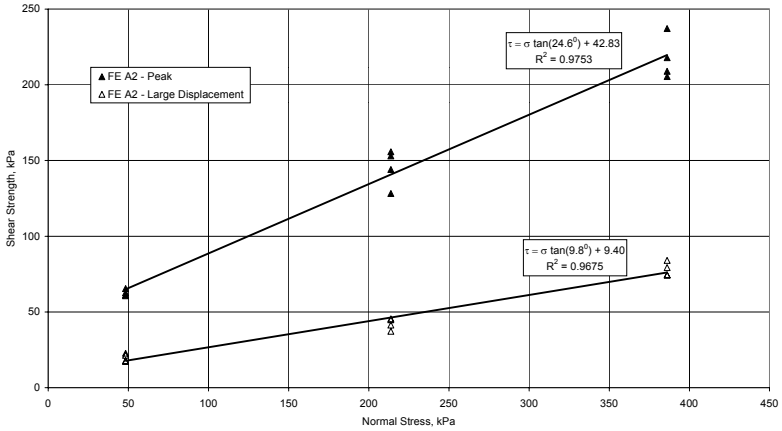

Figure 4.46: Peak and Large Displacement Shear Strength Failure Envelopes for GCL A (FE A2: t_H = 24 hours, t_C = 0 hours, and SDR = 0.5 mm/min); *Change in SDR from the Baseline*

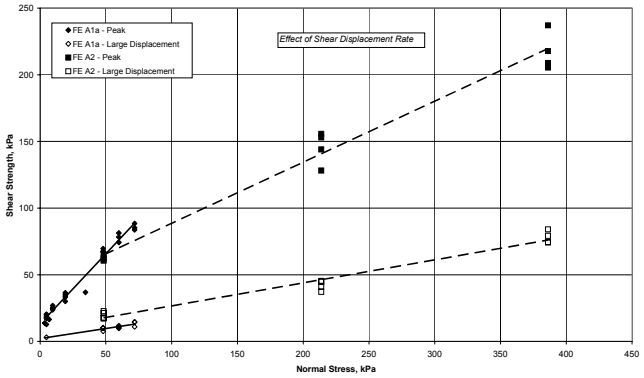

Figure 4.47: Comparison between Failure Envelopes A1 and A2

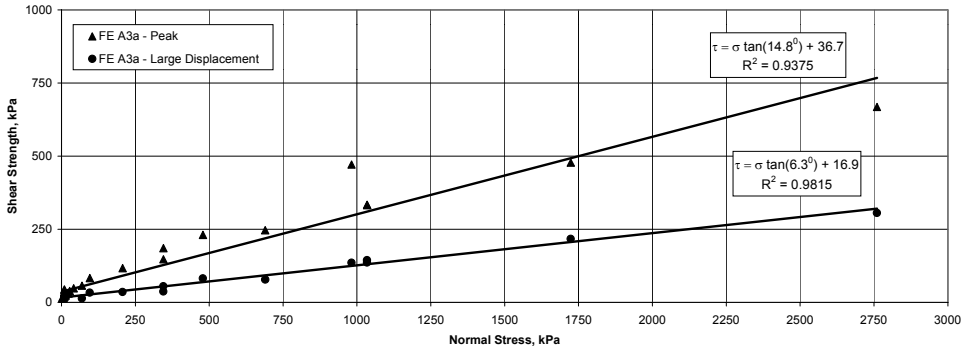

(a)

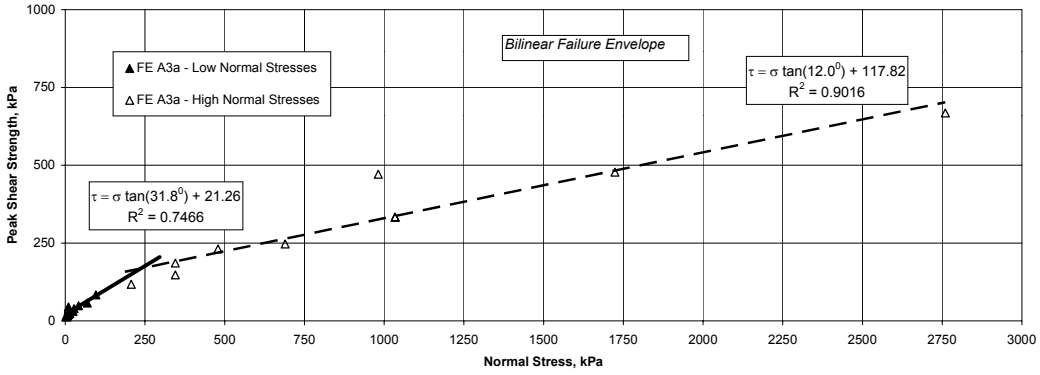

(b)

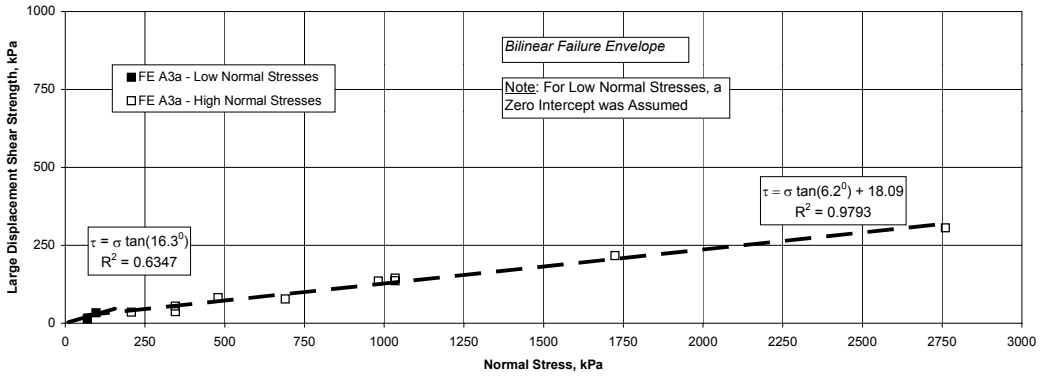

(c)

Figure 4.48: Peak and Large Displacement Shear Strength Failure Envelopes for GCL A (FE A3a: t_H = 48 hours, t_C = 0 hours, and SDR = 1.0 mm/min); (a) Linear Fit, (b) Bilinear Fit Peak, (c) Bilinear Fit Large Displacement

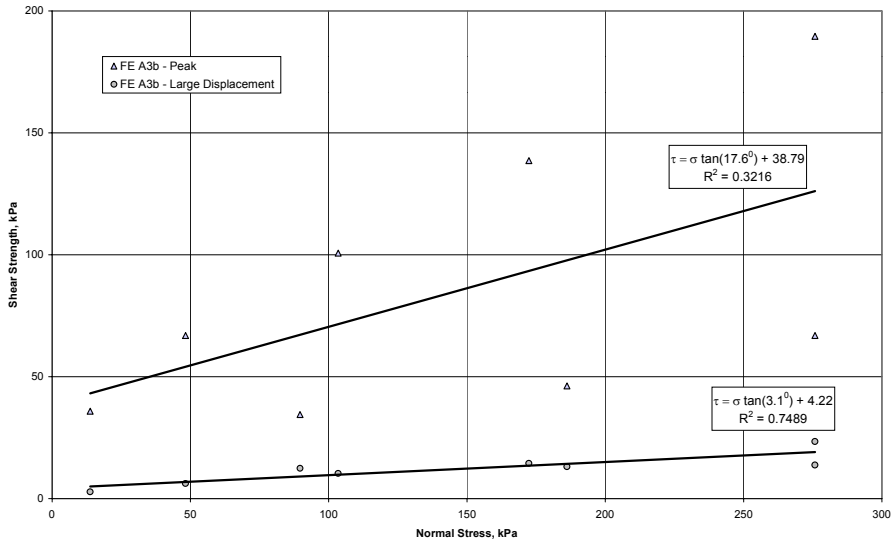

Figure 4.49: Peak and Large Displacement Shear Strength Failure Envelopes for GCL A (FE A3b: t_H = 48 hours, t_C = 0 hours, Hydration Normal Stress = 4.8 kPa, and SDR = 1.0 mm/min); *Change in t_H from the Baseline*

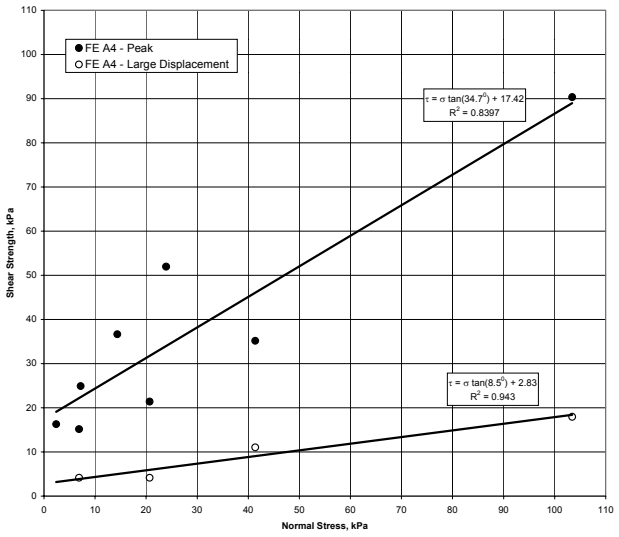

Figure 4.50: Peak and Large Displacement Shear Strength Failure Envelopes for GCL A (FE A4: t_H = 72 hours, t_C = 0 hours, and SDR = 1.0 mm/min); *Change in t_H from the Baseline*

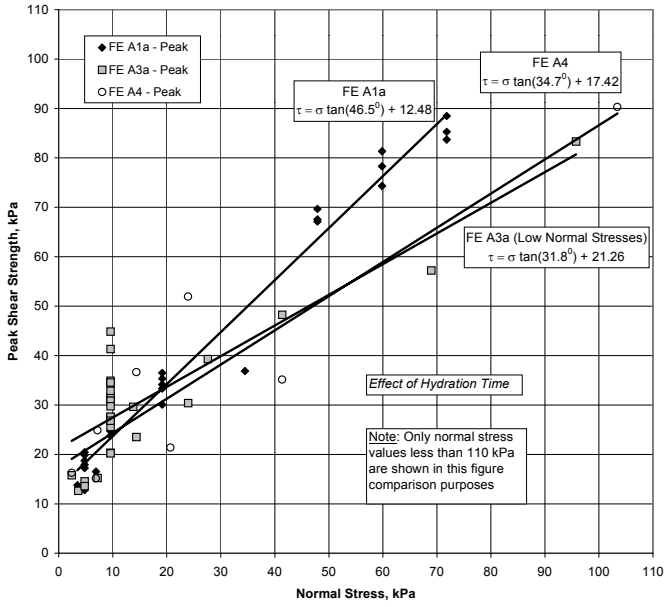

(a)

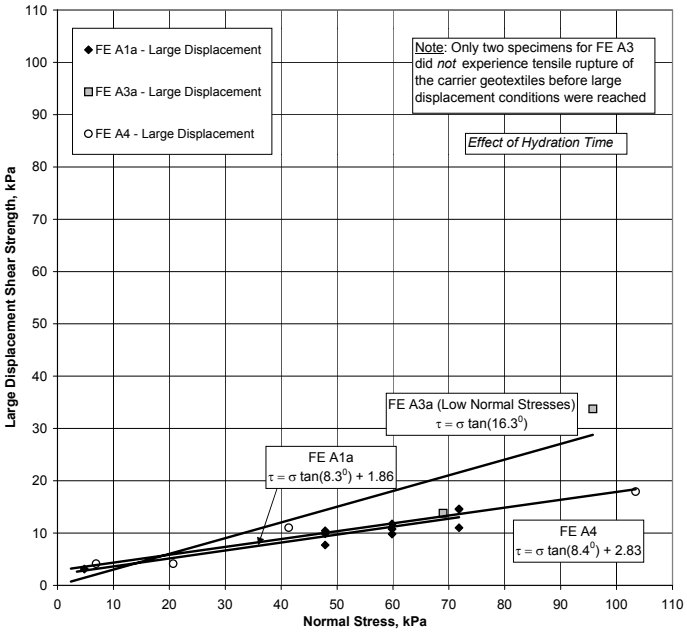

(b)

Figure 4.51: Peak and Large Displacement Shear Strength Failure Envelopes for GCL A (FE A1, A3 and A4: t_H = 24, 48 and 72 hours, respectively, t_C = 0 hours, and SDR = 1.0 mm/min); *Effect of Increasing t_H;* (a) Peak Shear Strength, (b) Large Displacement Shear Strength

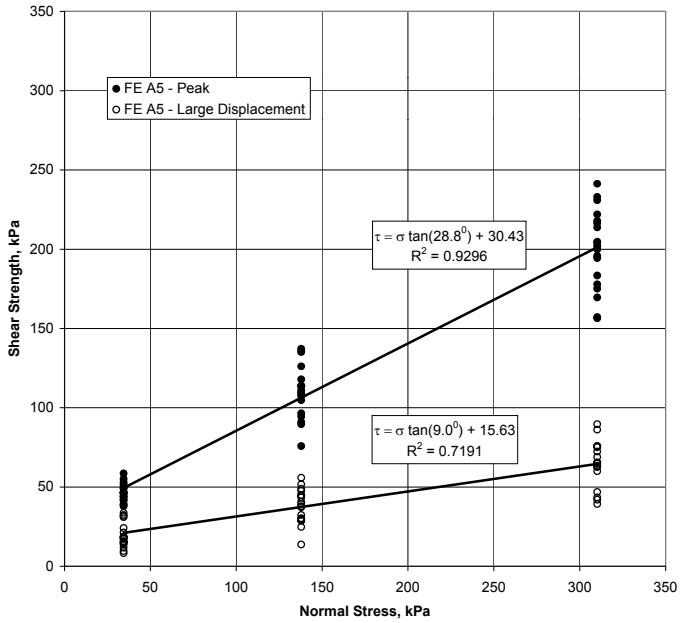

Figure 4.52: Peak and Large Displacement Shear Strength Failure Envelopes for GCL A (FE A5: t_H = 168 hours, t_C = 48 hours, and SDR = 0.1 mm/min); *Change in t_H, t_C and SDR from the Baseline*

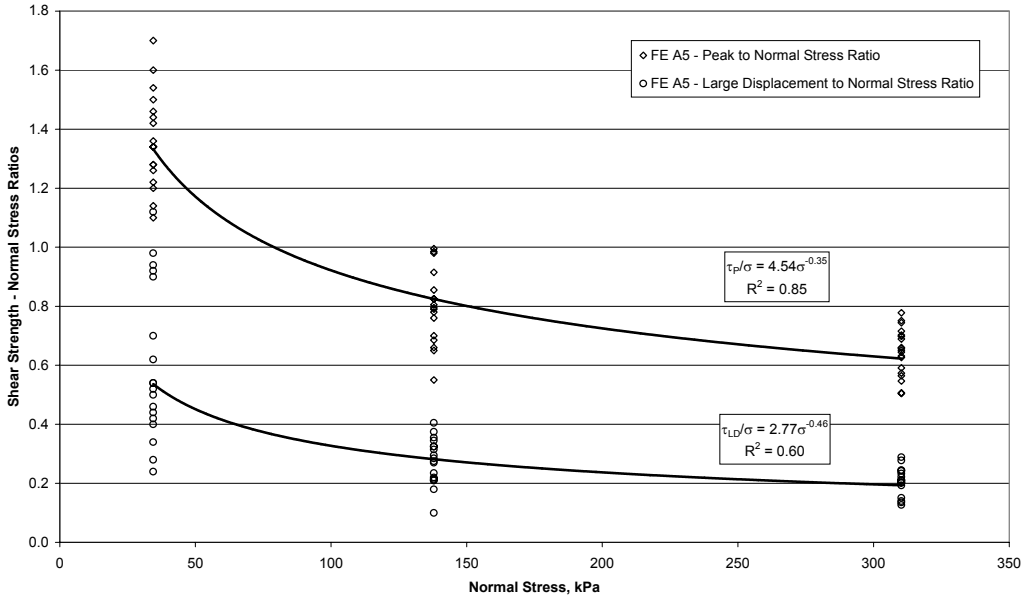

Figure 4.53: Ratios between Peak or Large Displacement Shear Strength and Normal Stress Plotted Against Normal Stress for GCL A (FE A5: t_H = 168 hours, t_C = 48hours, and SDR = 0.1 mm/min)

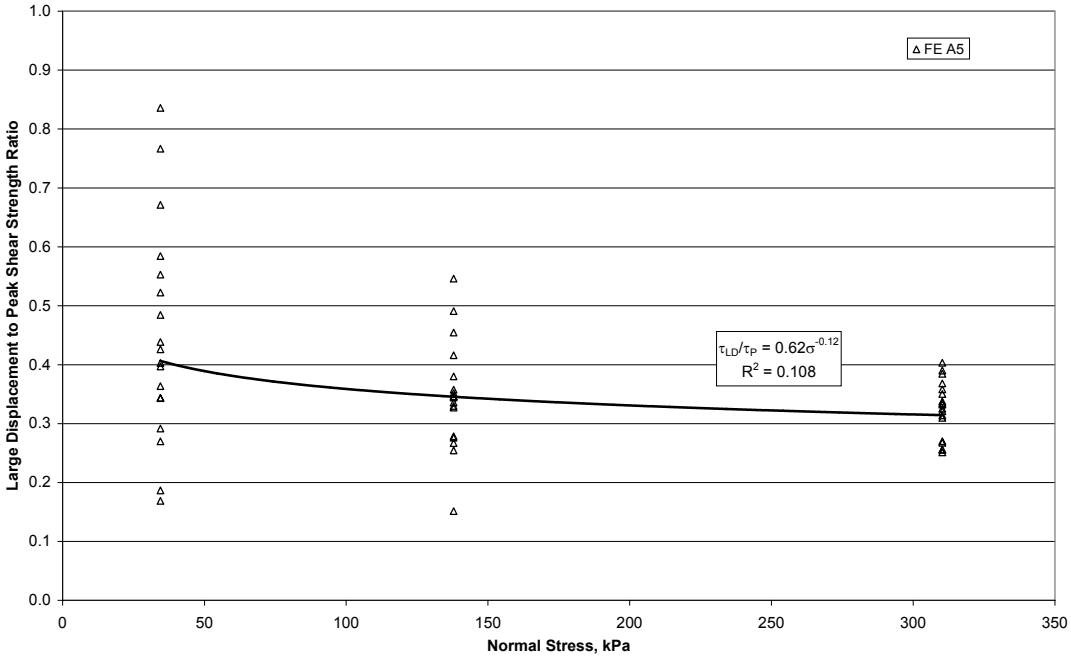

Figure 4.54: Ratio between the Large Displacement Shear Strength and Peak Shear Strengths Plotted Against Normal Stress for GCL A (FE A5: t_H = 168 hours, t_C = 48 hours, and SDR = 0.1 mm/min)

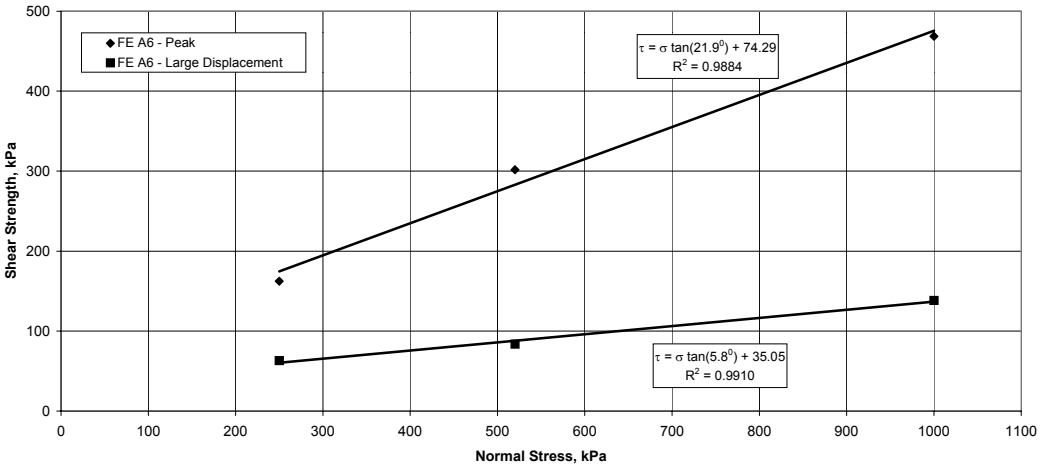

Figure 4.55: Peak and Large Displacement Shear Strength Failure Envelopes for GCL A (FE A6: Staged Hydration and Consolidation and SDR = 0.0015 mm/min); *Change in t_H, t_C and SDR from the Baseline*

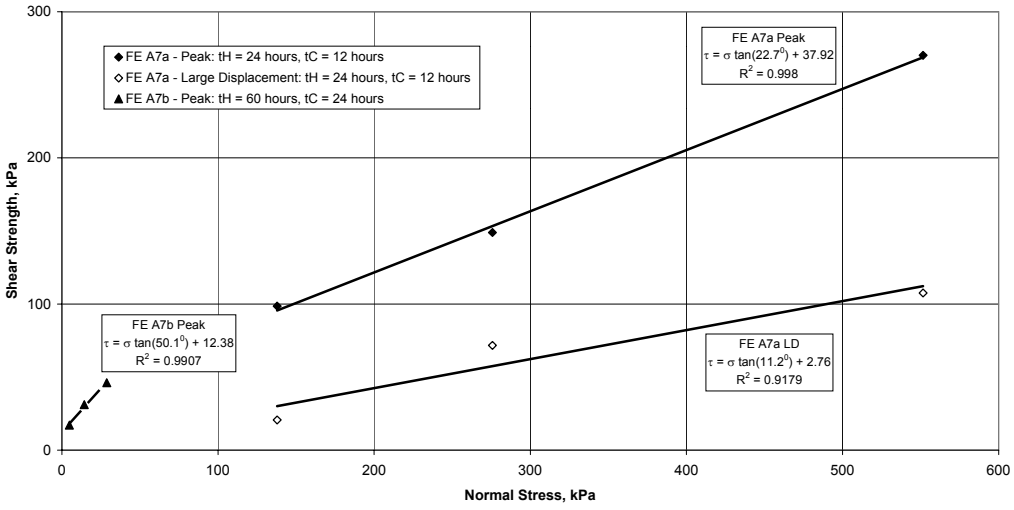

Figure 4.56: Peak and Large Displacement Shear Strength Failure Envelopes for GCL A (FE A7a and A7b: SDR = 1.0 mm/min); *Change in t_H and t_C from the Baseline*

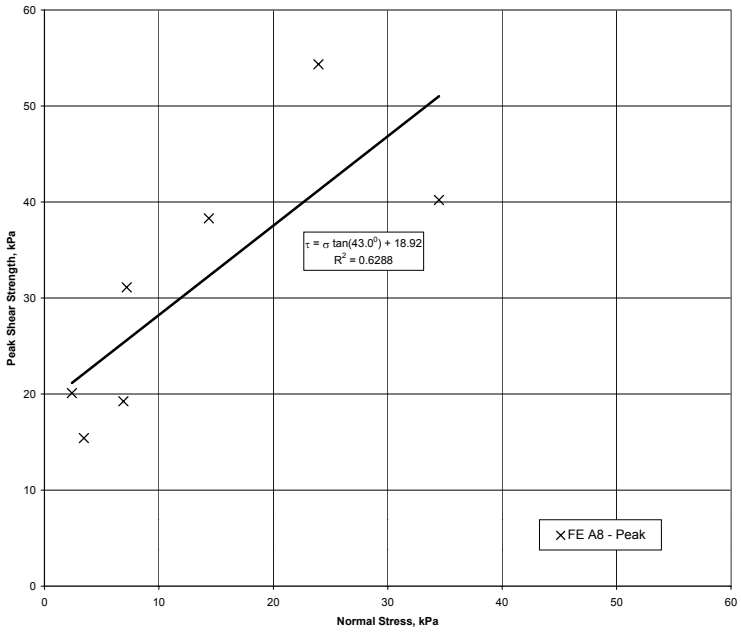

Figure 4.57: Peak Shear Strength Failure Envelope for GCL A (FE A8: Unhydrated and Unconsolidated, and SDR = 1.0 mm/min); *Change in t_H from the Baseline*

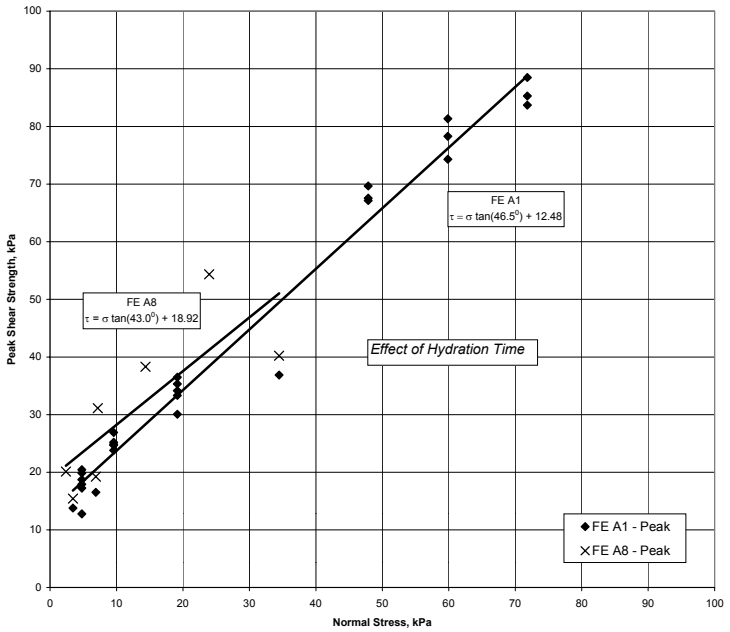

Figure 4.58: Peak and Large Displacement Shear Strength Failure Envelopes for GCL A (FE A1, A8: t_H = 24 and 0 hours, respectively, t_C = 0 hours, and SDR = 1.0 mm/min); *Effect of Decreasing t_H*

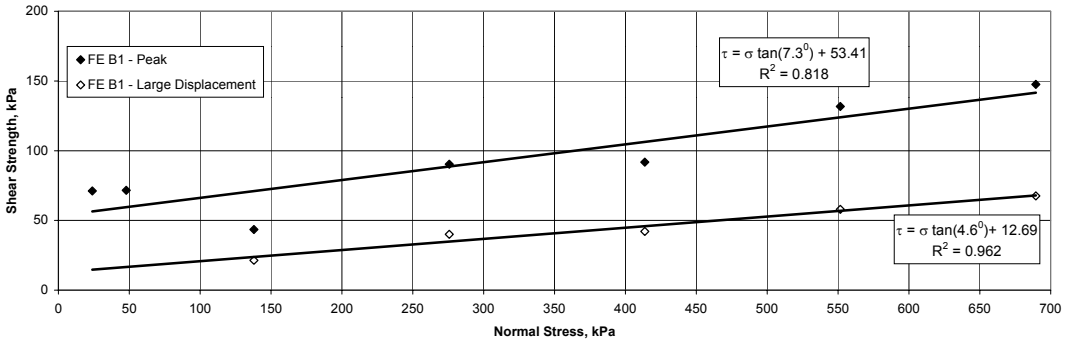

Figure 4.59: Peak and Large Displacement Shear Strength Failure Envelopes for GCL B (FE B1: t_H = 24 hours, t_C = 0 hours, and SDR = 1.0 mm/min); *Baseline Failure Envelope for GCL B*

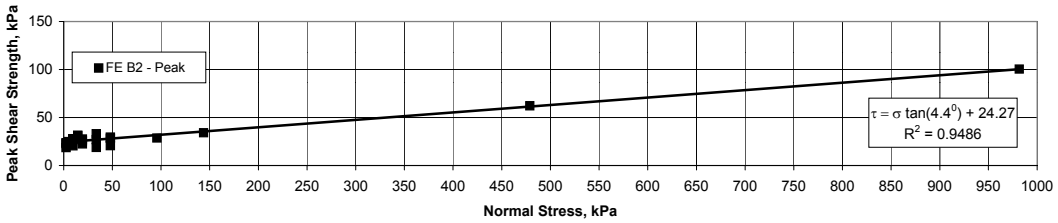

Figure 4.60: Peak Shear Strength Failure Envelopes for GCL B (FE B2: t_H = 48 hours, t_C = 0 hours, and SDR = 1.0 mm/min); *Change in t_H from the Baseline*

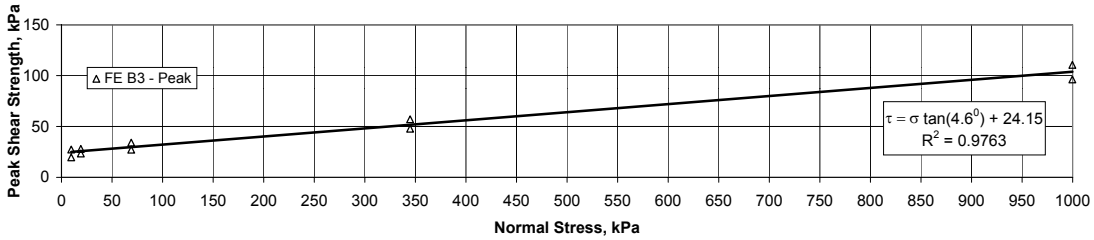

Figure 4.61: Peak Shear Strength Failure Envelopes for GCL B (FE B3: t_H = 96 hours, t_C = 0 hours, and SDR = 1.0 /min); *Change in t_H from the Baseline*

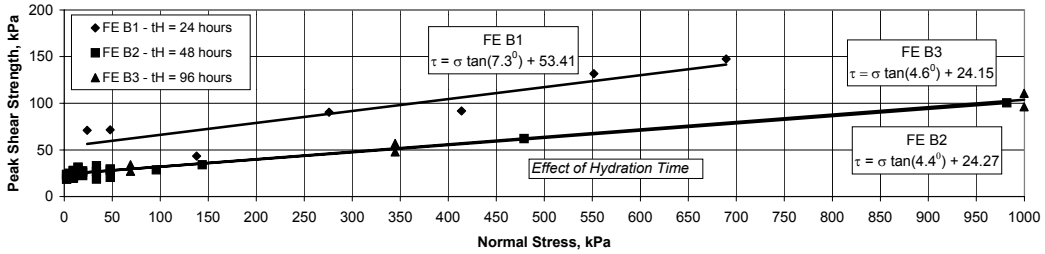

Figure 4.62: Peak Shear Strength Failure Envelope for GCL B (FE B1, B2 and B3); *Effect of Increasing t_H*

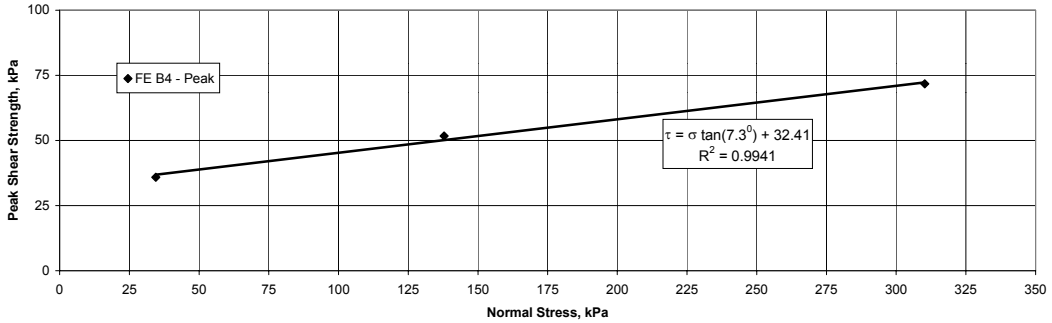

Figure 4.63: Peak Shear Strength Failure Envelope for GCL B (FE B4: t_H = 168 hrs, t_C = 48 hrs, and SDR = 0.1 mm/min); *Change in t_H, t_C and SDR from the Baseline*

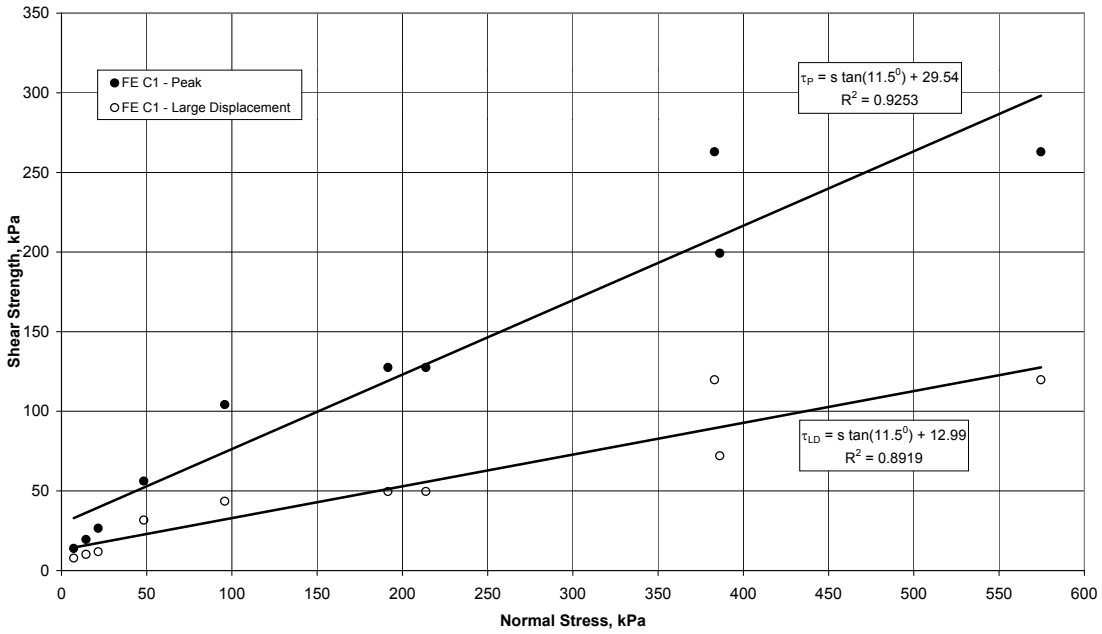

(a)

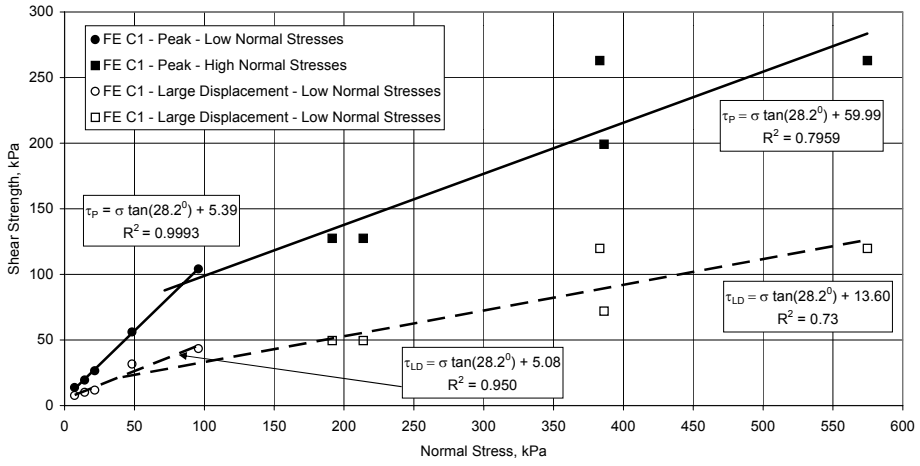

(b)

Figure 4.64: Peak and Large Displacement Shear Strength Failure Envelopes (FE C1: t_H = 24 hrs, t_C = 0 hrs, and SDR = 0.5 mm/min); (a) Linear Fit, (b) Bilinear Fit; *Baseline Failure Envelope for GCL C*

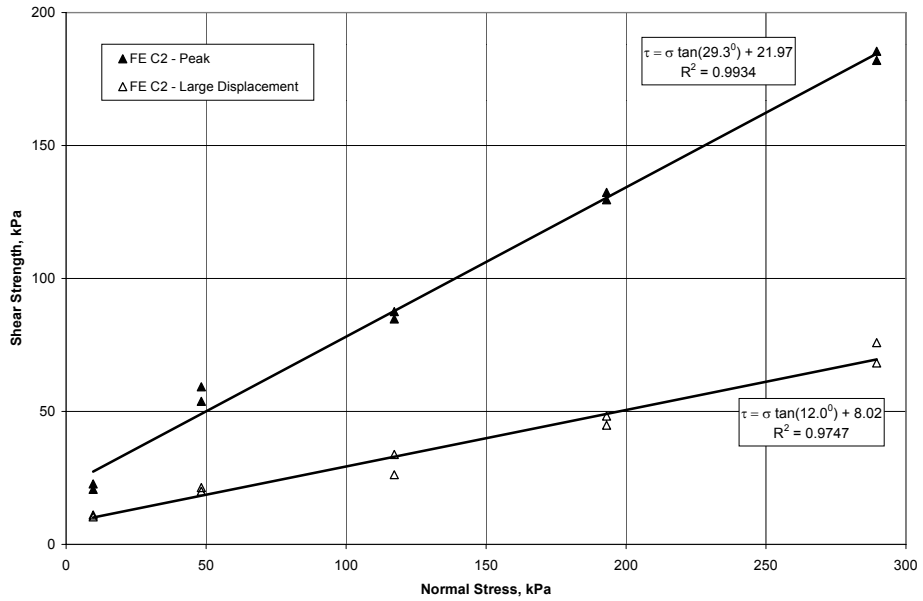

Figure 4.65: Peak and Large Displacement Shear Strength Failure Envelopes (FE C2: t_H = 24 hrs, t_C = 0 hrs, and SDR = 0.2 mm/min); *Change in SDR from the Baseline*

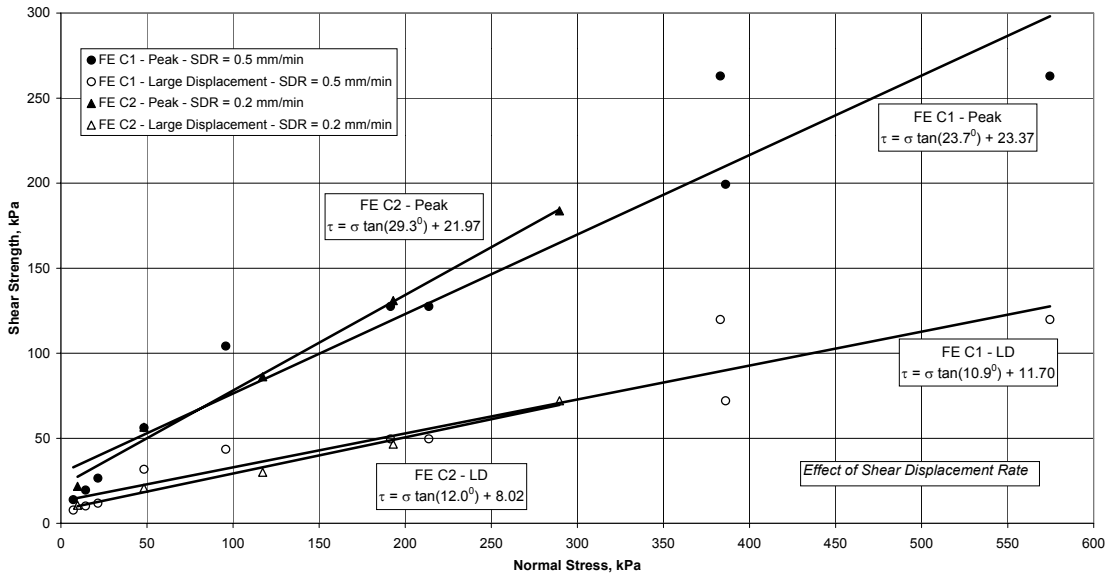

Figure 4.66: Comparison of Failure Envelopes for GCL C (FE C1, C2: t_H = 24, t_C = 0 hrs, and SDR = 0.5 and 0.2 mm/min, respectively); *Effect of Decreasing SDR*

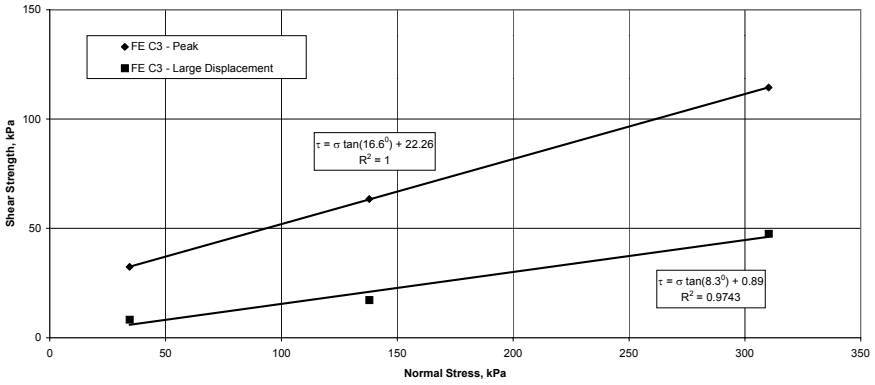

Figure 4.67: Peak and Large Displacement Shear Strength Failure Envelopes (FE C3: t_H = 168 hrs, t_C = 48 hrs, and SDR = 0.1 mm/min); *Change in t_H, t_C and SDR from the Baseline*

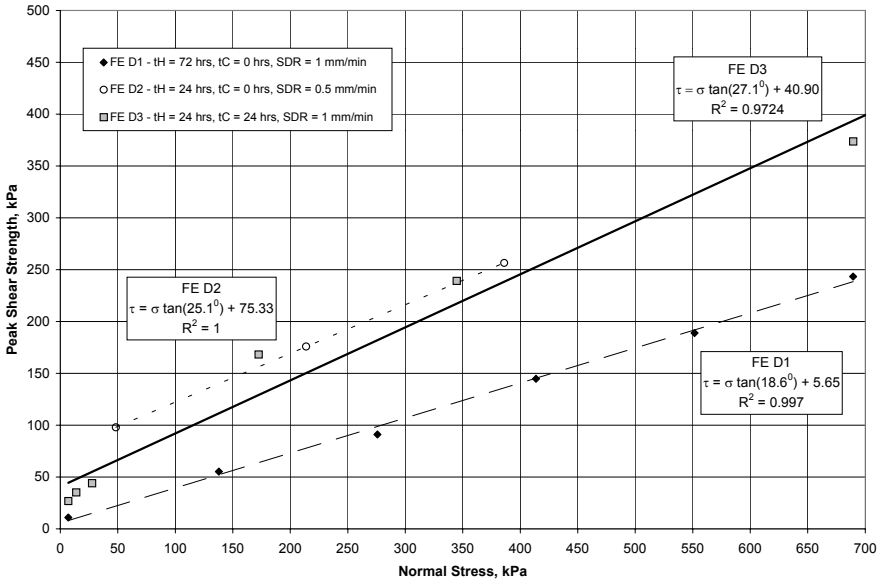

(a)

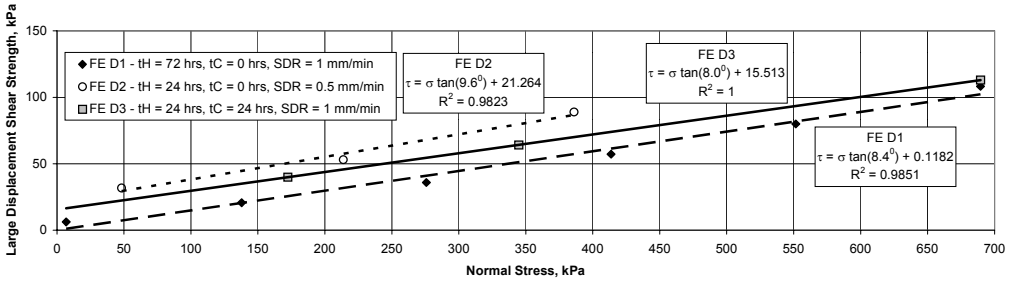

(b)

Figure 4.68: Shear Strength Failure Envelopes for GCL D (FE D1, D2 and D3: Different t_H, t_C and SDR)

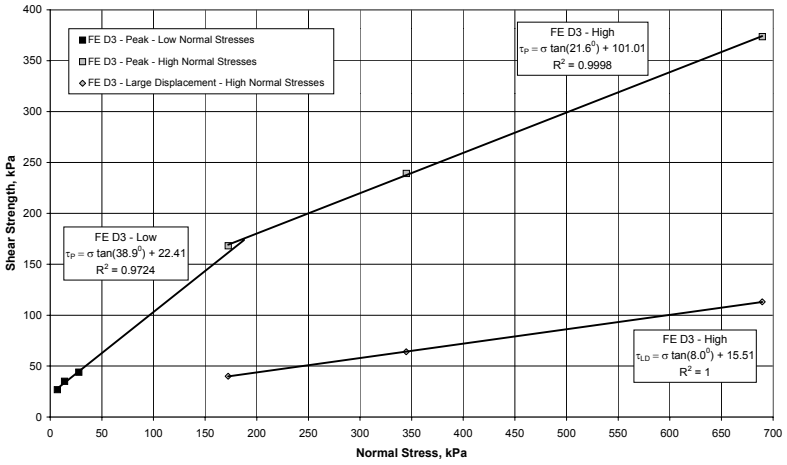

Figure 4.69: Bilinear Peak and Large Displacement Failure Envelopes for GCL D (FE D3: t_H = 24 hours, t_C = 24 hours, SDR = 1.0 mm/min)

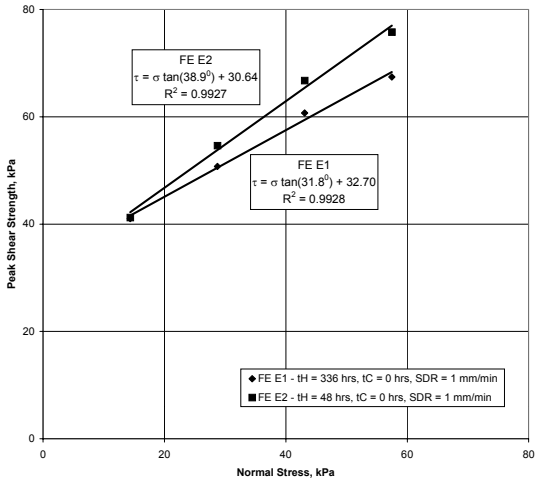

(a)

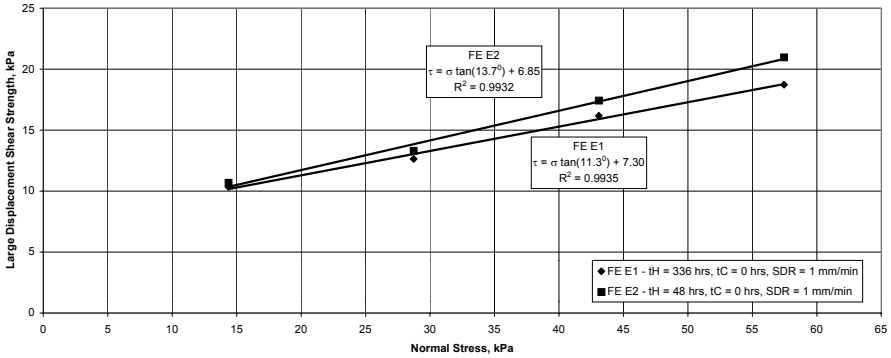

(b)

Figure 4.70: Shear Strength Failure Envelopes for GCL E (FE E1 and E2: Different t_H, No Consolidation, SDR = 1.0 mm/min); (a) Peak, (b) Large Displacement

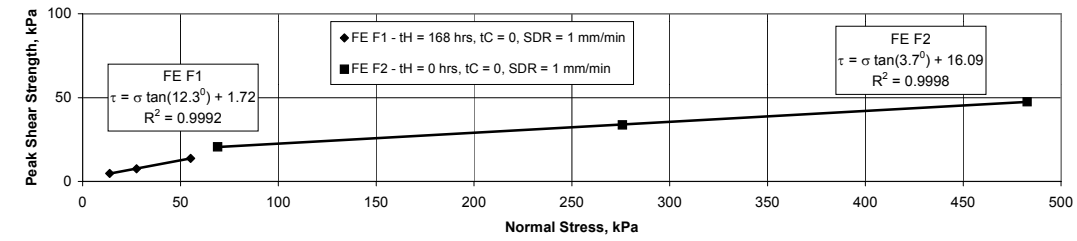

(a)

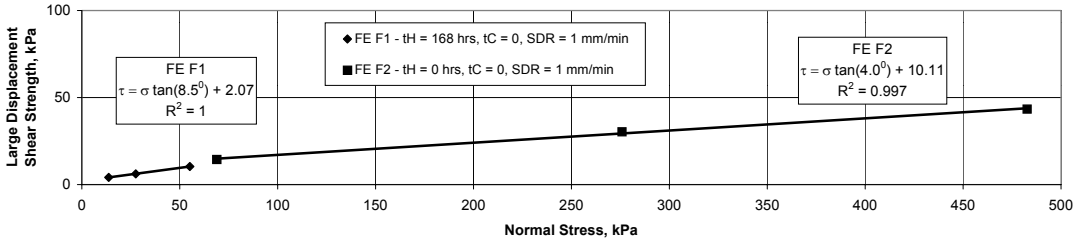

(b)

Figure 4.71: Shear Strength Failure Envelopes for GCL F (FE F1 and F2: Hydrated and Unhydrated GCLs, respectively, and SDR = 1.0 mm/min); (a) Peak Shear Strength, (b) Large Displacement Shear Strength

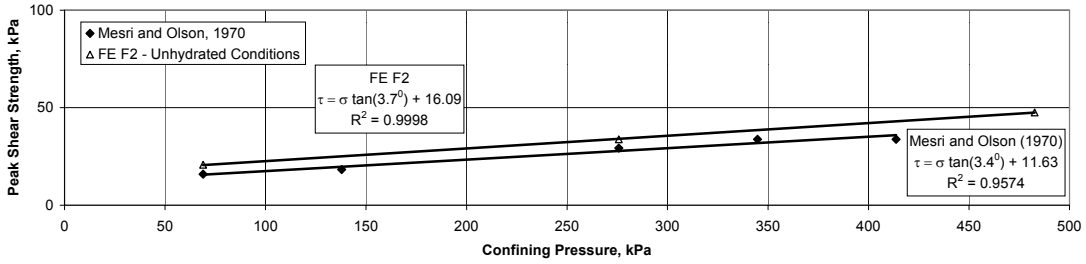

Figure 4.72: Comparison Plot Between Failure Envelope F2 and Total Stress Results of Triaxial Cell Tests on Sodium Montmorillonite Reported By Mesri and Olson (1970)

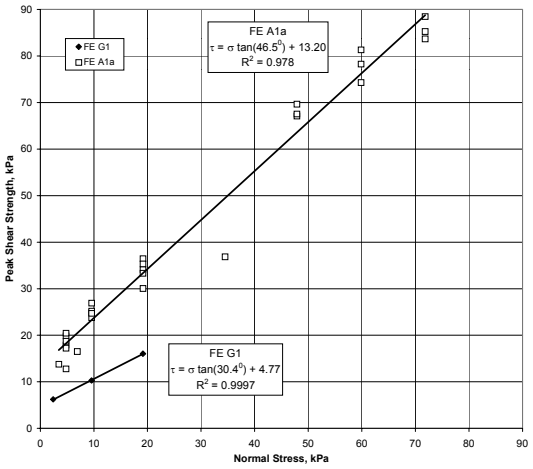

Figure 4.73: Peak and Large Displacement Shear Strength Failure Envelope for GCL G (FE G1: t_H = 24 hours, t_C = 0 hours, SDR = 1.0 mm/min)

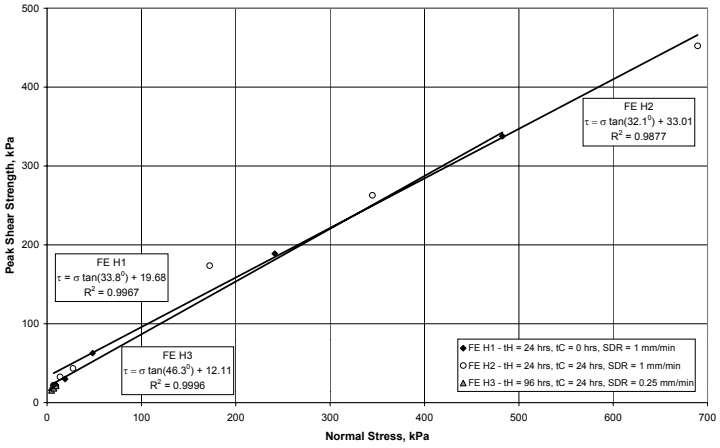

(a)

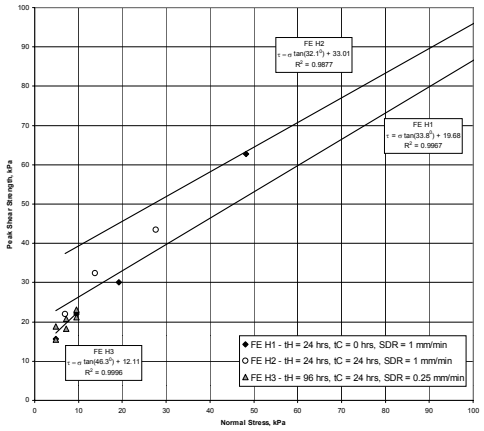

(b)

Figure 4.74: Peak Shear Strength Failure Envelopes for GCL H (FE H1, H2 and H3); (a) Full Normal Stress Range, (b) Detail of Low Normal Stresses

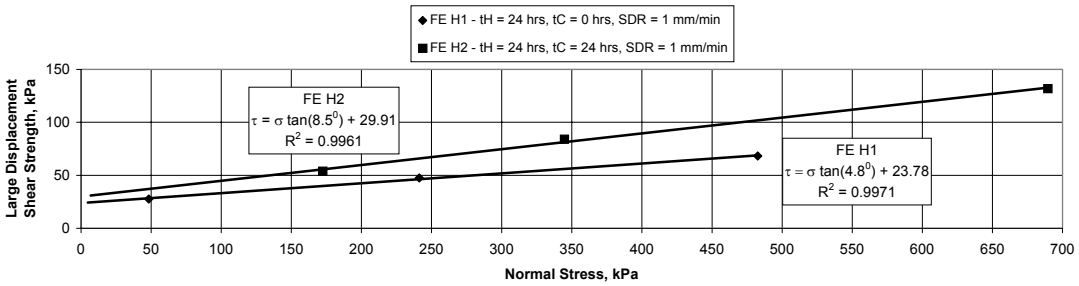

Figure 4.75: Large Displacement Shear Strength Failure Envelopes for GCL H (FE H1, H2 and H3)

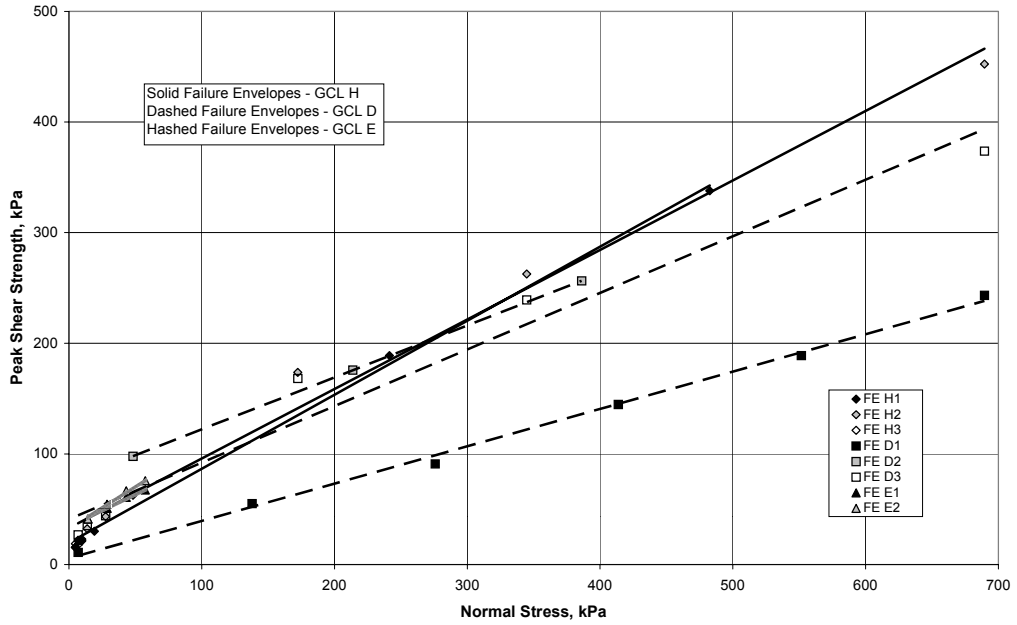

(a)

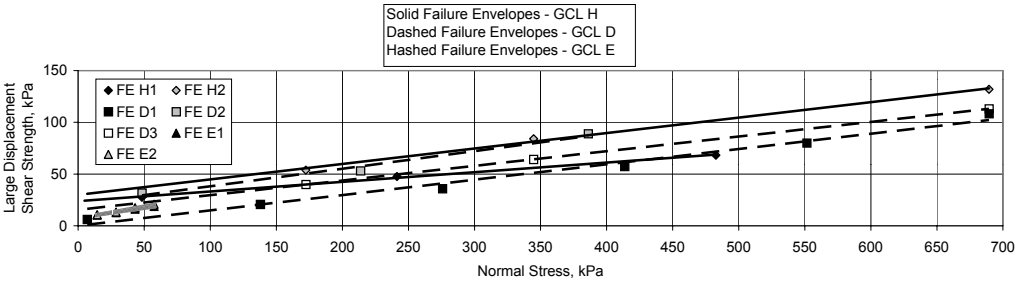

(b)

Figure 4.76: Comparison of Failure Envelopes D1, D2, D3, E1, E2, H1, H2 and H3; Effect of Thermal Bonding on Needle-Punched GCLs with Nonwoven Carrier Geotextiles; (a) Peak, (b) Large Displacement

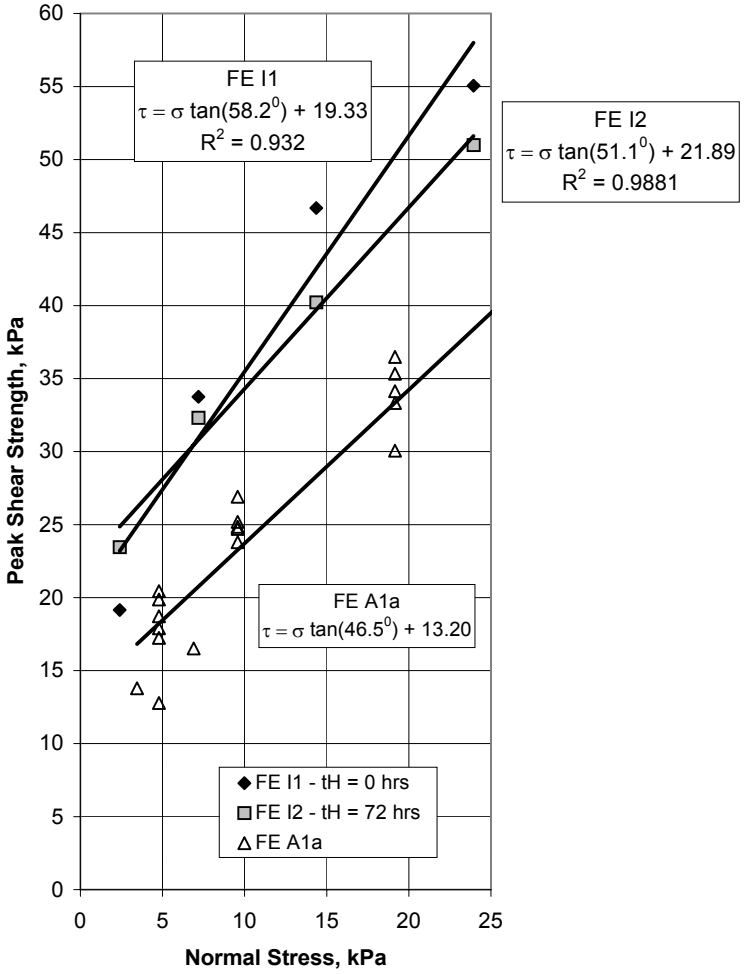

Figure 4.77: Peak Shear Strength Failure Envelopes for GCL I (FE I1 and I2, tH = 0 hours and 72 hours, Respectively, No Consolidation, SDR = 1.0 mm/min), with Failure Envelope A1a for Comparison

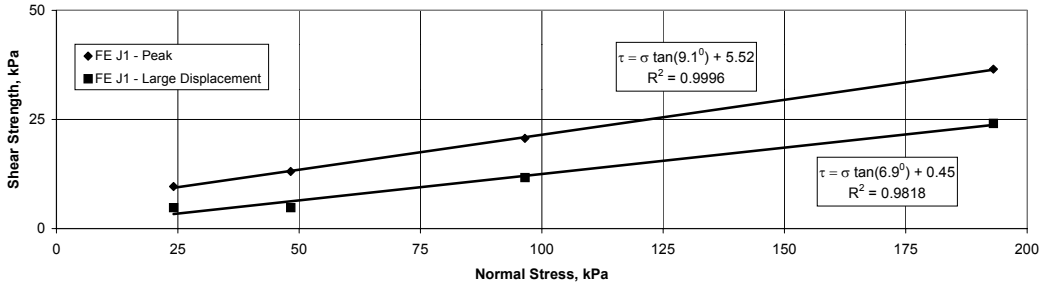

Figure 4.78: Peak and Large Displacement Shear Strength Failure Envelopes for GCL J (FE J1: t_C = 24 hours, t_C = 0 hours, SDR = 1.0 mm/min)

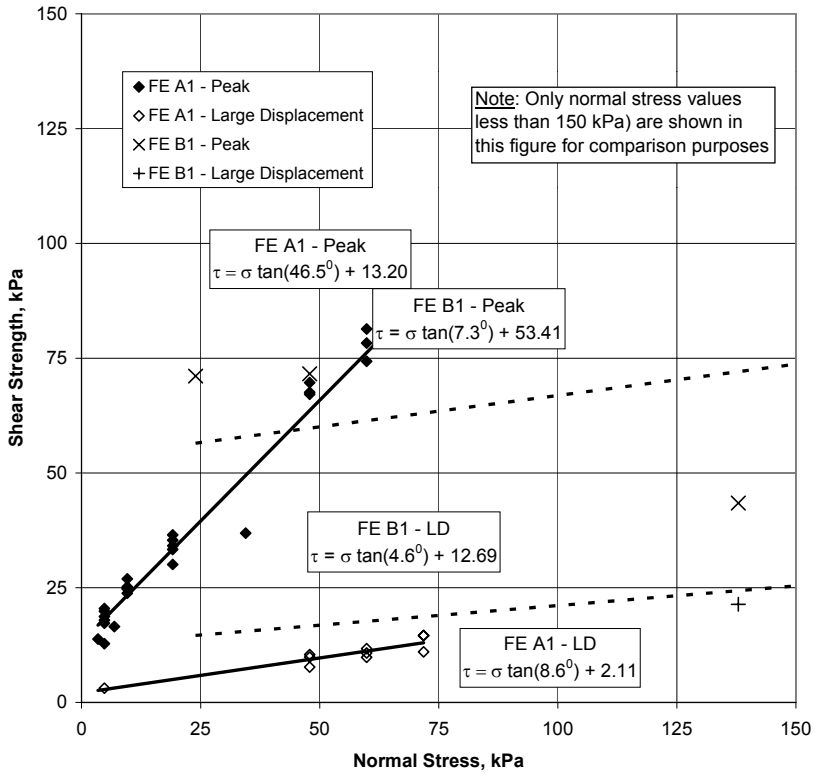

Figure 4.79: Comparison of the Peak and Large Displacement Failure Envelopes A1 and B1 (SDR = 1.0 mm/min, t_H = 24 hours, t_C = 0 hours)

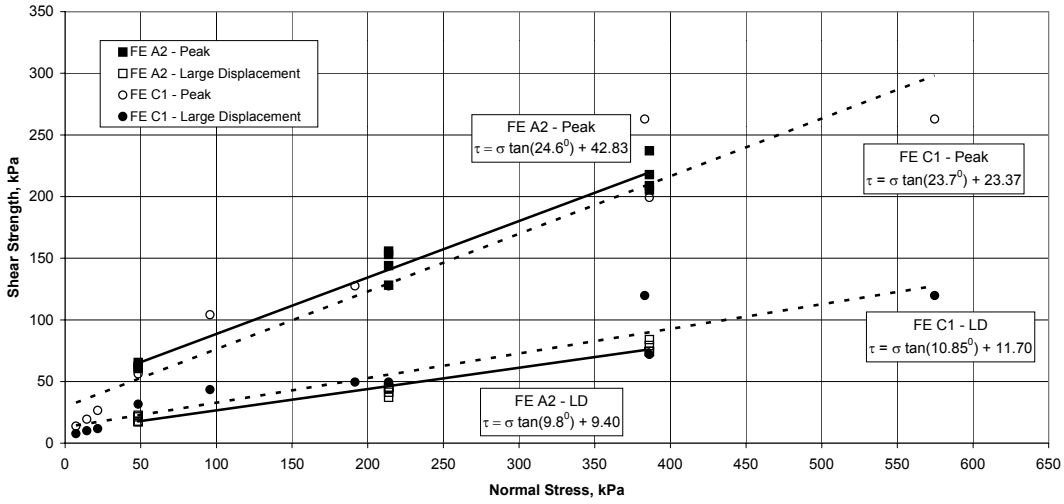

Figure 4.80: Comparison of the Peak and Large Displacement Failure Envelopes A2 and C1 (SDR = 0.5 mm/min, t_H = 24 hours, t_C = 0 hours)

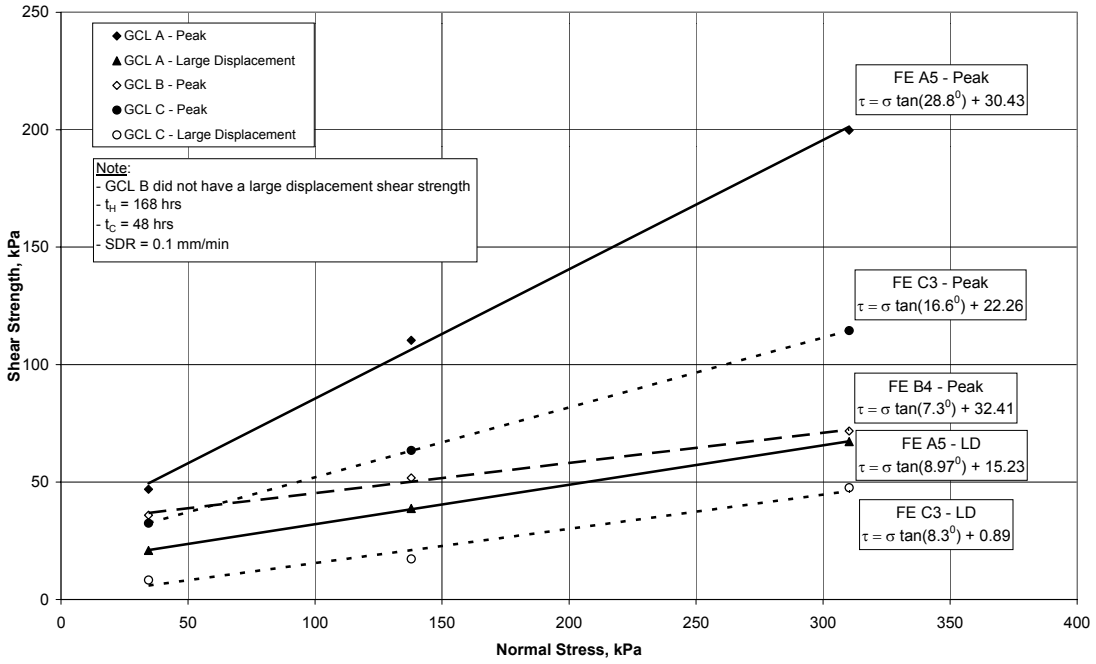

Figure 4.81: Comparison of the Peak and Large Displacement Failure Envelopes A5, B4 and C3 (SDR = 0.1 mm/min, t_H = 168 hours, t_C = 48 hours)

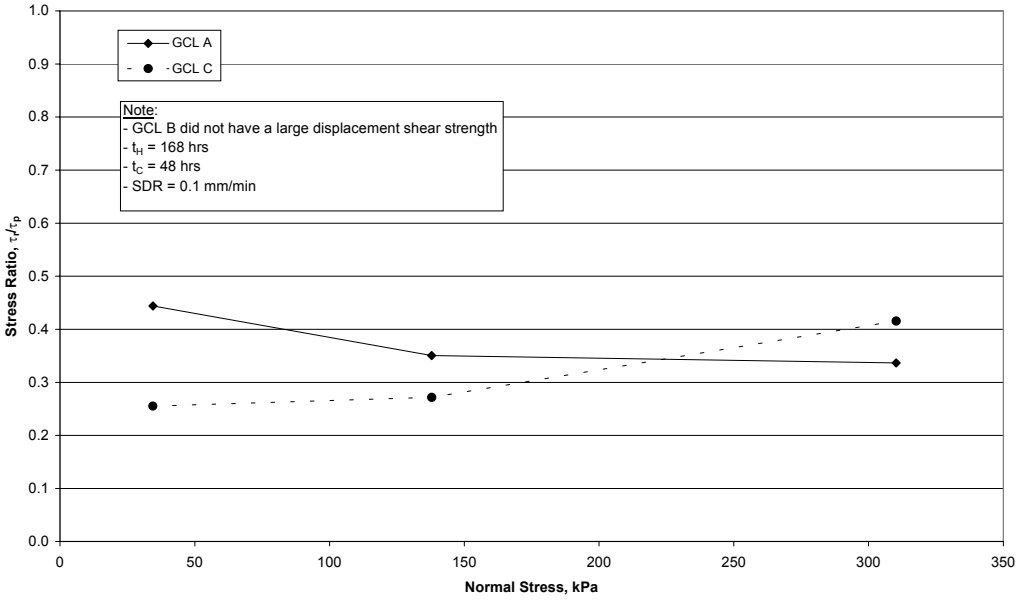

Figure 4.82: Comparison of the Peak and Large Displacement Shear Strength Ratios for Failure Envelopes A5, B4 and C3 (SDR = 0.1 mm/min, t_H = 168 hours, t_C = 48 hours)

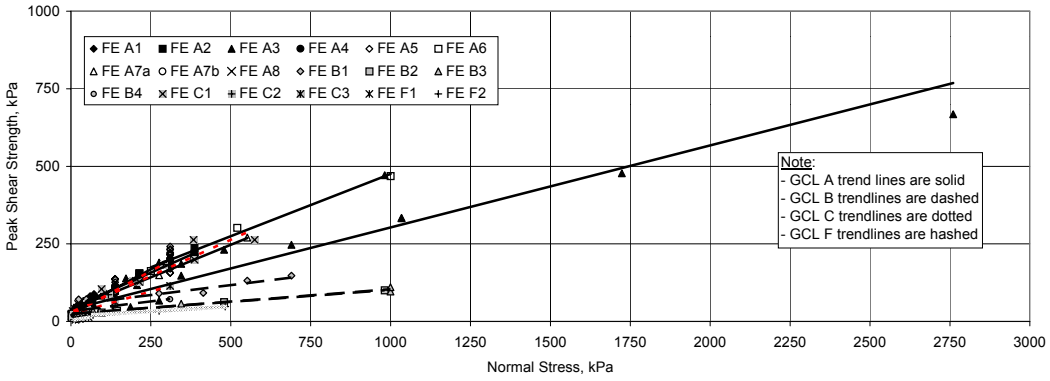

Figure 4.83: Comparison of Peak Failure Envelopes for GCLs A, B, C and F

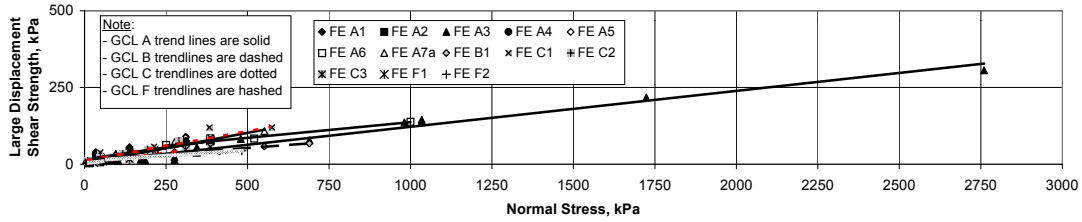

Figure 4.84: Comparison of Large Displacement Failure Envelopes for GCLs A, B, C and F

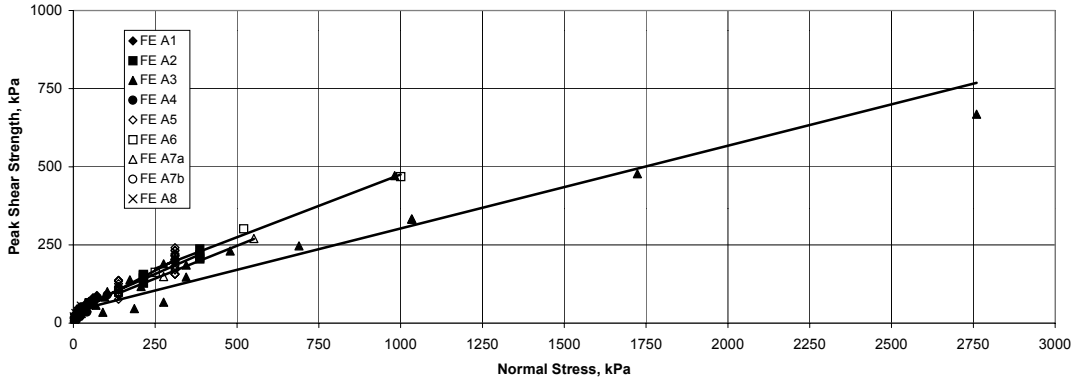

Figure 4.85: Comparison of Peak Shear Strength Failure Envelopes for GCLs A

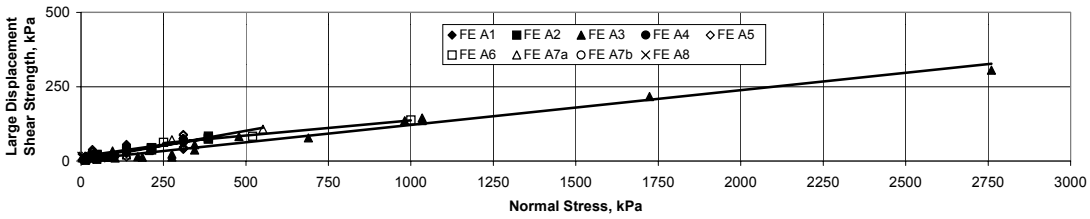

Figure 4.86: Comparison of Large Displacement Failure Envelopes for GCLs A

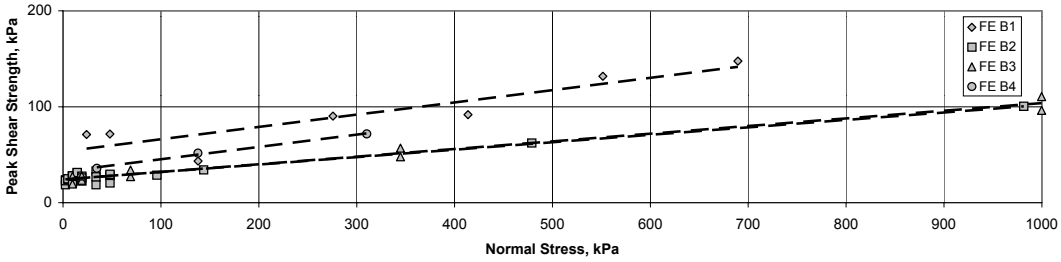

Figure 4.87: Comparison of Peak Shear Strength Failure Envelopes for GCLs B

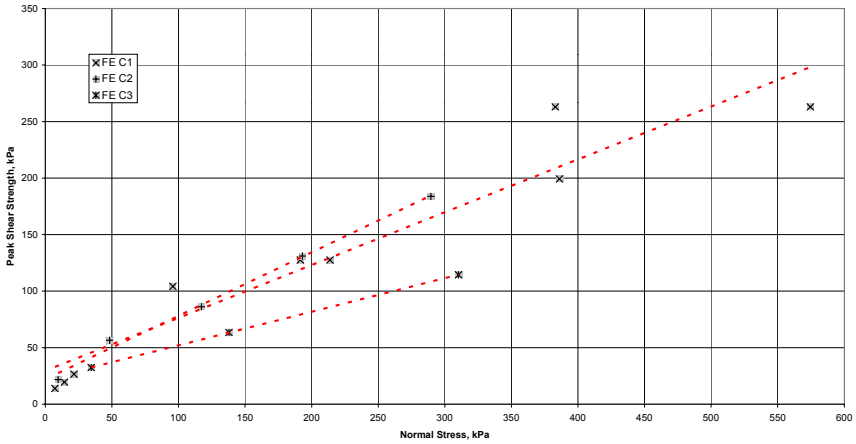

Figure 4.88: Comparison of Peak Shear Strength Failure Envelopes for GCLs C

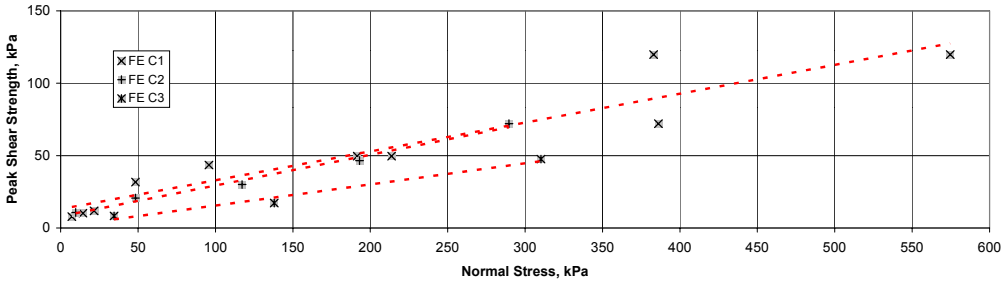

Figure 4.89: Comparison of Large Displacement Failure Envelopes for GCLs C

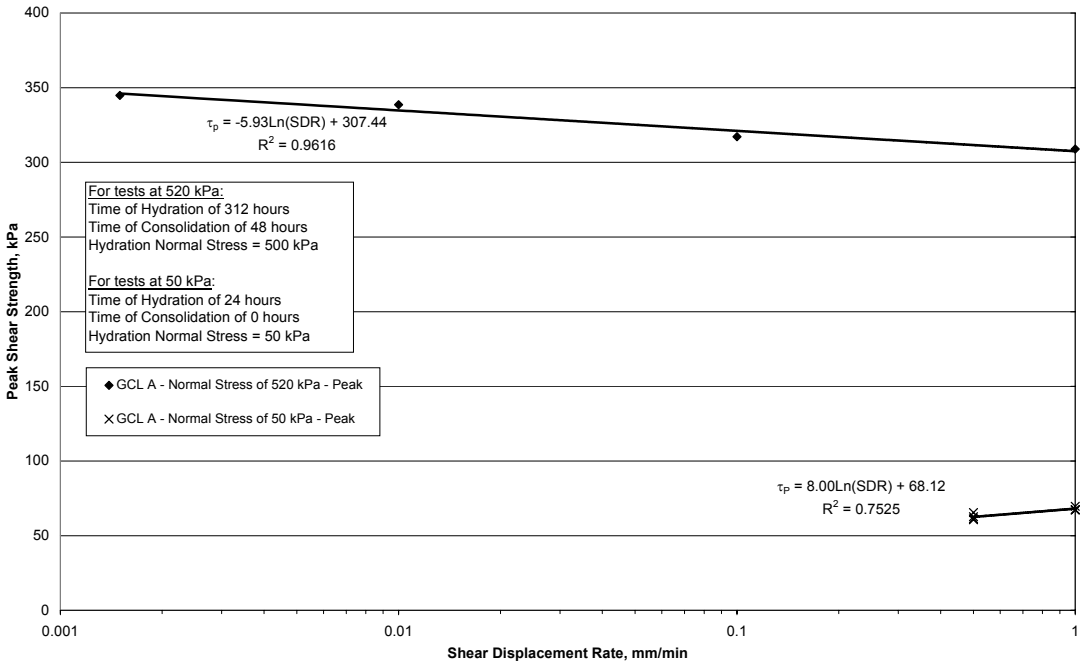

(a)

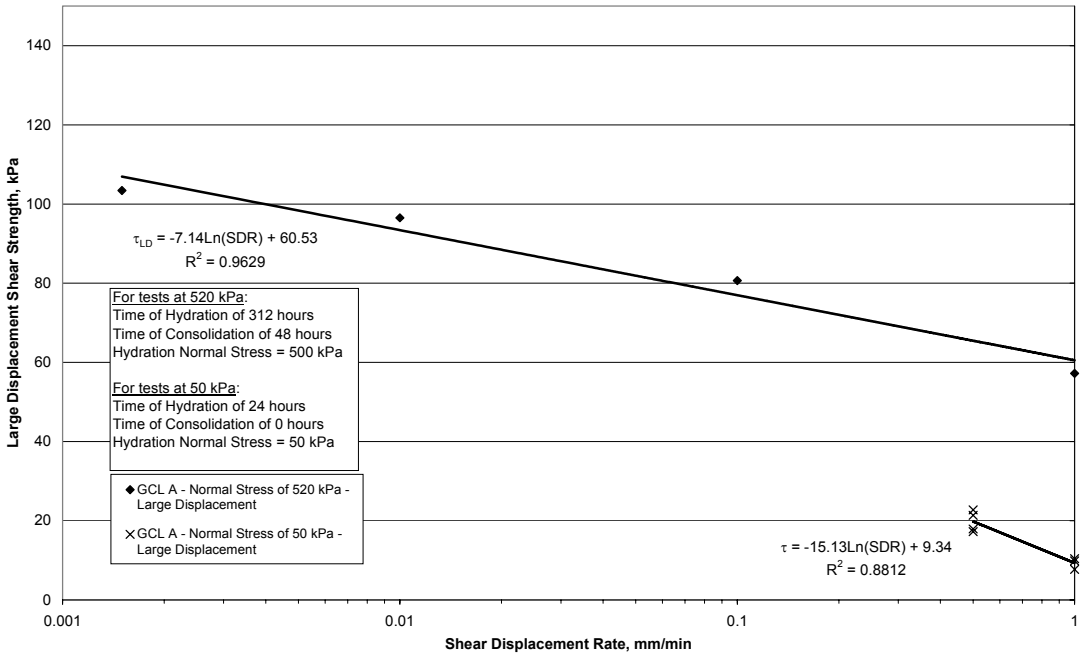

(b)

Figure 4.90: Effect of Shear Displacement Rate on the Shear Strength of GCL A for Low Normal Stress (50 kPa) and High Normal Stress (520 kPa); (a) Peak, (b) Large Displacement

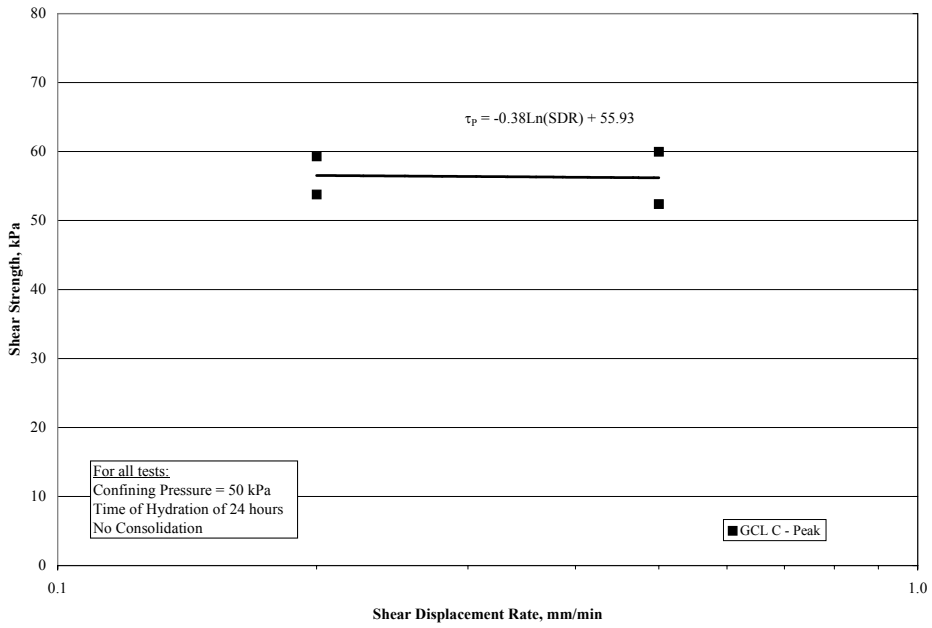

Figure 4.91: Effect of Shear Displacement Rate on the Shear Strength of GCL C; Normal Stress of 50 kPa

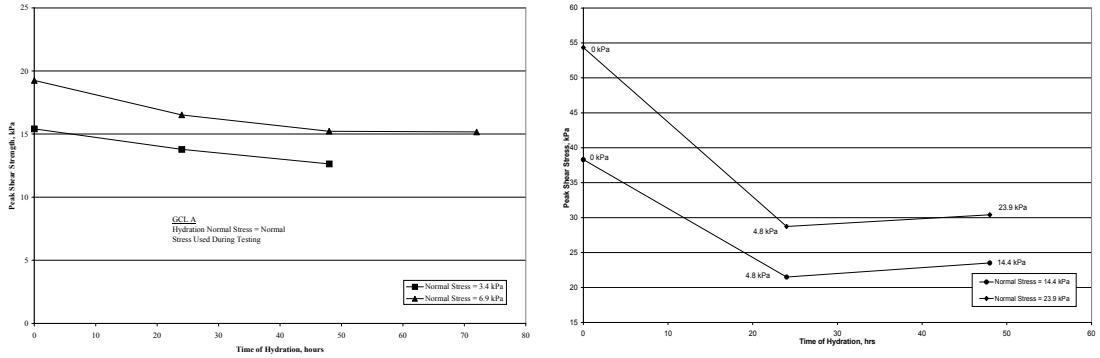

(a) (b)

Figure 4.92: Effect of the Time of Hydration on the Peak Shear Strength of GCL A (SDR = 1.0 mm/min, No Consolidation); (a) Hydration Normal Stress is Equal Normal Stress During Shearing, (b) Hydration Normal Stress Not Equal to Normal Stress During Shearing, Hydration Normal Stresses are Labeled

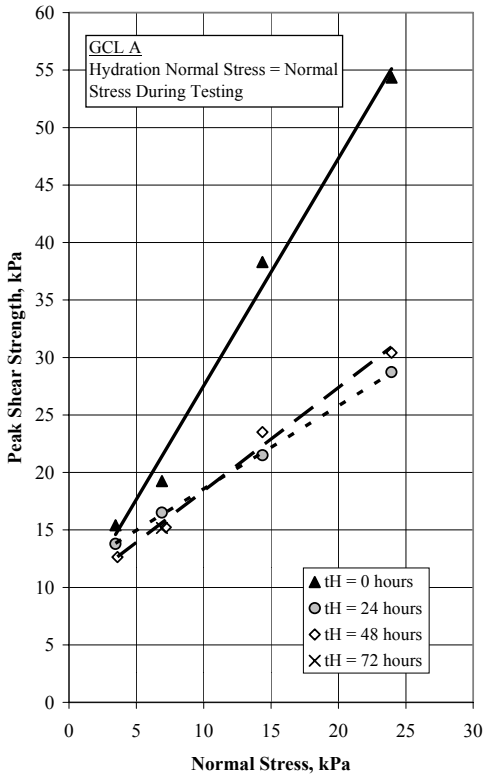

Figure 4.93: Effect of Time of Hydration on Peak Failure Envelopes for GCL A (Note: Hydration Normal Stress Equals Normal Stress During Shearing)

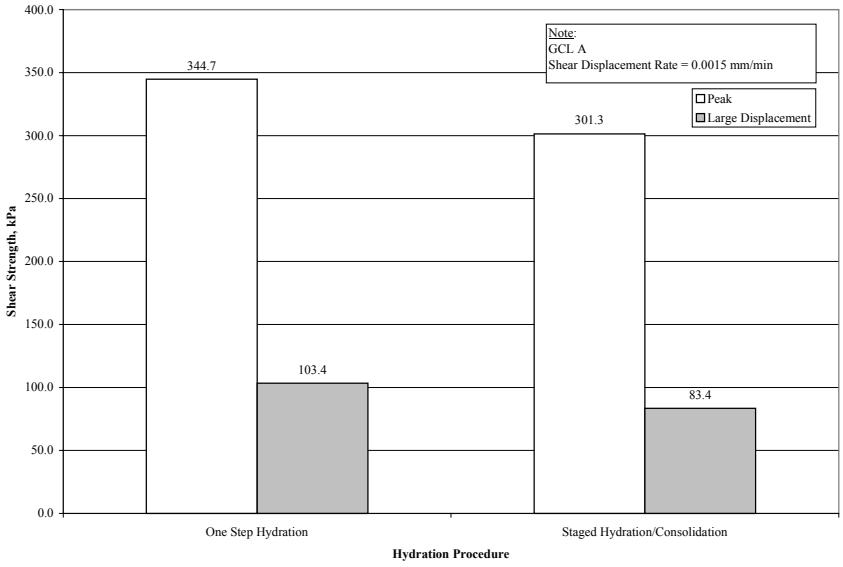

Figure 4.94: Effect of Hydration Procedure on GCL A

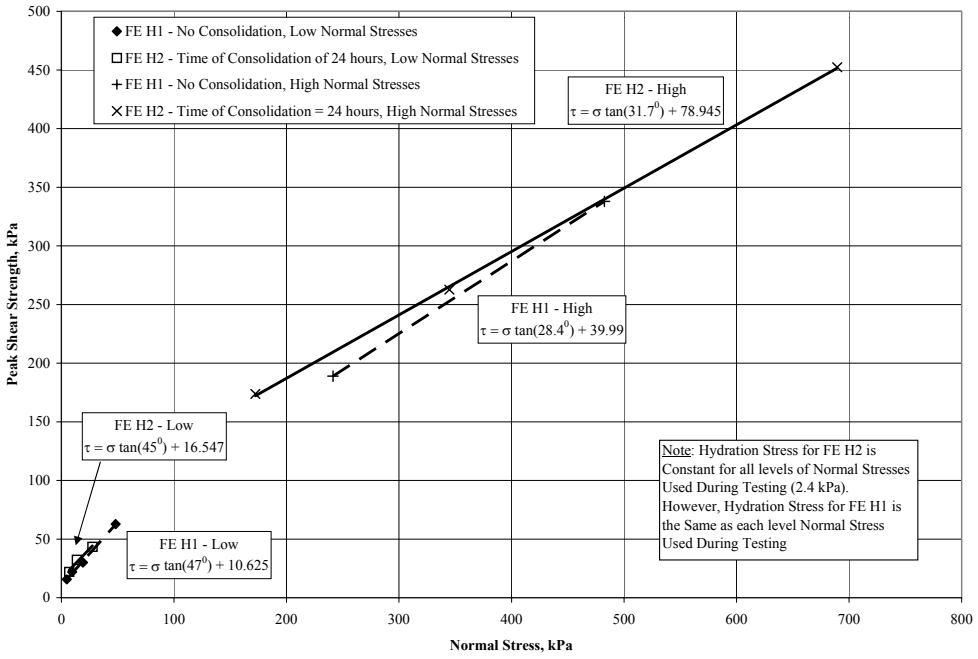

(a)

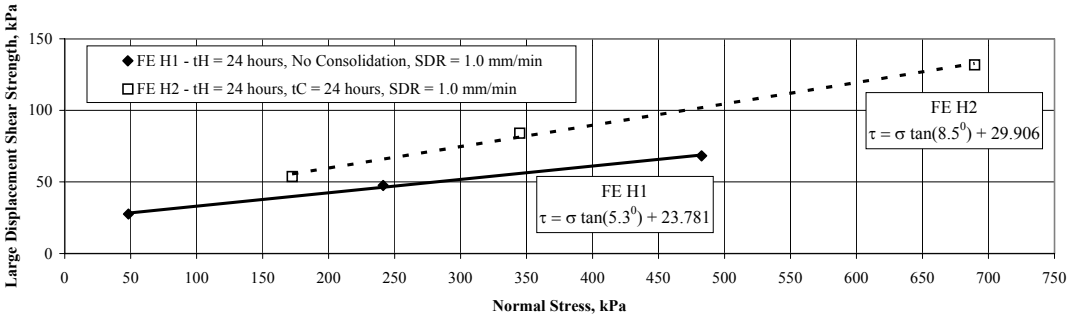

(b)

Figure 4.95: Effect of Consolidation on GCL H (a) Peak Shear Strength with High and Low Normal Stress Distributions, (b) Large Displacement Shear Strength

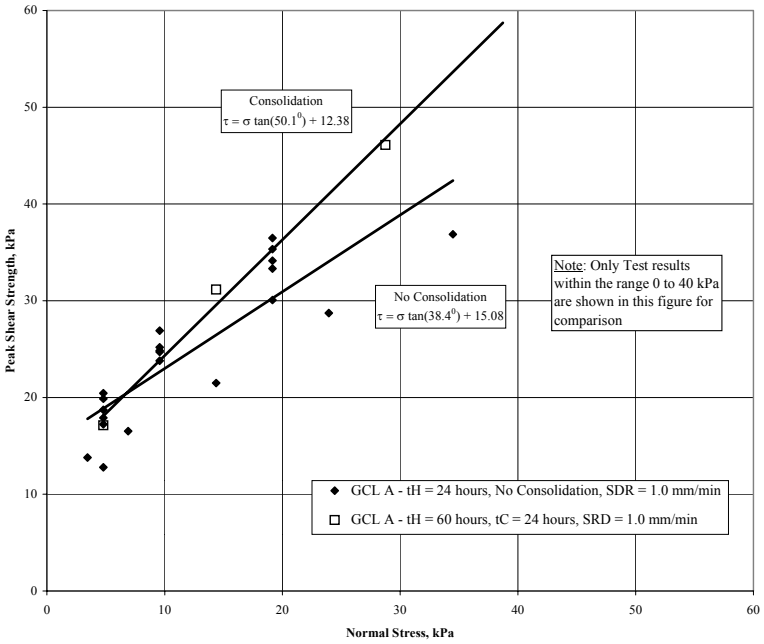

Figure 4.96: Effect of Consolidation on the Peak Shear Strength of GCL A

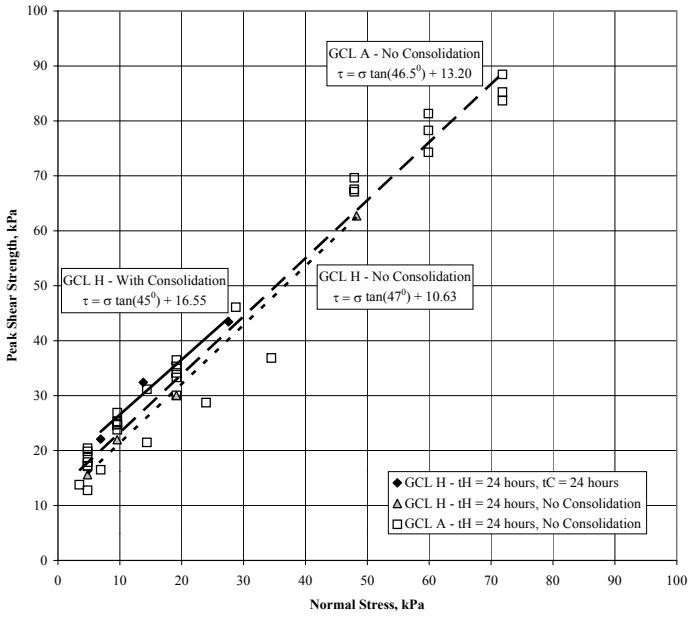

Figure 4.97: Comparison of the Effect of Consolidation on the Peak Shear Strengths of GCL A and GCL H (Low Ranges of Normal Stresses)

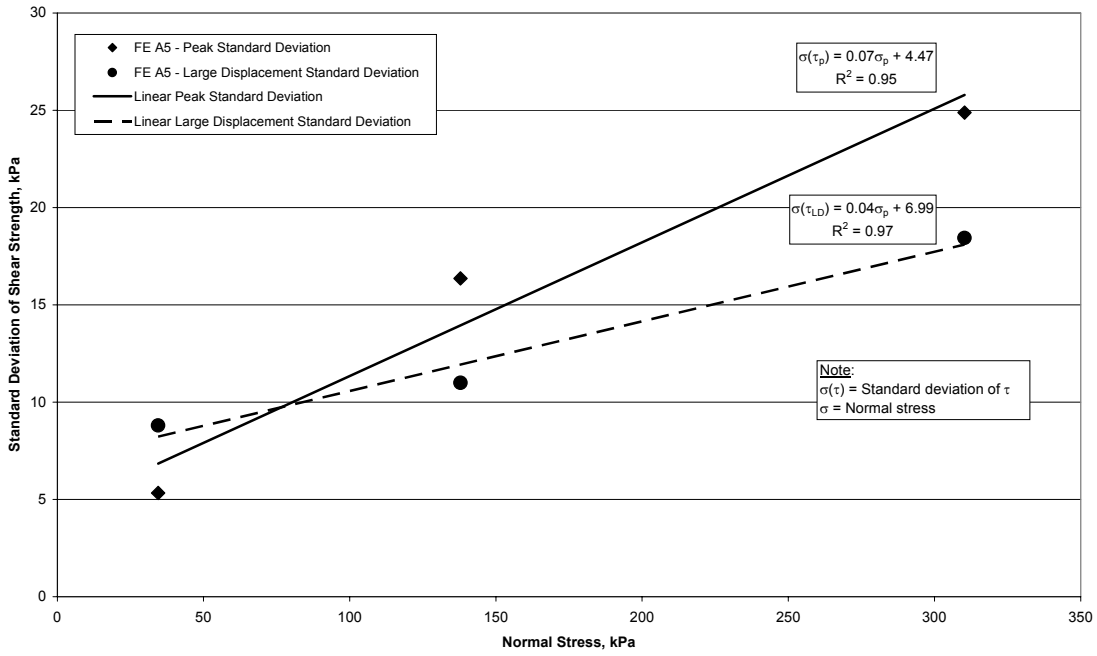

Figure 4.98: Variation in Standard Deviation of the Peak and Large Displacement Shear with Normal Stress for FE A5

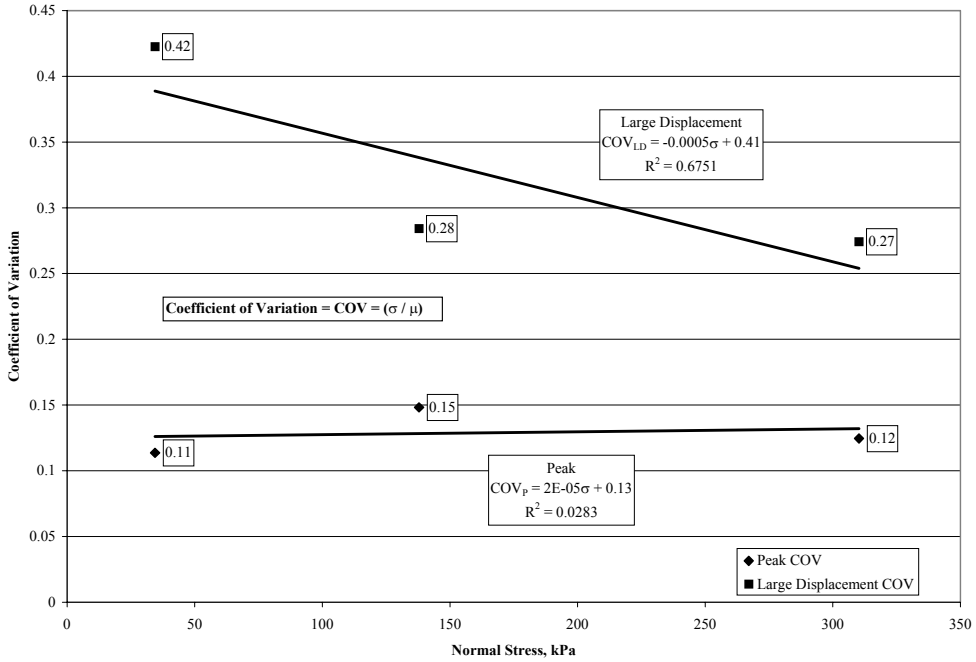

Figure 4.99: Variation in the Coefficient of Variation (COV) of the Peak and Large Displacement Shear with Normal Stress for FE A5

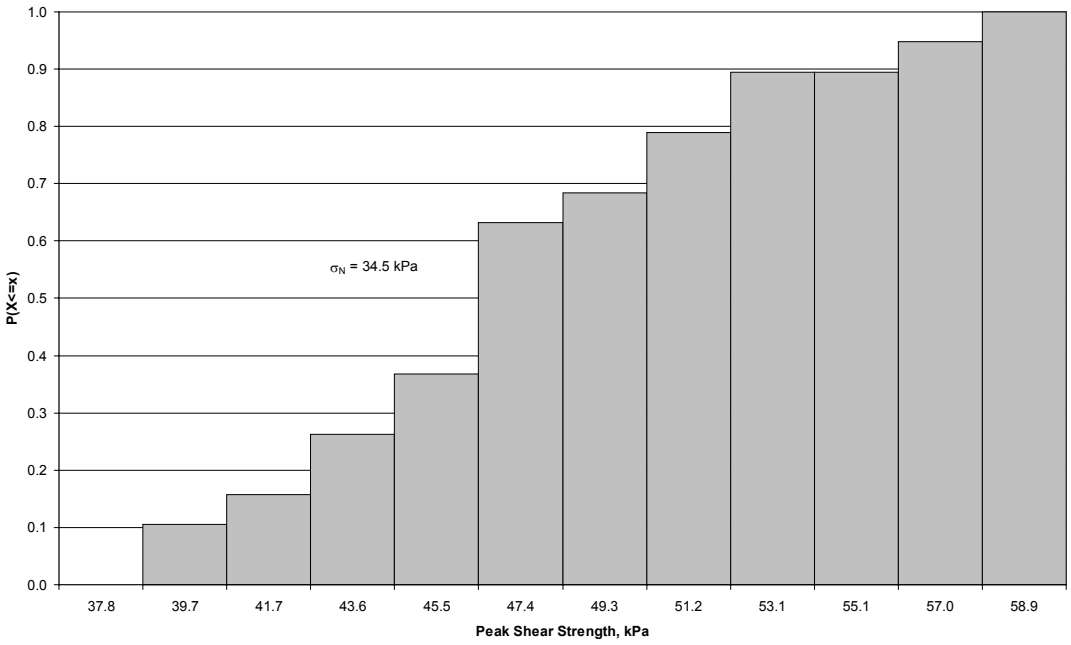

(a)

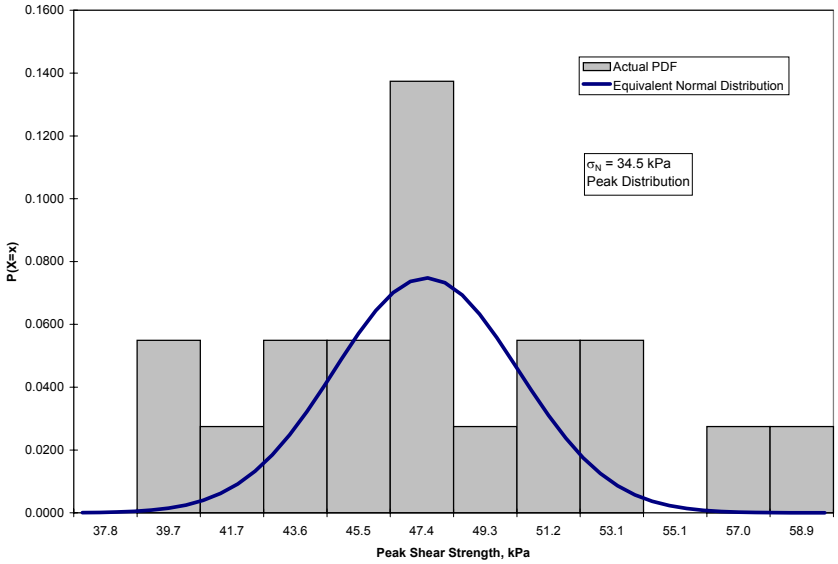

(b)

Figure 4.100: Variation in Peak Shear Strength of GCL A for a Constant Normal Stress of 34.5 kPa, t_H = 168 hrs, t_C = 48 hrs, and SDR = 0.1 mm/min (Failure Envelope A5); (a) Cumulative Distribution Function (CDF), (b) Probability Density Function (PDF) with an Equivalent Normal Distribution

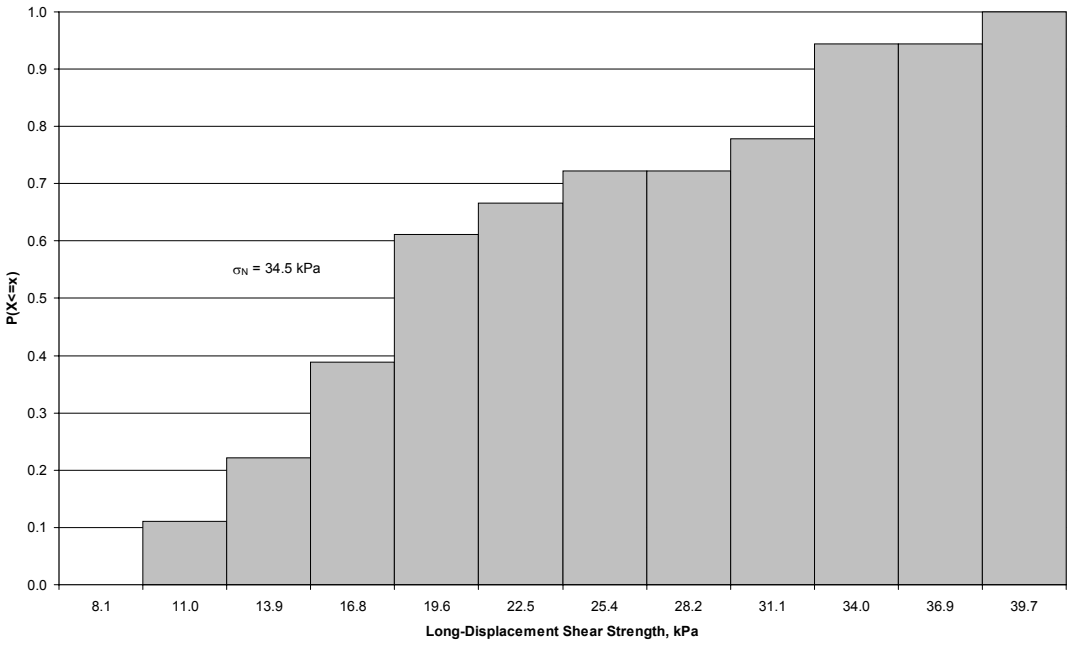

(a)

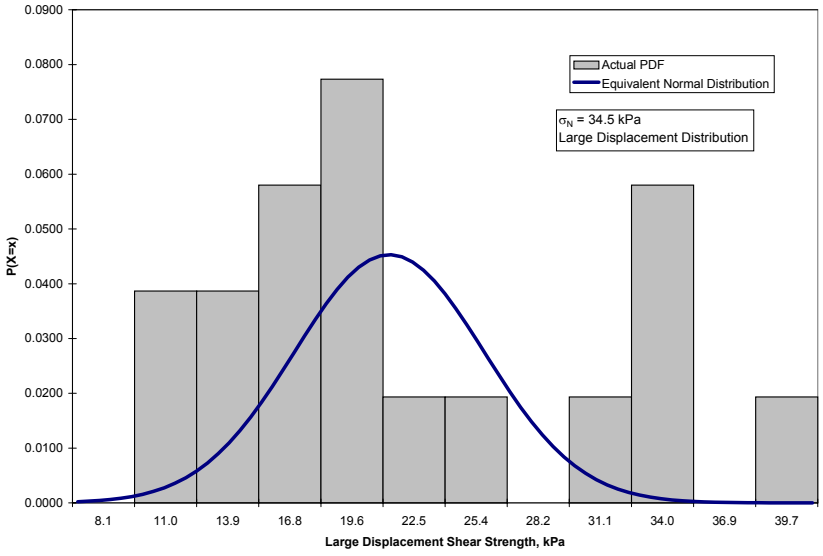

(b)

Figure 4.101: Variation in Large Displacement Shear Strength of GCL A for a Constant Normal Stress of 34.5 kPa, t_H = 168 hrs, t_C = 48 hrs, and SDR = 0.1 mm/min (Failure Envelope A5) ; (a) Cumulative Distribution Function (CDF), (b) Probability Density Function (PDF) with an Equivalent Normal Distribution

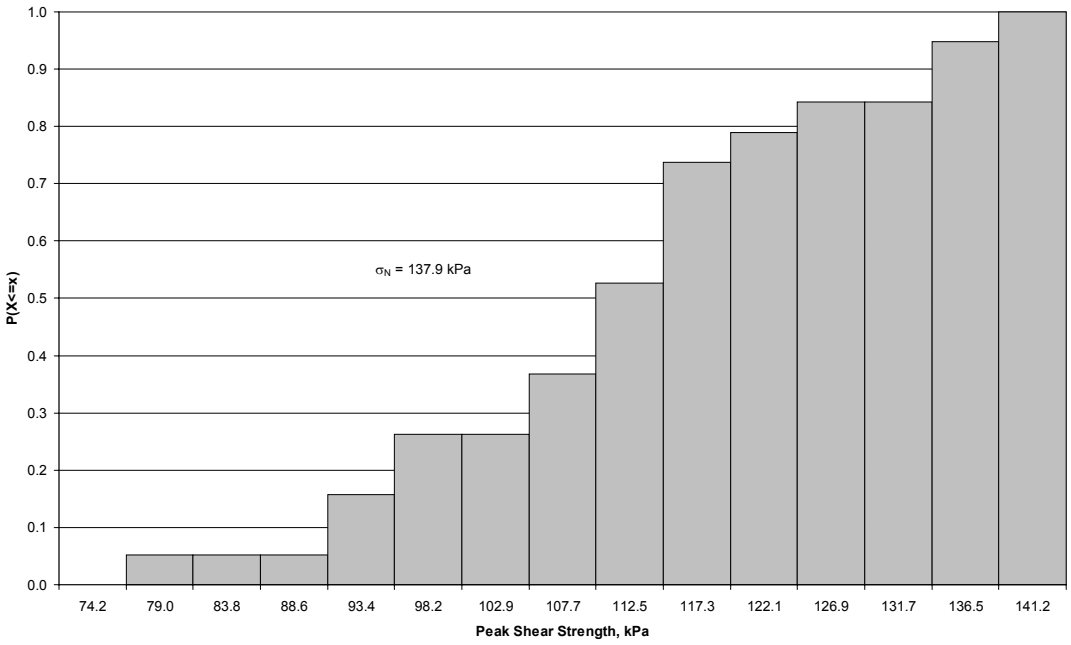

(a)

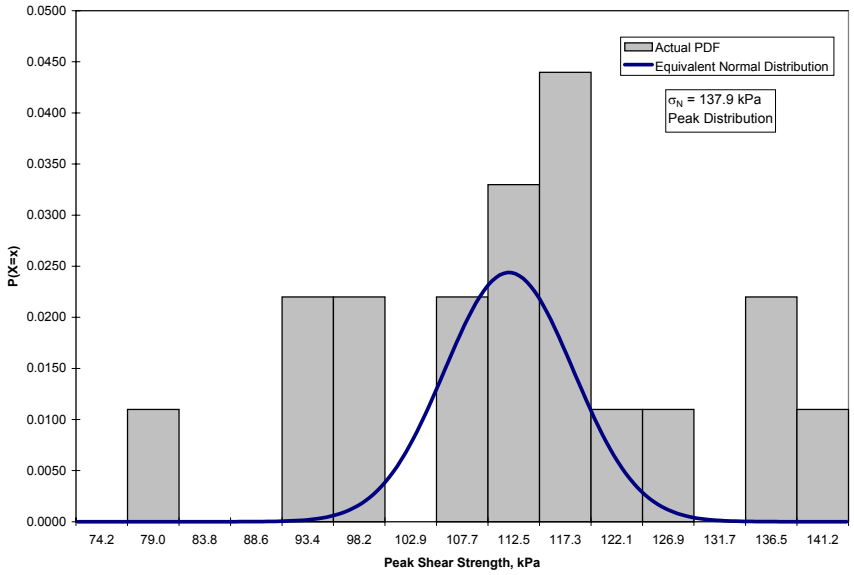

(b)

Figure 4.102: Variation in Peak Shear Strength of GCL A for a Constant Normal Stress of 137.9 kPa, t_H = 168 hrs, t_C = 48 hrs, and SDR = 0.1 mm/min (Failure Envelope A5) ; (a) Cumulative Distribution Function (CDF), (b) Probability Density Function (PDF) with an Equivalent Normal Distribution

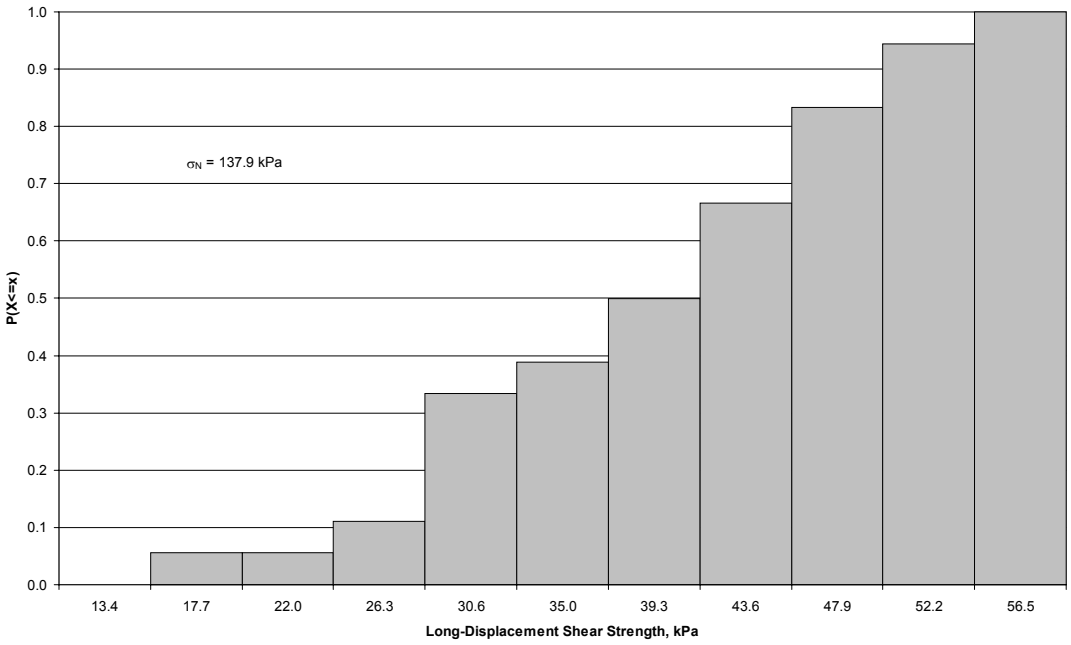

(a)

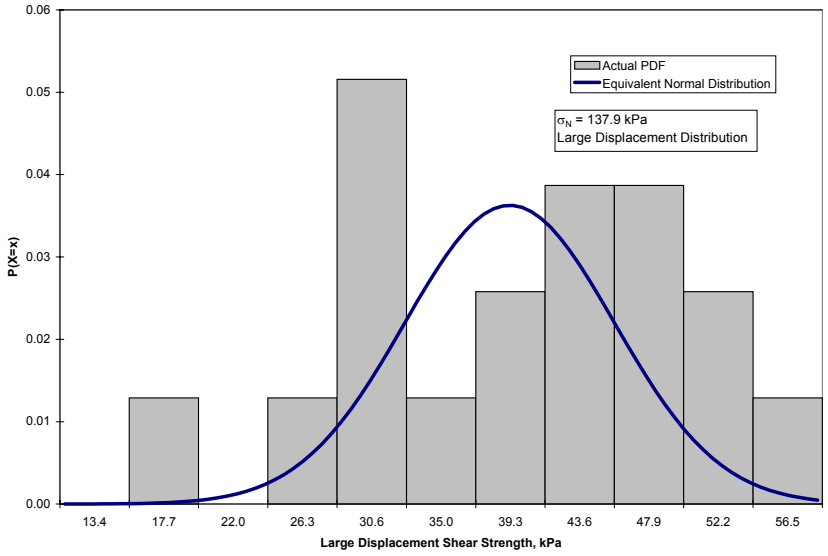

(b)

Figure 4.103: Variation in Large Displacement Shear Strength of GCL A for a Constant Normal Stress of 137.9 kPa, t_H = 168 hrs, t_C = 48 hrs, and SDR = 0.1 mm/min (Failure Envelope A5) ; (a) Cumulative Distribution Function (CDF), (b) Probability Density Function (PDF) with an Equivalent Normal Distribution

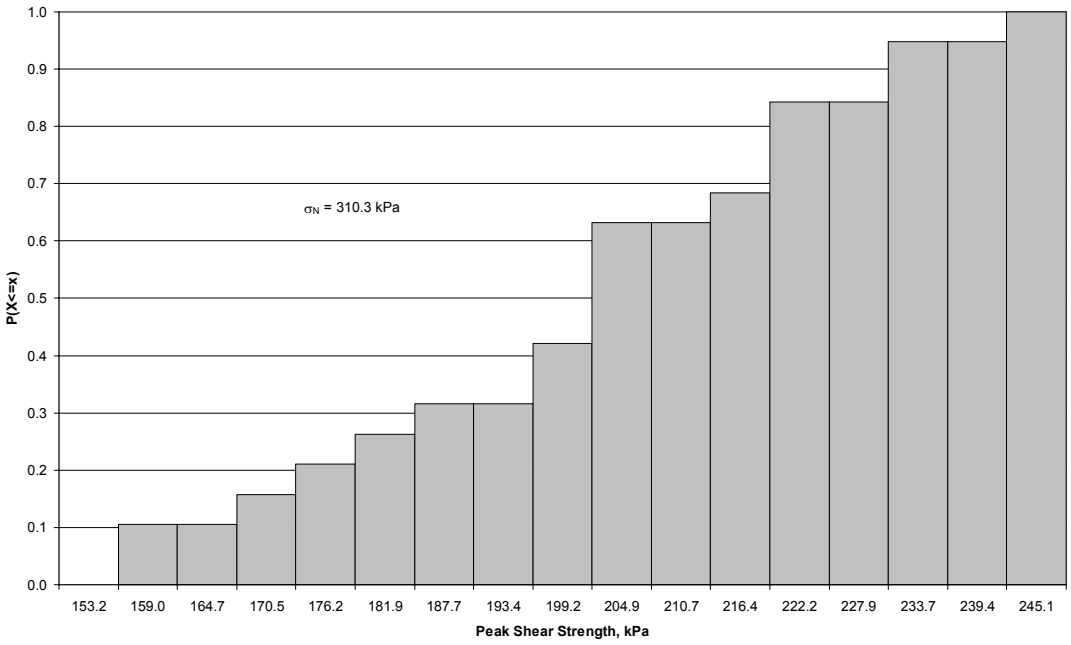

(a)

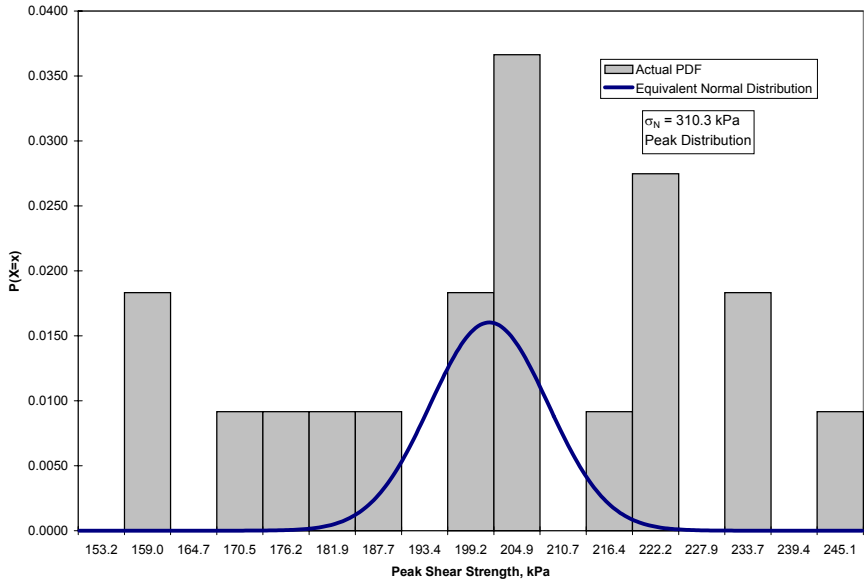

(b)

Figure 4.104: Variation in Peak Shear Strength of GCL A for a Constant Normal Stress of 310.3 kPa, t_H = 168 hrs, t_C = 48 hrs, and SDR = 0.1 mm/min (Failure Envelope A5) ; (a) Cumulative Distribution Function (CDF), (b) Probability Density Function (PDF) with an Equivalent Normal Distribution

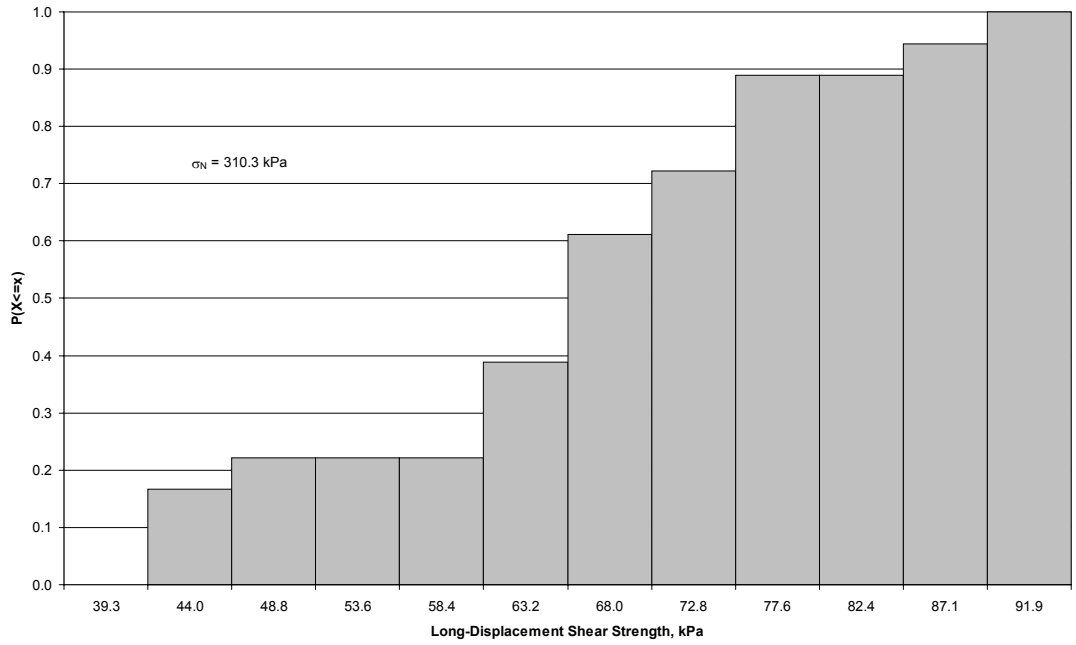

(a)

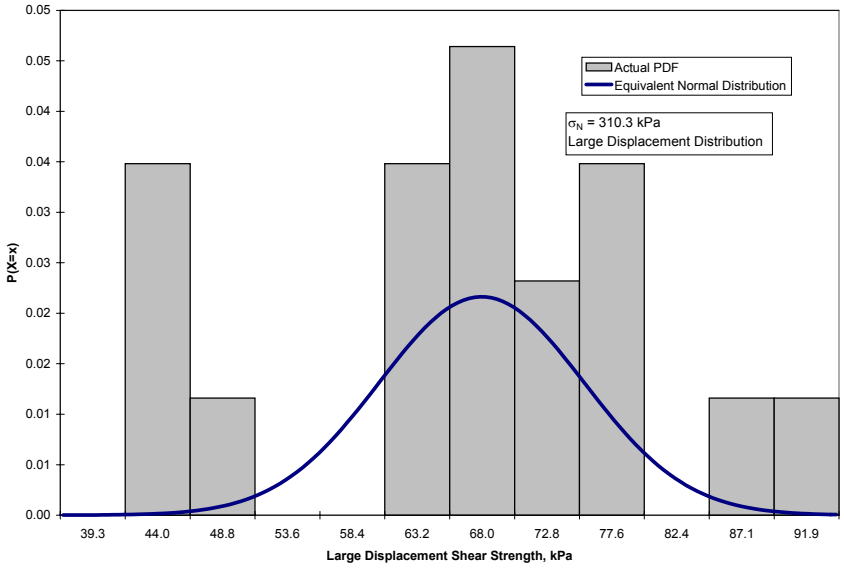

(b)

Figure 4.105: Variation in Large Displacement Shear Strength of GCL A for a Constant Normal Stress of 310.3 kPa, t_H = 168 hrs, t_C = 48 hrs, and SDR = 0.1 mm/min (Failure Envelope A5) ; (a) Cumulative Distribution Function (CDF), (b) Probability Density Function (PDF) with an Equivalent Normal Distribution

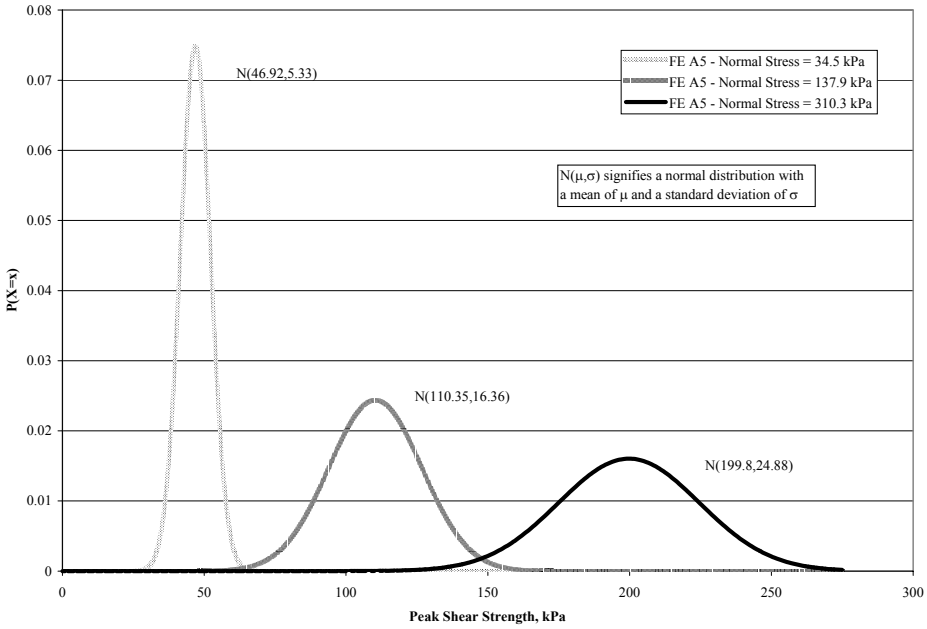

(a)

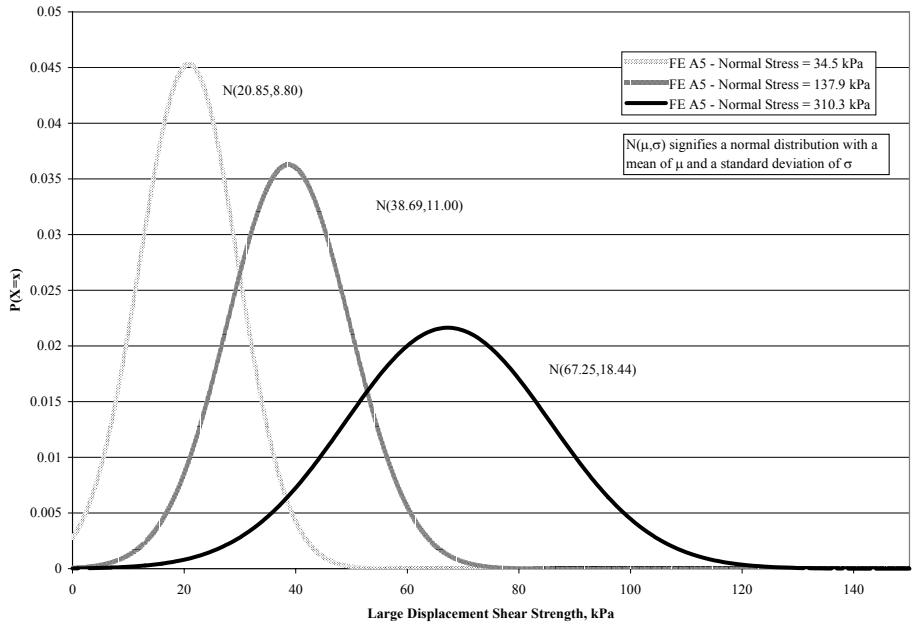

(b)

Figure 4.106: Probability Density Functions for Failure Envelope A5; (a) Peak Shear Strength Distributions, (b) Large Displacement Shear Strength Distributions

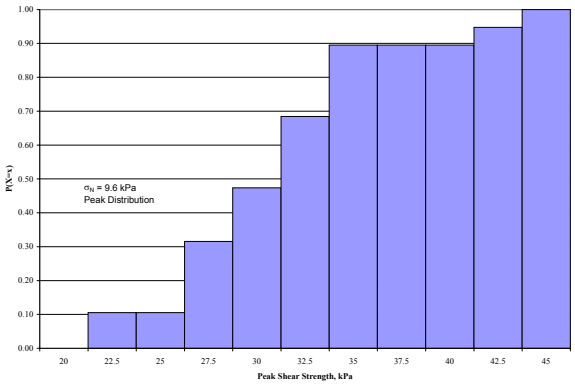

(a)

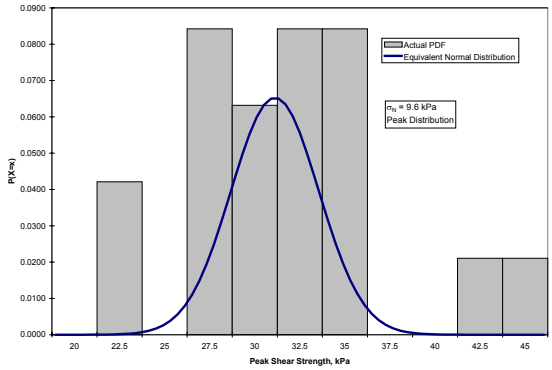

(b)

Figure 4.107: Variation in Peak Shear Strength of GCL A for a Constant Normal Stress of 9.6 kPa, (FE A3: t_H = 48 hrs, t_C = 0 hrs, and SDR = 1.0 mm/min); (a) Cumulative Distribution Function (CDF), (b) Probability Density Function (PDF) with an Equivalent Normal Distribution

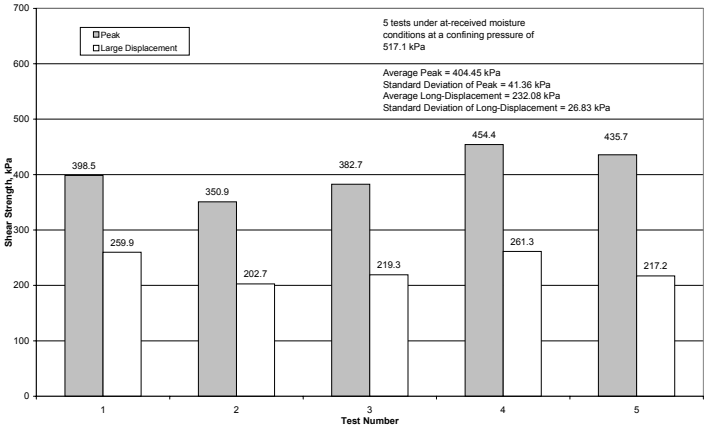

Figure 4.108: Variability in Peak and Large Displacement Shear Strength of GCL A Sheared at a Normal Stress of 517.1 kPa (No Hydration, No Consolidation, SDR = 1.0 mm/min)

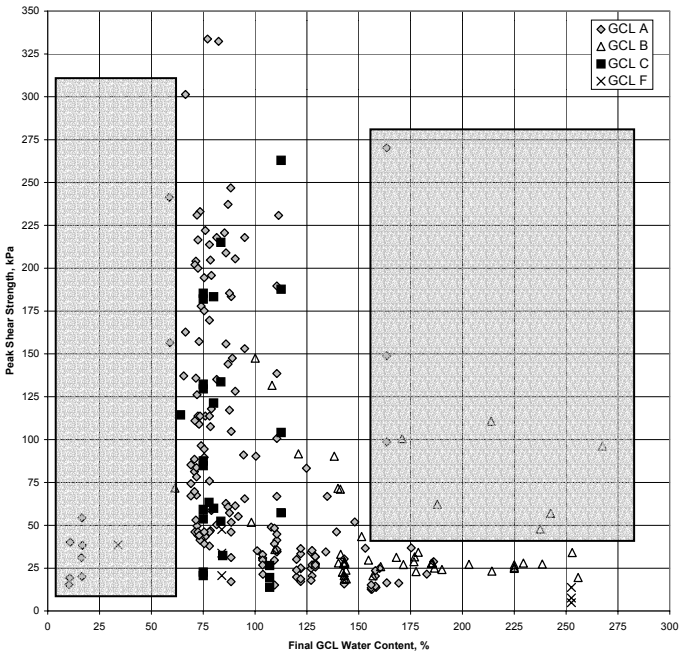

(a)

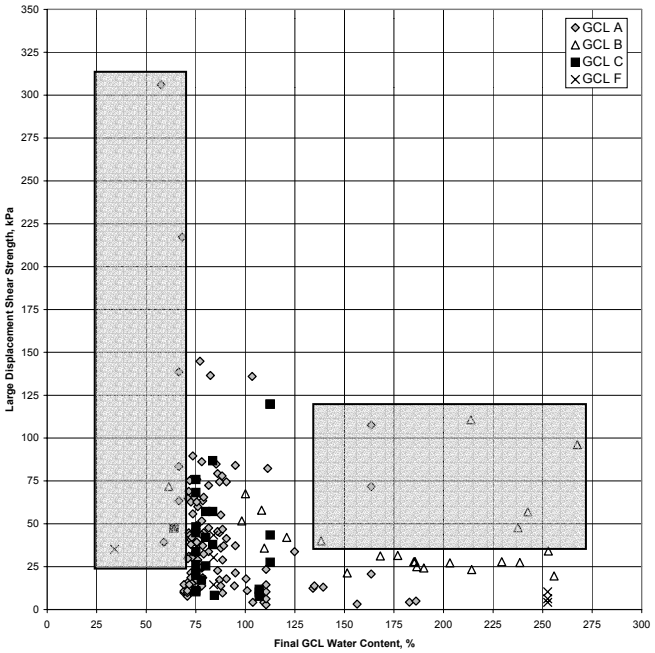

(b)

Figure 4.109: Final GCL Water Content as a Function of Shear Strength for All GCLs in the GCLSS Database, Outliers are Marked in Gray; (a) Peak, (b) Large Displacement

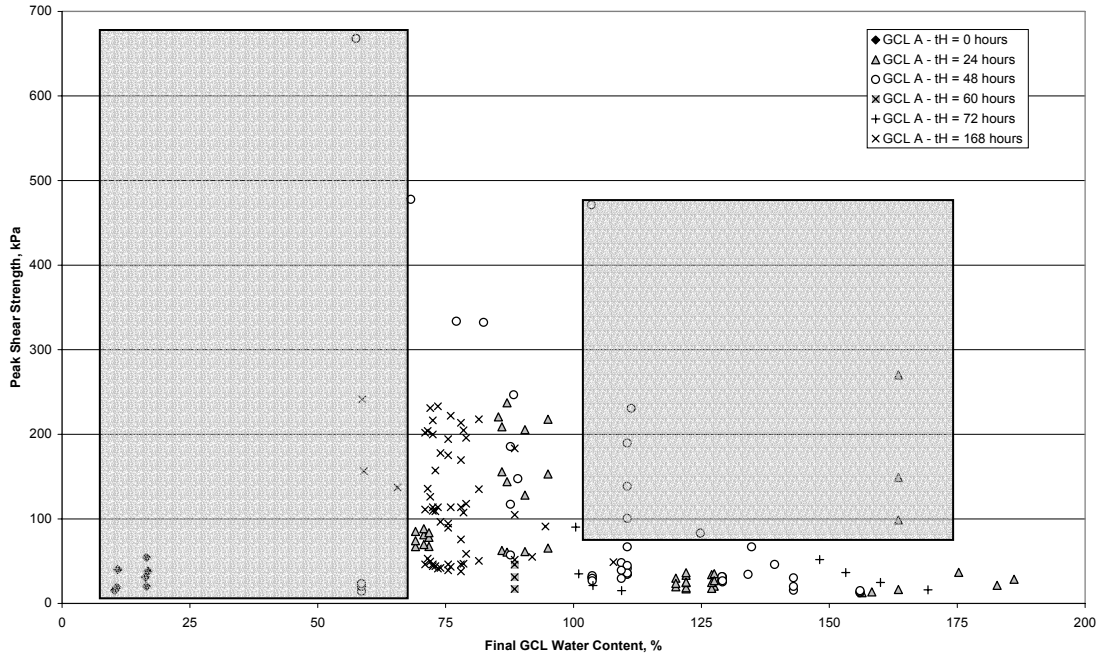

(a)

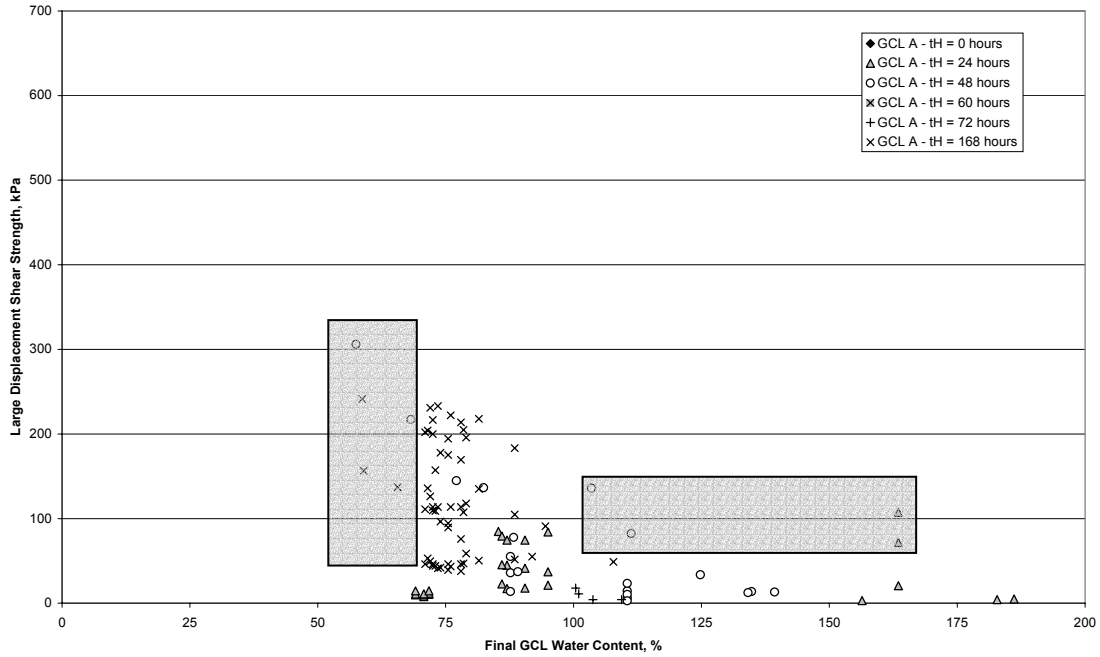

(b)

Figure 4.110: Final GCL Water Content as a Function of Shear Strength for GCL A, Effect of Time of Hydration, Outliers are Marked in Gray; (a) Peak, (b) Large Displacement

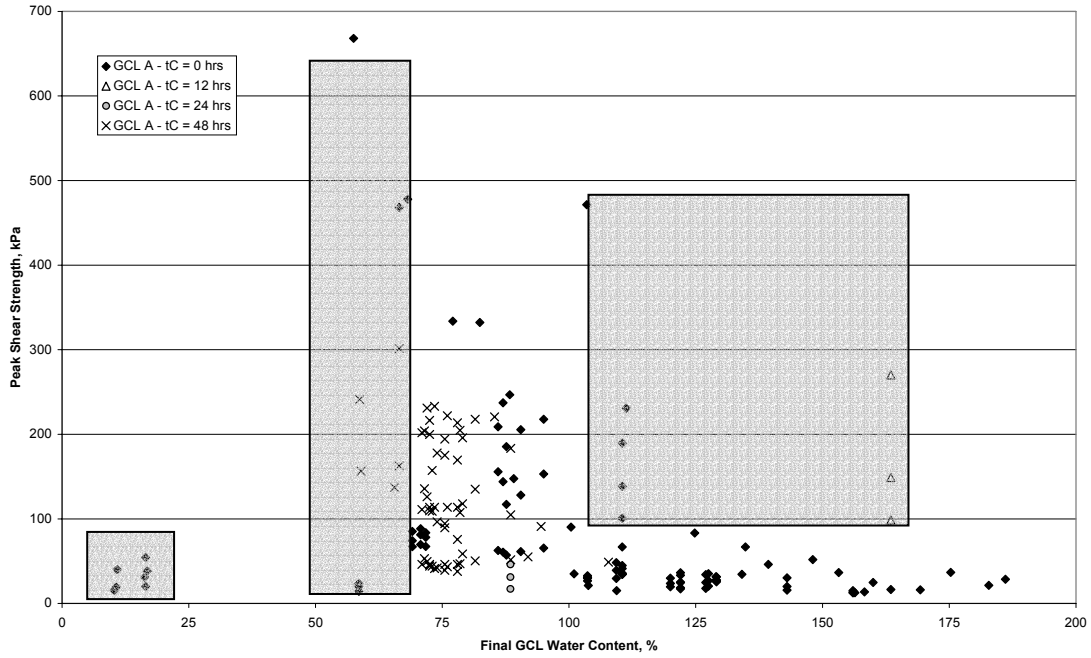

(a)

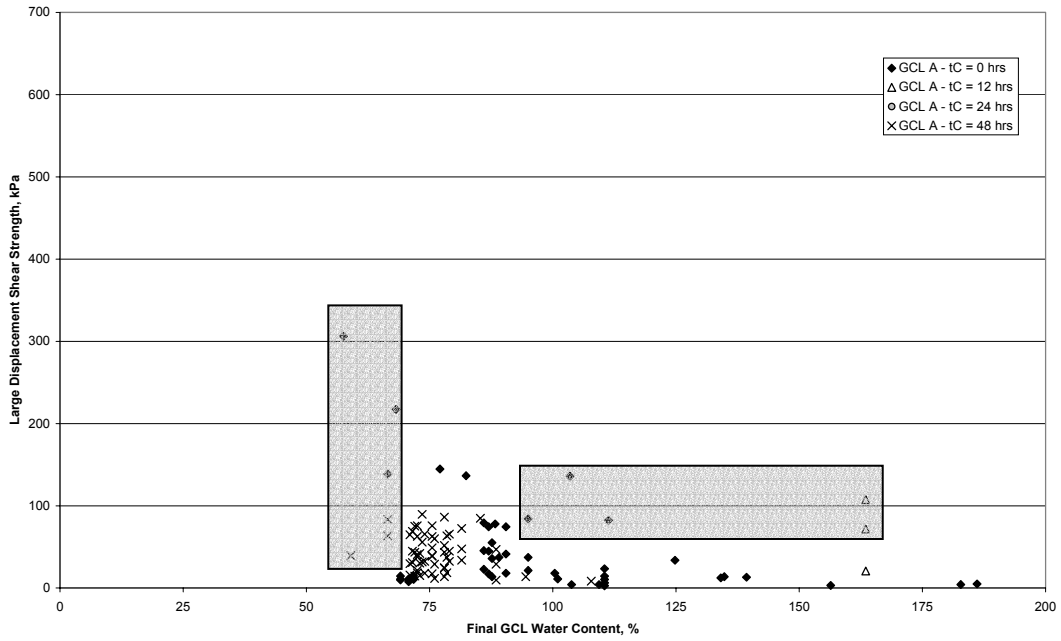

(b)

Figure 4.111: Final GCL Water Content as a Function of Shear Strength for GCL A, Effect of Time of Consolidation, Outliers are Marked in Gray; (a) Peak, (b) Large Displacement

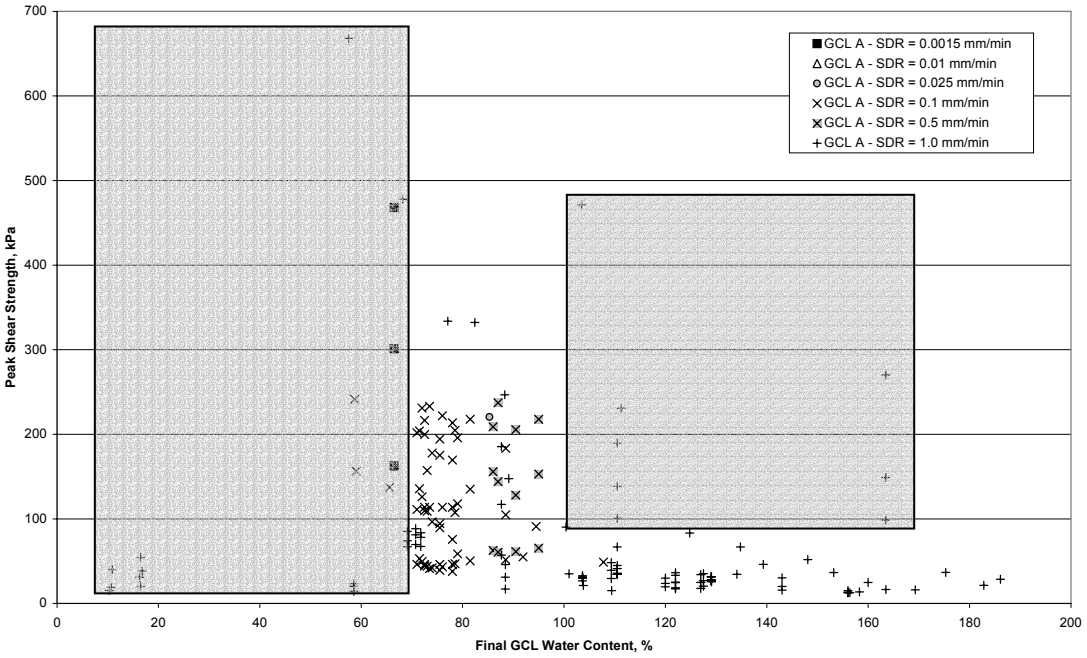

(a)

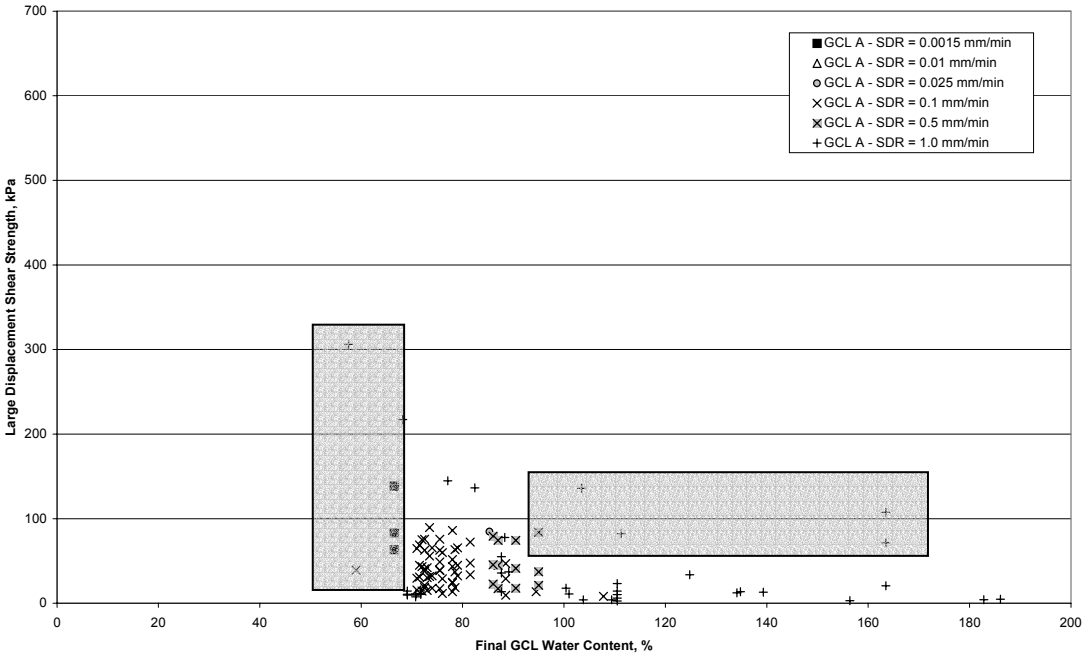

(b)

Figure 4.112: Final GCL Water Content as a Function of Shear Strength for GCL A, Effect of Shear Displacement Rate, Outliers are Marked in Gray; (a) Peak, (b) Large Displacement

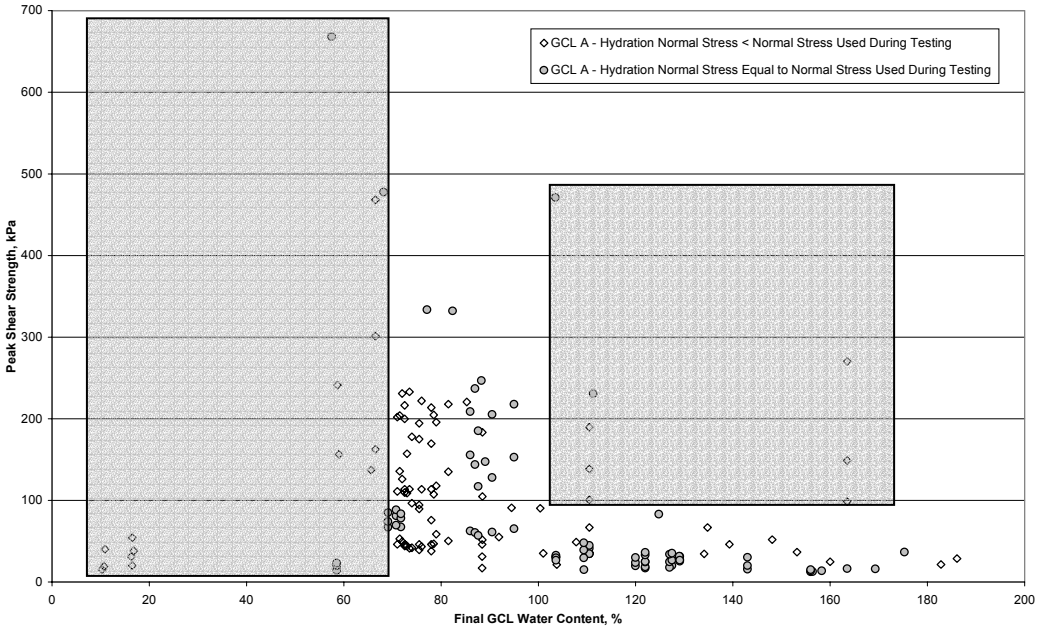

(a)

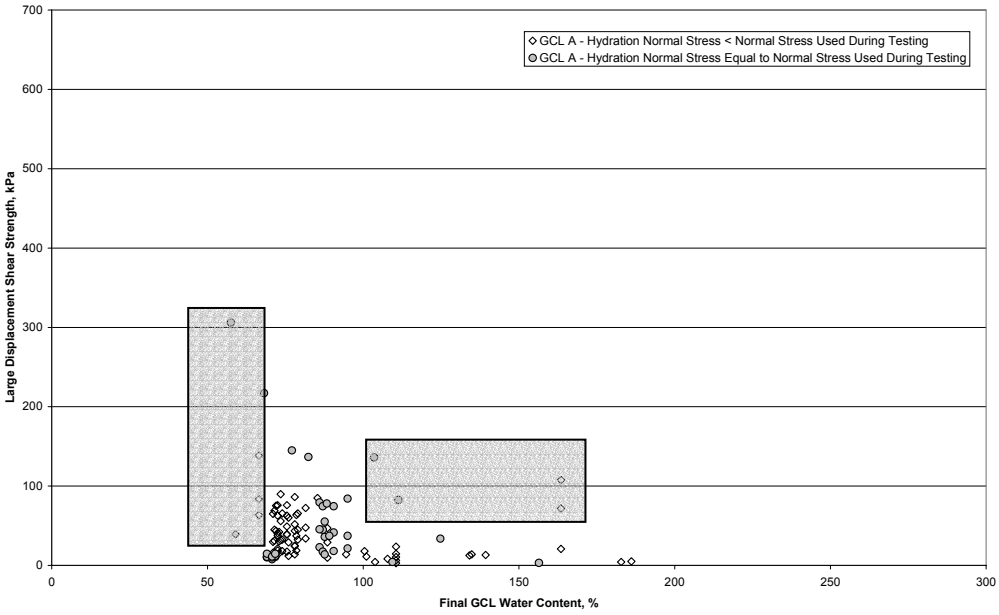

(b)

Figure 4.113: Final GCL Water Content as a Function of Large Displacement Shear Strength for GCL A, Effect of Order of Normal Stress Application, Outliers are Marked in Gray

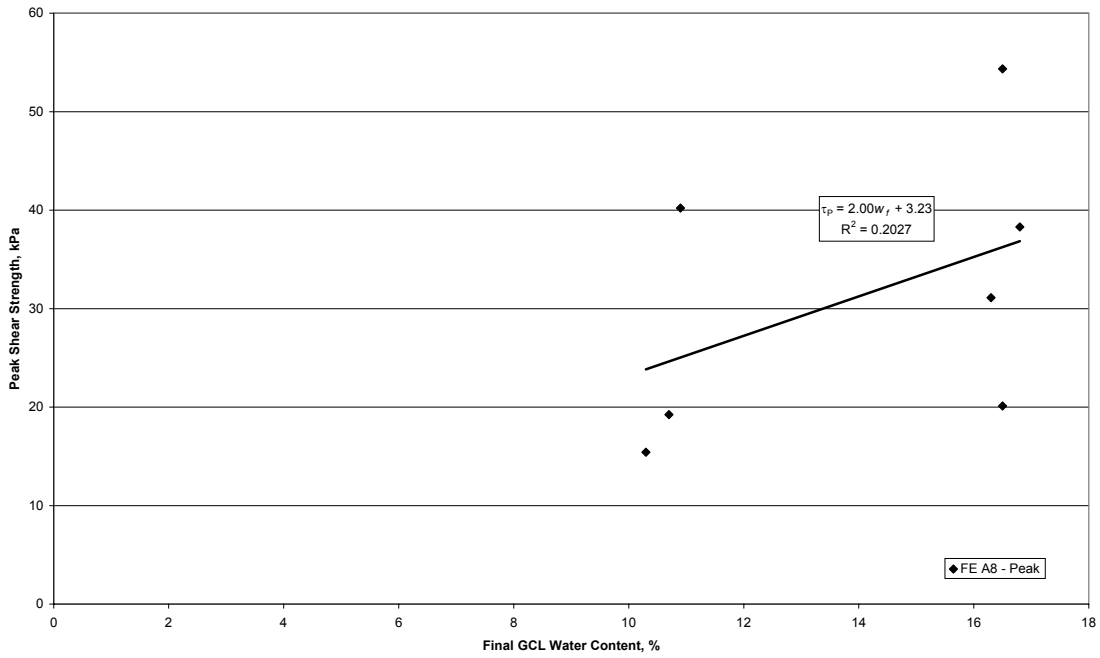

Figure 4.114: Variation in Peak Shear Strength with the Final GCL Water Content for Failure Envelope A8 (t_H = 0 hours, t_C = 0 hours, SDR = 1.0 mm/min)

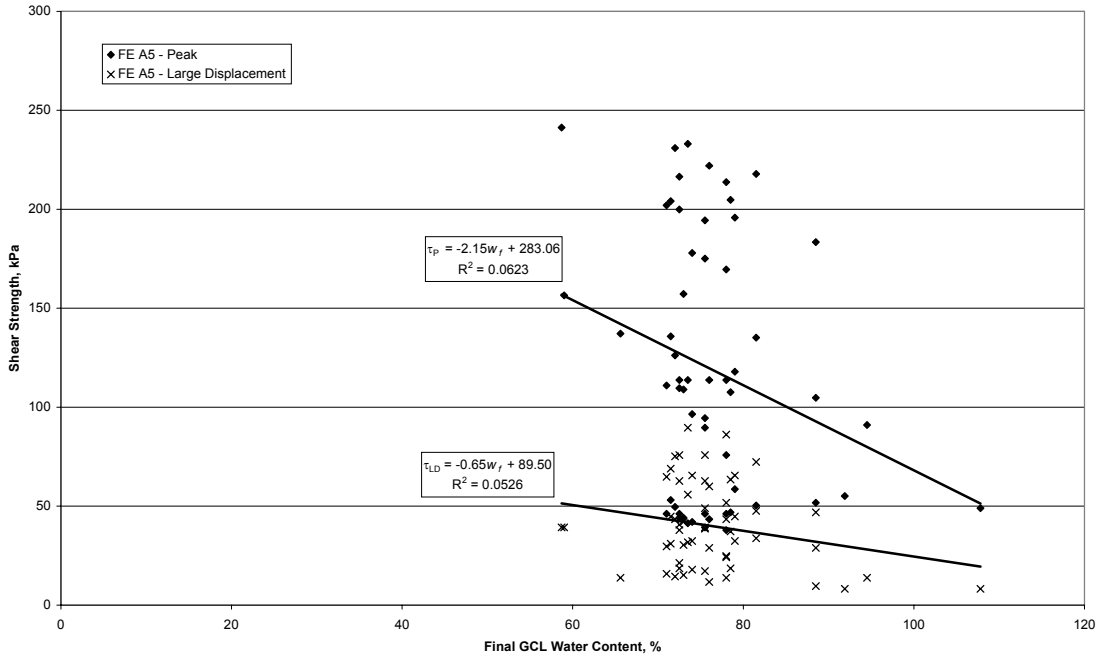

Figure 4.115: Variation in Shear Strength with the Final GCL Water Content for Failure Envelope A5 (t_H = 168 hours, t_C = 48 hours, SDR = 0.1 mm/min)

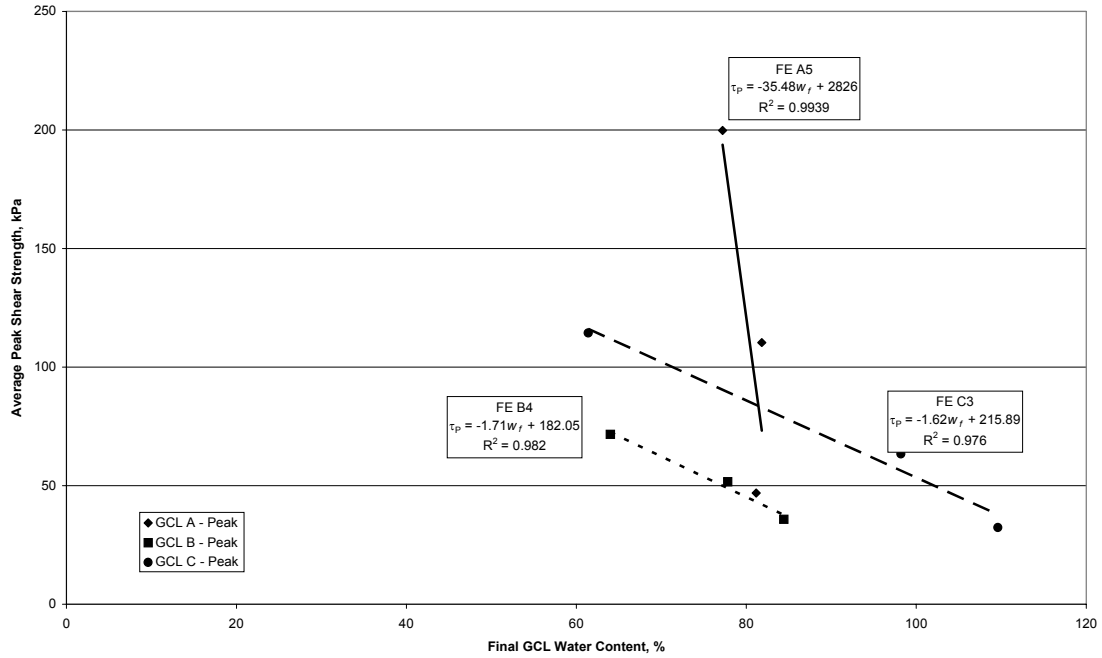

(a)

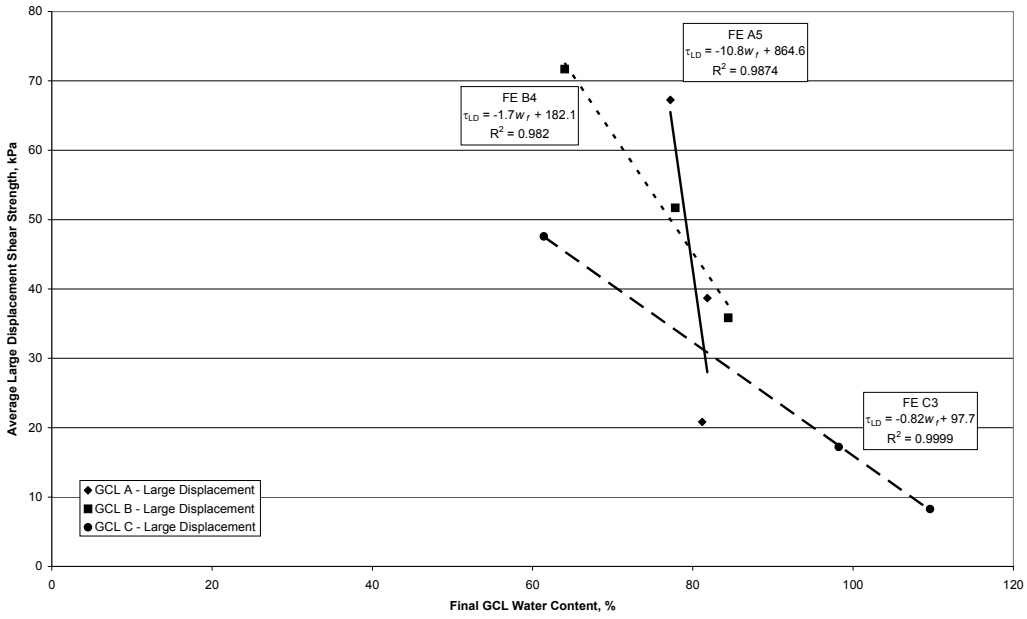

(b)

Figure 4.116: Variation in Average Shear Strength with the Final GCL Water Content for Three GCLs: (Failure Envelopes A5, B4 and C3: t_H = 168 hours, t_C = 48 hours, SDR = 0.1 mm/min); (a) Peak, (b) Large Displacement

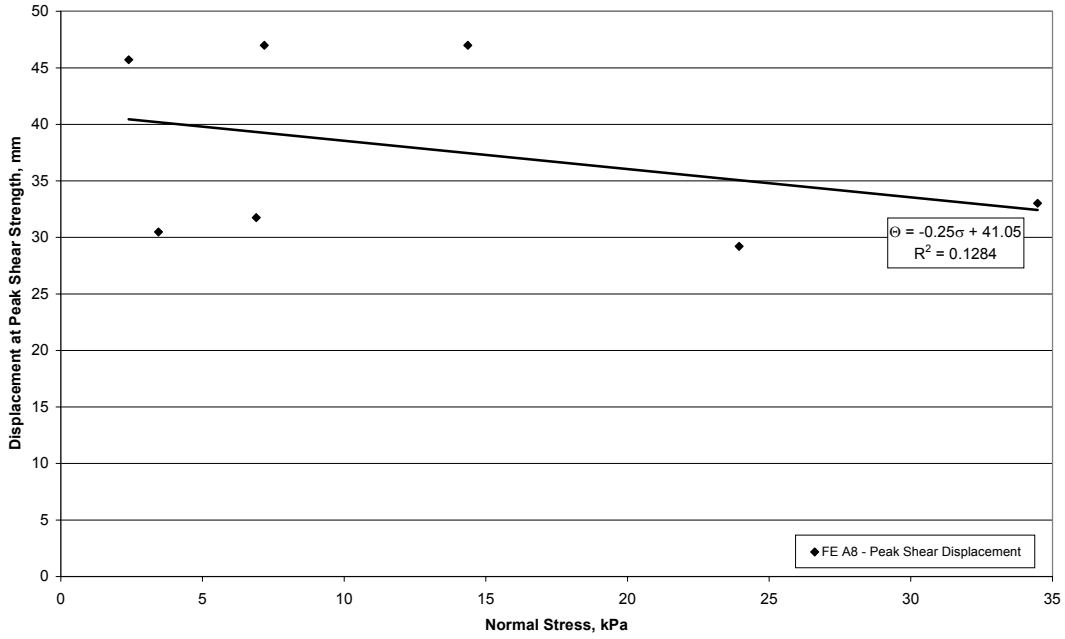

Figure 4.117: Variation in Displacement at Peak Shear Strength with Normal Stress for Failure Envelope A8 (t_H = 0 hours, t_C = 0 hours, SDR = 1.0 mm/min)

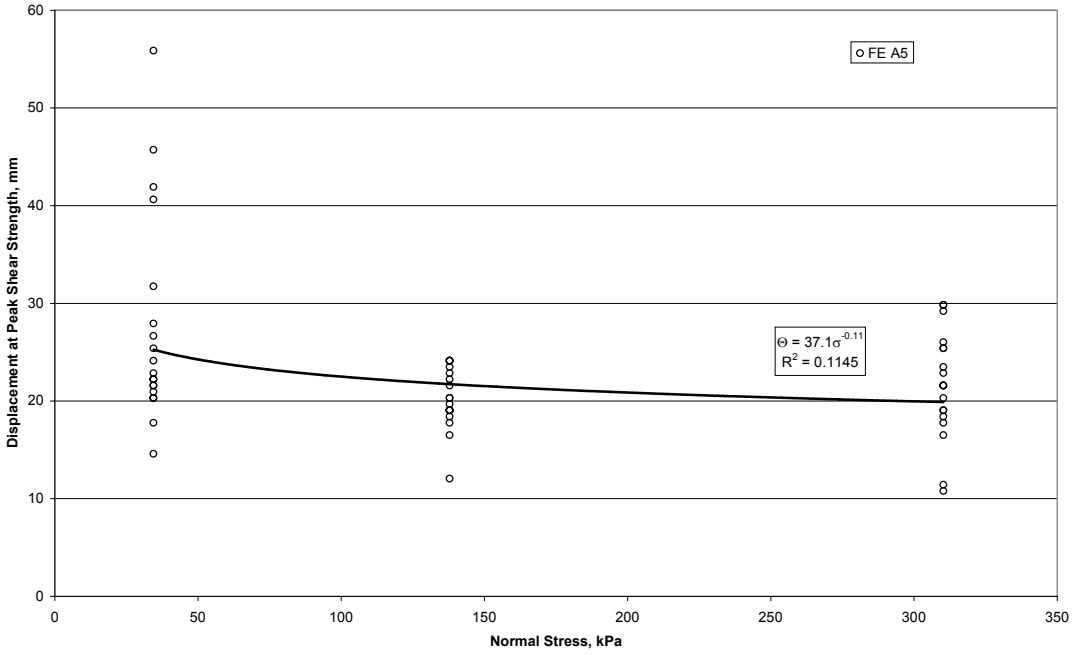

Figure 4.118: Variation in Displacement at Peak Shear Strength with Normal Stress for Failure Envelope A5 (t_H = 168 hours, t_C = 48 hours, SDR = 0.1 mm/min)

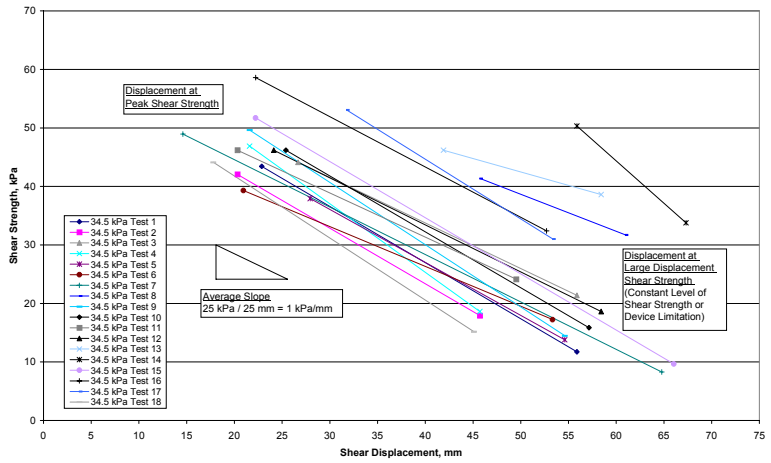

(a)

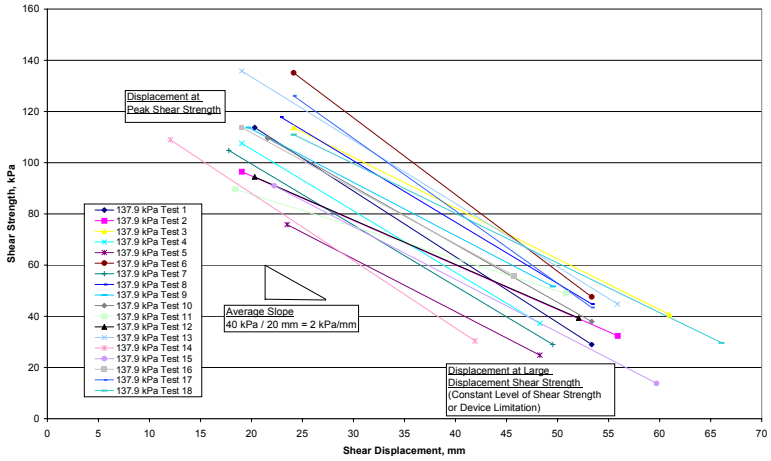

(b)

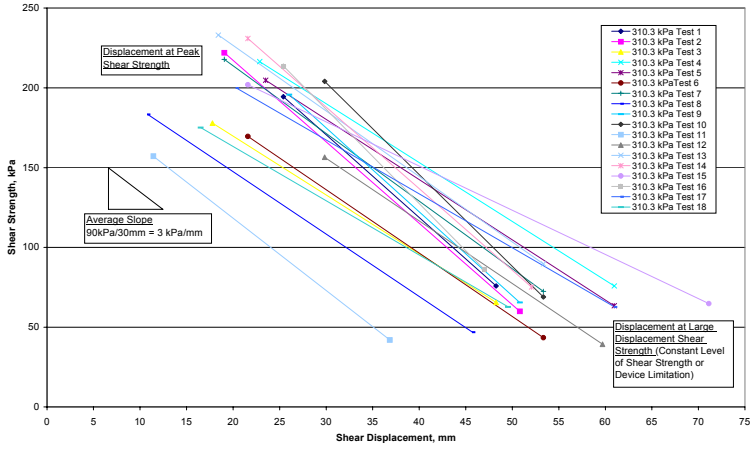

(c)

Figure 4.119: Movement from Displacement from Peak to Large Displacement Shear Strengths for Failure Envelope A5 (t_H = 168 hours, t_C = 48 hours, SDR = 0.1 mm/min); Normal Stress of (a) 34.5 kPa, (b) 137.9 kPa, (c) 310.3 kPa

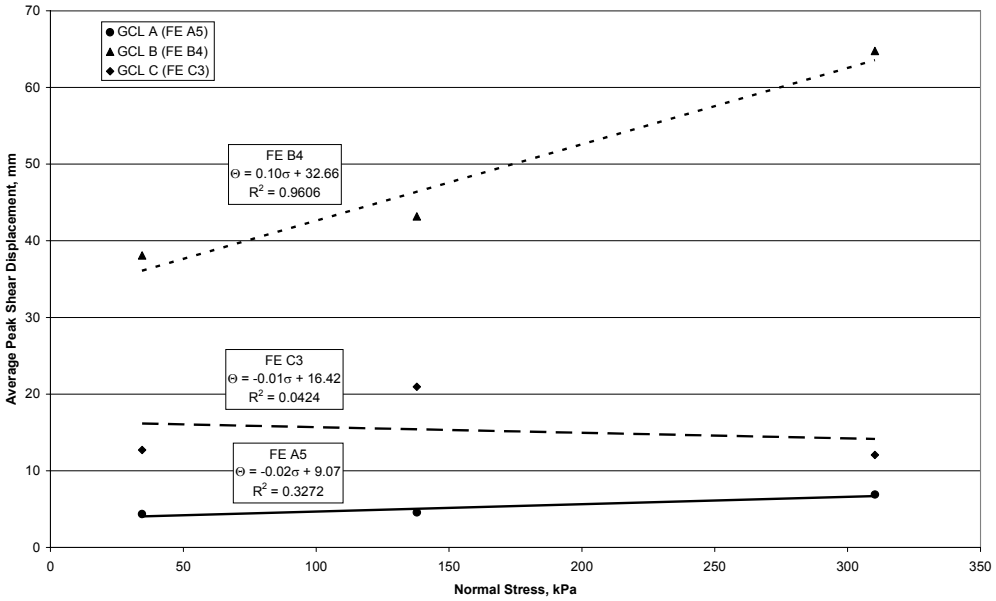

Figure 4.120: Variation in Displacement at Peak Shear Strength with Normal Stress for Failure Envelopes A5, B4 and C3 (t_H = 168 hours, t_C = 48 hours, SDR = 0.1 mm/min)

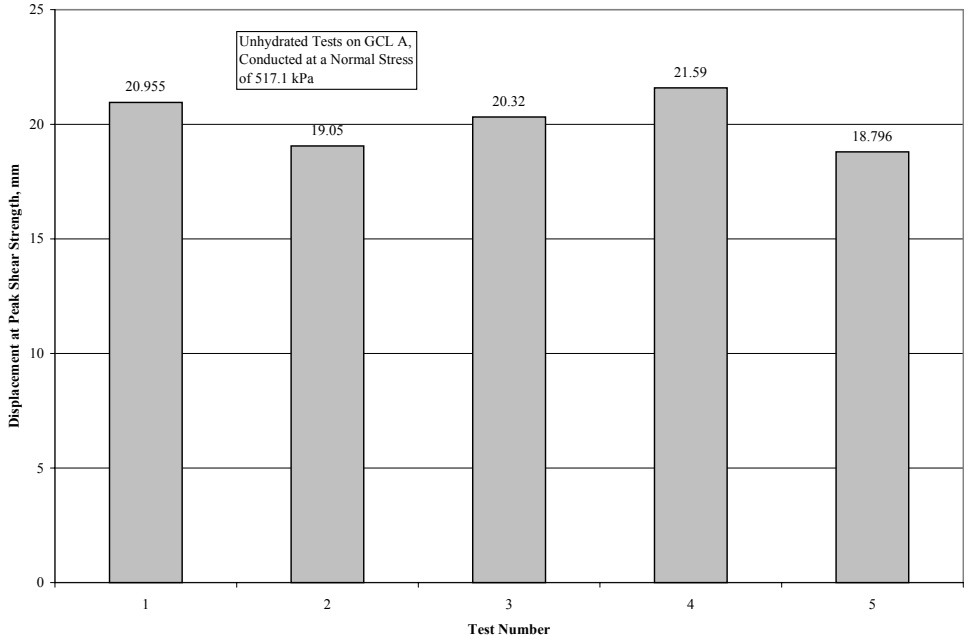

Figure 4.121: Variability in Displacement at Peak Shear Strength for GCL A Sheared at a Normal Stress of 517.1 kPa (No Hydration, No Consolidation, SDR = 1.0 mm/min)

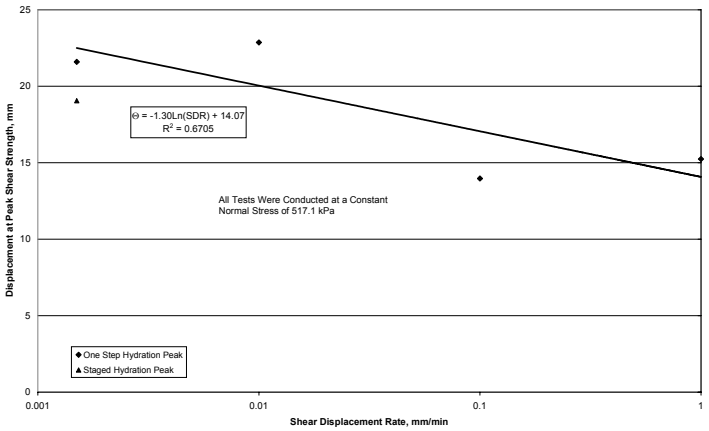

Figure 4.122: Displacement at Peak Shear Strength with Shear Displacement Rate for GCL A (Normal Stress of 517.1 kPa, t_H = 312 hours, t_C = 48 hours)

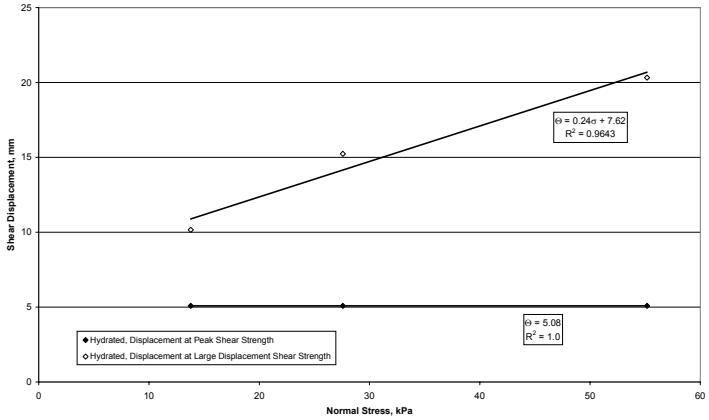

(a)

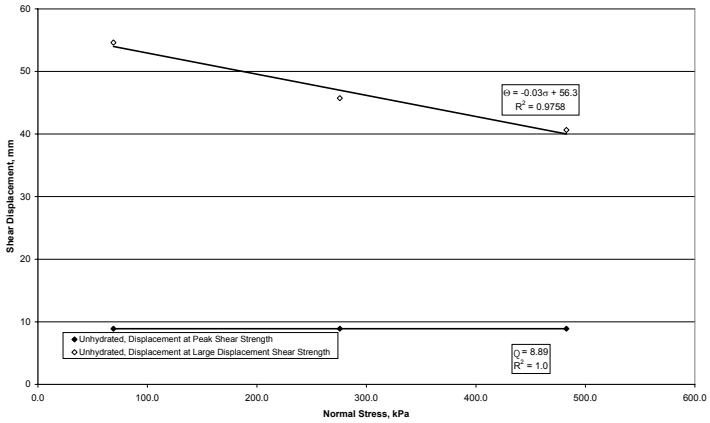

(b)

Figure 4.123: Variation in Displacement at Peak and Large Displacement Shear Strength for Unreinforced GCL Specimens (GCL F), (a) t_H = 168 hours, t_C = 0 hours, SDR = 1.0 mm/min; (b) t_H = 0 hours, t_C = 0 hours, SDR = 1.0 mm/min

5 Shear Strength of GCL-Geomembrane Interfaces

5.1 Overview of the Database of Interface Shear Strength of GCLs

5.1.1 The GCLSS Database

The Soil-Geosynthetics Interactions (SGI®) laboratory, formerly of GeoSyntec Consultants, performed 332 direct shear tests focusing on GCL-geomembrane interface shear strength since 1992. The data obtained from these tests was used for individual projects but has not been compiled for a global analysis until this point.

5.1.2 Information Included in the GCLSS Database

Test conditions and reporting of results for GCL-geomembrane direct shear tests conducted by the SGI® laboratory over the period 1992 to 2001 are consistent with the requirements of the standard for internal and interface shear strength resistance of GCLs, ASTM D6243. For each shear strength test series on a GCL in the GCLSS database, reported test conditions include the specimen preparation and confinement procedures, hydration procedure, times of hydration and consolidation, normal stresses applied during hydration, consolidation and testing, and shear displacement rate. For each individual test (under a single test normal stress) the SGI® laboratory reported the applied shear stress as a function of shear displacement, the corresponding peak and large-displacement shear strength values, and the change in GCL water content from unhydrated conditions to the completion of the test. Table 4.1 lists the variables used in the GCLSS database.

As pore pressures may not be accurately measured for a GCL-geomembrane interface in a direct shear device during shearing, a total stress approach is used in this chapter. To infer the pore water pressures generated during testing and thus the effective stress on the interface, the test conditions affecting the generation of pore water pressures (*i.e.* the times of hydration and consolidation and the shear displacement rate) are investigated.

5.1.3 Shear Strength Test Procedures

The procedures used by the SGI® laboratory for GCL interface testing are consistent with those discussed in section 4.1.3 of this report for internal GCL shear

strength testing. The major difference in the testing of GCL shear strength is the specimen confinement procedures.

Test specimens are prepared by first cutting sections of GCL and geomembrane with dimensions larger than the direct shear box. Typically, the geomembrane is placed atop a rigid layer of concrete sand, and the end opposite from the direction of shearing is clamped securely in place. GCL specimens are prepared by cutting sections of GCL with dimensions larger than the direct shear box, trimming the sections so that a flap of the upper carrier geotextile extends slightly in the direction of shear displacement. The GCL is typically affixed to the top box, and is placed in contact with a rigid wooden substrate with textured steel gripping surfaces to eliminate slippage between the carrier geotextile and the substrate. The upper carrier geotextile is wrapped around the rigid substrate, and is held in place with another set of rigid substrates. In this manner, if the top box is moved, the upper carrier geotextile of the GCL imparts a shear force on the interface between the GCL and the geomembrane. This test setup allows failure of the GCL-geomembrane interface as well as internal GCL failure, whichever has lower shear strength. A detail of the test setup is shown in Figure 2.6.

The GCL-geomembrane interface is typically hydrated and consolidated as a unit in order to model the hydration procedure for a GCL interface in the field. Often, several holes are placed in the geomembrane to allow a worst-case hydration scenario. A shear force is applied by pulling the GCL confined in the top box across the geomembrane in the stationary lower box. After testing, the location of the failure is verified to ensure that failure occurred at the interface between the GCL and the geomembrane.

5.2 Shear Strength Results and Preliminary Analysis

5.2.1 Background

Many different interface combinations of GCLs and geomembranes were tested by the SGI® laboratory over the period 1992 to 2001. Table 2.2 lists the different name designations for each of the GCLs tested for interface shear strength, and Table 2.4 lists the different name designations for the geomembranes tested for

interface shear strength. The GCLs are listed by capital letters beginning with *A*, while the geomembranes are listed by lower case letters beginning with *s*. The GCLs are listed by product type, and information on the carrier geosynthetics as well as the reinforcement characteristics is included. The GCLs that were tested for interface shear strength include:

- Bentomat® ST (GCL A)
- Claymax® 500SP (GCL B)
- Bentofix® NS (GCL C)
- Claymax® 200R (GCL F)
- Bentomat® CS (GCL G)
- GSE® Gundseal (GCL K)

The geomembranes may have different polymer types or texturing characteristics, which are listed in Table 2.3. These geomembranes include:

- Textured High Density Polyethylene (THDPE)
- Textured Very Low Density Polyethylene (TVLDPE)
- Textured Linear Low Density Polyethylene (TLLDPE)
- Smooth High Density Polyethylene (SHDPE)
- Smooth Very Low Density Polyethylene (SVLDPE)
- Smooth Linear Low Density Polyethylene (SLLDPE)
- Faille Finish and Smooth Finish Polyvinyl Chloride (PVC)

In Table 2.4, the geomembranes are listed by the manufacturing company, and the geomembrane polymer types produced by each manufacturer that were tested by the SGI® laboratory are listed. The analysis of the GCL interface shear strength test results in the GCLSS database is slightly more complex than the internal GCL test results. Many different interface combinations of GCLs and geomembranes are present in the database, and they may be grouped by GCL, geomembrane polymer, geomembrane texturing and geomembrane thickness. Geomembrane texturing has been reported to affect the interface shear strength in past studies, but the effects of the GCL characteristics, geomembrane polymer type and thickness on the interface shear strength have not been reported. A preliminary analysis is necessary to find the GCL and geomembrane characteristics that affect the interface shear strength so that

they may be investigated further in later sections of this chapter. The preliminary analysis includes a histogram analysis to present the different interface possibilities visually and an equivalent friction angle analysis to investigate the effect of each of the GCL and geomembrane characteristics on the interface shear strength.

5.2.2 Histogram Analysis

Figures 5.1 through 5.4 present histograms which characterize the different GCL-geomembrane interfaces. Figure 5.1 shows a histogram of the number of GCL-geomembrane interfaces of each geomembrane polymer groups. This figure shows that most of the geomembranes tested (244) are textured high density polyethylene (THDPE). Figure 5.2 shows a breakdown by the geomembrane manufacturers (see Table 2.4). The geomembrane polymer manufactured by one company may have different characteristics (*i.e.* manufacturing procedures related to creation of asperities or other texturing features on the geomembrane surface) than that manufactured by another company. Figure 5.3 shows a breakdown by GCL type. Each geomembrane polymer has interfaces with several GCLs. This allows analysis of the effect of the GCL reinforcement characteristics on the interface shear strength. Figure 5.4 shows a breakdown of Figure 5.1 by geomembrane thickness. There are several thicknesses for each geomembrane polymer. These three figures, although confusing, illustrate the many different material factors that must be considered in the shear strength analysis of a GCL-geomembrane interface.

5.2.3 Equivalent Friction Angle Analysis

Figures 5.5(a) and 5.5(b) show the peak and large-displacement shear strengths for all GCL-geomembrane interfaces. These figures show that the data is less variable than the internal GCL shear strength. Still, the variability increases with normal stress, as was the case for internal GCL shear strength. Also, as the data at low normal stresses appears to fall within the same bounds as the data at high normal stresses (*i.e.* the interfaces have small adhesion values), an equivalent friction angle analysis may be appropriate. As only three tests were conducted at normal stresses greater than 700 kPa, they will not be included in this particular analysis.

Table 5.1 lists 18 different sets of GCL-geomembrane interfaces that are investigated using an equivalent friction angle analysis. This table groups all of the GCL-geomembrane interfaces by the different geomembranes (sets 1 through 6), and also groups the GCL-textured HDPE geomembrane interfaces by the different GCLs (sets 7 through 10), geomembrane manufacturers (sets 11 through 15) and geomembrane thickness (sets 16 through 18). The details of the equivalent friction angle analysis are presented in Section 4.2.2. However, the definition of the equivalent friction angle is slightly different:

- The "average" equivalent friction angle is developed using linear regression techniques (Equation 4.1)
- The weighting factor for the standard deviation is the inverse of the normal stress (Equation 4.5), and the standard deviation is defined using standard linear regression techniques (Equation 4.7)
- The upper and lower equivalent friction angle bounds (Equations 4.8 and 4.9) on the data are defined by 2 standard deviations away from the average equivalent friction angle
- Data points for normal stresses greater than *700* kPa were not considered in the equivalent friction angle analysis

The only difference is the range of normal stresses over which the equivalent friction angle was developed (0 to 700 kPa instead of 0 to 550 kPa). The rationale of the wider normal stress range is that the interface shear strength results had significantly less scatter than the internal shear strength results. If the linear regression has a low R^2 value the accuracy of the upper and lower bounds is limited.

Figure 5.6 shows the peak shear strength values for all of the GCL-geomembrane interfaces in the database. The average equivalent friction angles for each geomembrane polymer type are also shown in this figure. All smooth geomembrane polymers are grouped together except for the faille/smooth finish PVC geomembranes, which have a significantly different shear strength behavior than the other smooth geomembranes. Figure 5.6(a) shows the full data set, while Figure 5.6(b) shows a detail for low normal stresses (*i.e.* below 50 kPa). A detail of low normal stresses is helpful as the majority of the shear strength tests were conducted at

low normal stresses, and they may significantly affect the results of the linear regression analysis. Figure 5.6(b) shows that there is not a significant adhesive component to the peak shear strength of the GCL-geomembrane interface. The textured VLDE geomembrane has the greatest peak equivalent friction angle, followed by the textured LLDPE, textured HDPE, PVC and smooth geomembranes. However, it should be noted that as the textured VLDPE, textured LLDPE and PVC geomembranes were tested only at low normal stresses. The difference in normal stress ranges between the VLDPE and HDPE interfaces will be investigated later in this section.

Figure 5.7 shows the large-displacement shear strength values for all of the GCL-geomembrane interfaces in the database. The average equivalent friction angles for each geomembrane polymer type are also included. Figure 5.7(a) shows the full data set while Figure 5.7(b) shows a detail of low normal stresses. There is a lower scatter in the large-displacement shear strength than in the peak shear strength. The order of large-displacement equivalent friction angles is similar in this figure to that for peak equivalent friction angles, except for the fact that the faille/smooth finished PVC geomembranes have a greater large-displacement equivalent friction angle than the textured HDPE geomembranes. This indicates that textured HDPE geomembranes show a large post-peak shear strength loss (*i.e.* large difference between peak and large displacement shear strength).

Figure 5.8 shows the shear strength values for all textured geomembrane interfaces in the database. This figure and all following figures in this section include two separate figures: (a) peak shear strength and (b) large-displacement shear strength. These figures include the average peak and large-displacement equivalent friction angles, respectively, as well as upper and lower equivalent friction angle bounds. Assessment of Figures 5.8(a) and 5.8(b) indicates that there is about an 8 degree drop in equivalent friction angle from peak to large-displacement conditions, and the upper and lower bounds have similar spread from the average equivalent friction angle for peak and large-displacement conditions. This implies that the variability in shear strength is similar for peak and large-displacement conditions for textured GCLs.

Figure 5.9 shows the shear strength values for all smooth geomembrane interfaces in the database. The peak equivalent friction angle for smooth geomembranes is less than textured geomembranes (10.0^0 for smooth geomembranes and 20.9^0 for textured geomembranes). The large-displacement friction angle for smooth geomembranes is also less than that for textured geomembranes, but there is not as significant a difference (9.4^0 for smooth geomembranes and 12.8^0 for textured geomembranes). Also, there is no significant post-peak shear strength loss for smooth geomembranes (10.0^0 to 9.4^0). This is most likely because there is no change in the interlocking capabilities from interface to interface. A non-linear failure envelope may be apparent from close inspection of these figures, as the low shear strength values are above the average equivalent failure envelope, and the higher shear strength values are below this line.

Figure 5.10 shows the shear strength of all textured HDPE geomembrane interfaces. The peak and large-displacement equivalent friction angles for the textured HDPE geomembranes are nearly the same as those for all textured geomembranes, as the majority of textured geomembranes are HDPE. This figure also includes shear strength test results for the interface between a textured HDPE geomembrane and a needle-punched GCL reported by other studies (Pavlik, 1997; Triplett and Fox, 2001). The data reported by other studies is not used to define the equivalent friction angles. The test results reported by Pavlik (1997) and Triplett and Fox (2001) are presented in Tables 5.1 and 5.2, respectively. These test results from other studies fall within the upper and lower equivalent friction angle bounds developed from the data in the GCLSS database. This indicates that the shear strength test results in the GCLSS database are consistent with those of past studies.

Figure 5.11 shows the peak and large-displacement shear strength values for all PVC geomembrane interfaces. All of these interfaces include GCL *A*, implying that differences in behavior are most likely the result of the geomembrane characteristics. It should be noted that the faille and smooth geomembrane interfaces have similar shear strength values. These geomembrane interfaces have higher peak equivalent friction angles than smooth geomembranes, and have only a slightly lower peak equivalent friction angle than textured HDPE geomembrane interfaces. The

large-displacement equivalent friction angle for the PVC geomembrane interfaces is greater than that of the textured HDPE geomembrane, which is because the PVC geomembrane interfaces have no reported post-peak shear strength loss. However, the average behavior for the textured HDPE geomembrane interface was developed from a wide range of normal stresses (2.4 to 969 kPa), while that for the PVC geomembrane interface was developed for normal stresses below 50 kPa.

Figure 5.12 shows the peak and large-displacement shear strength values for all textured VLDPE geomembrane interfaces. At low normal stresses, the textured VLDPE geomembrane interfaces have higher peak and large-displacement shear strength than the textured HDPE geomembranes. This is most likely due to the flexibility of the VLDPE geomembrane compared to the HDPE geomembrane. As shearing occurs, a flexible geomembrane may "plow" over the GCL, which in essence increases the contact area with the GCL and thus the interface shear strength (Dove and Frost, 1999). However, as the behavior of the textured VLDPE geomembrane is not investigated at higher normal stresses, the findings may not be generalized to higher normal stresses. The behavior of textured HDPE geomembranes at low normal stresses will be investigated later in this section. There is a relatively large scatter in the peak and large-displacement data points.

Figure 5.13 shows the peak and large-displacement shear strength values for all textured LLDPE geomembrane interfaces. The behavior of this interface is similar to that of the textured VLDPE geomembrane interface investigated in Figure 5.12, although the average peak and large-displacement equivalent friction angles for the textured LLDPE geomembrane interfaces are slightly lower.

Figure 5.14 shows the shear strength of all textured HDPE geomembrane interfaces, grouped by the GCL component of the interface. The GCL data points for interfaces involving GCLs *A* and *C*, lie between the upper and lower bounds (21.5^0 and 19.8^0, respectively). The peak shear strength data points for interfaces involving GCL *B* lie below the lower equivalent friction angle bound (13.2^0), and those for GCL *K* are generally lie above the upper equivalent friction angle bound (23.6^0). The behavior for these outlier points are discussed in detail later in this chapter.

The shear strength values for each of the GCL interfaces may be better understood by examining the values for each GCL separately. Figure 5.15 shows the peak and large-displacement shear strength values for all textured HDPE geomembrane interfaces with GCL *A*, grouped by geomembrane thickness and geomembrane manufacturer. Figure 5.15(a) shows that the interfaces with a 60-mil geomembrane *s* are well below lower equivalent friction angle bound, yet the interfaces with an 80-mil geomembrane *s* are within the range of one standard deviation above and below the average equivalent friction angle. This difference is most likely due to differences in test conditions, and is addressed later in this chapter. Figure 5.15(b) shows that the majority of the shear strength values fall within the upper and lower equivalent friction angle bounds for large-displacement conditions.

Figure 5.16 shows the peak and large-displacement shear strength values for all textured HDPE geomembrane interfaces with GCL *B*, grouped by geomembrane thickness and geomembrane manufacturer. This figure shows that the peak and large-displacement average equivalent friction angles for this interface are lower than the other textured HDPE geomembrane interfaces. The lower peak and large-displacement shear strength values may be due to the difference in interlocking characteristics of this stitch-bonded GCL when compared to that of needle-punched GCLs, or it may be due to the extrusion of different amounts of sodium bentonite for GCLs with different reinforcement characteristics. In addition, it should be noted that the upper and lower bounds are widely spread from the average equivalent friction angles. The difference is most likely due to differences in test conditions.

Figure 5.17 shows the peak and large-displacement shear strength values for all textured HDPE geomembrane interfaces with GCL *C*, grouped by geomembrane thickness and geomembrane manufacturer. It can be seen that the shear strength of interfaces between GCL *C* and geomembrane *s* generally lie below those for geomembrane *t* for both peak and large-displacement conditions. As geomembranes *s* and *t* are both textured HDPE, the difference in shear strength is most likely due to texturing differences between the two geomembrane manufacturers or the test conditions.

Figure 5.18 shows the peak and large-displacement shear strength values for all textured HDPE geomembrane interfaces with GCL *K*, grouped by geomembrane thickness and geomembrane manufacturer. The peak and large displacement equivalent friction angles for this interface are greater than those of all other GCL-geomembrane interfaces. This is due to the fact that GCL *K* is a geomembrane-backed layer of sodium bentonite placed in contact with another geomembrane on the sodium bentonite surface. In other words, this GCL-geomembrane interface is a layer of sodium bentonite sandwiched between two geomembranes. This interface was included with the analysis of the interface between the woven carrier geotextile of a GCL and a geomembrane because sodium bentonite often extrudes through the woven carrier geotextile, resulting in a layer of unreinforced sodium bentonite at the interface. Thus, the extruded bentonite from a GCL interface should behave similarly to an interface involving GCL *K*. Still, close inspection of the GCLSS database indicates that several of these interfaces were conducted under unhydrated conditions.

Figure 5.19 shows the same data points as Figure 5.14, but the data points are grouped geomembrane manufacturer. This figure shows that most of the equivalent friction angles for the geomembrane manufacturer sets are around 21^0. Geomembrane manufacturer *u* has slightly higher peak and large displacement equivalent friction angles (26.1 and 16.7^0, respectively) than the other geomembrane manufacturers. Geomembrane *t* has the lowest peak equivalent friction angle of 16.8^0. As mentioned above, the difference between the different interface sets is most likely due to specific geomembrane manufacturer texturing techniques.

Figure 5.20 shows the same data points as Figure 5.14, but the data points are grouped by geomembrane thickness. In other words, for each GCL interface, there are several different thicknesses of textured HDPE geomembranes in the GCLSS database. It should be noted that each GCL data point has a different symbol and is shaded according to the given thickness of the geomembrane. No clear trend can be found for the effect of the thickness of the geomembrane on the peak or large-displacement shear strength in these figures. The interface shear strength appears to be more sensitive to the GCL type and geomembrane manufacturer than the thickness of the geomembrane.

Table 5.4 summarizes the average peak and large-displacement equivalent friction angles for each set of GCL-geomembrane interfaces, grouped by geomembrane polymer. Also included in this table are the upper and lower equivalent friction angle bounds for peak and large-displacement shear strength. The textured VLDPE and LLDPE geomembrane interfaces have the highest peak and large-displacement equivalent friction angle for low normal stresses. The peak equivalent friction angle for all textured geomembrane interfaces is twice as large as that for smooth geomembrane interfaces, while the large-displacement equivalent friction angles are roughly the same.

Table 5.5 summarizes the peak and large-displacement equivalent friction angles for the sets of textured HDPE geomembrane interfaces. The first four rows show a comparison between the equivalent friction angles of interfaces with different GCLs. There are large differences depending on the reinforcement characteristics of the GCL. Stitch-bonded GCLs have the lowest shear strength, while thermally bonded needle-punched GCLs are only slightly weaker than needle-punched GCLs without thermal bonding. The next five rows show the HDPE geomembranes grouped by geomembrane manufacturer. There are slight differences in the equivalent friction angles, but the values are similar compared to the differences observed for different GCL types. Geomembrane *u* tended to have greater interface shear strength values than the other geomembrane manufacturers. The final three rows show the HDPE geomembranes divided by different geomembrane thicknesses. The findings indicate that there is no great difference in interface shear strength with geomembranes of different thickness.

An additional equivalent friction angle analysis that may prove enlightening is the investigation of the equivalent friction angles for the geomembrane polymer interfaces tested at normal stresses less than 50 kPa. As can be seen in Figures 5.6 and 5.7, all geomembrane polymers except for textured HDPE were tested at normal stresses less than approximately 50 kPa. The behavior of textured HDPE geomembranes should thus be investigated at low normal stresses for a more accurate comparison. Figure 5.21 shows the equivalent friction angles for the different geomembrane polymer interfaces developed for normal stresses less than 50 kPa.

This figure shows that at low normal stresses, the THDPE geomembrane interface peak and large-displacement equivalent friction angles are still less than those for the TVLDPE and TLLDPE geomembrane interfaces. This confirms the postulation that the flexibility of the geomembrane polymer is related to the GCL interface shear strength. The THDPE geomembrane interface large displacement equivalent friction angle is no longer less than that of the PVC geomembrane polymer interface, as observed in Figure 5.7. Table 5.6 summarizes the equivalent friction angles for normal stresses less than 50 kPa.

The findings of this preliminary analysis indicate that the GCL-geomembrane interfaces should be investigated in terms of geomembrane texturing characteristics, GCL types, geomembrane manufacturers, and specific test conditions.

5.3 Internal GCL Shear Strength Analysis

This section will group each of the different GCL-geomembrane interfaces by different test conditions to form relationships between the shear strength and normal stress (failure envelopes). In contrast to the previous section, the effects of the test conditions on the shear strength may be investigated directly. The effects of the shear displacement rate, the time of hydration and the time of consolidation will be investigated individually when all other testing conditions are held constant. The variability of peak and large displacement shear strength is also investigated. The final GCL water content and the displacement at peak shear strength are also discussed in detail.

5.3.1 Shear Force-Displacement Curves

During shearing, a constant displacement rate is applied to the direct shear box, and the required shear force to maintain this displacement rate is recorded with displacement. The maximum shear strength recorded during shearing is identified as the peak shear strength, and the stable level of shear stress obtained at the end of shearing is the large displacement shear strength.

Figures 5.22 through 5.33 present the shear force plotted against the shear displacement for different GCL-geomembrane interfaces (*i.e.* the shear force-

displacement curves). Each curve was selected to represent the shear force-displacement behavior of similar interfaces. As the area of the specimen is constant at 1 square foot (i.e. 300 mm by 300 mm) due to the slightly longer bottom box, the magnitude of the shear force (in lb) is equal to the shear stress (in psf).

Figures 5.22, 5.23 and 5.24 show several shear force-displacement curves for the interface between GCLs *A, B* and *C*, respectively, and an 80-mil textured HDPE geomembrane *s*. The test conditions for each of these interfaces are the same (t_H = 168 hours, t_C = 48 hours, SDR = 1.0 mm/min). Figure 5.22 shows that with increasing normal stress, GCL *A* interfaces show an increasing post-peak shear strength loss with increasing normal stress. The curves approach large-displacement conditions after a rapid decrease from peak conditions. Figure 5.23 shows a ductile shear force-displacement behavior for GCL *B* interfaces for larger normal stresses. GCL *B* interfaces do not have a large post-peak shear strength loss. The peak conditions for this interface occur at larger displacements than interfaces involving GCL *A*. Figure 5.24 shows that GCL *C* interfaces have similar behavior to those for interfaces involving GCL *A*, although the peak shear strength values are lower for the GCL *C* interfaces.

Figures 5.25, 5.26 and 5.27 show the shear force-displacement behavior for the interface between GCLs and different types of textured geomembranes. The curves for the interface between GCL *G* and a textured VLDPE geomembrane are found in Figure 5.25. The curves have similar shapes to interfaces between GCL *A* and a textured HDPE geomembrane interface shown in Figure 5.22. Figure 5.26 shows the shear force-displacement curves for the interface between GCL *A* and a textured LLDPE geomembrane. This interface behaves similarly to the textured VLDPE geomembrane interface, but displays less post-peak shear strength loss in shear strength. Figure 5.27 shows the shear force-displacement behavior for the interface between GCL *A* and a faille finish PVC geomembrane. The shear force-displacement behavior for this interface is significantly different from other textured geomembrane interfaces, as it experiences no post-peak shear strength loss. Instead, it appears to have similar shear force-displacement behavior to that observed for smooth geomembrane interfaces.

Figures 5.28, 5.29 and 5.30 show the shear force-displacement curves for interfaces with smooth HDPE, VLDPE and LLDPE geomembranes, respectively. All of these curves show similar patterns, with a steep initial modulus followed by a continuously increasing (hardening) behavior and no post-peak shear strength loss. Figure 5.30 shows the shear force-displacement behavior for the interface between GCL *A* and a smooth PVC geomembrane. The shear force-displacement behavior for this interface is similar to other smooth geomembrane interfaces, and also to the faille finish PVC geomembrane interface.

Figures 5.32 and 5.33 show the shear force-displacement curves for interfaces between GCL *K* and a textured HDPE geomembrane tested under unhydrated and hydrated conditions, respectively. GCL *K* is an unreinforced sodium bentonite layer adhered to a geomembrane backing layer. The curves for these interfaces are similar to those for the interface between the woven carrier geotextiles of GCLs *A* or *C* and a textured HDPE geomembrane shown in Figure 4.22 and 4.24. This may be because the extruded bentonite from GCLs *A* and *C* has similar shear force-displacement behavior to unreinforced sodium bentonite. However, there may be a large difference in the moisture and pore pressure conditions between the GCL *A* and *C* interfaces and those involving GCL *K* due to the encapsulation of the sodium bentonite between the carrier geomembrane of GCL *K* and the textured geomembrane. This encapsulation may result in two phenomena: (*i*) uneven hydration may occur in the sodium bentonite (*i.e.* only around holes in the carrier geomembrane), or (*ii*) drainage during shearing may not be adequate. The shear force-displacement curve for the GCL *K* interface reaches large-displacement shear strength at smaller displacements than the GCL *A* and *C* interfaces.

In summary, the shear force-displacement curves for the GCL-textured geomembrane interface are similar to that of the internal GCL interface, with a large post-peak shear strength loss. The curves for the GCL-smooth geomembrane interfaces show little post-peak shear strength loss. It is important to note that the large-displacement shear strengths recorded seem to correspond to residual shear strength values in most tests. The specific values of displacement at peak shear strength will be discussed in Section 5.3.8.

5.3.2 Effect of Test Conditions on Failure Envelopes

Using the information obtained in the preliminary analysis, each GCL–geomembrane interface may be classified by geomembrane texturing, GCL type, and geomembrane manufacturer to develop trends. In the GCLSS database, there are a total of 25 GCL-textured HDPE geomembrane failure envelopes, 5 GCL-textured VLDPE geomembrane failure envelopes, 5 GCL-textured LLDPE geomembrane failure envelopes, 4 GCL-smooth HDPE geomembrane interfaces, 2 GCL-smooth VLDPE geomembrane interfaces, 2 GCL-Smooth LLDPE geomembrane interfaces, and 3 GCL-PVC geomembrane interfaces. When multiple shear strength tests were conducted at the same normal stress level, averages and standard deviations were developed, and are presented in the tables. Due to the differences in test conditions as well as geomembrane texturing, GCL type, and geomembrane manufacturer, each of these failure envelopes has slightly different characteristics due to differences in the time of hydration, time of consolidation and shear displacement rate.

It is typically accepted that the adhesion of sodium bentonite clay is close to zero (Mesri and Olson, 1974), yet this section reports intercepts for some interfaces with magnitudes up to 45 kPa. However, this intercept should not be used to estimate the shear strength at normal stresses lower than the reported normal stress range.

Table 5.7 summarizes 51 different failure envelopes for different combinations of GCLs and geomembranes. The failure envelopes are grouped in the order: (*i*) geomembrane polymer, (*ii*) GCL, and (*iii*) geomembrane manufacturer. The table also lists the specific test conditions (*i.e.* the time of hydration, the time of consolidation and the shear displacement rate).

5.3.2.1 Textured HDPE Geomembrane Interfaces with GCL K

The first two failure envelopes investigated in this section (TH 1 and TH 2) include GCL *K*, which is the simplest to consider as it is a layer of sodium bentonite adhered to a geomembrane. Although this is not an interface between a woven geotextile and a geomembrane, it serves as a reference interface between sodium bentonite clay and a textured THDPE geomembrane. This interface is anticipated to

behave similarly to the interface between sodium bentonite extruded through the woven carrier geotextile of a GCL and a textured geomembrane.

Figure 5.34(a) shows peak failure envelopes TH 1 and TH 2 for GCL *K* and a textured HDPE geomembrane *u* tested under unhydrated and hydrated conditions, respectively. The test results for these failure envelopes are presented in Table 5.8. Peak failure envelope TH 2 has nearly the same peak shear strength as failure envelope TH 1, despite the fact that the sodium bentonite in failure envelope TH 2 is hydrated. The failure envelopes have a slightly different intercept value.

Figure 5.34(b) shows the large-displacement failure envelopes TH 1 and 2 for a hydrated GCL *K*, and a textured HDPE geomembrane *u*. The test results are presented in Table 5.8. Both failure envelopes show similar large-displacement shear strengths, with failure envelope TH 1 having slightly greater values, as would be expected of an unhydrated GCL. For failure envelope TH 1, the large-displacement shear strength is similar to the peak shear strength for comparatively low normal stresses. This is most likely the results of an adhesive failure similar to that reported by Eid and Stark (1997). That is, failure occurs at the interface between the sodium bentonite surface and the textured geomembrane for low normal stress levels. However, failure occurs within the adhesive bonding the sodium bentonite to the carrier geomembrane of GCL *K* for higher normal stresses. This behavior was not observed in large-displacement failure envelope TH 2, implying that the hydrated sodium bentonite at the interface between the GCL and the textured HDPE geomembrane is always the critical plane.

The relatively high shear strength of the interface between GCL *K* and a textured HDPE when hydrated may be explained by the fact that the sodium bentonite clay in GCL *K* is mixed with adhesives to obtain a cohesive bond between the soil particles when in unhydrated conditions. It is possible that the adhesives in the sodium bentonite may affect the shear strength behavior of fully hydrated sodium bentonite. Table 5.8 indicates that the sodium bentonite in GCL *K* reached an average water content of 131.6% when subjected to 48 hours of hydration, which is a very high water content, and should correspond to low shear strength in other GCL interfaces.

5.3.2.2 Textured HDPE Geomembrane Interfaces with GCL C

Figures 5.35 shows failure envelopes TH 3a and 3b for the interface between GCL *C* (thermal bonded) and a textured HDPE geomembrane *t*. The test results for this interface are presented in Table 5.9. Failure envelope TH 3a corresponds to the interface with an unhydrated GCL *C*, and failure envelope TH 3b corresponds to the interface with GCL *C* having a time of hydration of 1 hour. All other test conditions are the same. Failure envelope TH 3a may be used as a baseline failure envelope in comparing the changes in test results for all interfaces involving GCL *C* and a textured HDPE geomembrane. The short hydration period leads to slightly lower shear strength. Similar effects are found for the large-displacement failure envelopes, although the hydrated GCL *C* interface (TH 3b) has similar shear strength for peak and large-displacement conditions. The thermal bonded needle-punched fibers on the surface of GCL *C* act as asperities, which interlock with the asperities on the surface of the textured geomembranes. In addition, the rigid reinforcement connect of the thermal bonded GCL may lead to increased sodium bentonite extrusion during hydration.

Figure 5.36 shows failure envelopes TH 4a, 4b and 4c for the interface between GCL *C* and a textured HDPE geomembrane *t*. The test results for this interface are presented in Table 5.10. This figure allows the investigation of the effects of the shear displacement rate on the shear strength of this interface: failure envelope TH 4a corresponds to tests conducted at a shear displacement rate of 1.0 mm/min, failure envelope TH 4b corresponds to tests conducted at a shear displacement rate of 0.2 mm/min, and failure envelope TH 4c corresponds to tests conducted at a shear displacement rate of 0.025 mm/min. All other test conditions are constant. Figure 5.36(a) shows that a decreasing shear displacement rate leads to a change in friction angle, although there is not a clear trend from failure envelopes TH 4a to 4c. This is most likely the result of the different ranges of normal stresses for each of the failure envelopes. The differences in shear displacement rate have little influence on the peak and large displacement shear strength of these interfaces. The slight differences in shear strength may be due to variability in the amount of

bentonite extruded into the failure plane and variable interlocking between the GCL and the geomembrane asperities.

Figure 5.37 shows failure envelope TH 5 for the interface between GCL *C* and geomembrane *s*. The test results are presented in Table 5.11. This interface has a time of hydration of 168 hours, a time of consolidation of 48 hours and a shear displacement rate of 0.1 mm/min. The peak failure envelope has a lower friction angle and a lower intercept value than all of the failure envelopes involving GCL C and a textured HDPE geomembrane. However, the shear strength envelope for large-displacement shear strength is relatively consistent with those of the other failure envelopes.

The large-displacement failure envelopes for all interfaces with hydrated test conditions (TH 3b, 4a, 4b, 4c and 5) have greater shear strength than the interface with unhydrated conditions (TH 3a). However, the opposite is true for peak conditions. Unhydrated interfaces appear to place upper and lower bounds on the shear strength for interfaces between textured HDPE geomembranes and GCL *C* (thermal bonded).

5.3.2.3 Textured HDPE Geomembrane Interfaces with GCL A

Figure 5.38 shows failure envelope TH 6 for the interface between an unhydrated GCL *A* (needle-punched) and geomembrane *s*. The test results are presented in Table 5.12. This failure envelope serves as a baseline failure envelope for all GCL *A* interfaces that include different hydration times and shear displacement rates.

Figure 5.39 shows failure envelopes TH 7a, 7b and 7c for interfaces between GCL *A* and different textured HDPE geomembrane interfaces. The test results for these failure envelopes are presented in Table 5.13. These interfaces were tested with a time of hydration of 24 hours, no consolidation and a shear displacement rate of 1.0 mm/min. This failure envelope differs from the baseline failure envelope in terms of an increased time of hydration. As the test conditions, GCL type and geomembrane polymer are the same for these three failure envelopes, differences in shear strength are due to manufacturer differences in the geomembrane texturing. In general, the

failure envelopes show slight non-linear trends for both peak and large-displacement conditions. Figure 5.39(a) shows that peak failure envelopes are similar. Figure 5.39(b) shows that the large-displacement failure envelopes are also similar, but the data points in failure envelope TH 7b have significant scatter.

Figure 5.40 shows failure envelopes TH 8a, 8b and 8c for the interface between GCL *A* and a textured HDPE geomembrane. The test results for these failure envelopes are presented in Table 5.14. These interfaces were tested with an time of hydration of 48 hours, no consolidation and a shear displacement rate of 1.0 mm/min. This failure envelope differs from the baseline failure envelope in terms of an increased time of hydration. Similar to failure envelopes TH 7a, 7b and 7c, the GCL types, geomembrane polymer and test conditions are the same for failure envelope TH 8a, 8b and 8c, allowing comparison of the manufacturer differences in geomembrane texturing. For both peak and large-displacement conditions, failure envelopes TH 8b and 8c have similar shear strengths. For failure envelopes TH 8b and TH 8c, the increased time of hydration (t_H = 48 hours) resulted in lower peak shear strength values than those of failure envelopes TH 7a, 7b and 7c (t_H = 24 hours). Failure envelope TH 8a includes an interface with geomembrane *u*, which has the highest average equivalent friction angle of all textured HDPE geomembranes in the preliminary analysis. However, the large-displacement shear strengths for failure envelopes TH 8 and TH 7 are relatively the same.

Figure 5.41 shows failure envelopes TH 9a and 9b for the interface between GCL *A* and a textured HDPE geomembrane *u*. The test results are presented in Table 5.15. The interfaces have times of hydration similar to those found in TH 7 and TH 8, respectively, although they have different shear displacement rates of 0.2 and 0.1 mm/min. These two failure envelopes are similar. Peak failure envelope TH 9a has similar shear strength as failure envelopes TH 7a and 7c, and peak failure envelope TH 9b has higher shear strength than failure envelopes TH 8a, 8b and 8c. Failure envelope TH 9b has similar shear strength to failure envelope TH 8a as both include geomembrane *u*. The large-displacement failure envelopes for failure envelopes TH 9a and 9b are consistent with those of TH 7a, 7b, 7c, 8a, 8b and 8c. This implies that

the large-displacement shear strength is not particularly sensitive to the time of hydration or the shear displacement rate.

Figure 5.42 shows failure envelopes TH 10a and 10b for interfaces between GCL *A* and a textured HDPE geomembrane. The test results are presented in Table 5.16. These failure envelopes show the effect of consolidation on the interface shear strength, as failure envelope TH 10a has a time of hydration of 72 hours and a time of consolidation of 24 hours while failure envelope TH 10b has a time of hydration of 24 hours and a time of consolidation of 12 hours. Both failure envelopes have a shear displacement rate of 1.0 mm/min. Failure envelope TH 10a has the lowest peak and large-displacement shear strength values of any textured HDPE geomembrane interface. As no other interfaces between GCL *A* and a HDPE geomembrane have a similar time of hydration, it is difficult to distinguish the effects of the increased times of hydration or consolidation on the interface shear strength. Failure envelope TH 10b, has only slightly lower shear strength than failure envelope TH 7a, which has a similar time of hydration, shear displacement rate and geomembrane manufacturer. Typically, consolidation results in greater particle to particle interlocking capabilities. In this case, it appears that large times of hydration followed by a consolidation period result in a weaker interface. Still, when a GCL is consolidated, it is typically allowed to hydrate at low normal stresses, which allows more sodium bentonite extrusion from the GCL.

Figure 5.43 shows failure envelope TH 11 for an interface between GCL *A* and a textured HDPE geomembrane *s*. The test results are presented in Table 5.17 in terms of the test series (20 series). This failure envelope corresponds to a time of hydration of 168 hours, a time of consolidation of 48 hours and a shear displacement rate of 0.1 mm/min (similar to failure envelope TH 5). The test results show variability possible for shear strength results. This variability is possibly due to differences in amounts of sodium bentonite extruding from GCL *A*, or the variation in the density of needle-punching among GCL specimens. Needle-punching density is related to the amount of fiber reinforcements entangled on the surface of the GCL, which may be related to the interlocking capabilities of the interface (Triplett and Fox, 2001). The average peak and large-displacement shear strength envelopes for

this interface are similar to those for failure envelopes TH 7a and 7c, and are only slightly below failure envelopes TH 6 for unhydrated GCL *A* interfaces. However, the significant variability of the actual peak and large-displacement data should be emphasized.

Figure 5.44(a) shows the variation in the average ratios of the peak and large-displacement shear strength values to the normal stress. There is a non-linear decreasing trend in the peak and large-displacement ratios with increasing normal stress. The decreasing trends reach an asymptote at a normal stress of about 200 kPa. This implies that for high normal stresses, the ratio of the peak and large-displacement shear strength values to the normal stress becomes constant, allowing easier prediction of the shear strength. Figure 5.44(b) shows the variation in the average ratio of the large-displacement shear strength to the peak shear strength. The test results are presented in Table 5.17. A decreasing large-displacement to peak shear strength ratio implies a more significant post-peak shear strength loss for low normal stresses.

5.3.2.4 Textured HDPE Geomembrane Interfaces with GCL B

Figure 5.45 shows failure envelopes TH 12a and 12b for the interface between GCL *B* (stitch-bonded) and different textured HDPE geomembranes. The test results are presented in Table 5.18. Failure envelope TH 12a may be considered the baseline failure envelope for interfaces between GCL *B* and a textured HDPE geomembrane as the interfaces were tested with no hydration or consolidation. There is a slight difference in shear strength for failure envelopes TH 12a and 12b, which is most likely a result of the different geomembrane manufacturers. Assessment of Figures 5.45(a) and 5.45(b) shows that the peak and large-displacement shear strengths for the unhydrated interfaces are similar (*i.e.* small post-peak shear strength loss).

Figures 5.46 shows failure envelopes TH 13a and 13b for the interface between GCL *B* and different textured HDPE geomembranes, and the test values are presented in Table 5.19. These interfaces have a time of hydration of 24 hours, no consolidation and a shear displacement rate of 1.0 mm/min. The range of normal stresses for these failure envelopes is quite different, but the peak and large

displacement failure envelopes have similar trends. Both failure envelopes are below the unhydrated GCL *B* failure envelopes and all failure envelopes for GCLs *A* and *C*. The post-peak shear strength loss for these GCL *B* interfaces is also not as significant as for the GCL *A* and *C* interfaces. The trend in the two failure envelopes is similar to the bilinear failure envelopes developed in the internal GCL shear strength analysis (Chapter 4). Failure envelope TH 13b shows variability in peak shear strength values, although the failure envelopes fit the data well.

Figure 5.47 shows failure envelope TH 14 for interfaces between GCL *B* and a textured HDPE geomembrane *s*. The test results for this failure envelope are presented in Table 5.20. These interfaces have a time of hydration of 48 hours, no consolidation and a shear displacement rate of 1.0 mm/min. These failure envelopes have slightly lower peak and large-displacement shear strengths than failure envelopes TH 13a and 13b, yet the shear strength is still less than the unhydrated GCL *B* failure envelope (TH 12). This is expected, as an increased time of hydration should result in lower shear strength.

Figure 5.48 shows failure envelope TH 15 for an interface between GCL *B* and a textured HDPE geomembrane *s*. The test results are presented in Table 5.21. These interfaces have a time of hydration of 168 hours, a time of consolidation of 48 hours and a shear displacement rate of 0.1 mm/min (similar to failure envelope TH 5 and 11). The peak and large-displacement shear strength values for this interface are less than the other GCL B interfaces with textured HDPE geomembranes. This interface also does not display significant post-peak shear strength loss. This failure envelope is below failure envelope TH 13b, which includes the same geomembrane *s* but a shorter time of hydration, no consolidation and faster shear displacement rate.

5.3.2.5 Textured VLDPE Geomembrane Interfaces

Figure 5.49 shows failure envelopes TV 1a and 1b for the interfaces between GCL *G* and *B* and a textured VLDPE geomembrane *u*, respectively. The test results are presented in Table 5.22. The test conditions for these interfaces are the same: a time of hydration of 24 hours, no consolidation and a shear displacement rate of 1.0 mm/min. GCL *G* in failure envelope TV 1a is similar to GCL *A*, with needle-

punched fibers reinforcing a layer of sodium bentonite between woven and a non-woven carrier geotextiles. An adhesive is added to GCL *G* to prevent pullout of the needle-punched fibers from the woven carrier geotextile during GCL shearing. In failure envelope TV 1a, the hydration normal stress is one half that of failure envelope TV 1b. The failure envelopes for peak and large displacement shear strengths differ only in terms of the intercept value, which may be the result of the difference in hydration normal stress or the difference in the GCL types.

Figure 5.50 shows failure envelope TV 2 for the interface between GCL *B* and a 60-mil geomembrane *u*. The test results are presented in Table 5.22. This failure envelope has a time of hydration twice that in failure envelope TV 1a and TV 1b (48 hours), no consolidation and a shear displacement rate of 1.0 mm/min. As expected, failure envelope TV 2 has lower peak and large-displacement shear strength values than failure envelopes TV 1a and TV 1b.

Figure 5.51 shows failure envelopes TV 3a and 3b for the interface between GCL *B* and a textured VLDPE geomembrane *u*. The test results for these failure envelopes are presented in Table 5.22. The interfaces were tested under unhydrated conditions, with no consolidation and a shear displacement rate of 1.0 mm/min. Failure envelopes TV 3a and 3b have different woven carrier geotextiles attached to GCL *B*. TV 3a includes GCL *B* specimens with an Amoco 4030 carrier geotextile, and TV 3b includes GCL *B* specimens with a Clem HS carrier geotextile. The different carrier geotextiles result in different peak and large displacement shear strengths. The failure envelopes have similar friction angles but different intercept values for both peak and large displacement conditions. The negative intercept values for TH 3a is probably due to variability in test results and a limited amount of data points.

It should be noted that the peak friction angles for failure envelopes TV 1a, 1b, 2, 3a and 3b have higher shear strength than textured HDPE geomembrane interfaces tested at similar normal stresses. This is consistent with the conclusions of the equivalent friction angle analysis in Figure 5.20. Two direct comparisons may be made between the textured HDPE geomembrane interfaces and the textured VLDPE geomembrane interfaces at low normal stresses. TV 3a and 3b (Figure 5.51) may be

compared with TH 12a and 12b (Figure 5.45), all of which were conducted under unhydrated conditions. The textured VLDPE geomembrane interfaces have greater shear strength than the textured HDPE geomembrane interface. Along the same lines, TV 2 (Figure 5.50) may be compared with TH 14 (Figure 5.35), both of which were hydrated for 48 hours without consolidation and tested at a shear displacement rate of 1.0 mm/min. Again, the textured VLDPE geomembrane interface has higher shear strength. This assessment implies that the flexibility of the geomembrane is directly linked to the interface shear strength.

5.3.2.6 Textured LLDPE Geomembrane Interfaces

Figure 5.52 shows failure envelopes TL 1a and 1b for the interfaces between a textured LLDPE geomembrane *u* and GCLs *A* or *C*, respectively. The test results are presented in Table 5.23. The interfaces in these failure envelopes have similar times of hydration of 72 hours, no consolidation and a shear displacement rate of 1.0 mm/min. Failure envelope TL 1b shows lower shear strength than failure envelope TL 1a for both peak and large-displacement conditions. This implies that GCL *C* has higher interface shear strength than GCL *A* for interfaces with geomembrane *t*. The textured LLDPE geomembrane experiences less post-peak shear strength loss than textured HDPE geomembrane interfaces.

Figure 5.53 shows failure envelopes TL 2a and 2b for the interface between GCLs *A* or *C* and a textured LLDPE geomembrane *t*, respectively. The test results for these failure envelopes are presented in Table 5.23. These interfaces have similar test conditions to those in failure envelope TL 1a and 1b, but with a different geomembrane manufacturer type. The peak and large-displacement shear strengths are slightly less than those in failure envelopes TL 1a and 1b. Contrary to Figure 5.52, this implies that GCL *A* has higher interface shear strength than GCL *C* for interfaces with geomembrane *s*. This implies that the combination between geomembrane manufacturer and GCL type has a significant effect on the interface shear strength

Figure 5.54 shows failure envelope TL 3 for the interface between GCL *A* and a textured LLDPE geomembrane *t*. The test results for this failure envelope is

presented in Table 5.23. This interface for this failure envelope has similar test conditions to those found in failure envelope TL 1a, 1b, 2a and 2b, but it has a time of consolidation of 48 hours. When comparing the test results for the textured LLDPE geomembrane interfaces hydrated for 72 hours with no consolidation to failure envelope TV 3 it was found that failure envelopes TV 1a through 2b has greater shear strength than the consolidated failure envelope. This may be attributed to increased sodium bentonite extrusion due to the lower hydration normal stress.

Failure envelopes for the textured LLDPE geomembrane interfaces can be compared with tests on the textured HDPE and textured VLDPE geomembrane interfaces conducted under similar normal stress ranges. Although there is only one textured HDPE geomembrane interface hydrated for 72 hours, it has a time of consolidation of 24 hours (TH 10a). This failure envelope has lower shear strength than failure envelope TL 3 despite the 48 hours of consolidation for failure envelope TL 3. Failure envelope TV 2 (t_H = 48 hours) has lower peak shear strength than failure envelope TL 1a, 1b, 2a and 2b (t_H = 72 hours), despite the difference in times of hydration. Failure envelopes TV 1a and 1b (t_H = 24 hours) have greater peak shear strength than failure envelopes TL 1a, 1b, 2a and 2b (t_H = 72 hours). This may imply that textured VLDPE geomembrane interfaces are suitable applications where there is little possibility of hydration, while the textured LLDPE geomembranes are suitable applications where the possibility of hydration is likely.

5.3.2.7 Smooth HDPE Geomembrane Interfaces

Figure 5.55 shows failure envelopes SH 1a and 1b for the interface between a smooth HDPE geomembrane *t* and GCLs *B* or *C*, respectively. The test results for these failure envelopes are presented in Table 5.24. Failure envelope SH 1a includes interfaces between GCL *B* and geomembrane *t* with a time of hydration of 24 hours, no consolidation and a shear displacement rate of 1.0 mm/min. Failure envelope SH 1b includes interfaces between GCL *C* and geomembrane *t* with an increased time of hydration of 48 hours, no consolidation and a shear displacement rate of 1.0 mm/min. The peak shear strengths for both failure envelopes are lower than those of the textured HDPE geomembrane interfaces, with the exception of failure envelope TH

10a, which has a comparatively high peak friction angle (9.4^0). Despite the difference in the times of hydration, failure envelope SH 1a is only slightly above SH 1b (a reduction in friction angle from 11.1^0 to 8.8^0). The smooth geomembrane interfaces show no post-peak shear strength loss.

Figure 5.56 shows failure envelopes SH 2a and 2b for the interface between GCL *B* and geomembrane *u* and GCL *C* and geomembrane *t*, respectively. The test results for the failure envelopes are presented in Table 5.24. Both failure envelopes include the same test conditions: a time of hydration of 24 hours, no consolidation and a shear displacement rate of 0.2 mm/min. There is only a slight difference in friction angle from failure envelope SH 2a to SH 2b. The peak failure envelopes follow relatively linear trends, with FE S2b having a slight non-linearity. Figure 5.44(b) shows that the large-displacement conditions are the same as peak conditions for failure envelope SH 2a, but slightly lower for failure envelope SH2b (0.6^0). When comparing failure envelopes SH 2a and 2b with failure envelope SH 1a (which has a similar time of hydration but a higher shear displacement rate), failure envelopes SH 2a and 2b have lower shear strength than failure envelope SH 1a. An increase in the shear displacement rate typically results in a small decrease in shear strength.

The interfaces between smooth HDPE geomembranes and GCLs have little or no post-peak shear strength loss. This may be attributed to the lack of geomembrane asperities which interlock with the woven carrier geotextile of the GCL. For textured geomembranes, the interlocking connections fail at peak conditions, leading to a shear strength loss. The small post-peak shear strength loss for smooth geomembranes may be attractive to designers who prefer to design for large-displacement shear strength conditions but want to avoid the extra cost of a textured geomembrane. The large-displacement shear strength for failure envelope S1a is only slightly below than the large-displacement shear strength for failure envelopes TH 13a and 13b, all of which have same test conditions, normal stress ranges and GCLs.

5.3.2.8 Smooth VLDPE Geomembrane Interfaces

Figure 5.57 shows failure envelopes SV 1 and 2 for interfaces between GCLs and smooth VLDPE geomembranes. The test results for these failure envelopes are

shown in Table 5.24. Failure envelope SV 1 includes the interface between GCL *B* and geomembrane *u*, while failure envelope SV 2 includes the interface between GCL *A* and geomembrane *s*. The interfaces included in these failure envelopes had a time of hydration of 24 hours, no consolidation and a shear displacement rate of 1.0 mm/min. The failure envelopes have similar shear strengths, with only a small difference in intercept values. This implies that the GCL in the interface does not affect the shear strength of the interface. Similar to the smooth HDPE geomembranes, there was no post-peak shear strength loss. When comparing these failure envelopes to failure envelope S1b for a smooth HDPE geomembrane interface, the smooth VLDPE geomembranes interfaces have greater friction angles (14.1 and 14.0^0 for the SVLDPE geomembrane interfaces compared to 9.2 and 8.6^0 for the SHDPE geomembrane interfaces). This implies that smooth VLDPE geomembranes have better performance than smooth HDPE geomembranes at low normal stresses.

5.3.2.9 Smooth LLDPE Geomembrane Interfaces

Figure 5.58 shows failure envelopes SL 1 and 2 for the interface between different geomembranes and smooth LLDPE geomembranes. The test results for these failure envelopes are presented in Table 5.24. Failure envelope SL 1 includes the interface between GCL *A* and geomembrane *u*, tested with a time of hydration of 24 hours, no consolidation and a shear displacement rate of 1.0 mm/min. Despite the difference in test conditions, the peak friction angles for failure envelopes SL 1 and SL 2 are relatively the same. Failure envelope SL 1 experienced a small post-peak shear strength loss. Failure envelope SL 1 has slightly lower shear strength (a friction angle of 13.1^0) than the smooth VLDPE geomembrane failure envelopes SV 1 and 2 (friction angles of 14.1 and 14.0^0), yet it still has greater shear strength than the smooth HDPE geomembrane failure envelope SH 1a (a friction angle of 11.1^0) which all had similar test conditions and normal stress levels.

Failure envelope SL 2 includes the interface between GCL *F* and an unknown smooth LLDPE geomembrane, tested with a time of hydration of 168 hours, no consolidation and a shear displacement rate of 1.0 mm/min. This interface is unique as this interface has no fiber reinforcements in the failure plane. However, as the

geomembrane in this situation is not textured, the effect of the fiber reinforcements may not be investigated. The shear strength of this interface is similar to the other smooth LLDPE geomembrane interface.

5.3.2.10 PVC Geomembrane Interfaces

The PVC geomembrane interfaces tested by the SGI® laboratory had either a smooth or faille finish. The faille finish is a ridged surface treatment, similar to a file. The faille finish is typically embossed onto a PVC geomembrane, and is meant to provide better interlocking capabilities than asperities (texturing) used by other geomembrane manufacturers. Most of these geomembranes have dual surface, meaning that one side of the geomembrane is smooth while the other is faille. Shear strength tests on three PVC geomembrane interfaces are present in the GCLSS database: two PVC geomembranes with a smooth finish (geomembranes *x* and *z*), and one PVC geomembrane with a faille finish (geomembrane *y*).

Figure 5.59 and Table 5.25 show the peak failure envelopes PVC 1a, 1b and 1c for interfaces between GCL *A* and three different PVC geomembranes. The shear strength values of these interfaces are high when compared with the other geomembrane polymer interfaces. The friction angles for all of the PVC geomembrane failure envelopes are similar, although the faille finish geomembrane has a slightly greater intercept value. The performance of the PVC geomembrane with a faille finish in failure envelope PVC 1b has slightly lower shear strength than failure envelopes TH 8a, 8b and 8c, all of which have the same GCL and test conditions. PVC geomembranes are less expensive than THDPE geomembranes, so the slightly lower shear strength may be justified.

The smooth PVC interfaces have the greatest shear strength values of all of the smooth geomembrane interfaces. As mentioned, they have similar behavior to the faille finish PVC geomembrane interfaces and the textured HDPE geomembrane interfaces. The higher time of hydration for the faille-finish PVC geomembrane interface may imply that it is at the lower bound of shear strength for the faille-finish geomembranes. This may explain the proximity of the failure envelopes. However, the consolidated, smooth PVC geomembrane interface has similar behavior to the

PVC geomembrane interfaces without consolidation. This implies that the shear strength values of these PVC interfaces are all relatively constant with changing test conditions.

The higher strength of smooth PVC geomembranes has been attributed to the greater interface contact area during shear and the more "sticky" and flexible nature of the smooth side (EPI®, 1999). The faille finish PVC geomembranes have the advantage of allowing interlocking between the soil and the geomembrane, although a failure interface shift may occur at large-displacements (EPI®, 1999). This means that the soil remains interlocked with the geomembrane at failure, and another failure interface forms within the soil. This is similar to the plowing mechanism explained by Dove and Frost (1999) for flexible geomembranes.

5.3.2.11 Test Results Reported from Other Studies

As mentioned in the preliminary analysis, test results from other studies may be compared to the findings presented in this study (Pavlik, 1997; Triplett and Fox, 2001). Figure 5.60 and Table 5.2 show failure envelopes reported by Pavlik (1997) for the interface between GCL *A* and a textured HDPE geomembrane. Figure 5.61 and Table 5.3 show failure envelopes reported by Triplett and Fox (2001) for the interface between GCL *A* and a textured HDPE geomembrane. Pavlik (1997) developed a single failure envelope, and used the test results to investigate proper specimen conditioning procedures. Triplett and Fox (2001) developed three failure envelopes for the interfaces between GCL *A* and THDPE geomembranes *t* and *s*, respectively. This study investigated the differences in interface shear strength for geomembranes of a similar polymer but different manufacturer.

The failure envelopes from literature have friction angles that are consistent with similar interfaces found in the GCLSS database. Both Figures 5.60 and 5.61 show that reported intercept values are below 10 kPa, which is consistent with the failure envelopes developed in this study. The failure envelope developed by Pavlik (1997), is consistent with failure envelopes 8a, 8b and 8c, which were conducted under the same test conditions. Failure envelope 8a has the closest shear strength to that reported by Pavlik (1997). The smooth HDPE geomembrane interface tested by

Triplett and Fox (2001) is similar to SH 1a, and both interfaces have similar behavior despite the slower shear displacement rate used by Triplett and Fox (2001). Both failure envelopes TF 2 and TF 3 have similar test conditions and product types compared to failure envelope TH 9b, yet the failure envelopes are still slightly different. Failure envelope TH 9b was tested over a wider range of normal stresses, and has relatively low friction angle (19.3^0) and no intercept value. Failure envelope TF 2 predicts slightly lower peak shear strength, and failure envelope TF 3 predicts a significantly stronger failure envelope. These differences may be attributed to different testing procedures and variability. The three interfaces have similar large-displacement shear strength values.

5.3.2.12 Comparisons between Failure Envelopes

The failure envelopes developed for the different combinations between GCLs and geomembranes tested under different test conditions must be compared in detail to assess the shear strength behavior. This allows the determination of the most suitable GCL-geomembrane interface to use for different projects.

Table 5.26 summarizes the linear regression analysis for each peak and large-displacement failure envelope described in the previous section, with information on the normal stress range and the test conditions. This table presents the friction angle, the intercept value, as well as the R^2 value for the linear regression analysis for the peak and large-displacement conditions. A slight non-linear behavior is apparent from assessment of the R^2 values. This is especially evident from the figures described in this section that show test results from a wide range of normal stresses.

Table 5.26 shows that many of the failure envelopes for the GCL-geomembrane interfaces have small intercept values, implying that the shear strength behavior may be interpreted from the magnitude of the friction angle. This table shows that the majority of the interfaces tested under unhydrated conditions have friction angles ranging from 25 to 32^0, while those with a time of hydration of 24 hours have friction angles ranging from 15 to 30^0. Most of the interfaces that were consolidated had slightly lower friction angles than the other interfaces. The

interfaces that were tested at slower shear displacement rates generally had similar friction angles to interfaces tested at a shear displacement rate of 1.0 mm/min.

It is useful to compare failure envelopes on interfaces with the same test conditions, the same normal stress range, and the same geomembrane to investigate the effects of GCL type on the interface shear strength. Figure 5.62 shows a comparison between the failure envelopes of GCL K and GCL-textured HDPE geomembrane interfaces. Figure 5.61(a) shows failure envelopes TH 1, 3a, 6, 12a and 12b, all of which were not hydrated or consolidated, and shear displacement rates of 1.0 mm/min. Failure envelope TH 6 for GCL A has the highest shear strength, although the peak shear strength envelopes of all five interfaces are consistent. Figure 5.62(b) shows failure envelopes TH 2, 8a, 8b, 8c and 14, which have times of hydration of 48 hours, no consolidation and sheared at a displacement rate of 1.0 mm/min. This figure shows that the failure envelope for the unreinforced GCL K has the highest peak shear strength. As explained in section 5.3.2.1, this is most likely due to the affect of the adhesive on the shear strength, or uneven hydration throughout the GCL. In general, these five failure envelopes show consistent trends.

Figure 5.63 and Table 5.27 compare different aspects of failure envelopes for interfaces involving an 80-mil geomembrane *s* and different GCLs: TH 5 (GCL *C*), TH 11 (GCL *A*) and TH 15 (GCL *B*). All three of these failure envelopes include interfaces with a time of hydration of 168 hours, a time of consolidation of 48 hours and a shear displacement rate of 0.1 mm/min. GCL *A* is a needle-punched GCL, GCL B is a stitch-bonded GCL, and GCL *C* is a thermally bonded GCL.

As mentioned, the connection between the fiber reinforcements and the woven carrier geotextile of the GCL (*i.e.* rigid or flexible) may significantly affect the peak shear strength of a GCL-geomembrane interface. This connection affects the amount of sodium bentonite extruded into the interface between the GCL and the geomembrane, leading to different interface shear strength values. GCLs with rigid connections (such as GCLs *B*, *C* and *G*) do not the carrier geotextiles to expand freely with the sodium bentonite as it swells, so sodium bentonite will be extruded through the carrier geotextiles. GCLs with more flexible reinforcement connections or no reinforcements (GCL *As*, *F* and *K*) the carrier geotextiles to expand with the sodium

bentonite as the fiber reinforcements pull out of the carrier geotextile during swelling of the sodium bentonite. If the carrier geotextiles move with the sodium bentonite as it swells, the sodium bentonite will not extrude through the carrier geotextiles.

These postulations are supported by comparing the peak and large-displacement shear strength failure envelopes for the three interfaces shown in Figure 5.63. The failure envelope for the needle-punched GCL has the greatest friction angle of 20.7^0, while the failure envelopes for the thermally bonded GCL and the stitch-bonded GCL have lower friction angles of 17.9 and 9.8^0, respectively. However, the intercept value for the stitch-bonded GCL is the highest, suggesting that is may be suitable for low normal stress applications. These three interfaces have similar large-displacement shear strength behavior, with friction angles varying between 7.4^0 for the interface with GCL *B* and 12.3^0 for the interface with GCL *A*. This difference implies that either the surface characteristics of the GCL still affect the large-displacement shear strength of the interface (*i.e.* fiber reinforcements entangled in the shear plane), or that the amount of sodium bentonite in the interface affects the large-displacement shear strength.

The interlocking of the asperities of the geomembrane with the GCL appears to have three main effects on the interface shear strength: (*i*) during initial shearing, the connections between the geomembrane and the GCL carry the majority of the shear load, (*ii*) at peak conditions, the connections between the asperities and the GCL rupture results in a post-peak loss of shear strength, and (*iii*) the asperities removed during shearing increase the shear strength of the interface.

Figures 5.64(a) and 5.64(b) show the ratios of the peak and large-displacement shear strength values to the normal stress, respectively, for failure envelopes TH 5, TH 11 and T 15. A non-linear decreasing trend in the normalized peak shear strength is apparent with increasing normal stress for all three GCLs, although linear trends have R^2 values greater than 0.7. These figures show similar trends to those observed in Figure 5.48. Figure 5.64(c) shows the variation in the ratio of large-displacement to peak shear strength with normal stress. All three interfaces showed that there is a decrease in the post-peak shear strength loss with increasing normal stress, although the slope of this trend is not significant. This

figure shows that interfaces with GCL *B* had the largest post-peak softening, and the other two failure envelopes had roughly the same amount for all normal stresses. This may be attributed to the stitch-bonding in GCL *B* as opposed to the needle-punched surface found in GCLs *A* and *C*.

Comparison of the failure envelopes developed in this study allows identification of upper and lower bounds. Figures 5.65(a) and 5.65(b) present the peak and large-displacement failure envelopes for textured geomembrane interfaces in the GCLSS database, respectively. As the failure envelopes for other geomembrane polymers were developed for low normal stresses (*i.e.* 0-100 kPa), the large normal stress range in these figures (*i.e.* 0 to 1000 kPa), allows only the textured HDPE geomembrane failure envelopes to be assessed. Details of lower normal stresses will be discussed later in this section. For peak conditions, failure envelopes TH 10, 13 and 15 appear to define a lower bound on the failure envelopes, and failure envelopes TH 2 and 6 appear to define an upper bound. For large-displacement conditions, the same interfaces act as upper and lower bounds, although they are significantly closer together. The shear strength parameters characterizing these failure envelopes are presented in Table 5.26.

Figures 5.66(a) and 5.66(b) present the average peak and large-displacement failure envelopes, respectively, for the textured HDPE geomembrane interfaces. This figure is essentially the same figure as Figure 5.65, but the different failure envelopes are designated with trend lines. The peak failure envelopes for the interfaces with GCLs *A*, *K* and *C* have the highest shear strength. The peak failure envelopes for the interfaces with GCL *B* have the lowest shear strength. It is difficult to differentiate the failure envelopes for large-displacement conditions due to the close proximity of the failure envelopes, although GCL *A* and *K* have the highest shear strength values.

Figures 5.67(a) and 5.67(b) present the average peak and large-displacement failure envelopes for the textured VLDPE, LLDPE and PVC geomembrane interfaces, respectively. Most of the peak and large-displacement failure envelopes for these interfaces have similar friction angles. They differ by the intercept values. For peak and large-displacement conditions, the textured VLDPE geomembrane

interfaces have the greatest intercept values, while the PVC geomembrane interfaces have the lowest.

Figures 5.68(a) and 5.68(b) present the average peak and large-displacement failure envelopes for the smooth geomembrane interfaces, respectively. The failure envelopes for these interfaces have similar shear strength values. This figure shows that the smooth PVC geomembrane interfaces have the greatest peak and large-displacement shear strength values. All of the smooth geomembrane interfaces have similar large-displacement shear strength values.

5.3.3 Shear Displacement Rate Analysis

As mentioned in Chapter 3, studies investigating the effects of different test conditions on the shear strength behavior of the GCL-geomembrane interface reported that the peak and large-displacement shear strength values are not sensitive to the shear displacement rate.

Figures 5.69(a) and 5.69(b) show the effect of the shear displacement rate on the peak and large-displacement failure envelopes, respectively, for the interface between GCL *A* and textured HDPE geomembrane *u*. The envelopes correspond to a time of hydration of 24 hours, and no consolidation. For peak conditions, the failure envelope for the slower shear displacement rate of 0.2 mm/min is slightly below the envelope for 1.0 mm/min. For large-displacement conditions, the failure envelope for interface tested at the slower shear displacement rate of 0.2 mm/min is also below the envelope for 1.0 mm/min.

Figures 5.70(a) and 5.70(b) show the effect of the shear displacement rate on the peak and large-displacement shear strength values, respectively, for the interface between GCL *C* and a textured HDPE geomembrane *t* tested at three different normal stresses. The interface had a time of hydration of 24 hours, and no consolidation. The test results for these figures are presented in Table 5.28. For peak and large-displacement conditions, an increase in shear displacement rates from 0.025 mm/min to 1.0 mm/min did not result in significantly different shear strength values for three different normal stress levels. This figure shows that the shear strength is not significantly influenced by the shear displacement rate.

Figures 5.71(a) and 5.71(b) show the effect of the shear displacement rate on the peak and large-displacement shear strength values, respectively, for the interface between GCL *A* and a textured HDPE geomembrane *s* tested at three different normal stresses. The test results for these figures are presented in Table 5.29. The interface had a time of hydration of 48 hours, and no consolidation. This figure shows decreasing trends in peak and large-displacement shear strength for increasing shear displacement rates from 0.1 mm/min to 1.0 mm/min. The peak shear strength of the interfaces tested at higher normal stresses displayed a greater decrease in shear strength with increasing shear displacement rate. The difference in behavior shown in this figure with that observed in Figure 5.70 may be the result of the increased time of hydration, which may have allowed greater sodium bentonite extrusion.

Overall, the effect of the shear displacement rate on the GCL-geomembrane interface shear strength is less significant than for internal shear strength behavior. The effect of the shear displacement rate on the GCL-geomembrane interface shear strength is depends on the specific GCL and geomembrane types, as well as the time of hydration.

5.3.4 Time of Hydration Analysis

An increased time of hydration has been reported to lead to increased extrusion of sodium bentonite from the GCL, and subsequently to lower peak and large-displacement shear strength.

Figures 5.72(a) and 5.72(b) show the effect of the time of hydration on the peak and large-displacement failure envelopes, respectively, for the interface between GCL *C* and textured HDPE geomembrane *t*. Three different times of hydration were investigated for interfaces tested without consolidation and a constant shear displacement rate of 1.0 mm/min: 0, 1 and 24 hours. Increasing times of hydration appear to lead to decreasing peak and large-displacement intercept values. The difference is still quite slight.

Figures 5.73(a) and 5.73(b) show the effect of the time of hydration on the peak and large-displacement failure envelopes, respectively, for the interface between GCL *A* and a textured HDPE geomembrane *s*. Three different times of hydration

were investigated for interfaces tested without consolidation and a constant shear displacement rate of 1.0 mm/min: 0, 24 and 48 hours. Although the interface with no hydration was tested at a different normal stress range, it has significantly larger peak and large-displacement shear strength than the other interfaces. For the interfaces with times of hydration of 24 and 48 hours, there is not a significant change in the peak and large-displacement failure envelopes. This implies that times of hydration in excess of 24 hours seem adequate for interface shear strength testing.

Figures 5.74(a) and 5.74(b) show the effect of the time of hydration on the peak and large-displacement shear strength values, respectively, for the interface between GCL *A* and a textured HDPE geomembrane *s*, tested at four different normal stresses. The test results for this figure are presented in Table 5.30. It can be observed that there are large decreases in the peak and large-displacement shear strength values for times of hydration increasing from 0 to 24 hours, while there are smaller changes in peak and large-displacement shear strength values for times of hydration increasing from 24 to 48 hours. This decrease in both the peak and large shear strength values was more significant for the interfaces tested at a normal stress of 482.6 kPa than for the interfaces tested at a lower normal stress of 241.3 kPa. For increasing times of hydration from 24 hours to 48 hours, there is some scatter, but essentially no change in shear strength.

Figures 5.75(a) and 5.75(b) show the variation in peak and large-displacement shear strength values, respectively, with increasing times of hydration from 0 to 24 hours for the interface between GCL *B* and a textured HDPE geomembrane *s*. The test results for this figure are presented in Table 5.31. The trends are similar to those found in Figure 5.74, with a decrease in peak and large-displacement shear strength values with increasing times of hydration. There is again a larger decrease in shear strength for the interfaces tested at higher normal stresses.

Figure 5.76 along with the test results presented in Table 5.32 present a comparison of the peak and large-displacement shear strength values of the interface between GCL *B* and a textured HDPE geomembrane for different conditioning procedures. This figure shows that the interface with no hydration has the highest peak and large-displacement shear strength values, the interface with a time of

hydration of 24 hours and no consolidation is significantly weaker, and the interface with a time of hydration and a time of consolidation equal to 48 hours has the lowest peak and large-displacement shear strength values. This implies that increased hydration results in a decrease in interface shear strength, but a hydration period at a low normal stress followed by consolidation may be a more significant factor in interface shear strength behavior. This is discussed further in the next section.

Figure 5.77 along with the test results presented in Table 5.33 present a the effect of the time of hydration on the peak and large-displacement shear strength values of the interface between GCL *A* and a smooth PVC geomembrane *x* for different normal stress levels. As expected, the interface tested at 4.8 kPa with no hydration has higher peak shear strength than the interface with a time of hydration of 24 hours. The same interface tested at a normal stress of 12.0 kPa exhibits an increase in shear strength for an increase in time of hydration from 24 to 96 hours. This may be the result of variability, although the peak shear strength of 4.8 kPa for the interface with a time of hydration of 24 hours and 5.2 kPa for the interface with a time of hydration of 96 hours are not significantly different.

5.3.5 Time of Consolidation / Hydration Normal Stress Analysis

As observed in figure 5.76, the peak and large-displacement shear strength values of textured geomembrane interfaces were lower after a consolidation period following an initial hydration period. Although this may not be intuitive at first glance, the normal stresses used during hydration and consolidation should be noted. In Figure 5.76, the interface with a time of hydration of 24 hours and no consolidation had a hydration normal stress equal to the normal stress used during testing (689.5 kPa). However, the interface with a time of hydration of 24 hours and a time of consolidation of 48 hours had a lower, constant hydration normal stress for all tests (68.9 kPa). In this situation, the normal stress is increased to the level of normal stress used during shearing *after* the initial 24 hours of hydration. By comparison of these two situations, it is logical that less swelling occurs when the GCL is hydrated at a high normal stresses. So, less swelling and thus less extrusion occurred for the interface without consolidation than for the interface with consolidation. This implies

that the low hydration normal stress, not the consolidation procedure, resulted in the observed decrease in peak and large-displacement shear strength values.

Figures 5.78(a) and 5.78(b) show the effect of increasing the time of consolidation from 0 to 12 hours on the peak and large-displacement failure envelopes, respectively, for the interface between GCL *A* and a textured HDPE geomembrane *v*. The peak failure envelope for the interface with consolidation is below that of the interface without consolidation, and the large-displacement failure envelope for the interface with consolidation is above that of the interface without consolidation. The behavior for peak conditions is consistent with the shear strength results presented in Figure 5.76.

Figure 5.79 shows the effect of the time of consolidation on the peak and large-displacement shear strength values for the interface between GCL *A* and a textured HDPE geomembrane *v*. The test results for this figure are shown in Table 5.34. There is a decrease in peak shear strength with increasing times of consolidation and an increase in large-displacement shear strength with increasing consolidation.

Further evidence to these findings may be made from the comparison of failure envelopes TL 1b and 2b, for interfaces that were not consolidated, with failure envelope TL 3 for interfaces that were consolidated for a time of 48 hours. Failure envelope TL 3 has lower peak and large-displacement shear strength, implying that the consolidated interfaces is weaker than the interface that was not consolidated for all ranges of normal stress. Although the geomembrane polymers for the interfaces in these failure envelopes are the same, the geomembrane manufacturers are different.

5.3.6 Variability Analysis

The equivalent friction angle analysis and the failure envelope analyses show that the peak and large-displacement shear strength values for the GCL-geomembrane interface are highly variable. This variability may be quantified in the situations where there were multiple tests on a GCL-geomembrane interface conducted at the same normal stress and constant test conditions. Failure envelope TH 11 includes three sets of 20 tests conducted at different normal stresses. Statistical values

representing the peak and large displacement shear strengths for this failure envelope are presented in Table 5.35.

Figure 5.80 shows the standard deviation of the peak and large-displacement shear strength values for failure envelope TH 11. This figure shows that there is a large increase in variability with increasing normal stress. Figure 5.81 shows the variation in the Coefficient of Variation (COV) of the peak and large-displacement shear strength values with increasing normal stress. The coefficient of variation is a measure of variability similar to the standard of deviation, but includes the ratio of the standard deviation to the average value. This allows a "normalized" quantification of the variability. If a single test on a GCL interface is conducted, its test results may be multiplied by the COV to find a rough approximation of the standard deviation about that point.

The average and standard deviation of the peak and large-displacement data may be used to develop continuous probability distributions that are "equivalent" to the actual probability distributions for the data. It should be noted that this is not the actual procedure that would be taken when probabilistically characterizing the data, but this chapter focuses only on the change in variability with different normal stress levels. The actual probability distributions for the data may be developed as explained in section 4.3.6. Figures 5.82(a) and 5.82(b) show "equivalent" normal distributions for the peak and large-displacement shear strength values, respectively, for the interface between GCL *A* and a textured HDPE geomembrane *s* tested at different normal stresses. The test data for these figures is presented in Table 5.36. The trends in the variability of the peak and large-displacement shear strength values of this interface are similar to those for the internal GCL *A* shear strength shown in Figure 4.106.

Figure 5.83 shows the variation in the standard deviation for failure envelopes TH 5, 11 and 15. It is important to note that failure envelopes TH 5 and 15 included only 2 tests at each normal stress level, so the standard deviation of each may not be as statistically significant as that for failure envelope TH 11. Geomembrane interfaces with GCL *A* have the highest variability for peak and large-displacement conditions, most likely as the most test results were considered. The peak and large-

displacement failure envelopes for interfaces with GCLs *C* and *B* exhibit slight increases in variability with increasing normal stress. For all three failure envelopes, there was significantly more variability for peak conditions than for large-displacement conditions.

5.3.7 Analysis of the Final GCL Water Content

The final water content (w_f) for the sodium bentonite should decrease with increasing normal stress because of consolidation effects. This is confirmed in Figure 5.84, which shows the variation in w_f for different GCL-textured HDPE geomembrane interfaces. The final water content is directly related to the final void ratio (e_f) of the GCL if the sodium bentonite clay is fully saturated ($S_r = 1$) by the formula $e_f = w_f G_s$. The final void ratio of the sodium bentonite affected the internal shear strength of the sodium bentonite.

Figures 5.85(a) and 5.85(b) along with Table 5.36 show the variation in average peak and large-displacement shear strength values, respectively, with the average final GCL water content for three interfaces between different GCLs and a textured HDPE geomembrane *s* with the same test conditions. The interfaces with GCL *A* show little change in water content with increasing peak and large-displacement shear strength. The interfaces with GCL *B* and *C* both show decreasing water contents with increasing shear strength. This implies that lower sodium bentonite void ratios are related to lower GCL-geomembrane interface shear strength values.

Tables 5.37, 5.38 and 5.39 show the final water contents for failure envelopes TH 5, TH 11 and TH 15. The relationship between the average peak and large-displacement shear strength and the final GCL water content shows a large decrease in average shear strength with a small increase in final water content. Figure 5.86(a) and 5.84(b) show the variation in the peak and large-displacement shear strength values, respectively, with final GCL water content for failure envelope TH 11. There is significant scatter in the data, implying that the shear strength of this interface is not sensitive to the final void ratio of the sodium bentonite.

5.3.8 Analysis of Displacement at Peak Shear Strength

The displacement required to reach peak and large-displacement shear strength values may be a useful for design. Landfills typically experience large amounts of displacement over their design lives, Cowland (1997) states that domestic waste landfills can experience from 20-30 mm of displacement, due to waste settlement for landfill covers and down-drag for liner slopes. Byrne (1994) found that progressive strain softening led to the development of residual shear strength conditions at the Kettleman Hills landfill, resulting in failure. In Chapter 4, it was found that peak shear strength for the internal GCL analysis is typically mobilized within the first 5-15 mm of displacement, and that a rapid post-peak reduction in strength is apparent with increasing displacement.

Table 5.36 shows the average displacement at peak shear strength for interfaces between GCLs *A*, *B* and *C* and a textured HDPE geomembrane *s*. Also, Tables 5.37, 5.38 and 5.39 show the displacement at peak shear strength for the same interfaces involving GCLs *C* (TH 5), *A* (TH 11), and *B* (TH 15), respectively. Peak conditions for the GCL-geomembrane interface are developed within 2-20 mm of displacement. It should be noted that the large-displacement strength values in the GCLSS database were typically reported at the maximum displacement of the direct shear box, so they cannot be compared.

Figure 5.87 shows the variation in displacement at peak shear strength for interfaces between GCLs *A, B* and *C* and a textured HDPE geomembrane *s*. The displacement at peak shear strength for the interface involving GCL *A* is not sensitive to the normal stress. However, the interfaces involving GCLs *B* and *C* exhibit an increase in the amount of displacement required to reach peak conditions with increasing normal stress. The interface between GCL *C* and a textured HDPE geomembrane requires the least amount of displacement at peak shear strength.

Figure 5.88 shows the variation in displacement at peak shear strength for failure envelope TH 11, which shows the same average trend for this failure envelope presented in the previous figure but the actual data points are also presented. There is a slight upward trend in the average displacement required to reach peak and large-displacement conditions with increasing normal stress. The variability of the actual

displacement at peak shear strength values about the average does not show a conclusive trend with increasing normal stress.

Figure 5.89 shows the displacement from peak to large-displacement conditions for 20 interfaces involving GCL *A* and a textured HDPE geomembrane for normal stresses of 34.5, 137.9 and 310.3 kPa. Figures 5.89(a), 5.89(b) and 5.89(c) show lines connecting the peak strength level to the large-displacement strength level from a superimposed shear force-displacement curve. These figures show a large scatter in the shear force-displacement behavior. The slopes of the lines connecting the peak condition to the large-displacement condition on the different shear force-displacement curves are similar. In fact, the slopes of these lines increase non-linearly with normal stress. The slope for a normal stress of 34.5 kPa is 0.03 kPa/mm, the slope for a normal stress of 137.9 kPa is 0.8 kPa/mm and the slope for a normal stress of 310.3 kPa is 1.33 kPa/mm. This information may be useful for displacement-based seismic stability analysis (Newmark analyses).

5.4 Comparisons between Internal and Interface GCL Shear Strength

Chapter 4 of this report presented the shear strength results for different internal GCL interfaces. Direct comparison is possible between the failure envelopes for the internal GCL interfaces and the GCL-geomembrane interfaces tested under similar test conditions. For instance, internal GCL failure envelopes A5, B4 and C3 may be compared with the GCL-geomembrane failure envelopes TH 5, TH 11 and TH 15, all of which were hydrated for 168 hours, consolidated for 48 hours, and sheared at a displacement rate of 0.1 mm/min. Figures 5.90(a) and 5.90(b) shows the differences in peak and large-displacement shear strength values, respectively, for these six interfaces. The averages and standard deviations for the peak and large-displacement shear strength values are presented in Table 5.40 for these failure envelopes. The interfaces involving GCL *A* have greatest shear strength, with the GCL *A*-geomembrane interfaces being weaker than the internal GCL *A* interface. GCL *B* is typically the weakest in terms of both internal GCL shear strength and interface shear strength. The large-displacement failure envelopes for the internal GCL interfaces are typically greater than the GCL-geomembrane interfaces, most

likely due to the effect of the ruptured fiber reinforcements dragging through the shear zone.

It should be noted that internal GCL shear strength is higher, but approximately parallel (*i.e.* similar friction angle) to its GCL-geomembrane interface shear strength. This may have significant importance, as if the internal GCL shear strength is known, the trend in the interface GCL-geomembrane shear strength may be estimated by lowering the intercept value by a certain amount (*i.e.* GCL A has 50% higher internal peak shear strength than its interface shear strength for all normal stress ranges).

Figure 5.90(c) shows the displacement at peak shear strength values for the six abovementioned failure envelopes. The averages and standard deviations for the displacement at peak shear strength values and final GCL water contents are presented in Table 5.41 for these failure envelopes. The stitch-bonded GCLs have the greatest displacement at peak shear strength values for internal or interface conditions. Also, the needle-punched GCL (GCL *A*) has greater displacement at peak shear strength values for internal and interface conditions than the thermal bonded GCL (GCL *C*). Again, it should be noted that for the internal GCL, the trend in displacement at peak shear strength with normal stress is roughly parallel to that for its GCL-geomembrane interface.

Table 4.32 present the shear strength failure envelope parameters (c_A and δ) representing the internal GCL shear strength for different test conditions at a range of normal stresses. Table 5.26 shows the same information for the GCL-geomembrane interface shear strength failure envelopes. They should facilitate comparison between the interfaces tested under similar normal stress ranges and test conditions. The failure envelopes for the internal GCL interfaces generally have higher shear strength for similar GCL interfaces and similar test conditions.

Several studies have identified the fact that in an interface system with a GCL and a geomembrane, internal or interface failure depends on the normal stress during shearing (Eid and Stark, 1997; Gilbert *et. al.*, 1997). Gilbert et. al. (1997) proposed that for low normal stresses (*i.e.* landfill cover conditions) failure occurs at the interface, while for high normal stresses (*i.e.* landfill liner conditions) failure occurs

internally in the GCL. Although when comparing the failure envelopes for failure envelopes A5, B4, C3, TH 5, TH 11 and TH 15, it was found that on the most part, the internal GCL interfaces had failure envelopes with greater shear strength.

5.5 Summary and Conclusions

5.5.1 Summary

The database for GCL-geomembrane interface shear strength evaluated in this study is probably the largest compilation such tests available, with a total of 332 tests on different GCLs, conducted at different normal stresses and test conditions. This database was compiled from a single laboratory, which eliminates a significant source of variability in testing procedures. This database extends the scarce information currently available for GCL-geomembrane interface shear strength.

Analysis of the database was performed using different approaches. Equivalent friction angles were developed for different sets of interfaces to identify the sensitivity of the peak and large-displacement shear strength to different geomembrane polymer types and GCLs. A failure envelope analysis for interfaces with similar test conditions was conducted to investigate the changes in shear strength for different GCLs with normal stress. Based on the conclusions of the failure envelope analysis, the effects of the shear displacement rate, time of hydration, and time of consolidation (or hydration normal stress) on the peak and large-displacement shear strength values were investigated. In addition, the variability in shear strength under constant test conditions, the relationship between the shear strength and the final water content, and the variation in the displacement at peak shear strength were also investigated. The GCL-geomembrane interface shear strength was also compared with the internal GCL shear strength. The findings of these analyses generally confirm and expand the findings of previous studies investigated as part of the state-of-the-art review in Chapter 3.

5.5.2 Conclusions

The findings this study may be summarized as follows:

a) Peak equivalent friction angles (σ = 0 to 700 kPa): $\phi_{THDPE} = 21.0^0$, $\phi_{TLLDPE} = 31.7^0$, $\phi_{TLLDPE} = 29.8^0$, $\phi_{PVC} = 18.9^0$, $\phi_{Smooth} = 10.0^0$

b) Textured geomembrane interfaces had higher interface shear strength ($\phi_{EQ,Peak} = 21^0$) than smooth geomembrane interfaces ($\phi_{EQ,Peak} = 10^0$)

c) The flexibility of the geomembrane was found to be associated with the interface shear strength. This was proposed to be due to a "plowing" mechanism that allows a greater contact area during shear.

d) Large-displacement equivalent friction angles (σ = 0 to 700 kPa): $\phi_{THDPE} = 12.7^0$, $\phi_{TLLDPE} = 25.1^0$, $\phi_{TLLDPE} = 22.6^0$, $\phi_{PVC} = 18.9^0$, $\phi_{Smooth} = 9.4^0$

e) Textured geomembrane interfaces experienced a very large post-peak shear strength loss, while smooth geomembrane interfaces experienced very little post-peak shear strength loss.

f) For low normal stresses (*i.e.* 0 to 50 kPa) the order in magnitude of peak and large-displacement equivalent friction angles is still the same as above.

g) Peak equivalent friction angles for THDPE interfaces: $\phi_{GCL\ A} = 21.5^0$ (needle-punched), $\phi_{GCL\ B} = 13.2^0$ (stitch-bonded), $\phi_{GCL\ C} = 19.8^0$ (thermal bonded), $\phi_{GCL\ K} = 26.3^0$ (Unreinforced – GM backed)

h) Large-displacement equivalent friction angles for THDPE interfaces: $\phi_{GCL\ A} = 12.5^0$ (needle-punched), $\phi_{GCL\ B} = 9.9^0$ (stitch-bonded), $\phi_{GCL\ C} = 13.4^0$ (thermal bonded), $\phi_{GCL\ K} = 16.2^0$ (Unreinforced – GM backed)

i) For textured geomembrane interfaces, needle-punched GCLs had higher interface shear strength than thermal bonded and stitch-bonded GCLs. This was proposed to be due to the difference in fiber reinforcements entangled on the woven carrier geotextile of the GCL, as well as different amounts of sodium bentonite extrusion from the GCL during hydration.

j) For smooth geomembrane interfaces, the interface shear strength is not sensitive to the GCL product.

k) Peak equivalent friction angles for THDPE interfaces: $\phi_{GM\ s} = 20.8^0$, $\phi_{GM\ t} = 16.8^0$, $\phi_{GM\ u} = 26.1^0$, $\phi_{GM\ v} = 21.3^0$, $\phi_{GM\ w} = 20.8^0$

l) Large-displacement equivalent friction angles for THDPE interfaces: $\phi_{GM\ s} = 13.0^0$, $\phi_{GM\ t} = 10.6^0$, $\phi_{GM\ u} = 16.7^0$, $\phi_{GM\ v} = 11.9^0$, $\phi_{GM\ w} = 10.4^0$

m) The interface shear strength was closely related to the geomembrane polymer and to the specific geomembrane manufacturer. This was proposed to be due to differences in texturing characteristics.

n) The interface shear strength was not sensitive to the geomembrane thickness

The failure envelope analysis (*i.e.* effects of normal stress and different test conditions on the GCL-geomembrane shear strength) may be summarized as follows:

o) The failure envelopes for the GCL-geomembrane interfaces did not have large adhesion components to the shear strength. This implies that interlocking between the GCL and the geomembrane is not present at low normal stresses.

p) The interface shear strength was not particularly sensitive to the shear displacement rate. Slight decreasing trends in shear strength with increasing shear displacement rates were observed for GCLs with longer times of hydration, although the change in shear strength was small.

q) Unhydrated conditions result in the highest shear strength for the GCL-geomembrane interface, as there is little sodium bentonite extrusion and maximum interlocking.

r) Little decrease in shear strength for times of hydration beyond 24 hours was observed.

s) The hydration normal stress was found to be closely related to the interface shear strength. Higher hydration normal stresses do not allow swelling of the sodium bentonite, so sodium bentonite will not extrude into the interface. The opposite is true for low hydration normal stresses.

t) It was observed that consolidation leads to lower shear strength. However, it was also observed that when a GCL is to be consolidated, it is allowed to hydrate at a low hydration normal stress, which implies that increased sodium bentonite extrusion may occur. Thus the lower shear strength observed for consolidated GCL-geomembrane interfaces was determined to be the result of the hydration normal stress.

u) The peak and large-displacement shear strength values for the GCL-textured geomembrane interface were found to be highly variable, though the variability was not as significant as observed for internal GCL shear strength.

Some possible explanations for the observed behavior are summarized as follows:

v) Shear strength behavior of different GCL-geomembrane interfaces was proposed to be due to (*i*) the interlocking of the asperities of the geomembrane (if any) and the woven carrier geotextile of the GCL (or any reinforcement fibers present on the surface), or (*ii*) extrusion of sodium bentonite from the GCL into the interface.

w) The interlocking of the asperities of the geomembrane with the GCL appears to have three main effects on the interface shear strength: (*i*) during initial shearing, the connections between the geomembrane and the GCL carry the majority of the shear load, (*ii*) at peak conditions, the connections between the asperities and the GCL rupture results in a post-peak loss of shear strength, and (*iii*) the asperities removed during shearing increase the shear strength of the interface.

x) It was also proposed that the differences in shear strength between needle-punched thermally bonded GCLs are related to the interlocking capabilities of thermally bonded GCLs. The thermally bonded fiber reinforcements present on the surface of the GCL act as small asperities which may have different interlocking capabilities than entangled needle-punched fibers. Interfaces with stitch-bonded GCLs have little fiber reinforcement presence on the surface of the GCL, implying that interlocking is minimal for this type of GCL.

y) Extruded bentonite was proposed to have two purposes in decreasing interface shear strength: (*i*) it lubricates the connections between needle-punched fibers and the geomembrane asperities, and (*ii*) it creates a layer of unreinforced bentonite which is weaker than the internal shear strength of a reinforced GCL or the shear strength of a geomembrane-woven geotextile interface.

z) The extrusion of bentonite was proposed to depend on several factors, such as the time of hydration, the level of confining stress during hydration, the type of fiber reinforcement connection (i.*e.* rigid or flexible) and possibly the specific woven carrier geotextile of the GCL. Rigid fiber reinforcement connections in thermal bonded and stitch-bonded GCLs may lead to greater sodium bentonite extrusion as the carrier geotextiles are not allowed to expand with the sodium bentonite during hydration.

Table 5.1: GCL-Geomembrane Interface Sets

GCL-Geomembrane Interface Set	Set Description		
1	Textured GM Interfaces		
2	Smooth GM Interfaces		
3	THDPE GM Interfaces		
4	PVC GM Interfaces		
5	TVLDPE GM Interfaces		
6	TLLDPE GM Interfaces		
7	THDPE Geomembrane Interfaces	GCL	A
8			B
9			C
10			K
11		Geomembrane Manufacturer	s
12			t
13			u
14			v
15			w
16		Geomembrane Thickness	40mil
17			60mil
18			80mil

Table 5.2: Shear Strength Test Results for Interfaces between the Woven Geotextile of GCL A and a THDPE Geomembrane Reported by Pavlik (1997); t_H = 48 hours, t_C = 0 hours, SDR = 1 mm/min

GCL Name	Geomembrane Type	Normal Stress (kPa)	Peak Shear Strength (kPa)	Large Displacement Shear Strength (kPa)	Peak Displacement (mm)	Large Displacement (mm)
A	60-mil THDPE	7	8.3	5.9	1.5	66
A	60-mil THDPE	14	10.4	6.3	3.6	79
A	60-mil THDPE	28	15.2	9.4	3	79

Table 5.3: Shear Strength Test Results for Interfaces between the Woven Geotextile of GCL A and Different Geomembranes Reported by Triplett and Fox (2001); t_H = 48 hours, t_C = 0 hours, SDR = 0.1 mm/min

Failure Envelope Name	GCL Name	Geomembrane Name	Geomembrane Type	Normal Stress (kPa)	SDR (mm/min)	Peak Shear Strength (kPa)	Large Displacement (200 mm) Shear Strength (kPa)	Peak Displacement (mm)
TF 1	A	40-mil t	GM-SHDPE	6.9	0.1	1.4	1.3	0.600
TF 1	A	40-mil t	GM-SHDPE	72.2	0.1	12.8	10.5	0.600
TF 1	A	40-mil t	GM-SHDPE	141	0.1	25.1	20.3	0.900
TF 1	A	40-mil t	GM-SHDPE	279	0.1	48.4	36.3	1.500
TF 1	A	40-mil t	GM-SHDPE	486	0.1	84.4	61.8	2.400
TF 1	A	40-mil t	GM-SHDPE	72.2	0.01	12.6	9.9	0.800
TF 1	A	40-mil t	GM-SHDPE	72.2	1	12.9	9.3	0.600
TF 1	A	40-mil t	GM-SHDPE	72.2	10	12.5	11.9	0.600
TF 2	A	40-mil t	GM-THDPE	6.9	0.1	4.8	2.2	9.800
TF 2	A	40-mil t	GM-THDPE	72.2	0.1	31.4	18.0	18.300
TF 2	A	40-mil t	GM-THDPE	141	0.1	58.1	32.6	9.700
TF 2	A	40-mil t	GM-THDPE	279	0.1	83.6	47.2	14.400
TF 2	A	40-mil t	GM-THDPE	486	0.1	138.7	72.4	14.300
TF 2	A	40-mil t	GM-THDPE	72.2	0.01	36.3	19.1	8.800
TF 2	A	40-mil t	GM-THDPE	72.2	1	30.5	17.3	9.700
TF 2	A	40-mil t	GM-THDPE	72.2	10	37.7	18.5	7.900
TF 3	A	40-mil s	GM-THDPE	6.9	0.1	3.5	1.8	8.800
TF 3	A	40-mil s	GM-THDPE	72.2	0.1	32.2	19.4	7.000
TF 3	A	40-mil s	GM-THDPE	141	0.1	49.9	28.2	14.600
TF 3	A	40-mil s	GM-THDPE	279	0.1	123.9	60.9	10.000
TF 3	A	40-mil s	GM-THDPE	72.2	0.01	29.5	18.8	13.000
TF 3	A	40-mil s	GM-THDPE	72.2	1	24.8	16.6	15.700
TF 3	A	40-mil s	GM-THDPE	72.2	10	29.4	15.3	6.400

Table 5.4: Equivalent Friction Angles for GCL-Geomembrane Sets

Interface Set	Set Description	Peak				Large Displacement			
		Equivalent Friction Angle (Degrees)	Standard Deviation Equivalent Friction Angle (Degrees)	Upper Bound Equivalent Friction Angle (Degrees)	Lower Bound Equivalent Friction Angle (Degrees)	Equivalent Friction Angle (Degrees)	Standard Deviation Equivalent Friction Angle (Degrees)	Upper Bound Equivalent Friction Angle (Degrees)	Lower Bound Equivalent Friction Angle (Degrees)
1	Textured GM Interfaces	21.0	5.8	26.8	15.1	12.7	6.4	19.1	6.3
2	Smooth GM Interfaces	10.0	4.5	14.4	5.5	9.4	4.4	13.8	4.9
3	THDPE GM Interfaces	21.0	3.8	24.8	17.1	12.7	4.2	16.9	8.5
4	PVC GM Interfaces	18.9	4.0	22.9	14.9	18.9	4.0	22.9	14.9
5	TVLDPE GM Interfaces	31.7	13.0	44.7	18.7	25.1	12.6	37.7	12.5
6	TLLDPE GM Interfaces	29.8	4.2	34.0	25.6	22.6	3.1	25.7	19.5

Note: Equivalent friction angle defined for the normal stress range 0-700 kPa for each interface set

Table 5.5: Equivalent Friction Angles for GCL-THDPE Geomembrane Sets

Interface Set	THDPE Geomembrane Interface Description		Peak Equivalent Friction Angle (Degrees)	Large Displacement Equivalent Friction Angle (Degrees)
7	GCL	A	21.5	12.5
8		B	13.2	9.9
9		C	19.8	13.4
10		K	26.3	16.2
11	Geomembrane Manufacturer	s	20.8	13.0
12		t	16.8	10.6
13		u	26.1	16.7
14		v	21.3	11.9
15		w	20.8	10.4
16	Geomembrane Thickness	40mil	23.0	11.3
17		60mil	20.5	12.3
18		80mil	21.5	13.4

Note: Equivalent friction angle defined for the normal stress range 0-700 kPa for each interface set

Table 5.6: Equivalent Friction Angles (Defined for Less than 50 kPa) for Different GCL-Geomembrane Interfaces for *Low* Normal Stresses

Interface Description	Peak Equivalent Friction Angle (Degrees)	Large Displacement Equivalent Friction Angle (Degrees)
THDPE GM	26.9	19.6
TVLDPE GM	31.7	25.1
TLLDPE GM	30.6	24.3
PVC GM	18.9	18.9
Smooth GM	13.7	12.7

Note: Equivalent friction angle defined for the normal stress range 0- 50 kPa

Table 5.7: Failure Envelopes for Different GCL-Geomembrane Interfaces

Failure Envelope Number	Interface Characteristics				Test Conditions		
	Geomembrane Interface Description	Failure Envelope Name	GCL	Geomembrane	SDR (mm/min)	Time of Hydration (hrs)	Time of Consolidation (hrs)
1	Textured HDPE	TH 1	K	60-mil u	1.000	Unhydrated	0
2		TH 2	K	60-mil u	1.000	48	0
3		TH 3a	C	40-mil t	1.000	Unhydrated	0
4		TH 3b	C	60-mil t	1.000	1	0
5		TH 4a	C	60-mil t	1.000	24	0
6		TH 4b	C	60-mil t	0.200	24	0
7		TH 4c	C	60-mil t	0.025	24	0
8		TH 5	C	80-mil t	0.100	168	48
9		TH 6	A	80-mil s	1.000	Unhydrated	0
10		TH 7a	A	60/80-mil v	1.000	24	0
11		TH 7b	A	60/80-mil s	1.000	24	0
12		TH 7c	A	80-mil w	1.000	24	0
13		TH 8a	A	60-mil u	1.000	48	0
14		TH 8b	A	80-mil w	1.000	48	0
15		TH 8c	A	60-mil s	1.000	48	0
16		TH 9a	A	60-mil u	0.200	24	0
17		TH 9b	A	60-mil s	0.100	48	0
18		TH 10a	A	60-mil t	1.000	72	24
19		TH 10b	A	80-mil v	1.000	24	12
20		TH 11	A	80-mil s	0.100	168	48
21		TH 12a	B	60-mil s	1.000	Unhydrated	0
22		TH 12b	B	60-mil t	1.000	Unhydrated	0
23		TH 13a	B	40/60-mil t	1.000	24	0
24		TH 13b	B	60-mil s	1.000	24	0
25		TH 14	B	40/60-mil s	1.000	48	0
26		TH 15	B	80-mil s	0.100	168	48
27	TVLDPE	TV 1a	G	40-mil u	1.000	24	0
28		TV 1b	B	60-mil t	1.000	24	0
29		TV 2	B	60-mil u	1.000	48	0
30		TV 3a	B (Amoco)	60-mil u	1.000	Unhydrated	0
31		TV 3b	B (Clem)	60-mil u	1.000	Unhydrated	0
32	TLLDPE	TL 1a	C	40-mil u	1.000	72	0
33		TL 1b	A	40-mil u	1.000	72	0
34		TL 2a	C	40-mil t	1.000	72	0
35		TL 2b	A	40-mil t	1.000	72	0
36		TL 3	A	40-mil s	1.000	72	48
37	Smooth HDPE	SH 1a	B	60-mil t	1.000	24	0
38		SH 1b	C	60-mil t	1.000	48	0
39		SH 2a	B	60-mil u	0.200	24	0
40		SH 2b	C	60-mil t	0.200	24	0
41	Smooth VLDPE	SV 1	B	40-mil u	1.000	24	0
42		SV 2	A	40-mil s	1.000	24	0
43	Smooth LLDPE	SL 1	A	60-mil u	1.000	24	0
44		SL 2	F	40-mil	1.000	168	0
45	PVC	PVC 1a	A	30-mil x (Smooth)	1.000	24	0
46		PVC 1b	A	40-mil y (Faille)	1.000	48	0
47		PVC 1c	A	40-mil z (Smooth)	0.050	24	48
48	Pavlik (1997)	P 1	B	60- mil THDPE	1.000	48	0
49	Triplett and Fox (2001)	TF 1	A	40-mil t (Smooth)	0.100	48	0
50		TF 2	A	40-mil t (Textured)	0.100	48	0
51		TF 3	A	40-mil s (Textured)	0.100	48	0

Baseline Failure Envelope

Table 5.8: Shear Strength Tests on the Interface between a GCL and a Textured HDPE Geomembrane; Failure Envelopes TH 1 and TH 2 (Different Times of Hydration, No Consolidation, SDR = 1.0 mm/min)

Failure Envelope Name	GCL Name	Geomembrane Name	Normal Stress (kPa)	Peak Shear Strength (kPa)	Large Displacement Shear Strength (kPa)	Hydration Time (hrs)	Hydration Normal Stress (kPa)	Final GCL Water Content (%)
TH 1	K	60-mil s	68.9	58.6	54.5	0	0	15.3
	K	60-mil s	206.8	115.8	111.0	0	0	15.1
	K	60-mil s	344.7	187.5	111.0	0	0	15
TH 2	K	60-mil u	241.3	120.0	71.7	48	241.3	131.6
	K	60-mil u	482.6	245.5	148.2	48	482.6	131.6
	K	60-mil u	723.9	386.1	242.0	48	723.9	131.6
	K	60-mil u	965.3	483.3	288.2	48	965.3	131.6

Table 5.9: Shear Strength Tests on the Interface between GCL C and a Textured HDPE Geomembrane; Failure Envelope TH 3 (Different Times of Hydration, No Consolidation, SDR = 1.0 mm/min)

Failure Envelope Name	GCL Name	Geomembrane Name	Normal Stress (kPa)	Peak Shear Strength (kPa)	Large Displacement Shear Strength (kPa)	Time of Hydration (hrs)	Hydration Normal Stress (kPa)	Final GCL Water Content (%)
TH 3a	C	40-mil t	16.8	14.1	8.0	0	0.0	14.9
	C	40-mil t	143.6	72.3	40.5	0	0.0	14.8
	C	40-mil t	335.2	158.5	81.9	0	0.0	14.5
	C	40-mil t	670.3	275.8	123.5	0	0.0	14.2
TH 3b	C	60-mil t	20.7	9.0	6.9	1	20.7	78.5
	C	60-mil t	41.4	17.2	13.1	1	20.7	73.5
	C	60-mil t	62.1	24.7	18.6	1	20.7	84.6

Table 5.10: Shear Strength Tests on the Interface between GCL C and a Textured HDPE Geomembrane; Failure Envelope TH 4 (Same Times of Hydration, No Consolidation, Different Shear Displacement Rates)

Failure Envelope Name	GCL Name	Geomembrane Name	Normal Stress (kPa)	Peak Shear Strength (kPa)	Mean Peak Shear Strength (kPa)	Standard Deviation Peak Shear Strength (kPa)	Large Displacement Shear Strength (kPa)	Mean Large Displacement Shear Strength (kPa)	Standard Deviation Large Displacement Shear Strength (kPa)	Shear Displacement Rate (mm/min)	Time of Hydration (hrs)	Hydration Normal Stress (kPa)	Final GCL Water Content (%)
TH 4a	C	60-mil t	34.5	14.5	14.5	0.0	10.3	10.3	0.0	1.0	24	13.8	105.5
	C	60-mil t	68.9	30.3	30.3	0.0	22.1	22.1	0.0	1.0	24	13.8	105.5
	C	60-mil t	137.9	59.3	59.3	0.0	40.7	40.7	0.0	1.0	24	13.8	105.5
TH 4b	C	60-mil t	9.6	4.6	4.9	0.4	3.2	3.7	0.8	0.2	24	57.5	81.5
	C	60-mil t	9.6	5.1			4.3			0.2	24	57.5	80
	C	60-mil t	47.9	27.0	26.4	0.8	18.2	18.7	0.7	0.2	24	57.5	81.5
	C	60-mil t	47.9	25.9			19.2			0.2	24	57.5	80
	C	60-mil t	95.8	44.5	43.0	2.0	29.7	30.6	1.2	0.2	24	57.5	81.5
	C	60-mil t	95.8	41.6			31.5			0.2	24	57.5	80
	C	60-mil t	191.5	72.0	74.1	3.0	46.0	46.3	0.4	0.2	24	57.5	81.5
	C	60-mil t	191.5	76.2			46.6			0.2	24	57.5	80
	C	60-mil t	335.2	114.5	115.8	1.8	85.2	83.7	2.2	0.2	24	57.5	81.5
	C	60-mil t	335.2	117.1			82.1			0.2	24	57.5	80
TH 4c	C	60-mil t	34.5	15.2	15.2	0.0	11.7	11.7	0.0	0.025	24	13.8	105.5
	C	60-mil t	68.9	27.6	27.6	0.0	22.1	22.1	0.0	0.025	24	13.8	105.5
	C	60-mil t	137.9	57.9	57.9	0.0	45.5	45.5	0.0	0.025	24	13.8	105.5

Statistical Results

Table 5.11: Shear Strength Tests on the Interface between GCL C and a Textured HDPE Geomembrane; Failure Envelope TH 5 (t_H = 168 hours, t_C = 48 hours, SDR = 0.1 mm/min)

Failure Envelope Name	GCL Name	Geomembrane Name	Normal Stress (kPa)	Peak Shear Strength (kPa)	Mean Peak Shear Strength (kPa)	Standard Deviation Peak Shear Strength (kPa)	Large Displacement Shear Strength (kPa)	Mean Large Displacement Shear Strength (kPa)	Standard Deviation Large Displacement Shear Strength (kPa)	Hydration Normal Stress (kPa)	Consolidation Normal Stress (kPa)	Final GCL Water Content (%)
TH 5	C	80-mil s	34.5	13.1	14.5	2.0	9.7	9.7	0.0	20.7	34.5	101.1
	C	80-mil s	34.5	15.9			9.7			20.7	34.5	101.3
	C	80-mil s	137.9	45.5	49.0	4.9	23.4	28.6	7.3	20.7	137.9	93.8
	C	80-mil s	137.9	52.4			33.8			20.7	137.9	74.2
	C	80-mil s	310.3	107.6	103.8	5.4	61.4	60.3	1.5	20.7	310.3	82.0
	C	80-mil s	310.3	100.0			59.3			20.7	310.3	66.8

Statistical Results

Table 5.12: Shear Strength Tests on the Interface between GCL A and a Textured HDPE Geomembrane; Failure Envelope TH 6 (No Hydration, No Consolidation, SDR = 1.0 mm/min)

Failure Envelope Name	GCL Name	Geomembrane Name	Normal Stress (kPa)	Peak Shear Strength (kPa)	Large Displacement Shear Strength (kPa)	Final GCL Water Content (%)
TH 6	A	80-mil s	241.3	133.1	85.5	20.5
	A	80-mil s	482.6	313.7	142.7	20.5
	A	80-mil s	965.3	488.8	300.6	20.5

Table 5.13: Shear Strength Tests on the Interface between GCL A and a Textured HDPE Geomembrane; Failure Envelope TH 7 (t_H = 24 hours, t_C = 0 hours, SDR = 1.0 mm/min

Failure Envelope Name	GCL Name	Geomembrane Name	Normal Stress (kPa)	Peak Shear Strength (kPa)	Mean Peak Shear Strength (kPa)	Standard Deviation Peak Shear Strength (kPa)	Large Displacement Shear Strength (kPa)	Mean Large Displacement Shear Strength (kPa)	Standard Deviation Large Displacement Shear Strength (kPa)	Hydration Normal Stress (kPa)	Final GCL Water Content (%)
TH 7a	A	60/80-mil v	6.9	3.4	3.4	0.0	2.8	2.8	0.0	6.9	88.5
	A	60/80-mil v	13.8	6.9	6.9	0.0	4.8	4.8	0.0	13.8	88.5
	A	60/80-mil v	27.6	11.7	11.7	0.0	9.7	9.7	0.0	27.6	88.5
	A	60/80-mil v	34.5	15.9	15.7	1.3	13.1	10.5	1.8	34.5	75.5
	A	60/80-mil v	34.5	16.5			9.7			34.5	75.5
	A	60/80-mil v	34.5	13.8			9.0			34.5	75.5
	A	60/80-mil v	34.5	16.5			10.3			34.5	75.5
	A	60/80-mil v	68.9	29.0	31.2	6.9	20.7	19.8	3.8	68.9	75.5
	A	60/80-mil v	68.9	40.7			23.4			68.9	75.5
	A	60/80-mil v	68.9	31.0			20.7			68.9	75.5
	A	60/80-mil v	68.9	24.1			14.5			68.9	75.5
	A	60/80-mil v	137.9	58.6	60.0	7.4	35.2	34.3	2.1	137.9	75.5
	A	60/80-mil v	137.9	68.9			33.8			137.9	75.5
	A	60/80-mil v	137.9	61.4			36.5			137.9	75.5
	A	60/80-mil v	137.9	51.0			31.7			137.9	75.5
	A	60/80-mil v	172.4	84.1	73.5	8.1	53.1	43.8	8.3	172.4	61.0
	A	60/80-mil v	172.4	76.5			56.5			172.4	61.0
	A	60/80-mil v	172.4	75.8			42.1			172.4	61.0
	A	60/80-mil v	172.4	64.1			40.7			172.4	61.0
	A	60/80-mil v	172.4	79.3			44.1			172.4	61.0
	A	60/80-mil v	172.4	73.1			36.5			172.4	61.0
	A	60/80-mil v	172.4	61.4			33.8			172.4	61.0
	A	60/80-mil v	344.7	149.6	138.5	16.5	86.2	75.1	8.9	344.7	61.0
	A	60/80-mil v	344.7	147.5			82.7			344.7	61.0
	A	60/80-mil v	344.7	142.0			80.0			344.7	61.0
	A	60/80-mil v	344.7	135.8			73.1			344.7	61.0
	A	60/80-mil v	344.7	148.9			75.2			344.7	61.0
	A	60/80-mil v	344.7	142.7			67.6			344.7	61.0
	A	60/80-mil v	344.7	102.7			60.7			344.7	61.0
	A	60/80-mil v	689.5	305.4	264.6	31.8	155.1	139.9	16.3	689.5	61.0
	A	60/80-mil v	689.5	281.3			143.4			689.5	61.0
	A	60/80-mil v	689.5	260.6			139.3			689.5	61.0
	A	60/80-mil v	689.5	264.1			144.1			689.5	61.0
	A	60/80-mil v	689.5	273.7			157.2			689.5	61.0
	A	60/80-mil v	689.5	265.4			131.0			689.5	61.0
	A	60/80-mil v	689.5	201.3			108.9			689.5	61.0
TH 7b	A	60/80-mil s	6.9	4.8	4.6	0.4	4.1	3.9	0.4	6.9	150.0
	A	60/80-mil s	6.9	4.1			3.4			6.9	161.0
	A	60/80-mil s	6.9	4.8			4.1			6.9	108.6
	A	60/80-mil s	13.8	8.3	8.3	0.0	5.5	5.5	0.0	13.8	153.0
	A	60/80-mil s	20.7	15.9	15.9	0.0	11.0	11.0	0.0	6.9	101.0
	A	60/80-mil s	27.6	15.2	15.2	0.0	6.9	6.9	0.0	13.8	155.0
	A	60/80-mil s	41.4	20.7	20.7	0.0	13.8	13.8	0.0	6.9	104.4
	A	60/80-mil s	68.9	47.6	36.5	9.7	28.3	20.9	6.4	68.9	134.0
	A	60/80-mil s	68.9	29.6			16.5			68.9	124.2
	A	60/80-mil s	68.9	32.4			17.9			68.9	102.0
	A	60/80-mil s	103.4	38.6	38.6	0.0	22.8	29.0	0.0	6.9	105.9
	A	60/80-mil s	137.9	54.5	54.5	0.0	29.0	64.1	0.0	137.9	105.9
	A	60/80-mil s	206.8	99.3	99.3	0.0	64.1	104.8	0.0	68.9	125.0
	A	60/80-mil s	241.3	82.7	82.7	0.0	39.3	17.9	0.0	68.9	102.0
	A	60/80-mil s	344.7	157.2	157.2	0.0	104.8	39.3	0.0	68.9	114.4
	A	60/80-mil s	482.6	126.9	126.9	0.0	69.6	69.6	0.0	68.9	102.0
TH 7c	A	80-mil w	68.9	43.4	35.9	10.7	23.4	21.0	3.4	68.9	126.8
	A	80-mil w	68.9	28.3			18.6			68.9	132.6
	A	80-mil w	206.8	106.9	95.1	16.6	50.3	43.4	9.8	206.8	112.1
	A	80-mil w	206.8	83.4			36.5			206.8	113.3
	A	80-mil w	344.7	144.8	135.5	13.2	67.6	60.7	9.8	344.7	104.2
	A	80-mil w	344.7	126.2			53.8			344.7	103.8

Statistical Results

Table 5.14: Shear Strength Tests on the Interface between GCL A and a Textured HDPE Geomembrane; Failure Envelope TH 8 (t_H = 48 hours, t_C = 0 hours, SDR = 1.0 mm/min)

Failure Envelope Name	GCL Name	Geomembrane Name	Normal Stress (kPa)	Peak Shear Strength (kPa)	Large Displacement Shear Strength (kPa)	Hydration Normal Stress (kPa)	Final GCL Water Content (%)
TH 8a	A	60-mil u	51.7	25.5	17.9	51.7	127.3
	A	60-mil u	206.8	76.5	64.8	103.4	115.1
	A	60-mil u	103.4	42.1	35.2	206.8	113.5
TH 8b	A	80-mil w	89.6	29.0	22.1	4.8	126.9
	A	80-mil w	186.2	60.7	35.2	4.8	123.2
	A	80-mil w	275.8	71.0	42.7	4.8	144
TH 8c	A	60-mil s	51.7	29.0	13.8	51.7	123.7
	A	60-mil s	68.9	17.9	10.3	68.9	65.6
	A	60-mil s	103.4	48.3	26.2	103.4	115.1
	A	60-mil s	206.8	73.1	46.9	206.8	105.7
	A	60-mil s	206.8	55.8	34.5	206.8	65.6
	A	60-mil s	344.7	86.2	53.8	344.7	65.6

Table 5.15: Shear Strength Tests on the Interface between GCL A and a Textured HDPE Geomembrane; Failure Envelope TH 9 (Different Times of Hydration, No Consolidation, Different Shear Displacement Rates)

Failure Envelope Name	GCL Name	Geomembrane Name	Normal Stress (kPa)	Peak Shear Strength (kPa)	Mean Peak Shear Strength (kPa)	Standard Deviation Peak Shear Strength (kPa)	Large Displacement Shear Strength (kPa)	Mean Large Displacement Shear Strength (kPa)	Standard Deviation Large Displacement Shear Strength (kPa)	Shear Displacement Rate (mm/min)	Hydration Time (hrs)	Hydration Normal Stress (kPa)	Final GCL Water Content (%)
TH 9a	A	60-mil u	9.6	5.6	5.8	0.4	4.8	4.9	0.1	0.2	24	57.5	74.5
	A	60-mil u	9.6	6.1			5.0			0.2	24	57.5	71.5
	A	60-mil u	47.9	17.8	18.1	0.4	12.9	12.9	0.0	0.2	24	57.5	74.5
	A	60-mil u	47.9	18.4			12.8			0.2	24	57.5	71.5
	A	60-mil u	95.8	37.3	37.0	0.4	26.7	27.0	0.4	0.2	24	57.5	74.5
	A	60-mil u	95.8	36.7			27.2			0.2	24	57.5	71.5
	A	60-mil u	191.5	76.8	72.9	5.5	47.9	46.4	2.0	0.2	24	57.5	74.5
	A	60-mil u	191.5	69.1			45.0			0.2	24	57.5	71.5
	A	60-mil u	287.3	106.3	101.9	6.3	65.0	61.5	4.9	0.2	24	57.5	74.5
	A	60-mil u	287.3	97.5			58.0			0.2	24	57.5	71.5
TH 9b	A	60-mil s	68.9	24.8	24.8	0.0	17.9	17.9	0.0	0.1	48	68.9	59.6
	A	60-mil s	206.8	71.0	71.0	0.0	42.7	42.7	0.0	0.1	48	206.8	59.6
	A	60-mil s	344.7	121.3	121.3	0.0	64.8	64.8	0.0	0.1	48	344.7	59.6

Statistical Results

Table 5.16: Shear Strength Tests on the Interface between GCL A and a Textured HDPE Geomembrane; Failure Envelope TH 10 (Different Times of Hydration, Different Times of Consolidation, SDR = 1.0 mm/min)

Failure Envelope Name	GCL Name	Geomembrane Name	Normal Stress (kPa)	Peak Shear Strength (kPa)	Large Displacement Shear Strength (kPa)	Hydration Time (hrs)	Hydration Normal Stress (kPa)	Consolidation Time (hrs)	Consolidation Normal Stress (kPa)	Final GCL Water Content (%)
TH 10a	A	60-mil t	172.4	53.8	32.4	72	6.9	24	172.4	88
	A	60-mil t	413.7	89.6	54.5	72	6.9	24	413.7	88
	A	60-mil t	689.5	139.3	66.9	72	6.9	24	689.5	88
TH 10b	A	80-mil v	137.9	51.0	34.5	24	68.9	12	137.9	164.5
	A	80-mil v	275.8	104.1	73.1	24	68.9	12	275.8	164.5
	A	80-mil v	551.6	199.9	117.9	24	68.9	12	551.6	164.5

Table 5.17: Shear Strength Tests on the Interface between GCL A and a Textured HDPE Geomembrane s; Failure Envelope TH 11 (t_H = 168 hours, t_C = 48 hours, SDR = 0.1 mm/min)

Failure Envelope Name/ Series Number	Normal Stress (kPa	Peak Shear Strength (kPa)	Large Displacement Shear Strength (kPa)	τ_p/σ	τ_{LD}/σ	τ_{LD}/τ_p	Hydration Normal Stress (kPa)	Consolidation Normal Stress (kPa)	Final GCL Water Content (%)
TH 11 1	34.5	20.0	13.8	0.58	0.40	0.69	20.7	34.5	61.0
	137.9	53.8	30.3	0.39	0.22	0.56	20.7	137.9	61.0
	310.3	123.4	78.6	0.40	0.25	0.64	20.7	310.3	61.0
TH 11 2	34.5	17.2	13.8	0.50	0.40	0.80	20.7	34.5	62.5
	137.9	50.3	33.1	0.37	0.24	0.66	20.7	137.9	62.5
	310.3	122.0	73.8	0.39	0.24	0.60	20.7	310.3	62.5
TH 11 3	34.5	20.0	12.4	0.58	0.36	0.62	20.7	34.5	73.0
	137.9	42.7	26.2	0.31	0.19	0.61	20.7	137.9	73.0
	310.3	98.6	68.3	0.32	0.22	0.69	20.7	310.3	73.0
TH 11 4	34.5	19.3	13.1	0.56	0.38	0.68	20.7	34.5	73.5
	137.9	51.7	33.1	0.38	0.24	0.64	20.7	137.9	73.5
	310.3	110.3	66.9	0.36	0.22	0.61	20.7	310.3	73.5
TH 11 5	34.5	17.2	11.0	0.50	0.32	0.64	20.7	34.5	76.0
	137.9	44.1	24.8	0.32	0.18	0.56	20.7	137.9	76.0
	310.3	100.0	57.2	0.32	0.18	0.57	20.7	310.3	76.0
TH 11 6	34.5	16.5	11.0	0.48	0.32	0.67	20.7	34.5	75.0
	137.9	63.4	43.4	0.46	0.32	0.68	20.7	137.9	75.0
	310.3	120.7	72.4	0.39	0.23	0.60	20.7	310.3	75.0
TH 11 7	34.5	19.3	9.7	0.56	0.28	0.50	20.7	34.5	83.5
	137.9	77.2	37.2	0.56	0.27	0.48	20.7	137.9	83.5
	310.3	155.1	80.0	0.50	0.26	0.52	20.7	310.3	83.5
TH 11 8	34.5	18.6	12.4	0.54	0.36	0.67	20.7	34.5	78.0
	137.9	64.1	37.9	0.47	0.28	0.59	20.7	137.9	78.0
	310.3	99.3	74.5	0.32	0.24	0.75	20.7	310.3	78.0
TH 11 9	34.5	14.5	9.7	0.42	0.28	0.67	20.7	34.5	71.5
	137.9	65.5	35.9	0.48	0.26	0.55	20.7	137.9	71.5
	310.3	99.3	68.9	0.32	0.22	0.69	20.7	310.3	71.5
TH 11 10	34.5	24.1	13.1	0.70	0.38	0.54	20.7	34.5	87.0
	137.9	53.1	31.0	0.39	0.23	0.58	20.7	137.9	72.3
	310.3	132.4	60.7	0.43	0.20	0.46	20.7	310.3	67.4
TH 11 11	34.5	18.6	11.7	0.54	0.34	0.63	20.7	34.5	89.7
	137.9	46.2	25.5	0.34	0.19	0.55	20.7	137.9	70.3
	310.3	117.9	60.0	0.38	0.19	0.51	20.7	310.3	51.7
TH 11 12	34.5	18.6	14.5	0.54	0.42	0.78	20.7	34.5	84.6
	137.9	60.0	37.9	0.44	0.28	0.63	20.7	137.9	64.2
	310.3	101.4	64.1	0.33	0.21	0.63	20.7	310.3	63.8
TH 11 13	34.5	16.5	12.4	0.48	0.36	0.75	20.7	34.5	74.0
	137.9	49.6	31.7	0.36	0.23	0.64	20.7	137.9	74.0
	310.3	120.7	73.1	0.39	0.24	0.61	20.7	310.3	74.0
TH 11 14	34.5	27.6	15.2	0.80	0.44	0.55	20.7	34.5	72.0
	137.9	82.7	37.9	0.60	0.28	0.46	20.7	137.9	72.0
	310.3	169.6	84.8	0.55	0.27	0.50	20.7	310.3	72.0
TH 11 15	34.5	25.5	15.9	0.74	0.46	0.62	20.7	34.5	69.5
	137.9	76.5	46.9	0.56	0.34	0.61	20.7	137.9	69.5
	310.3	148.2	94.5	0.48	0.30	0.64	20.7	310.3	69.5
TH 11 16	34.5	31.7	19.3	0.92	0.56	0.61	20.7	34.5	73.5
	137.9	84.8	46.9	0.62	0.34	0.55	20.7	137.9	73.5
	310.3	149.6	91.7	0.48	0.30	0.61	20.7	310.3	73.5
TH 11 17	34.5	21.4	13.8	0.62	0.40	0.65	20.7	34.5	71.0
	137.9	57.9	34.5	0.42	0.25	0.60	20.7	137.9	71.0
	310.3	138.6	77.2	0.45	0.25	0.56	20.7	310.3	71.0
TH 11 18	34.5	17.2	14.5	0.50	0.42	0.84	20.7	34.5	67.5
	137.9	69.6	37.9	0.51	0.28	0.54	20.7	137.9	67.5
	310.3	135.8	81.4	0.44	0.26	0.60	20.7	310.3	67.5
TH 11 19	34.5	18.6	11.7	0.54	0.34	0.63	20.7	34.5	76.0
	137.9	59.3	31.0	0.43	0.23	0.52	20.7	137.9	76.0
	310.3	120.7	75.2	0.39	0.24	0.62	20.7	310.3	76.0
TH 11 20	34.5	19.3	13.8	0.56	0.40	0.71	20.7	34.5	74.5
	137.9	46.9	28.3	0.34	0.21	0.60	20.7	137.9	74.5
	310.3	122.0	63.4	0.39	0.20	0.52	20.7	310.3	74.5

Table 5.18: Shear Strength Tests on the Interface between GCL B and a Textured HDPE Geomembrane; Failure Envelope TH 12 (No Hydration, No Consolidation, SDR = 1.0 mm/min)

Failure Envelope Name	GCL Name	Geomembrane Name	Normal Stress (kPa)	Peak Shear Strength (kPa)	Mean Peak Shear Strength (kPa)	Standard Deviation Peak Shear Strength (kPa)	Large Displacement Shear Strength (kPa)	Mean Large Displacement Shear Strength (kPa)	Standard Deviation Large Displacement Shear Strength (kPa)	Final GCL Water Content (%)
TH 12a	B	60-mil s	12.0	5.7	7.1	1.9	5.3	6.0	1.0	18.2
	B	60-mil s	12.0	8.4			6.7			18.4
	B	60-mil s	23.9	9.6	11.6	2.9	7.7	9.5	2.5	18.4
	B	60-mil s	23.9	13.6			11.3			18.5
	B	60-mil s	47.9	18.2	22.4	5.9	13.2	17.4	5.9	18.2
	B	60-mil s	47.9	26.6			21.5			18.2
TH 12b	B	60-mil t	2.4	2.2	2.2	0.0	1.9	1.9	0.0	18.1
	B	60-mil t	9.6	6.8	6.8	0.0	5.5	5.5	0.0	18.0
	B	60-mil t	19.2	13.7	13.7	0.0	11.1	11.1	0.0	18.2
	B	60-mil t	33.5	22.5	22.5	0.0	15.9	15.9	0.0	18.3
	B	60-mil t	47.9	29.4	29.4	0.0	20.8	20.8	0.0	18.2

Statistical Results

Table 5.19: Shear Strength Tests on the Interface between GCL B and a Textured HDPE Geomembrane; Failure Envelope TH 13 (t_H = 24 hours, No Consolidation, SDR = 1.0 mm/min)

Failure Envelope Name	GCL Name	Geomembrane Name	Normal Stress (kPa)	Peak Shear Strength (kPa)	Mean Peak Shear Strength (kPa)	Standard Deviation Peak Shear Strength (kPa)	Large Displacement Shear Strength (kPa)	Mean Large Displacement Shear Strength (kPa)	Standard Deviation Large Displacement Shear Strength (kPa)	Hydration Normal Stress (kPa)	Final GCL Water Content (%)
TH 13a	B	40/60-mil t	2.4	2.0	1.3	1.0	1.6	1.1	0.7	4.8	135.0
	B	40/60-mil t	2.4	0.6			0.6			4.8	135.0
	B	40/60-mil t	6.9	6.2	6.6	0.5	4.1	4.5	0.5	13.8	140.3
	B	40/60-mil t	6.9	6.9			4.8			13.8	140.0
	B	40/60-mil t	9.6	7.1	5.0	3.0	6.1	4.5	2.3	4.8	135.0
	B	40/60-mil t	9.6	2.9			2.9			4.8	135.0
	B	40/60-mil t	19.2	13.6	10.9	3.8	9.8	8.7	1.5	4.8	135.0
	B	40/60-mil t	19.2	8.2			7.7			4.8	135.0
	B	40/60-mil t	27.6	15.9	15.9	0.0	10.3	10.7	0.5	13.8	120.3
	B	40/60-mil t	27.6	15.9			11.0			13.8	130.4
	B	40/60-mil t	33.5	18.7	15.9	4.0	14.0	12.9	1.7	4.8	135.0
	B	40/60-mil t	33.5	13.1			11.7			4.8	135.0
	B	40/60-mil t	47.9	16.4	21.3	6.9	13.1	15.9	4.0	4.8	135.0
	B	40/60-mil t	47.9	26.2			18.7			4.8	135.0
	B	40/60-mil t	55.2	22.1	22.1	0.0	11.7	11.7	0.0	13.8	121.5
	B	40/60-mil t	55.2	22.1			11.7			13.8	110.3
	B	40/60-mil t	103.4	35.2	35.2	0.0	20.0	20.0	0.0	13.8	120.8
	B	40/60-mil t	103.4	35.2			20.0			13.8	110.2
TH 13b	B	60-mil s	68.9	24.1	19.7	6.3	19.3	15.5	5.4	68.9	146.0
	B	60-mil s	68.9	15.2			11.7			68.9	163.2
	B	60-mil s	137.9	26.2	26.2	0.0	18.6	18.6	0.0	137.9	154.6
	B	60-mil s	206.8	66.9	66.9	0.0	38.6	38.6	0.0	68.9	136.4
	B	60-mil s	275.8	54.5	54.5	0.0	42.7	42.7	0.0	275.8	140.1
	B	60-mil s	344.7	107.6	107.6	0.0	64.1	64.1	0.0	68.9	128.5
	B	60-mil s	413.7	82.0	82.0	0.0	56.5	56.5	0.0	413.7	116.1
	B	60-mil s	551.6	108.2	108.2	0.0	83.4	83.4	0.0	551.6	105.3
	B	60-mil s	689.5	133.1	133.1	0.0	95.8	95.8	0.0	689.5	95.4

Statistical Results

Table 5.20: Shear Strength Tests on the Interface between GCL B and a Textured HDPE Geomembrane; Failure Envelope TH 14 (t_H = 48 hours, No Consolidation, SDR = 1.0 mm/min)

Failure Envelope Name	GCL Name	Geomembrane Name	Normal Stress (kPa)	Peak Shear Strength (kPa)	Large Displacement Shear Strength (kPa)	Hydration Normal Stress (kPa)	Final GCL Water Content (%)
TH 14	B	40-mil s	6.9	2.3	2.3	6.9	170.6
	B	60-mil s	12.0	5.5	4.8	12.0	141.1
	B	40-mil s	13.8	4.7	4.6	13.8	160.3
	B	60-mil s	23.9	9.8	7.4	12.0	141.5
	B	40-mil s	27.6	8.9	8.6	27.6	156
	B	60-mil s	47.9	17.2	11.3	12.0	141.4

Table 5.21: Shear Strength Tests on the Interface between GCL B and a Textured HDPE Geomembrane; Failure Envelope TH 15 (t_H = 168 hours, t_C = 48 hours, SDR = 0.1 mm/min)

Failure Envelope Name	GCL Name	Geomembrane Name	Normal Stress (kPa)	Peak Shear Strength (kPa)	Mean Peak Shear Strength (kPa)	Standard Deviation Peak Shear Strength (kPa)	Large Displacement Shear Strength (kPa)	Mean Large Displacement Shear Strength (kPa)	Standard Deviation Large Displacement Shear Strength (kPa)	Hydration Normal Stress (kPa)	Consolidation Normal Stress (kPa)	Final GCL Water Content (%)
TH 15	B	80-mil s	34.5	12.4	12.1	0.5	11.0	10.7	0.5	20.7	34.5	103.3
	B	80-mil s	34.5	11.7			10.3			20.7	34.5	106.0
	B	80-mil s	137.9	35.2	37.9	3.9	29.6	30.3	1.0	20.7	137.9	64.1
	B	80-mil s	137.9	40.7			31.0			20.7	137.9	77.1
	B	80-mil s	310.3	59.3	61.0	2.4	48.3	47.2	1.5	20.7	310.3	63.5
	B	80-mil s	310.3	62.7			46.2			20.7	310.3	76.9

Statistical Results

Table 5.22: Shear Strength Tests on the Interface between a GCL and a Textured VLDPE Geomembrane; Failure Envelopes TV 1, 2 and 3 (Different Times of Hydration, No Consolidation, SDR = 1.0 mm/min)

Failure Envelope Number	GCL Name	Geomembrane Name	Normal Stress (kPa)	Peak Shear Strength (kPa)	Large Displacement Shear Strength (kPa)	Hydration Time (hrs)	Hydration Normal Stress (kPa)	Final GCL Water Content (%)
TV 1a	G	40-mil u	2.4	5.5	4.1	24	2.4	140.7
	G	40-mil u	9.6	10.8	6.2	24	2.4	108.2
	G	40-mil u	19.2	16.5	11.5	24	2.4	122.5
TV1b	B	60-mil t	2.4	2.3	1.9	24	4.8	141.1
	B	60-mil t	9.6	8.9	5.8	24	4.8	141.7
	B	60-mil t	19.2	15.0	10.8	24	4.8	141.5
	B	60-mil t	33.5	22.0	17.3	24	4.8	140.6
	B	60-mil t	47.9	29.9	21.5	24	4.8	141.2
TV 2	B	60-mil u	12.0	8.4	7.4	48	12.0	140.4
	B	60-mil u	23.9	13.2	11.0	48	12.0	141.4
	B	60-mil u	47.9	20.6	14.8	48	12.0	141.7
TV 3a	B - With Amoco 4034 Geotextiles	60-mil u	12.0	7.2	5.3	0	0.0	18.1
	B - With Amoco 4034 Geotextiles	60-mil u	23.9	12.2	9.6	0	0.0	18.3
	B - With Amoco 4034 Geotextiles	60-mil u	47.9	28.5	21.5	0	0.0	18
TV 3b	B - With Clem HS Geotextiles	60-mil u	12.0	10.3	7.9	0	0.0	18.2
	B - With Clem HS Geotextiles	60-mil u	23.9	17.7	14.4	0	0.0	18.2
	B - With Clem HS Geotextiles	60-mil u	47.9	33.3	26.6	0	0.0	18.1

Table 5.23: Shear Strength Tests on the Interface between a GCL and a Textured LLDPE Geomembrane; Failure Envelopes TL 1, 2 and 3 (Different Times of Hydration and Consolidation, SDR = 1.0 mm/min)

Failure Envelope Name	GCL Name	Geomembrane Name	Normal Stress (kPa)	Peak Shear Strength (kPa)	Large Displacement Shear Strength (kPa)	Shear Displacement Rate (mm/min)	Hydration Time (hrs)	Hydration Normal Stress (kPa)	Consolidation Time (hrs)	Consolidation Normal Stress (kPa)	Final GCL Water Content (%)
TL 1a	C	40-mil u	6.9	6.2	4.8	1.0	72	6.9	0	0.0	94
	C	40-mil u	13.8	9.7	7.6	1.0	72	13.8	0	0.0	94
	C	40-mil u	27.6	17.9	14.5	1.0	72	27.6	0	0.0	94
	C	40-mil u	55.2	33.1	24.1	1.0	72	55.2	0	0.0	94
TL 1d	A	40-mil u	6.9	5.5	3.4	1.0	72	6.9	0	0.0	107.5
	A	40-mil u	13.8	10.3	7.6	1.0	72	13.8	0	0.0	107.5
	A	40-mil u	27.6	17.2	13.8	1.0	72	27.6	0	0.0	107.5
	A	40-mil u	55.2	32.4	24.8	1.0	72	55.2	0	0.0	107.5
TL 2a	C	40-mil t	6.9	4.1	3.4	1.0	72	6.9	0	0.0	84.5
	C	40-mil t	13.8	7.6	5.5	1.0	72	13.8	0	0.0	84.5
	C	40-mil t	27.6	13.8	10.3	1.0	72	27.6	0	0.0	84.5
	C	40-mil t	55.2	29.6	19.3	1.0	72	55.2	0	0.0	84.5
TL 2b	A	40-mil t	6.9	5.5	3.4	1.0	72	6.9	0	0.0	114
	A	40-mil t	13.8	9.7	6.9	1.0	72	13.8	0	0.0	114
	A	40-mil t	27.6	16.5	11.7	1.0	72	27.6	0	0.0	114
	A	40-mil t	55.2	29.6	20.7	1.0	72	55.2	0	0.0	114
TL 3	A	40-mil s	4.8	2.0	1.8	1.0	72	0.0	48	4.8	205.5
	A	40-mil s	12.0	4.9	4.4	1.0	72	0.0	48	12.0	205.5
	A	40-mil s	19.2	7.4	5.9	1.0	72	0.0	48	19.2	205.5

Table 5.24: Shear Strength Tests on the Interface between a GCL and Smooth Geomembranes; Failure Envelopes SH 1 and 2, SV 1 and 2 and SL 1 and 2 (Different Times of Hydration, No Consolidation, SDR = 1.0 mm/min)

Failure Envelope Name	GCL Name	Geomembrane Name	Geomembrane Type	Normal Stress (kPa)	Peak Shear Strength (kPa)	Mean Peak Shear Strength (kPa)	Standard Deviation Peak Shear Strength (kPa)	Large Displacement Shear Strength (kPa)	Mean Large Displacement Shear Strength (kPa)	Standard Deviation Large Displacement Shear Strength (kPa)	Shear Displacement Rate (mm/min)	Hydration Time (hrs)	Hydration Normal Stress (kPa)	Final GCL Water Content (%)
SH 1a	B	60-mil t	HDPE	2.4	1.0	1.0	0.0	1.0	1.0	0.0	1.0	24	4.8	#N/A
	B	60-mil t	HDPE	9.6	2.4	2.4	0.0	2.4	2.4	0.0	1.0	24	4.8	#N/A
	B	60-mil t	HDPE	19.2	4.1	4.1	0.0	4.1	4.1	0.0	1.0	24	4.8	#N/A
	B	60-mil t	HDPE	33.5	7.4	7.4	0.0	7.4	7.4	0.0	1.0	24	4.8	#N/A
	B	60-mil t	HDPE	47.9	9.7	9.7	0.0	9.7	9.7	0.0	1.0	24	4.8	#N/A
SH 1b	C	60-mil t	HDPE	10.3	2.8	2.8	0.0	2.8	2.8	0.0	1.0	48	10.3	144.4
	C	60-mil t	HDPE	27.6	4.8	4.8	0.0	4.8	4.8	0.0	1.0	48	10.3	152.3
	C	60-mil t	HDPE	68.9	11.7	11.7	0.0	11.7	11.7	0.0	1.0	48	10.3	145.9
SH 2a	B	60-mil u	HDPE	9.6	4.5	4.2	0.3	3.8	3.6	0.3	0.2	24	57.5	73.6
	B	60-mil u	HDPE	9.6	4.0			3.4			0.2	24	57.5	72.9
	B	60-mil u	HDPE	47.9	12.8	13.3	0.7	10.8	11.9	1.7	0.2	24	57.5	73.6
	B	60-mil u	HDPE	47.9	13.7			13.1			0.2	24	57.5	72.9
	B	60-mil u	HDPE	95.8	16.9	18.9	2.9	16.5	17.5	1.4	0.2	24	57.5	73.6
	B	60-mil u	HDPE	95.8	21.0			18.4			0.2	24	57.5	72.9
	B	60-mil u	HDPE	191.5	37.3	35.7	2.3	36.7	35.2	2.2	0.2	24	57.5	73.6
	B	60-mil u	HDPE	191.5	34.1			33.6			0.2	24	57.5	72.9
	B	60-mil u	HDPE	287.3	52.3	49.9	3.4	51.8	49.0	4.0	0.2	24	57.5	73.6
	B	60-mil u	HDPE	287.3	47.4			46.2			0.2	24	57.5	72.9
SH 2b	C	60-mil t	HDPE	9.7	2.8	2.8	0.0	2.8	2.4	0.5	0.2	24	55.2	76
	C	60-mil t	HDPE	9.7	2.8			2.1			0.2	24	55.2	74
	C	60-mil t	HDPE	48.3	10.3	11.0	1.0	8.3	9.3	1.5	0.2	24	55.2	76
	C	60-mil t	HDPE	48.3	11.7			10.3			0.2	24	55.2	74
	C	60-mil t	HDPE	117.2	24.8	24.8	0.0	20.7	20.3	0.5	0.2	24	55.2	76
	C	60-mil t	HDPE	117.2	24.8			20.0			0.2	24	55.2	74
	C	60-mil t	HDPE	193.1	30.3	32.8	3.4	29.0	30.7	2.4	0.2	24	55.2	76
	C	60-mil t	HDPE	193.1	35.2			32.4			0.2	24	55.2	74
	C	60-mil t	HDPE	289.6	46.2	45.9	0.5	44.1	41.7	3.4	0.2	24	55.2	76
	C	60-mil t	HDPE	289.6	45.5			39.3			0.2	24	55.2	74
SV 1	B	40-mil u	VLDPE	2.4	1.0	1.0	0.0	1.0	1.0	0.0	1.0	24	2.4	155.2
	B	40-mil u	VLDPE	9.6	2.9	2.9	0.0	2.9	2.9	0.0	1.0	24	9.6	130.5
	B	40-mil u	VLDPE	19.2	5.5	5.5	0.0	5.5	5.5	0.0	1.0	24	19.2	108.1
SV 2	A	40-mil s	VLDPE	14.4	3.8	3.8	0.0	3.8	3.8	0.0	1.0	24	4.8	141.6
	A	40-mil s	VLDPE	23.9	6.2	6.2	0.0	6.2	6.2	0.0	1.0	24	4.8	147
SL 1	A	60-mil u	LLDPE	13.8	3.4	3.4	0.0	2.8	2.8	0.0	1.0	24	13.8	97.5
	A	60-mil u	LLDPE	24.1	6.9	6.9	0.0	6.2	6.2	0.0	1.0	24	24.1	97.5
	A	60-mil u	LLDPE	34.5	8.3	8.3	0.0	7.6	7.6	0.0	1.0	24	34.5	97.5
SL 2	F	40-mil	LLDPE	13.8	3.4	3.4	0.0	3.4	3.4	0.0	1.0	168	13.8	188.5
	F	40-mil	LLDPE	27.6	6.9	6.9	0.0	6.9	6.9	0.0	1.0	168	27.6	188.5
	F	40-mil	LLDPE	55.2	12.4	12.4	0.0	12.4	12.4	0.0	1.0	168	55.2	188.5

Statistical Results

Table 5.25: Shear Strength Tests on the Interface between GCL A and a Smooth or Faille Finish PVC Geomembrane; Failure Envelopes PVC 1 a, b and c (Different Times of Hydration and Consolidation, SDR = 1.0 mm/min)

Failure Envelope Name	GCL Name	Geomembrane Name	Normal Stress (kPa)	Peak Shear Strength (kPa)	Large Displacement Shear Strength (kPa)	Final GCL Water Content (%)	Hydration Time (hrs)	Hydration Normal Stress (kPa)	Consolidation Time (hrs)	Consolidation Normal Stress (kPa)	Shear Displacement Rate (mm/min)
PVC 1a	A	40-mil x (Smooth)	2.4	1.2	1.2	172.6	24	0.0	48	2.4	0.05
	A	40-mil x (Smooth)	4.8	2.2	2.2	172.6	24	0.0	48	4.8	0.05
	A	40-mil x (Smooth)	35.9	10.9	10.9	172.6	24	0.0	48	35.9	0.05
PVC 1b	A	30-mil y (Faille)	13.8	5.5	5.5	90.2	48	13.8	0	0.0	1.0
	A	30-mil y (Faille)	27.6	10.3	10.3	90.2	48	27.6	0	0.0	1.0
	A	30-mil y (Faille)	41.4	13.8	13.8	90.2	48	41.4	0	0.0	1.0
PVC 1c	A	40-mil z (Smooth)	4.8	1.8	1.8	173.2	24	4.8	0	0.0	1.0
	A	40-mil z (Smooth)	14.4	4.9	4.9	179.7	24	4.8	0	0.0	1.0
	A	40-mil z (Smooth)	23.9	8.2	8.2	179.0	24	4.8	0	0.0	1.0

Table 5.26: Linear Best-Fit Line Results for All GCL-Geomembrane Failure Envelopes

Failure Envelope Number	Interface Characteristics				Test Conditions				Peak			Large Displacement		
	Geomembrane Interface Type	Failure Envelope Number	GCL	Geomembrane	SDR (mm/min)	Time of Hydration (hrs)	Time of Consolidation (hrs)	Normal Stress Range (kPa)	Friction Angle (Degrees)	Intercept Value (kPa)	R^2 Value	Friction Angle (Degrees)	Intercept Value (kPa)	R^2 Value
1	Textured HDPE	TH 1	K	60-mil u	1.000	0	0	69-345	25.1	23.96	0.9958	11.6	49.76	0.7500
2		TH 2	K	60-mil u	1.000	48	0	241-965	27.0	1.03	0.9951	17.1	1.72	0.9843
3		TH 3a	C	40-mil t	1.000	0	0	16-670	21.8	13.88	0.9950	9.9	12.83	0.9713
4		TH 3b	C	60-mil t	1.000	1	0	20-62	20.9	1.21	0.9992	15.8	1.14	0.9988
5		TH 4a	C	60-mil t	1.000	24	0	34-138	23.3	0.00	0.9995	16.2	1.03	0.9964
6		TH 4b	C	60-mil t	0.200	24	0	9.6-335	18.3	7.92	0.9889	13.1	4.86	0.9881
7		TH 4c	C	60-mil t	0.025	24	0	34-138	22.6	0.00	0.9978	18.2	0.00	0.9991
8		TH 5	C	80-mil t	0.100	168	48	34-310	17.9	3.74	0.9929	10.4	3.30	0.9792
9		TH 6	A	80-mil s	1.000	0	0	241-965	25.3	45.51	0.9609	16.8	6.55	0.9946
10		TH 7a	A	60/80-mil v	1.000	24	0	6.9-689	20.7	5.83	0.9705	11.0	6.71	0.9965
11		TH 7b	A	60/80-mil s	1.000	24	0	6.9-483	17.6	9.73	0.8834	10.5	6.08	0.3809
12		TH 7c	A	80-mil w	1.000	24	0	38-345	19.9	14.11	0.9356	8.2	11.98	0.9944
13		TH 8a	A	60-mil u	1.000	48	0	51-103	18.2	8.27	0.9999	16.7	3.10	0.9985
14		TH 8b	A	80-mil w	1.000	48	0	89-276	12.8	11.77	0.9319	6.4	12.84	0.9828
15		TH 8c	A	60-mil s	1.000	48	0	51-345	12.2	16.39	0.8606	8.4	6.65	0.8848
16		TH 9a	A	60-mil u	0.200	24	0	9.6-287	19.4	2.63	0.9923	11.7	4.44	0.9894
17		TH 9b	A	60-mil s	0.100	48	0	68-345	19.3	0.00	0.9994	9.6	6.66	0.9988
18		TH 10a	A	60-mil t	1.000	72	24	172-690	9.4	23.78	0.9993	3.8	23.12	0.9610
19		TH 10b	A	80-mil v	1.000	24	12	138-552	19.7	3.10	0.9970	11.1	12.07	0.9785
20		TH 11	A	80-mil s	0.100	168	48	34-310	20.7	7.43	0.9065	12.3	5.13	0.9294
21		TH 12a	B	60-mil s	1.000	0	0	12-48	23.3	1.60	0.8396	17.7	2.03	0.7606
22		TH 12b	B	60-mil t	1.000	0	0	2.4-48	31.2	1.29	0.9950	22.5	1.73	0.9852
23		TH 13a	B	40/60-mil t	1.000	24	0	2.4-103	17.9	3.93	0.8810	9.8	4.13	0.7965
24		TH 13b	B	60-mil s	1.000	24	0	68-690	10.4	12.32	0.9132	7.7	6.66	0.9619
25		TH 14	B	40/60-mil s	1.000	48	0	6.9-48	19.3	0.38	0.9728	12.0	1.81	0.9441
26		TH 15	B	80-mil s	0.100	168	48	34-310	9.8	9.16	0.9608	7.3	8.67	0.9631
27	TVLDPE	TV 1a	G	40-mil u	1.000	24	0	2.4-19.2	33.2	4.15	0.9967	24.2	2.61	0.9761
28		TV 1b	B	60-mil t	1.000	24	0	2.4-48	30.3	2.46	0.9892	23.5	1.66	0.9869
29		TV 2	B	60-mil u	1.000	48	0	12-48	18.6	4.67	0.9956	11.3	5.51	0.9709
30		TV 3a	B (Amoco)	60-mil u	1.000	0	0	12-48	31.2	-0.96	0.9888	24.7	-0.72	0.9944
31		TV 3b	B (Clem)	60-mil u	1.000	0	0	12-48	32.7	2.51	0.9999	27.4	1.80	0.9998
32	TLLDPE	TL 1a	C	40-mil u	1.000	72	0	6.9-55.2	29.3	2.22	0.9996	21.9	2.37	0.9936
33		TL 1b	A	40-mil u	1.000	72	0	6.9-55.2	28.8	2.19	0.9986	23.5	1.17	0.9954
34		TL 2a	C	40-mil t	1.000	72	0	6.9-55.2	27.9	0.12	0.9970	18.3	1.11	0.9997
35		TL 2b	A	40-mil t	1.000	72	0	6.9-55.2	26.3	2.55	0.9987	19.3	1.65	0.9952
36		TL 3	A	40-mil s	1.000	72	48	4.8-19.2	20.6	0.23	0.9979	15.8	0.65	0.9762
37	Smooth HDPE	SH 1a	B	60-mil t	1.000	24	0	2.4-48	11.1	0.53	0.9967	11.1	0.53	0.9967
38		SH 1b	C	60-mil t	1.000	48	0	10-69	8.8	0.90	0.9954	8.8	0.90	0.9954
39		SH 2a	B	60-mil u	0.200	24	0	9.6-287	9.2	3.94	0.9866	9.2	2.86	0.9871
40		SH 2b	C	60-mil t	0.200	24	0	9.7-290	8.6	3.62	0.9760	8.0	2.44	0.9830
41	Smooth VLDPE	SV 1	B	40-mil u	1.000	24	0	2.4-19.2	14.1	0.40	0.9909	14.1	0.40	0.9909
42		SV 2	A	40-mil s	1.000	24	0	14.4-23.9	14.0	0.24	1.0000	14.0	0.24	1.0000
43	Smooth LLDPE	SL 1	A	60-mil u	1.000	24	0	13.8-34.5	13.1	0.57	0.9423	13.1	-0.11	0.9423
44		SL 2	F	40-mil	1.000	168	0	13.8-55.2	12.1	0.69	0.9967	12.1	0.69	0.9967
45	PVC	PVC 1a	A	30-mil x (Smooth)	1.000	24	0	13.8-41	16.7	1.66	0.9908	16.7	1.66	0.9908
46		PVC 1b	A	40-mil y (Faille)	1.000	48	0	4.8-24	18.5	0.18	0.9997	18.5	0.18	0.9997
47		PVC 1c	A	40-mil z (Smooth)	0.050	24	48	2.4-36	15.9	0.65	0.9993	15.9	0.65	0.9993
48	Pavlik (1997)	P 1	B	60- mil THDPE	1.000	48	0	7-28	18.3	5.90	0.9990	9.9	4.35	0.9485
49	Triplett and Fox (2001)	TF 1	A	40-mil t (Smooth)	0.100	48	0	6.9-279	9.8	0.35	1.0000	7.1	1.41	0.9988
50		TF 2	A	40-mil t (Textured)	0.100	48	0	6.9-280	14.9	10.57	0.9846	8.0	6.19	0.9737
51		TF 3	A	40-mil s (Textured)	0.100	48	0	6.9-281	23.6	-2.24	0.9844	12.0	1.16	0.9904

Table 5.27: Comparison of the Average Shear Strengths for Failure Envelopes TH 5, TH 11 and TH 15 (t_H = 168 hours, t_C = 48 hours, SDR = 0.1 mm/min)

.

Failure Envelope	GCL	Geomembrane Description	Number of Tests	Normal Stress (kPa)	Mean Peak Shear Strength (kPa)	Standard Deviation of the Peak Shear Strength (kPa)	Mean Large Displacement Shear Strength (kPa)	Standard Deviation of the Large Displacement Shear Strength (kPa)	τ_p/σ Ratio	τ_r/σ Ratio	τ_r/τ_p Ratio
TH 5	GCL C	80-mil s	20	34.5	14.5	2.0	9.7	0.0	0.42	0.28	0.67
	GCL C	80-mil s	20	137.9	49.0	4.9	28.6	7.3	0.36	0.21	0.58
	GCL C	80-mil s	20	310.3	103.8	5.4	60.3	1.5	0.33	0.19	0.58
TH 11	GCL A	80-mil s	2	34.5	20.1	4.2	13.1	2.2	0.58	0.38	0.65
	GCL A	80-mil s	2	137.9	56.0	12.8	34.6	6.4	0.41	0.25	0.62
	GCL A	80-mil s	2	310.3	124.3	20.4	73.3	10.1	0.40	0.24	0.59
TH 15	GCL B	80-mil s	2	34.5	12.1	0.5	10.7	0.5	0.35	0.31	0.89
	GCL B	80-mil s	2	137.9	37.9	3.9	30.3	1.0	0.28	0.22	0.80
	GCL B	80-mil s	2	310.3	61.0	2.4	47.2	1.5	0.20	0.15	0.77

Table 5.28: Effect of the Shear Displacement Rate on the Interface between GCL C and a 60 mil Textured HDPE GM t (t_H = 24 hours, Hydration Normal Stress = 13.8 kPa, Average Final Water Content = 105%, No Consolidation)

GCL Name	Geomembrane Name	Normal Stress (kPa)	Mean Peak Shear Strength (kPa)	Mean Large Displacement Shear Strength (kPa)	Shear Displacement Rate (mm/min)
C	60-mil t	34.5	14.5	10.3	1.0
C	60-mil t	34.5	15.2	11.7	0.025
C	60-mil t	68.9	30.3	22.1	1.0
C	60-mil t	68.9	27.6	22.1	0.025
C	60-mil t	137.9	59.3	40.7	1.0
C	60-mil t	137.9	57.9	45.5	0.025

Table 5.29: Effect of the Shear Displacement Rate on the Interface between GCL A and a 60 mil Textured HDPE GM s (t_H = 48 hours, No Consolidation)

GCL Name	Geomembrane Name	Normal Stress (kPa)	Peak Shear Strength (kPa)	Large Displacement Shear Strength (kPa)	Shear Displacement Rate (mm/min)
A	60-mil s	68.9	17.9	10.3	1.0
A	60-mil s	68.9	24.8	17.9	0.1
A	60-mil s	206.8	73.1	46.9	1.0
A	60-mil s	206.8	55.8	34.5	1.0
A	60-mil s	206.8	71.0	42.7	0.1
A	60-mil s	344.7	86.2	53.8	1.0
A	60-mil s	344.7	121.3	64.8	0.1

Table 5.30: Effect of the Time of Hydration on the Interface between GCL A and a 60/80 mil Textured HDPE GM s (No Consolidation, SDR = 1.0 mm/min)

GCL Name	Geomembrane Name	Normal Stress (kPa)	Peak Shear Strength (kPa)	Large Displacement Shear Strength (kPa)	Final GCL Water Content (%)	Time of Hydration (hrs)
A	60-mil s	68.9	31.0	17.2	102	24
A	60-mil s	68.9	17.9	10.3	65.6	48
A	60-mil s	103.4	38.6	22.8	105.9	24
A	60-mil s	103.4	48.3	26.2	115.1	48
A	80-mil s	241.3	133.1	85.5	20.5	0
A	60-mil s	241.3	82.7	39.3	102	24
A	80-mil s	482.6	313.7	142.7	20.5	0
A	60-mil s	482.6	126.9	69.6	102	24

Table 5.31: Effect of the Time of Hydration on the Interface between GCL B and a 60 mil Textured HDPE GM s (No Consolidation, SDR = 1.0 mm/min)

GCL Name	Geomembrane Name	Normal Stress (kPa)	Peak Shear Strength (kPa)	Large Displacement Shear Strength (kPa)	Final GCL Water Content (%)	Time of Hydration (hrs)
B	60-mil s	12.0	5.7	5.3	18.2	0
B	60-mil s	12.0	8.4	6.7	18.4	0
B	60-mil s	12.0	5.5	4.8	141.1	48
B	60-mil s	23.9	9.6	7.7	18.4	0
B	60-mil s	23.9	13.6	11.3	18.5	0
B	60-mil s	23.9	9.8	7.4	141.5	48
B	60-mil s	47.9	18.2	13.2	18.2	0
B	60-mil s	47.9	26.6	21.5	18.2	0
B	60-mil s	47.9	17.2	11.3	141.4	48

Table 5.32: Effect of Different Hydration and Consolidation Times on the Shear Strength of the Interface between GCL B and textured HDPE geomembrane; Constant Normal Stress of 698.5 kPa (SDR = 1.0 mm/min)

Series Number	GCL Name	Geomembrane Name	Normal Stress (kPa)	Peak Shear Strength (kPa)	Large Displacement Shear Strength (kPa)	Hydration Time (hrs)	Hydration Normal Stress (kPa)	Consolidation Time (hrs)	Consolidation Normal Stress (kPa)	Final GCL Water Content (%)
1	B	80-mil t	689.5	238.6	182.7	0	0.0	0	0.0	21.5
2	B	80-mil t	689.5	114.5	95.1	24	68.9	48	689.5	152.3
3	B	60-mil s	689.5	133.1	95.8	24	689.5	0	0.0	163.1

Table 5.33: Statistical Results for the Shear Strength Tests on the Interface between GCL A and a Smooth PVC Geomembrane; Effect of Different Hydration Procedures (SDR = 1.0 mm/min)

Series Number	GCL Name	Geomembrane Name	Normal Stress (kPa)	Peak Shear Strength (kPa)	Large Displacement Shear Strength (kPa)	Hydration Time (hrs)	Hydration Normal Stress (kPa)	Consolidation Time (hrs)	Consolidation Normal Stress (kPa)	Final GCL Water Content (%)
1	A	40-mil x	4.8	2.4	2.4	0	0.0	0	0.0	44.9
2	A	40-mil x	4.8	1.9	1.9	24	0.0	24	4.8	87.0
3	A	40-mil x	12.0	4.8	4.8	24	12.0	0	0.0	80.9
4	A	40-mil x	12.0	5.2	5.2	96	12.0	0	0.0	82.2

Table 5.34: Effect of the Time of Consolidation on the Interface between GCL A and a 60 mil Textured HDPE GM v (t_H = 48 hours, No Consolidation)

GCL Name	Geomembrane Name	Normal Stress (kPa)	Peak Shear Strength (kPa)	Large Displacement Shear Strength (kPa)	Final GCL Water Content (%)	Time of Consolidation (hrs)
A	80-mil v	137.9	58.6	35.2	75.5	0
A	80-mil v	137.9	68.9	33.8	75.5	0
A	80-mil v	137.9	61.4	36.5	75.5	0
A	80-mil v	137.9	51.0	31.7	75.5	0
A	80-mil v	137.9	51.0	34.5	164.5	12

Table 5.35: Variability of the Interface between GCL A and Geomembrane *s*, Listed by Test Series (FE TH 11, t_H = 168 hours, t_C = 48 hours, SDR = 0.1 mm/min)

Failure Envelope	Statistical Values	σ = 34.5 kPa		σ = 137.9 kPa		σ = 310.3 kPa	
		Peak Shear Strength (kPa)	Large Displacement Shear Strength (kPa)	Peak Shear Strength (kPa)	Large Displacement Shear Strength (kPa)	Peak Shear Strength (kPa)	Large Displacement Shear Strength (kPa)
TH 11	Average	20.10	13.13	59.98	34.58	124.28	73.33
	St. Dev.	4.17	2.22	12.83	6.40	20.44	10.10
	COV	0.21	0.17	0.21	0.19	0.16	0.14

Table 5.36: Comparison of the Displacements at Peak Shear Strength and Final Water Contents for Failure Envelopes TH 5, TH 11 and TH 15 (tH = 168 hours, tC = 48 hours, SDR = 0.1 mm/min)

Failure Envelope	GCL	Geomembrane Description	Number of Tests	Mean Displacement at Peak Shear Strength (mm)	Standard Deviation of the Displacement at Peak Shear Strength (mm)	Mean Final GCL Water Content (%)	Standard Deviation of the Final GCL Water Content (%)
TH 5	GCL C	80-mil s	20	2.22	0.45	101.2	0.1
	GCL C	80-mil s	20	9.84	0.45	84.0	13.9
	GCL C	80-mil s	20	11.56	0.18	74.4	10.7
TH 11	GCL A	80-mil s	2	10.48	4.79	74.7	7.3
	GCL A	80-mil s	2	11.09	3.24	71.9	5.3
	GCL A	80-mil s	2	12.96	5.66	70.7	7.0
TH 15	GCL B	80-mil s	2	12.70	3.59	104.7	1.9
	GCL B	80-mil s	2	26.67	5.39	70.6	9.2
	GCL B	80-mil s	2	33.34	1.35	70.2	9.5

Table 5.37: Displacements at Peak Shear Strength and Final Water Contents for Failure Envelope TH 5 (t_H = 168 hours, t_C = 48 hours, SDR = 0.1 mm/min)

GCL Description	Geomembrane Description	Normal Stress (kPa)	Peak Shear Strength (kPa)	Displacement at Peak Shear Strength (mm)	Final GCL Water Content (%)
C	80-mil s	34.5	13.1	1.91	101.1
C	80-mil s	34.5	15.9	2.54	101.3
C	80-mil s	137.9	45.5	10.16	93.8
C	80-mil s	137.9	52.4	9.53	74.2
C	80-mil s	310.3	107.6	11.68	82.0
C	80-mil s	310.3	100.0	11.43	66.8

Table 5.38: Displacements at Peak Shear Strength and Final Water Contents for Failure Envelope TH 11 (t_H = 168 hours, t_C = 48 hours, SDR = 0.1 mm/min)

Failure Envelope Name / Series Number	Geomembrane Manufacturer	Normal Stress (kPa)	Peak Shear Strength (kPa)	Large Displacement Shear Strength (kPa)	Displacement at Peak Shear Strength (mm)	Final GCL Water Content (%)	Displacement at Large Displacement Shear Strength (mm)
TH 11 1	80-mil s	34.5	20.0	13.8	19.05	61	53.34
	80-mil s	137.9	53.8	30.3	11.43	61	38.10
	80-mil s	310.3	123.4	78.6	11.43	61	45.09
TH 11 2	80-mil s	34.5	17.2	13.8	1.27	62.5	22.86
	80-mil s	137.9	50.3	33.1	10.80	62.5	41.91
	80-mil s	310.3	122.0	73.8	7.62	62.5	50.17
TH 11 3	80-mil s	34.5	20.0	12.4	10.16	73	50.17
	80-mil s	137.9	42.7	26.2	11.43	73	42.55
	80-mil s	310.3	98.6	68.3	10.80	73	48.26
TH 11 4	80-mil s	34.5	19.3	13.1	8.89	73.5	50.17
	80-mil s	137.9	51.7	33.1	10.80	73.5	45.72
	80-mil s	310.3	110.3	66.9	7.62	73.5	26.67
TH 11 5	80-mil s	34.5	17.2	11.0	7.62	76	24.13
	80-mil s	137.9	44.1	24.8	7.62	76	33.02
	80-mil s	310.3	100.0	57.2	7.62	76	38.10
TH 11 6	80-mil s	34.5	16.5	11.0	8.89	75	42.55
	80-mil s	137.9	63.4	43.4	12.70	75	49.53
	80-mil s	310.3	120.7	72.4	16.51	75	51.44
TH 11 7	80-mil s	34.5	19.3	9.7	18.42	83.5	55.88
	80-mil s	137.9	77.2	37.2	15.88	83.5	50.80
	80-mil s	310.3	155.1	80.0	28.58	83.5	53.34
TH 11 8	80-mil s	34.5	18.6	12.4	11.43	78	38.10
	80-mil s	137.9	64.1	37.9	7.62	78	48.90
	80-mil s	310.3	99.3	74.5	18.80	78	52.71
TH 11 9	80-mil s	34.5	14.5	9.7	12.70	71.5	17.78
	80-mil s	137.9	65.5	35.9	8.26	71.5	43.18
	80-mil s	310.3	99.3	68.9	16.51	71.5	27.94
TH 11 10	80-mil s	34.5	24.1	13.1	3.81	87	45.72
	80-mil s	137.9	53.1	31.0	11.68	72.3	53.34
	80-mil s	310.3	132.4	60.7	16.51	67.4	52.07
TH 11 11	80-mil s	34.5	18.6	11.7	11.43	89.7	45.72
	80-mil s	137.9	46.2	25.5	13.97	70.3	54.61
	80-mil s	310.3	117.9	60.0	12.45	51.7	46.99
TH 11 12	80-mil s	34.5	18.6	14.5	8.26	84.6	40.64
	80-mil s	137.9	60.0	37.9	7.62	64.2	46.99
	80-mil s	310.3	101.4	64.1	12.70	63.8	46.36
TH 11 13	80-mil s	34.5	16.5	12.4	13.97	74	43.18
	80-mil s	137.9	49.6	31.7	12.70	74	58.42
	80-mil s	310.3	120.7	73.1	12.70	74	60.96
TH 11 14	80-mil s	34.5	27.6	15.2	11.43	72	48.26
	80-mil s	137.9	82.7	37.9	15.24	72	63.50
	80-mil s	310.3	169.6	84.8	15.24	72	55.25
TH 11 15	80-mil s	34.5	25.5	15.9	8.89	69.5	56.52
	80-mil s	137.9	76.5	46.9	8.26	69.5	31.12
	80-mil s	310.3	148.2	94.5	7.62	69.5	61.60
TH 11 16	80-mil s	34.5	31.7	19.3	19.05	73.5	57.79
	80-mil s	137.9	84.8	46.9	19.05	73.5	59.69
	80-mil s	310.3	149.6	91.7	19.05	73.5	53.34
TH 11 17	80-mil s	34.5	21.4	13.8	7.62	71	57.15
	80-mil s	137.9	57.9	34.5	7.62	71	57.15
	80-mil s	310.3	138.6	77.2	5.08	71	53.34
TH 11 18	80-mil s	34.5	17.2	14.5	6.99	67.5	11.43
	80-mil s	137.9	69.6	37.9	6.99	67.5	45.72
	80-mil s	310.3	135.8	81.4	6.35	67.5	33.02
TH 11 19	80-mil s	34.5	18.6	11.7	5.72	76	43.18
	80-mil s	137.9	59.3	31.0	10.80	76	46.99
	80-mil s	310.3	120.7	75.2	9.53	76	53.34
TH 11 20	80-mil s	34.5	19.3	13.8	13.97	74.5	45.72
	80-mil s	137.9	46.9	28.3	11.43	74.5	52.07
	80-mil s	310.3	122.0	63.4	16.51	74.5	52.71
				Average	**11.38**	**73.05**	**46.31**
				St. Dev.	**4.73**	**6.31**	**11.12**
				COV	**0.42**	**0.09**	**0.24**

Note: Large displacement is reported when the shear strength has reached a constant level, it still should not be used as the residual displacement

Table 5.39: Displacements at Peak Shear Strength and Final GCL Water Contents for Failure Envelope TH 15 (t_H = 168 hours, t_C = 48 hours, SDR = 0.1 mm/min)

GCL Description	Geomembrane Description	Normal Stress (kPa)	Peak Shear Strength (kPa)	Displacement at Peak Shear Strength (mm)	Final GCL Water Content (%)
B	80-mil s	34.5	12.4	15.24	103.3
B	80-mil s	34.5	11.7	10.16	106
B	80-mil s	137.9	35.2	30.48	64.1
B	80-mil s	137.9	40.7	22.86	77.1
B	80-mil s	310.3	59.3	34.29	63.5
B	80-mil s	310.3	62.7	32.39	76.9

Table 5.40: Comparison of the Average Shear Strengths for Internal GCL Failure Envelopes A5, B4 and C3 and the Average Shear Strengths for GCL-GM Interface Failure Envelopes TH 5, TH 11 and TH 15 (t_H = 168 hours, t_C = 48 hours, SDR = 0.1 mm/min)

Failure Envelope Name and Description			Number of Tests	Normal Stress (kPa)	Mean Peak Shear Strength (kPa)	Standard Deviation Peak Shear Strength (kPa)	Mean Large Displacement Shear Strength (kPa)	Standard Deviation Large Displacement Shear Strength (kPa)
A5	GCL A	Internal	19	34.5	46.9	5.3	20.8	8.8
	GCL A	Internal	19	137.9	110.4	16.4	38.7	11.0
	GCL A	Internal	19	310.3	199.8	24.9	67.2	18.4
B4	GCL B	Internal	1	34.5	35.9	#N/A	35.9	#N/A
	GCL B	Internal	1	137.9	51.7	#N/A	51.7	#N/A
	GCL B	Internal	1	310.3	71.7	#N/A	71.7	#N/A
C3	GCL C	Internal	1	34.5	32.4	#N/A	8.3	#N/A
	GCL C	Internal	1	137.9	63.4	#N/A	17.2	#N/A
	GCL C	Internal	1	310.3	114.5	#N/A	47.6	#N/A
TH 5	GCL C	80-mil THDPE s	2	34.5	14.5	2.0	9.7	0.0
	GCL C	80-mil THDPE s	2	137.9	49.0	4.9	28.6	7.3
	GCL C	80-mil THDPE s	2	310.3	103.8	5.4	60.3	1.5
TH 11	GCL A	80-mil THDPE s	20	34.5	20.1	4.2	13.1	2.2
	GCL A	80-mil THDPE s	20	137.9	56.0	12.8	34.6	6.4
	GCL A	80-mil THDPE s	20	310.3	124.3	20.4	73.3	10.1
TH 15	GCL B	80-mil THDPE s	2	34.5	12.1	0.5	10.7	0.5
	GCL B	80-mil THDPE s	2	137.9	37.9	3.9	30.3	1.0
	GCL B	80-mil THDPE s	2	310.3	61.0	2.4	47.2	1.5

Table 5.41: Comparison of the Average Displacements at Peak Shear Strength and Average Final Water Contents for Internal and Interface GCL Failure Envelopes A5, B4, C3, TH 5, TH 11 and TH 15 (t_H = 168 hours, t_C = 48 hours, SDR = 0.1 mm/min)

Failure Envelope Name and Description			Mean Displacement at Peak Shear Strength (mm)	Standard Deviation Displacement at Peak Shear Strength (mm)	Mean Final GCL Water Content (%)	Standard Deviation of the Final GCL Water Content (%)
A5	GCL A	Internal	27.6	10.8	78.4	9.0
	GCL A	Internal	20.4	3.2	76.3	6.5
	GCL A	Internal	21.6	5.4	74.1	6.8
B4	GCL B	Internal	38.1	#N/A	84.4	#N/A
	GCL B	Internal	43.18	#N/A	77.8	#N/A
	GCL B	Internal	64.77	#N/A	64.0	#N/A
C3	GCL C	Internal	12.7	#N/A	109.6	#N/A
	GCL C	Internal	21.0	#N/A	98.2	#N/A
	GCL C	Internal	12.1	#N/A	61.4	#N/A
TH 5	GCL C	80-mil THDPE s	2.2	0.4	101.2	0.1
	GCL C	80-mil THDPE s	9.8	0.4	84.0	13.9
	GCL C	80-mil THDPE s	11.6	0.2	74.4	10.7
TH 11	GCL A	80-mil THDPE s	10.5	4.8	74.7	7.3
	GCL A	80-mil THDPE s	11.1	3.2	71.9	5.3
	GCL A	80-mil THDPE s	13.0	5.7	70.7	7.0
TH 15	GCL B	80-mil THDPE s	12.7	3.6	104.7	1.9
	GCL B	80-mil THDPE s	26.7	5.4	70.6	9.2
	GCL B	80-mil THDPE s	33.3	1.3	70.2	9.5

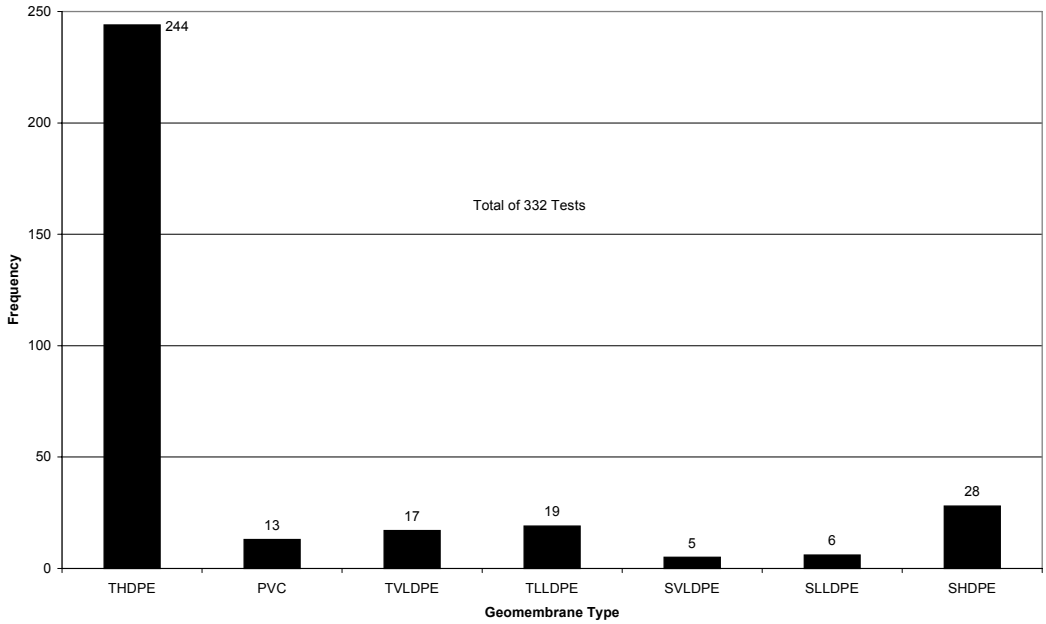

Figure 5.1: Histogram of the Number of GCL-Geomembrane Interface Tests on Each Type of Geomembrane

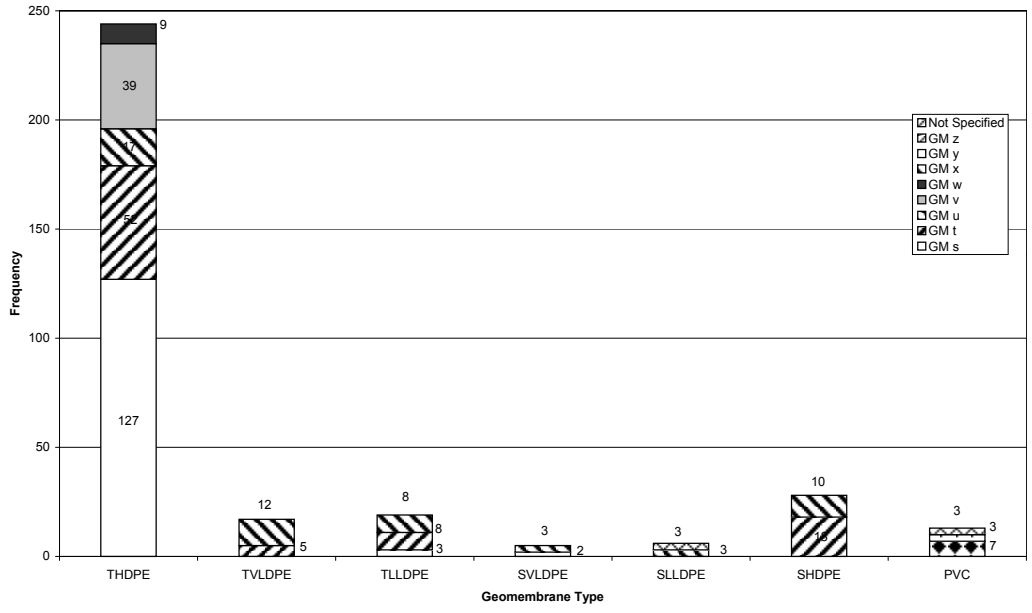

Figure 5.2: Histogram of the Number of GCL-Geomembrane Interface Tests on Each Type of Geomembrane, Identifying Geomembrane Manufacturer

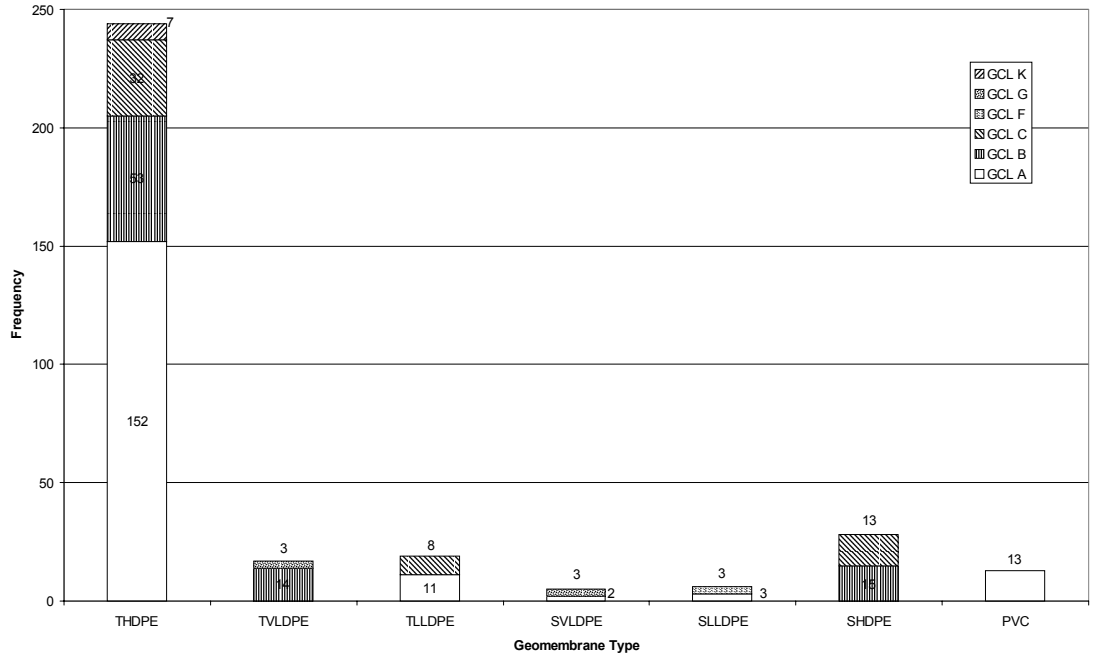

Figure 5.3: Histogram of the Number of GCL-Geomembrane Interface Tests on Each Type of Geomembrane, Identifying GCL Types

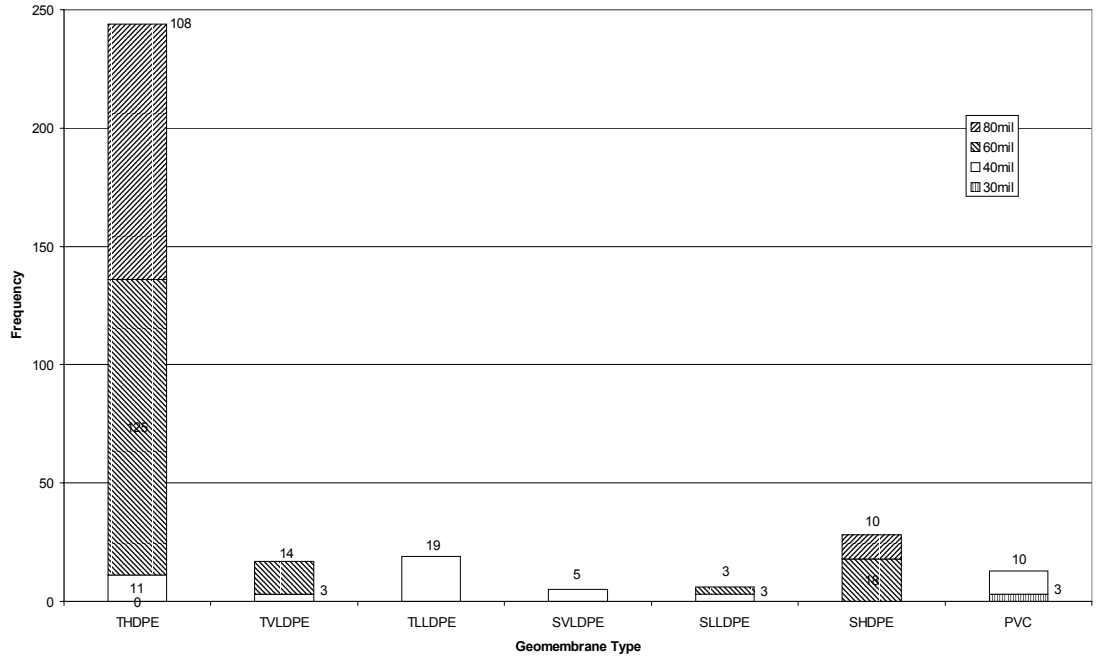

Figure 5.4: Histogram of the Number of GCL-Geomembrane Interface Tests on Each Type of Geomembrane, Identifying Geomembrane Thickness

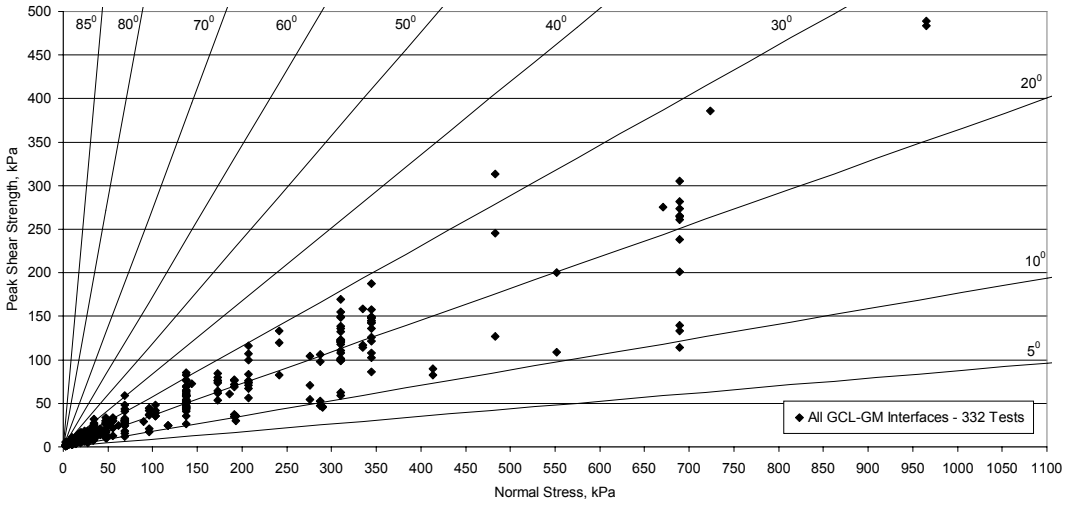

(a)

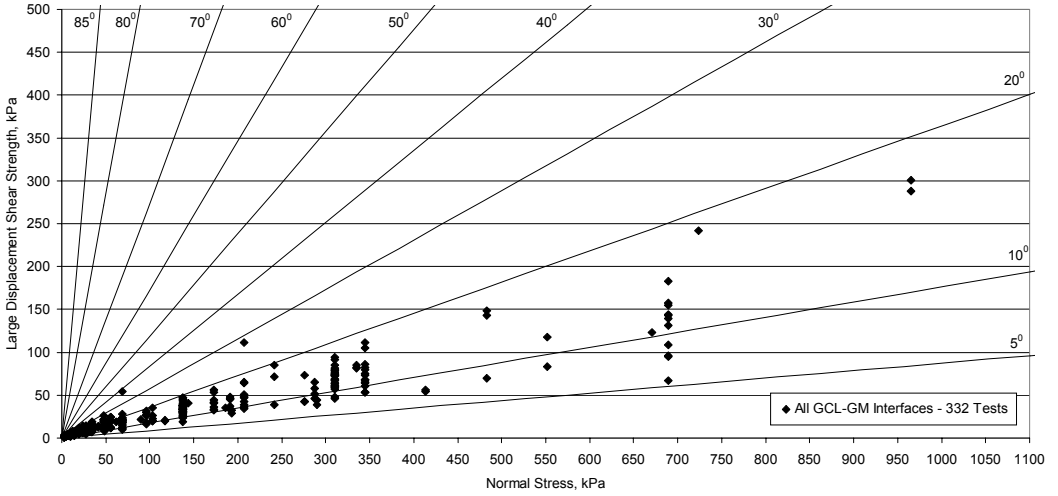

(b)

Figure 5.5: Shear Strength of All GCL-Geomembrane Interfaces; (a) Peak, (b) Large-Displacement

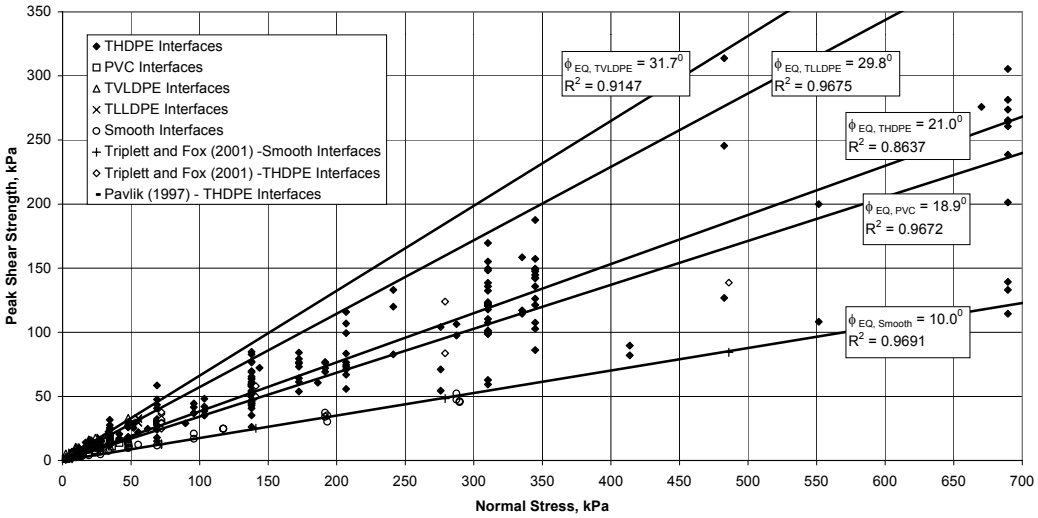

(a)

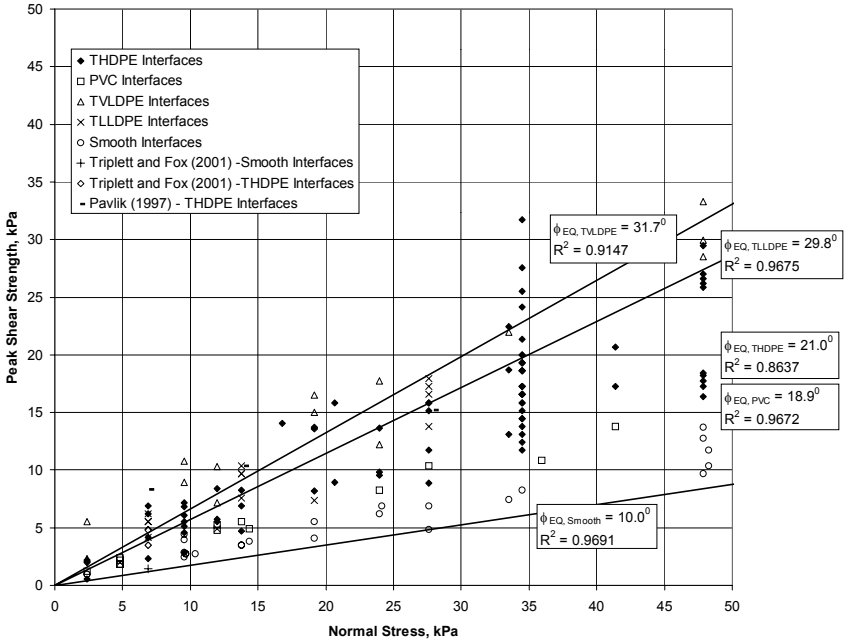

(b)

Figure 5.6: Peak Shear Strengths of All GCL-Geomembrane Interfaces (with Average Equivalent Friction Angles); (a) Full Data Set, (b) Detail of Low Normal Stresses

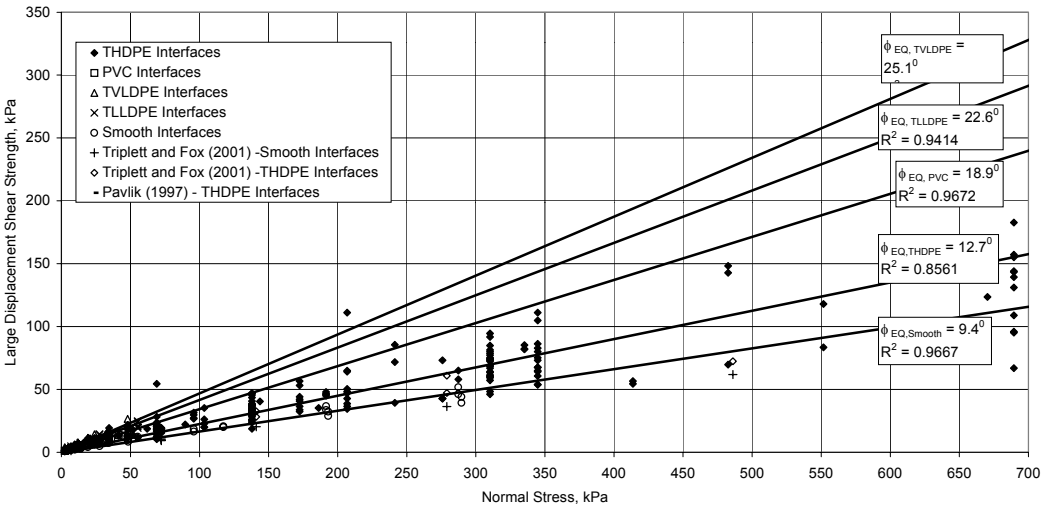

(a)

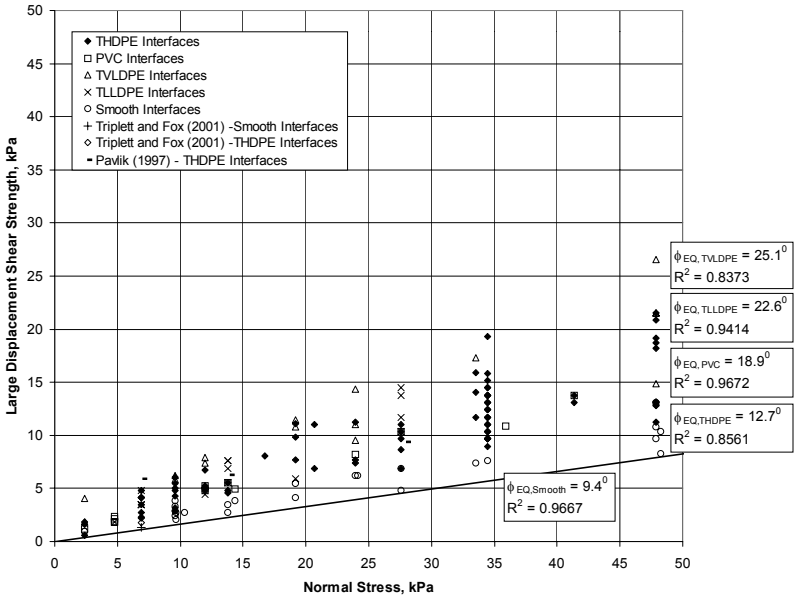

(b)

Figure 5.7: Large Displacement Shear Strengths of All GCL-Geomembrane Interfaces (with Average Equivalent Friction Angles); (a) Full Data Set, (b) Detail of Low Normal Stresses

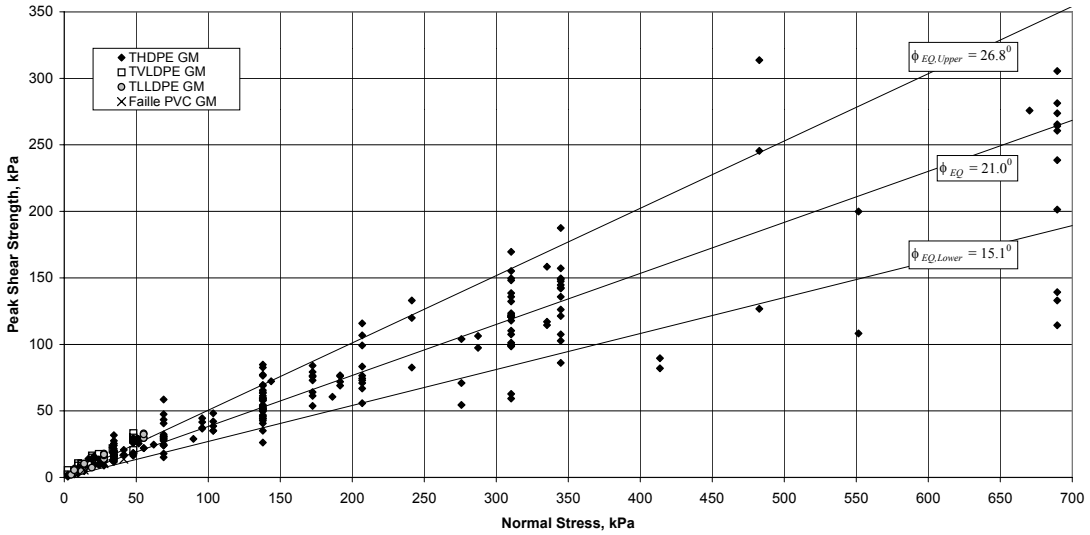

(a)

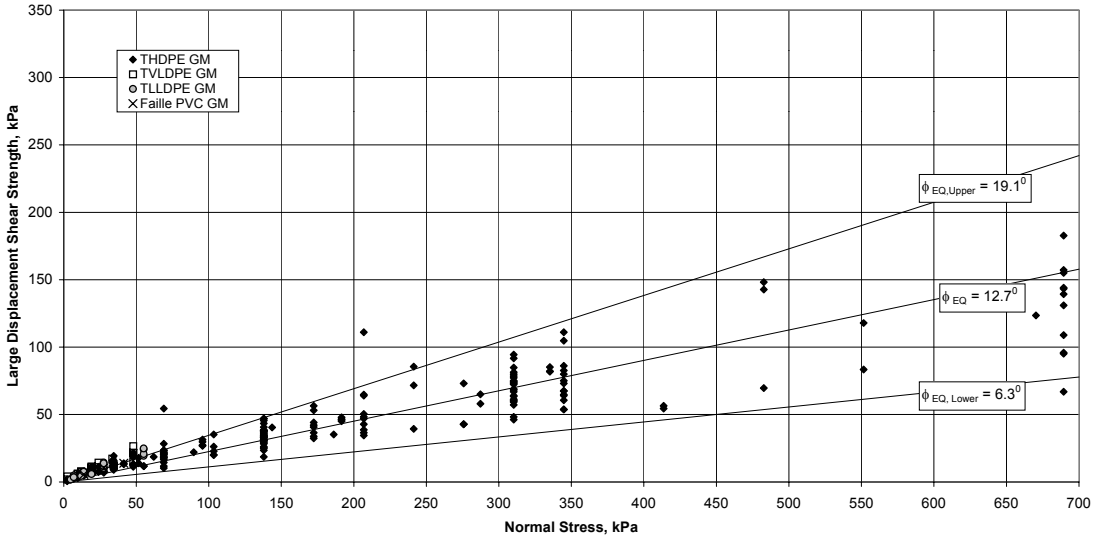

(b)

Figure 5.8: Shear Strength of all Textured Geomembrane Interfaces with the Equivalent, Upper Bound and Lower Bound Equivalent Friction Angles; (a) Peak Shear Strength, (b) Large Displacement Shear Strength

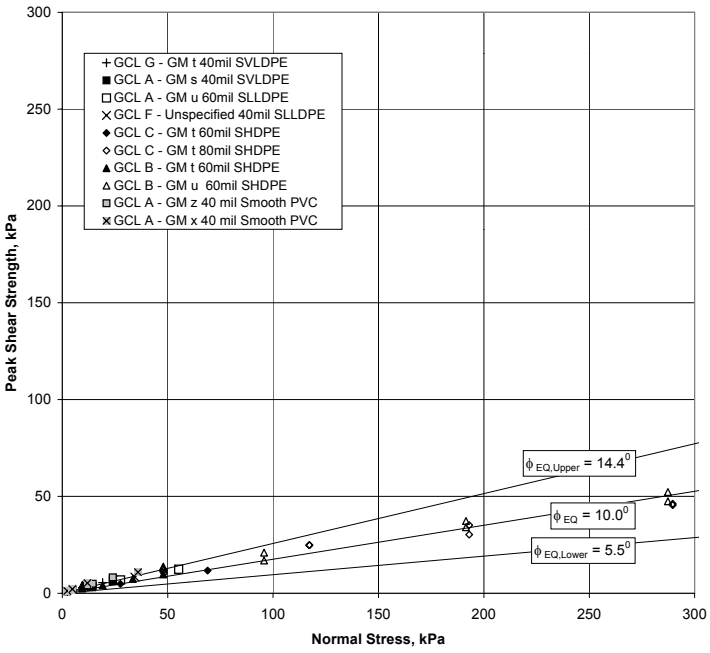

(a)

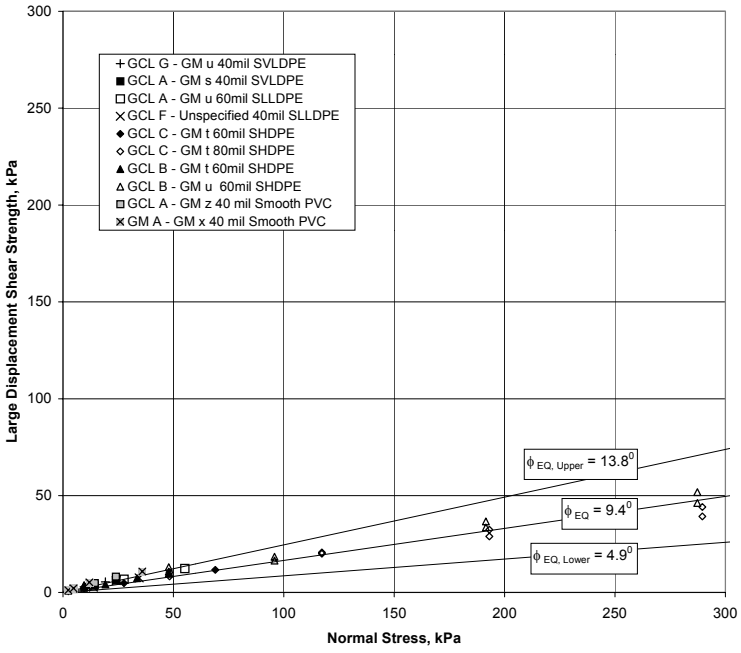

(b)

Figure 5.9: Shear Strength of all Smooth Geomembrane Interfaces with the Equivalent, Upper Bound and Lower Bound Equivalent Friction Angles; (a) Peak Shear Strength; (b) Large Displacement Shear Strength

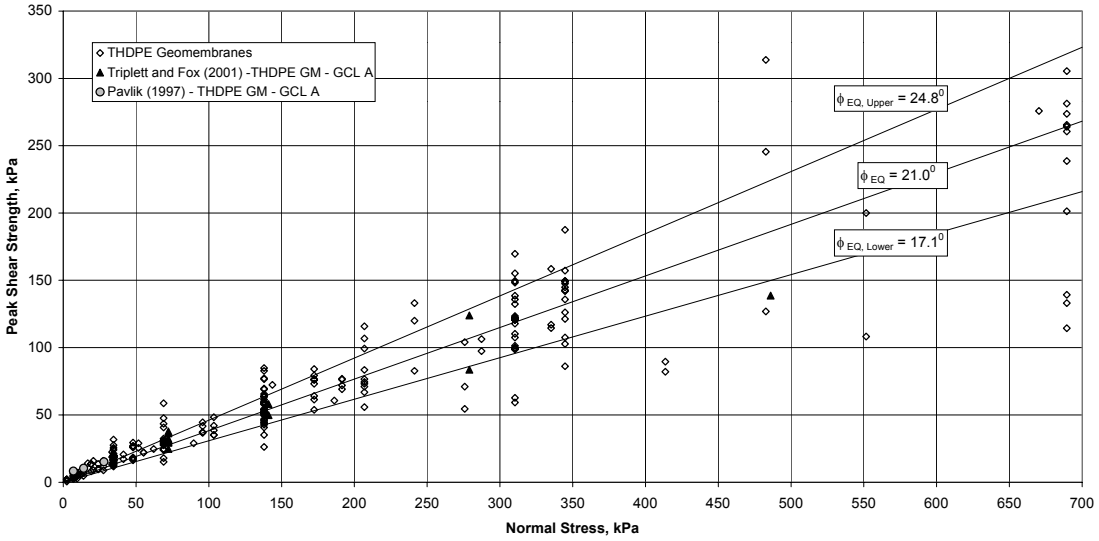

(a)

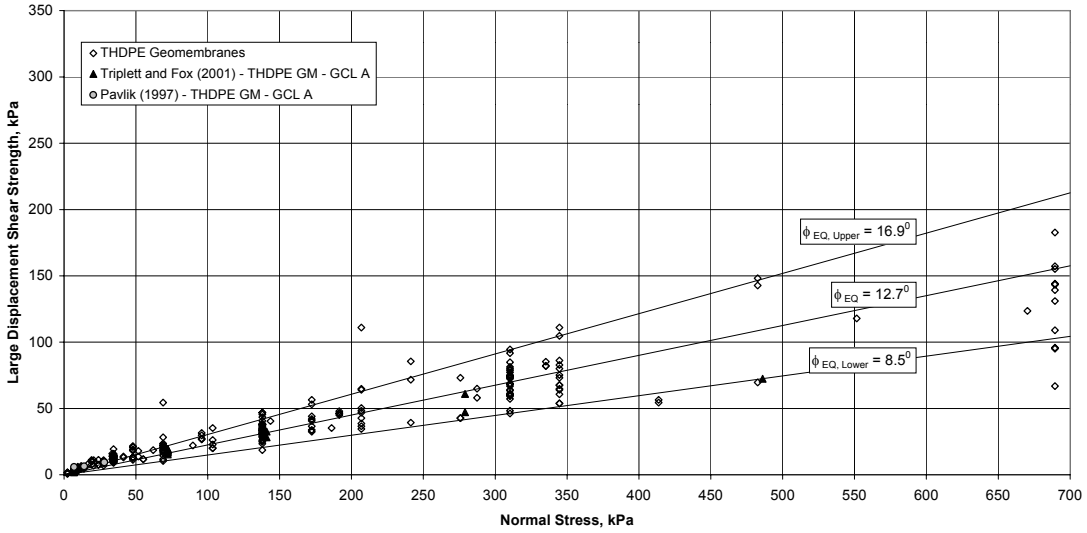

(b)

Figure 5.10: Shear Strength of all Textured HDPE Geomembrane Interfaces with the Equivalent, Upper Bound and Lower Bound Equivalent Friction Angles, with Test Results from Other Studies; (a) Peak Shear Strength, (b) Large Displacement Shear Strength

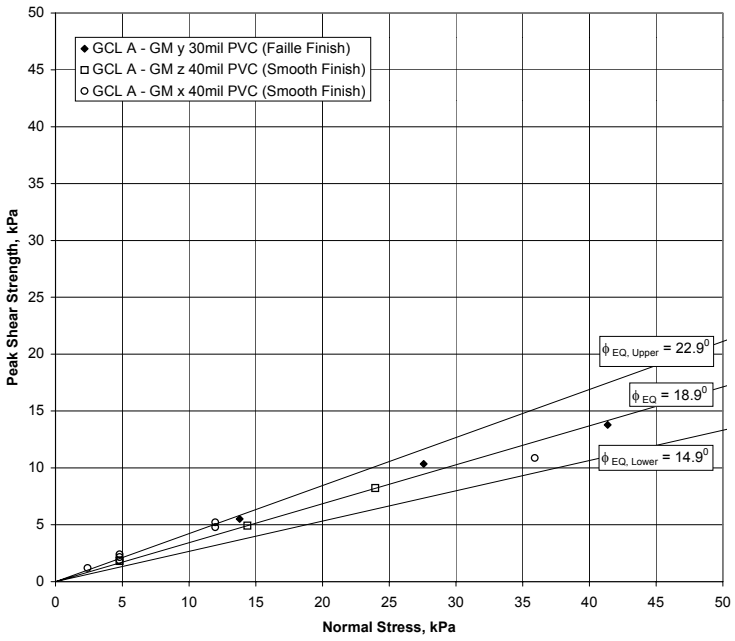

(a)

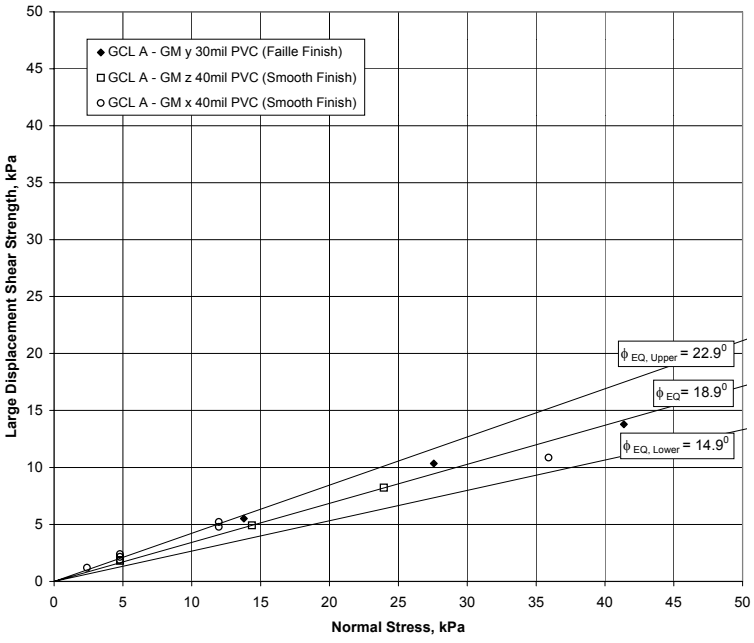

(b)

Figure 5.11: Shear Strength of all PVC Geomembrane Interface with the Equivalent, Upper Bound and Lower Bound Equivalent Friction Angles; (a) Peak Shear Strength; (a) Peak Shear Strength, (b) Large Displacement Shear Strength

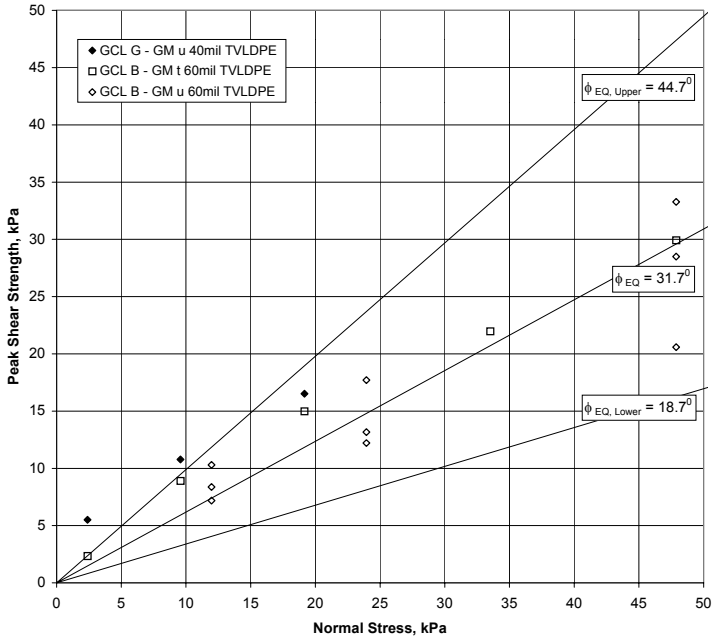

(a)

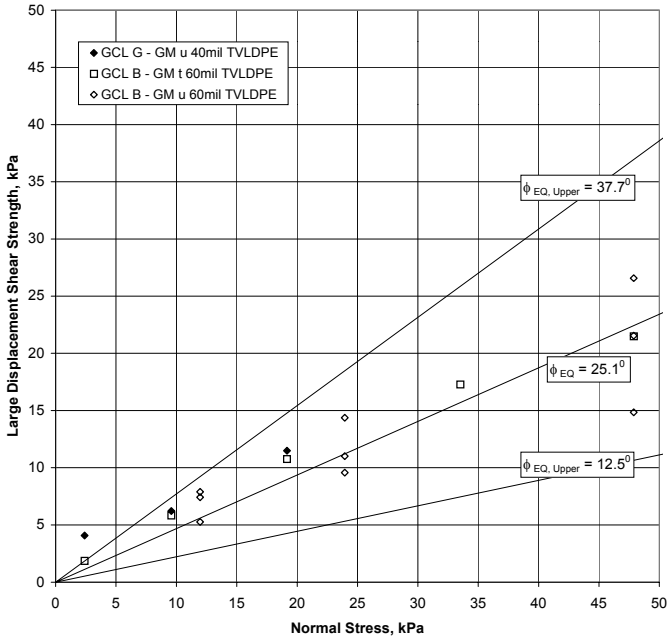

(b)

Figure 5.12: Shear Strength of all Textured VLDPE Geomembrane Interface with the Equivalent, Upper Bound and Lower Bound Equivalent Friction Angles; (a) Peak Shear Strength; (a) Peak Shear Strength, (b) Large Displacement Shear Strength

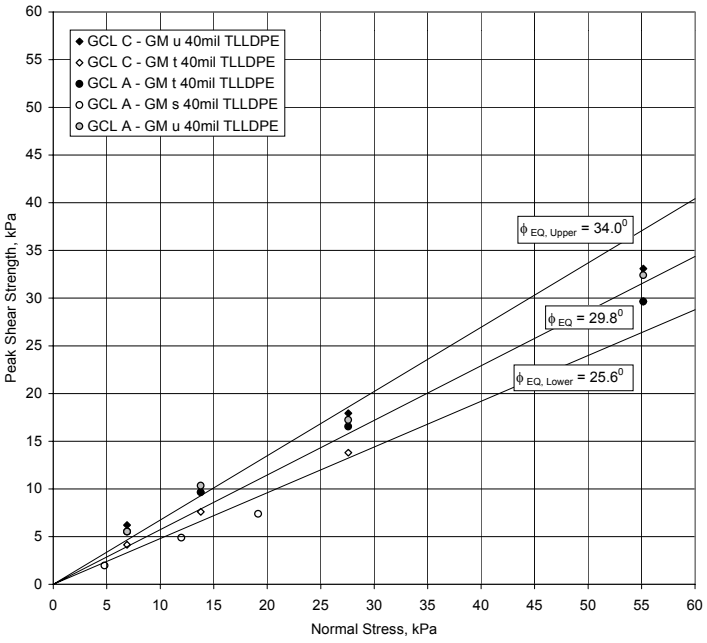

(a)

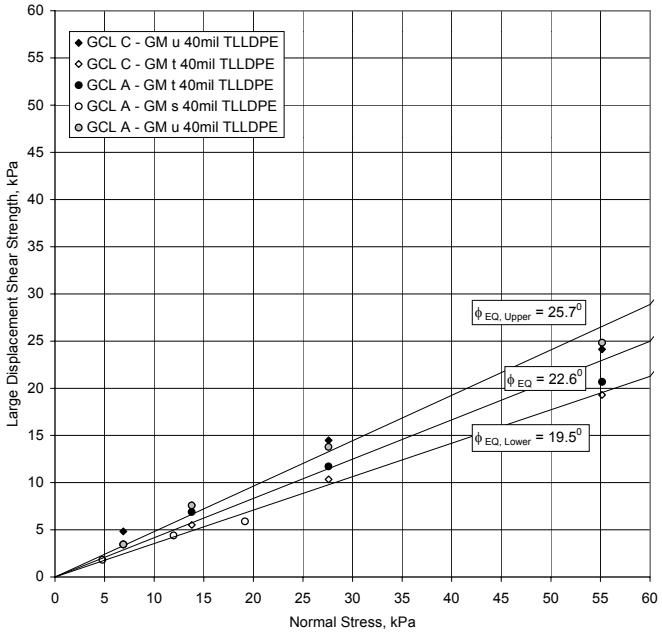

(b)

Figure 5.13: Shear Strength of all Textured LLDPE Geomembrane Interface with the Equivalent, Upper Bound and Lower Bound Equivalent Friction Angles; (a) Peak Shear Strength; (a) Peak Shear Strength, (b) Large Displacement Shear Strength

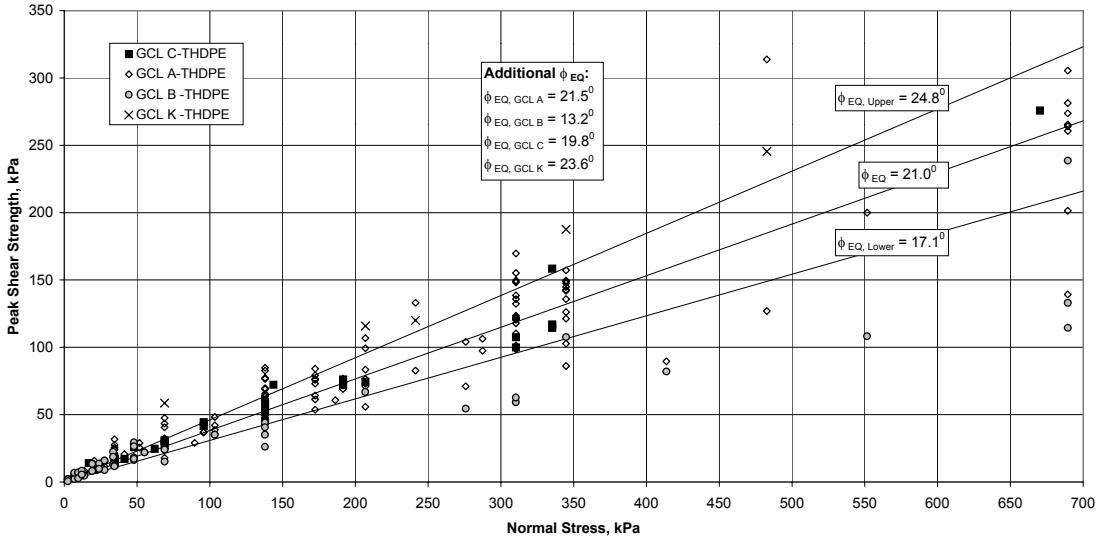

(a)

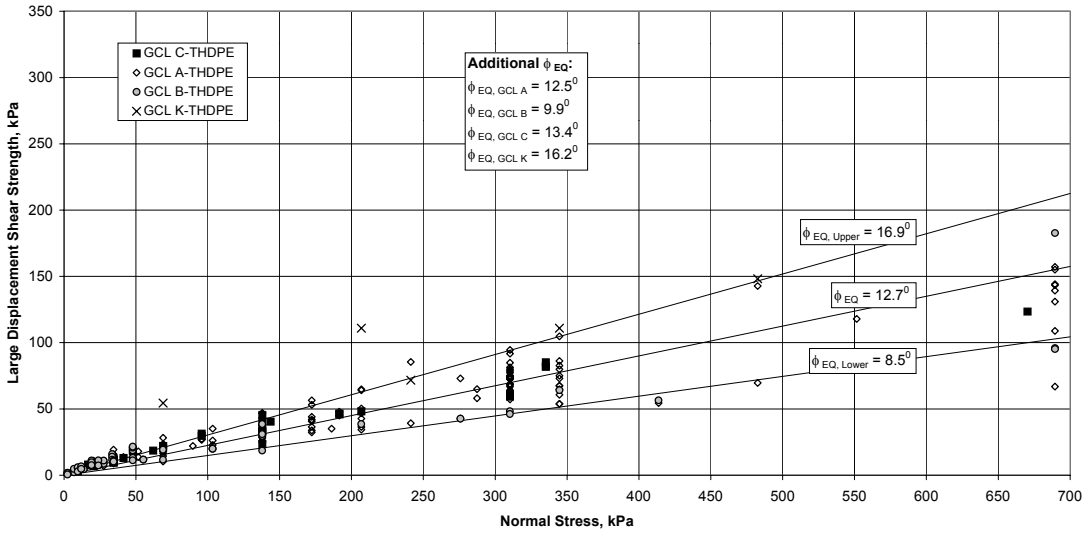

(b)

Figure 5.14: Shear Strength of all Textured HDPE Geomembrane Interfaces (Separated by GCL Interface) with the Equivalent, Upper Bound and Lower Bound Equivalent Friction Angles; (a) Peak Shear Strength; (a) Peak Shear Strength, (b) Large Displacement Shear Strength

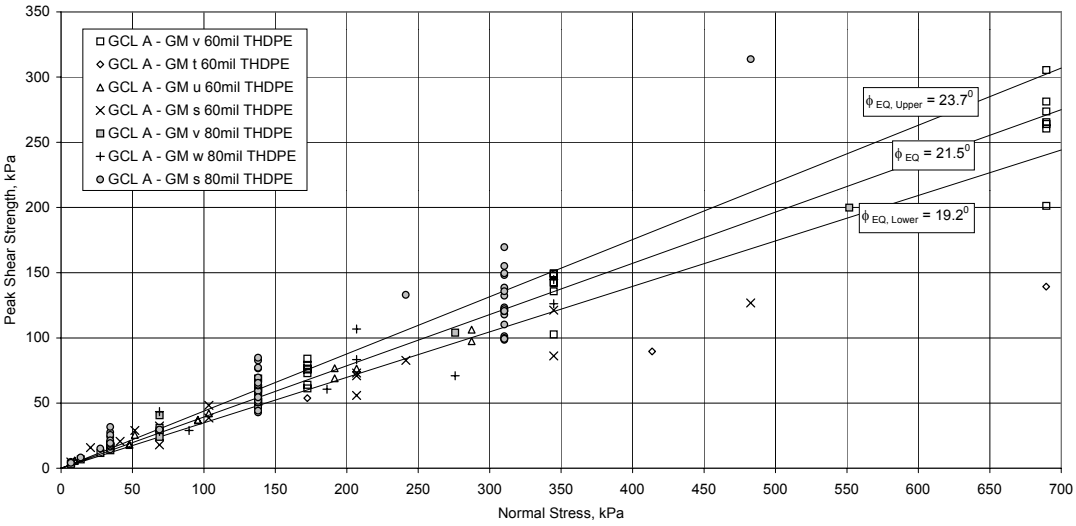

(a)

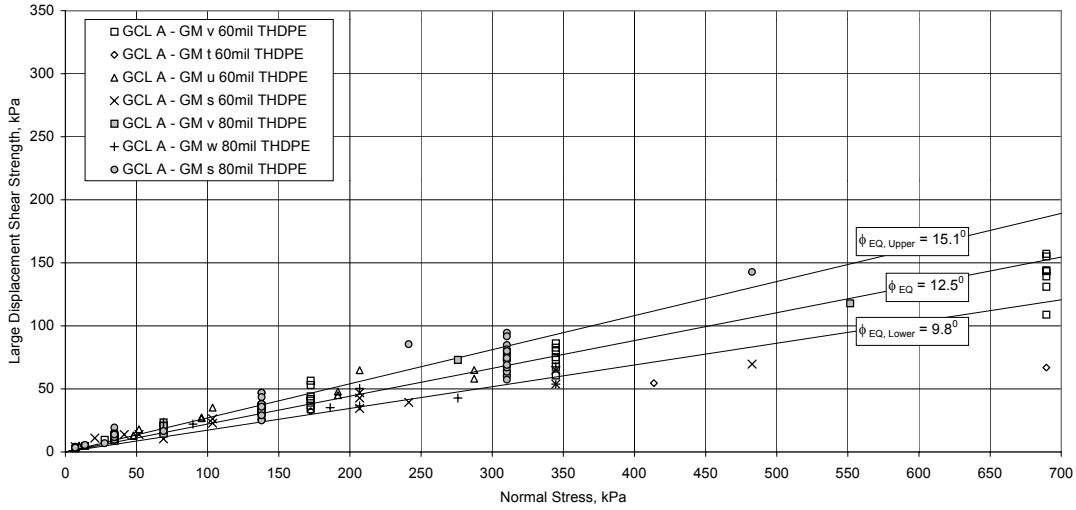

(b)

Figure 5.15: Shear Strength of all GCL A Interfaces with a Textured HDPE Geomembrane with the Equivalent, Upper Bound and Lower Bound Equivalent Friction Angles; (a) Peak Shear Strength; (a) Peak Shear Strength, (b) Large Displacement Shear Strength

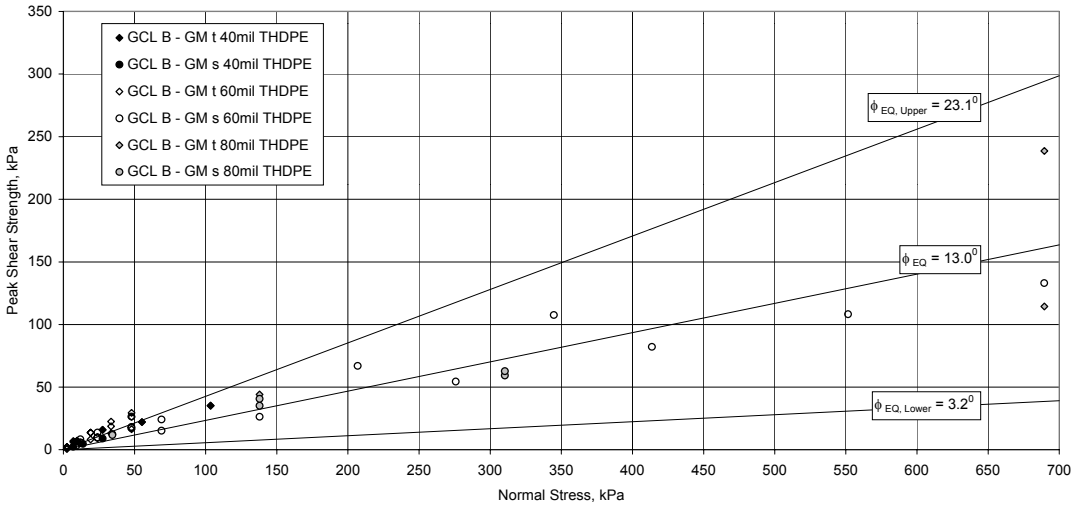

(a)

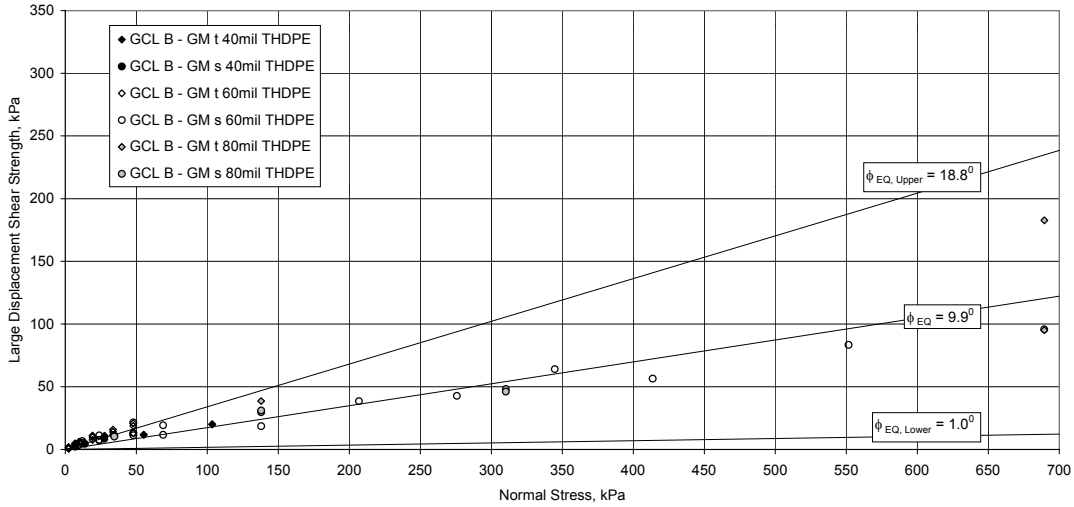

(b)

Figure 5.16: Shear Strength of all GCL B Interfaces with a Textured HDPE Geomembrane with the Equivalent, Upper Bound and Lower Bound Equivalent Friction Angles; (a) Peak Shear Strength; (a) Peak Shear Strength, (b) Large Displacement Shear Strength

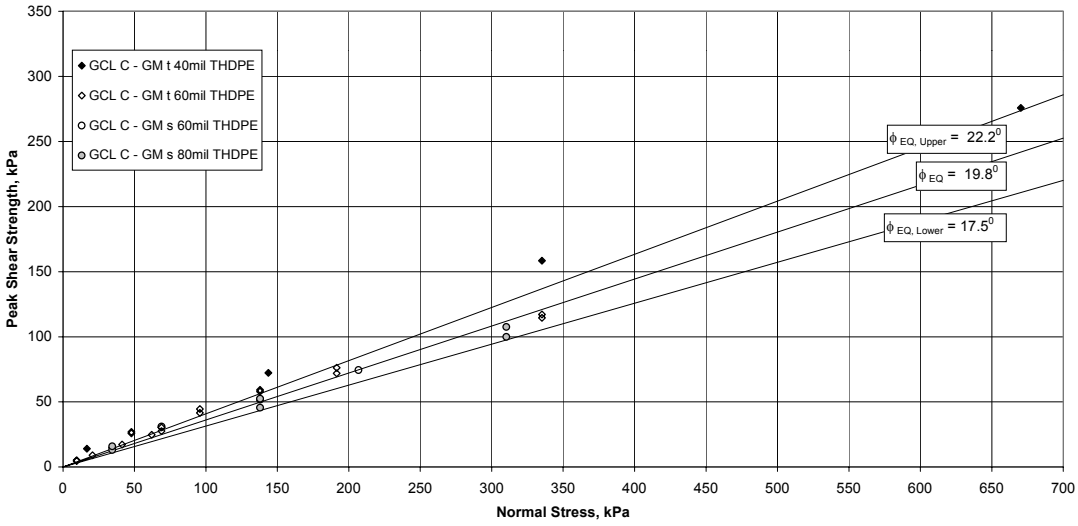

(a)

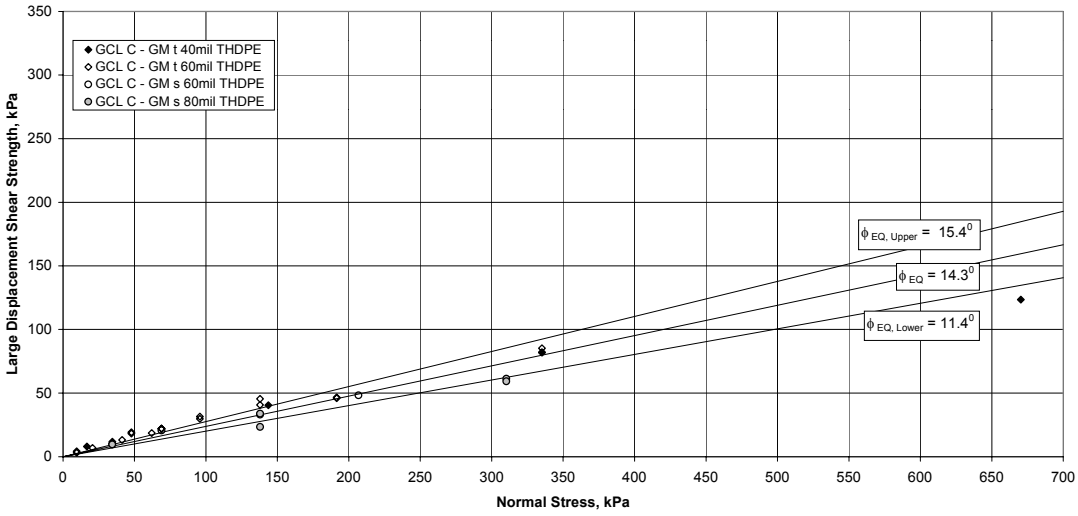

(b)

Figure 5.17: Shear Strength of all GCL C Interfaces with a Textured HDPE Geomembrane with the Equivalent, Upper Bound and Lower Bound Equivalent Friction Angles; (a) Peak Shear Strength; (a) Peak Shear Strength, (b) Large Displacement Shear Strength

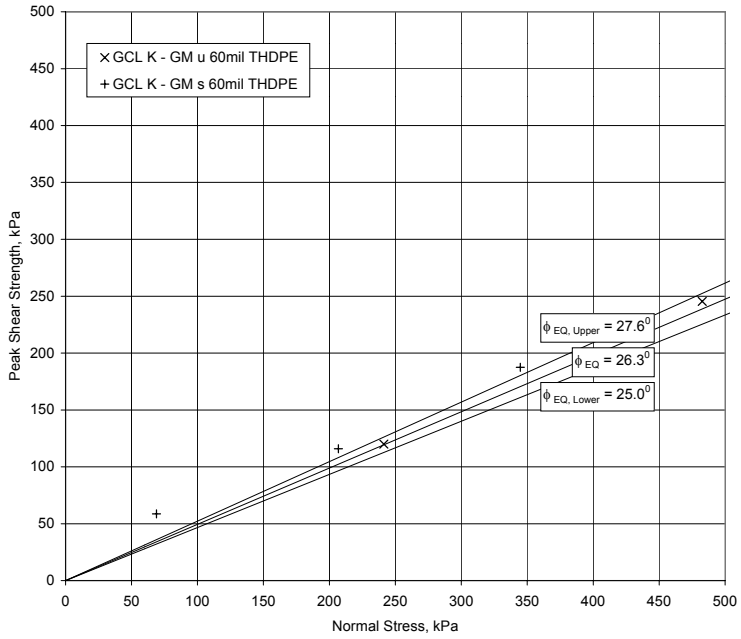

(a)

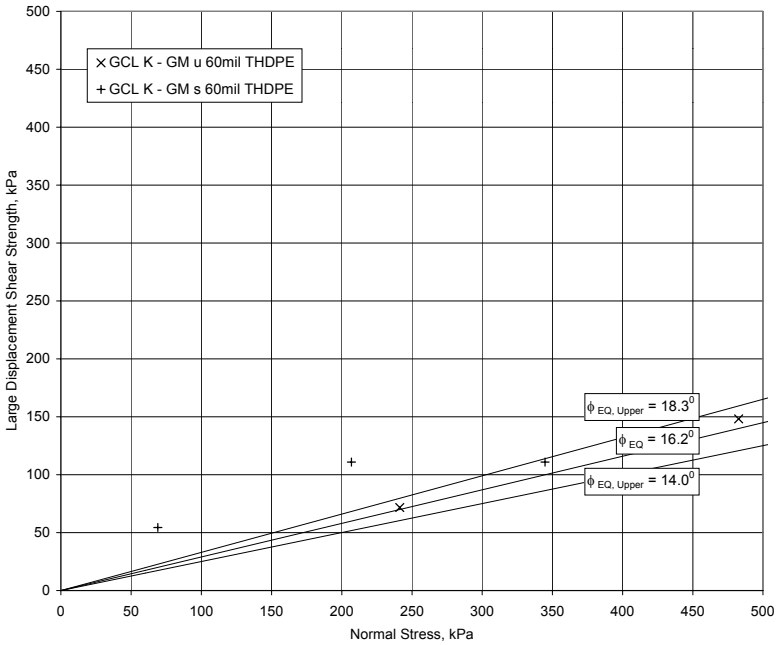

(b)

Figure 5.18: Shear Strength of all GCL K Interfaces with a Textured HDPE Geomembrane with the Equivalent, Upper Bound and Lower Bound Equivalent Friction Angles; (a) Peak Shear Strength; (a) Peak Shear Strength, (b) Large Displacement Shear Strength

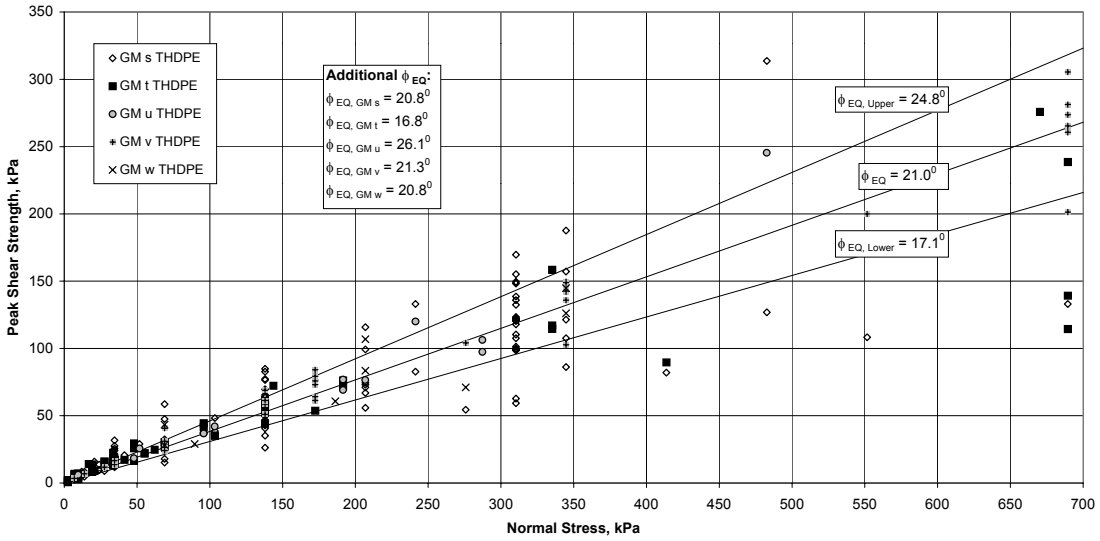

(a)

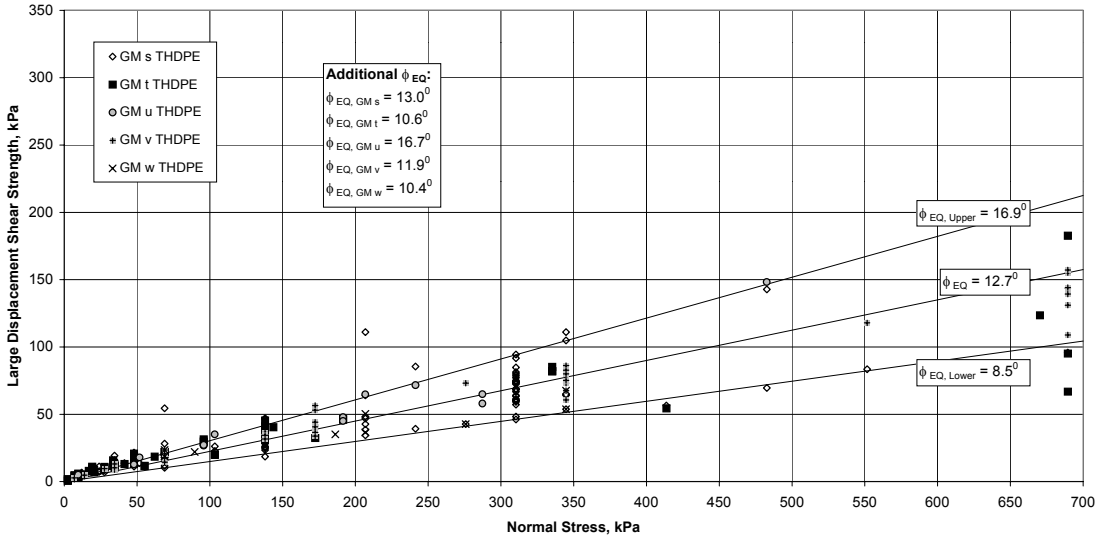

(b)

Figure 5.19: Shear Strength of all Textured HDPE Geomembrane Interfaces (Separated by Geomembrane Manufacturer) with the Equivalent, Upper Bound and Lower Bound Equivalent Friction Angles; (a) Peak Shear Strength; (a) Peak Shear Strength, (b) Large Displacement Shear Strength

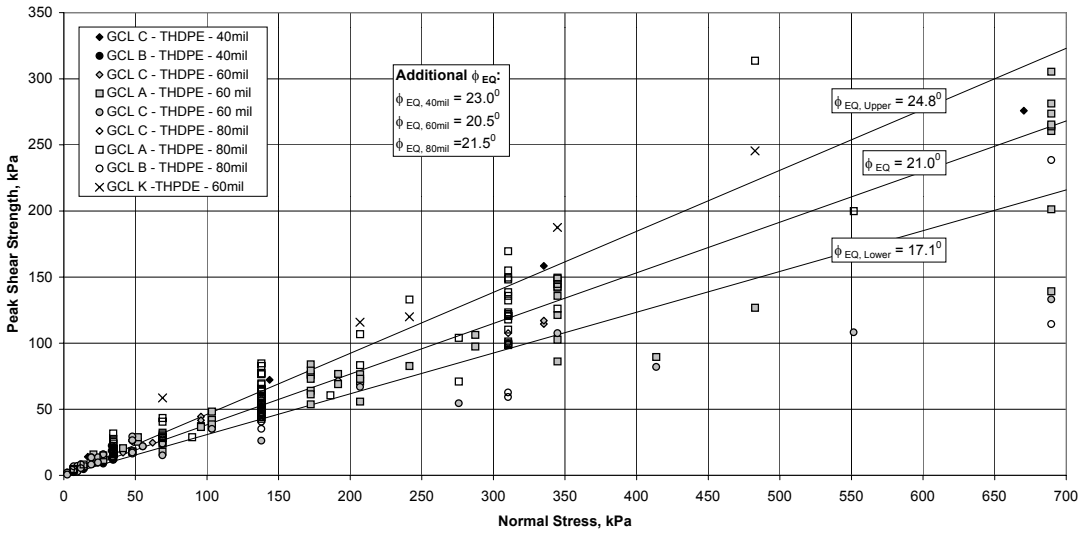

(a)

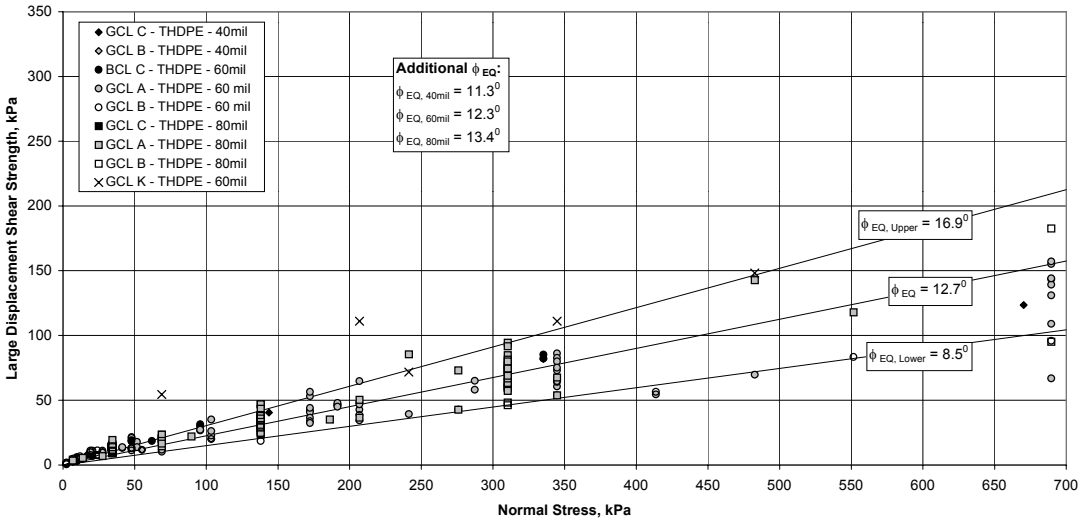

(b)

Figure 5.20: Shear Strength of all Textured HDPE Geomembrane Interfaces (Separated by Geomembrane Thickness) with the Equivalent, Upper Bound and Lower Bound Equivalent Friction Angles; (a) Peak Shear Strength; (a) Peak Shear Strength, (b) Large Displacement Shear Strength

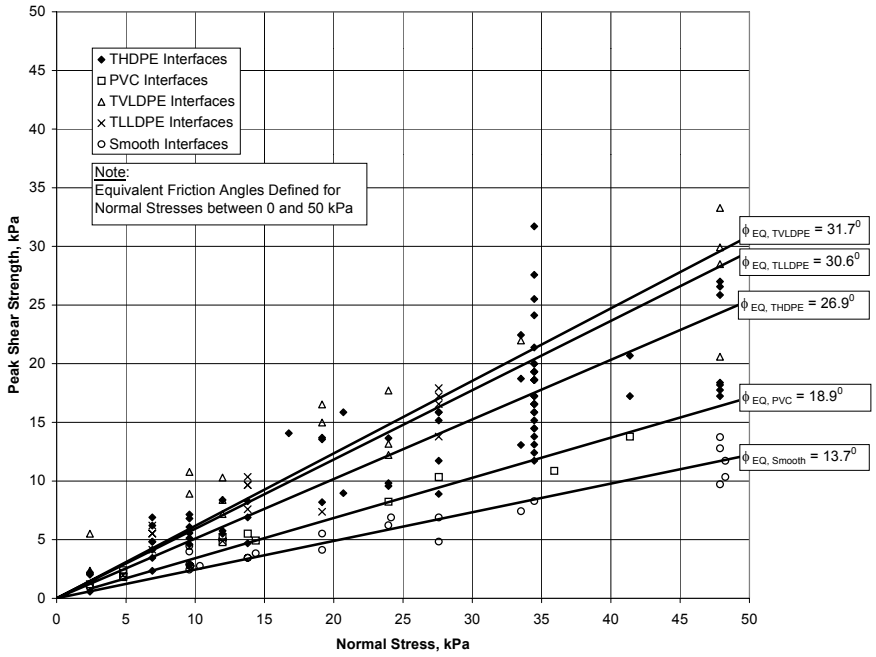

(a)

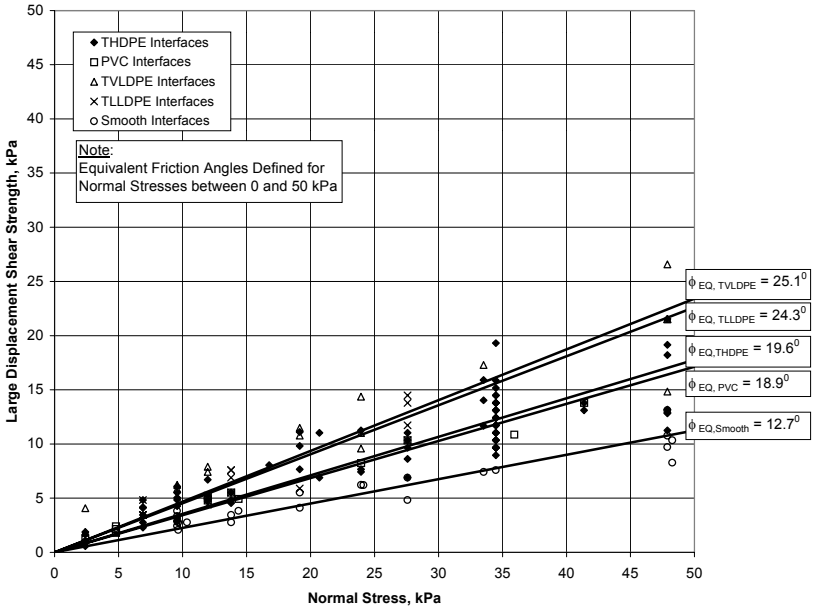

(b)

Figure 5.21: Shear Strength of all GCL-Geomembrane Interfaces at Low Normal Stress; *with the Equivalent Friction Angles for Normal Stresses Less than 50 kPa*; (a) Peak Shear Strength, (b) Large Displacement Shear Strength

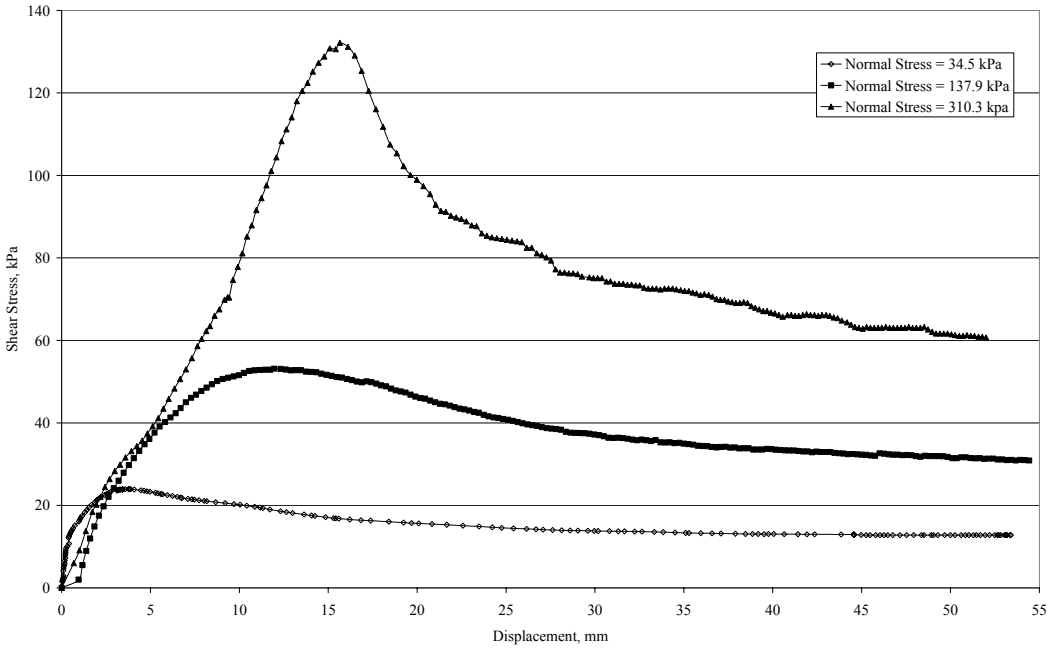

Figure 5.22: Shear Force-Displacement Curves for the Interface between a Hydrated GCL A and an 80-mil Textured HDPE Geomembrane s (t_H = 168 hours, t_C = 48 hours, SDR = 0.1 mm/min)

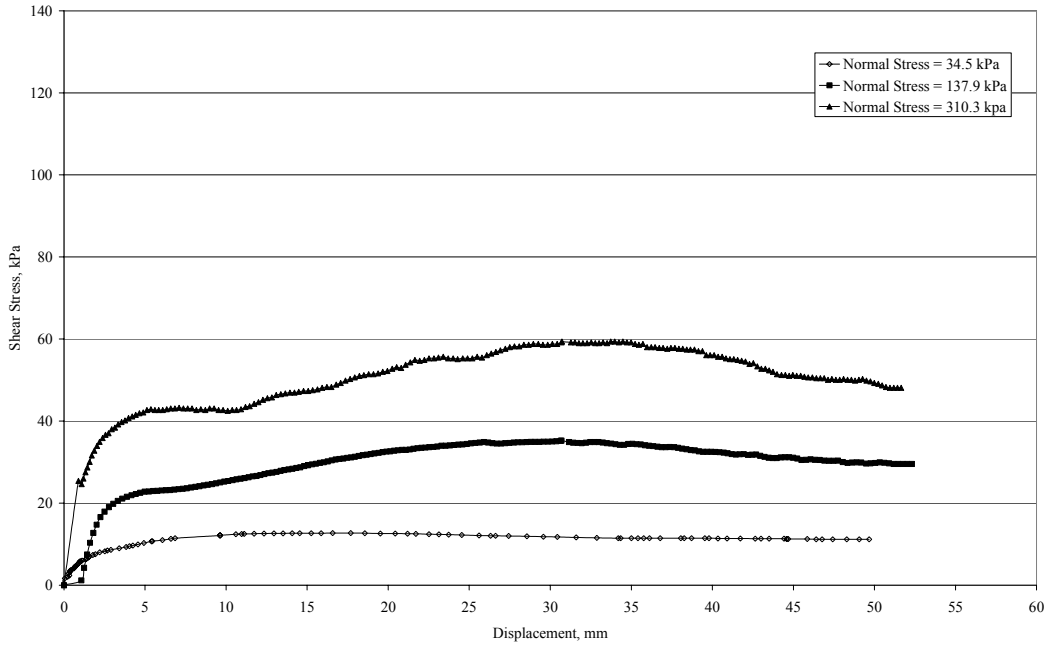

Figure 5.23: Shear Force-Displacement Curves for the Interface between a Hydrated GCL B and an 80-mil Textured HDPE Geomembrane s (t_H = 168 hours, t_C = 48 hours, SDR = 0.1 mm/min)

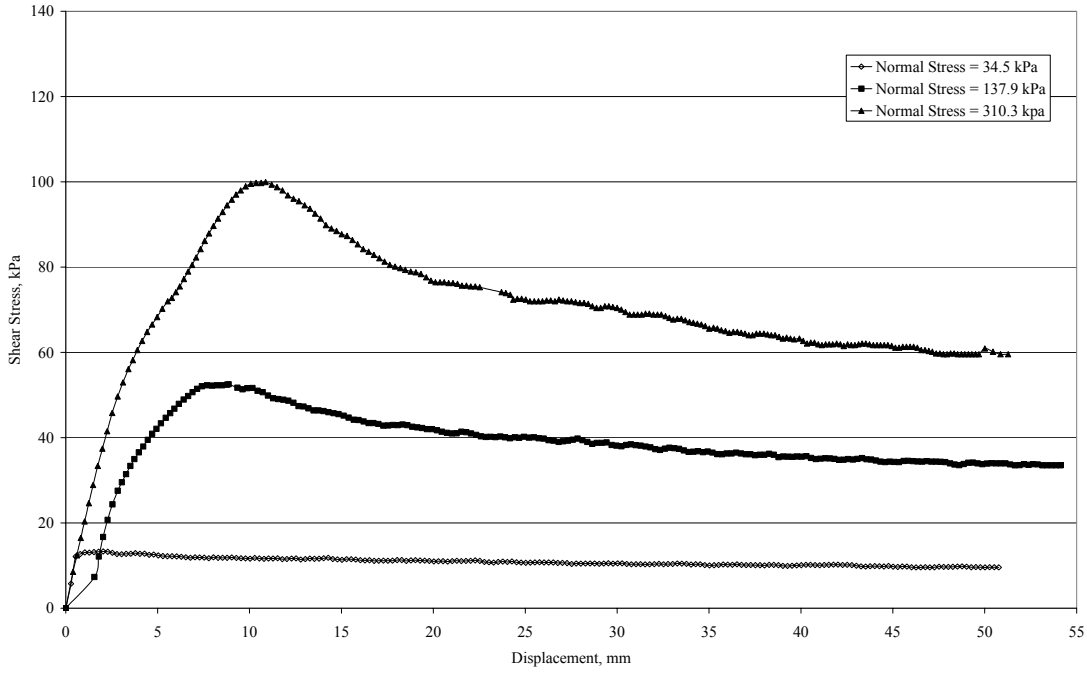

Figure 5.24: Shear Force-Displacement Curves for the Interface between a Hydrated GCL C and an 80-mil Textured HDPE Geomembrane s (t_H = 168 hours, t_C = 48 hours, SDR = 0.1 mm/min)

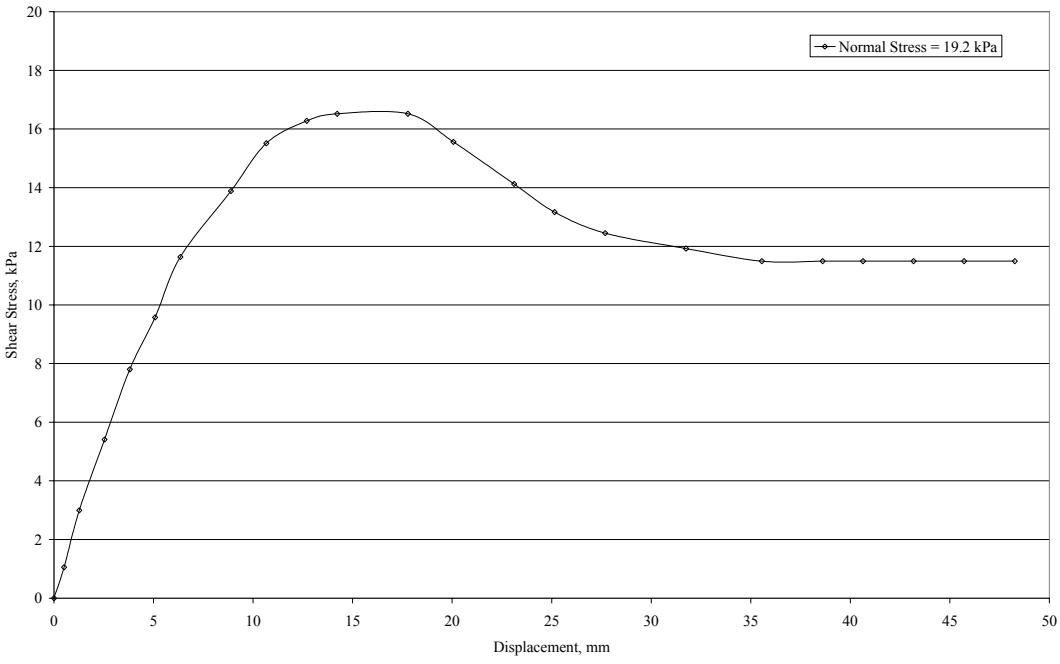

Figure 5.25: Shear Force-Displacement Curves for the Interface between a Hydrated Needle-Punched GCL and a Textured VLDPE Geomembrane

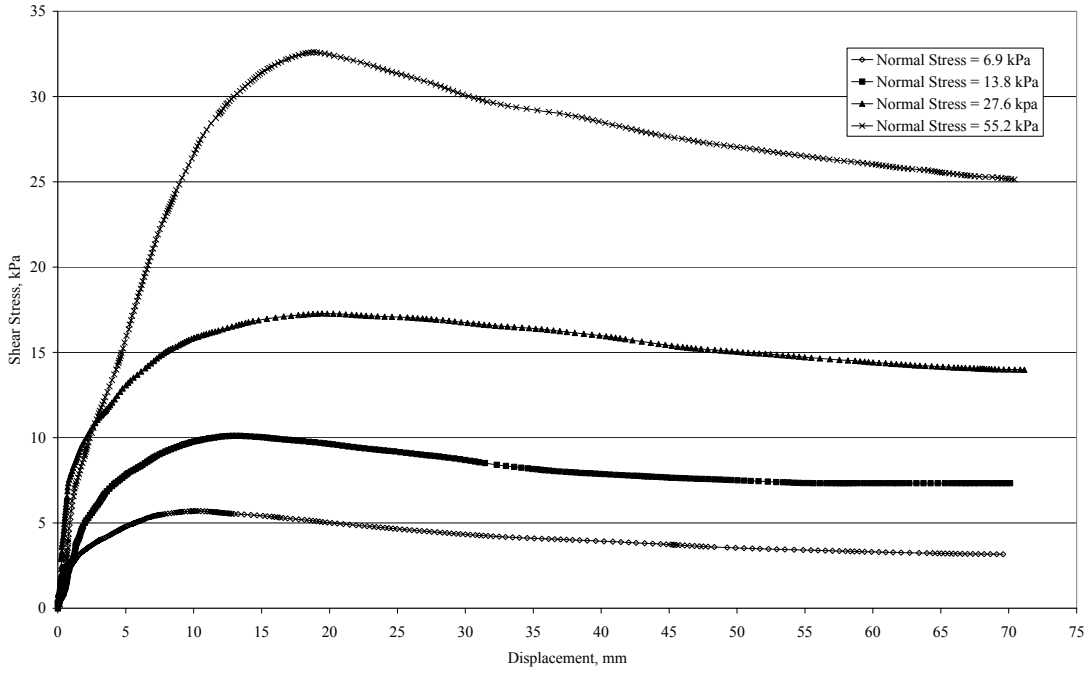

Figure 5.26: Shear Force-Displacement Curves for the Interface between a Hydrated Needle-Punched GCL and a Textured LLDPE Geomembrane

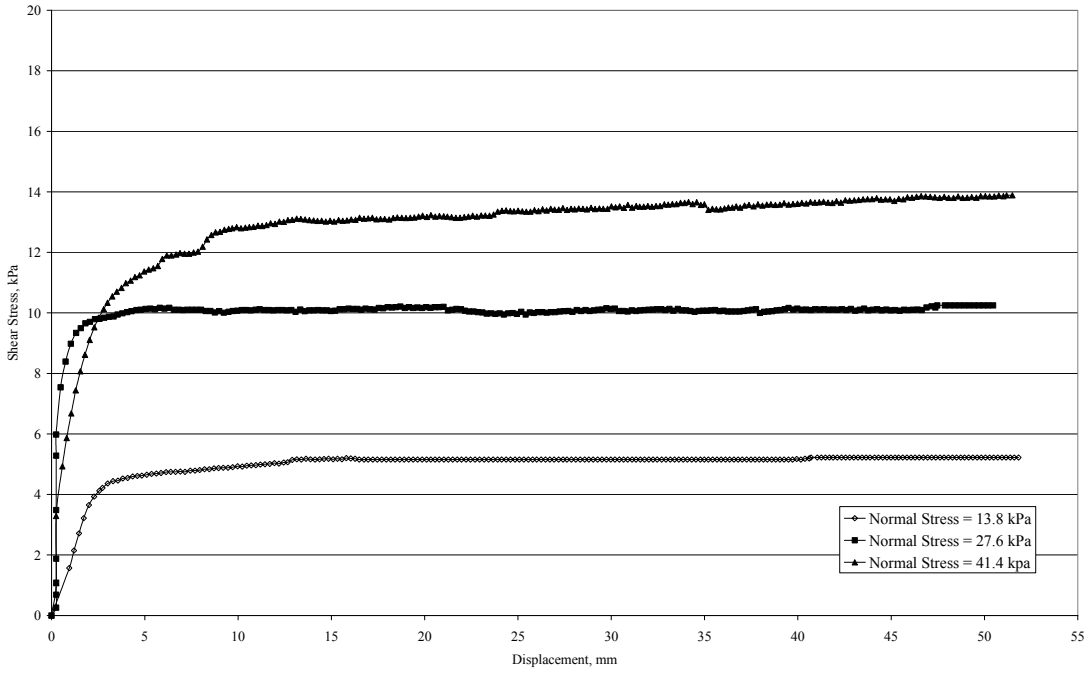

Figure 5.27: Shear Force-Displacement Curves for the Interface between a Hydrated Needle-Punched GCL and a Faille Finish PVC Geomembrane

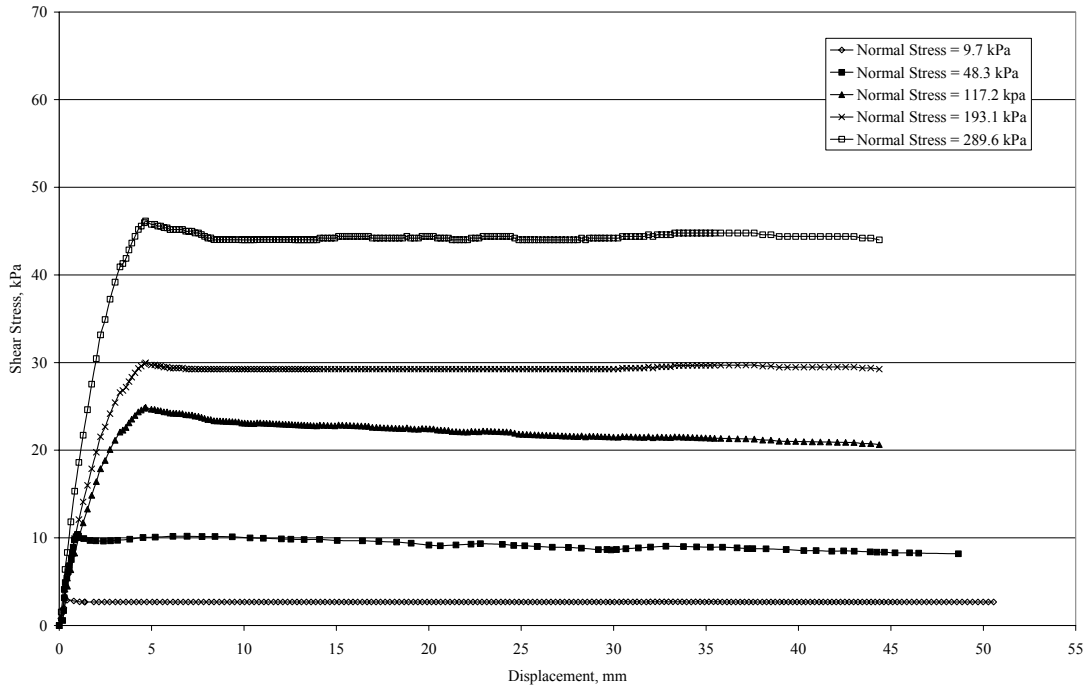

Figure 5.28: Shear Force-Displacement Curves for the Interface between a Hydrated Needle-Punched GCL and a Smooth HDPE Geomembrane

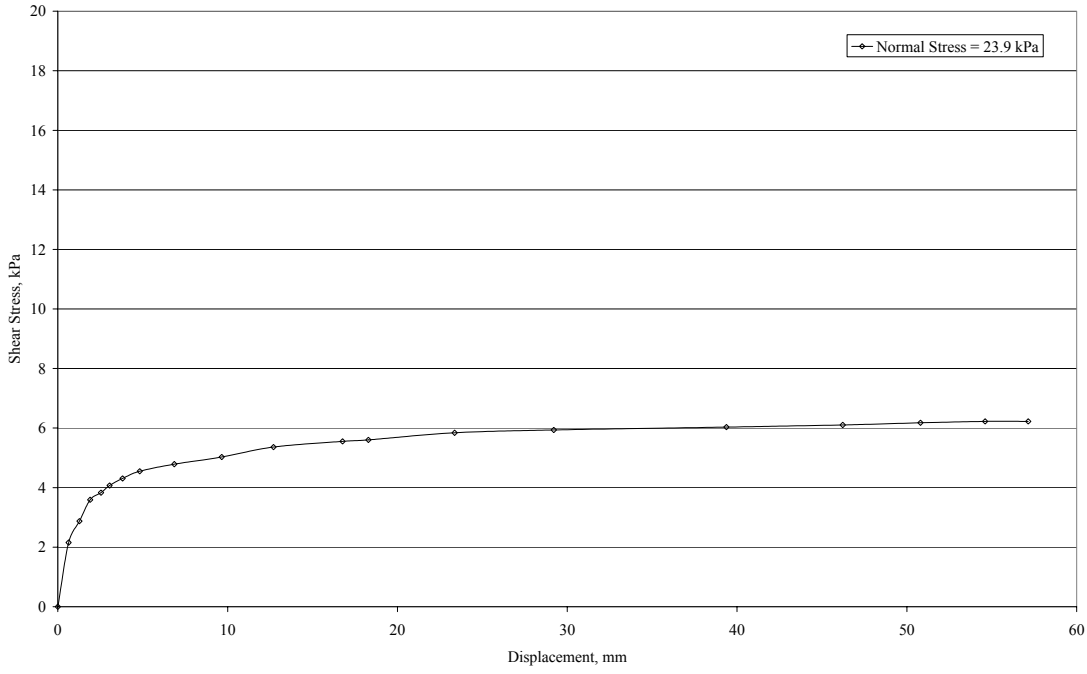

Figure 5.29: Shear Force-Displacement Curves for the Interface between a GCL and a Smooth VLDPE Geomembrane

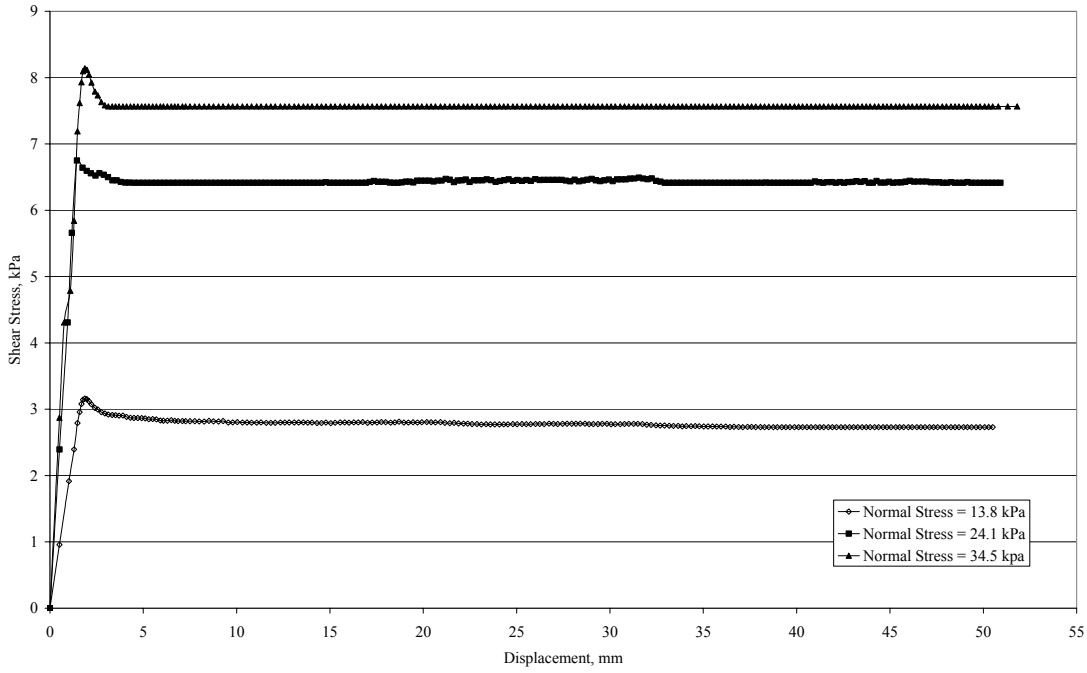

Figure 5.30: Shear Force-Displacement Curves for the Interface between a Hydrated GCL and a Smooth LLDPE Geomembrane

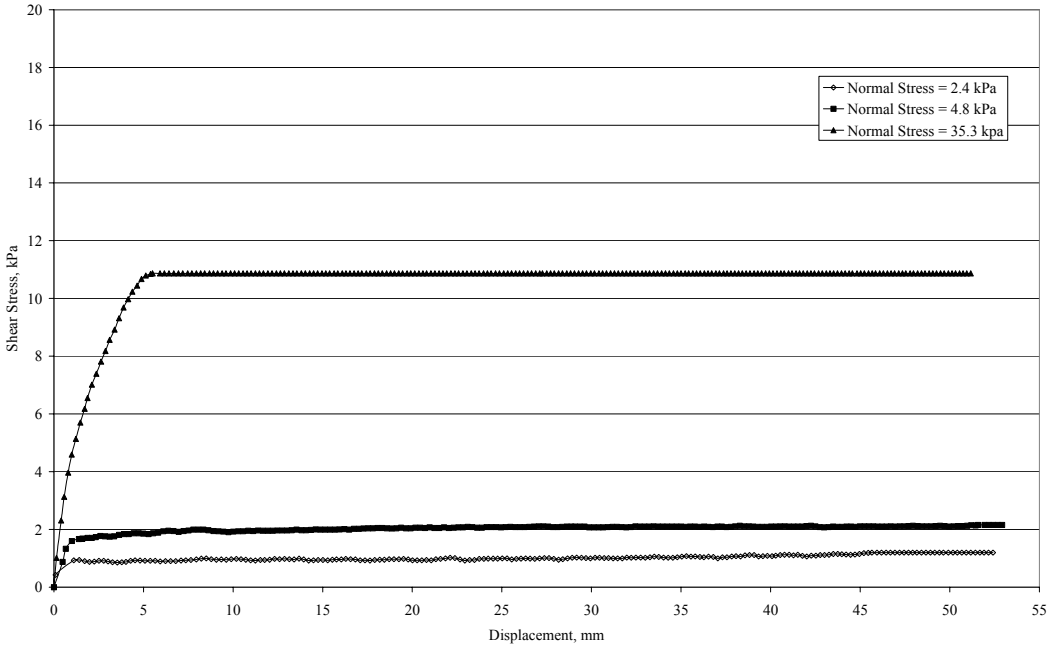

Figure 5.31: Shear Force-Displacement Curves for the Interface between a Hydrated GCL and a Smooth PVC Geomembrane

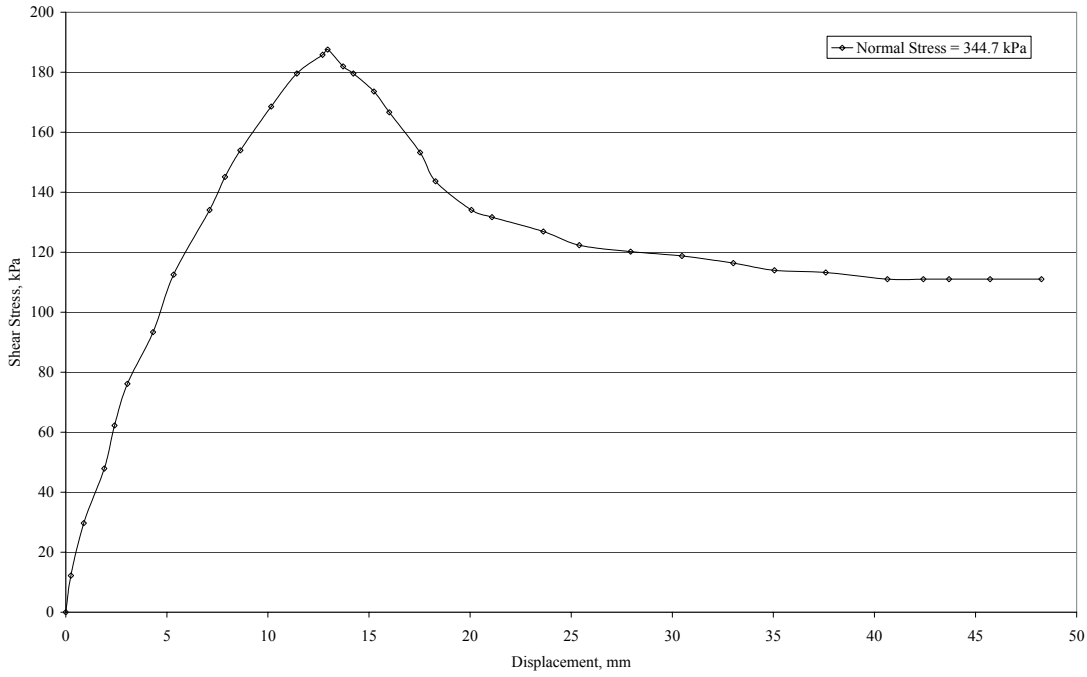

Figure 5.32: Shear Force-Displacement Curves for the Interface between an Unhydrated, Unreinforced Geomembrane-Backed GCL and a Textured HDPE Geomembrane

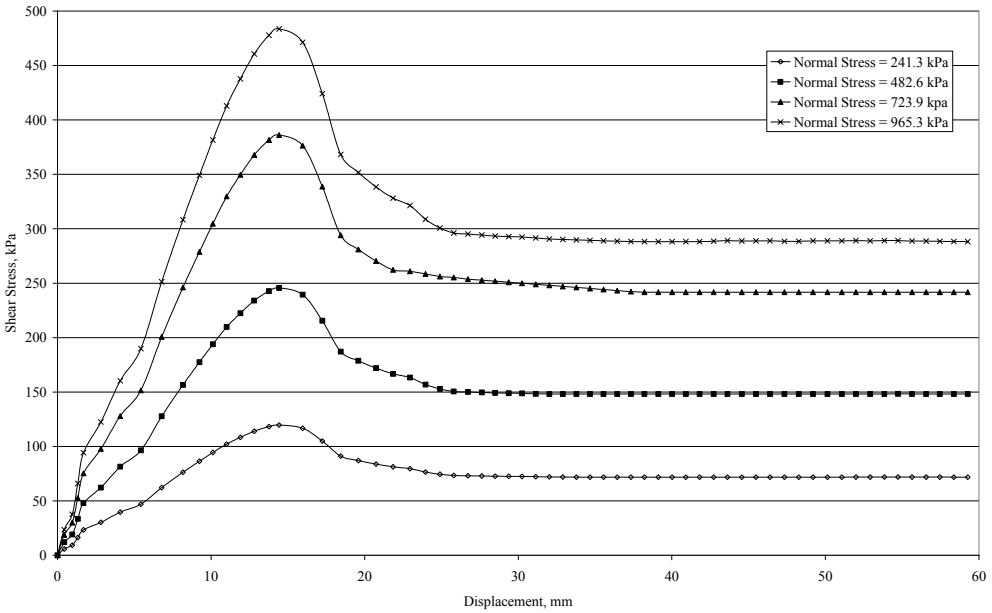

Figure 5.33: Shear Force-Displacement Curves for the Interface between a Hydrated, Unreinforced Geomembrane-Backed GCL and a Textured HDPE Geomembrane

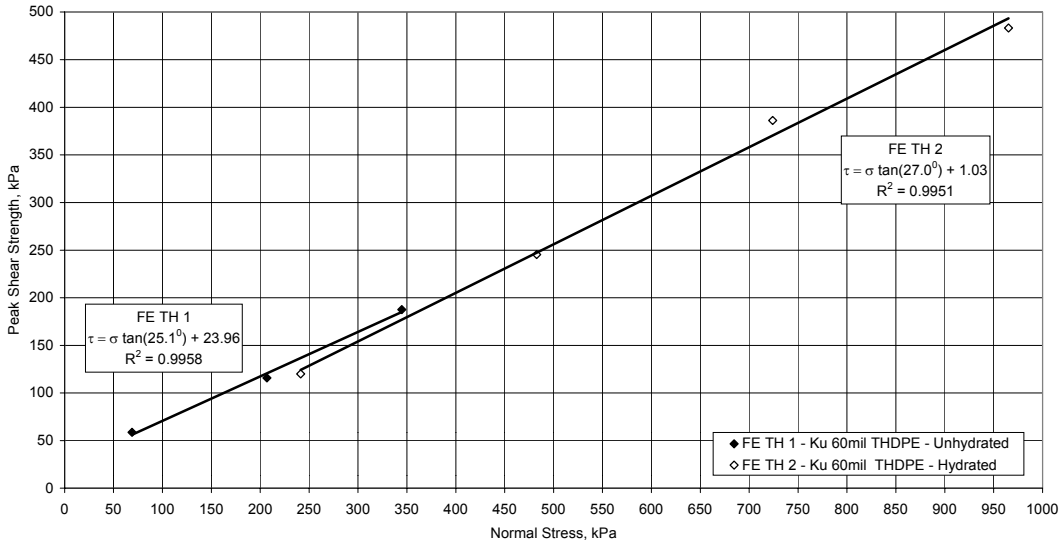

(a)

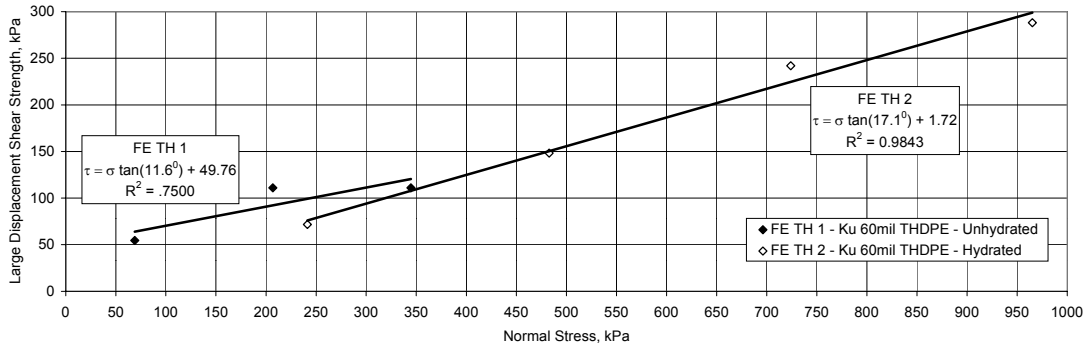

(b)

Figure 5.34: Failure Envelopes for an Unreinforced Geomembrane-Backed GCL and a Textured HDPE Geomembrane (FE TH 1 and 2: GCL K and GM u, t_H = 0 and 48 hours, respectively, t_C = 0 hours and SDR = 1.0 mm/min); (a) Peak, (b) Large Displacement

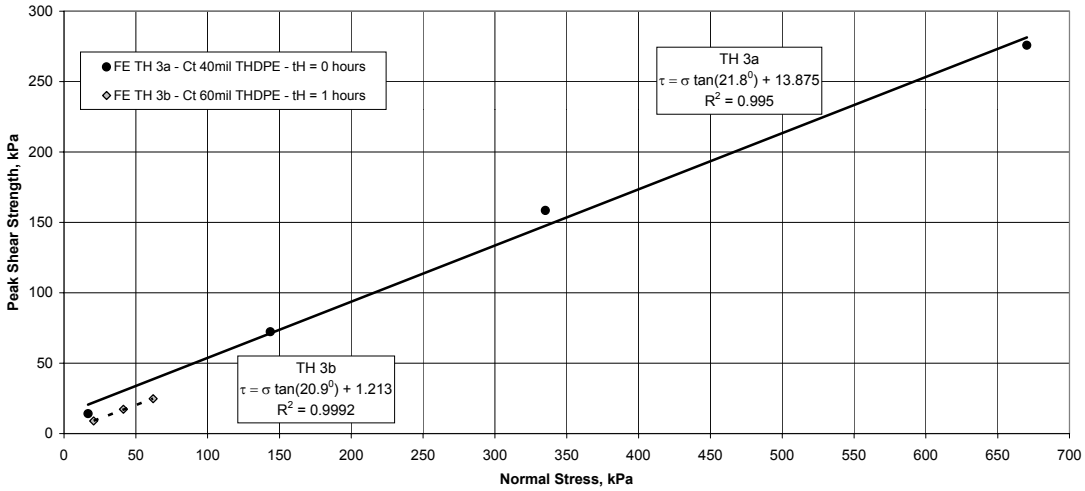

(a)

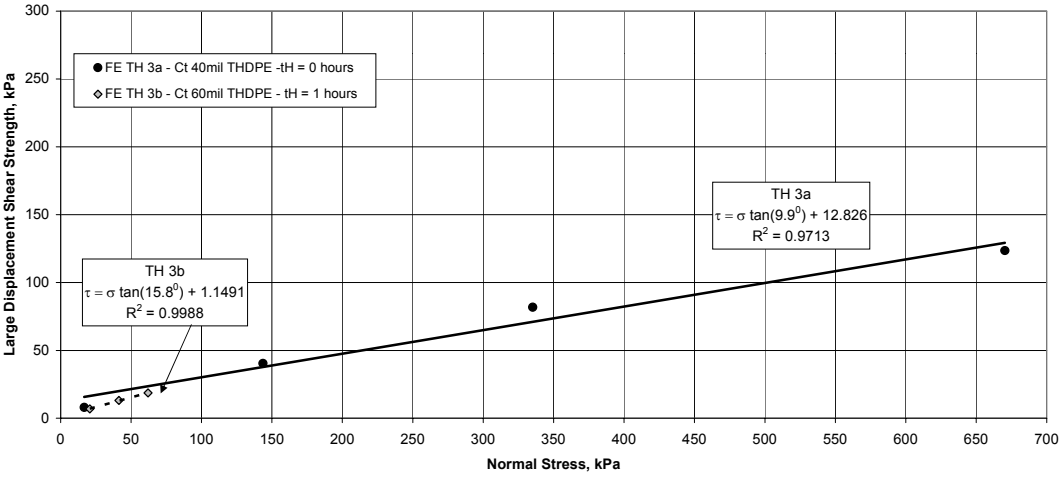

(b)

Figure 5.35: Failure Envelopes for the Interface between GCL C and a Textured HDPE Geomembrane (FE TH 3a and 3b: GCL C and GM t, t_H = 0 and 1 hours, respectively, No Consolidation and SDR = 1.0 mm/min) ; (a) Peak, (b) Large Displacement

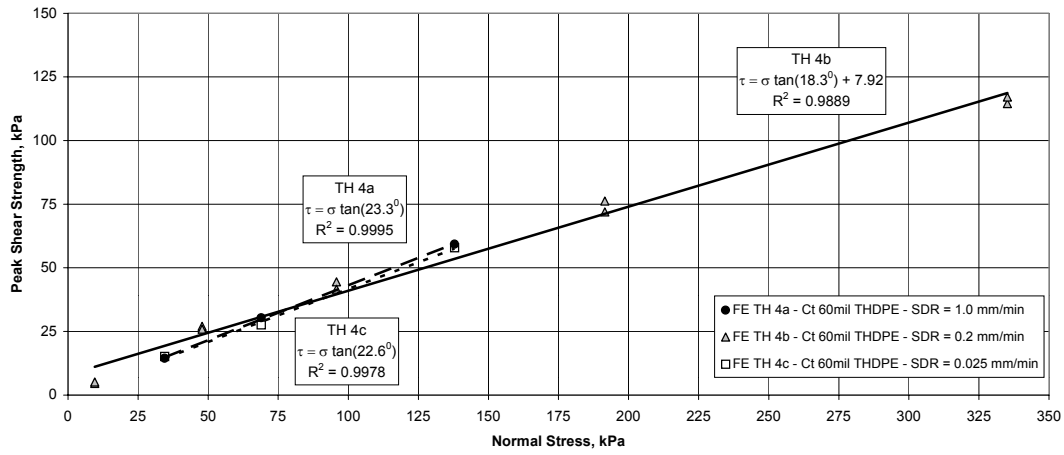

(a)

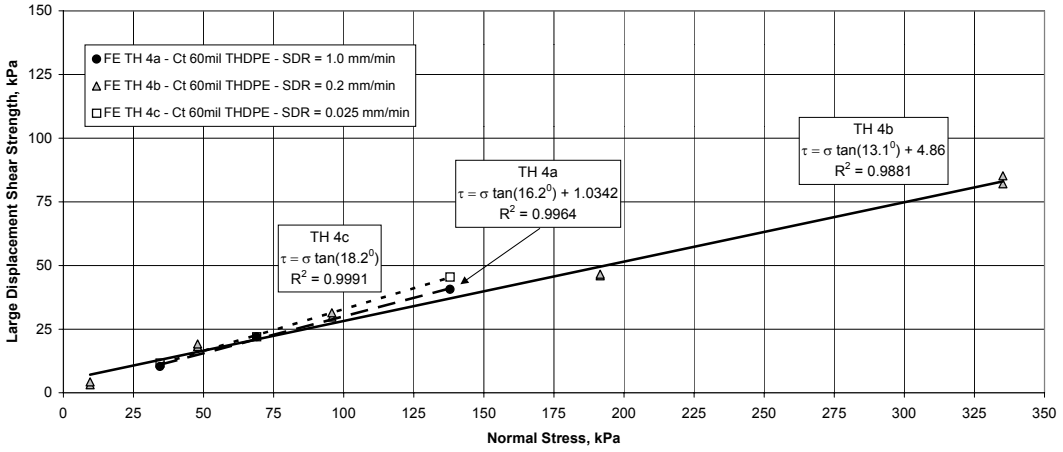

(b)

Figure 5.36: Failure Envelopes for the Interface between GCL C and a Textured HDPE Geomembrane (FE TH 4a, 4b and 4c: GCL C and GM t, t_H = 24 hours, No Consolidation and SDR = 1.0, 0.2 and 0.025 mm/min, respectively); (a) Peak, (b) Large Displacement

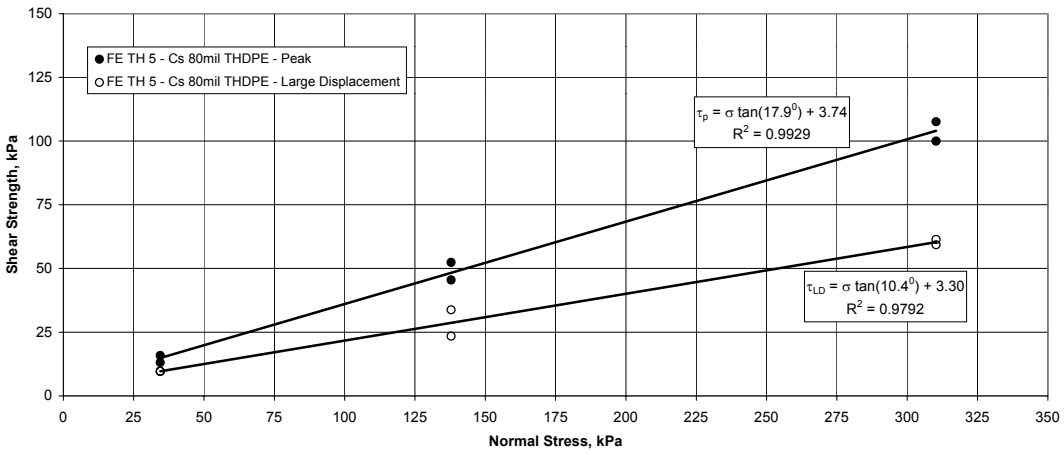

Figure 5.37: Failure Envelopes for the Interface between GCL C and a Textured HDPE Geomembrane (FE TH 5: GCL C and GM s, t_H = 168 hours, t_C = 48 hours and SDR = 0.1 mm/min)

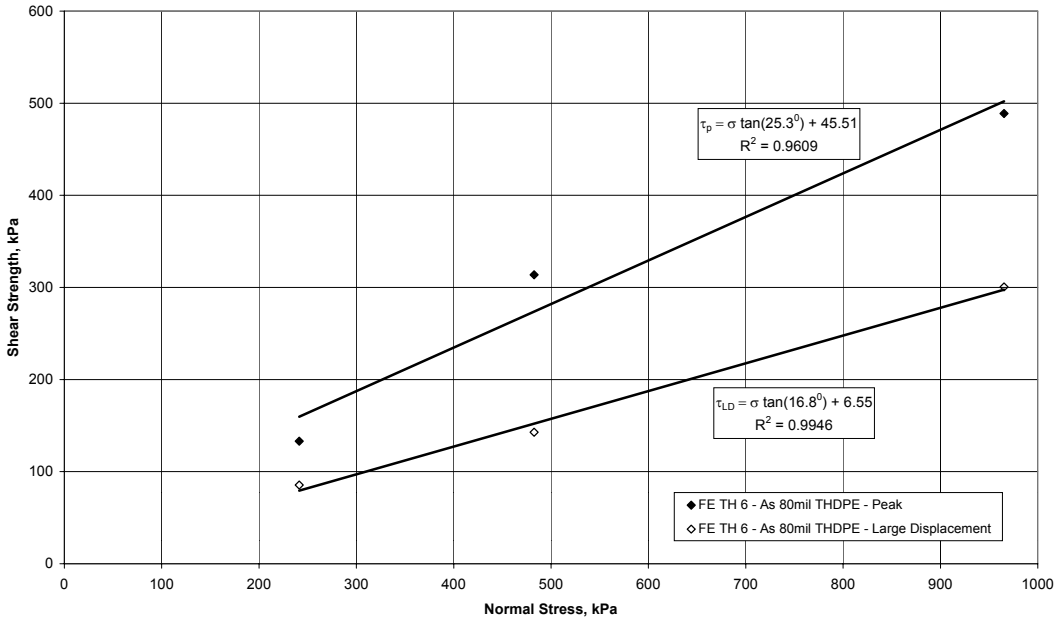

Figure 5.38: Failure Envelopes for the Interface between GCL A and a Textured HDPE Geomembrane (FE TH 6: GCL A and GM s, t_H = 0 hours, t_C = 0 hours and SDR = 1.0 mm/min)

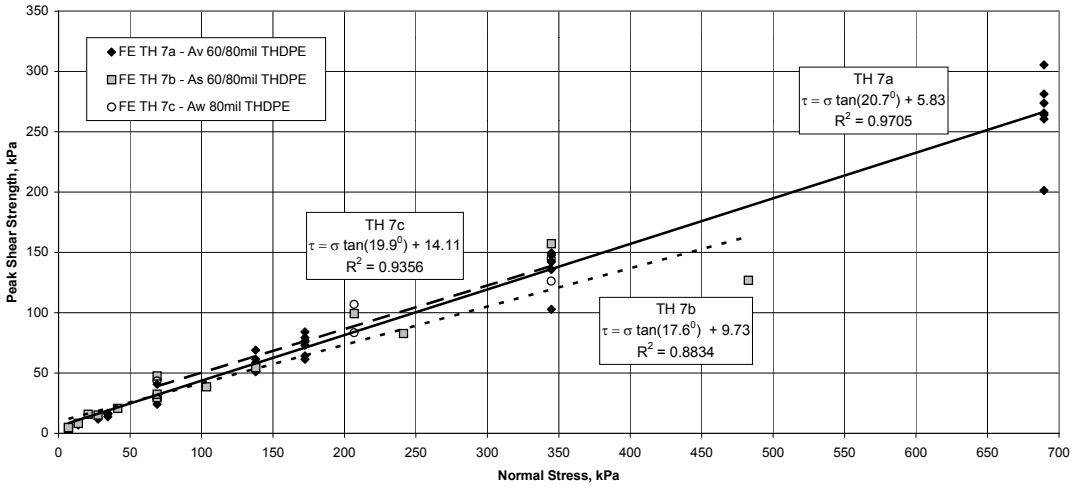

(a)

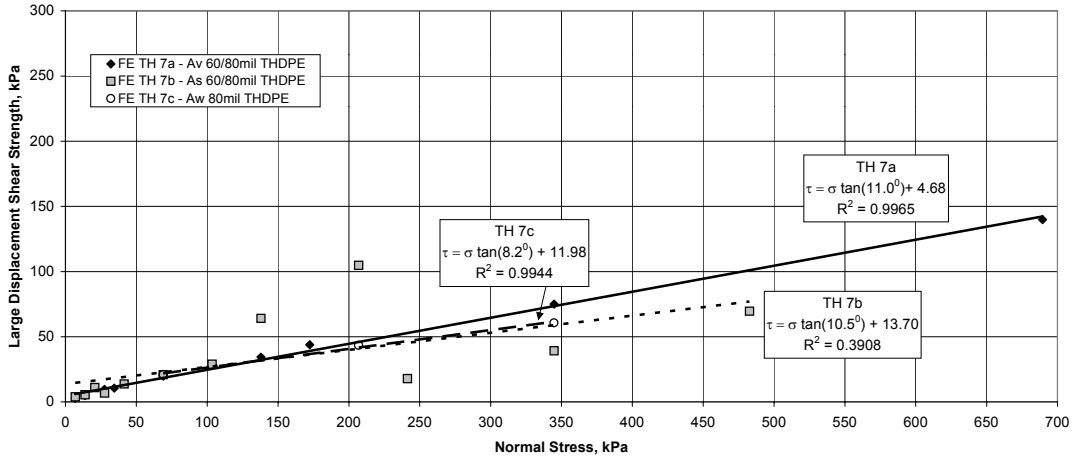

(b)

Figure 5.39: Failure Envelopes for the Interface between GCL A and a Textured HDPE Geomembrane (FE TH 7a, 7b, and 7c: GCL A and Different Geomembranes, t_H = 24 hours, t_C = 0 hours and SDR = 1.0 mm/min); (a) Peak, (b) Large Displacement

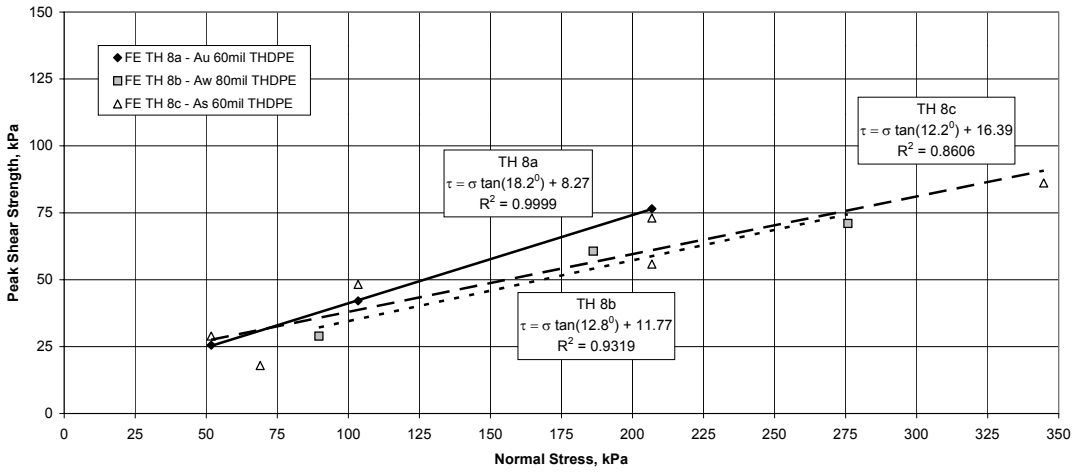

(a)

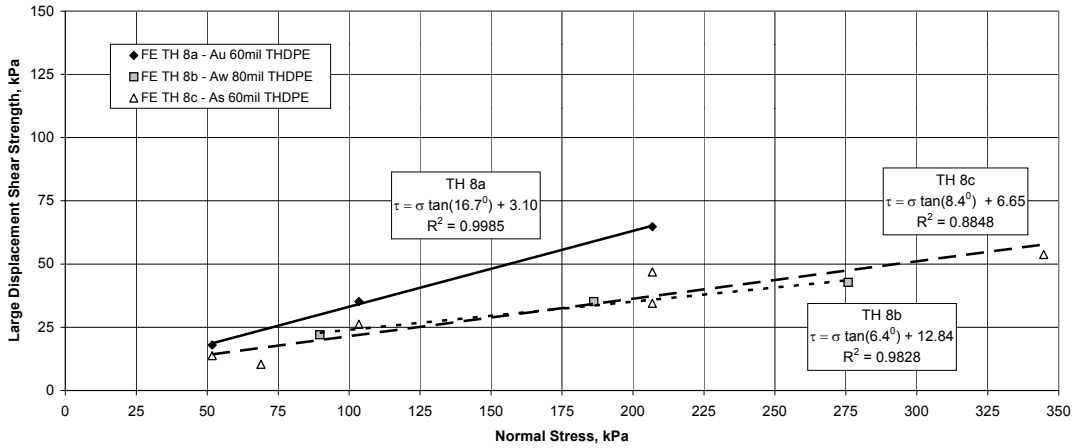

(b)

Figure 5.40: Failure Envelopes for the Interface between GCL A and a Textured HDPE Geomembrane (FE TH 8a, 8b and 8c: GCL A and Different Geomembranes, t_H = 48 hours, t_C = 0 hours and SDR = 1.0 mm/min); (a) Peak, (b) Large Displacement

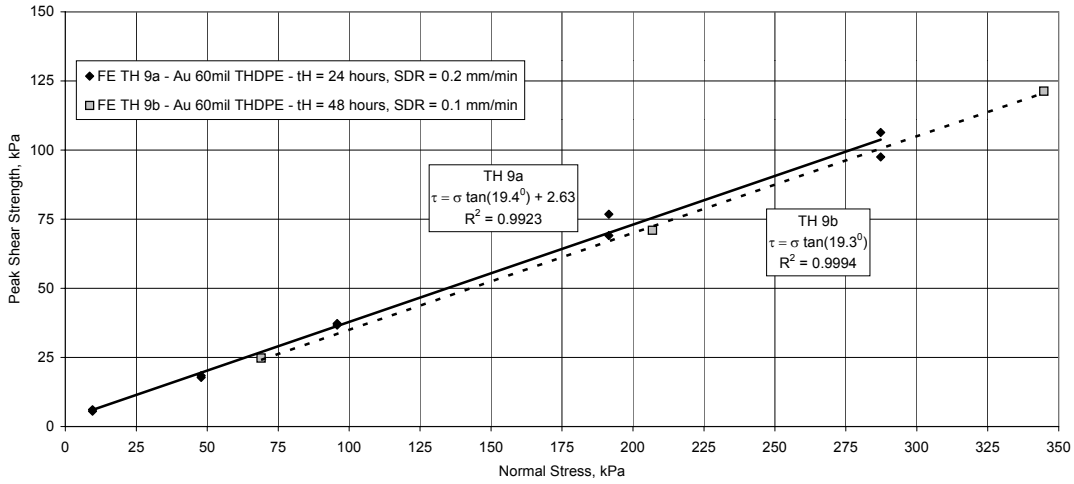

(a)

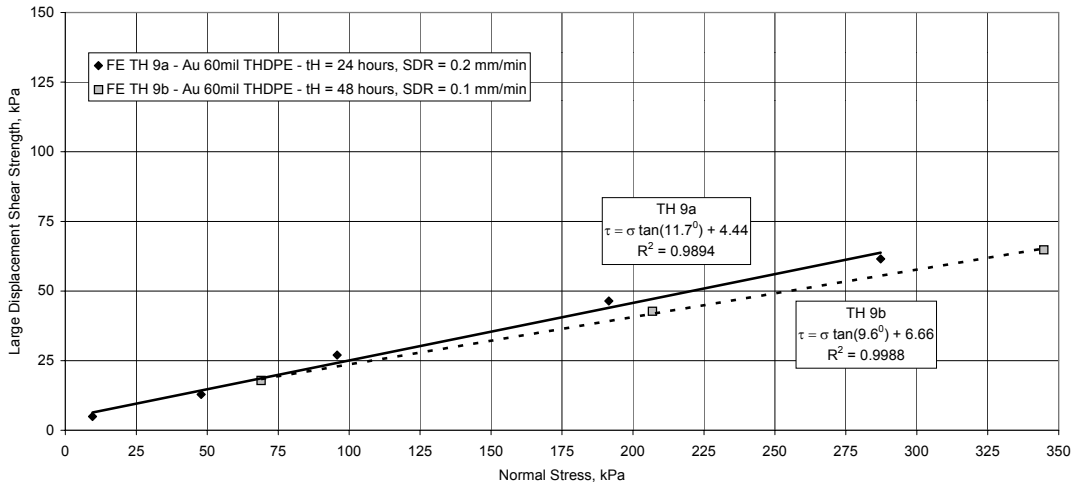

(b)

Figure 5.41: Failure Envelopes for the Interface between GCL A and a Textured HDPE Geomembrane (FE TH 9a and 9b: GCL A and Different Geomembranes, t_H = 24 and 48 hours, respectively, No Consolidation and SDR = 0.2 and 0.1 mm/min, respectively); (a) Peak, (b) Large Displacement

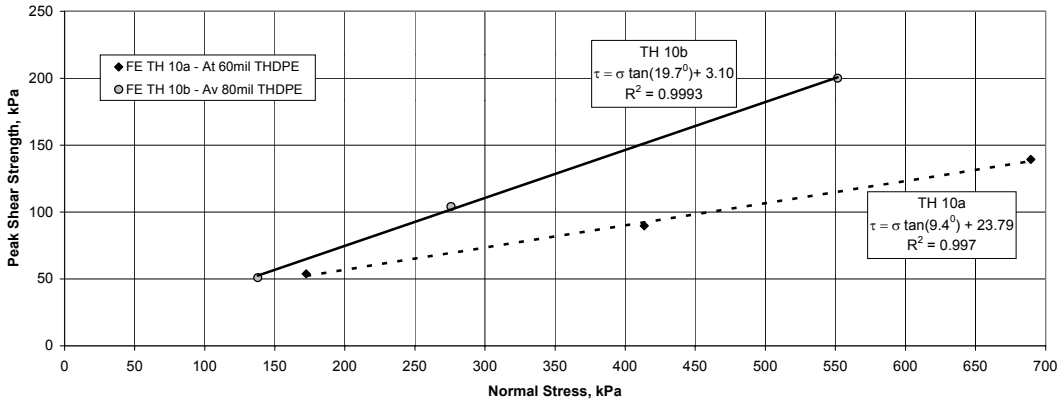

(a)

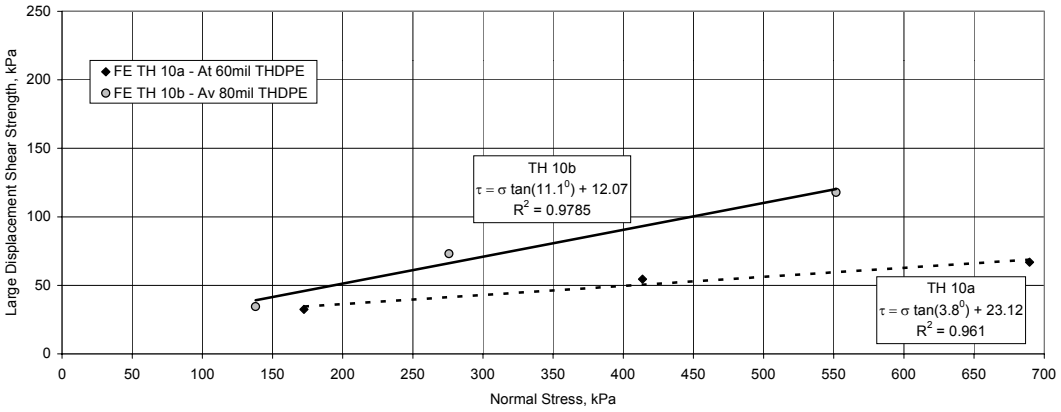

(b)

Figure 5.42: Failure Envelopes for the Interface between GCL A and a Textured HDPE Geomembrane (FE TH 10a and 10b: GCL A and Different Geomembranes, t_H = 72 and 24 hours, respectively, t_C = 24 and 12 hours, respectively, and SDR = 1.0 mm/min); (a) Peak, (b) Large Displacement

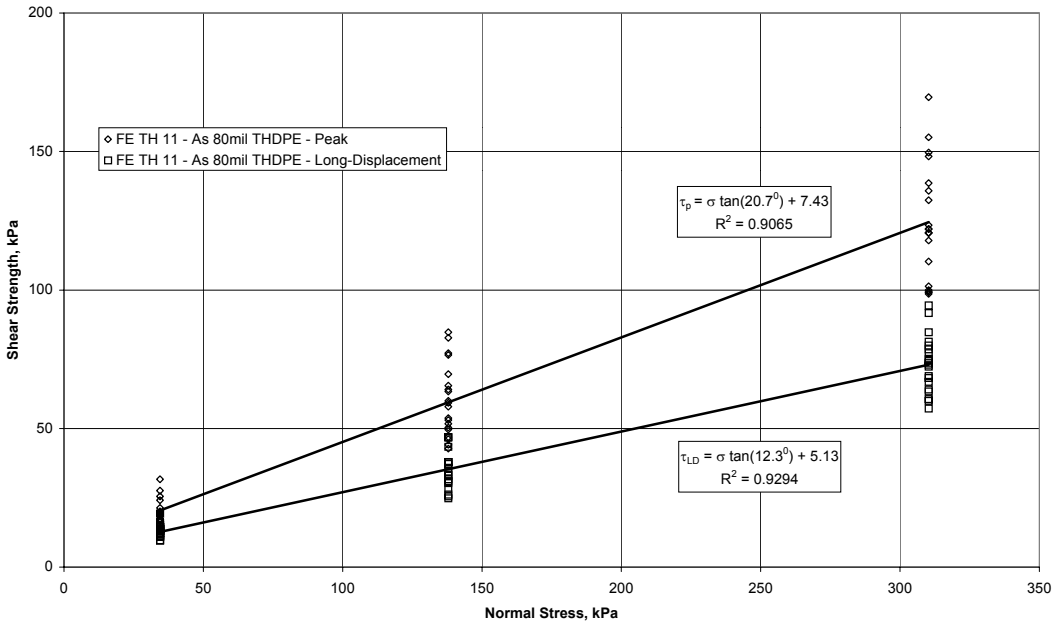

Figure 5.43: Failure Envelopes for the Interface between GCL A and a Textured HDPE Geomembrane (FE TH 11: GCL A and GM s, t_H = 168 hours, t_C = 48 hours and SDR = 0.1 mm/min)

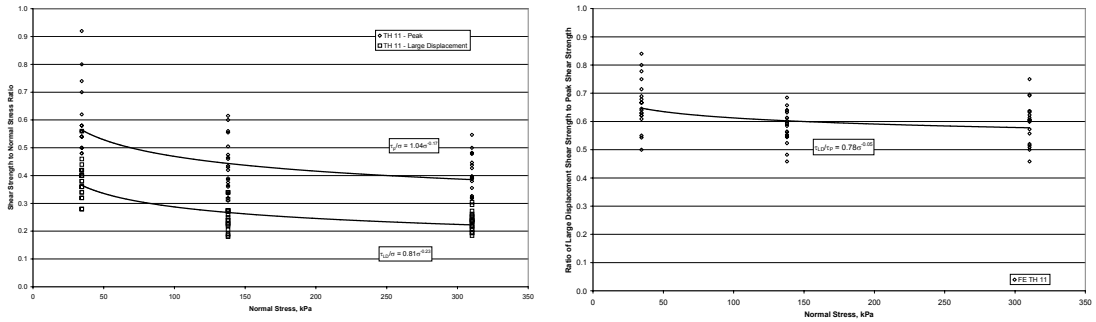

(a) (b)

Figure 5.44: Shear Strength Ratios for Failure Envelope TH 11 (GCL A and GM s, t_H = 168 hours, t_C = 48 hours and SDR = 0.1 mm/min); (a) Ratios of Peak and Large Displacement Shear Strengths to Normal Stress, (b) Ratio of Large Displacement Shear Strength to Peak Shear Strength

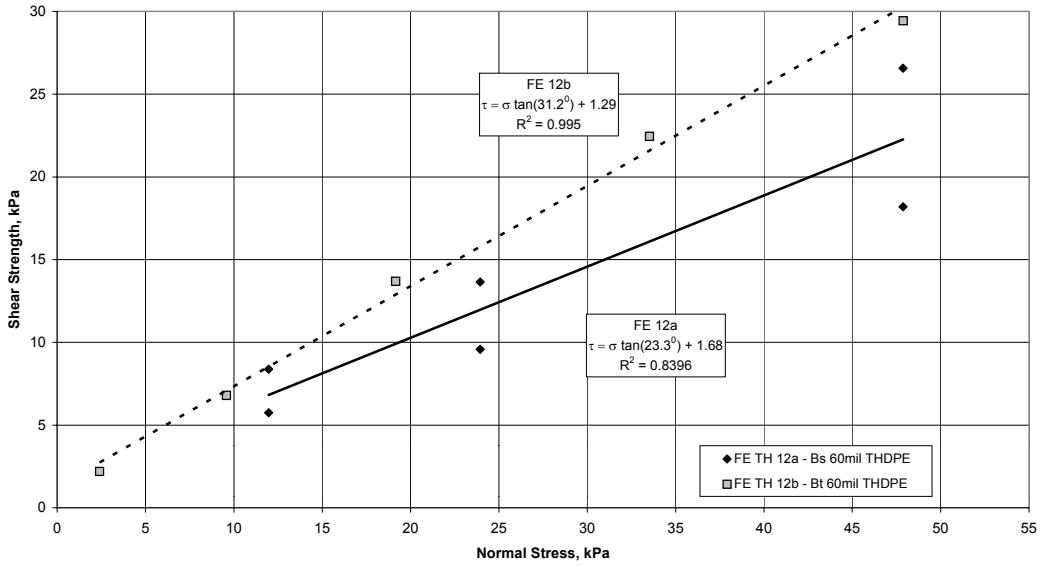

(a)

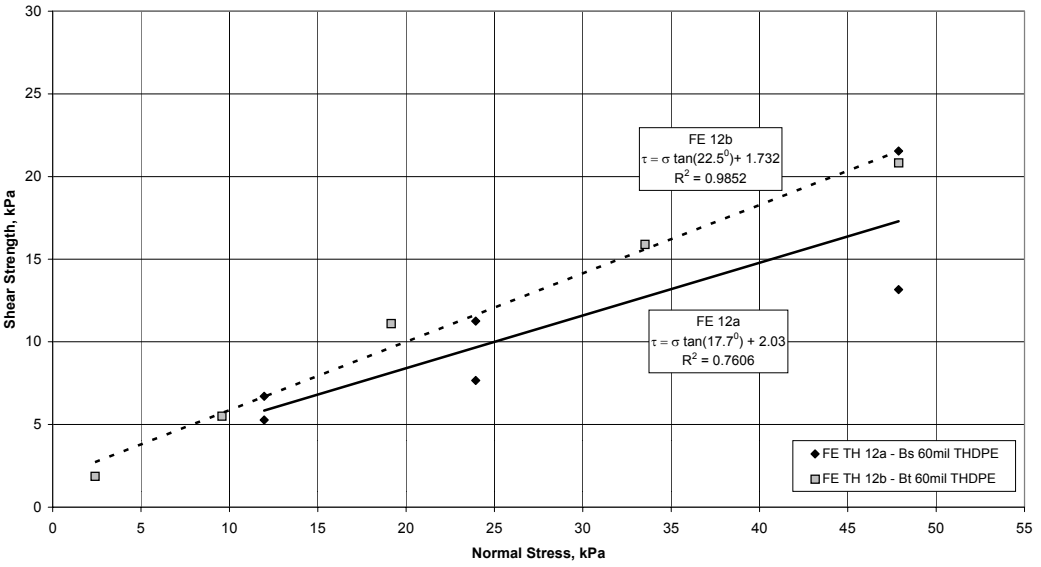

(b)

Figure 5.45: Failure Envelopes for the Interface between GCL B and a Textured HDPE Geomembrane (FE TH 12a and 12b: GCL B and GM s or t, respectively, t_H = 0 hours, t_C = 0 hours and SDR = 1.0 mm/min); (a) Peak, (b) Large Displacement

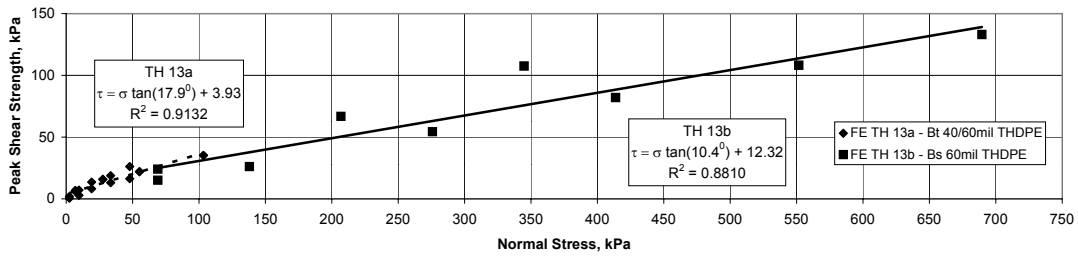

(a)

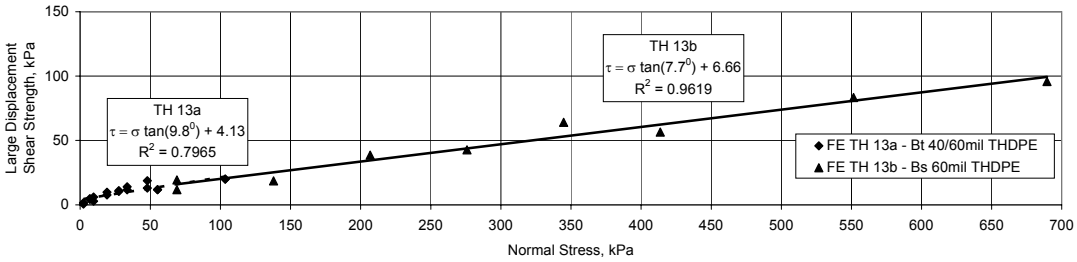

(b)

Figure 5.46: Failure Envelopes for the Interface between GCL B and a Textured HDPE Geomembrane (FE TH 13a and 13b: GCL B and Different Geomembranes, t_H = 24 hours, t_C = 0 hours and SDR = 1.0 mm/min); (a) Peak, (b) Large Displacement

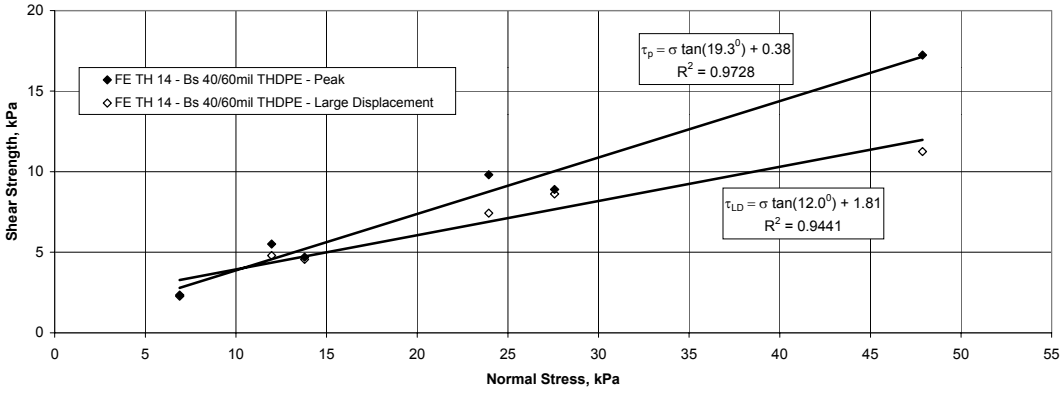

Figure 5.47: Failure Envelopes for the Interface between GCL B and a Textured HDPE Geomembrane (FE TH 14: GCL B and GM s, t_H = 48 hours, t_C = 0 hours and SDR = 1.0 mm/min)

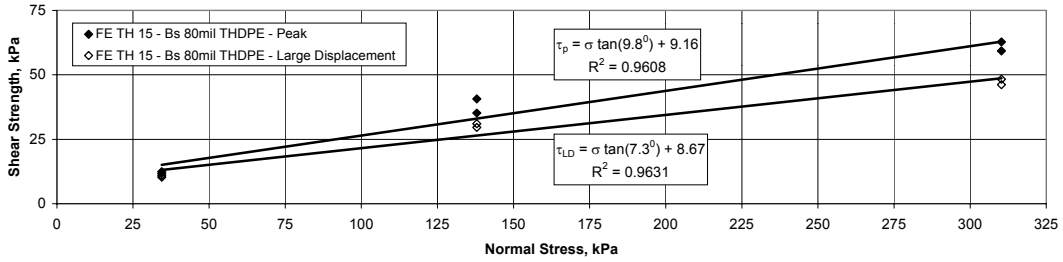

Figure 5.48: Shear Failure Envelopes for the Interface between GCL B and a Textured HDPE Geomembrane (FE TH 15: GCL B and GM s, t_H = 168 hours, t_C = 48 hours and SDR = 0.1 mm/min)

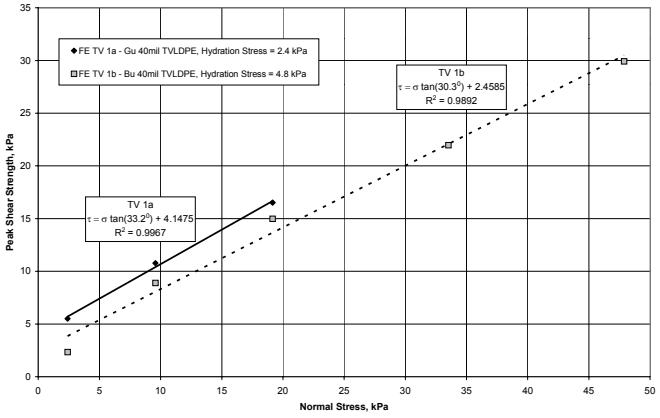

(a)

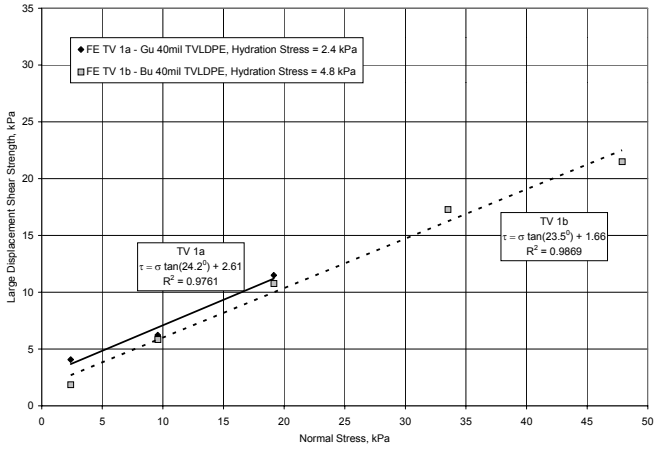

(b)

Figure 5.49: Failure Envelopes for the Interface between a GCL and a Textured VLDPE Geomembrane (FE TV 1a and 1b: GCLs G or B and GM t, t_H = 24 hours, t_C = 0 hours and SDR = 1.0 mm/min); (a) Peak, (b) Large Displacement

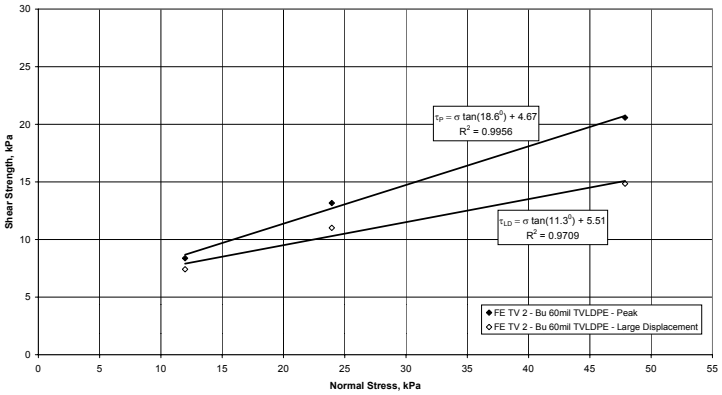

Figure 5.50: Failure Envelopes for the Interface between a GCL and a Textured VLDPE Geomembrane (FE TV 2: GCL B and GM t, t_H = 48 hours, t_C = 0 hours and SDR = 1.0 mm/min)

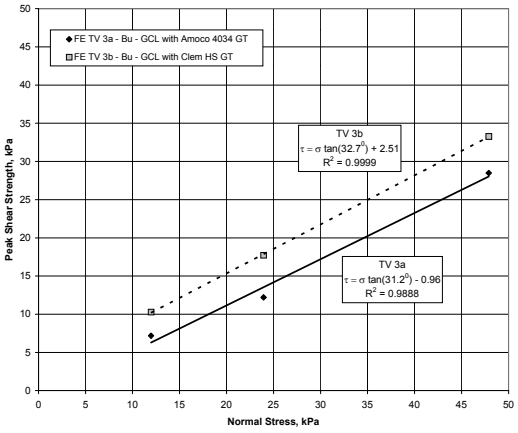

(a)

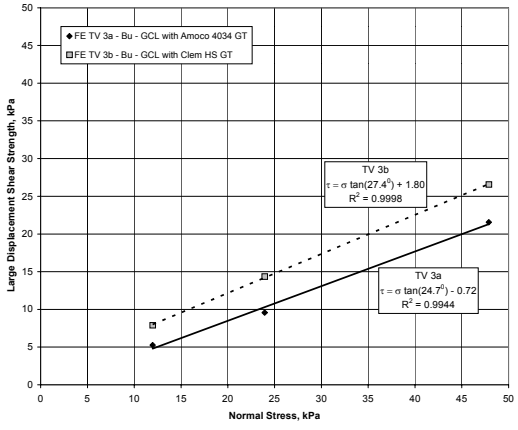

(b)

Figure 5.51: Failure Envelopes for the Interface between a GCL and a Textured VLDPE Geomembrane (FE TV 3a and 3b: GCL B and GM u with Amoco or Clem Geotextiles, respectively, t_H = 0 hours, t_C = 0 hours and SDR = 1.0 mm/min); (a) Peak, (b) Large Displacement

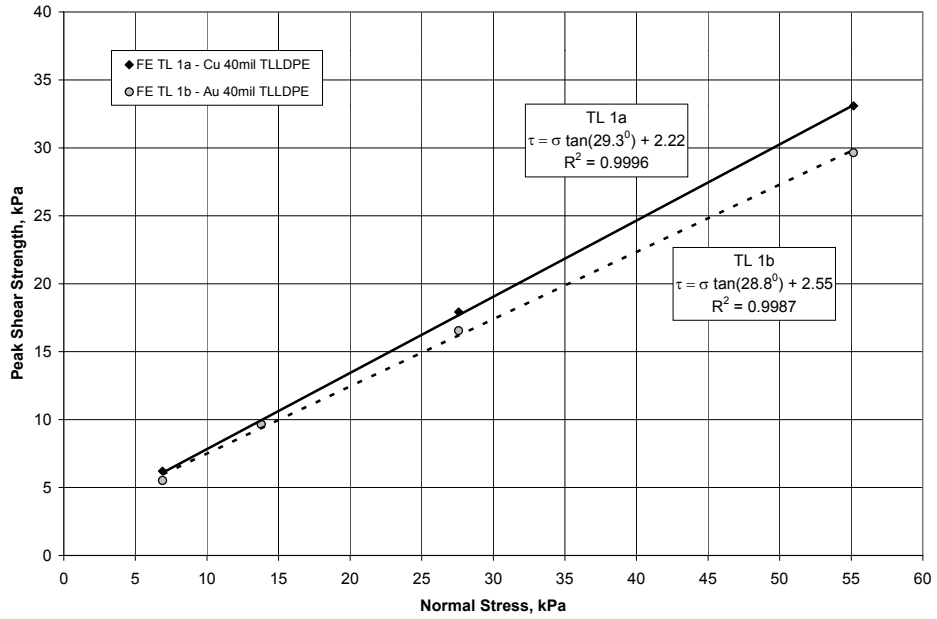

(a)

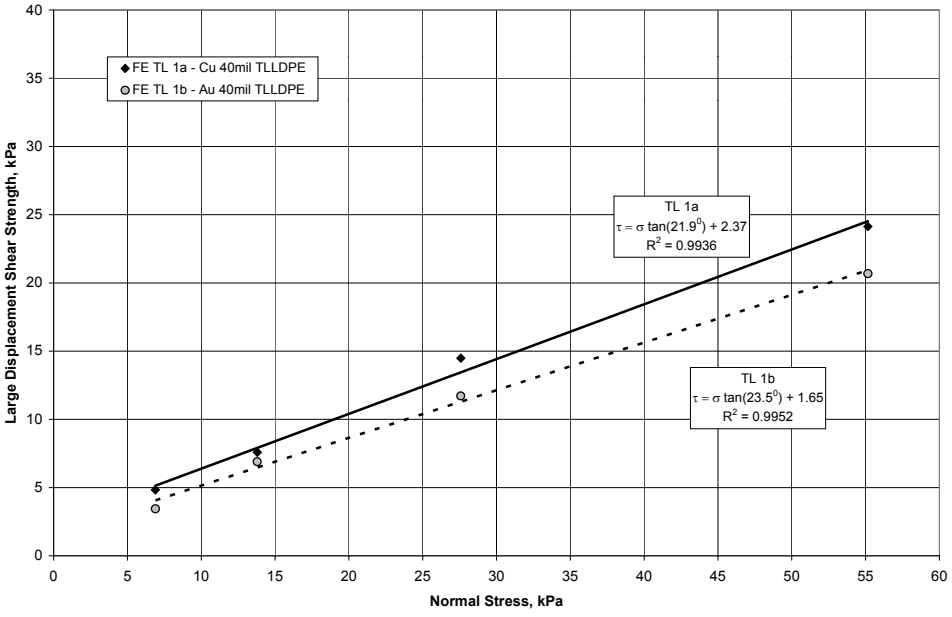

(b)

Figure 5.52: Failure Envelopes for the Interface between a GCL and a Textured LLDPE Geomembrane (FE TL 1a and 1b: GCLs C and A and GM u, t_H = 72 hours, t_C = 0 hours and SDR = 1.0 mm/min); (a) Peak, (b) Large Displacement

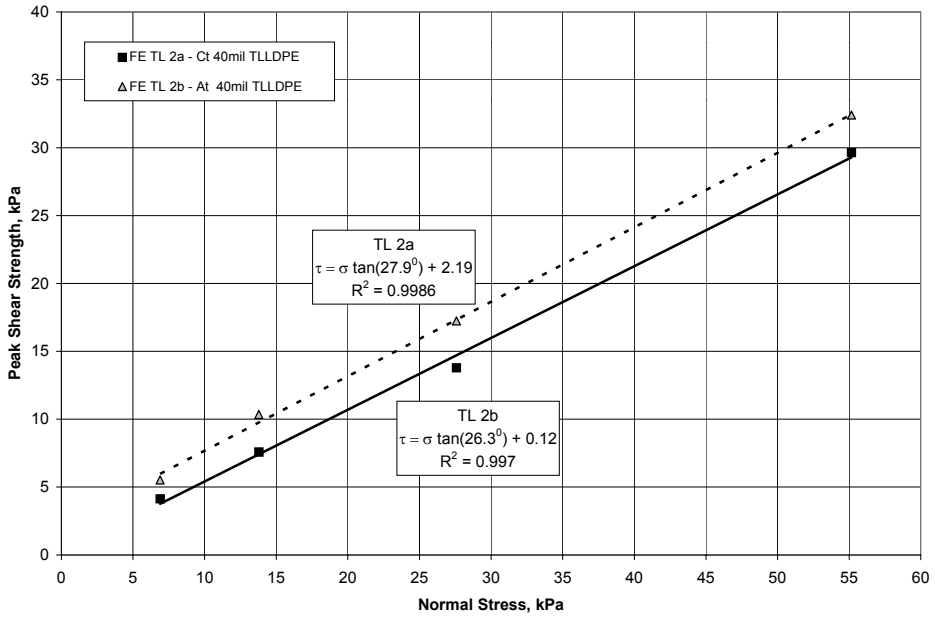

(a)

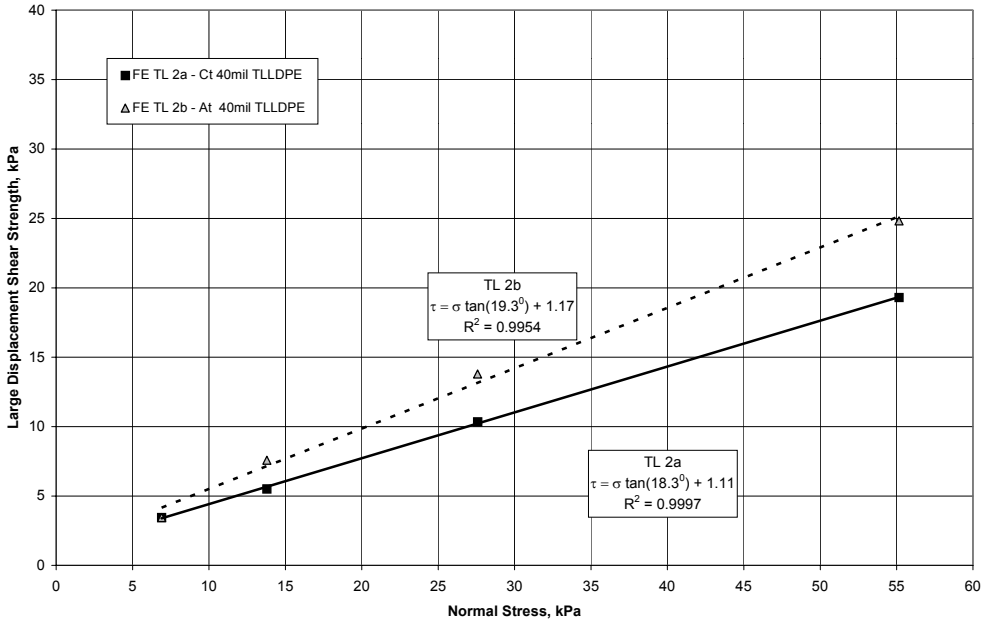

(b)

Figure 5.53: Failure Envelopes for the Interface between a GCL and a Textured LLDPE Geomembrane (FE TL 2a and 2b: GCLs C and A and GM t, t_H = 72 hours, t_C = 0 hours and SDR = 1.0 mm/min) ; (a) Peak, (b) Large Displacement

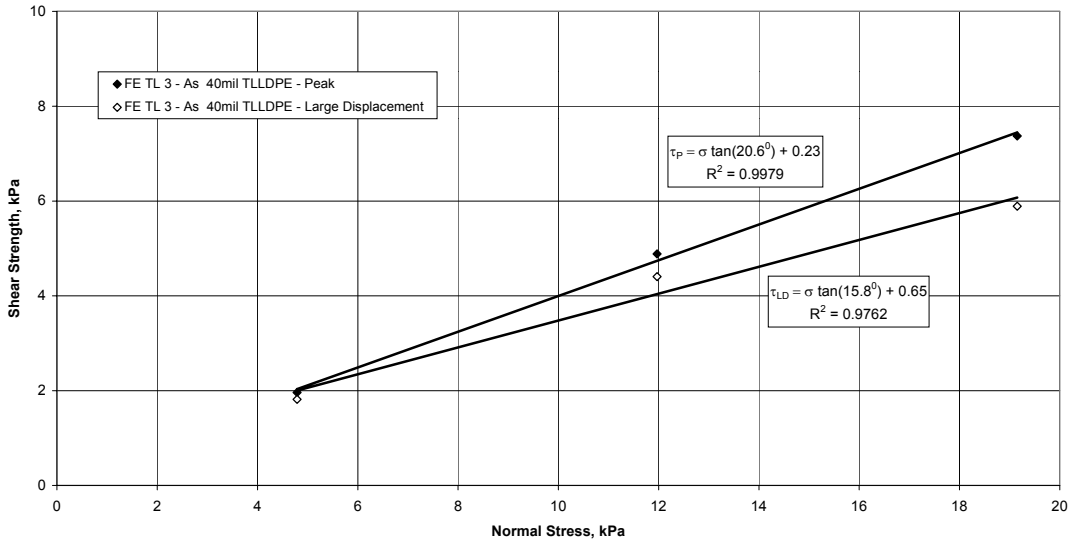

Figure 5.54: Failure Envelopes for the Interface between a GCL and a Textured LLDPE Geomembrane (FE TL 3: GCL A and GM s, t_H = 72 hours, t_C = 48 hours and SDR = 1.0 mm/min)

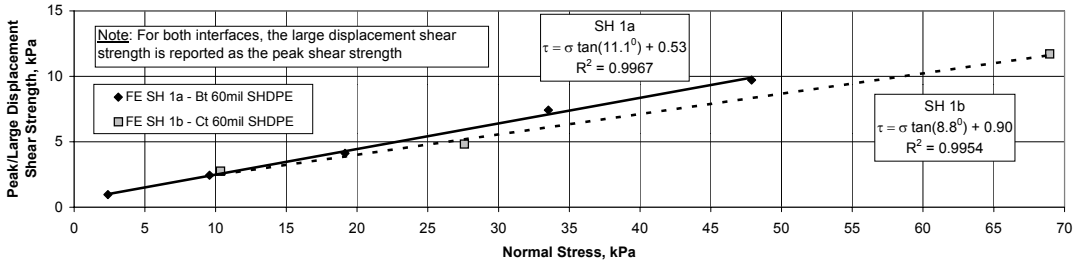

Figure 5.55: Failure Envelopes for the Interface between a GCL and a Smooth HDPE Geomembrane (FE SH 1a and 1b: GCL B and C and GM t, t_H = 24 and 48 hours, respectively, No Consolidation, and SDR = 1.0 mm/min)

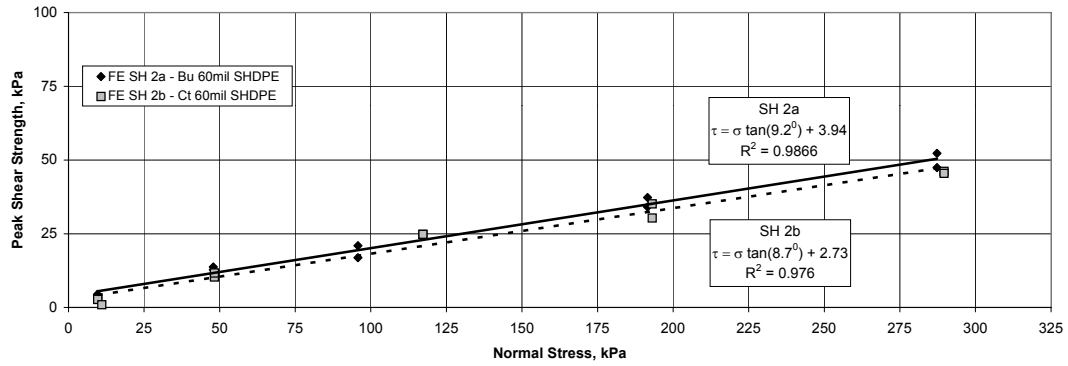

(a)

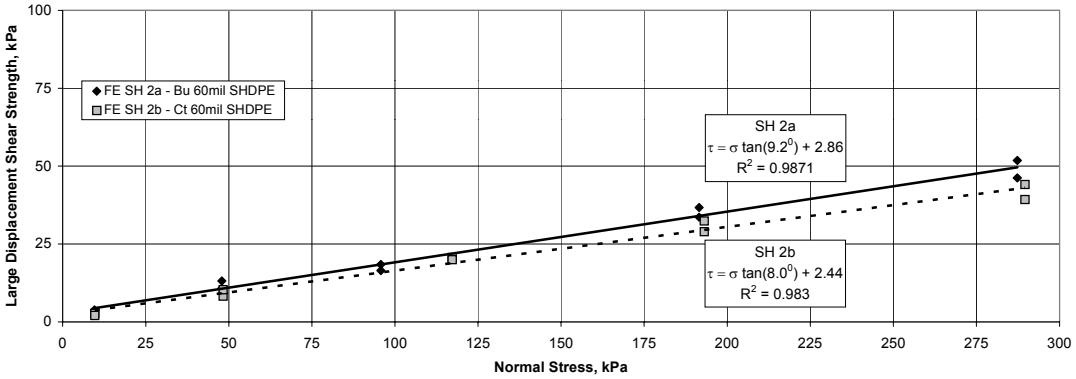

(b)

Figure 5.56: Failure Envelopes for the Interface between a GCL and a Smooth HDPE Geomembrane (FE SH 2a: GCL B and GM u, t_H = 24 hours, t_C = 0 hours and SDR = 0.2 mm/min; 2b: GCL C and GM t, t_H = 24 hours, t_C = 0 hours and SDR = 0.2 mm/min)

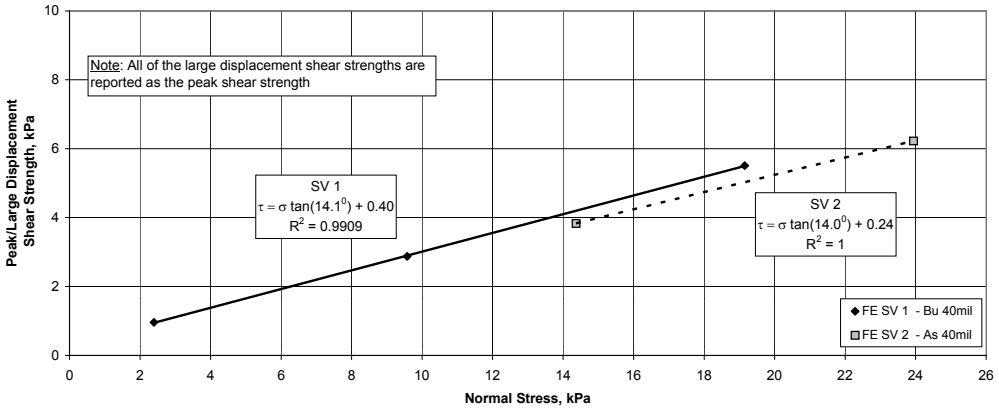

Figure 5.57: Failure Envelopes for the Interface between a GCL and a Smooth VLDPE Geomembrane (FE SV 1 and SV 2: t_H = 24 hours, No Consolidation and SDR = 1.0 mm/min)

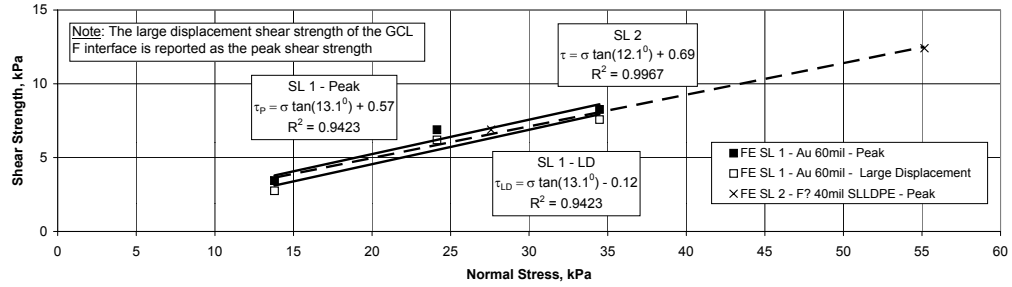

Figure 5.58: Failure Envelopes for the Interface between a GCL and a Smooth LLDPE Geomembrane (FE SL 1 and 2, t_H = 24 and 168 hours, respectively, No Consolidation and SDR = 1.0 mm/min)

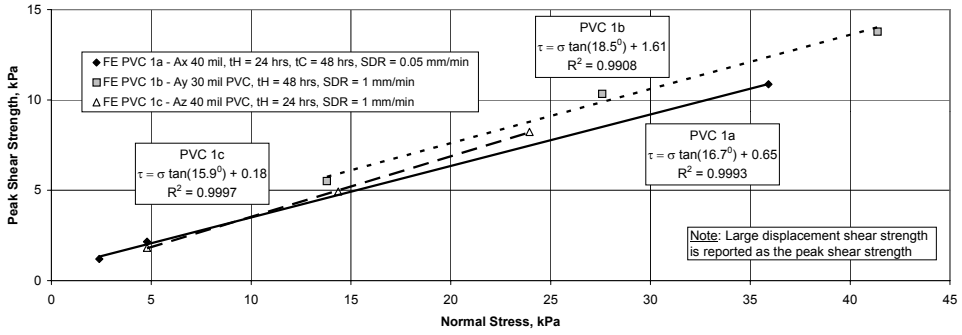

Figure 5.59: Peak Failure Envelopes for the Interface between a GCL and a PVC Geomembrane (FE PVC 1a, 1b and 1c: t_H = 48, 24 and 24 hours, respectively, No Consolidation, SDR = 1.0, 1.0 and 0.05 mm/min, respectively)

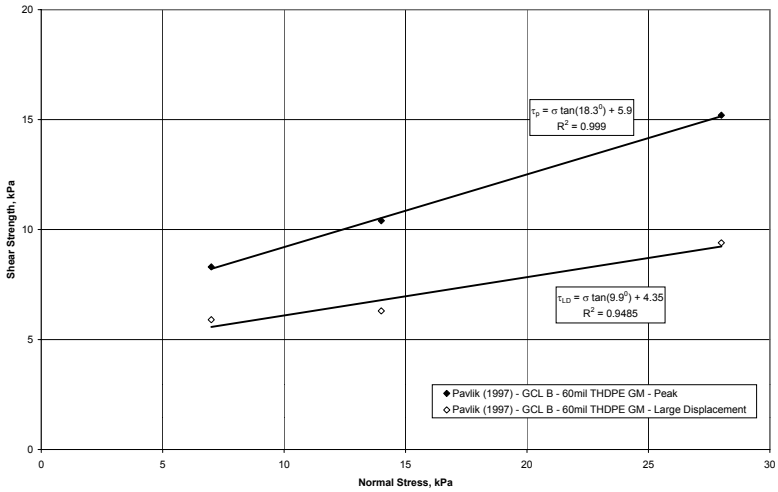

Figure 5.60: Failure Envelopes Reported by Pavlik (1997) for the Interface between GCL A and a 60 mil Textured HDPE Geomembrane (t_H = 48 hours, t_C = 0 hours, SDR = 1.0 mm/min)

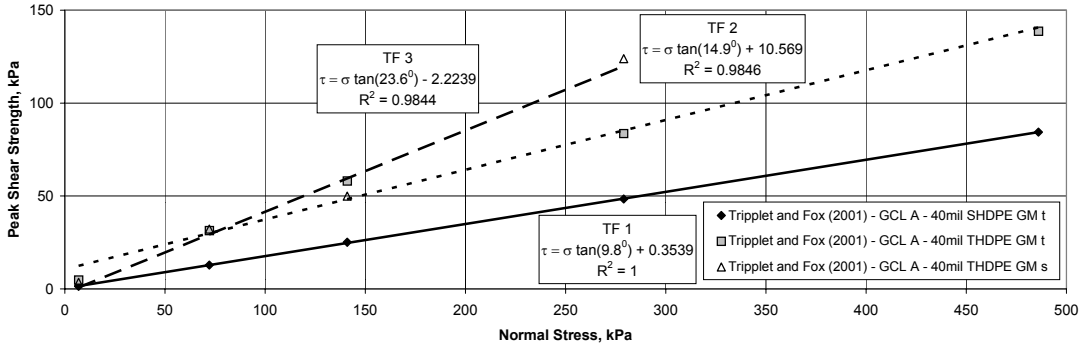

(a)

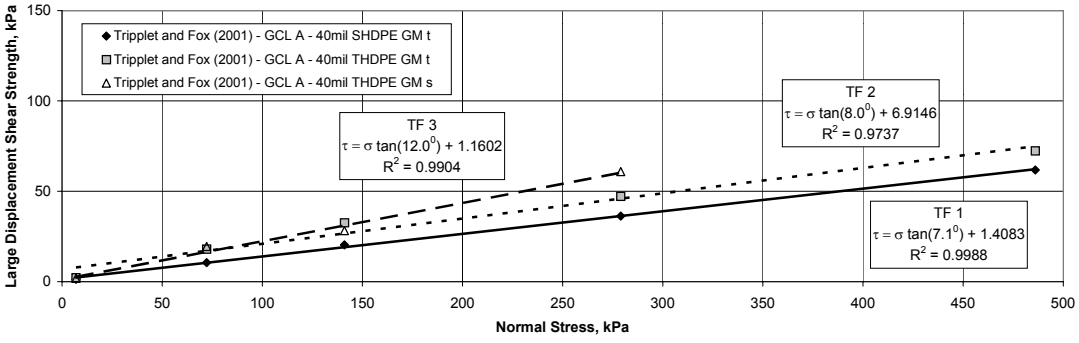

(b)

Figure 5.61: Failure Envelopes Reported by Triplett and Fox (2001) for the Interface between GCL A and a 40 mil Smooth or Textured HDPE Geomembrane (t_H = 48 hours, t_C = 0 hours, SDR = 0.1 mm/min); (a) Peak, (b) Large Displacement

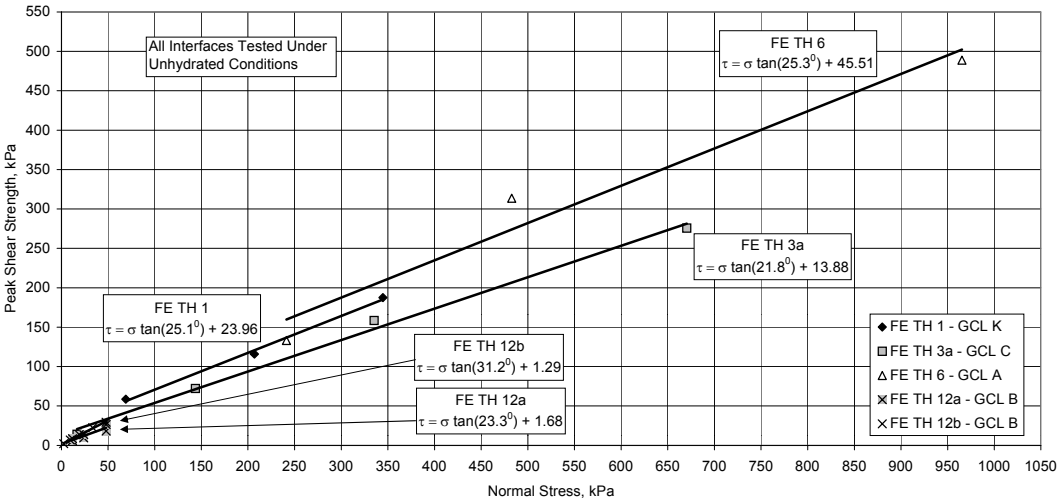

(a)

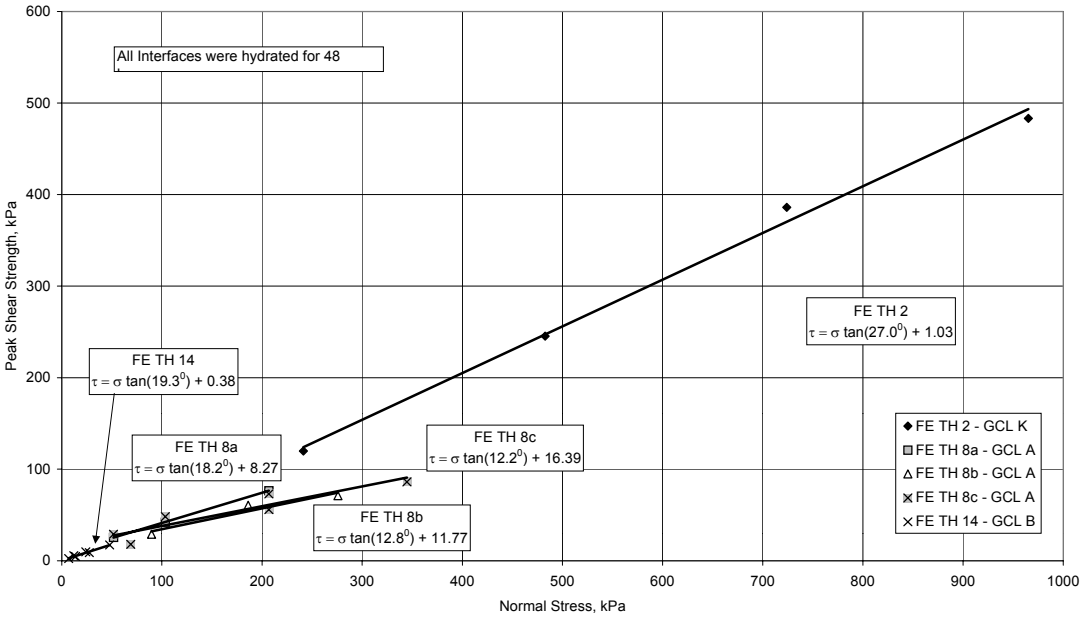

(b)

Figure 5.62: Comparison of Peak Failure Envelopes for Interfaces between GCL K and a Textured HDPE Geomembrane with Those for Other GCL-Textured HDPE Geomembrane Interfaces (No Consolidation, SDR = 1.0 mm/min); (a) t_H = 0 hours, (b) t_H = 48 hours

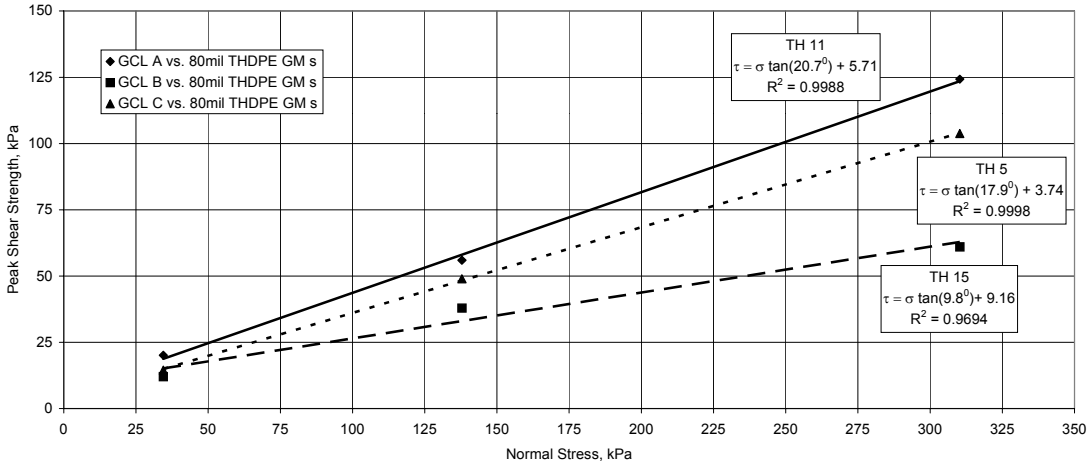

(a)

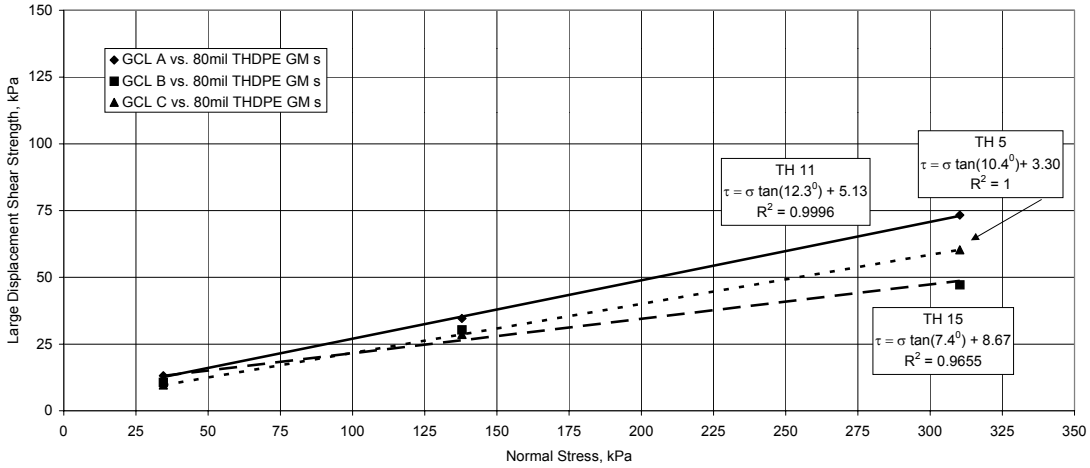

(b)

Figure 5.63: Comparison of Failure Envelopes TH 5, 11 and 15 (t_H = 168 hours, t_C = 48 hours and SDR = 0.1 mm/min); (a) Peak, (b) Large Displacement

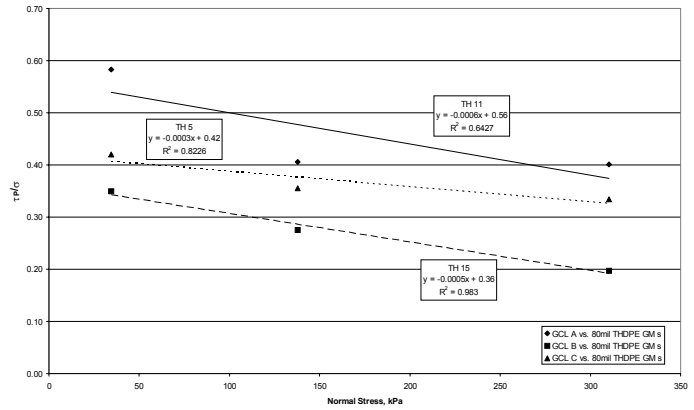

(a)

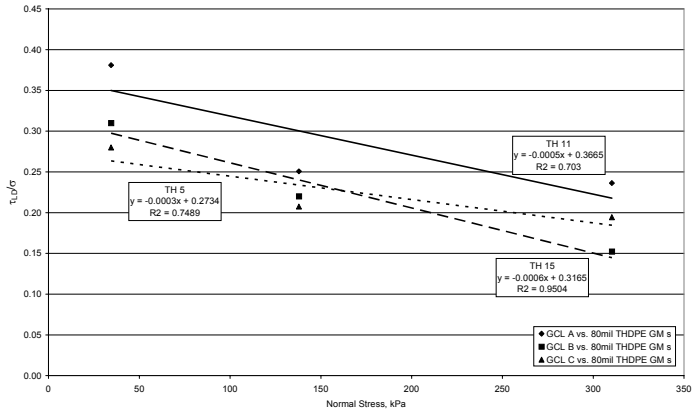

(b)

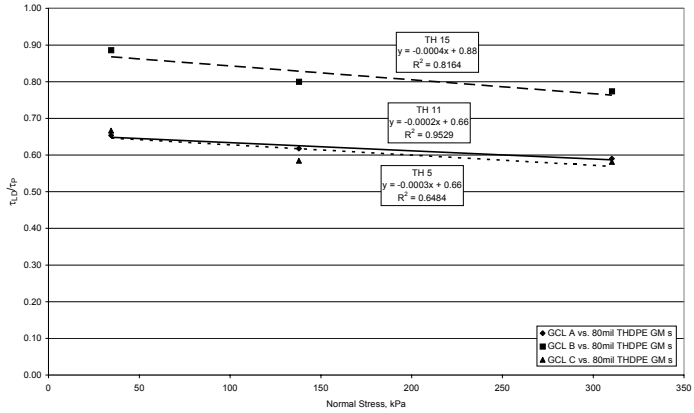

(c)

Figure 5.64: Variation in Shear Strength Ratios with Normal Stress for Failure Envelopes 5, 11 and 15 (t_H = 168 hours, t_C = 48 hours and SDR = 0.1 mm/min); (a) Peak Shear Strength Ratio, (b) Large Displacement Shear Strength Ratio, (c) Displacement Shear Strength to Peak Shear Strength Ratio

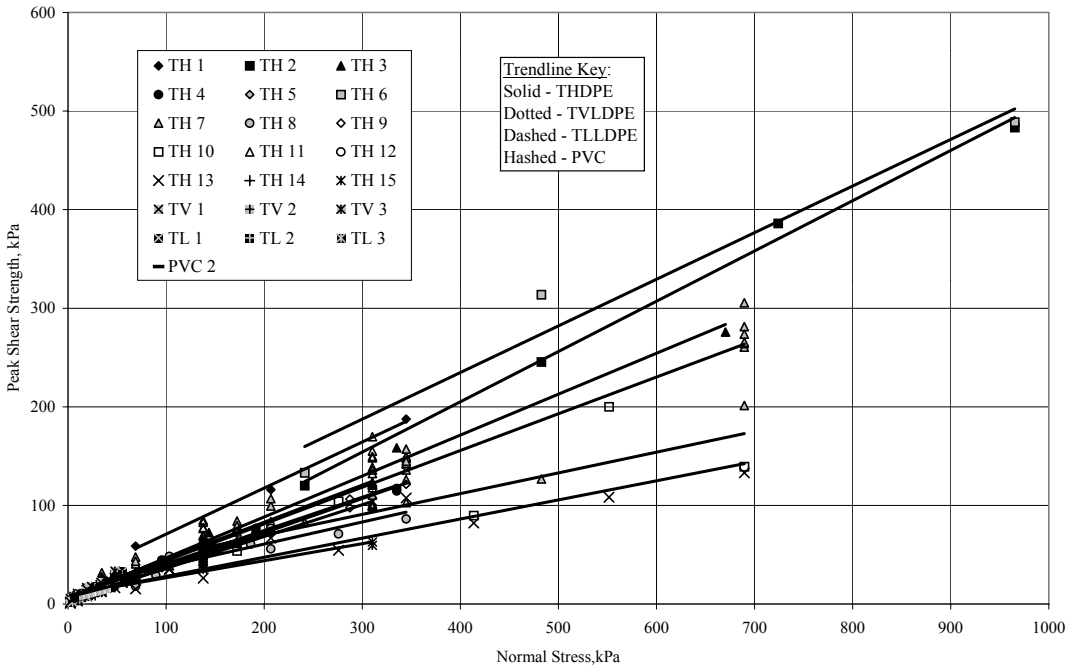

(a)

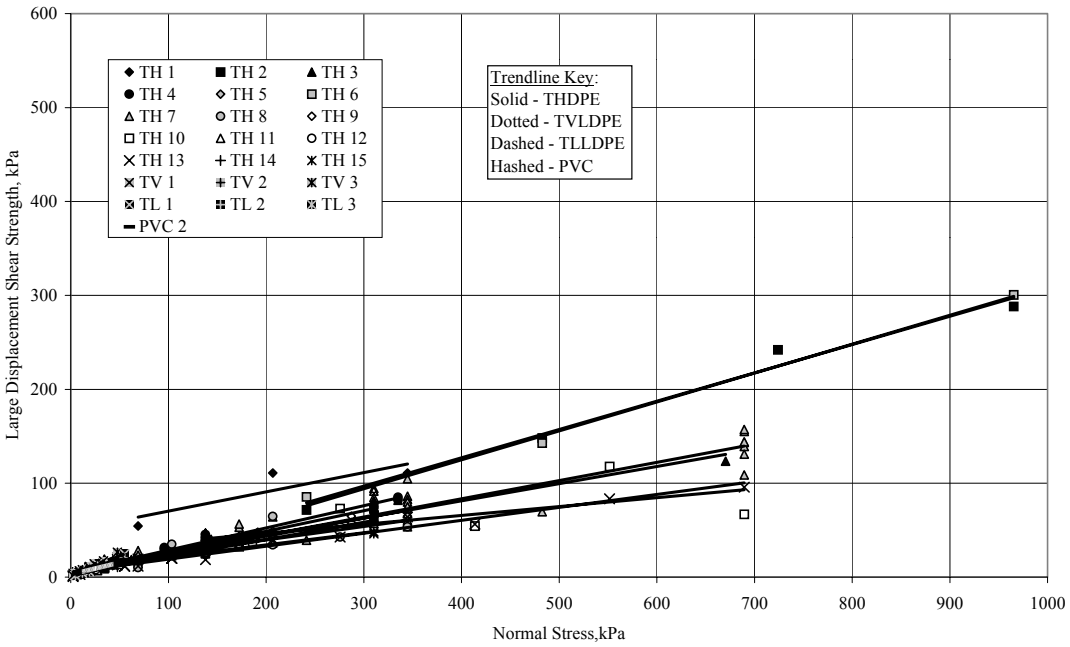

(b)

Figure 5.65: All Failure Envelopes for Textured Geomembrane Interfaces; (a) Peaks, (b) Large Displacement

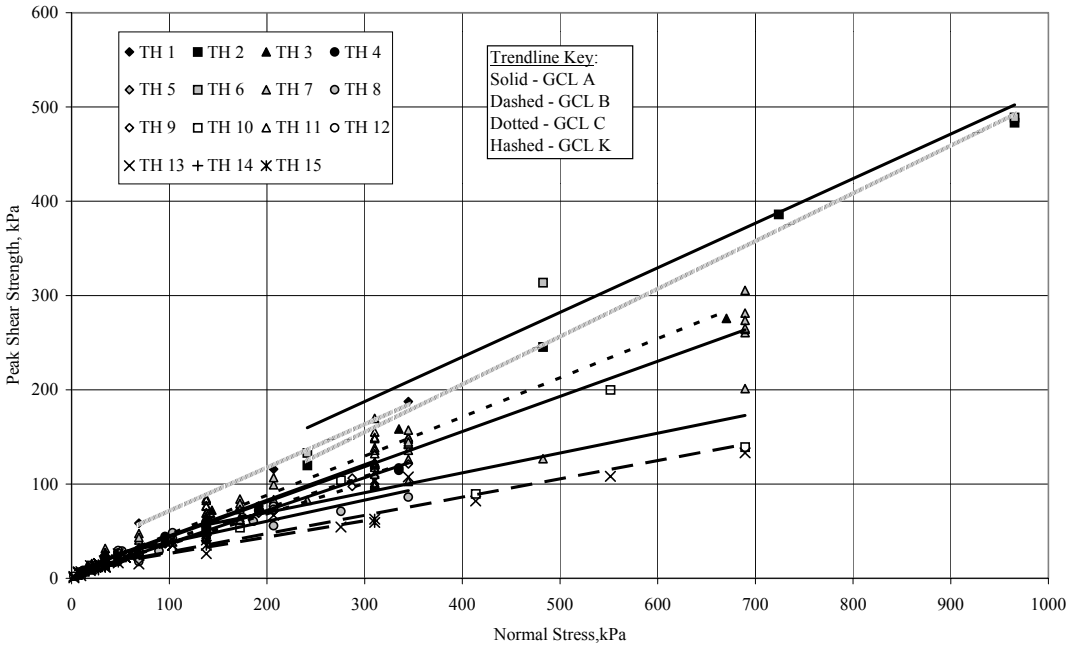

(a)

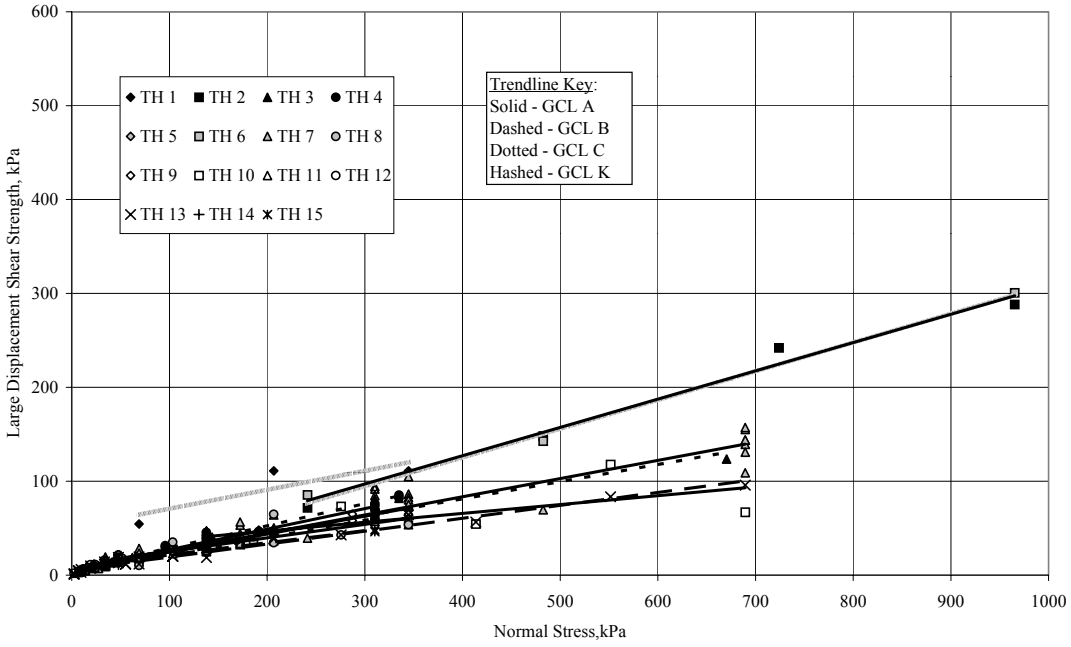

(b)

Figure 5.66: All Failure Envelopes for Textured HDPE Geomembrane Interfaces; (a) Peaks, (b) Large Displacement

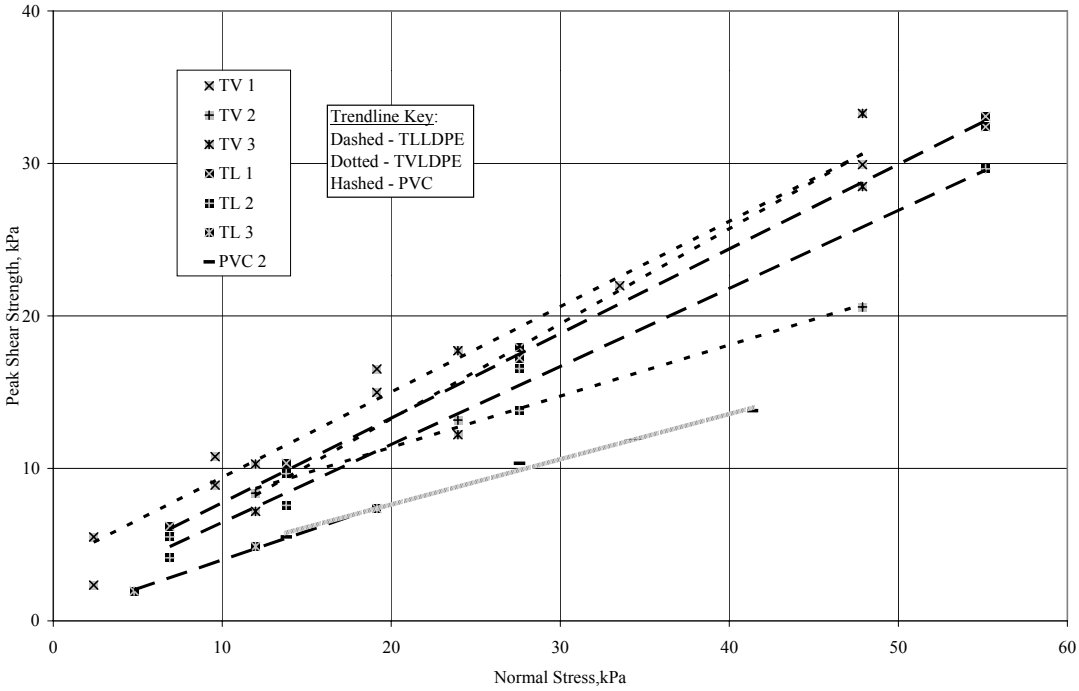

(a)

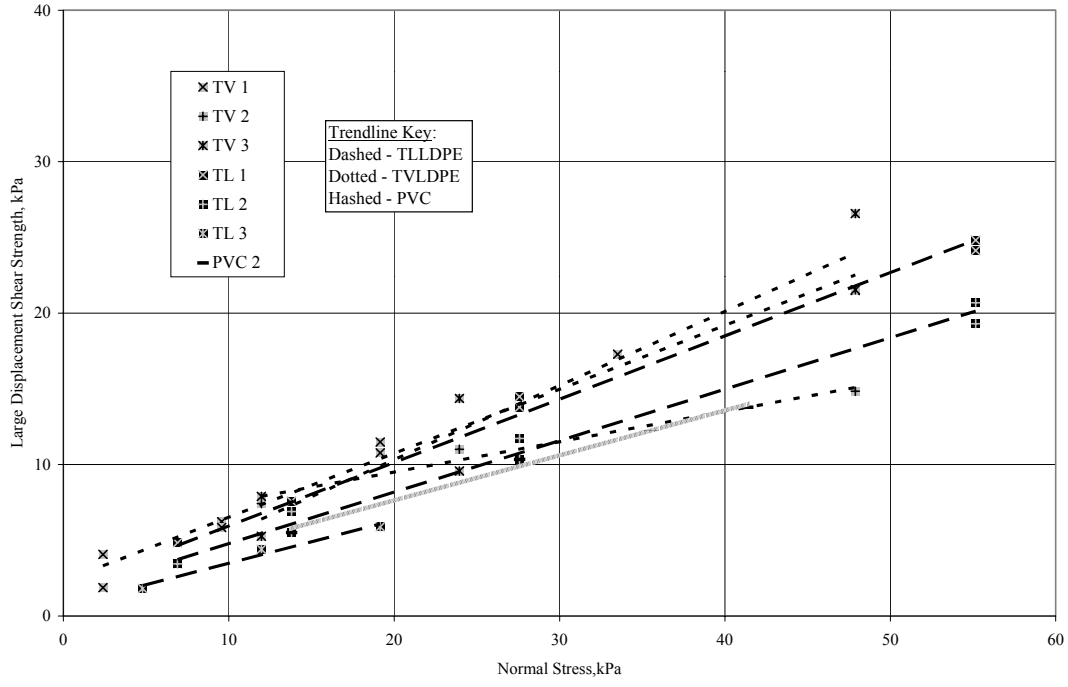

(b)

Figure 5.67: All Failure Envelopes for All Textured VLDPE, LLDPE and PVC Geomembrane Interfaces; (a) Peaks, (b) Large Displacement

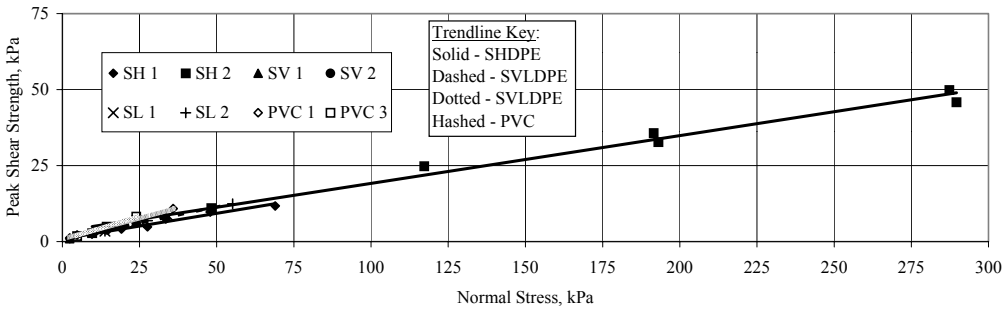

(a)

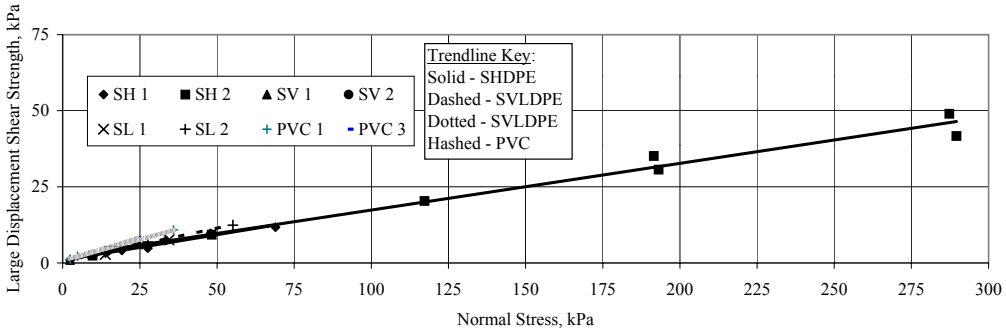

(b)

Figure 5.68: All Failure Envelopes for Smooth Geomembrane Interfaces; (a) Peaks, (b) Large Displacement

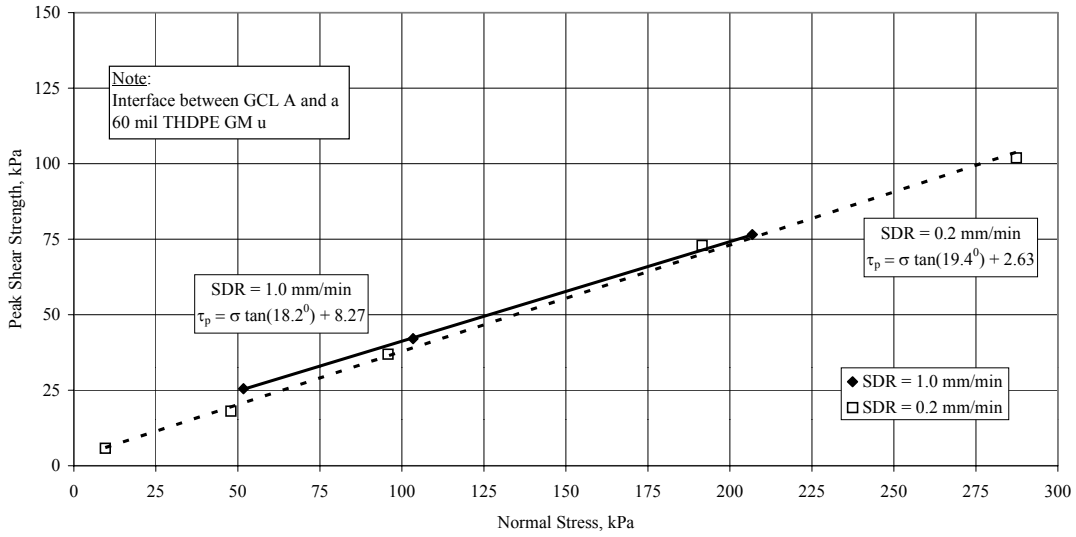

(a)

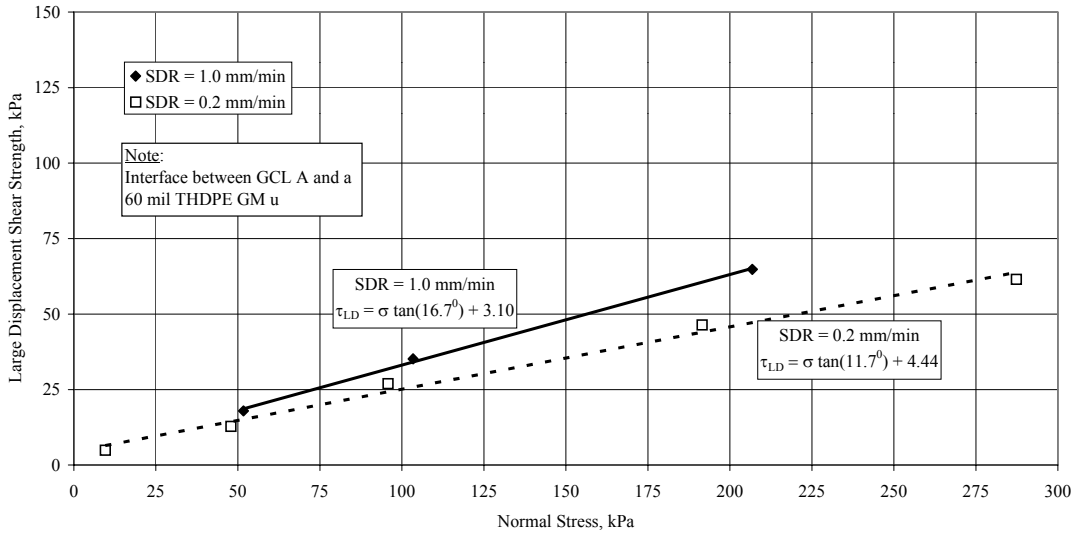

(b)

Figure 5.69: Effect of the Shear Displacement Rate on the Shear Strength of the Interface between GCL A and a 60 mil Textured HDPE GM u (t_H = 24 hours, No Consolidation); (a) Peak, (b) Large Displacement

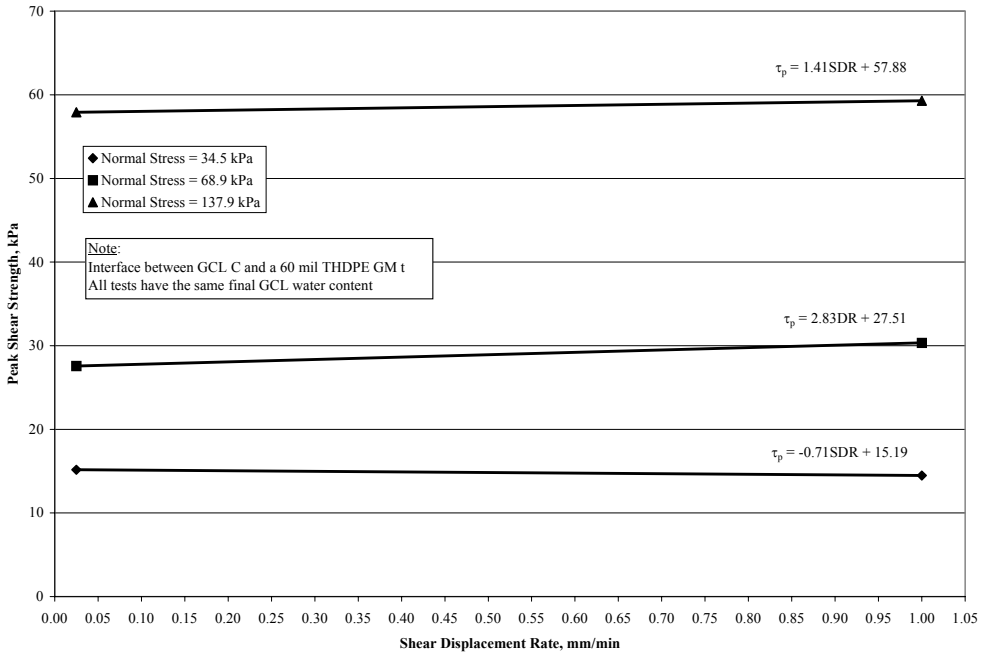

(a)

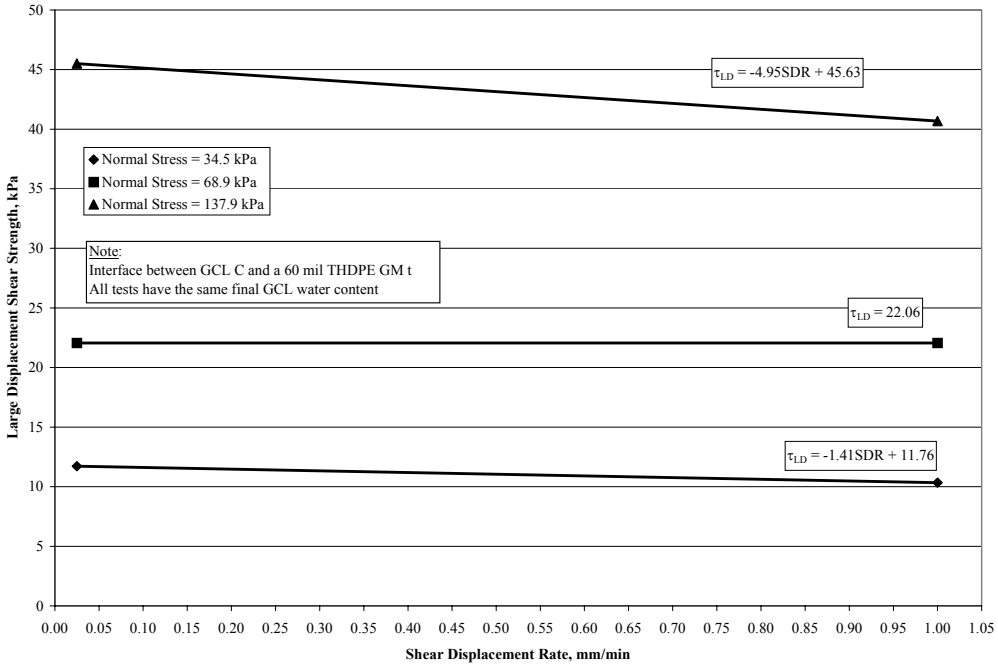

(b)

Figure 5.70: Effect of the Shear Displacement Rate on the Shear Strength of the Interface between GCL C and a 60 mil Textured HDPE GM t (t_H = 24 hours, No Consolidation); (a) Peak, (b) Large Displacement

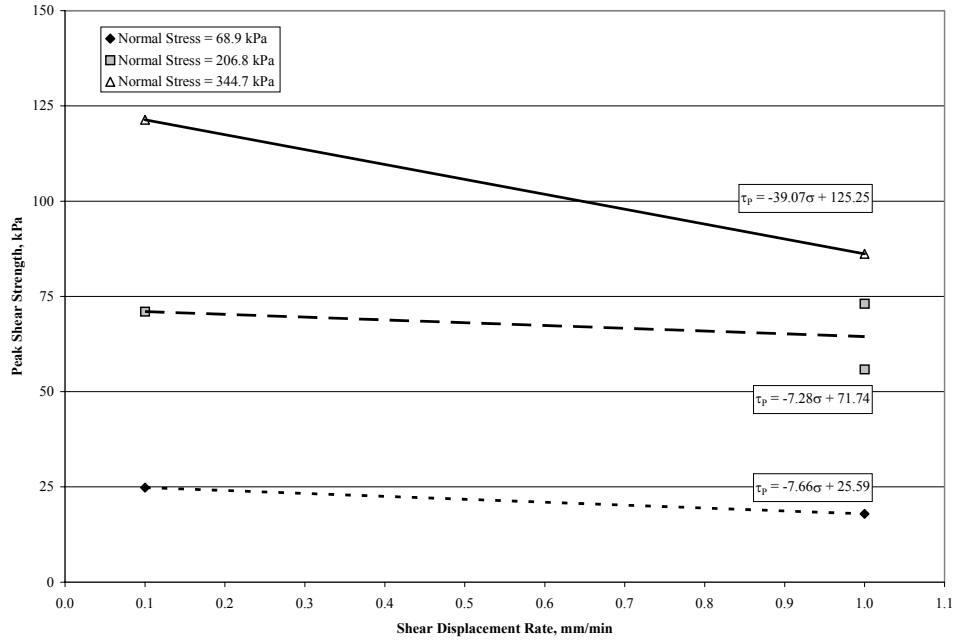

(a)

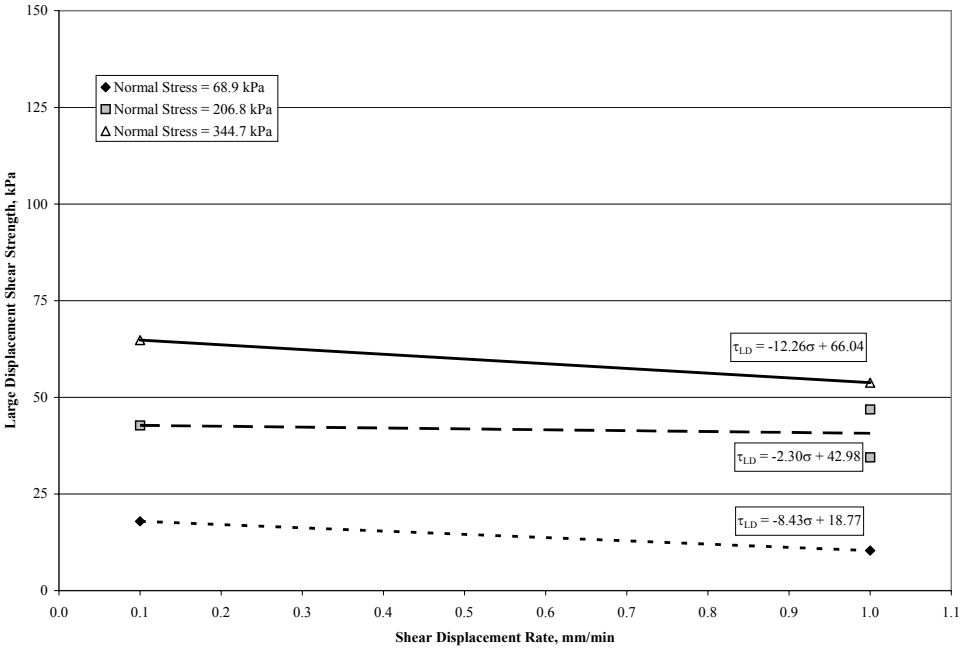

(b)

Figure 5.71: Effect of the Shear Displacement Rate on the Shear Strength of Interface between GCL A and a 60 mil Textured HDPE GM s (t_H = 48 hours, No Consolidation); (a) Peak, (b) Large Displacement

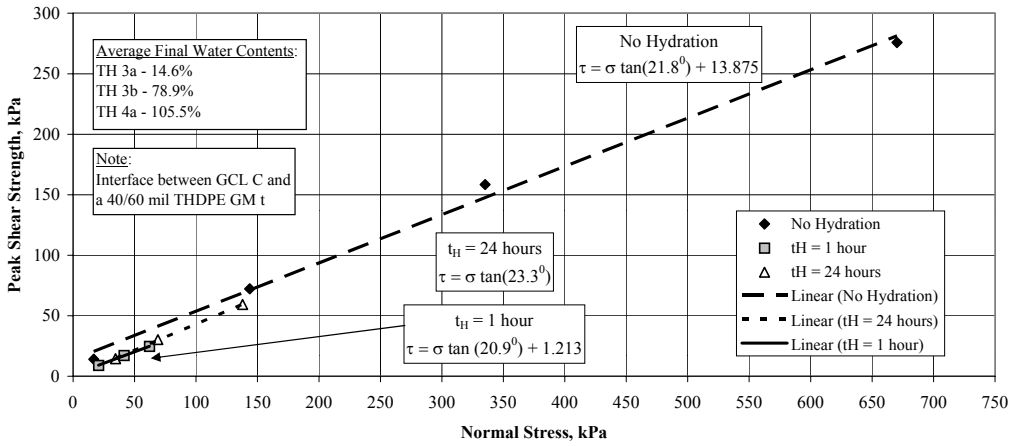

(a)

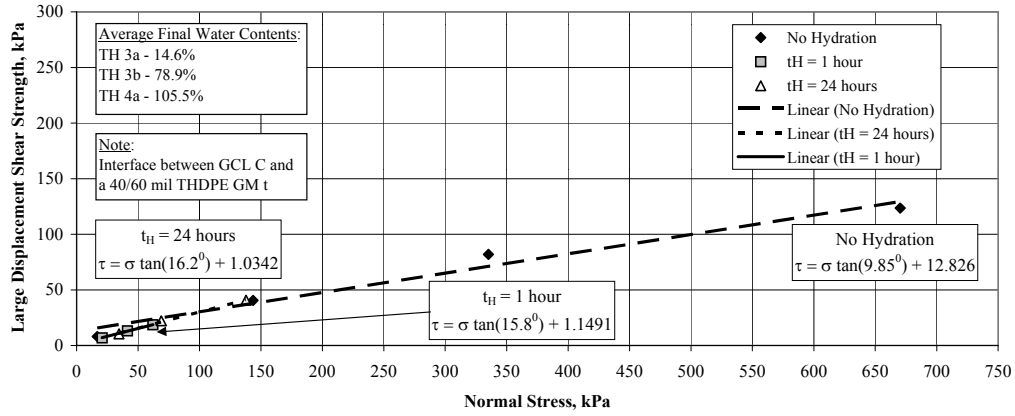

(b)

Figure 5.72: Effect of the Time of Hydration on the Shear Strength of the Interface between GCL C and a 40/60 mil Textured HDPE GM t (No Consolidation, SDR = 1.0 mm/min); (a) Peak, (b) Large Displacement

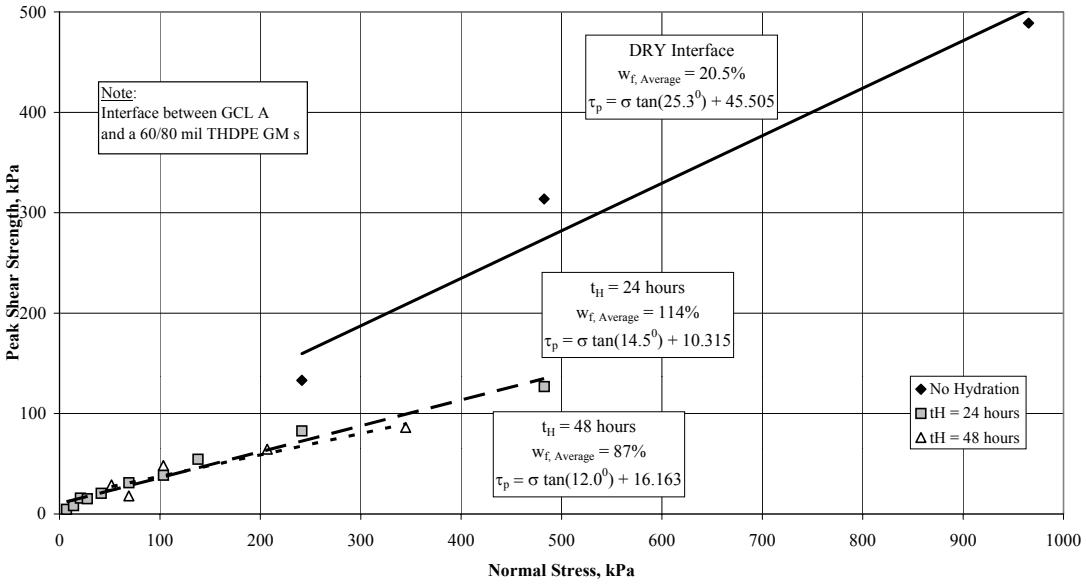

(a)

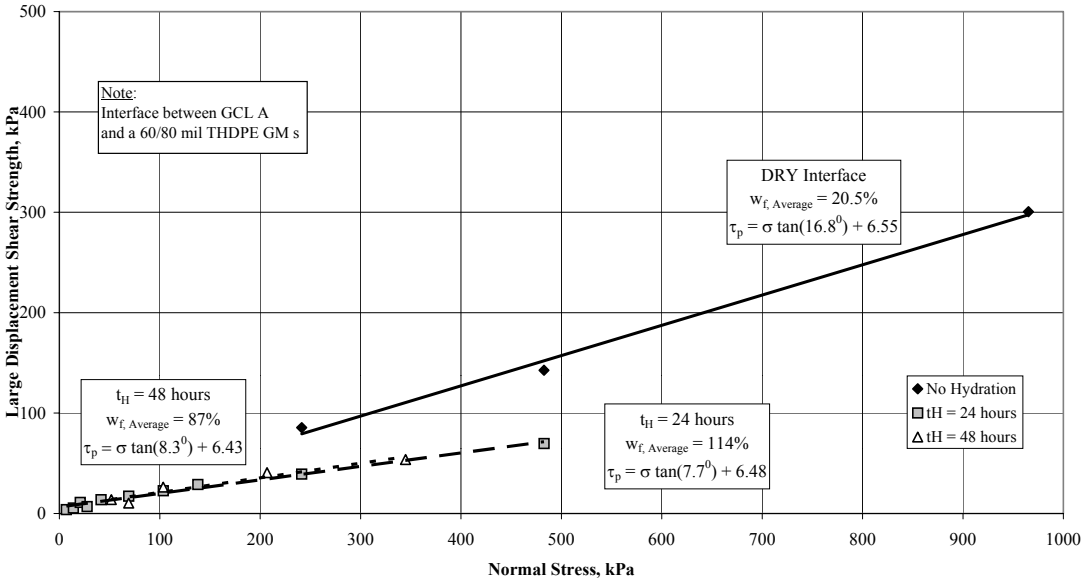

(b)

Figure 5.73: Effect of the Time of Hydration on the Shear Strength of the Interface between GCL A and a 60/80 mil Textured HDPE GM s (No Consolidation, SDR = 1.0 mm/min); (a) Peak, (b) Large Displacement

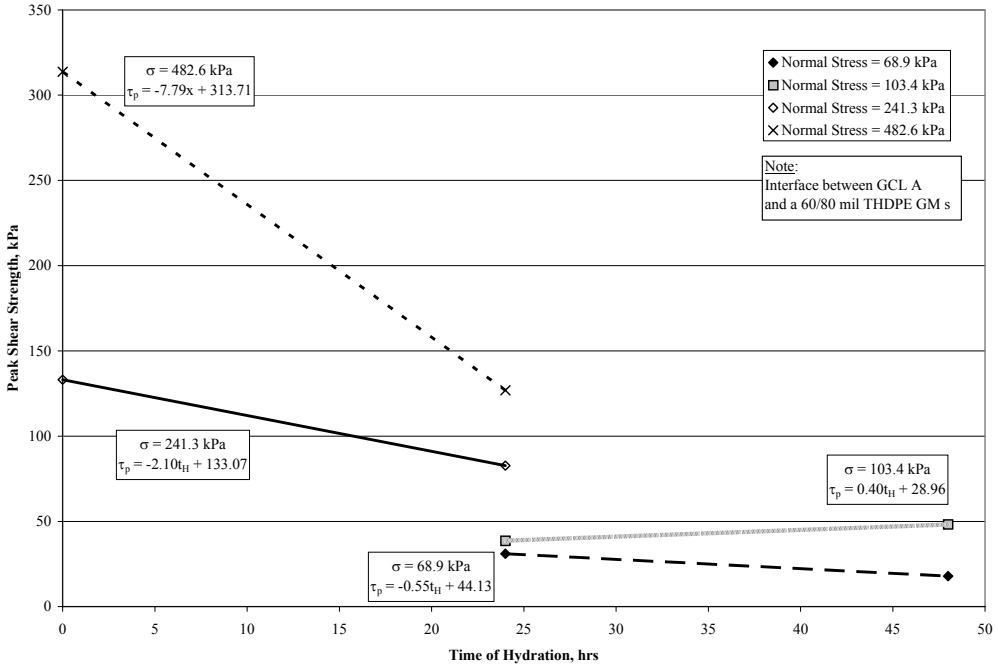

(a)

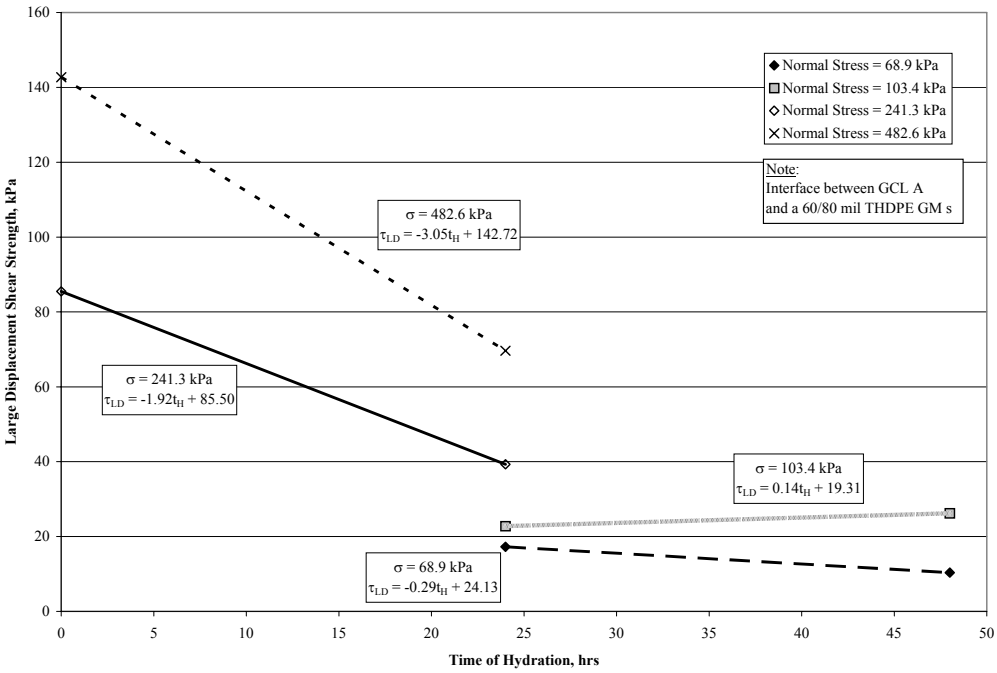

(b)

Figure 5.74: Effect of the Time of Hydration on the Shear Strength of the Interface between GCL A and a 60/80 mil Textured HDPE GM s (No Consolidation, SDR = 1.0 mm/min); (a) Peak, (b) Large Displacement

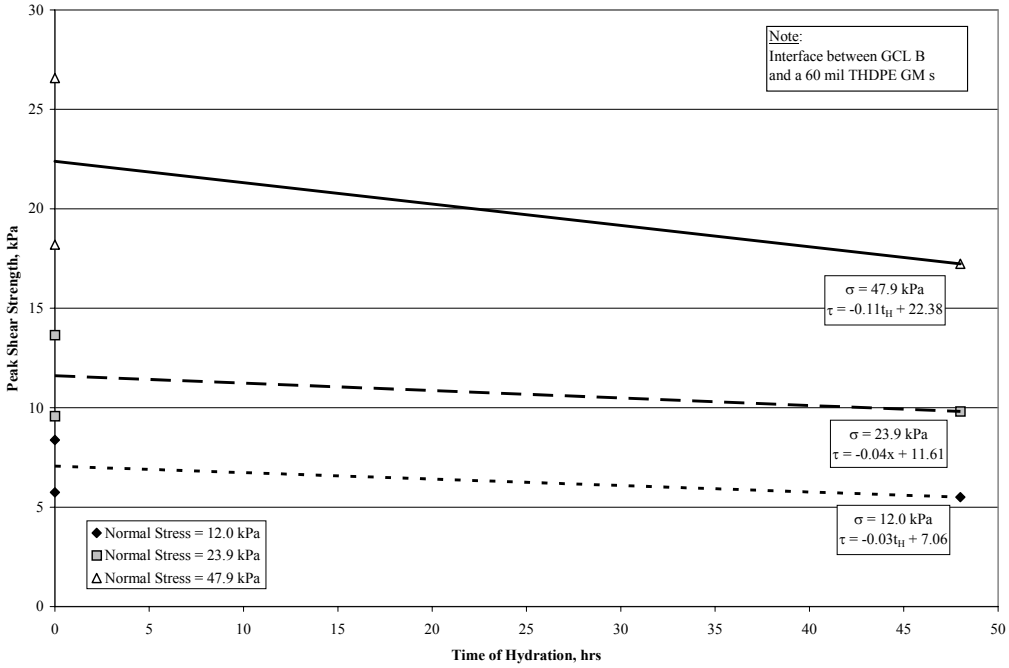

(a)

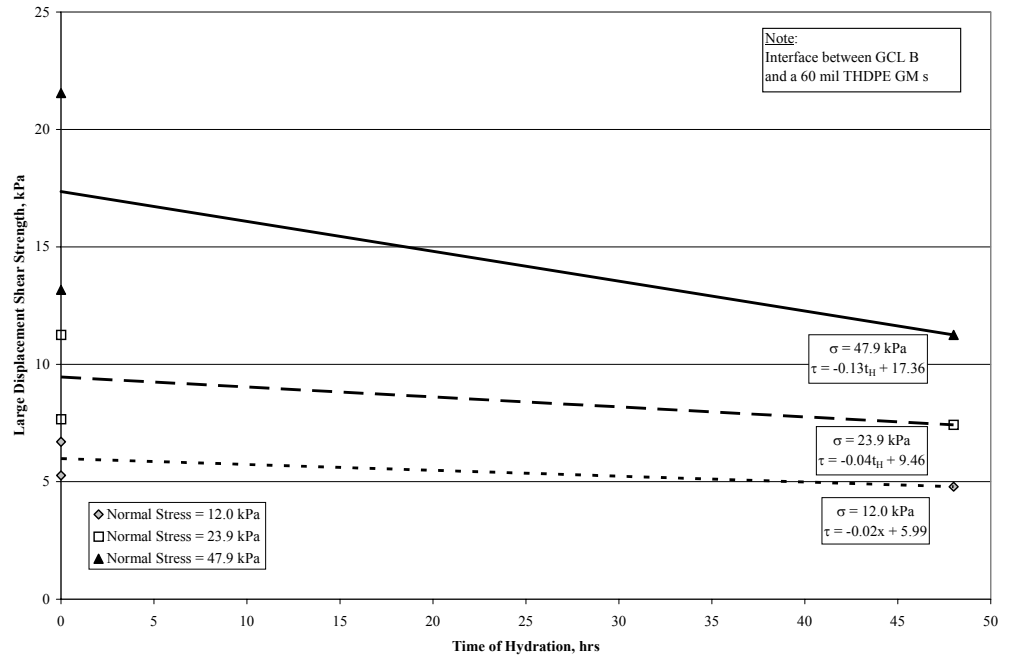

(b)

Figure 5.75: Effect of the Time of Hydration on the Shear Strength of the Interface between GCL B and a 60 mil Textured HDPE GM s (No Consolidation, SDR = 1.0 mm/min); (a) Peak, (b) Large Displacement

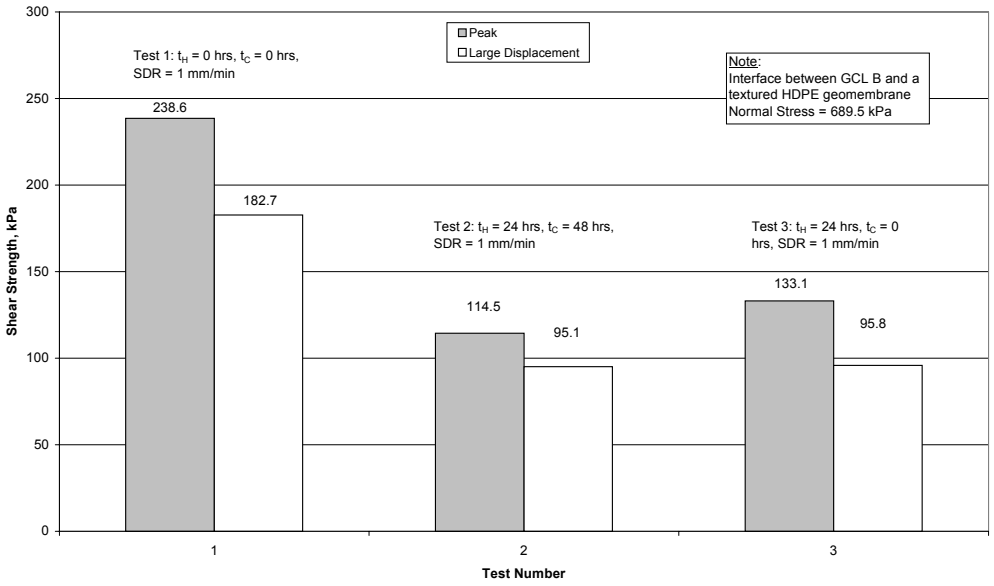

Figure 5.76: Effect of Different Hydration Procedures on the Shear Strength of the Interface between GCL B and a Textured HDPE geomembrane (Constant Normal Stress Level of 689.5 kPa for all Interfaces, Consolidated Interface has a Hydration Normal Stress of 68.9 kPa)

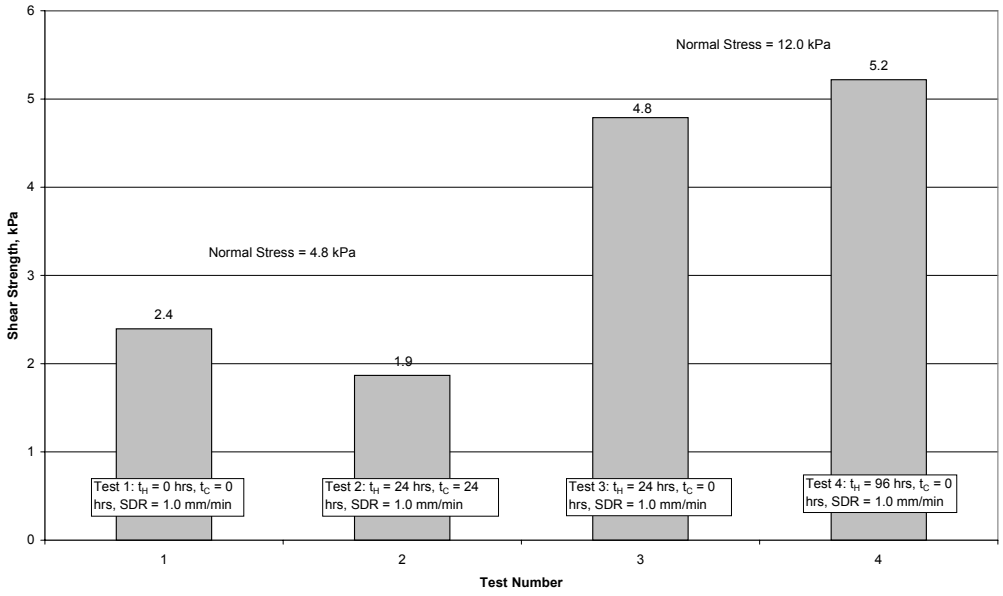

Figure 5.77: Shear Strength of the Interface between GCL A and a Smooth 40-mil PVC Geomembrane x; Different Hydration Procedures for Different Normal Stress Levels

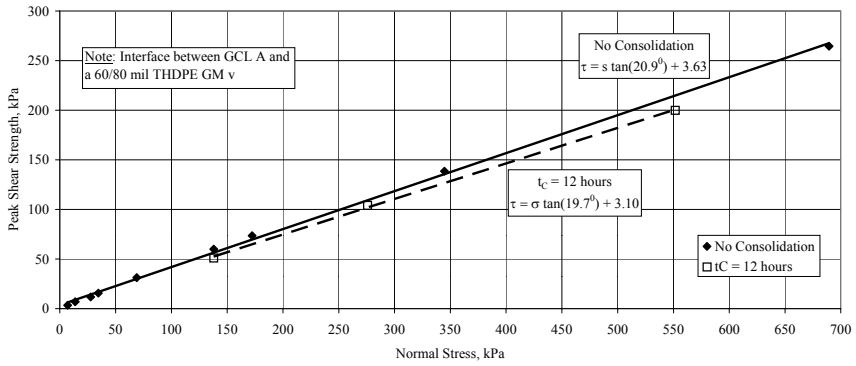

(a)

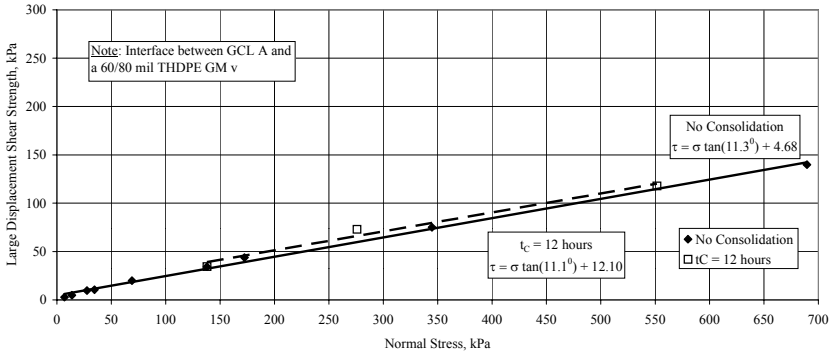

(b)

Figure 5.78: Effect of the Time of Consolidation on the Failure Envelopes for the Interface between GCL A and a 80 mil Textured HDPE GM v (Consolidated Interface has a Hydration Normal Stress of 68.9 kPa, SDR = 1.0 mm/min); (a) Peak, (b) Large Displacement

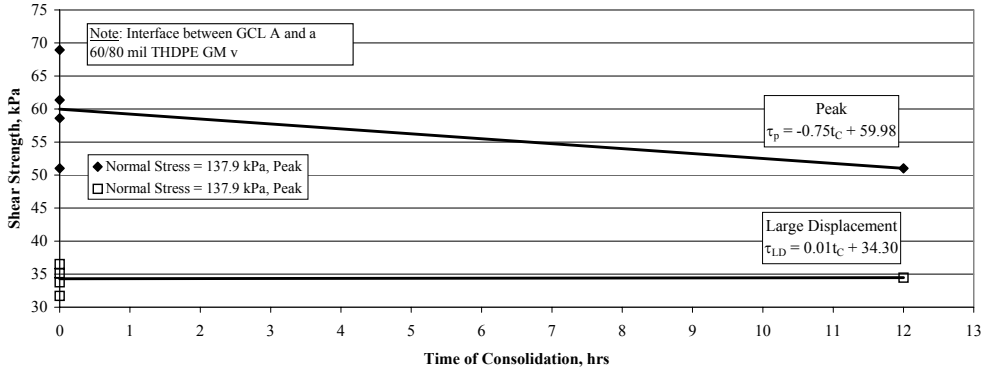

Figure 5.79: Effect of the Time of Consolidation on the Shear Strength of the Interface between GCL A and a 80 mil Textured HDPE GM v (Consolidated Interface has a Hydration Normal Stress of 68.9 kPa, SDR = 1.0 mm/min)

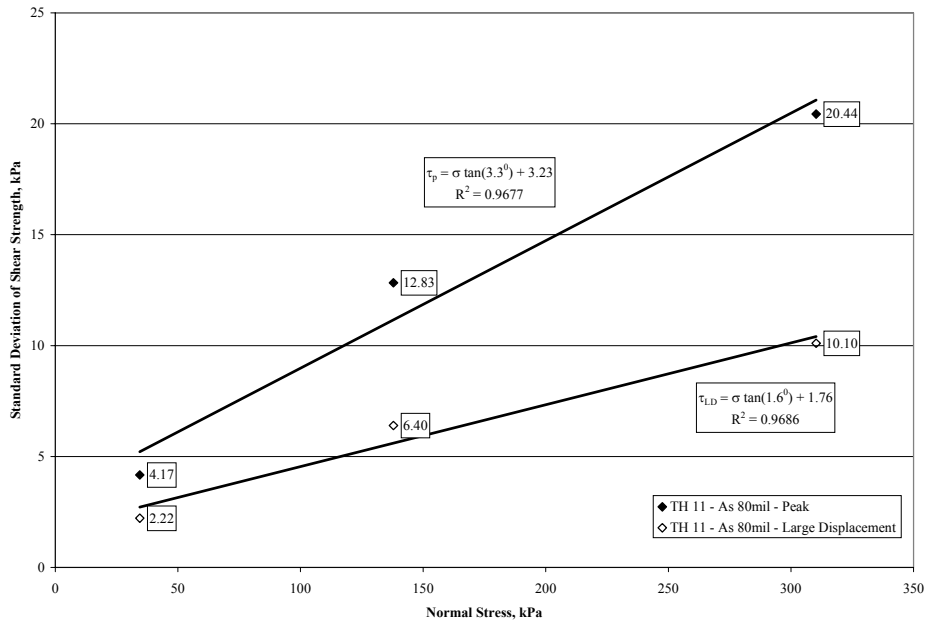

Figure 5.80: Standard Deviation of Peak and Large Displacement Shear Strengths for Failure Envelope TH 11 (t_H = 168 hours, t_C = 48 hours and SDR = 0.1 mm/min)

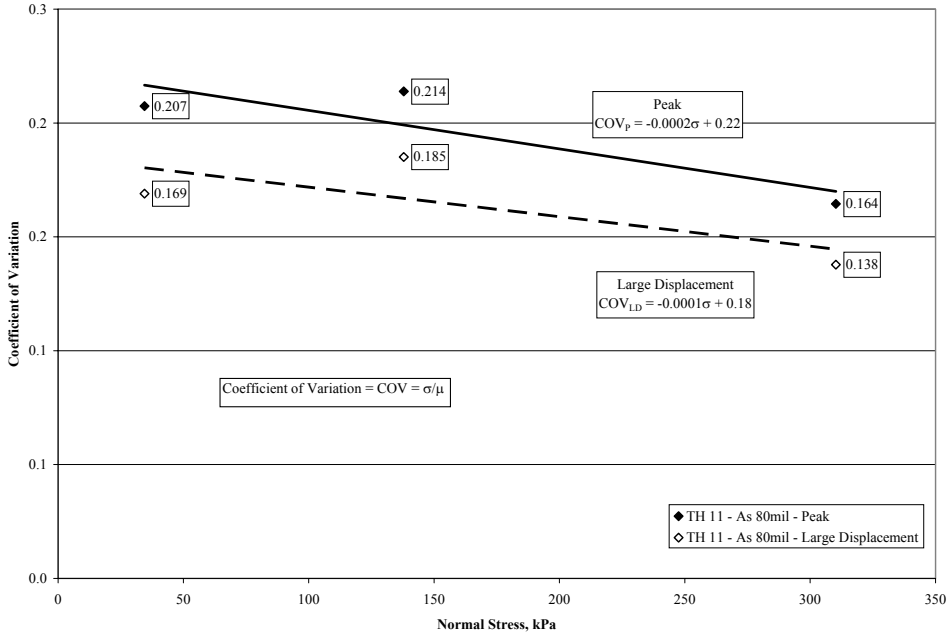

Figure 5.81: Coefficients of Variation for the Peak and Large displacement Shear Strengths for Failure Envelope TH 11 (t_H = 168 hours, t_C = 48 hours and SDR = 0.1 mm/min)

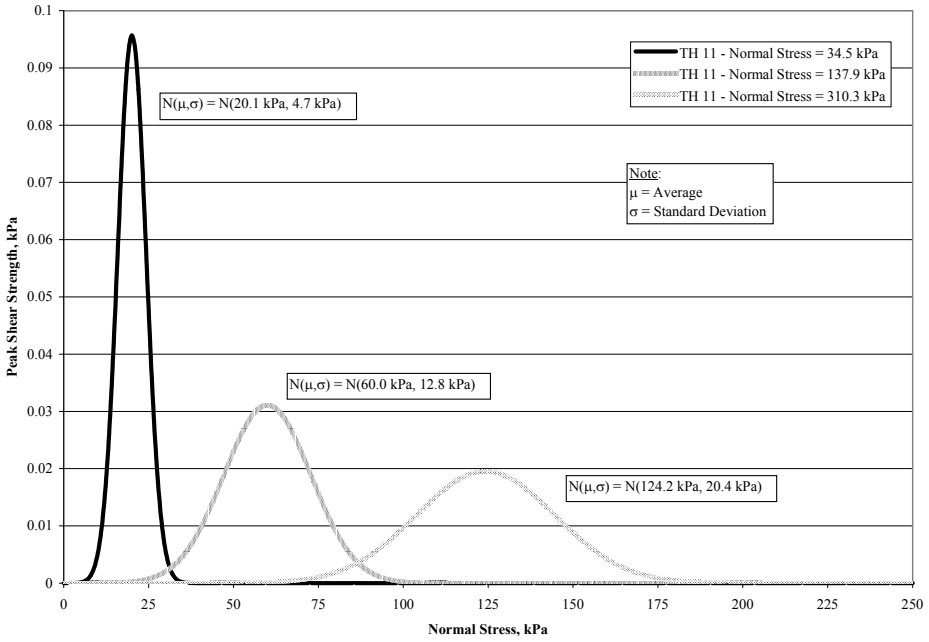

(a)

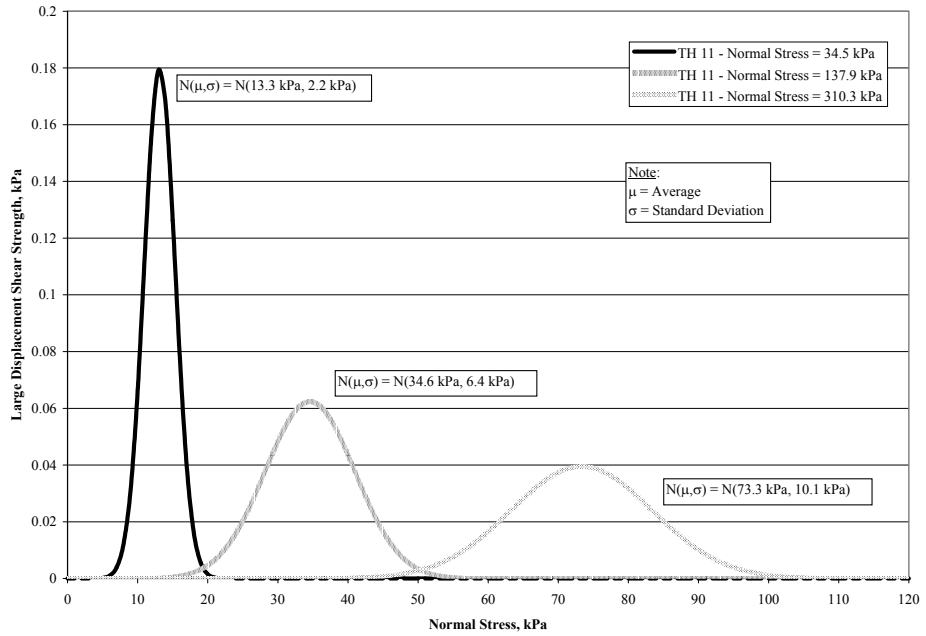

(b)

Figure 5.82: Equivalent Normal Probability Density Functions for the Shear Strength of the Interface between GCL A and an 80 mil Textured HDPE GM s (t_H = 168 hours, t_C = 48 hours and SDR = 0.1 mm/min); (a) Peak, (b) Large Displacement

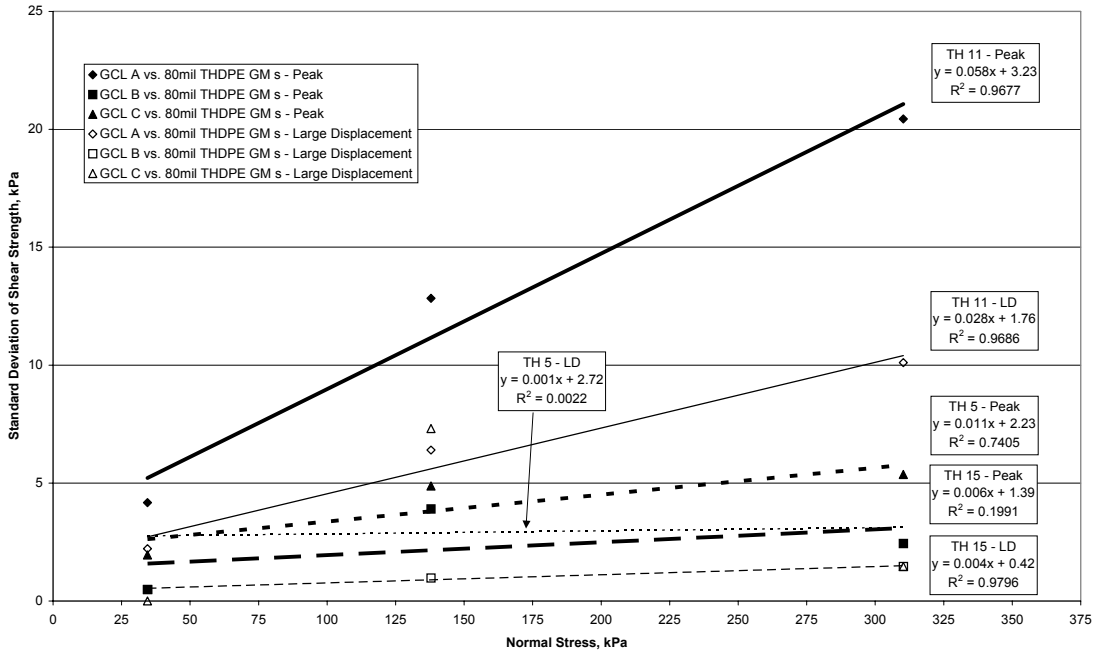

Figure 5.83: Standard Deviation of Peak and Large Displacement Shear Strengths for Failure Envelopes TH 5, 11 and 15 (t_H = 168 hours, t_C = 48 hours and SDR = 0.1 mm/min)

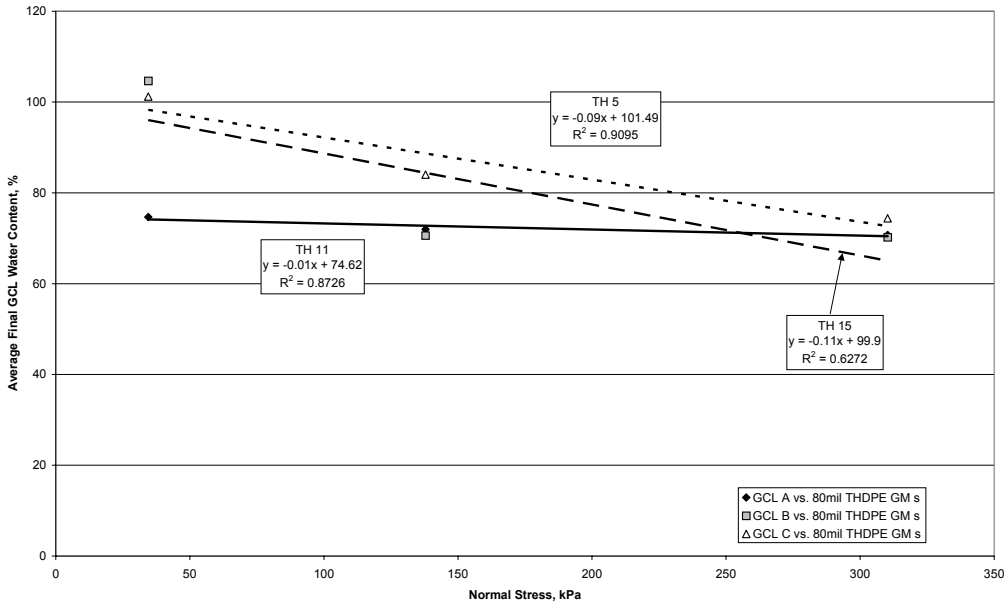

Figure 5.84: Variation in the Average Final GCL Water Content with Normal Stress for Three GCL-Textured HDPE Geomembrane Interfaces; Constant Test Condition with t_H = 168 hours, t_C = 48 hours, SDR = 0.1 mm/min

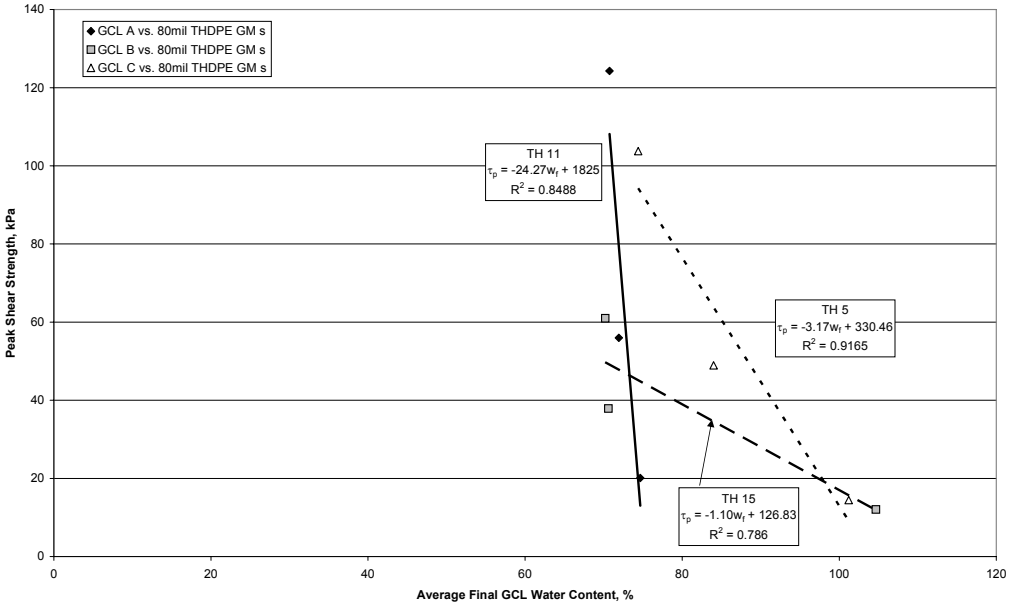

(a)

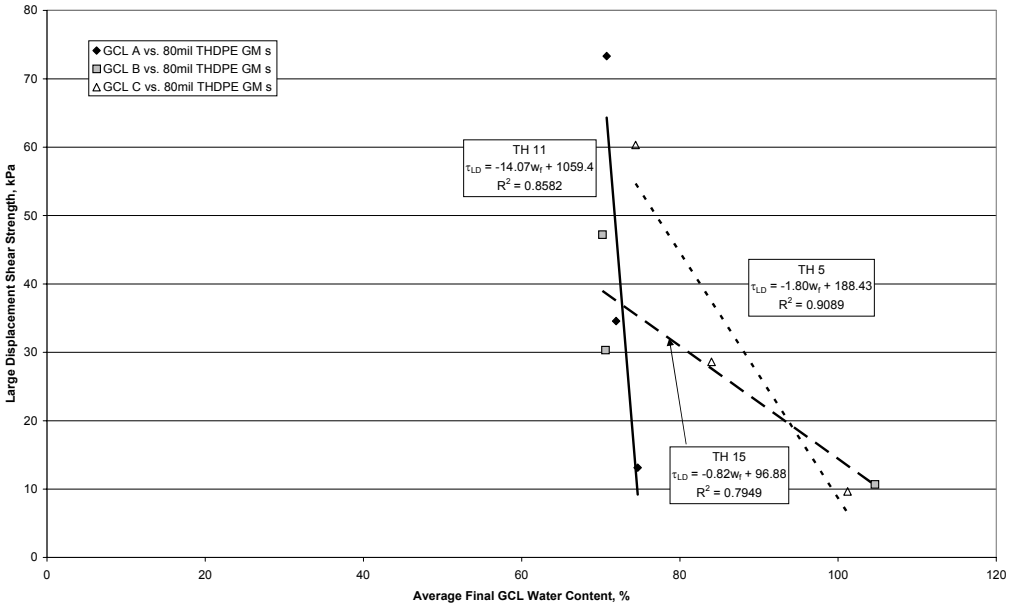

(b)

Figure 5.85: Relationships between the Average Shear Strength and the Average Final GCL Water Content for Failure Envelopes TH 5, 11 and 15 (t_H = 168 hours, t_C = 48 hours, SDR = 0.1 mm/min); (a) Peak, (b) Large Displacement

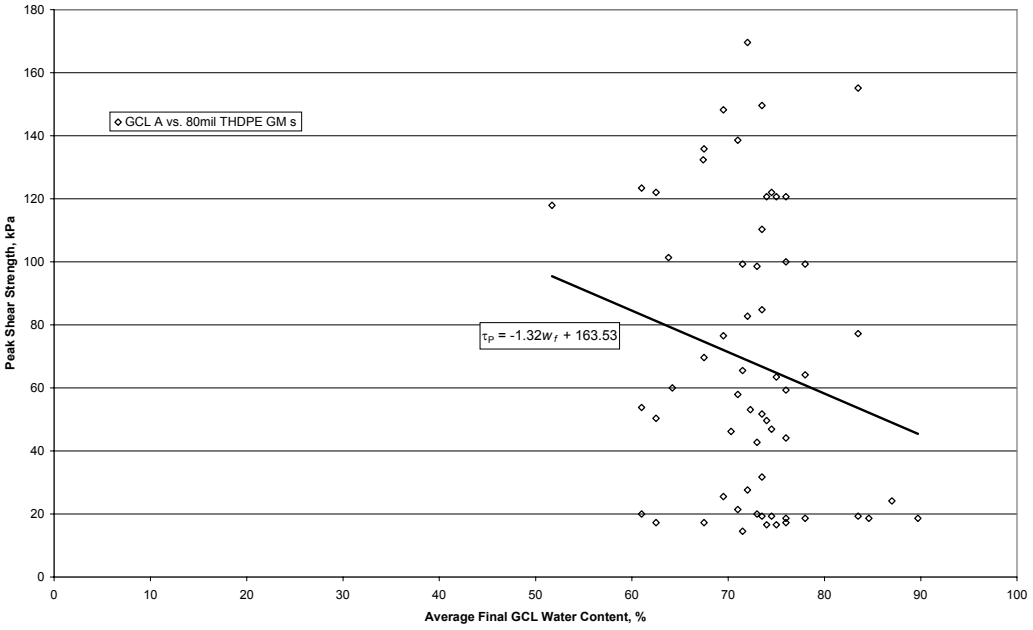

(a)

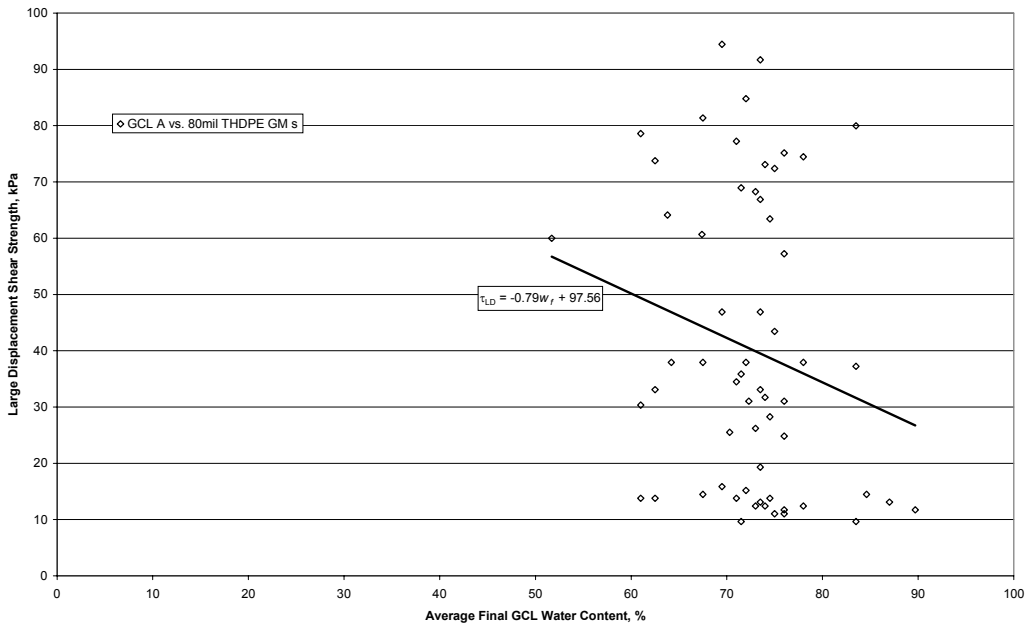

(b)

Figure 5.86: Relationship between the Shear Strength and the Final GCL Water Content for Failure Envelope TH 11 (t_H = 168 hours, t_C = 48 hours, SDR = 0.1 mm/min); (a) Peak, (b) Large Displacement

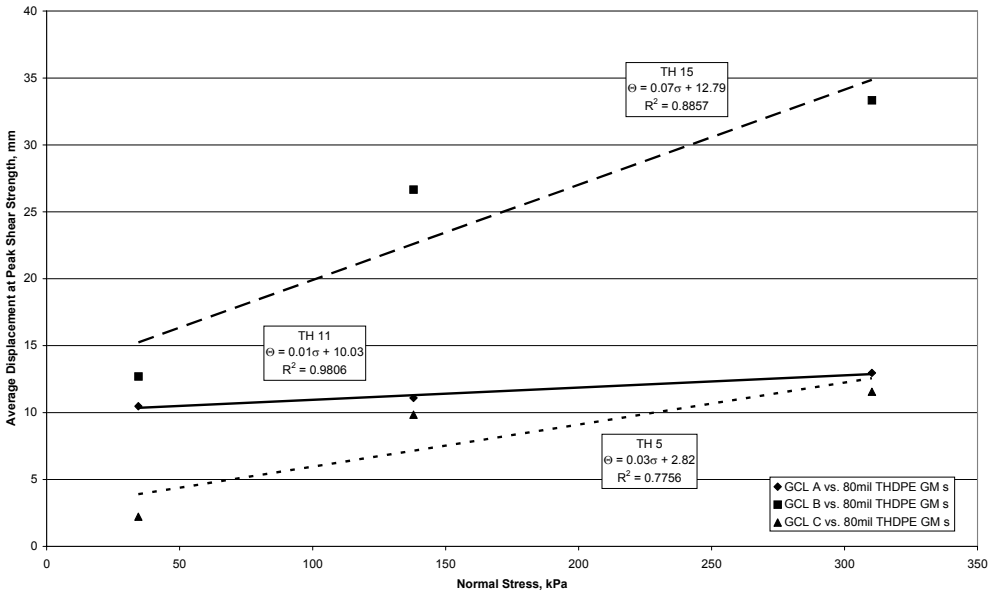

Figure 5.87: Displacement at Peak Shear Strength for Failure Envelopes TH 5, 11, and 15 (t_H = 168 hours, t_C = 48 hours, SDR = 0.1 mm/min)

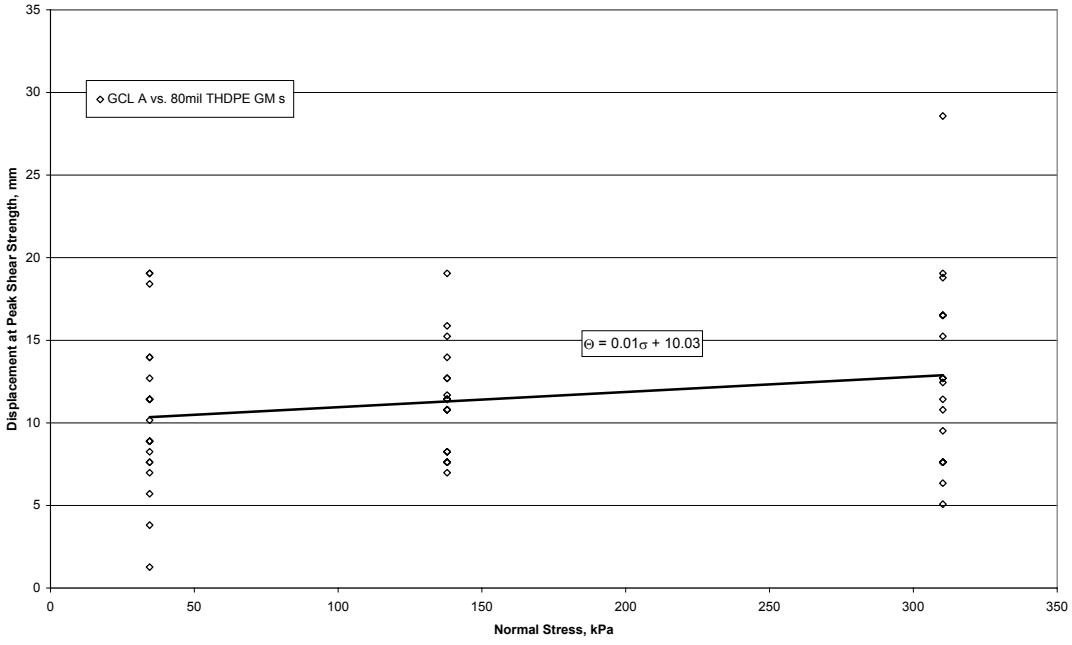

Figure 5.88: Displacement at Peak Shear Strength for Failure Envelope TH 11 (t_H = 168 hours, t_C = 48 hours, SDR = 0.1 mm/min)

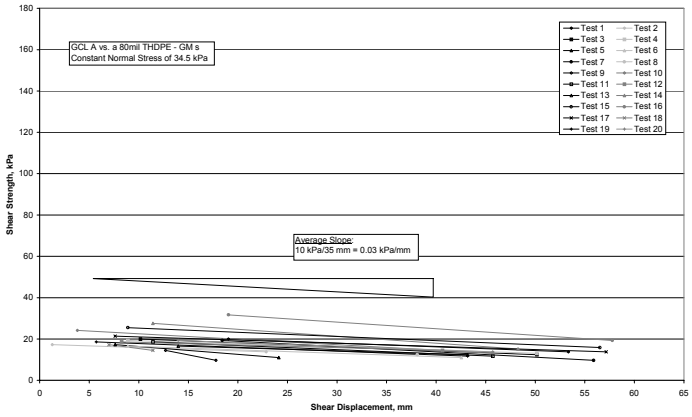

(a)

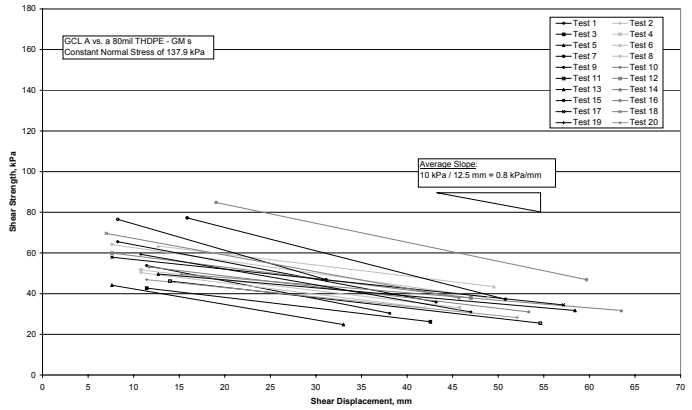

(b)

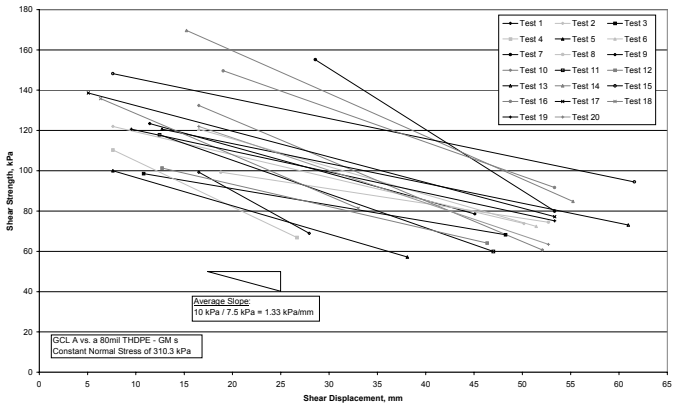

(c)

Figure 5.89: Displacement from Peak to Large Displacement Shear Strengths for the Interface between GCL A and a 80 mil Textured HDPE GM (t_H = 168 hours, t_C = 48 hours, SDR = 0.1 mm/min), Normal Stresses of (a) 34.5 kPa, (b) 137.9 kPa, (c) 310.3 kPa

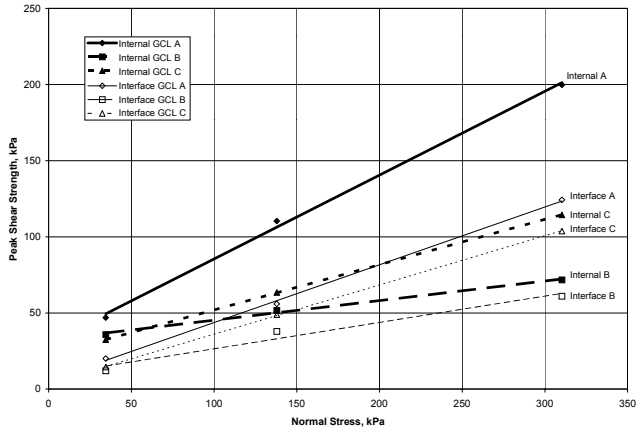

(a)

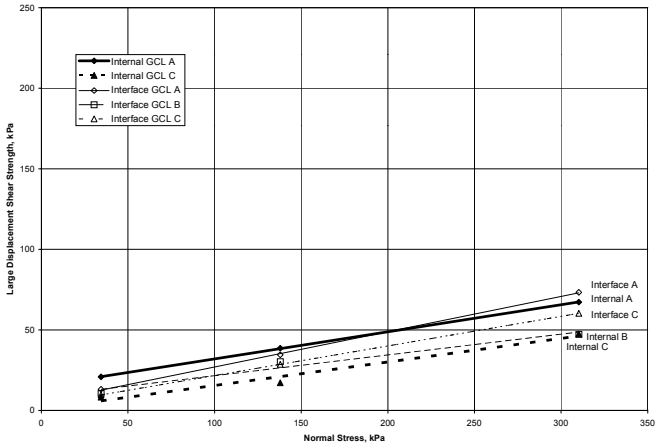

(b)

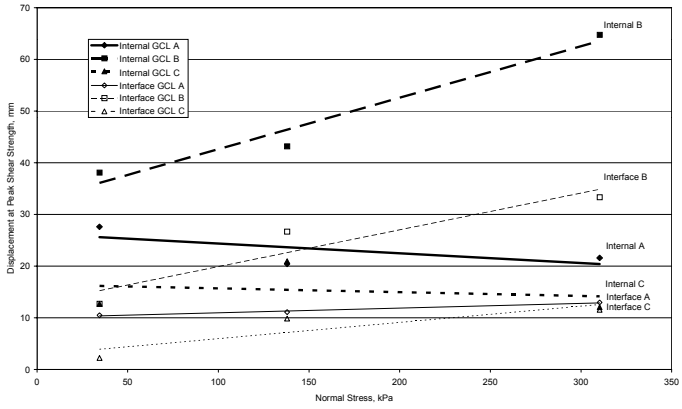

(c)

Figure 5.90: Comparison between Average Behavior for Internal GCL Failure envelopes A5, B4, C3, and GCL-GM Interface Failure Envelopes TH 5, TH 11 and TH 15 (a) Peak Shear Strength, (b) Large Displacement Shear Strength; (c) Displacements at Peak Shear Strength

6 Application to Geotechnical Design

6.1 Introduction

As mentioned in previous chapters of this report, the internal and interface GCL shear strengths are key design concerns, especially as they may potentially be highly variable. Design of layered geosynthetic systems involving consideration of the interface shear strength has been investigated in the past, yet there has not been a reasonable quantification of the variability of the shear strength parameters. The use of probability and reliability concepts, with the incorporation of correlation (or inter-dependence) between the random variables, may provide insight to this problem if there is a significant amount of data available to quantify the variability of different random variables. As the GCLSS database provides a large amount of test results, it is a suitable source of data for a probability-based analysis. This chapter will provide new insights into the applications of a database of shear strength test results through probability and reliability based design of layered systems.

The objective of this chapter is to introduce the concept of reliability-based design as a means of quantifying GCL shear strength variability in slope design. Specifically, these concepts are used for infinite slope stability analysis which, in spite of its simplicity, represents a common design problem for cover systems. Direct shear test results for different internal GCL and GCL-geomembrane interfaces obtained from the GCLSS database will be analyzed to quantify the variability of the shear strength parameters.

6.2 Conventional Approach to Infinite Slope Design

Design of geotechnical structures must take into account the uncertainty in the material properties, unexpected conditions, and errors in any simplifying assumptions. Although an infinite slope is a simple system, full understanding of all of the resisting and disturbing mechanisms in the slope is challenging. A failure plane may be defined anywhere through the slope where the shear strength equals the shear stress required for equilibrium. Conventional slope designs use the concept of a safety factor to ensure that the slope is safe. The safety factor (FS) is defined as:

$$FS = \frac{\text{Shear Strength}}{\text{Shear Stress}} \qquad \text{Eq. 6.1}$$

When the shear stress approaches the shear strength, the slope will fail and move downhill in the direction of gravity.

Figure 6.1(a) shows a typical infinite cover slope, and Figure 6.1(b) shows a free-body diagram with the relevant forces acting on the GCL layer. For equilibrium, the component of the weight normal to the interface must be equal to the normal force along the interface:

$$N = W \sin\psi \qquad \text{Eq. 6.2}$$

where N is the normal force on the interface, W is the weight of the cover soil, and ψ is the slope angle (this notation is used to avoid confusion with the reliability index, β). The failure plane for the slope will be located at the interface or inside of the GCL as the sodium bentonite layer is typically the weakest interface in a layered slope (*i.e.* the lowest friction angle). The normal force on the interface may be related to the shear resistance, T, of the interface:

$$T = c_A L + N \tan\delta = W \sin\psi \qquad \text{Eq. 6.3}$$

where c_A is the adhesion of the interface, δ is the friction angle of the weakest interface, and L is the slope length of the free-body. In addition, the weight of soil above the interface is equal to:

$$W = tL\gamma \qquad \text{Eq. 6.4}$$

where t is the thickness of the slope, and γ is the unit weight of the cover soil. An equation for the safety factor for a cohesive soil can be represented by:

$$FS = \frac{\text{Shear Strength}}{\text{Shear Stress}} = \frac{c_A L + \gamma Lt \cos\psi \tan\delta}{\gamma Lt \sin\psi} \qquad \text{Eq. 6.5}$$

which may be simplified to:

$$FS = \frac{c_A}{\gamma t \sin\psi} + \frac{\tan\delta}{\tan\psi} \qquad \text{Eq. 6.6}$$

It can be seen from Equation 6.6 that the safety factor for an infinite slope depends on the geometry of the slope and the material characteristics, both of which may be variable. The mean values for the shear strength parameters may be used to simulate the behavior of the most likely situation. Still, in this equation, the variability of the

shear strength about the mean value is not considered. Instead, the variability of the parameters is typically handled in conventional slope design by penalizing the actual shear strength of the slope. In other words, a slope that is actually safe at an angle of repose of 30^0 may be designed at 20^0 if the variability of the parameters is high.

6.3 Introduction to Probability and Reliability Based Design Concepts

6.3.1 Background

Geotechnical engineering deals with uncertainty on a regular basis, as the entire soil continuum is beneath the ground surface. Its actual behavior cannot be observed directly, but must be implied by failure back-analysis or other means. Several phenomena may lead to uncertainty in geotechnical engineering, including the limitations of mathematical theories, differences in field and laboratory conditions, heterogeneity, anisotropy, incorrect calculation of loads and effects, and many others. Also, there often is not necessarily a unique solution that will lead to the optimal combination between safety and efficient use of materials. Tests to measure material properties of a soil may be accurate only for the soil near the test location, but it is possible for these properties to vary with location.

Reliability based design combines the concepts of mechanics of materials with probability and statistics to understand the behavior of a system when variability and uncertainty are considered. Mechanics of materials provides a mathematical framework for understanding physical phenomena, while probabilistic and statistic concepts provide an understanding of the variability of each parameter representing a material phenomenon. Reliability based design is useful as it provides a method of quantifying the safety of a system and examining inter-dependence between random variables. Geotechnical structures designed using reliability methods have a more consistent level of risk and a more efficient use of materials and space (Ang and Tang, 1975). Layered systems on slopes are an example of a geotechnical system that can be designed using reliability methods. On a slope, the layers each have similar loading conditions (assuming negligible thicknesses of layers), and each provides a resistance to shear failure independent from other layers.

6.3.2 Random Variables

Before explanation of the concepts of reliability based design, a short background in probability is provided herein. Further discussion of the following topics may be found in Ang and Tang (1975). A random variable is a variable that is capable of taking any value from a given range of values. A deterministic variable, for comparison, is one that can take only one value. In geotechnical problems, typical deterministic variables are the unit weight of water, applied loads or surcharges, and surface geometric variables (i.e. the height and length of a slope, the angle of inclination of a slope). Random variables encountered are the material properties of the soil at each location in the subsurface continuum (*e.g.* adhesion and friction angle), strength conditions (*i.e.* anisotropy or dilatancy effects, attainment of peak or residual conditions, *etc.*), and subsurface geometric variables.

A random variable may be characterized in many ways, but the most common is the determination of a central value, and a dispersion value, often referred to as the first and second moments of a group of data. The central value, or mean, is the most probable value, and is calculated similar to the centroid of a collection of different areas or weights:

$$E(x) = \mu_x = \Sigma x_i P(x_i) \qquad \text{Eq. 6.7}$$

Where x is the set of values that a certain measure may attain and $P(x)$ is the probability of each value. The variance of a set of data is a measure of the dispersion of data about the central value. A commonly used term is the standard deviation, which is simply the square root of the variance. The variance and standard deviation may be calculated by the equations:

$$\mathrm{Var}(x) = s^2(x) = \Sigma(x_i - \mu_x)^2 P(x_i) \qquad \text{Eq. 6.8}$$

$$s(x) = \sqrt{Var(x)} \qquad \text{Eq. 6.9}$$

where $s(x)$ is the standard deviation, x_i is the particular value from a group of data, μ_x is the mean of the data, and $P(x_i)$ is the probability of occurrence for the particular value x_i.

6.3.6 Limit State Analysis

If probabilistic distributions have been developed for each of the material properties for a soil, the material properties c_A and δ may be assembled into equations representing the resistance to shear loading on a given failure plane:

$$R = c_A(\mu_{c_A}, s_{c_A}) + \sigma_n \tan\delta(\mu_\delta, s_\delta) \qquad \text{Eq. 6.10}$$

where R is the resistance of the soil to shear stress, s_n is the normal stress on the interface, and μ and s are the standard deviation of the shear strength parameters. The disturbing load on the failure plane may be difficult to formulate as it depends on the loading situation and the geometry of the slope. In its simplest form, the shear disturbance on the interface can be represented by the equation:

$$Q = \tau_a(\mu_{\tau_a}, s_{\tau_a}) \qquad \text{Eq. 6.11}$$

where τ_a is the applied shear stress on the interface, which may be a random variable. A safety margin can then be developed, by finding the difference between the resistance and load:

$$M = R - Q \qquad \text{Eq. 6.12}$$

where M is the safety margin for a single interface, R is the resistance of the interface to shear loading, and Q is the load applied to the interface. As R and Q are random variables, then it follows that M is a random variable. In order to find the standard deviation of the safety margin, a first-order, second method approach described by Duncan (2000) or Monte Carlo simulation could be used.

A limit state equation can be developed by setting the safety margin to zero, which effectively brings the situation to the failure point where resistance equals the applied load. The usefulness of a limit state equation is explained in the formulation of the reliability index in the next section.

6.3.7 The Reliability Index

The reliability index is a dimensionless measure of how likely the resistance or a component or system will be less than the applied load. In particular, the log-normal reliability index is particularly used in engineering problems, as the log-normal distribution is always greater than zero (Ang and Tang, 1975). Many

engineering parameters only have a physical significance when positive. The log-normal reliability index may be expressed in terms of the safety margin as follows (Ang and Tang, 1984):

$$\beta_{ln} = \frac{\ln(E(M))}{\sqrt{V(R)^2 + V(Q)^2}} \qquad \text{Eq. 6.13}$$

where β_{ln} is the log-normal reliability index, *E(M)* is the mean of the safety margin and *V(R)* and V(Q) are the coefficient of variation for the resistance and load, respectively.

In addition, the log-normal reliability index may be calculated in terms of the safety factor as follows (Duncan, 2000):

$$\beta_{ln} = \frac{\ln\left(\frac{E(FS)}{\sqrt{1+V(FS)^2}}\right)}{\sqrt{\ln(1+V(FS)^2)}} \qquad \text{Eq. 6.14}$$

where β_{ln} is the log-normal reliability index, *E(FS)* is the mean safety margin and *V(M)* is the coefficient of variation of the safety margin. The coefficient of variation of the safety margin is defined as (Duncan 2000):

$$V(FS) = \frac{E(FS)}{s(FS)} \qquad \text{Eq. 6.15}$$

where *s(FS)* is the standard deviation of the safety factor, which can be defined using the approach of Duncan (2000) or Monte Carlo simulation.

The probability of failure corresponding to either of these reliability indices may also be calculated as follows (Ang and Tang, 1984):

$$P_f = \Phi(-\beta) = 1 - \Phi(\beta) \qquad \text{Eq. 6.16}$$

where Φ is the CDF function for the standard normal distribution.

6.4 Reliability Based Design/Analysis of Infinite Slopes

6.4.1 Background

The first-order, second-method approach, explained by Duncan (2000) for several different geotechnical applications, may be used to analyze the shear strength

of the internal or interface GCL shear strength in a layered system on a slope. This approach may be broken into five steps:

1. Define the mean safety factor *E(FS)* for the infinite slope (Equation 6.6) using the mean values of each parameter (Equation 6.7)
2. Calculate the standard deviations of the parameters (Equation 6.9)
3. Compute the safety factor with each parameter increased by one standard deviation (FS_i^+), and decreased by one standard deviation (FS_i^-) holding all other parameters held equal to their mean values. Find the difference between these two safety factors ($\Delta FS_i = FS_i^+ - FS_i^-$). Find the standard deviation of the safety factor using a Taylor Series Expansion:

$$s_{FS} = \sqrt{\left(\frac{\Delta FS_{\psi}}{2}\right)^2 + \left(\frac{\Delta FS_{t}}{2}\right)^2 + \left(\frac{\Delta FS_{C_A}}{2}\right)^2 + \left(\frac{\Delta FS_{\phi}}{2}\right)^2 + \left(\frac{\Delta FS_{\gamma}}{2}\right)^2} \qquad \text{Eq. 6.17}$$

   where ΔFS_{ψ} is the safety factor difference for the slope angle, ΔFS_t is the safety factor difference for the cover soil thickness, ΔFS_{CA} is the safety factor difference for the adhesion, ΔFS_{ϕ} is the safety factor difference for the slope angle, ΔFS_{γ} is the safety factor difference for the unit weight of the cover soil.
4. Calculate the coefficient of variation, *V(FS)* using Equation 6.15
5. Use *E(FS)* and *V(FS)* to find the reliability index according to Equation 6.14, and then calculate the probability of failure, P_f, according to Equation 6.16

6.4.2 Definition of Variables

The safety factor and the probability of failure for an infinite slope, which may be suitable for analysis of cover systems (Figures 6.1(a) and 6.1(b)) is calculated herein for different slope angles, ψ. The standard deviation of slope angle is fixed at 0.5^0. The unit weight of the soil overlying the interface has a mean of 20 kN/m^3 and a standard deviation of 1.5 kN/m^3. Two cover soil thicknesses, t_1 and t_2, will be considered, with mean values of 1 and 3 m, respectively, and each with a standard deviation of 0.1 m.

Definition of the mean and standard deviation for the intercept value and friction angle is straightforward. As an example, failure envelopes A5 and TH 11

from the GCLSS database for internal GCL and GCL-geomembrane interface shear strengths, respectively, are selected to conduct statistical and reliability based design procedures. For failure envelope A5, internal shear strength tests were conducted on GCL A, and for failure envelope TH 11, interface shear strength tests were conducted on the interface between GCL A and a textured HDPE geomembrane *s*. All of the tests were conducted under the exact same conditions: a time of hydration of 168 hours, a time of consolidation of 48 hours, and a shear displacement rate of 0.1 mm/min. For failure envelopes A5 and TH 11, 19 and 20 series, respectively, of three tests (at different normal stresses) were assembled. The intercept value and friction angle were then defined for each series. The mean and standard deviation of the intercept value and friction angle for all series were defined to represent the variability of each failure envelope. Tables 6.1 and 6.2 present the mean and standard deviation for the intercept value and friction angles representing internal GCL and GCL-geomembrane interface shear strength.

For the peak internal GCL shear strength data shown in Table 6.1, the intercept value has a mean and standard deviation of 30.43 kPa and 8.61 kPa, respectively, and the friction angle had a mean and standard deviation of 28.71^0 and 3.88^0, respectively. For the large-displacement data, the intercept value has a mean and standard deviation of 15.63 kPa and 9.49 kPa, respectively, and the friction angle had a mean and standard deviation of 8.96^0 and 2.43^0, respectively.

For the peak GCL-geomembrane interface shear strength data shown in Table 6.2, the intercept value has a mean and standard deviation of 7.43 kPa and 5.11 kPa, respectively, and the peak friction angle had a mean and standard deviation of 20.60^0 and 3.25^0, respectively. For the large-displacement data, the intercept value has a mean and standard deviation of 5.27 kPa and 2.47 kPa, respectively, and the friction angle had a mean and standard deviation of 12.28^0 and 1.81^0, respectively.

6.4.3 Formulation of Infinite Slope Problem

For each slope angle value, the mean safety factor and the probability of failure are calculated according to Equations 6.6 and 6.16 for the internal GCL and GCL-geomembrane interface peak and large-displacement shear strength values. The

factors of safety and the probabilities of failure may be plotted versus the slope angle to define a "reliability-based design chart". The reliability based charts for the peak and large displacement internal GCL shear strengths are presented in Figures 6.2 and 6.3. Similarly, the reliability based charts for the peak and large displacement GCL-geomembrane interface shear strengths are presented in Figures 6.4 and 6.5.

For design, a target probability of failure may be selected for a given soil cover thickness. From the reliability based chart, the corresponding safety factor may be found. Next the required slope angle may be found. Figure 6.6 shows Figure 6.4 with arrows highlighting a typical design process for the peak shear strength of a GCL-Geomembrane interface. For example, a target probability of failure of 0.01 was selected for a slope with a height of 1 meter is used. From the safety factor-probability of failure relationship, a safety factor of 2.3 is found. In a conventional analysis, this would appear very conservative. However, a probability of failure of 0.01 implies that 1 slope out of 100 is likely to fail. From the slope angle-safety factor relationship, a maximum slope angle of 19^0 can exist without exceeding the target probability of failure.

For analysis, the reverse process may be used. First, the actual slope angle is observed in the field. The safety factor may then be found from the reliability based chart, and the corresponding probability of failure may be found. Figure 6.7 shows Figure 6.2 with arrows highlighting a typical analysis process for the large-displacement internal shear strength of a GCL. For example, a slope angle of 20^0 with a slope cover thickness of 3 meters is used. From the slope-angle-safety factor relationship, the safety factor is found to be 1.2. From the safety factor-probability of failure relationship, the actual probability of failure was found to be 0.4. This is a very high probability of failure. Although the GCL is less likely to reach peak conditions for this same slope ($P_f \sim 0$ from Figure 6.2), the probability of failure is quite high for large-displacement conditions.

A conventional slope design may define the mean safety factor, but it provides no insight into the effects of the variability of the variables that are included in the definition of the safety factor. The design calculation in Figure 6.8 shows that a mean safety factor of 2.3 actually corresponds to a probability of failure of 0.01, while the

analysis calculation in Figure 6.9 shows that a safety factor of 1.2 corresponds to a probability of failure of 0.4. Although the factor of safety in Figure 6.8 is greater than 1.0, this does not assure that the probability of failure is close to zero. It must be noted that there is no fixed relationship between the probability of failure and the factor of safety that applies to all interfaces. The ability to distinguish the affects of variability emphasizes the usefulness of the reliability based design and analysis method to fully understand the behavior of a GCL slope.

6.7 Conclusions

This chapter presents an application of the data from the GCLSS database related to probability and reliability based design concepts. Using these concepts, it was possible to define reliability based design charts for a slope involving a GCL. The results of a conventional safety factor design of slopes were compared to reliability based design. The usefulness of reliability based design was stressed. The analysis techniques presented in this chapter may be useful in the design of engineering structures that use layered interfaces for hydraulic barriers or reinforcement.

Table 6.1: Development of Peak and Large Displacement Failure Envelope Parameters *c* and ϕ for an Internal GCL *A* Interface (t_H = 168 hours, t_C = 48 hours and SDR = 0.1 mm/min)

GCL Name	Shear Strength Data				Peak Failure Envelope		Large Displacement Failure	
	Normal Stress (kPa	Peak Shear Strength (kPa)	Large Displacement Shear Strength (kPa)	Average Final GCL Water Content (%)	Peak Friction Angle (Degrees)	Peak Intercept (kPa)	Large Displacement Friction Angle (Degrees)	Large Displacement Intercept (kPa)
A5 1	34.5	37.9	13.8	78.0	25.84	16.55	6.14	10.05
	137.9	75.8	24.8	78.0				
	310.3	169.6	43.4	78.0				
A5 2	34.5	46.9	18.6	78.5	29.75	27.78	9.17	13.79
	137.9	107.6	37.2	78.5				
	310.3	204.8	63.4	78.5				
A5 3	34.5	42.1	17.9	74.0	26.12	26.59	9.90	10.54
	137.9	96.5	32.4	74.0				
	310.3	177.9	65.5	74.0				
A5 4	34.5	50.3	33.8	81.5	30.73	38.81	7.99	28.66
	137.9	135.1	47.6	81.5				
	310.3	217.9	72.4	81.5				
A5 5	34.5	41.4	31.7	73.5	34.79	17.63	11.78	25.51
	137.9	113.8	55.8	73.5				
	310.3	233.0	89.6	73.5				
A5 6	34.5	46.2	24.1	78.0	31.16	27.28	12.54	18.22
	137.9	113.8	51.7	78.0				
	310.3	213.7	86.2	78.0				
A5 7	34.5	46.2	18.6	72.5	28.99	29.45	9.00	14.28
	137.9	109.6	37.9	72.5				
	310.3	199.9	62.7	72.5				
A5 8	34.5	49.6	14.5	72.0	33.12	30.63	12.21	9.55
	137.9	126.2	43.4	72.0				
	310.3	231.0	75.2	72.0				
A5 9	34.5	46.2	38.6	75.5	25.19	27.97	4.96	36.15
	137.9	89.6	49.0	75.5				
	310.3	175.1	62.7	75.5				
A5 10	34.5	39.3	17.2	75.5	29.44	18.62	11.99	9.95
	137.9	94.5	39.3	75.5				
	310.3	194.4	75.8	75.5				
A5 11	34.5	46.2	15.9	71.0	29.30	29.45	10.22	7.78
	137.9	111.0	29.6	71.0				
	310.3	202.0	64.8	71.0				
A5 12	34.5	55.2	#N/A	91.9	33.73	37.13	#N/A	#N/A
	137.9	137.2	#N/A	65.6				
	310.3	241.3	#N/A	58.7				
A5 13	34.5	49.0	8.3	107.8	21.26	36.25	6.62	1.77
	137.9	91.0	13.8	94.5				
	310.3	156.5	39.3	59.0				
A5 14	34.5	44.1	15.2	73.0	21.64	39.60	5.40	13.99
	137.9	108.9	30.3	73.0				
	310.3	157.2	42.1	73.0				
A5 15	34.5	53.1	31.0	71.5	28.01	45.41	7.84	26.10
	137.9	135.8	44.8	71.5				
	310.3	204.1	68.9	71.5				
A5 16	34.5	43.4	11.7	76.0	32.84	22.56	9.95	5.32
	137.9	113.8	29.0	76.0				
	310.3	222.0	60.0	76.0				
A5 17	34.5	58.6	32.4	79.0	26.24	44.82	6.84	28.27
	137.9	117.9	44.8	79.0				
	310.3	195.8	65.5	79.0				
A5 18	34.5	51.7	9.7	88.5	25.42	36.84	7.51	7.29
	137.9	104.8	29.0	88.5				
	310.3	183.4	46.9	88.5				
A5 19	34.5	44.1	21.4	72.5	31.88	24.72	11.21	14.09
	137.9	113.8	40.7	72.5				
	310.3	216.5	75.8	72.5				
			Average		**28.71**	**30.43**	**8.96**	**15.63**
			Standard Deviation		**3.88**	**8.61**	**2.43**	**9.49**
			COV		**0.14**	**0.28**	**0.27**	**0.61**

Table 6.2: Development of Peak and Large Displacement Failure Envelope Parameters *c* and ϕ for the Interface between GCL *A* and an 80-mil Geomembrane *s* (t_H = 168 hours, t_C = 48 hours and SDR = 0.1 mm/min)

GCL Name	Shear Strength Data				Peak Failure Envelope		Large Displacement Failure	
	Normal Stress (kPa	Peak Shear Strength (kPa)	Large Displacement Shear Strength (kPa)	Final Water Content (%)	Peak Friction Angle (Degrees)	Peak Intercept (kPa)	Large Displacement Friction Angle (Degrees)	Large Displacement Intercept (kPa)
TH 11 1	34.5	20.0	13.8	61.0	20.70	4.92	13.47	2.36
	137.9	53.8	30.3	61.0				
	310.3	123.4	78.6	61.0				
TH 11 2	34.5	17.2	13.8	62.5	20.99	1.48	12.37	4.92
	137.9	50.3	33.1	62.5				
	310.3	122.0	73.8	62.5				
TH 11 3	34.5	20.0	12.4	73.0	16.12	7.29	11.68	2.36
	137.9	42.7	26.2	73.0				
	310.3	98.6	68.3	73.0				
TH 11 4	34.5	19.3	13.1	73.5	18.32	7.19	11.04	6.30
	137.9	51.7	33.1	73.5				
	310.3	110.3	66.9	73.5				
TH 11 5	34.5	17.2	11.0	76.0	16.83	5.12	9.63	3.74
	137.9	44.1	24.8	76.0				
	310.3	100.0	57.2	76.0				
TH 11 6	34.5	16.5	11.0	75.0	20.45	6.89	12.24	7.39
	137.9	63.4	43.4	75.0				
	310.3	120.7	72.4	75.0				
TH 11 7	34.5	19.3	9.7	83.5	26.03	5.32	14.27	1.38
	137.9	77.2	37.2	83.5				
	310.3	155.1	80.0	83.5				
TH 11 8	34.5	18.6	12.4	78.0	15.83	15.07	12.61	5.61
	137.9	64.1	37.9	78.0				
	310.3	99.3	74.5	78.0				
TH 11 9	34.5	14.5	9.7	71.5	16.50	12.12	12.01	3.94
	137.9	65.5	35.9	71.5				
	310.3	99.3	68.9	71.5				
TH 11 10	34.5	24.1	13.1	87.0	21.77	5.61	9.78	7.19
	137.9	53.1	31.0	72.3				
	310.3	132.4	60.7	67.4				
TH 11 11	34.5	18.6	11.7	89.7	20.09	2.07	10.07	3.84
	137.9	46.2	25.5	70.3				
	310.3	117.9	60.0	51.7				
TH 11 12	34.5	18.6	14.5	84.6	16.38	12.71	10.05	10.34
	137.9	60.0	37.9	64.2				
	310.3	101.4	64.1	63.8				
TH 11 13	34.5	16.5	12.4	74.0	20.86	0.98	12.52	3.35
	137.9	49.6	31.7	74.0				
	310.3	120.7	73.1	74.0				
TH 11 14	34.5	27.6	15.2	72.0	27.20	10.64	14.28	5.02
	137.9	82.7	37.9	72.0				
	310.3	169.6	84.8	72.0				
TH 11 15	34.5	25.5	15.9	69.5	23.85	12.31	15.86	6.70
	137.9	76.5	46.9	69.5				
	310.3	148.2	94.5	69.5				
TH 11 16	34.5	31.7	19.3	73.5	22.89	20.78	14.69	10.44
	137.9	84.8	46.9	73.5				
	310.3	149.6	91.7	73.5				
TH 11 17	34.5	21.4	13.8	71.0	23.24	3.55	13.05	4.53
	137.9	57.9	34.5	71.0				
	310.3	138.6	77.2	71.0				
TH 11 18	34.5	17.2	14.5	67.5	23.04	5.81	13.68	5.42
	137.9	69.6	37.9	67.5				
	310.3	135.8	81.4	67.5				
TH 11 19	34.5	18.6	11.7	76.0	20.23	6.89	13.10	1.87
	137.9	59.3	31.0	76.0				
	310.3	120.7	75.2	76.0				
TH 11 20	34.5	19.3	13.8	74.5	20.76	1.77	10.34	5.81
	137.9	46.9	28.3	74.5				
	310.3	122.0	63.4	74.5				
			Average		**20.60**	**7.56**	**12.28**	**5.27**
			Standard Deviation		**3.34**	**5.21**	**1.81**	**2.47**
			COV		**0.16**	**0.69**	**0.15**	**0.47**

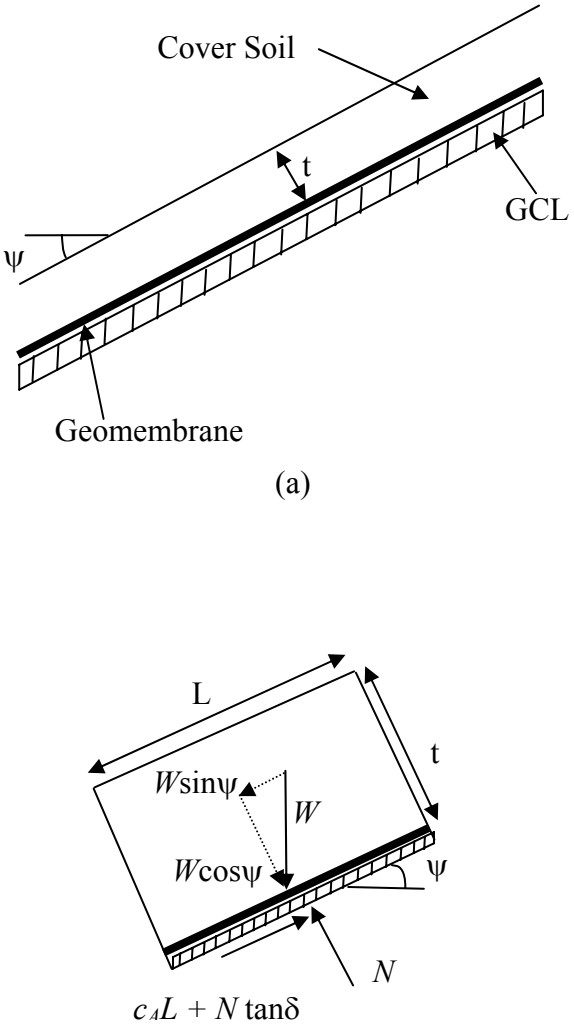

Figure 6.1: Definition of Variables for an Infinite Slope Situation; (a) Names of Different Layers, (b) Free-Body Diagram

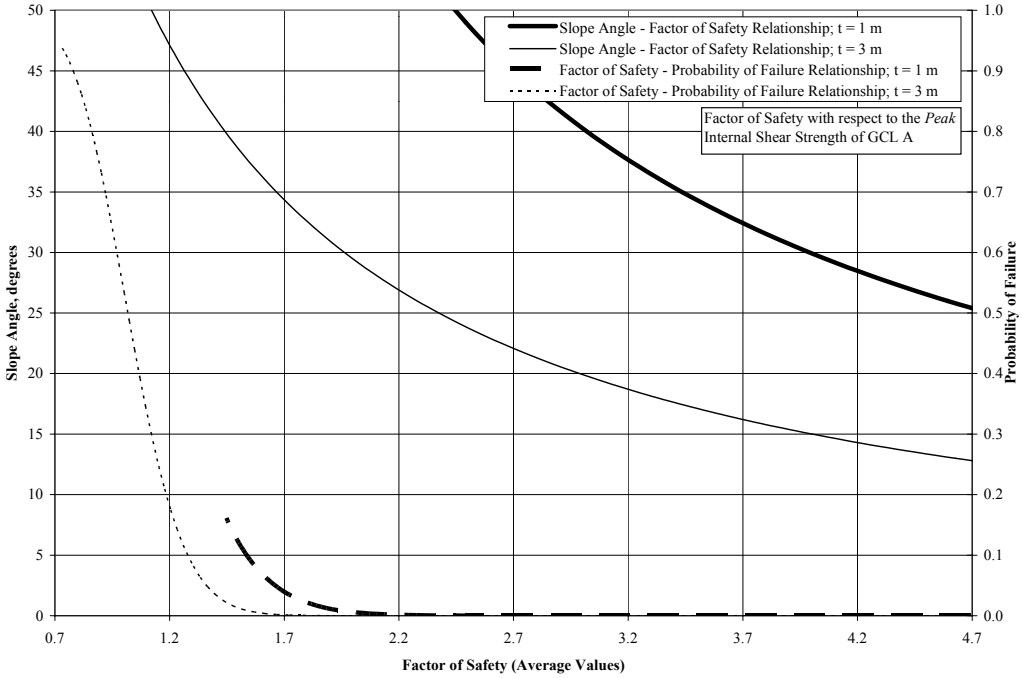

Figure 6.2: Reliability Based Design Chart for Internal GCL Shear Strength; Peak

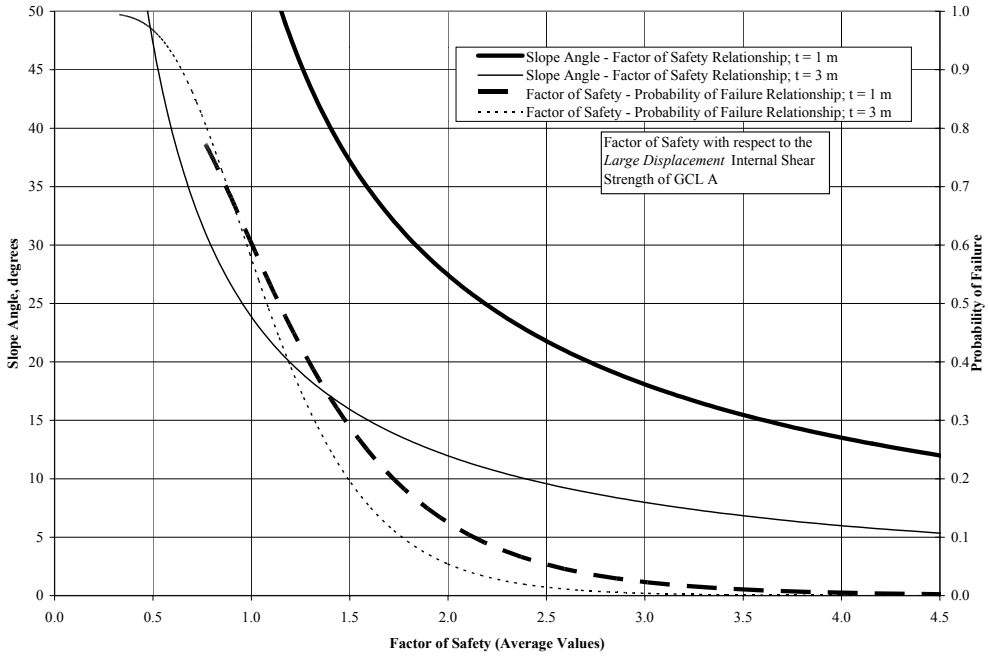

Figure 6.3: Reliability Based Design Chart for Internal GCL Shear Strength; Large Displacement

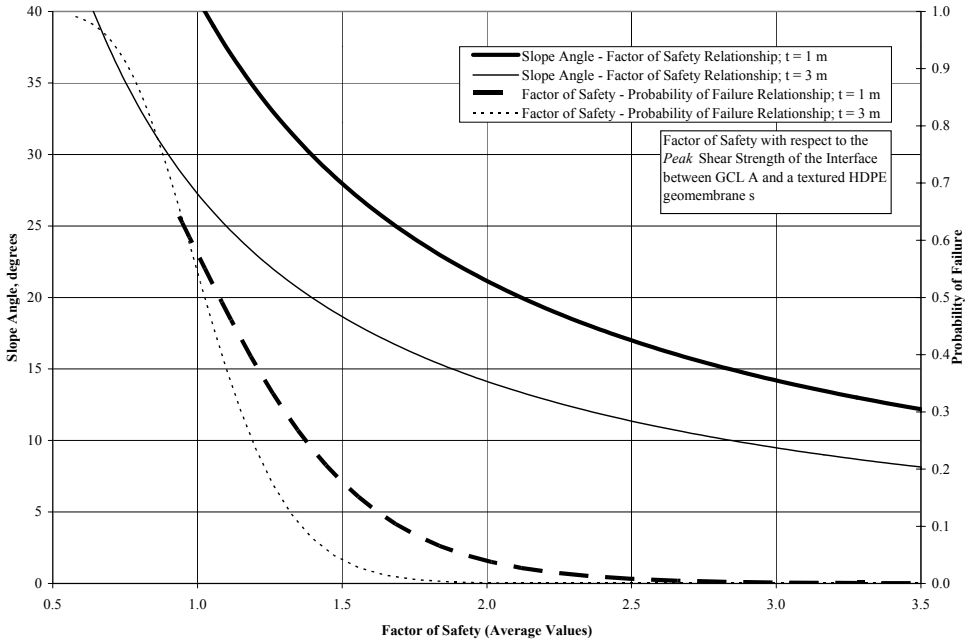

Figure 6.4: Reliability Based Design Chart for Shear Strength of the GCL-Geomembrane Interface; Peak

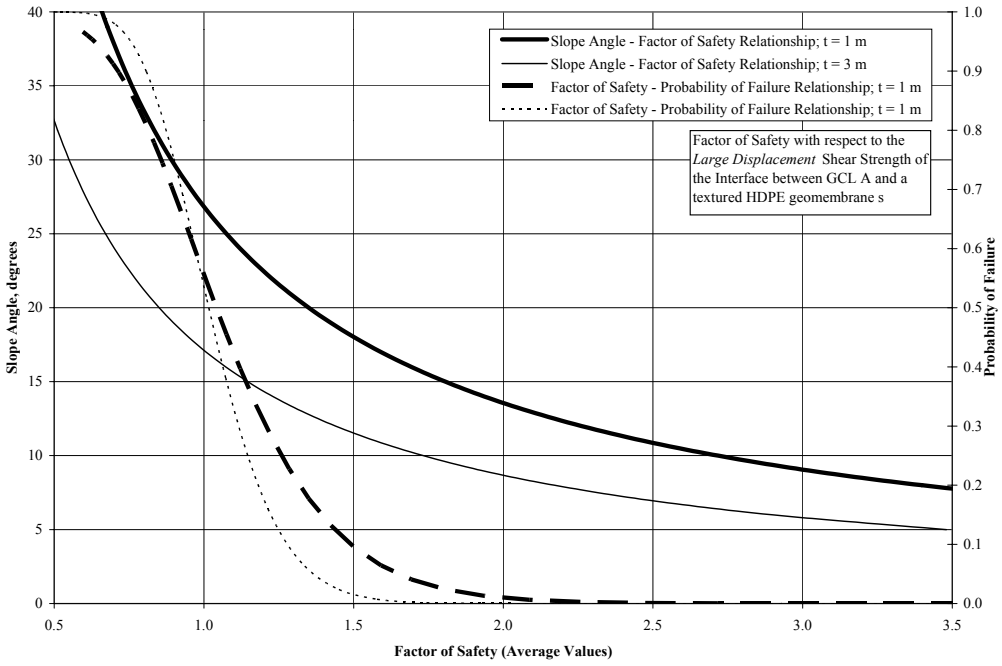

Figure 6.5: Reliability Based Design Chart for Shear Strength of the GCL-Geomembrane Interface; Large Displacement

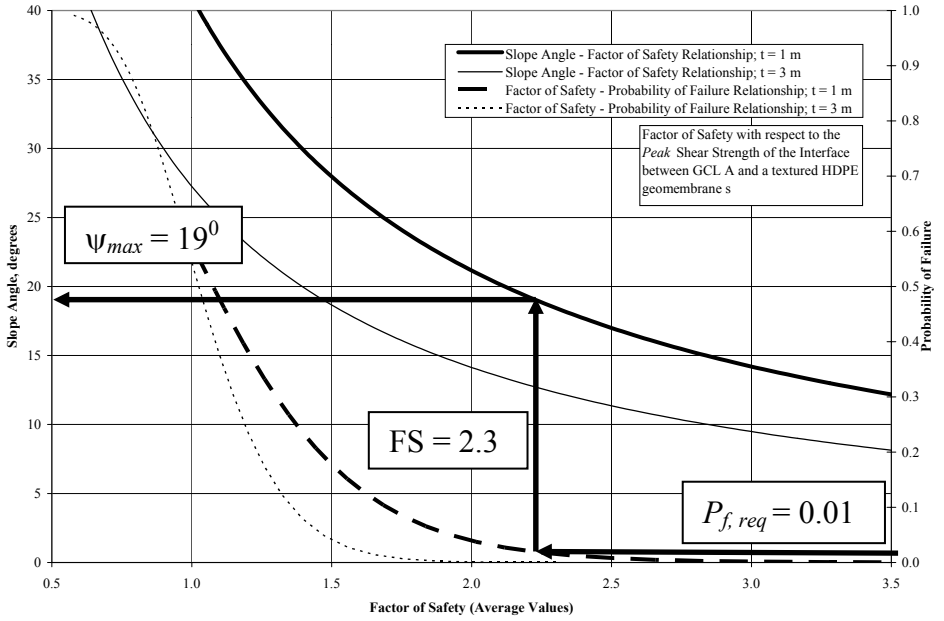

Figure 6.6: Reliability Based Chart for Peak GCL-Geomembrane Interface Shear Strength; Arrows for Reliability Based *Design* of a Slope with Height of 1 meters and Required Probability of Failure of 0.01

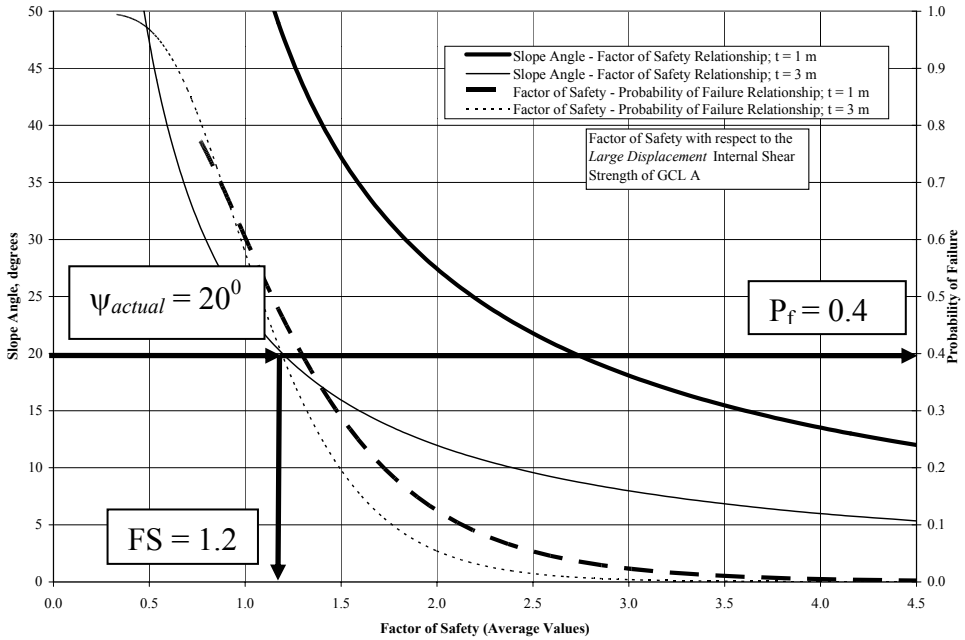

Figure 6.7: Reliability Based Chart for Large Displacement Internal GCL Shear Strength; Arrows for Reliability Based *Analysis* of a Slope with a Height of 3 meters and a Slope Angle of 20^0

7 Summary and Conclusions

7.1 Summary

The low internal and interface shear strengths of GCLs in layered systems as well as the variability of direct shear test results are significant concerns that must be addressed by designers of hydraulic barriers involving GCLs. This report provides understanding of these concerns by summarizing past discussions on GCL internal and interface shear strength, as well as presenting new findings and design applications. A thorough grasp on the behavior of the materials involved in GCLs and critical GCL interfaces (*i.e.* sodium bentonite clay, GCLs and geomembranes) was initially presented. In addition, the basic concepts of shear strength testing for these materials were introduced. A state-of-the-art literature review on issues affecting internal and interface GCL shear strength was included in this report. This review evaluates reported responses of GCLs to different testing parameters such as the time of hydration, time of consolidation, shear displacement rate, and normal stresses during hydration, consolidation and testing. The review also presents several mechanisms that have been suggested to explain the internal and interface shear strength behavior of GCLs as well as the shear strength behavior of sodium bentonite clay.

A significant database of shear strength results (*i.e.* the GCLSS database) was presented in this report. The GCLSS database is probably the largest compilation of GCL shear strength test results available, with a total of 320 internal GCL test results and 332 GCL-geomembrane interface test results. The direct shear tests were conducted at different confining pressures with different test conditions, as the test results were generated for specific projects. A significant amount of information is present, and it has the advantage of being compiled from a single laboratory, which eliminates a significant source of variability in testing procedures. The GCLSS database extends the scarce database of shear strength information currently available for GCL internal and interface shear strength. Two important features of the GCLSS database should be highlighted: (*i*) the test conditions used by the SGI® laboratory are consistent with the current standard, ASTM D6234, even before it was officially issued, and (*ii*) the wide range of normal stresses at which the GCL specimens were

sheared. This implies that all of the shear strength test results are consistent with current test procedures, may be compared to new test results and are applicable to the design of both landfill cover and base liner systems.

This report analyzes both the internal and interface GCL shear strength. Ranges of effective friction angles were developed for different sets of GCLs or test conditions to identify the sensitivity of the peak and large-displacement shear strength to different material characteristics or test conditions. Correlation coefficients between the different strength parameters were developed for further understanding of the trends in the shear strength observed in the effective friction angle analysis, which may also be useful for probabilistic analyses. A failure envelope analysis for GCLs with similar test conditions was conducted to investigate the changes in shear strength for different GCLs with normal stress. Based on the conclusions of the failure envelope analysis, the effects of the time of hydration, the time of consolidation, the shear displacement rate on the peak and large-displacement shear strengths were investigated. In addition, the variability in shear strength under constant test conditions, the relationship between the shear strength and the final water content, and the variation in the displacement at peak shear strength were also investigated.

7.2 Conclusions on Internal GCL Shear Strength

The wide range of normal stresses and test conditions are suitable for investigation of the behavior of the internal GCL shear strength. Trends in the shear strength data were developed with the normal stress, time of hydration, time of consolidation, shear displacement rate, final GCL water content, and shear displacement at failure. In addition, the variability of the internal GCL shear strength was investigated using statistical methods. In general, it was found that the GCL internal shear strength increases with increasing normal stresses, times of consolidation and shear displacement rates at low normal stresses (i.e. below 100 kPa), and that it decreases with increasing times of hydration, and shear displacement rates at high normal stresses (*i.e.* above 200 kPa). The variability of the internal GCL

shear strength was found to increase with normal stress, and that the variability in the peak shear strength was greater than the large-displacement shear strength.

The shear strength envelopes evaluated in the analysis of the GCLSS database typically show non-linear trends for a wide range of normal stresses. A bilinear failure envelope for high and low normal stresses was employed in these situations. For low normal stresses, the friction angle was comparatively high while the intercept value was low, and for high normal stresses, the friction angle was low while the intercept was high. The intersection between the high and low normal stress failure envelopes fell within the range of the swell pressure of reinforced GCLs (*i.e.* 100-200 kPa). The swelling behavior of sodium bentonite potentially may have a large affect on the shear strength of GCLs.

Non-thermally bonded needle-punched GCLs were found to have higher peak shear strengths than thermally bonded needle-punched GCLs, stitch-bonded GCLs and unreinforced GCLs. Different mechanisms are suggested for differences in shear strength behavior, such as the swelling of sodium bentonite, extrusion of sodium bentonite from the GCL, fiber reinforcement rupture, fiber reinforcement pullout from the GCL carrier geotextiles, and GCL-geomembrane interlocking. In addition, it was found that reinforced GCLs had higher large-displacement shear strengths than unreinforced GCLs. Needle-punched GCLs were found to have higher large-displacement shear strengths than stitch-bonded GCLs.

7.3 Conclusions on GCL-Geomembrane Interface Shear Strength

The shear strength of the interface between a GCL and a geomembrane is consistently below the internal GCL shear strength. In general, it was found that the interface shear strength increases with increasing times of hydration, that it decreases with increasing times of consolidation, and that it is unaffected by changing shear displacement rates. The decrease in shear strength with increasing times of consolidation was attributed to the low hydration normal stress used when GCLs were subsequently consolidated. Similar to the internal GCL shear strength, a large amount of variability in the GCL-geomembrane interface shear strength was

observed. The variability tended to increase with normal stress, and was greater for peak shear strength than large-displacement shear strength.

Unhydrated conditions result in the highest shear strength for the GCL-geomembrane interface, as there is little sodium bentonite extrusion and maximum interlocking between the GCL and the geomembrane. Encapsulation of the sodium bentonite between two geomembranes (*i.e.* interfaces involving GCL *K*) results in shear strength values similar to unreinforced, unhydrated sodium bentonite.

It was found that the type of GCL may significantly affect the interface shear strength. The non-thermally bonded needle-punched GCLs (GCL *A*) have greater peak shear strength than interfaces with other GCLs. The interfaces between thermally bonded needle-punched GCLs (*i.e.* GCL *C*) and a textured geomembrane have lower shear strength values than those of non-thermally bonded needle-punched GCLs. Interfaces involving stitch-bonded GCLs (*i.e.* GCL B) and a geomembrane have lower shear strength than needle-punched GCLs for both textured and smooth geomembranes. The shear strength of the smooth geomembrane interfaces is not sensitive to the GCL product involved in the interface.

This study found that geomembrane polymers (*i.e.* LLDPE, VLDPE, HDPE, or PVC) have a significant effect on peak and large displacement shear strengths. In addition, the similar geomembrane polymers manufactured by different companies were found to have slightly different peak and large displacement shear strengths. These differences are most likely due to different texturing procedures used by different manufactures rather than different polymer types. Geomembrane thickness was found to have little effect on the shear strength of a GCL-geomembrane interface.

7.4 Suggestions for Laboratory Procedures

When designing a slope that includes GCL, it is anticipated that laboratory testing will be required to investigate the effects of site-specific conditions. This report has many conclusions that aid in the formulation of a successful laboratory testing program:

- The amount of hydration necessary to decrease the shear strength to an unacceptable level should be quantified. Further reduction in shear strength is seldom observed for times of hydration beyond 48 hours.
- It should be identified if the GCL in the field hydrates before the application of a normal stress in the field. To decrease the amount of bentonite extrusion and to ensure good frictional connection between the geomembrane asperities and the carrier geotextile of the GCL, a large normal stress may be applied before hydration (in the field and in the laboratory). This also prevents the need to consolidate the specimen after hydration, saving time.
- The shear displacement rate used in the laboratory should be slow enough (i.e. below 1.0 mm/min) to ensure drained conditions throughout shearing. However, the magnitude of the shear displacement rate required to obtain the lowest shear strength for different levels of normal stress should be understood. For low normal stresses, the lowest shear strength is obtained at slow shear displacement rates (i.e. 0.0015 mm/min). For high normal stresses, the lowest shear strength is obtained at fast shear displacement rates (*i.e.* 1.0 mm/min).
- Trends should not be interpolated from low normal stresses to high normal stresses or vice-versa.

This chapter presents an application of the data from the GCLSS database related to probability and reliability based design concepts. Using these concepts, it was possible to define reliability based design charts for a slope involving a GCL. The differences in reliability based design and conventional stability design methods were discussed. The analysis techniques presented in this chapter may be useful in the design of engineering structures that use layered interfaces for hydraulic barriers or reinforcement.

References

Ang, A., and Tang, W. (1975). Probability Concepts in Engineering Planning and Design, Volume I – Basic Principles. John Wiley and Sons, Inc.

Ang, A. and Tang, W. (1984). Probability Concepts in Engineering Planning and Design, Volume II – Decision, Risk, and Reliability. John Wiley & Sons, Inc.

Arthur, J.R.F., Dalili, A. and Dunstan, T. (1988). "Sixth Geotechnique Symposium in Print: The Engineering Application of Direct and Simple Shear Testing." Geotechnique, 38(1), 139-154.

ASTMD5321. (1992). "Standard Test Method for Determining the Coefficient of Soil and Geosynthetic of Geosynthetic and Geosynthetic Friction by the Direct Shear Method." American Society of Testing and Materials, West Conshocken, Pennsylvania, USA.

ASTMD6243. (1998). "Standard Test Method for Determining the Internal and Interface Shear Resistance of Geosynthetic Clay Liner by the Direct Shear Method." American Society of Testing and Materials, West Conshocken, Pennsylvania, USA.

Bachus, R. C., and Swan, R. H. (1993). "Shear Strength of Geosynthetic Clay Liners." Geosynthetic Clay Liner Workshop, USEPA, Cincinnati, OH.

Bemben, S., and Schulze, D. (1997). "Shear Strength of Reinforced Geosynthetic Clay Liner (Discussion)." Journal of Geotechnical and Geoenvironmental Engineering, ASCE, 124(12), 1177-1178.

Berard, J. F. (1997). "Evaluation of Needle-Punched Geosynthetic Clay Liners Internal Friction." Geosynthetics '97, St. Paul, MI, 351-362.

Bonaparte, R., Othman, M. A., Rad, N. S., Swan, R. H., and Vander Linde, D. L. (1996). "Appendix F: Evaluation of Various Aspects of GCL Performance." Report of 1995 Workshop on Geosynthetic Clay Liners, D. E. Daniel and H. Scranton, B., eds., Cincinnati, OH, F1-F34.

Bouazza, A. (2002). "Geosynthetic Clay Liners." Geotextiles and Geomembranes, 20, 3-17.

Code of Federal Regulations, 40 CFR. "Protection of Environment." The office of the Federal Register National Archives and Records Administration. U.S.

Printing Office, Washington, D.C. 40 CFR 258, pp. 355-392 and 40 CFR 264, pp. 154-330.

Daniel, D. E., and Shan, H. Y. (1991). "Results of Direct Shear Tests on Hydrated Bentonitic Blankets." Geotechnical Engineering Center, University of Texas at Austin, Austin, TX.

Daniel, D. E., Shan, H. Y., and Anderson, J. D. (1993). "Effects of Partial Wetting on the Performance of the Bentonite Component of a Geosynthetic Clay Liner." Geosynthetics '97, St. Paul, MN.

Daniel, D. E., Carson, D. A., Bonaparte, R., Koerner, R. M., and Scranton, H. B. (1998). "Slope Stability of Geosynthetic Clay Liner Test Plots." Journal of Geotechnical and Geoenvironmental Engineering, ASCE, 124(7), 628-637.

Dove, J. E., and Frost, J. D. (1999). "Peak Friction Behavior of Smooth Geomembrane-Particle Interfaces." Journal of Geotechnical and Geoenvironmental Engineering, ASCE, 125(7), 544-555.

Duncan, J. M. (2000). "Factors of Safety and Reliability in Geotechnical Engineering." Journal of Geotechnical and Geoenvironmental Engineering, ASCE, 126(4), 307-316.

Eid, H. T., and Stark, T. D. (1997). "Shear Behavior of an Unreinforced Geosynthetic Clay Liner." Geosynthetics International, IFAI, 4(6), 645-659.

Eid, H. T., Stark, T. D., and Doerfler, C. K. (1999). "Effect of Shear Displacement Rate on Internal Shear Strength of a Reinforced Geosynthetic Clay Liner." Geosynthetics International, IFAI, 6(3), 219-239.

Environmental Protection, Inc. (1999). "PVC Geomembrane Interface Strengths." PGI Technical Bulletin. PVC Geomembrane Institute, University of Illinois. Urbana, IL.

Feki, N., Garcin, P., and Berroir, G. (1996). "Shear Strength Tests on Geosynthetic Liner Systems." Geosynthetics: Applications, Design and Construction, D. Groot, D. Hoedt, and Termaat, eds., A.A. Balkema, Rotterdam, The Netherlands, 787-794.

Feki, N., Garcin, P., Faure, Y., Gourc, J., and Berroir, G. (1997). "Shear Strength of Geosynthetic Clay Liner Systems." Geosynthetics '97, St. Paul, MN, 899-912.

Fox, P. J., Scheithe, J. R., and Rowland, M. G. (1997). "Shear Strength of Reinforced Geosynthetic Clay Liner (Discussion)." Journal of Geotechnical and Geoenvironmental Engineering, ASCE, 124(12), 1178-1179.

Fox, P. J., Rowland, M. G., and Scheithe, J. R. (1998). "Internal Shear Strength of Three Geosynthetic Clay Liners." Journal of Geotechnical and Geoenvironmental Engineering, ASCE, 124(10), 933-944.

Fox, P. J. (1998). "Research on Geosynthetic Clay Liners at Purdue University." Geotechnical News, 16(1), 35-40.

Frobel, R. K. (1996). "Geosynthetic Clay Liners, Part Four: Interface and Internal Shear Strength Determination." Geosynthetics Fabric Report, October/November, 20-23.

Geosyntec Consultants. (1995). "Testing Procedure: Interface and Internal Direct Shear Testing." Soil-Geosynthetics Interaction Testing Laboratory, Atlanta, GA.

Gilbert, R. B., Fernandez, F. F., and Horsfield, D. (1996). "Shear Strength of a Reinforced Clay Liner." Journal of Geotechnical and Geoenvironmental Engineering, ASCE, 122(4), 259-266.

Gilbert, R. B., Scranton, H. B., and Daniel, D. E. (1997). "Shear Strength Testing for Geosynthetic Clay Liners." Testing and Acceptance Criteria for Geosynthetic Clay Liners, L. Well, ed., American Society for Testing and Materials, Philadelphia, 121-138.

Gilbert, R. B., Fernandez, F. F., and Horsfield, D. (1997). "Shear Strength of Reinforced Geosynthetic Clay Liner (Discussion Closure)." Journal of Geotechnical and Geoenvironmental Engineering, ASCE, 124(12), 1179-1180.

Giroud, J. P., Darrasse, J., and Bachus, R. C. (1993). "Hyperbolic Expression for Soil-Geosynthetic or Geosynthetic Interface Shear Strength." Geotextiles and Geomembranes, 12, 275-286.

Hewitt, R. D., Soydemir, C., Stulgis, R. P., and Coombs, M. T. (1997). "Effect of Normal Stress During Hydration and Shear on the Shear Strength of GCL/Textured Geomembrane Interfaces." Testing and Acceptance Criteria for

Geosynthetic Clay Liners, L. Well, ed., American Society for Testing and Materials, Philadelphia, 55-71.

Koerner, R. M., Martin, J. P., and Koerner, G. R. (1986). "Shear strength parameters between geomembranes and cohesive soil." Geotextiles and Geomembranes, 4(1), 21-30.

Koerner, R. M. (1996). "Geosynthetic Clay Liners, Part One: An Overview." Geosynthetics Fabric Report, May, 22-24.

Koerner, R. M. (1999). Designing With Geosynthetics, Prentice Hall, Inc., New Jersey.

Kovacevic Zelic, B., Znidarcic, D., and Kovacic, D. (2002). "Shear Strength Testing on Claymax 200R." 7th International Conference on Geosynthetics, Nice, France.

Kulhawy, F. H. (1990). Manual on Estimating Soil Properties for Foundation Design, Electric Power Research Institute Report EL-6800, Palo Alto, California.

Lake, C. G., and Rowe, R. K. (2000). "Swelling Characteristics of Needle-Punched, Thermally Treated Geosynthetic Clay Liners." Geotextiles and Geomembranes, 18, 77-101.

Lambe, W.T. and Whitman, R.V. (1969). Soil Mechanics. Massachusetts Institute of Technology. John Wiley and Sons, New York.

Ling, H. I., Pamuk, A., Dechasakulsom, M., Mohri, Y., and Burke, C. (2001). "Interactions between PVC Geomembranes and Compacted Clays." Journal of Geotechnical and Geoenvironmental Engineering, ASCE, 127(11), 950-954.

Lupini, J. F., Skinner, A. E., and Vaughan, P. R. (1981). "The Drained Residual Strength of Cohesive Soils." Geotechnique, 31(2), 181-213.

Marr, W. A. (2001). "Interface and Internal Shear Testing Procedures to Obtain Peak and Residual Values." 15th GRI Conference: Hot Topics in Geosynthetics (Peak/Residual; RECMs; Installation; Concerns), Houston, TX, 1-27.

Mesri, G., and Olson, R. E. (1970). "Shear Strength of Montmorillonite." Geotechnique, 20(3), 261-270.

Mitchell, J.K. (1994). Fundamentals of Soil Behavior. University of California, Berkeley. John Wiley and Sons, New York.

Muller-Vonmoos, M., and Loken, T. (1989). "The Shearing Behavior of Clays." Applied Clay Science, 4(2), 125-141.

Neter, J., and Wasserman, W. (1974). Applied Linear Statistical Models: Regression, Analysis of Variance and Experimental Designs, Richard D. Irwin, Inc., Homewood, Illinois.

Pavlik, K. L. (1997). "U.S. Army Corps of Engineers GCL Interface Testing Program." Geosynthetics '97, St. Paul, MN, 877-884.

Petrov, R. J., Rowe, R. K., and Quigley, R. M. (1997). "Selected Factors Influencing GCL Hydraulic Conductivity." *Journal of Geotechnical and Geoenvironmental Engineering, ASCE*, 123(8), 683-695.

Richardson, G. N. (1997). "GCL Internal Shear Strength Requirements." Geosynthetics Fabric Report, March, 20-25.

Sharma, H. D., Hullings, D. E., and Greguras, R. F. (1997). "Interface Strength Tests and Application to Landfill Design." Geosynthetics '97, St. Paul, MI, 913.

Siebken, J. R., Swan Jr., R. H., and Yuan, Z. (1996). "Short Term Creep Shear Characteristics for Geosynthetic Clay Liners." Testing and Acceptance Criteria for Geosynthetic Clay Liners, L. Well, ed., American Society for Testing and Materials, Philadelphia.

Skempton, A. W. (1985). "Residual Strength of Clays in Landslides, Folded Strata and the Laboratory." Geotechnique, 35(1), 3-18.

Snow, M., Mansour, R., Swan Jr., R. H., and Kavazanjian Jr., E. (1998). "Variability of Interface Shear Strengths." Sixth International Conference on Geosynthetics, Roseville, MN, 315-320.

Stark, T. D., and Eid, H. T. (1996). "Shear Behavior of a Reinforced Geosynthetic Clay Liner." Geosynthetics International, IFAI, 3(6), 771-785.

Stark, T. D. (1998). "Bentonite Migration in Geosynthetic Clay Liners." Sixth International Conference on Geosynthetics, Roseville, MN, 315-320.

Stark, T. D., Arellano, D., Evans, W. D., Wilson, V. L., and Gonda, J. M. (1998). "Unreinforced Geosynthetic Clay Liner Case History." Geosynthetics International, IFAI, 5(5), 521-544.

Stoewahse, C., Nixon, N., Jones, D. R. V., Blumel, W., and Kamugisha, P. (2002). "Geosynthetic Interface Shear Behavior." Ground Engineering, February 2002, 35-41.

Swan Jr., R. H., Yuan, Z., and Bachus, R. C. (1996). "Factors Influencing Laboratory Measurement of the Internal and Interface Shear Strength of GCLs." American Society for Testing and Materials Symposium on Testing and Acceptance Criteria for Geosynthetic Clay Liners, Atlanta, GA.

Swan Jr., R. H., Yuan, Z., and Bachus, R. C. (1999). "Key Factors Influencing Laboratory Measurement of the Internal and Interface Shear Strength of GCLs." American Society for Testing and Material Symposium on Grips, Clamps, Clamping Techniques and Strain Measurement for Testing Geosynthetics, Memphis, TN.

Trauger, R. J., Swan Jr., R. H., and Yuan, Z. (1996). "Long-Term Shear Strength Behavior of a Needle-Punched Geosynthetic Clay Liner." Testing and Acceptance Criteria for Geosynthetic Clay Liners, L. Well, ed., American Society for Testing and Materials, Philadelphia.

Triplett, E. J., and Fox, P. J. (2001). "Shear Strength of HDPE Geomembrane/Geosynthetic Clay Liner Interfaces." Journal of Geotechnical and Geoenvironmental Engineering, ASCE, 127(7), 543-552.

von Maubeuge, K. P., and Ehrenberg, H. (2000). "Comparison of Peel Bond and Shear Tensile Test Methods for Needle-Punched Geosynthetic Clay Liners." Geotextiles and Geomembranes, 18, 203-214.

Williams, N. D., and Houlihan, M. (1986). "Evaluation of Friction Coefficients between Geomembranes, Geotextiles and Related Products." Proc., Third International Conference on Geotextiles, 891-896.

Wroth, C. P. (1987). The Behavior of Normally Consolidated Clay as Observed in Undrained Direct Shear Tests. *Geotechnique*, 37, No. 1, 37-43.

Appendix A

The GCLSS Database

Internal GCL Interfaces

GCL Manufacturer	GCL Description	Normal Stress (kPa)	Peak Shear Strength (kPa)	Large Displacement Shear Strength (kPa)	GCL Final Water Content (%)	Hydration Time (hrs)	Hydration Normal Stress (kPa)	Consolidation Time (hrs)	Consolidation Normal Stress (kPa)	Shear Displacement Rate (mm/min)	Hydration Procedure	Reinforcement Type
Bentofix	NS	7.2	13.9	7.8	107	24	7.2	0	0.0	0.5	Soaked in Tap Water	NP W-NW, TB
Bentofix	NS	9.7	20.7	10.3	75	24	55.2	0	0.0	0.2	Soaked in Tap Water	NP W-NW, TB
Bentofix	NS	9.7	22.8	11.0	75	24	55.2	0	0.0	0.2	Soaked in Tap Water	NP W-NW, TB
Bentofix	NS	14.4	19.5	10.2	107	24	14.4	0	0.0	0.5	Soaked in Tap Water	NP W-NW, TB
Bentofix	NS	21.5	26.6	11.8	107	24	21.5	0	0.0	0.5	Soaked in Tap Water	NP W-NW, TB
Bentofix	NS	34.5	32.4	8.3	84.4	168	20.7	48	34.5	0.1	Soaked in Tap Water	NP W-NW, TB
Bentofix	NS	48.3	53.8	20.0	75	24	55.2	0	0.0	0.2	Soaked in Tap Water	NP W-NW, TB
Bentofix	NS	48.3	59.3	21.4	75	24	55.2	0	0.0	0.2	Soaked in Tap Water	NP W-NW, TB
Bentofix	NS	48.3	60.0	25.5	80	24	48.3	0	0.0	0.5	Soaked in Tap Water	NP W-NW, TB
Bentofix	NS	48.3	52.4	37.9	83.5	24	48.3	0	0.0	0.5	Soaked in Tap Water	NP W-NW, TB
Bentofix	NS	95.8	57.4	27.6	112.5	24	95.8	0	0.0	0.5	Soaked in Tap Water	NP W-NW, TB
Bentofix	NS	117.2	87.6	26.2	75	24	55.2	0	0.0	0.2	Soaked in Tap Water	NP W-NW, TB
Bentofix	NS	117.2	84.8	33.8	75	24	55.2	0	0.0	0.2	Soaked in Tap Water	NP W-NW, TB
Bentofix	NS	137.9	63.4	17.2	77.8	168	20.7	48	137.9	0.1	Soaked in Tap Water	NP W-NW, TB
Bentofix	NS	191.5	104.2	43.5	112.5	24	191.5	0	0.0	0.5	Soaked in Tap Water	NP W-NW, TB
Bentofix	NS	193.1	132.4	48.3	75	24	55.2	0	0.0	0.2	Soaked in Tap Water	NP W-NW, TB
Bentofix	NS	193.1	129.6	44.8	75	24	55.2	0	0.0	0.2	Soaked in Tap Water	NP W-NW, TB
Bentofix	NS	213.7	121.3	42.1	80	24	213.7	0	0.0	0.5	Soaked in Tap Water	NP W-NW, TB
Bentofix	NS	213.7	133.8	57.2	83.5	24	213.7	0	0.0	0.5	Soaked in Tap Water	NP W-NW, TB
Bentofix	NS	289.6	182.0	75.8	75	24	55.2	0	0.0	0.2	Soaked in Tap Water	NP W-NW, TB
Bentofix	NS	289.6	185.5	68.3	75	24	55.2	0	0.0	0.2	Soaked in Tap Water	NP W-NW, TB
Bentofix	NS	310.3	114.5	47.6	64	168	20.7	48	310.3	0.1	Soaked in Tap Water	NP W-NW, TB
Bentofix	NS	383.0	187.8	119.8	112.5	24	383.0	0	0.0	0.5	Soaked in Tap Water	NP W-NW, TB
Bentofix	NS	386.1	183.4	57.2	80	24	386.1	0	0.0	0.5	Soaked in Tap Water	NP W-NW, TB
Bentofix	NS	386.1	215.1	86.9	83.5	24	386.1	0	0.0	0.5	Soaked in Tap Water	NP W-NW, TB
Bentofix	NS	574.6	263.0	119.8	112.5	24	574.6	0	0.0	0.5	Soaked in Tap Water	NP W-NW, TB
Bentofix	NW	6.9	11.0	6.2	109.5	72	6.9	0	0.0	1	Soaked in Tap Water	NP NW-NW, TB
Bentofix	NW	6.9	26.9	#N/A	86	24	3.4	24	6.9	1	Soaked in Tap Water	NP NW-NW, TB
Bentofix	NW	13.8	35.2	#N/A	86	24	3.4	24	13.8	1	Soaked in Tap Water	NP NW-NW, TB
Bentofix	NW	27.6	44.1	#N/A	86	24	3.4	24	27.6	1	Soaked in Tap Water	NP NW-NW, TB
Bentofix	NW	48.3	97.9	31.7	83.5	24	48.3	0	0.0	0.5	Soaked in Tap Water	NP NW-NW, TB
Bentofix	NW	137.9	55.2	20.7	109.5	72	6.9	0	0.0	1	Soaked in Tap Water	NP NW-NW, TB
Bentofix	NW	172.4	168.2	40.0	86	24	3.4	24	172.4	1	Soaked in Tap Water	NP NW-NW, TB
Bentofix	NW	213.7	175.8	53.1	83.5	24	213.7	0	0.0	0.5	Soaked in Tap Water	NP NW-NW, TB
Bentofix	NW	275.8	91.0	35.9	109.5	72	6.9	0	0.0	1	Soaked in Tap Water	NP NW-NW, TB
Bentofix	NW	344.7	239.2	64.1	86	24	3.4	24	344.7	1	Soaked in Tap Water	NP NW-NW, TB
Bentofix	NW	386.1	256.5	88.9	83.5	24	386.1	0	0.0	0.5	Soaked in Tap Water	NP NW-NW, TB
Bentofix	NW	413.7	144.8	57.2	109.5	72	6.9	0	0.0	1	Soaked in Tap Water	NP NW-NW, TB
Bentofix	NW	551.6	188.9	80.0	109.5	72	6.9	0	0.0	1	Soaked in Tap Water	NP NW-NW, TB
Bentofix	NW	689.5	243.4	108.2	109.5	72	6.9	0	0.0	1	Soaked in Tap Water	NP NW-NW
Bentofix	NW	689.5	373.7	113.1	86	24	3.4	24	689.5	1	Soaked in Tap Water	NP NW-NW, TB
Bentofix	NW	1379.0	633.6	226.8	103.9	24	1379.0	0	0.0	1	Soaked in Tap Water	NP NW-NW, TB
Bentofix	NWL	14.4	41.0	10.3	104.85	336	14.4	0	0.0	1	Soaked in Tap Water	NP NW-NW, TB
Bentofix	NWL	14.4	41.2	10.7	104.85	48	14.4	0	0.0	1	Soaked in Tap Water	NP NW-NW, TB
Bentofix	NWL	28.7	50.8	12.6	104.85	336	28.7	0	0.0	1	Soaked in Tap Water	NP NW-NW, TB
Bentofix	NWL	28.7	54.6	13.3	104.85	48	28.7	0	0.0	1	Soaked in Tap Water	NP NW-NW, TB
Bentofix	NWL	43.1	60.7	16.2	104.85	336	43.1	0	0.0	1	Soaked in Tap Water	NP NW-NW, TB
Bentofix	NWL	43.1	66.7	17.4	104.85	48	43.1	0	0.0	1	Soaked in Tap Water	NP NW-NW, TB
Bentofix	NWL	57.5	67.4	18.7	104.85	336	57.5	0	0.0	1	Soaked in Tap Water	NP NW-NW, TB
Bentofix	NWL	57.5	75.8	21.0	104.85	48	57.5	0	0.0	1	Soaked in Tap Water	NP NW-NW, TB
Bentomat	DN	4.8	18.8	#N/A	217	96	0.0	24	4.8	0.25	Soaked in Tap Water	NP NW-NW
Bentomat	DN	4.8	15.6	#N/A	147.05	24	4.8	0	0.0	1	Soaked in Tap Water	NP NW-NW
Bentomat	DN	4.8	15.5	#N/A	217	96	0.0	24	4.8	0.25	Soaked in Tap Water	NP NW-NW
Bentomat	DN	6.9	22.1	#N/A	120.5	24	3.4	24	6.9	1	Soaked in Tap Water	NP NW-NW
Bentomat	DN	7.2	20.8	#N/A	217	96	0.0	24	7.2	0.25	Soaked in Tap Water	NP NW-NW
Bentomat	DN	7.2	18.3	#N/A	217	96	0.0	24	7.2	0.25	Soaked in Tap Water	NP NW-NW
Bentomat	DN	9.6	23.1	#N/A	217	96	0.0	24	9.6	0.25	Soaked in Tap Water	NP NW-NW
Bentomat	DN	9.6	21.2	#N/A	217	96	0.0	24	9.6	0.25	Soaked in Tap Water	NP NW-NW
Bentomat	DN	9.6	22.0	#N/A	147.05	24	9.6	0	0.0	1	Soaked in Tap Water	NP NW-NW
Bentomat	DN	13.8	32.4	#N/A	120.5	24	3.4	24	13.8	1	Soaked in Tap Water	NP NW-NW
Bentomat	DN	19.2	30.0	#N/A	147.05	24	19.2	0	0.0	1	Soaked in Tap Water	NP NW-NW
Bentomat	DN	27.6	43.4	#N/A	120.5	24	3.4	24	27.6	1	Soaked in Tap Water	NP NW-NW
Bentomat	DN	48.3	62.7	27.6	72	24	48.3	0	0.0	1	Soaked in Tap Water	NP NW-NW
Bentomat	DN	172.4	173.7	53.8	85	24	3.4	24	172.4	1	Soaked in Tap Water	NP NW-NW
Bentomat	DN	241.3	188.9	47.6	72	24	241.3	0	0.0	1	Soaked in Tap Water	NP NW-NW
Bentomat	DN	344.7	262.7	84.1	85	24	3.4	24	344.7	1	Soaked in Tap Water	NP NW-NW
Bentomat	DN	482.6	337.8	68.3	72	24	482.6	0	0.0	1	Soaked in Tap Water	NP NW-NW
Bentomat	DN	689.5	452.3	131.9	85	24	3.4	24	689.5	1	Soaked in Tap Water	NP NW-NW
Bentomat	HS	2.4	23.5	#N/A	168.8	72	2.4	0	0.0	1	Soaked in Tap Water	NP W-NW
Bentomat	HS	2.4	19.2	#N/A	20.9	0	0.0	0	0.0	1	As Received	NP W-NW
Bentomat	HS	7.2	32.3	#N/A	194.8	72	2.4	0	0.0	1	Soaked in Tap Water	NP W-NW
Bentomat	HS	7.2	33.8	#N/A	20.6	0	0.0	0	0.0	1	As Received	NP W-NW
Bentomat	HS	14.4	40.2	#N/A	154.8	72	2.4	0	0.0	1	Soaked in Tap Water	NP W-NW
Bentomat	HS	14.4	46.7	#N/A	21.8	0	0.0	0	0.0	1	As Received	NP W-NW
Bentomat	HS	23.9	51.0	#N/A	162	72	2.4	0	0.0	1	Soaked in Tap Water	NP W-NW
Bentomat	HS	23.9	55.1	#N/A	21.6	0	0.0	0	0.0	1	As Received	NP W-NW
Bentomat	ST	2.4	20.1	#N/A	16.5	0	0.0	0	0.0	1	As Received	NP W-NW
Bentomat	ST	2.4	15.8	#N/A	143	48	2.4	0	0.0	1	Soaked in Tap Water	NP W-NW
Bentomat	ST	2.4	16.3	#N/A	169.3	72	2.4	0	0.0	1	Soaked in Tap Water	NP W-NW
Bentomat	ST	3.4	15.4	#N/A	10.3	0	0.0	0	0.0	1	As Received	NP W-NW
Bentomat	ST	3.4	13.8	#N/A	158.3	24	3.4	0	0.0	1	Soaked in Tap Water	NP W-NW
Bentomat	ST	3.6	12.6	#N/A	156	48	3.6	0	0.0	1	Soaked in Tap Water	NP W-NW
Bentomat	ST	4.8	12.8	3.1	156.4	24	4.8	0	0.0	1	Submerged in Tap	NP W-NW
Bentomat	ST	4.8	19.9	#N/A	120	24	4.8	0	0.0	1	Soaked in Tap Water	NP W-NW
Bentomat	ST	4.8	17.9	#N/A	127	24	4.8	0	0.0	1	Soaked in Tap Water	NP W-NW
Bentomat	ST	4.8	18.7	#N/A	122	24	4.8	0	0.0	1	Soaked in Tap Water	NP W-NW
Bentomat	ST	4.8	17.2	#N/A	122	24	4.8	0	0.0	1	Soaked in Tap Water	NP W-NW
Bentomat	ST	4.8	20.4	#N/A	127.5	24	4.8	0	0.0	1	Soaked in Tap Water	NP W-NW
Bentomat	ST	4.8	14.6	#N/A	58.5615	48	4.8	0	0.0	1	Soaked in Tap Water	NP W-NW
Bentomat	ST	4.8	13.6	#N/A	156	48	4.8	0	0.0	1	Soaked in Tap Water	NP W-NW
Bentomat	ST	4.8	17.1	#N/A	88.45	60	6.9	24	4.8	1	Soaked in Tap Water	NP W-NW
Bentomat	ST	6.9	15.2	4.1	109.4	72	6.9	0	0.0	1	Soaked in Tap Water	NP W-NW
Bentomat	ST	6.9	16.5	#N/A	163.5	24	6.9	0	0.0	1	Soaked in Tap Water	NP W-NW
Bentomat	ST	6.9	19.2	#N/A	10.7	0	0.0	0	0.0	1	As Received	NP W-NW
Bentomat	ST	7.2	15.2	#N/A	156	48	7.2	0	0.0	1	Soaked in Tap Water	NP W-NW
Bentomat	ST	7.2	24.9	#N/A	160	72	2.4	0	0.0	1	Soaked in Tap Water	NP W-NW
Bentomat	ST	7.2	31.1	#N/A	16.3	0	0.0	0	0.0	1	As Received	NP W-NW
Bentomat	ST	9.6	23.8	#N/A	120	24	9.6	0	0.0	1	Soaked in Tap Water	NP W-NW
Bentomat	ST	9.6	24.8	#N/A	127	24	9.6	0	0.0	1	Soaked in Tap Water	NP W-NW
Bentomat	ST	9.6	25.2	#N/A	122	24	9.6	0	0.0	1	Soaked in Tap Water	NP W-NW
Bentomat	ST	9.6	24.7	#N/A	122	24	9.6	0	0.0	1	Soaked in Tap Water	NP W-NW
Bentomat	ST	9.6	26.9	#N/A	127.5	24	9.6	0	0.0	1	Soaked in Tap Water	NP W-NW
Bentomat	ST	9.6	25.6	#N/A	129.1	48	9.6	0	0.0	1	Soaked in Tap Water	NP W-NW
Bentomat	ST	9.6	31.6	#N/A	129.1	48	9.6	0	0.0	1	Soaked in Tap Water	NP W-NW
Bentomat	ST	9.6	27.6	#N/A	129	48	9.6	0	0.0	1	Soaked in Tap Water	NP W-NW
Bentomat	ST	9.6	27.2	#N/A	129	48	9.6	0	0.0	1	Soaked in Tap Water	NP W-NW

Bentomat	ST	9.6	31.7	#N/A	129	48	9.6	0	0.0	1	Soaked in Tap Water	NP W-NW
Bentomat	ST	9.6	26.9	#N/A	129.1	48	9.6	0	0.0	1	Soaked in Tap Water	NP W-NW
Bentomat	ST	9.6	34.6	#N/A	110.5	48	9.6	0	0.0	1	Soaked in Tap Water	NP W-NW
Bentomat	ST	9.6	27.6	#N/A	129.1	48	9.6	0	0.0	1	Soaked in Tap Water	NP W-NW
Bentomat	ST	9.6	30.8	#N/A	103.65	48	9.6	0	0.0	1	Soaked in Tap Water	NP W-NW
Bentomat	ST	9.6	30.9	#N/A	103.65	48	9.6	0	0.0	1	Soaked in Tap Water	NP W-NW
Bentomat	ST	9.6	32.9	#N/A	103.65	48	9.6	0	0.0	1	Soaked in Tap Water	NP W-NW
Bentomat	ST	9.6	29.7	#N/A	103.65	48	9.6	0	0.0	1	Soaked in Tap Water	NP W-NW
Bentomat	ST	9.6	34.9	#N/A	110.5	48	9.6	0	0.0	1	Soaked in Tap Water	NP W-NW
Bentomat	ST	9.6	26.8	#N/A	103.65	48	9.6	0	0.0	1	Soaked in Tap Water	NP W-NW
Bentomat	ST	9.6	20.3	#N/A	58.5615	48	9.6	0	0.0	1	Soaked in Tap Water	NP W-NW
Bentomat	ST	9.6	20.2	#N/A	143	48	9.6	0	0.0	1	Soaked in Tap Water	NP W-NW
Bentomat	ST	9.6	41.3	#N/A	110.5	48	9.6	0	0.0	1	Soaked in Tap Water	NP W-NW
Bentomat	ST	9.6	44.9	#N/A	110.5	48	9.6	0	0.0	1	Soaked in Tap Water	NP W-NW
Bentomat	ST	9.6	34.6	#N/A	110.5	48	9.6	0	0.0	1	Soaked in Tap Water	NP W-NW
Bentomat	ST	13.8	35.9	2.8	110.5	48	4.8	0	0.0	1	Soaked in Tap Water	NP W-NW
Bentomat	ST	13.8	29.6	#N/A	109.35	48	13.8	0	0.0	1	Soaked in Tap Water	NP W-NW
Bentomat	ST	14.4	36.6	#N/A	153.2	72	2.4	0	0.0	1	Soaked in Tap Water	NP W-NW
Bentomat	ST	14.4	21.5	4.3	182.8	24	4.8	0	0.0	1	Submerged in Tap	NP W-NW
Bentomat	ST	14.4	38.3	#N/A	16.8	0	0.0	0	0.0	1	As Received	NP W-NW
Bentomat	ST	14.4	23.5	#N/A	58.5615	48	14.4	0	0.0	1	Soaked in Tap Water	NP W-NW
Bentomat	ST	14.4	31.2	#N/A	88.45	60	6.9	24	14.4	1	Soaked in Tap Water	NP W-NW
Bentomat	ST	19.2	30.1	#N/A	120	24	19.2	0	0.0	1	Soaked in Tap Water	NP W-NW
Bentomat	ST	19.2	34.1	#N/A	127	24	19.2	0	0.0	1	Soaked in Tap Water	NP W-NW
Bentomat	ST	19.2	36.5	#N/A	122	24	19.2	0	0.0	1	Soaked in Tap Water	NP W-NW
Bentomat	ST	19.2	33.3	#N/A	122	24	19.2	0	0.0	1	Soaked in Tap Water	NP W-NW
Bentomat	ST	19.2	35.3	#N/A	127.5	24	19.2	0	0.0	1	Soaked in Tap Water	NP W-NW
Bentomat	ST	20.7	21.4	4.1	103.8	72	6.9	0	0.0	1	Soaked in Tap Water	NP W-NW
Bentomat	ST	23.9	52.0	#N/A	148.1	72	2.4	0	0.0	1	Soaked in Tap Water	NP W-NW
Bentomat	ST	23.9	28.7	4.9	186.1	24	4.8	0	0.0	1	Submerged in Tap	NP W-NW
Bentomat	ST	23.9	54.3	#N/A	16.5	0	0.0	0	0.0	1	As Received	NP W-NW
Bentomat	ST	23.9	30.4	#N/A	143	48	23.9	0	0.0	1	Soaked in Tap Water	NP W-NW
Bentomat	ST	27.6	39.3	#N/A	109.35	48	27.6	0	0.0	1	Soaked in Tap Water	NP W-NW
Bentomat	ST	28.7	46.1	#N/A	88.45	60	6.9	24	28.7	1	Soaked in Tap Water	NP W-NW
Bentomat	ST	34.5	40.2	#N/A	10.9	0	0.0	0	0.0	1	As Received	NP W-NW
Bentomat	ST	34.5	36.9	#N/A	175.3	24	34.5	0	0.0	1	Soaked in Tap Water	NP W-NW
Bentomat	ST	34.5	37.9	13.8	78	168	20.7	48	34.5	0.1	Soaked in Tap Water	NP W-NW
Bentomat	ST	34.5	46.9	18.6	78.5	168	20.7	48	34.5	0.1	Soaked in Tap Water	NP W-NW
Bentomat	ST	34.5	42.1	17.9	74	168	20.7	48	34.5	0.1	Soaked in Tap Water	NP W-NW
Bentomat	ST	34.5	50.3	33.8	81.5	168	20.7	48	34.5	0.1	Soaked in Tap Water	NP W-NW
Bentomat	ST	34.5	41.4	31.7	73.5	168	20.7	48	34.5	0.1	Soaked in Tap Water	NP W-NW
Bentomat	ST	34.5	46.2	24.1	78	168	20.7	48	34.5	0.1	Soaked in Tap Water	NP W-NW
Bentomat	ST	34.5	46.2	18.6	72.5	168	20.7	48	34.5	0.1	Soaked in Tap Water	NP W-NW
Bentomat	ST	34.5	49.6	14.5	72	168	20.7	48	34.5	0.1	Soaked in Tap Water	NP W-NW
Bentomat	ST	34.5	46.2	38.6	75.5	168	20.7	48	34.5	0.1	Soaked in Tap Water	NP W-NW
Bentomat	ST	34.5	39.3	17.2	75.5	168	20.7	48	34.5	0.1	Soaked in Tap Water	NP W-NW
Bentomat	ST	34.5	46.2	15.9	71	168	20.7	48	34.5	0.1	Soaked in Tap Water	NP W-NW
Bentomat	ST	34.5	55.2	#N/A	91.9	168	20.7	48	34.5	0.1	Soaked in Tap Water	NP W-NW
Bentomat	ST	34.5	49.0	8.3	107.8	168	20.7	48	34.5	0.1	Soaked in Tap Water	NP W-NW
Bentomat	ST	34.5	44.1	15.2	73	168	20.7	48	34.5	0.1	Soaked in Tap Water	NP W-NW
Bentomat	ST	34.5	53.1	31.0	71.5	168	20.7	48	34.5	0.1	Soaked in Tap Water	NP W-NW
Bentomat	ST	34.5	43.4	11.7	76	168	20.7	48	34.5	0.1	Soaked in Tap Water	NP W-NW
Bentomat	ST	34.5	58.6	32.4	79	168	20.7	48	34.5	0.1	Soaked in Tap Water	NP W-NW
Bentomat	ST	34.5	51.7	9.7	88.5	168	20.7	48	34.5	0.1	Soaked in Tap Water	NP W-NW
Bentomat	ST	34.5	44.1	21.4	72.5	168	20.7	48	34.5	0.1	Soaked in Tap Water	NP W-NW
Bentomat	ST	41.4	35.2	11.0	101	72	6.9	0	0.0	1	Soaked in Tap Water	NP W-NW
Bentomat	ST	41.4	48.3	#N/A	109.35	48	41.4	0	0.0	1	Soaked in Tap Water	NP W-NW
Bentomat	ST	47.9	69.7	7.7	70.75	24	47.9	0	0.0	1	Soaked in Tap Water	NP W-NW
Bentomat	ST	47.9	67.1	9.9	69.1	24	47.9	0	0.0	1	Soaked in Tap Water	NP W-NW
Bentomat	ST	47.9	67.6	10.4	71.75	24	47.9	0	0.0	1	Soaked in Tap Water	NP W-NW
Bentomat	ST	48.3	62.7	22.8	86	24	48.3	0	0.0	0.5	Soaked in Tap Water	NP W-NW
Bentomat	ST	48.3	65.5	21.4	95	24	48.3	0	0.0	0.5	Soaked in Tap Water	NP W-NW
Bentomat	ST	48.3	60.7	17.2	87	24	48.3	0	0.0	0.5	Soaked in Tap Water	NP W-NW
Bentomat	ST	48.3	61.4	17.9	90.5	24	48.3	0	0.0	0.5	Soaked in Tap Water	NP W-NW
Bentomat	ST	48.3	66.9	6.2	110.5	48	4.8	0	0.0	1	Soaked in Tap Water	NP W-NW
Bentomat	ST	59.9	81.3	9.8	70.75	24	59.9	0	0.0	1	Soaked in Tap Water	NP W-NW
Bentomat	ST	59.9	74.3	10.8	69.1	24	59.9	0	0.0	1	Soaked in Tap Water	NP W-NW
Bentomat	ST	59.9	78.3	11.7	71.75	24	59.9	0	0.0	1	Soaked in Tap Water	NP W-NW
Bentomat	ST	68.9	57.2	13.8	87.65	48	68.9	0	0.0	1	Soaked in Tap Water	NP W-NW
Bentomat	ST	71.8	88.5	11.0	70.75	24	71.8	0	0.0	1	Soaked in Tap Water	NP W-NW
Bentomat	ST	71.8	85.3	14.6	69.1	24	71.8	0	0.0	1	Soaked in Tap Water	NP W-NW
Bentomat	ST	71.8	83.7	14.6	71.75	24	71.8	0	0.0	1	Soaked in Tap Water	NP W-NW
Bentomat	ST	89.6	34.5	12.4	134.1	48	4.8	0	0.0	1	Soaked in Tap Water	NP W-NW
Bentomat	ST	95.8	83.3	33.8	124.8	48	95.8	0	0.0	1	Soaked in Tap Water	NP W-NW
Bentomat	ST	103.4	90.3	17.9	100.4	72	6.9	0	0.0	1	Soaked in Tap Water	NP W-NW
Bentomat	ST	103.4	100.7	10.3	110.5	48	4.8	0	0.0	1	Soaked in Tap Water	NP W-NW
Bentomat	ST	137.9	98.6	20.7	163.5	24	68.9	12	137.9	1	Soaked in Tap Water	NP W-NW
Bentomat	ST	137.9	113.8	40.7	72.5	168	20.7	48	137.9	0.1	Soaked in Tap Water	NP W-NW
Bentomat	ST	137.9	113.8	51.7	78	168	20.7	48	137.9	0.1	Soaked in Tap Water	NP W-NW
Bentomat	ST	137.9	75.8	24.8	78	168	20.7	48	137.9	0.1	Soaked in Tap Water	NP W-NW
Bentomat	ST	137.9	107.6	37.2	78.5	168	20.7	48	137.9	0.1	Soaked in Tap Water	NP W-NW
Bentomat	ST	137.9	96.5	32.4	74	168	20.7	48	137.9	0.1	Soaked in Tap Water	NP W-NW
Bentomat	ST	137.9	135.1	47.6	81.5	168	20.7	48	137.9	0.1	Soaked in Tap Water	NP W-NW
Bentomat	ST	137.9	113.8	55.8	73.5	168	20.7	48	137.9	0.1	Soaked in Tap Water	NP W-NW
Bentomat	ST	137.9	109.6	37.9	72.5	168	20.7	48	137.9	0.1	Soaked in Tap Water	NP W-NW
Bentomat	ST	137.9	126.2	43.4	72	168	20.7	48	137.9	0.1	Soaked in Tap Water	NP W-NW
Bentomat	ST	137.9	89.6	49.0	75.5	168	20.7	48	137.9	0.1	Soaked in Tap Water	NP W-NW
Bentomat	ST	137.9	94.5	39.3	75.5	168	20.7	48	137.9	0.1	Soaked in Tap Water	NP W-NW
Bentomat	ST	137.9	111.0	29.6	71	168	20.7	48	137.9	0.1	Soaked in Tap Water	NP W-NW
Bentomat	ST	137.9	137.2	#N/A	65.6	168	20.7	48	137.9	0.1	Soaked in Tap Water	NP W-NW
Bentomat	ST	137.9	91.0	13.8	94.5	168	20.7	48	137.9	0.1	Soaked in Tap Water	NP W-NW
Bentomat	ST	137.9	108.9	30.3	73	168	20.7	48	137.9	0.1	Soaked in Tap Water	NP W-NW
Bentomat	ST	137.9	135.8	44.8	71.5	168	20.7	48	137.9	0.1	Soaked in Tap Water	NP W-NW
Bentomat	ST	137.9	113.8	29.0	76	168	20.7	48	137.9	0.1	Soaked in Tap Water	NP W-NW
Bentomat	ST	137.9	117.9	44.8	79	168	20.7	48	137.9	0.1	Soaked in Tap Water	NP W-NW
Bentomat	ST	137.9	104.8	29.0	88.5	168	20.7	48	137.9	0.1	Soaked in Tap Water	NP W-NW
Bentomat	ST	172.4	138.6	14.5	110.5	48	4.8	0	0.0	1	Soaked in Tap Water	NP W-NW
Bentomat	ST	186.2	46.2	13.1	139.3	48	4.8	0	0.0	1	Soaked in Tap Water	NP W-NW
Bentomat	ST	206.8	117.2	35.9	87.65	48	206.8	0	0.0	1	Soaked in Tap Water	NP W-NW
Bentomat	ST	213.7	155.8	45.5	86	24	213.7	0	0.0	0.5	Soaked in Tap Water	NP W-NW
Bentomat	ST	213.7	153.1	37.2	95	24	213.7	0	0.0	0.5	Soaked in Tap Water	NP W-NW
Bentomat	ST	213.7	144.1	44.8	87	24	213.7	0	0.0	0.5	Soaked in Tap Water	NP W-NW
Bentomat	ST	213.7	128.2	41.4	90.5	24	213.7	0	0.0	0.5	Soaked in Tap Water	NP W-NW
Bentomat	ST	250.0	162.7	63.4	66.5	144	8.0	252	250.0	0.0015	Staged H/C	NP W-NW

Bentomat	ST	275.8	66.9	13.8	134.8	48	4.8	0	0.0	1	Soaked in Tap Water	NP W-NW
Bentomat	ST	275.8	189.6	23.4	110.5	48	4.8	0	0.0	1	Soaked in Tap Water	NP W-NW
Bentomat	ST	275.8	148.9	71.7	163.5	24	68.9	12	275.8	1	Soaked in Tap Water	NP W-NW
Bentomat	ST	310.3	216.5	75.8	72.5	168	20.7	48	310.3	0.1	Soaked in Tap Water	NP W-NW
Bentomat	ST	310.3	213.7	86.2	78	168	20.7	48	310.3	0.1	Soaked in Tap Water	NP W-NW
Bentomat	ST	310.3	169.6	43.4	78	168	20.7	48	310.3	0.1	Soaked in Tap Water	NP W-NW
Bentomat	ST	310.3	204.8	63.4	78.5	168	20.7	48	310.3	0.1	Soaked in Tap Water	NP W-NW
Bentomat	ST	310.3	177.9	65.5	74	168	20.7	48	310.3	0.1	Soaked in Tap Water	NP W-NW
Bentomat	ST	310.3	217.9	72.4	81.5	168	20.7	48	310.3	0.1	Soaked in Tap Water	NP W-NW
Bentomat	ST	310.3	233.0	89.6	73.5	168	20.7	48	310.3	0.1	Soaked in Tap Water	NP W-NW
Bentomat	ST	310.3	199.9	62.7	72.5	168	20.7	48	310.3	0.1	Soaked in Tap Water	NP W-NW
Bentomat	ST	310.3	231.0	75.2	72	168	20.7	48	310.3	0.1	Soaked in Tap Water	NP W-NW
Bentomat	ST	310.3	175.1	62.7	75.5	168	20.7	48	310.3	0.1	Soaked in Tap Water	NP W-NW
Bentomat	ST	310.3	194.4	75.8	75.5	168	20.7	48	310.3	0.1	Soaked in Tap Water	NP W-NW
Bentomat	ST	310.3	202.0	64.8	71	168	20.7	48	310.3	0.1	Soaked in Tap Water	NP W-NW
Bentomat	ST	310.3	241.3	#N/A	58.7	168	20.7	48	310.3	0.1	Soaked in Tap Water	NP W-NW
Bentomat	ST	310.3	156.5	39.3	59	168	20.7	48	310.3	0.1	Soaked in Tap Water	NP W-NW
Bentomat	ST	310.3	157.2	42.1	73	168	20.7	48	310.3	0.1	Soaked in Tap Water	NP W-NW
Bentomat	ST	310.3	204.1	68.9	71.5	168	20.7	48	310.3	0.1	Soaked in Tap Water	NP W-NW
Bentomat	ST	310.3	222.0	60.0	76	168	20.7	48	310.3	0.1	Soaked in Tap Water	NP W-NW
Bentomat	ST	310.3	195.8	65.5	79	168	20.7	48	310.3	0.1	Soaked in Tap Water	NP W-NW
Bentomat	ST	310.3	183.4	46.9	88.5	168	20.7	48	310.3	0.1	Soaked in Tap Water	NP W-NW
Bentomat	ST	344.7	185.5	55.2	87.65	48	344.7	0	0.0	1	Soaked in Tap Water	NP W-NW
Bentomat	ST	344.7	147.5	37.2	89.1	48	344.7	0	0.0	1	Soaked in Tap Water	NP W-NW
Bentomat	ST	344.7	220.6	84.8	85.3	24	6.9	48	344.7	0.025	Soaked in Tap Water	NP W-NW
Bentomat	ST	386.1	237.2	74.5	87	24	386.1	0	0.0	0.5	Soaked in Tap Water	NP W-NW
Bentomat	ST	386.1	205.5	74.5	90.5	24	386.1	0	0.0	0.5	Soaked in Tap Water	NP W-NW
Bentomat	ST	386.1	208.9	79.3	86	24	386.1	0	0.0	0.5	Soaked in Tap Water	NP W-NW
Bentomat	ST	386.1	217.9	84.1	95	24	386.1	0	0.0	0.5	Soaked in Tap Water	NP W-NW
Bentomat	ST	478.8	230.8	82.4	111.3	48	478.8	0	0.0	1	Soaked in Tap Water	NP W-NW
Bentomat	ST	517.1	344.7	103.4		312	496.4	48	517.1	0.0015	Soaked in Tap Water	NP W-NW
Bentomat	ST	517.1	338.5	96.5		312	496.4	48	517.1	0.01	Soaked in Tap Water	NP W-NW
Bentomat	ST	517.1	317.2	80.7		312	496.4	48	517.1	0.1	Soaked in Tap Water	NP W-NW
Bentomat	ST	517.1	308.9	57.2		312	496.4	48	517.1	1	Soaked in Tap Water	NP W-NW
Bentomat	ST	517.1	301.3	83.4	66.5	48	62.5	132	500.0	0.0015	Staged H/C	NP W-NW
Bentomat	ST	517.1	398.5	259.9		0	0.0	0	0.0	1	As Received	NP W-NW
Bentomat	ST	517.1	350.9	202.7		0	0.0	0	0.0	1	As Received	NP W-NW
Bentomat	ST	517.1	382.7	219.3		0	0.0	0	0.0	1	As Received	NP W-NW
Bentomat	ST	517.1	454.4	261.3		0	0.0	0	0.0	1	As Received	NP W-NW
Bentomat	ST	517.1	435.7	217.2		0	0.0	0	0.0	1	As Received	NP W-NW
Bentomat	ST	551.6	270.3	107.6	163.5	24	68.9	12	551.6	1	Soaked in Tap Water	NP W-NW
Bentomat	ST	689.5	246.8	77.9	88.3	48	689.5	0	0.0	1	Soaked in Tap Water	NP W-NW
Bentomat	ST	981.5	471.4	136.0	103.5	48	981.5	0	0.0	1	Soaked in Tap Water	NP W-NW
Bentomat	ST	992.8	468.2	138.6	66.5	144	8.0	504	1000.0	0.0015	Staged H/C	NP W-NW
Bentomat	ST	1034.2	333.7	144.8	77.1	48	1034.2	0	0.0	1	Soaked in Tap Water	NP W-NW
Bentomat	ST	1034.2	332.3	136.5	82.4	48	1034.2	0	0.0	1	Soaked in Tap Water	NP W-NW
Bentomat	ST	1723.7	477.8	217.2	68.2	48	1723.7	0	0.0	1	Soaked in Tap Water	NP W-NW
Bentomat	ST	2757.9	668.1	306.1	57.5	48	2757.9	0	0.0	1	Soaked in Tap Water	NP W-NW
Bentomat	CS	2.4	6.2	#N/A	144.6	48	2.4	0	0.0	1	Soaked in Tap Water	NP W-NW
Bentomat	CS	9.6	10.3	#N/A	120	48	9.6	0	0.0	1	Soaked in Tap Water	NP W-NW
Bentomat	CS	19.2	16.0	#N/A	100.2	48	19.2	0	0.0	1	Soaked in Tap Water	NP W-NW
Geobent	N-U	24.1	9.7	4.8	103	24	24.1	0	0.0	1	Soaked in Tap Water	NP - W-NW
Geobent	N-U	48.3	13.1	4.8	103	24	48.3	0	0.0	1	Soaked in Tap Water	NP - W-NW
Geobent	N-U	96.5	20.7	11.7	103	24	96.5	0	0.0	1	Soaked in Tap Water	NP - W-NW
Geobent	N-U	193.1	36.5	24.1	103	24	193.1	0	0.0	1	Soaked in Tap Water	NP - W-NW
Claymax	500SP	2.4	18.7	#N/A	144	48	4.8	0	0.0	1	Soaked in Tap Water	SB, W-W
Claymax	500SP	2.4	23.8	#N/A	143.8	48	4.8	0	0.0	1	Soaked in Tap Water	SB, W-W
Claymax	500SP	2.4	23.0	#N/A	177.6	48	4.8	0	0.0	1	Soaked in Tap Water	SB, W-W
Claymax	500SP	4.8	24.2	#N/A	190.1	48	4.8	0	0.0	1	Soaked in Tap Water	SB, W-W
Claymax	500SP	4.8	25.0	#N/A	186.5	48	4.8	0	0.0	1	Soaked in Tap Water	SB, W-W
Claymax	500SP	9.6	19.6	#N/A	255.8	96	7.2	0	0.0	1	Soaked in Tap Water	SB, W-W
Claymax	500SP	9.6	27.4	#N/A	238.5	96	7.2	0	0.0	1	Soaked in Tap Water	SB, W-W
Claymax	500SP	9.6	27.8	#N/A	185	48	9.6	0	0.0	1	Soaked in Tap Water	SB, W-W
Claymax	500SP	9.6	28.0	#N/A	185.6	48	9.6	0	0.0	1	Soaked in Tap Water	SB, W-W
Claymax	500SP	9.6	27.6	#N/A	143.3	48	9.6	0	0.0	1	Soaked in Tap Water	SB, W-W
Claymax	500SP	9.6	28.1	#N/A	140.2	48	4.8	0	0.0	1	Soaked in Tap Water	SB, W-W
Claymax	500SP	9.6	20.6	#N/A	156.9	48	4.8	0	0.0	1	Soaked in Tap Water	SB, W-W
Claymax	500SP	13.8	26.9	#N/A	225	168	13.8	0	0.0	1	Soaked in Tap Water	SB, W-W
Claymax	500SP	14.4	31.3	#N/A	168.1	48	14.4	0	0.0	1	Soaked in Tap Water	SB, W-W
Claymax	500SP	14.4	31.6	#N/A	176.9	48	14.4	0	0.0	1	Soaked in Tap Water	SB, W-W
Claymax	500SP	19.2	23.3	#N/A	214.2	96	7.2	0	0.0	1	Soaked in Tap Water	SB, W-W
Claymax	500SP	19.2	27.9	#N/A	229.4	96	7.2	0	0.0	1	Soaked in Tap Water	SB, W-W
Claymax	500SP	19.2	27.7	#N/A	142.7	48	4.8	0	0.0	1	Soaked in Tap Water	SB, W-W
Claymax	500SP	19.2	22.6	#N/A	142.1	48	4.8	0	0.0	1	Soaked in Tap Water	SB, W-W
Claymax	500SP	19.2	25.9	#N/A	160.6	48	4.8	0	0.0	1	Soaked in Tap Water	SB, W-W
Claymax	500SP	23.9	71.1	#N/A	141.1	24	12.0	0	0.0	1	Soaked in Tap Water	SB, W-W
Claymax	500SP	27.6	24.8	#N/A	225	168	27.6	0	0.0	1	Soaked in Tap Water	SB, W-W
Claymax	500SP	33.5	18.8	#N/A	143.1	48	4.8	0	0.0	1	Soaked in Tap Water	SB, W-W
Claymax	500SP	33.5	33.1	#N/A	141.3	48	4.8	0	0.0	1	Soaked in Tap Water	SB, W-W
Claymax	500SP	33.5	27.1	#N/A	171.5	48	4.8	0	0.0	1	Soaked in Tap Water	SB, W-W
Claymax	500SP	34.5	35.9	#N/A	109.6	168	20.7	48	34.5	0.1	Soaked in Tap Water	SB, W-W
Claymax	500SP	47.9	20.7	#N/A	143	48	4.8	0	0.0	1	Soaked in Tap Water	SB, W-W
Claymax	500SP	47.9	28.4	#N/A	143.3	48	4.8	0	0.0	1	Soaked in Tap Water	SB, W-W
Claymax	500SP	47.9	29.7	#N/A	154.7	48	4.8	0	0.0	1	Soaked in Tap Water	SB, W-W
Claymax	500SP	47.9	71.6	#N/A	140	24	12.0	0	0.0	1	Soaked in Tap Water	SB, W-W
Claymax	500SP	55.2	25.5	#N/A	225	168	55.2	0	0.0	1	Soaked in Tap Water	SB, W-W
Claymax	500SP	68.9	27.2	#N/A	203.2	96	7.2	0	0.0	1	Soaked in Tap Water	SB, W-W
Claymax	500SP	68.9	34.1	#N/A	252.9	96	7.2	0	0.0	1	Soaked in Tap Water	SB, W-W
Claymax	500SP	95.8	28.7	#N/A	176.6	48	4.8	0	0.0	1	Soaked in Tap Water	SB, W-W
Claymax	500SP	137.9	43.4	21.4	151.4	24	137.9	0	0.0	1	Soaked in Tap Water	SB, W-W
Claymax	500SP	137.9	51.7	#N/A	98.2	168	20.7	48	137.9	0.1	Soaked in Tap Water	SB, W-W
Claymax	500SP	143.6	34.2	#N/A	178.7	48	4.8	0	0.0	1	Soaked in Tap Water	SB, W-W
Claymax	500SP	275.8	90.3	40.0	138.2	24	275.8	0	0.0	1	Soaked in Tap Water	SB, W-W
Claymax	500SP	310.3	71.7	#N/A	61.4	168	20.7	48	310.3	0.1	Soaked in Tap Water	SB, W-W

Claymax	500SP	344.7	47.8	#N/A	237.5	96	7.2	0	0.0	1	Soaked in Tap Water	SB, W-W
Claymax	500SP	344.7	57.0	#N/A	242.5	96	7.2	0	0.0	1	Soaked in Tap Water	SB, W-W
Claymax	500SP	413.7	91.7	42.1	120.9	24	413.7	0	0.0	1	Soaked in Tap Water	SB, W-W
Claymax	500SP	478.8	62.2	#N/A	187.9	48	4.8	0	0.0	1	Soaked in Tap Water	SB, W-W
Claymax	500SP	551.6	131.7	57.9	108.2	24	551.6	0	0.0	1	Soaked in Tap Water	SB, W-W
Claymax	500SP	689.5	147.5	67.6	100.1	24	689.5	0	0.0	1	Soaked in Tap Water	SB, W-W
Claymax	500SP	981.5	100.5	#N/A	170.9	48	4.8	0	0.0	1	Soaked in Tap Water	SB, W-W
Claymax	500SP	999.7	96.2	#N/A	267.5	96	7.2	0	0.0	1	Soaked in Tap Water	SB, W-W
Claymax	500SP	999.7	110.6	#N/A	213.8	96	7.2	0	0.0	1	Soaked in Tap Water	SB, W-W
Claymax	200R	13.8	4.8	4.1	252.5	168	13.8	0	0.0	1	Soaked in Tap Water	UN - W-NW
Claymax	200R	27.6	7.6	6.2	252.5	168	27.6	0	0.0	1	Soaked in Tap Water	UN - W-NW
Claymax	200R	55.2	13.8	10.3	252.5	168	55.2	0	0.0	1	Soaked in Tap Water	UN - W-NW
Claymax	200R	68.9	20.7	14.5	84	0	0.0	0	0.0	1	As Received	UN - W-NW
Claymax	200R	275.8	38.6	35.2	34	0	0.0	14	275.8	0.1	As Received	UN - W-NW
Claymax	200R	275.8	33.8	30.3	84	0	0.0	0	0.0	1	As Received	UN - W-NW
Claymax	200R	482.6	47.6	43.4	84	0	0.0	0	0.0	1	As Received	UN - W-NW

GCL Geomembrane Interfaces

GCL Manufacturer	GCL Description	Geomembrane Manufacturer	Geomembrane Description	Geomembrane Type	Normal Stress (kPa)	Peak Shear Strength (kPa)	Large Displacement Shear Strength (kPa)	GCL Initial Water Content (%)	GCL Final Water Content (%)	Hydration Time (hrs)	Hydration Normal Stress (kPa)	Consolidation Time (hrs)	Consolidation Normal Stress (kPa)	Shear Displacement Rate (mm/min)	Hydration Procedure
Gundle	Gundseal	Polyflex	60-mil	GM-THDPE	241.3	120.0	71.7	28.3	131.6	48	241.3	0	0.0	1	Soaked in Tap Water
Gundle	Gundseal	Polyflex	60-mil	GM-THDPE	482.6	245.5	148.2	28.3	131.6	48	482.6	0	0.0	1	Soaked in Tap Water
Gundle	Gundseal	Polyflex	60-mil	GM-THDPE	723.9	386.1	242.0	28.3	131.6	48	723.9	0	0.0	1	Soaked in Tap Water
Gundle	Gundseal	Polyflex	60-mil	GM-THDPE	965.3	483.3	288.2	28.3	131.6	48	965.3	0	0.0	1	Soaked in Tap Water
Gundle	Gundseal	GSE	60-mil	GM-THDPE	68.9	58.6	54.5	15	15.3	0	0.0	0	0.0	1	As Received
Gundle	Gundseal	GSE	60-mil	GM-THDPE	206.8	115.8	111.0	15.5	15.1	0	0.0	0	0.0	1	As Received
Gundle	Gundseal	GSE	60-mil	GM-THDPE	344.7	187.5	111.0	15.5	15	0	0.0	0	0.0	1	As Received
Bentofix	NS	NSC	40-mil	GM-THDPE	16.8	14.1	8.0	15.1	14.9	0	0.0	0	0.0	1	As Received
Bentofix	NS	NSC	40-mil	GM-THDPE	143.6	72.3	40.5	15.1	14.8	0	0.0	0	0.0	1	As Received
Bentofix	NS	NSC	40-mil	GM-THDPE	335.2	158.5	81.9	15.1	14.5	0	0.0	0	0.0	1	As Received
Bentofix	NS	NSC	40-mil	GM-THDPE	670.3	275.8	123.5	15.1	14.2	0	0.0	0	0.0	1	As Received
Bentofix	NS	NSC	60-mil	GM-THDPE	9.6	4.6	3.2	8.9	81.5	24	57.5	0	0.0	0.2	Soaked in Tap Water
Bentofix	NS	NSC	60-mil	GM-THDPE	9.6	5.1	4.3	8.3	80	24	57.5	0	0.0	0.2	Soaked in Tap Water
Bentofix	NS	NSC	60-mil	GM-THDPE	20.7	9.0	6.9	11.3	78.5	1	20.7	0	0.0	1	Submerged in Tap
Bentofix	NS	NSC	60-mil	GM-THDPE	34.5	14.5	10.3	7.85	105.5	24	13.8	0	0.0	1	Soaked in Tap Water
Bentofix	NS	NSC	60-mil	GM-THDPE	34.5	15.2	11.7	7.85	105.5	24	13.8	0	0.0	0.025	Soaked in Tap Water
Bentofix	NS	NSC	60-mil	GM-THDPE	41.4	17.2	13.1	11.1	73.5	1	20.7	0	0.0	1	Submerged in Tap
Bentofix	NS	NSC	60-mil	GM-THDPE	47.9	27.0	18.2	8.9	81.5	24	57.5	0	0.0	0.2	Soaked in Tap Water
Bentofix	NS	NSC	60-mil	GM-THDPE	47.9	25.9	19.2	8.3	80	24	57.5	0	0.0	0.2	Soaked in Tap Water
Bentofix	NS	NSC	60-mil	GM-THDPE	62.1	24.7	18.6	11.2	84.6	1	20.7	0	0.0	1	Submerged in Tap
Bentofix	NS	NSC	60-mil	GM-THDPE	68.9	30.3	22.1	7.85	105.5	24	13.8	0	0.0	1	Soaked in Tap Water
Bentofix	NS	NSC	60-mil	GM-THDPE	68.9	27.6	22.1	7.85	105.5	24	13.8	0	0.0	0.025	Soaked in Tap Water
Bentofix	NS	NSC	60-mil	GM-THDPE	95.8	44.5	29.7	8.9	81.5	24	57.5	0	0.0	0.2	Soaked in Tap Water
Bentofix	NS	NSC	60-mil	GM-THDPE	95.8	41.6	31.5	8.3	80	24	57.5	0	0.0	0.2	Soaked in Tap Water
Bentofix	NS	NSC	60-mil	GM-THDPE	137.9	59.3	40.7	7.85	105.5	24	13.8	0	0.0	1	Soaked in Tap Water
Bentofix	NS	NSC	60-mil	GM-THDPE	137.9	57.9	45.5	7.85	105.5	24	13.8	0	0.0	0.025	Soaked in Tap Water
Bentofix	NS	NSC	60-mil	GM-THDPE	191.5	72.0	46.0	8.9	81.5	24	57.5	0	0.0	0.2	Soaked in Tap Water
Bentofix	NS	NSC	60-mil	GM-THDPE	191.5	76.2	46.6	8.3	80	24	57.5	0	0.0	0.2	Soaked in Tap Water
Bentofix	NS	NSC	60-mil	GM-THDPE	335.2	114.5	85.2	8.9	81.5	24	57.5	0	0.0	0.2	Soaked in Tap Water
Bentofix	NS	NSC	60-mil	GM-THDPE	335.2	117.1	82.1	8.3	80	24	57.5	0	0.0	0.2	Soaked in Tap Water
Bentofix	NS	GSE	60-mil	GM-THDPE	68.9	31.0	20.7	7.2	90	24	5.7	15	68.9	1	Soaked in Tap Water
Bentofix	NS	GSE	60-mil	GM-THDPE	137.9	51.7	33.1	7.2	90	24	5.7	15	137.9	1	Soaked in Tap Water
Bentofix	NS	GSE	60-mil	GM-THDPE	206.8	74.5	48.3	7.2	90	24	5.7	15	206.8	1	Soaked in Tap Water
Bentofix	NS	GSE	80-mil	GM-THDPE	34.5	13.1	9.7	6.9	101.1	168	20.7	48	34.5	0.1	Soaked in Tap Water
Bentofix	NS	GSE	80-mil	GM-THDPE	34.5	15.9	9.7	7	101.3	168	20.7	48	34.5	0.1	Soaked in Tap Water
Bentofix	NS	GSE	80-mil	GM-THDPE	137.9	45.5	23.4	7	93.8	168	20.7	48	137.9	0.1	Soaked in Tap Water
Bentofix	NS	GSE	80-mil	GM-THDPE	137.9	52.4	33.8	6.9	74.2	168	20.7	48	137.9	0.1	Soaked in Tap Water
Bentofix	NS	GSE	80-mil	GM-THDPE	310.3	107.6	61.4	7	82	168	20.7	48	310.3	0.1	Soaked in Tap Water
Bentofix	NS	GSE	80-mil	GM-THDPE	310.3	100.0	59.3	6.9	66.8	168	20.7	48	310.3	0.1	Soaked in Tap Water
Bentomat	ST	Serrot	60-mil	GM-THDPE	6.9	3.4	2.8	16	88.5	24	6.9	0	0.0	1	Soaked in Tap Water
Bentomat	ST	Serrot	60-mil	GM-THDPE	13.8	6.9	4.8	16	88.5	24	13.8	0	0.0	1	Soaked in Tap Water
Bentomat	ST	Serrot	60-mil	GM-THDPE	27.6	11.7	9.7	16	88.5	24	27.6	0	0.0	1	Soaked in Tap Water
Bentomat	ST	Serrot	60-mil	GM-THDPE	172.4	84.1	53.1	21.2	61	24	172.4	0	0.0	1	Soaked in Tap Water
Bentomat	ST	Serrot	60-mil	GM-THDPE	172.4	76.5	56.5	21.2	61	24	172.4	0	0.0	1	Soaked in Tap Water
Bentomat	ST	Serrot	60-mil	GM-THDPE	172.4	75.8	42.1	21.2	61	24	172.4	0	0.0	1	Soaked in Tap Water
Bentomat	ST	Serrot	60-mil	GM-THDPE	172.4	64.1	40.7	21.2	61	24	172.4	0	0.0	1	Soaked in Tap Water
Bentomat	ST	Serrot	60-mil	GM-THDPE	172.4	79.3	44.1	21.2	61	24	172.4	0	0.0	1	Soaked in Tap Water
Bentomat	ST	Serrot	60-mil	GM-THDPE	172.4	73.1	36.5	21.2	61	24	172.4	0	0.0	1	Soaked in Tap Water
Bentomat	ST	Serrot	60-mil	GM-THDPE	172.4	61.4	33.8	21.2	61	24	172.4	0	0.0	1	Soaked in Tap Water
Bentomat	ST	Serrot	60-mil	GM-THDPE	344.7	149.6	86.2	21.2	61	24	344.7	0	0.0	1	Soaked in Tap Water
Bentomat	ST	Serrot	60-mil	GM-THDPE	344.7	147.5	82.7	21.2	61	24	344.7	0	0.0	1	Soaked in Tap Water
Bentomat	ST	Serrot	60-mil	GM-THDPE	344.7	142.0	80.0	21.2	61	24	344.7	0	0.0	1	Soaked in Tap Water
Bentomat	ST	Serrot	60-mil	GM-THDPE	344.7	135.8	73.1	21.2	61	24	344.7	0	0.0	1	Soaked in Tap Water
Bentomat	ST	Serrot	60-mil	GM-THDPE	344.7	148.9	75.2	21.2	61	24	344.7	0	0.0	1	Soaked in Tap Water
Bentomat	ST	Serrot	60-mil	GM-THDPE	344.7	142.7	67.6	21.2	61	24	344.7	0	0.0	1	Soaked in Tap Water
Bentomat	ST	Serrot	60-mil	GM-THDPE	344.7	102.7	60.7	21.2	61	24	344.7	0	0.0	1	Soaked in Tap Water
Bentomat	ST	Serrot	60-mil	GM-THDPE	689.5	305.4	155.1	21.2	61	24	689.5	0	0.0	1	Soaked in Tap Water
Bentomat	ST	Serrot	60-mil	GM-THDPE	689.5	281.3	143.4	21.2	61	24	689.5	0	0.0	1	Soaked in Tap Water
Bentomat	ST	Serrot	60-mil	GM-THDPE	689.5	260.6	139.3	21.2	61	24	689.5	0	0.0	1	Soaked in Tap Water
Bentomat	ST	Serrot	60-mil	GM-THDPE	689.5	264.1	144.1	21.2	61	24	689.5	0	0.0	1	Soaked in Tap Water
Bentomat	ST	Serrot	60-mil	GM-THDPE	689.5	273.7	157.2	21.2	61	24	689.5	0	0.0	1	Soaked in Tap Water
Bentomat	ST	Serrot	60-mil	GM-THDPE	689.5	265.4	131.0	21.2	61	24	689.5	0	0.0	1	Soaked in Tap Water
Bentomat	ST	Serrot	60-mil	GM-THDPE	689.5	201.3	108.9	21.2	61	24	689.5	0	0.0	1	Soaked in Tap Water
Bentomat	ST	NSC	60-mil	GM-THDPE	172.4	53.8	32.4	21.4	88	72	6.9	24	172.4	1	Soaked in Tap Water
Bentomat	ST	NSC	60-mil	GM-THDPE	413.7	89.6	54.5	21.4	88	72	6.9	24	413.7	1	Soaked in Tap Water
Bentomat	ST	NSC	60-mil	GM-THDPE	689.5	139.3	66.9	21.4	88	72	6.9	24	689.5	1	Soaked in Tap Water
Bentomat	ST	Polyflex	60-mil	GM-THDPE	9.6	5.6	4.8	11.5	74.5	24	57.5	0	0.0	0.2	Soaked in Tap Water
Bentomat	ST	Polyflex	60-mil	GM-THDPE	9.6	6.1	5.0	11.8	71.5	24	57.5	0	0.0	0.2	Soaked in Tap Water
Bentomat	ST	Polyflex	60-mil	GM-THDPE	47.9	17.8	12.9	11.5	74.5	24	57.5	0	0.0	0.2	Soaked in Tap Water
Bentomat	ST	Polyflex	60-mil	GM-THDPE	47.9	18.4	12.8	11.8	71.5	24	57.5	0	0.0	0.2	Soaked in Tap Water
Bentomat	ST	Polyflex	60-mil	GM-THDPE	51.7	25.5	17.9	20	127.3	48	51.7	0	0.0	1	Soaked in Tap Water
Bentomat	ST	Polyflex	60-mil	GM-THDPE	95.8	37.3	26.7	11.5	74.5	24	57.5	0	0.0	0.2	Soaked in Tap Water
Bentomat	ST	Polyflex	60-mil	GM-THDPE	95.8	36.7	27.2	11.8	71.5	24	57.5	0	0.0	0.2	Soaked in Tap Water
Bentomat	ST	Polyflex	60-mil	GM-THDPE	103.4	42.1	35.2	20	113.5	48	103.4	0	0.0	1	Soaked in Tap Water
Bentomat	ST	Polyflex	60-mil	GM-THDPE	191.5	76.8	47.9	11.5	74.5	24	57.5	0	0.0	0.2	Soaked in Tap Water
Bentomat	ST	Polyflex	60-mil	GM-THDPE	191.5	69.1	45.0	11.8	71.5	24	57.5	0	0.0	0.2	Soaked in Tap Water
Bentomat	ST	Polyflex	60-mil	GM-THDPE	206.8	76.5	64.8	20	115.1	48	206.8	0	0.0	1	Soaked in Tap Water
Bentomat	ST	Polyflex	60-mil	GM-THDPE	287.3	106.3	65.0	11.5	74.5	24	57.5	0	0.0	0.2	Soaked in Tap Water
Bentomat	ST	Polyflex	60-mil	GM-THDPE	287.3	97.5	58.0	11.8	71.5	24	57.5	0	0.0	0.2	Soaked in Tap Water
Bentomat	ST	GSE	60-mil	GM-THDPE	68.9	47.6	28.3	23.9	134	24	68.9	0	0.0	1	Soaked in Tap Water
Bentomat	ST	GSE	60-mil	GM-THDPE	206.8	99.3	64.1	23.9	125	24	68.9	0	0.0	1	Soaked in Tap Water
Bentomat	ST	GSE	60-mil	GM-THDPE	344.7	157.2	104.8	23.9	114.4	24	68.9	0	0.0	1	Soaked in Tap Water
Bentomat	ST	GSE	60-mil	GM-THDPE	6.9	4.8	4.1	6	108.6	24	6.9	0	0.0	1	Soaked in Tap Water
Bentomat	ST	GSE	60-mil	GM-THDPE	20.7	15.9	11.0	6	101	24	6.9	0	0.0	1	Soaked in Tap Water
Bentomat	ST	GSE	60-mil	GM-THDPE	41.4	20.7	13.8	6	104.4	24	6.9	0	0.0	1	Soaked in Tap Water
Bentomat	ST	GSE	60-mil	GM-THDPE	51.7	29.0	13.8	20	123.7	48	51.7	0	0.0	1	Soaked in Tap Water
Bentomat	ST	GSE - H.F-F.F	60-mil	GM-THDPE	68.9	32.4	17.9	15.3	102	24	68.9	0	0.0	1	Soaked in Tap Water
Bentomat	ST	GSE	60-mil	GM-THDPE	68.9	17.9	10.3	21.1	65.6	48	68.9	0	0.0	1	Soaked in Tap Water
Bentomat	ST	GSE	60-mil	GM-THDPE	68.9	24.8	17.9	21.1	59.55	48	68.9	0	0.0	0.1	Soaked in Tap Water
Bentomat	ST	GSE	60-mil	GM-THDPE	103.4	38.6	22.8	6	105.9	24	6.9	0	0.0	1	Soaked in Tap Water
Bentomat	ST	GSE	60-mil	GM-THDPE	103.4	48.3	26.2	20	115.1	48	103.4	0	0.0	1	Soaked in Tap Water
Bentomat	ST	GSE	60-mil	GM-THDPE	206.8	73.1	46.9	20	105.7	48	206.8	0	0.0	1	Soaked in Tap Water
Bentomat	ST	GSE	60-mil	GM-THDPE	206.8	55.8	34.5	21.1	65.6	48	206.8	0	0.0	1	Soaked in Tap Water
Bentomat	ST	GSE	60-mil	GM-THDPE	206.8	71.0	42.7	21.1	59.55	48	206.8	0	0.0	0.1	Soaked in Tap Water
Bentomat	ST	GSE - H.F-F.F	60-mil	GM-THDPE	241.3	82.7	39.3	15.3	102	24	68.9	0	0.0	1	Soaked in Tap Water
Bentomat	ST	GSE	60-mil	GM-THDPE	344.7	86.2	53.8	21.1	65.6	48	344.7	0	0.0	1	Soaked in Tap Water
Bentomat	ST	GSE	60-mil	GM-THDPE	344.7	121.3	64.8	21.1	59.55	48	344.7	0	0.0	0.1	Soaked in Tap Water
Bentomat	ST	GSE - H.F-F.F	60-mil	GM-THDPE	482.6	126.9	69.6	15.3	102	24	68.9	0	0.0	1	Soaked in Tap Water
Bentomat	ST	Serrot	80-mil	GM-THDPE	34.5	15.9	13.1	18.95	75.5	24	34.5	0	0.0	1	Soaked in Tap Water
Bentomat	ST	Serrot	80-mil	GM-THDPE	34.5	16.5	9.7	18.95	75.5	24	34.5	0	0.0	1	Soaked in Tap Water
Bentomat	ST	Serrot	80-mil	GM-THDPE	34.5	13.8	9.0	18.95	75.5	24	34.5	0	0.0	1	Soaked in Tap Water
Bentomat	ST	Serrot	80-mil	GM-THDPE	34.5	16.5	10.3	18.95	75.5	24	34.5	0	0.0	1	Soaked in Tap Water
Bentomat	ST	Serrot	80-mil	GM-THDPE	68.9	29.0	20.7	18.95	75.5	24	68.9	0	0.0	1	Soaked in Tap Water
Bentomat	ST	Serrot	80-mil	GM-THDPE	68.9	40.7	23.4	18.95	75.5	24	68.9	0	0.0	1	Soaked in Tap Water
Bentomat	ST	Serrot	80-mil	GM-THDPE	68.9	31.0	20.7	18.95	75.5	24	68.9	0	0.0	1	Soaked in Tap Water
Bentomat	ST	Serrot	80-mil	GM-THDPE	68.9	24.1	14.5	18.95	75.5	24	68.9	0	0.0	1	Soaked in Tap Water

Bentomat	ST	Serrot	80-mil	GM-THDPE	137.9	58.6	35.2	18.95	75.5	24	137.9	0	0.0	1	Soaked in Tap Water
Bentomat	ST	Serrot	80-mil	GM-THDPE	137.9	68.9	33.8	18.95	75.5	24	137.9	0	0.0	1	Soaked in Tap Water
Bentomat	ST	Serrot	80-mil	GM-THDPE	137.9	61.4	36.5	18.95	75.5	24	137.9	0	0.0	1	Soaked in Tap Water
Bentomat	ST	Serrot	80-mil	GM-THDPE	137.9	51.0	31.7	18.95	75.5	24	137.9	0	0.0	1	Soaked in Tap Water
Bentomat	ST	Serrot	80-mil	GM-THDPE	137.9	51.0	34.5	20.4	164.5	24	68.9	12	137.9	1	Soaked in Tap Water
Bentomat	ST	Serrot	80-mil	GM-THDPE	275.8	104.1	73.1	20.4	164.5	24	68.9	12	275.8	1	Soaked in Tap Water
Bentomat	ST	Serrot	80-mil	GM-THDPE	551.6	199.9	117.9	20.4	164.5	24	68.9	12	551.6	1	Soaked in Tap Water
Bentomat	ST	SLT	80-mil	GM-THDPE	68.9	43.4	23.4	15.3	126.8	24	68.9	0	0.0	1	Soaked in Tap Water
Bentomat	ST	SLT	80-mil	GM-THDPE	68.9	28.3	18.6	15.3	132.6	24	68.9	0	0.0	1	Soaked in Tap Water
Bentomat	ST	SLT	80-mil	GM-THDPE	89.6	29.0	22.1	12.8	126.9	48	4.8	0	0.0	1	Soaked in Tap Water
Bentomat	ST	SLT	80-mil	GM-THDPE	186.2	60.7	35.2	12.8	123.2	48	4.8	0	0.0	1	Soaked in Tap Water
Bentomat	ST	SLT	80-mil	GM-THDPE	206.8	106.9	50.3	15.3	112.1	24	206.8	0	0.0	1	Soaked in Tap Water
Bentomat	ST	SLT	80-mil	GM-THDPE	206.8	83.4	36.5	15.3	113.3	24	206.8	0	0.0	1	Soaked in Tap Water
Bentomat	ST	SLT	80-mil	GM-THDPE	275.8	71.0	42.7	12.8	144	48	4.8	0	0.0	1	Soaked in Tap Water
Bentomat	ST	SLT	80-mil	GM-THDPE	344.7	144.8	67.6	15.3	104.2	24	344.7	0	0.0	1	Soaked in Tap Water
Bentomat	ST	SLT	80-mil	GM-THDPE	344.7	126.2	53.8	15.3	103.8	24	344.7	0	0.0	1	Soaked in Tap Water
Bentomat	ST	GSE	80-mil	GM-THDPE	6.9	4.8	4.1	18.1	150	24	6.9	0	0.0	1	Soaked in Tap Water
Bentomat	ST	GSE	80-mil	GM-THDPE	6.9	4.1	3.4	10	161	24	13.8	0	0.0	1	Soaked in Tap Water
Bentomat	ST	GSE	80-mil	GM-THDPE	13.8	8.3	5.5	10.7	153	24	13.8	0	0.0	1	Soaked in Tap Water
Bentomat	ST	GSE	80-mil	GM-THDPE	27.6	15.2	6.9	11.4	155	24	13.8	0	0.0	1	Soaked in Tap Water
Bentomat	ST	GSE	80-mil	GM-THDPE	34.5	20.0	13.8	23.8	61	168	20.7	48	34.5	0.1	Soaked in Tap Water
Bentomat	ST	GSE	80-mil	GM-THDPE	34.5	17.2	13.8	20.2	62.5	168	20.7	48	34.5	0.1	Soaked in Tap Water
Bentomat	ST	GSE	80-mil	GM-THDPE	34.5	20.0	12.4	21.1	73	168	20.7	48	34.5	0.1	Soaked in Tap Water
Bentomat	ST	GSE	80-mil	GM-THDPE	34.5	19.3	13.1	19.9	73.5	168	20.7	48	34.5	0.1	Soaked in Tap Water
Bentomat	ST	GSE	80-mil	GM-THDPE	34.5	17.2	11.0	21.2	76	168	20.7	48	34.5	0.1	Soaked in Tap Water
Bentomat	ST	GSE	80-mil	GM-THDPE	34.5	16.5	11.0	21.4	75	168	20.7	48	34.5	0.1	Soaked in Tap Water
Bentomat	ST	GSE	80-mil	GM-THDPE	34.5	19.3	9.7	17.8	83.5	168	20.7	48	34.5	0.1	Soaked in Tap Water
Bentomat	ST	GSE	80-mil	GM-THDPE	34.5	18.6	12.4	22.6	78	168	20.7	48	34.5	0.1	Soaked in Tap Water
Bentomat	ST	GSE	80-mil	GM-THDPE	34.5	14.5	9.7	21.6	71.5	168	20.7	48	34.5	0.1	Soaked in Tap Water
Bentomat	ST	GSE	80-mil	GM-THDPE	34.5	24.1	13.1	14.8	87	168	20.7	48	34.5	0.1	Soaked in Tap Water
Bentomat	ST	GSE	80-mil	GM-THDPE	34.5	18.6	11.7	22.2	89.7	168	20.7	48	34.5	0.1	Soaked in Tap Water
Bentomat	ST	GSE	80-mil	GM-THDPE	34.5	18.6	14.5	14.2	84.6	168	20.7	48	34.5	0.1	Soaked in Tap Water
Bentomat	ST	GSE	80-mil	GM-THDPE	34.5	16.5	12.4	22.5	74	168	20.7	48	34.5	0.1	Soaked in Tap Water
Bentomat	ST	GSE	80-mil	GM-THDPE	34.5	27.6	15.2	22.9	72	168	20.7	48	34.5	0.1	Soaked in Tap Water
Bentomat	ST	GSE	80-mil	GM-THDPE	34.5	25.5	15.9	22.7	69.5	168	20.7	48	34.5	0.1	Soaked in Tap Water
Bentomat	ST	GSE	80-mil	GM-THDPE	34.5	31.7	19.3	23.2	73.5	720	20.7	48	34.5	0.1	Soaked in Tap Water
Bentomat	ST	GSE	80-mil	GM-THDPE	34.5	21.4	13.8	21.5	71	168	20.7	48	34.5	0.1	Soaked in Tap Water
Bentomat	ST	GSE	80-mil	GM-THDPE	34.5	17.2	14.5	23.7	67.5	168	20.7	48	34.5	0.1	Soaked in Tap Water
Bentomat	ST	GSE	80-mil	GM-THDPE	34.5	18.6	11.7	23	76	168	20.7	48	34.5	0.1	Soaked in Tap Water
Bentomat	ST	GSE	80-mil	GM-THDPE	34.5	19.3	13.8	21.6	74.5	168	20.7	48	34.5	0.1	Soaked in Tap Water
Bentomat	ST	GSE	80-mil	GM-THDPE	68.9	29.6	16.5	18.1	124.2	24	68.9	0	0.0	1	Soaked in Tap Water
Bentomat	ST	GSE	80-mil	GM-THDPE	137.9	53.1	31.0	14.8	72.3	168	20.7	48	137.9	0.1	Soaked in Tap Water
Bentomat	ST	GSE	80-mil	GM-THDPE	137.9	46.2	25.5	22.2	70.3	168	20.7	48	137.9	0.1	Soaked in Tap Water
Bentomat	ST	GSE	80-mil	GM-THDPE	137.9	60.0	37.9	14.2	64.2	168	20.7	48	137.9	0.1	Soaked in Tap Water
Bentomat	ST	GSE	80-mil	GM-THDPE	137.9	49.6	31.7	22.5	74	168	20.7	48	137.9	0.1	Soaked in Tap Water
Bentomat	ST	GSE	80-mil	GM-THDPE	137.9	82.7	37.9	22.9	72	168	20.7	48	137.9	0.1	Soaked in Tap Water
Bentomat	ST	GSE	80-mil	GM-THDPE	137.9	76.5	46.9	22.7	69.5	168	20.7	48	137.9	0.1	Soaked in Tap Water
Bentomat	ST	GSE	80-mil	GM-THDPE	137.9	84.8	46.9	23.2	73.5	720	20.7	48	137.9	0.1	Soaked in Tap Water
Bentomat	ST	GSE	80-mil	GM-THDPE	137.9	57.9	34.5	21.5	71	168	20.7	48	137.9	0.1	Soaked in Tap Water
Bentomat	ST	GSE	80-mil	GM-THDPE	137.9	69.6	37.9	23.7	67.5	168	20.7	48	137.9	0.1	Soaked in Tap Water
Bentomat	ST	GSE	80-mil	GM-THDPE	137.9	59.3	31.0	23	76	168	20.7	48	137.9	0.1	Soaked in Tap Water
Bentomat	ST	GSE	80-mil	GM-THDPE	137.9	46.9	28.3	21.6	74.5	168	20.7	48	137.9	0.1	Soaked in Tap Water
Bentomat	ST	GSE	80-mil	GM-THDPE	137.9	53.8	30.3	23.8	61	168	20.7	48	137.9	0.1	Soaked in Tap Water
Bentomat	ST	GSE	80-mil	GM-THDPE	137.9	50.3	33.1	20.2	62.5	168	20.7	48	137.9	0.1	Soaked in Tap Water
Bentomat	ST	GSE	80-mil	GM-THDPE	137.9	42.7	26.2	21.1	73	168	20.7	48	137.9	0.1	Soaked in Tap Water
Bentomat	ST	GSE	80-mil	GM-THDPE	137.9	51.7	33.1	19.9	73.5	168	20.7	48	137.9	0.1	Soaked in Tap Water
Bentomat	ST	GSE	80-mil	GM-THDPE	137.9	44.1	24.8	21.2	76	168	20.7	48	137.9	0.1	Soaked in Tap Water
Bentomat	ST	GSE	80-mil	GM-THDPE	137.9	63.4	43.4	21.4	75	168	20.7	48	137.9	0.1	Soaked in Tap Water
Bentomat	ST	GSE	80-mil	GM-THDPE	137.9	77.2	37.2	17.8	83.5	168	20.7	48	137.9	0.1	Soaked in Tap Water
Bentomat	ST	GSE	80-mil	GM-THDPE	137.9	64.1	37.9	22.6	78	168	20.7	48	137.9	0.1	Soaked in Tap Water
Bentomat	ST	GSE	80-mil	GM-THDPE	137.9	65.5	35.9	21.6	71.5	168	20.7	48	137.9	0.1	Soaked in Tap Water
Bentomat	ST	GSE	80-mil	GM-THDPE	137.9	54.5	29.0	18.1	105.9	24	137.9	0	0.0	1	Soaked in Tap Water
Bentomat	ST	GSE	80-mil	GM-THDPE	241.3	133.1	85.5	20.5	20.5	0	0.0	0	0.0	1	As Received
Bentomat	ST	GSE	80-mil	GM-THDPE	310.3	132.4	60.7	14.8	67.4	168	20.7	48	310.3	0.1	Soaked in Tap Water
Bentomat	ST	GSE	80-mil	GM-THDPE	310.3	117.9	60.0	22.2	51.7	168	20.7	48	310.3	0.1	Soaked in Tap Water
Bentomat	ST	GSE	80-mil	GM-THDPE	310.3	101.4	64.1	14.2	63.8	168	20.7	48	310.3	0.1	Soaked in Tap Water
Bentomat	ST	GSE	80-mil	GM-THDPE	310.3	120.7	73.1	22.5	74	168	20.7	48	310.3	0.1	Soaked in Tap Water
Bentomat	ST	GSE	80-mil	GM-THDPE	310.3	169.6	84.8	22.9	72	168	20.7	48	310.3	0.1	Soaked in Tap Water
Bentomat	ST	GSE	80-mil	GM-THDPE	310.3	148.2	94.5	22.7	69.5	168	20.7	48	310.3	0.1	Soaked in Tap Water
Bentomat	ST	GSE	80-mil	GM-THDPE	310.3	149.6	91.7	23.2	73.5	720	20.7	48	310.3	0.1	Soaked in Tap Water
Bentomat	ST	GSE	80-mil	GM-THDPE	310.3	138.6	77.2	21.5	71	168	20.7	48	310.3	0.1	Soaked in Tap Water
Bentomat	ST	GSE	80-mil	GM-THDPE	310.3	135.8	81.4	23.7	67.5	168	20.7	48	310.3	0.1	Soaked in Tap Water
Bentomat	ST	GSE	80-mil	GM-THDPE	310.3	120.7	75.2	23	76	168	20.7	48	310.3	0.1	Soaked in Tap Water
Bentomat	ST	GSE	80-mil	GM-THDPE	310.3	122.0	63.4	21.6	74.5	168	20.7	48	310.3	0.1	Soaked in Tap Water
Bentomat	ST	GSE	80-mil	GM-THDPE	310.3	123.4	78.6	23.8	61	168	20.7	48	310.3	0.1	Soaked in Tap Water
Bentomat	ST	GSE	80-mil	GM-THDPE	310.3	122.0	73.8	20.2	62.5	168	20.7	48	310.3	0.1	Soaked in Tap Water
Bentomat	ST	GSE	80-mil	GM-THDPE	310.3	98.6	68.3	21.1	73	168	20.7	48	310.3	0.1	Soaked in Tap Water
Bentomat	ST	GSE	80-mil	GM-THDPE	310.3	110.3	66.9	19.9	73.5	168	20.7	48	310.3	0.1	Soaked in Tap Water
Bentomat	ST	GSE	80-mil	GM-THDPE	310.3	100.0	57.2	21.2	76	168	20.7	48	310.3	0.1	Soaked in Tap Water
Bentomat	ST	GSE	80-mil	GM-THDPE	310.3	120.7	72.4	21.4	75	168	20.7	48	310.3	0.1	Soaked in Tap Water
Bentomat	ST	GSE	80-mil	GM-THDPE	310.3	155.1	80.0	17.8	83.5	168	20.7	48	310.3	0.1	Soaked in Tap Water
Bentomat	ST	GSE	80-mil	GM-THDPE	310.3	99.3	74.5	22.6	78	168	20.7	48	310.3	0.1	Soaked in Tap Water
Bentomat	ST	GSE	80-mil	GM-THDPE	310.3	99.3	68.9	21.6	71.5	168	20.7	48	310.3	0.1	Soaked in Tap Water
Bentomat	ST	GSE	80-mil	GM-THDPE	482.6	313.7	142.7	20.5	20.5	0	0.0	0	0.0	1	As Received
Bentomat	ST	GSE	80-mil	GM-THDPE	965.3	488.8	300.6	20.5	20.5	0	0.0	0	0.0	1	As Received
Claymax	500SP	NSC	40-mil	GM-THDPE	6.9	6.2	4.1	54.7	140.3	24	13.8	0	0.0	1	Soaked in Tap Water
Claymax	500SP	NSC	40-mil	GM-THDPE	27.6	15.9	10.3	54.7	120.3	24	13.8	0	0.0	1	Soaked in Tap Water
Claymax	500SP	NSC	40-mil	GM-THDPE	55.2	22.1	11.7	54.7	110.3	24	13.8	0	0.0	1	Soaked in Tap Water
Claymax	500SP	NSC	40-mil	GM-THDPE	103.4	35.2	20.0	54.7	110.2	24	13.8	0	0.0	1	Soaked in Tap Water
Claymax	500SP	GSE	40-mil	GM-THDPE	6.9	2.3	2.3	12.6	170.6	48	6.9	0	0.0	1	Soaked in Tap Water
Claymax	500SP	GSE	40-mil	GM-THDPE	13.8	4.7	4.6	12.6	160.3	48	13.8	0	0.0	1	Soaked in Tap Water
Claymax	500SP	GSE	40-mil	GM-THDPE	27.6	8.9	8.6	12.6	156	48	27.6	0	0.0	1	Soaked in Tap Water
Claymax	500SP	NSC	60-mil	GM-THDPE	2.4	2.2	1.9	18.1	18.1	0	0.0	0	0.0	1	As Received
Claymax	500SP	NSC	60-mil	GM-THDPE	2.4	2.0	1.6	0	0	24	4.8	0	0.0	1	Soaked in Tap Water
Claymax	500SP	NSC	60-mil	GM-THDPE	2.4	0.6	0.6	0	0	24	4.8	0	0.0	1	Soaked in Tap Water
Claymax	500SP	NSC	60-mil	GM-THDPE	4.8	28.6	18.7	0	0	24	4.8	0	0.0	1	Soaked in Tap Water
Claymax	500SP	NSC	60-mil	GM-THDPE	6.9	6.9	4.8	53	140	24	13.8	0	0.0	1	Soaked in Tap Water
Claymax	500SP	NSC	60-mil	GM-THDPE	9.6	6.8	5.5	18	18	0	0.0	0	0.0	1	As Received
Claymax	500SP	NSC	60-mil	GM-THDPE	9.6	7.1	6.1	0	0	24	4.8	0	0.0	1	Soaked in Tap Water
Claymax	500SP	NSC	60-mil	GM-THDPE	9.6	2.9	2.9	0	0	24	4.8	0	0.0	1	Soaked in Tap Water
Claymax	500SP	NSC	60-mil	GM-THDPE	19.2	13.7	11.1	18.2	18.2	0	0.0	0	0.0	1	As Received
Claymax	500SP	NSC	60-mil	GM-THDPE	19.2	13.6	9.8	0	0	24	4.8	0	0.0	1	Soaked in Tap Water
Claymax	500SP	NSC	60-mil	GM-THDPE	19.2	8.2	7.7	0	0	24	4.8	0	0.0	1	Soaked in Tap Water
Claymax	500SP	NSC	60-mil	GM-THDPE	27.6	15.9	11.0	53	130.4	24	13.8	0	0.0	1	Soaked in Tap Water

Claymax	500SP	NSC	60-mil	GM-THDPE	33.5	22.5	15.9	18.3	18.3	0	0.0	0	0.0	1	As Received
Claymax	500SP	NSC	60-mil	GM-THDPE	33.5	18.7	14.0	0	0	24	4.8	0	0.0	1	Soaked in Tap Water
Claymax	500SP	NSC	60-mil	GM-THDPE	33.5	13.1	11.7	0	0	24	4.8	0	0.0	1	Soaked in Tap Water
Claymax	500SP	NSC	60-mil	GM-THDPE	47.9	29.4	20.8	18.2	18.2	0	0.0	0	0.0	1	As Received
Claymax	500SP	NSC	60-mil	GM-THDPE	47.9	16.4	13.1	0	0	24	4.8	0	0.0	1	Soaked in Tap Water
Claymax	500SP	NSC	60-mil	GM-THDPE	55.2	22.1	11.7	53	121.5	24	13.8	0	0.0	1	Soaked in Tap Water
Claymax	500SP	NSC	60-mil	GM-THDPE	103.4	35.2	20.0	53	120.8	24	13.8	0	0.0	1	Soaked in Tap Water
Claymax	500SP	GSE	60-mil	GM-THDPE	12.0	5.7	5.3	18.3	18.2	0	0.0	0	0.0	1	As Received
Claymax	500SP	GSE	60-mil	GM-THDPE	12.0	8.4	6.7	18.5	18.4	0	0.0	0	0.0	1	As Received
Claymax	500SP	GSE	60-mil	GM-THDPE	12.0	5.5	4.8	18.3	141.1	48	12.0	0	0.0	1	Soaked in Tap Water
Claymax	500SP	GSE	60-mil	GM-THDPE	23.9	9.6	7.7	18.4	18.4	0	0.0	0	0.0	1	As Received
Claymax	500SP	GSE	60-mil	GM-THDPE	23.9	13.6	11.3	18.7	18.5	0	0.0	0	0.0	1	As Received
Claymax	500SP	GSE	60-mil	GM-THDPE	23.9	9.8	7.4	18.5	141.5	48	12.0	0	0.0	1	Soaked in Tap Water
Claymax	500SP	GSE	60-mil	GM-THDPE	47.9	18.2	13.2	18.3	18.2	0	0.0	0	0.0	1	As Received
Claymax	500SP	GSE	60-mil	GM-THDPE	47.9	26.6	21.5	18.4	18.2	0	0.0	0	0.0	1	As Received
Claymax	500SP	GSE	60-mil	GM-THDPE	47.9	17.2	11.3	18.5	141.4	48	12.0	0	0.0	1	Soaked in Tap Water
Claymax	500SP	GSE	60-mil	GM-THDPE	68.9	24.1	19.3	33.9	146	24	68.9	0	0.0	1	Soaked in Tap Water
Claymax	500SP	GSE	60-mil	GM-THDPE	68.9	15.2	11.7	26.5	163.2	24	68.9	0	0.0	1	Soaked in Tap Water
Claymax	500SP	GSE	60-mil	GM-THDPE	137.9	26.2	18.6	26.5	154.6	24	137.9	0	0.0	1	Soaked in Tap Water
Claymax	500SP	GSE	60-mil	GM-THDPE	206.8	66.9	38.6	33.9	136.4	24	68.9	0	0.0	1	Soaked in Tap Water
Claymax	500SP	GSE	60-mil	GM-THDPE	275.8	54.5	42.7	26.5	140.1	24	275.8	0	0.0	1	Soaked in Tap Water
Claymax	500SP	GSE	60-mil	GM-THDPE	344.7	107.6	64.1	33.9	128.5	24	68.9	0	0.0	1	Soaked in Tap Water
Claymax	500SP	GSE	60-mil	GM-THDPE	413.7	82.0	56.5	32.5	116.1	24	413.7	0	0.0	1	Soaked in Tap Water
Claymax	500SP	GSE	60-mil	GM-THDPE	551.6	108.2	83.4	32.5	105.3	24	551.6	0	0.0	1	Soaked in Tap Water
Claymax	500SP	GSE	60-mil	GM-THDPE	689.5	133.1	95.8	32.5	95.4	24	689.5	0	0.0	1	Soaked in Tap Water
Claymax	500SP	NSC	80-mil	GM-THDPE	689.5	114.5	95.1	22	152.3	24	68.9	48	689.5	1	Soaked in Tap Water
Claymax	500SP	NSC	80-mil	GM-THDPE	137.9	44.1	38.6	21.9	163.1	42	137.9	0	0.0	1	Soaked in Tap Water
Claymax	500SP	NSC	80-mil	GM-THDPE	689.5	238.6	182.7	21.9	21.5	0	0.0	0	0.0	1	As Received
Claymax	500SP	GSE	80-mil	GM-THDPE	34.5	12.4	11.0	27.3	103.3	168	20.7	48	34.5	0.1	Soaked in Tap Water
Claymax	500SP	GSE	80-mil	GM-THDPE	34.5	11.7	10.3	23.7	106	168	20.7	48	34.5	0.1	Soaked in Tap Water
Claymax	500SP	GSE	80-mil	GM-THDPE	137.9	35.2	29.6	27.3	64.1	168	20.7	48	137.9	0.1	Soaked in Tap Water
Claymax	500SP	GSE	80-mil	GM-THDPE	137.9	40.7	31.0	23.7	77.1	168	20.7	48	137.9	0.1	Soaked in Tap Water
Claymax	500SP	GSE	80-mil	GM-THDPE	310.3	59.3	48.3	27.3	63.5	168	20.7	48	310.3	0.1	Soaked in Tap Water
Claymax	500SP	GSE	80-mil	GM-THDPE	310.3	62.7	46.2	23.7	76.9	168	20.7	48	310.3	0.1	Soaked in Tap Water
Bentomat	ST	EL	30-mil	GM-FPVC	13.8	5.5	5.5	22.3	90.15	48	13.8	0	0.0	1	Soaked in Tap Water
Bentomat	ST	EL	30-mil	GM-FPVC	27.6	10.3	10.3	22.3	90.15	48	27.6	0	0.0	1	Soaked in Tap Water
Bentomat	ST	EL	30-mil	GM-FPVC	41.4	13.8	13.8	22.3	90.15	48	41.4	0	0.0	1	Soaked in Tap Water
Bentomat	ST	EPI	40-mil	GM-SPVC	4.8	1.8	1.8	17.8	173.2	24	4.8	0	0.0	1	Submerged in Tap
Bentomat	ST	EPI	40-mil	GM-SPVC	14.4	4.9	4.9	17.7	179.7	24	4.8	0	0.0	1	Submerged in Tap
Bentomat	ST	EPI	40-mil	GM-SPVC	23.9	8.2	8.2	17.7	179	24	4.8	0	0.0	1	Submerged in Tap
Bentomat	ST	Watersaver	40-mil	GM-SPVC	4.8	2.4	2.4	78.6	44.85	0	0.0	0	0.0	1	Spray with Tap Water
Bentomat	ST	Watersaver	40-mil	GM-SPVC	12.0	4.8	4.8	21.5	80.9	24	12.0	0	0.0	1	Soaked in Tap Water
Bentomat	ST	Watersaver	40-mil	GM-SPVC	12.0	5.2	5.2	21.5	82.2	96	12.0	0	0.0	1	Soaked in Tap Water
Bentomat	ST	Watersaver	40-mil	GM-SPVC	4.8	1.9	1.9	21.6	86.95	24	0.0	24	4.8	1	Soaked in Tap Water
Bentomat	ST	Watersaver	40-mil	GM-SPVC	2.4	1.2	1.2	97.1	172.55	24	0.0	48	2.4	0.05	Soaked in Tap Water
Bentomat	ST	Watersaver	40-mil	GM-SPVC	4.8	2.2	2.2	97.1	172.55	24	0.0	48	4.8	0.05	Soaked in Tap Water
Bentomat	ST	Watersaver	40-mil	GM-SPVC	35.9	10.9	10.9	97.1	172.55	24	0.0	48	35.9	0.05	Soaked in Tap Water
Bentomat	CS	Polyflex	40-mil	GM-TVLDPE	2.4	5.5	4.1	9.9	140.7	24	2.4	0	0.0	1	Soaked in Tap Water
Bentomat	CS	Polyflex	40-mil	GM-TVLDPE	9.6	10.8	6.2	9.9	108.2	24	9.6	0	0.0	1	Soaked in Tap Water
Bentomat	CS	Polyflex	40-mil	GM-TVLDPE	19.2	16.5	11.5	9.9	122.5	24	19.2	0	0.0	1	Soaked in Tap Water
Claymax	500SP	NSC	60-mil	GM-TVLDPE	2.4	2.3	1.9	18.3	141.1	24	4.8	0	0.0	1	Soaked in Tap Water
Claymax	500SP	NSC	60-mil	GM-TVLDPE	9.6	8.9	5.8	18.8	141.7	24	4.8	0	0.0	1	Soaked in Tap Water
Claymax	500SP	NSC	60-mil	GM-TVLDPE	19.2	15.0	10.8	18.5	141.5	24	4.8	0	0.0	1	Soaked in Tap Water
Claymax	500SP	NSC	60-mil	GM-TVLDPE	33.5	22.0	17.3	18.2	140.6	24	4.8	0	0.0	1	Soaked in Tap Water
Claymax	500SP	NSC	60-mil	GM-TVLDPE	47.9	29.9	21.5	18.6	141.2	24	4.8	0	0.0	1	Soaked in Tap Water
Claymax	500SP	Polyflex	60-mil	GM-TVLDPE	12.0	7.2	5.3	18.2	18.1	0	0.0	0	0.0	1	As Received
Claymax	500SP	Polyflex	60-mil	GM-TVLDPE	12.0	10.3	7.9	18.2	18.2	0	0.0	0	0.0	1	As Received
Claymax	500SP	Polyflex	60-mil	GM-TVLDPE	23.9	12.2	9.6	18.4	18.3	0	0.0	0	0.0	1	As Received
Claymax	500SP	Polyflex	60-mil	GM-TVLDPE	23.9	17.7	14.4	18.3	18.2	0	0.0	0	0.0	1	As Received
Claymax	500SP	Polyflex	60-mil	GM-TVLDPE	47.9	28.5	21.5	18.1	18	0	0.0	0	0.0	1	As Received
Claymax	500SP	Polyflex	60-mil	GM-TVLDPE	47.9	33.3	26.6	18.3	18.1	0	0.0	0	0.0	1	As Received
Claymax	500SP	Polyflex	60-mil	GM-TVLDPE	12.0	8.4	7.4	18.5	140.4	48	250.0	0	0.0	1	Soaked in Tap Water
Claymax	500SP	Polyflex	60-mil	GM-TVLDPE	23.9	13.2	11.0	18.2	141.4	48	250.0	0	0.0	1	Soaked in Tap Water
Claymax	500SP	Polyflex	60-mil	GM-TVLDPE	47.9	20.6	14.8	18.4	141.7	48	250.0	0	0.0	1	Soaked in Tap Water
Bentofix	NS	Polyflex	40-mil	GM-TLLDPE	6.9	6.2	4.8	9.6	94	72	6.9	0	0.0	1	Soaked in Tap Water
Bentofix	NS	Polyflex	40-mil	GM-TLLDPE	13.8	9.7	7.6	9.6	94	72	13.8	0	0.0	1	Soaked in Tap Water
Bentofix	NS	Polyflex	40-mil	GM-TLLDPE	27.6	17.9	14.5	9.6	94	72	27.6	0	0.0	1	Soaked in Tap Water
Bentofix	NS	Polyflex	40-mil	GM-TLLDPE	55.2	33.1	24.1	9.6	94	72	55.2	0	0.0	1	Soaked in Tap Water
Bentofix	NS	NSC	40-mil	GM-TLLDPE	6.9	4.1	3.4	9.2	84.5	72	6.9	0	0.0	1	Soaked in Tap Water
Bentofix	NS	NSC	40-mil	GM-TLLDPE	13.8	7.6	5.5	9.2	84.5	72	13.8	0	0.0	1	Soaked in Tap Water
Bentofix	NS	NSC	40-mil	GM-TLLDPE	27.6	13.8	10.3	9.2	84.5	72	27.6	0	0.0	1	Soaked in Tap Water
Bentofix	NS	NSC	40-mil	GM-TLLDPE	55.2	29.6	19.3	9.2	84.5	72	55.2	0	0.0	1	Soaked in Tap Water
Bentomat	ST	NSC	40-mil	GM-TLLDPE	27.6	16.5	11.7	26.3	114	72	27.6	0	0.0	1	Soaked in Tap Water
Bentomat	ST	NSC	40-mil	GM-TLLDPE	55.2	29.6	20.7	26.3	114	72	55.2	0	0.0	1	Soaked in Tap Water
Bentomat	ST	NSC	40-mil	GM-TLLDPE	6.9	5.5	3.4	26.3	114	72	6.9	0	0.0	1	Soaked in Tap Water
Bentomat	ST	NSC	40-mil	GM-TLLDPE	13.8	9.7	6.9	26.3	114	72	13.8	0	0.0	1	Soaked in Tap Water
Bentomat	ST	GSE	40-mil	GM-TLLDPE	4.8	2.0	1.8	82.8	205.5	72	0.0	48	4.8	1	Soaked in Tap Water
Bentomat	ST	GSE	40-mil	GM-TLLDPE	12.0	4.9	4.4	82.8	205.5	72	0.0	48	12.0	1	Soaked in Tap Water
Bentomat	ST	GSE	40-mil	GM-TLLDPE	19.2	7.4	5.9	82.8	205.5	72	0.0	48	19.2	1	Soaked in Tap Water
Bentomat	ST	Polyflex	40-mil	GM-TLLDPE	6.9	5.5	3.4	26.3	107.5	72	6.9	0	0.0	1	Soaked in Tap Water
Bentomat	ST	Polyflex	40-mil	GM-TLLDPE	13.8	10.3	7.6	26.3	107.5	72	13.8	0	0.0	1	Soaked in Tap Water
Bentomat	ST	Polyflex	40-mil	GM-TLLDPE	27.6	17.2	13.8	26.3	107.5	72	27.6	0	0.0	1	Soaked in Tap Water
Bentomat	ST	Polyflex	40-mil	GM-TLLDPE	55.2	32.4	24.8	26.3	107.5	72	55.2	0	0.0	1	Soaked in Tap Water
Bentomat	CS	Polyflex	40-mil	GM-SVLDPE	2.4	1.0	1.0	9.2	155.2	24	2.4	0	0.0	1	Soaked in Tap Water
Bentomat	CS	Polyflex	40-mil	GM-SVLDPE	9.6	2.9	2.9	9.2	130.5	24	9.6	0	0.0	1	Soaked in Tap Water
Bentomat	CS	Polyflex	40-mil	GM-SVLDPE	19.2	5.5	5.5	9.2	108.1	24	19.2	0	0.0	1	Soaked in Tap Water
Bentomat	ST	GSE	40-mil	GM-SVLDPE	14.4	3.8	3.8	17.5	141.6	24	4.8	0	0.0	1	Submerged in Tap
Bentomat	ST	GSE	40-mil	GM-SVLDPE	23.9	6.2	6.2	17.6	147	24	4.8	0	0.0	1	Submerged in Tap
Claymax	200R	Not Specified	40-mil	GM-SLLDPE	13.8	3.4	3.4	32.9	188.5	168	13.8	0	0.0	1	Soaked in Tap Water
Claymax	200R	Not Specified	40-mil	GM-SLLDPE	27.6	6.9	6.9	32.9	188.5	168	27.6	0	0.0	1	Soaked in Tap Water
Claymax	200R	Not Specified	40-mil	GM-SLLDPE	55.2	12.4	12.4	32.9	188.5	168	55.2	0	0.0	1	Soaked in Tap Water
Bentomat	ST	Polyflex	60-mil	GM-SLLDPE	13.8	3.4	2.8	18.6	97.5	24	13.8	0	0.0	1	Soaked in Tap Water
Bentomat	ST	Polyflex	60-mil	GM-SLLDPE	24.1	6.9	6.2	18.6	97.5	24	24.1	0	0.0	1	Soaked in Tap Water
Bentomat	ST	Polyflex	60-mil	GM-SLLDPE	34.5	8.3	7.6	18.6	97.5	24	34.5	0	0.0	1	Soaked in Tap Water

Bentofix	NS	NSC	60-mil	GM-SHDPE	10.3	2.8	2.8	11.1	144.4	48	10.3	0	0.0	1	Soaked in Tap Water
Bentofix	NS	NSC	60-mil	GM-SHDPE	27.6	4.8	4.8	11.1	152.3	48	10.3	0	0.0	1	Soaked in Tap Water
Bentofix	NS	NSC	60-mil	GM-SHDPE	68.9	11.7	11.7	11.1	145.9	48	10.3	0	0.0	1	Soaked in Tap Water
Bentofix	NS	NSC	80-mil	GM-SHDPE	9.7	2.8	2.8	7.5	76	24	55.2	0	0.0	0.2	Soaked in Tap Water
Bentofix	NS	NSC	80-mil	GM-SHDPE	9.7	2.8	2.1	7.8	74	24	55.2	0	0.0	0.2	Soaked in Tap Water
Bentofix	NS	NSC	80-mil	GM-SHDPE	48.3	10.3	8.3	7.5	76	24	55.2	0	0.0	0.2	Soaked in Tap Water
Bentofix	NS	NSC	80-mil	GM-SHDPE	48.3	11.7	10.3	7.8	74	24	55.2	0	0.0	0.2	Soaked in Tap Water
Bentofix	NS	NSC	80-mil	GM-SHDPE	117.2	24.8	20.7	7.5	76	24	55.2	0	0.0	0.2	Soaked in Tap Water
Bentofix	NS	NSC	80-mil	GM-SHDPE	117.2	24.8	20.0	7.8	74	24	55.2	0	0.0	0.2	Soaked in Tap Water
Bentofix	NS	NSC	80-mil	GM-SHDPE	193.1	30.3	29.0	7.5	76	24	55.2	0	0.0	0.2	Soaked in Tap Water
Bentofix	NS	NSC	80-mil	GM-SHDPE	193.1	35.2	32.4	7.8	74	24	55.2	0	0.0	0.2	Soaked in Tap Water
Bentofix	NS	NSC	80-mil	GM-SHDPE	289.6	46.2	44.1	7.5	76	24	55.2	0	0.0	0.2	Soaked in Tap Water
Bentofix	NS	NSC	80-mil	GM-SHDPE	289.6	45.5	39.3	7.8	74	24	55.2	0	0.0	0.2	Soaked in Tap Water
Claymax	500SP	NSC	60-mil	GM-SHDPE	2.4	1.0	1.0	0	0	24	4.8	0	0.0	1	Soaked in Tap Water
Claymax	500SP	NSC	60-mil	GM-SHDPE	9.6	2.4	2.4	0	0	24	4.8	0	0.0	1	Soaked in Tap Water
Claymax	500SP	NSC	60-mil	GM-SHDPE	19.2	4.1	4.1	0	0	24	4.8	0	0.0	1	Soaked in Tap Water
Claymax	500SP	NSC	60-mil	GM-SHDPE	33.5	7.4	7.4	0	0	24	4.8	0	0.0	1	Soaked in Tap Water
Claymax	500SP	NSC	60-mil	GM-SHDPE	47.9	9.7	9.7	0	0	24	4.8	0	0.0	1	Soaked in Tap Water
Claymax	500SP	Polyflex	60-mil	GM-SHDPE	9.6	4.5	3.8	21.6	73.6	24	57.5	0	0.0	0.2	Soaked in Tap Water
Claymax	500SP	Polyflex	60-mil	GM-SHDPE	9.6	4.0	3.4	21.4	72.9	24	57.5	0	0.0	0.2	Soaked in Tap Water
Claymax	500SP	Polyflex	60-mil	GM-SHDPE	47.9	12.8	10.8	21.6	73.6	24	57.5	0	0.0	0.2	Soaked in Tap Water
Claymax	500SP	Polyflex	60-mil	GM-SHDPE	47.9	13.7	13.1	21.4	72.9	24	57.5	0	0.0	0.2	Soaked in Tap Water
Claymax	500SP	Polyflex	60-mil	GM-SHDPE	95.8	16.9	16.5	21.6	73.6	24	57.5	0	0.0	0.2	Soaked in Tap Water
Claymax	500SP	Polyflex	60-mil	GM-SHDPE	95.8	21.0	18.4	21.4	72.9	24	57.5	0	0.0	0.2	Soaked in Tap Water
Claymax	500SP	Polyflex	60-mil	GM-SHDPE	191.5	37.3	36.7	21.6	73.6	24	57.5	0	0.0	0.2	Soaked in Tap Water
Claymax	500SP	Polyflex	60-mil	GM-SHDPE	191.5	34.1	33.6	21.4	72.9	24	57.5	0	0.0	0.2	Soaked in Tap Water
Claymax	500SP	Polyflex	60-mil	GM-SHDPE	287.3	52.3	51.8	21.6	73.6	24	57.5	0	0.0	0.2	Soaked in Tap Water
Claymax	500SP	Polyflex	60-mil	GM-SHDPE	287.3	47.4	46.2	21.4	72.9	24	57.5	0	0.0	0.2	Soaked in Tap Water

Appendix B:

Glossary of Terms

Glossary of Terms

Asperity – A texturing feature used in HDPE, VLDPE and LLDPE geomembranes which typically consists of small polymeric bits of material adhered to the face of the geomembrane, meant to interlock with a soil or geosynthetic interface

Confined Swell Pressure – This is the level of confining pressure at which sodium bentonite clay will not swell beyond its initial height

Direct Shear Device – Device used for shear strength testing that function by confining a specimen between two boxes and translating one of the boxes in relation to the other by pushing the box

Faille Finish – A texturing feature used in PVC geomembranes, similar to the surface of a file with a system of ridges

Failure Envelope – For a given interface, this is the relationship between the peak or residual shear stress and the normal stress applied to an interface. An interface may have a combination of shear and normal stresses below the failure envelope (safe) or along the failure envelope (failed), but not above the failure envelope (impossible)

GCL – Geosynthetic Clay Liner, a layer of powdered or granular bentonite clay attached to confining geosynthetics

Geomembrane – A planar, polymeric material that is used as a hydration barrier, typically in conjunction with a GCL

Hydration – The process in which sodium bentonite absorbs water and swells. GCLs are typically hydrated through soaking in tap water

Mohr-Coulomb Failure Criterion – Linear approximation of the failure envelope for an interface, the slope which is the tangent of the friction angle and the ordinate-intercept is the adhesion, or shear strength at zero normal stress

Platen – A porous rigid plate (plywood, stone or metal) that is used to confine a GCL in a shear testing device, meant to prevent wrinkling of the GCL while providing a distributed shear force and allowing water to flow in and out of the specimen

Ring Shear Device – Device used for shear strength testing that functions by placing a ring-shaped specimen between two rigid plates, and then rotating the top rigid plate in relation to the bottom rigid plate

Sodium Bentonite – A clay soil with very high plasticity that has the ability to hydrate to water contents in the range of 180-200%; the sodium bentonite soil matrix provides water suction that attracts water from surrounding soils, and will swell significantly during hydration

SGI® – Soil-Geosynthetics Interaction Laboratory, formerly a division of GeoSyntec Consultants

Appendix C:

GCL Manufacturer's Specifications

CETCO® LINING TECHNOLOGIES

Certified Properties

BENTOMAT® ST CERTIFIED PROPERTIES

MATERIAL PROPERTY	TEST METHOD	TEST FREQUENCY $ft^2(m^2)$	REQUIRED VALUES
Bentonite Swell Index[1]	ASTM D 5890	1 per 50 tonnes	24mL/2g min
Bentonite Fluid Loss[1]	ASTM D 5891	1 per 50 tonnes	18mL max
Bentonite Mass/Area[2]	ASTM D 5993	40,000ft^2 (4,000m^2)	0.75lb/ft^2 (3.6 kg/m^2) min
GCL Grab Strength[3]	ASTM D 4632	200,000ft^2 (20,000m^2)	90lbs (400 N) MARV
GCL Peel Strength[3]	ASTM D 4632	40,000ft^2 (4,000m^2)	15lbs (65 N) min
GCL Index Flux[4]	ASTM D 5887	Weekly	1 x $10^{-8}m^3/m^2$/sec max
GCL Permeability[4]	ASTM D 5887	Weekly	5 x 10^{-9}cm/sec max
GCL Hydrated Internal Shear Strength[5]	ASTM D 5321	Periodic	500psf (24 kPa) typical

Bentomat ST is a reinforced GCL consisting of a layer of sodium bentonite between a woven and a nonwoven geotextile, which are needlepunched together.

Notes

1 Bentonite property tests performed at a bentonite processing facility before shipment to CETCO's GCL production facilities.

2 Bentonite mass/area reported at 0 percent moisture content.

3 All tensile testing is performed in the machine direction, with results as minimum average roll values unless otherwise indicated.

4 Index flux and permeability testing with deaired distilled/deionized water at 80psi (551kPa) cell pressure, 77psi (531kPa) headwater pressure and p75psi (517kPa) tailwater pressure. Reported value is equivalent to 925gal/acre/day. This flux value is equivalent to a permeability of 5x10^{-9} cm/sec for typical GCL thickness. This flux value should not be used for equivalency calculations unless the gradients used represent field conditions. A flux test using gradients that represent field conditions must be performed to determine equivalency. The last 20 weekly values prior the end of the production date of the supplied GCL may be provided.

5 Peak value measured at 200psf (10kPa) normal stress. Site-specific materials, GCL products, and test conditions must be used to verify internal and interface strength of the proposed design.

CETCO® LINING TECHNOLOGIES

1500 West Shure Drive Arlington Heights, IL 60004 USA 800.527.9948 Fax 847.577.5571
For the most up-to-date product information please visit our website, www.cetco.com
A wholly owned subsidiary of AMCOL International Corporation

Revised 5.02

CETCO® LINING TECHNOLOGIES

Certified Properties

BENTOMAT® DN CERTIFIED PROPERTIES

MATERIAL PROPERTY	TEST METHOD	TEST FREQUENCY ft²(m²)	REQUIRED VALUES
Bentonite Swell Index[1]	ASTM D 5890	1 per 50 tonnes	24mL/2g min
Bentonite Fluid Loss[1]	ASTM D 5891	1 per 50 tonnes	18mL max
Bentonite Mass/Area[2]	ASTM D 5993	40,000ft^2 (4,000 m^2)	0.75lb/ft^2 (3.6 kg/m^2) min
GCL Grab Strength[3]	ASTM D 4632	200,000ft^2(20,000 m^2)	150lbs (660 N) MARV
GCL Peel Strength[3]	ASTM D 4632	40,000ft^2 (4,000 m^2)	15lbs (65 N) min.
GCL Index Flux[4]	ASTM D 5887	Weekly	1 x 10^{-8}m^3/m^2/sec max
GCL Permeability[4]	ASTM D 5887	Weekly	5 x 10^{-9}cm/sec max
GCL Hydrated Internal Sheer Strength[5]	ASTM D 5321	Periodic	500psf (24kPa) typical

Bentomat DN is a reinforced GCL consisting of a layer of sodium bentonite between two nonwoven geotextiles, which are needlepunched together.

Notes

1 Bentonite property tests performed at a bentonite processing facility before shipment to CETCO's GCL production facilities.

2 Bentonite mass/area reported at 0 percent moisture content.

3 All tensile testing is performed in the machine direction, with results as minimum average roll values unless otherwise indicated.

4 Index flux and permeability testing with deaired distilled/deionized water at 80psi (551kPa) cell pressure, 77psi (531kPa) headwater pressure and 75psi (517kPa) tailwater pressure. Reported value is equivalent to 925gal/acre/day. This flux value is equivalent to a permeability of 5x10^{-9} cm/sec for typical GCL thickness. This flux value should not be used for equivalency calculations unless the gradients used represent field conditions. A flux test using gradients that represent field conditions must be performed to determine equivalency. The last 20 weekly values prior the end of the production date of the supplied GCL may be provided.

5 Peak value measured at 200psf (10kPa) normal stress. Site-specific materials, GCL products, and test conditions must be used to verify internal and interface strength of the proposed design.

CETCO® LINING TECHNOLOGIES

1500 West Shure Drive Arlington Heights, IL 60004 USA 800.527.9948 Fax 847.577.5571
For the most up-to-date product information please visit our website, www.cetco.com
A wholly owned subsidiary of AMCOL International Corporation

Revised 5.02

CETCO® LINING TECHNOLOGIES

Certified Properties

CLAYMAX® 200R CERTIFIED PROPERTIES

MATERIAL PROPERTY	TEST METHOD	TEST FREQUENCY $ft^2(m^2)$	REQUIRED VALUES
Bentonite Swell Index[1]	ASTM D 5890	1 per 50 tonnes	24mL/2g min
Bentonite Fluid Loss[1]	ASTM D 5891	1 per 50 tonnes	18mL max
Bentonite Mass/Area[2]	ASTM D 5993	40,000ft^2 (4,000 m^2)	0.75lb/ft^2 (3.6 kg/m^2)
GCL Grab Strength[3]	ASTM D 4632	200,000ft^2 (20,000 m^2)	100lbs (445 N) MARV
GCL Peel Strength[3]	ASTM D 4632	N/A	N/A
GCL Index Flux[4]	ASTM D 5887	Weekly	1 x $10^{-8}m^3/m^2$/sec max
GCL Permeability[4]	ASTM D 5887	Weekly	5 x 10^{-9}cm/sec max
GCL Hydrated Internal Shear Strength[5]	ASTM D 5321	Periodic	50 psf (2.4 kPa) typical

Claymax 200R is an unreinforced GCL consisting of a layer of sodium bentonite between two nonwoven geotextiles which are continuously adhered together.

Notes

1 Bentonite property tests performed at a bentonite processing facility before shipment to CETCO's GCL production facilities.
2 Bentonite mass/area reported at 0 percent moisture content.
3 All tensile testing is performed in the machine direction, with results as minimum average roll values unless otherwise indicated.
4 Index flux and permeability testing with deaired distilled/deionized water at 80psi (551kPa) cell pressure, 77psi (531kPa) headwater pressure and 75psi (517kPa) tailwater pressure. Reported value is equivalent to 925gal/acre/day. This flux value is equivalent to a permeability of $5x10^{-9}$ cm/sec for typical GCL thickness. This flux value should not be used for equivalency calculations unless the gradients used represent field conditions. A flux test using gradients that represent field conditions must be performed to determine equivalency. The last 20 weekly values prior the end of the production date of the supplied GCL may be provided.
5 Peak value measured at 200psf (10kPa) normal stress. Site-specific materials, GCL products, and test conditions must be used to verify internal and interface strength of the proposed design.

CETCO® LINING TECHNOLOGIES

1500 West Shure Drive Arlington Heights, IL 60004 USA 800.527.9948 Fax 847.577.5571
For the most up-to-date product information please visit our website, www.cetco.com
A wholly owned subsidiary of AMCOL International Corporation

Revised 5.02

BENTOFIX® NS

Thermal Lock NS Geosynthetic Clay Liner (GCL)

Bentofix Thermal Lock "NS" is a needlepunch reinforced GCL comprised of a uniform layer of granular sodium bentonite encapsulated between a slit-film woven and a virgin staple fiber nonwoven geotextile. The needlepunched fibers are thermally fused to the woven geotextile to enhance the reinforcing bond.

Product Specifications

GEOTEXTILE PROPERTIES	TEST METHOD	MINIMUM TEST FREQUENCY	VALUE (ENGLISH)	VALUE (SI)
Cap Nonwoven (Mass/Unit Area)	ASTM D 5261	1/200,000 sq ft (1/20,000 sq m)	6.0 oz/yd^2 MARV	200 g/m^2 MARV
Woven Scrim (Mass/Unit Area)	ASTM D 5261	1/200,000 sq ft (1/20,000 sq m)	3.1 oz/yd^2 MARV	105 g/m^2 MARV
BENTONITE PROPERTIES				
Swell Index	ASTM D 5890	1/100,000 lbs (50,000 kg)	24 ml/2 g min	24 ml/2 g min
Moisture Content	ASTM D 4643	1/100,000 lbs (50,000 kg)	12% max	12% max
Fluid Loss	ASTM D 5891	1/100,000 lbs (50,000 kg)	18 ml max	18 ml max
FINISHED GCL PROPERTIES				
Bentonite (Mass/Unit Area)[1]	ASTM D 5993	1/40,000 sq ft (1/4,000 sq m)	0.893 lb/sq ft MARV	4.34 kg/m^2 MARV
Grab Strength[2]	ASTM D 4632	1/40,000 sq ft (1/4,000 sq m)	95 lbs MARV	422 N MARV
Grab Elongation[2]	ASTM D 4632	1/40,000 sq ft (1/4,000 sq m)	100% Typical	100% Typical
Peel Strength[3]	ASTM D 4632	1/40,000 sq ft (1/4,000 sq m)	15 lbs min	66 N
Permeability[4]	ASTM D 5084	1/100,000 sq ft (1/10,000 sq m)	5 x 10^{-9} cm/sec max	5 x 10^{-9} cm/sec max
Index Flux[4]	ASTM D 5887	1/Week	1 x 10^{-8} m^3/m^2/sec max	1 x 10^{-8} m^3/m^2/sec max
Internal Shear Strength[5]	ASTM D 6243	Periodic	500 psf Typical	24 kPa Typical
DIMENSIONS				
Width x Length	Nominal	Every Roll	15.5 x 150 ft	4.7 x 45.72 m
Area per Roll	Nominal	Every Roll	2325 ft^2	216 m^2
Packaged Weight	Typical	Every Roll	2600 lbs	1179 kg

NOTES:

[1] Oven-dried measurement. Equates to 1.0 lb when indexed to a 12% moisture content.
[2] Measured at maximum peak, in weakest principal direction. Elongation is provided for reference only.
[3] Modified to use a 4-inch wide grip. The maximum peak of five specimens averaged.
[4] De-Aired Tap Water @ 5 psi maximum effective confining stress and 2 psi head.
[5] Typical peak value for specimen hydrated for 24 hours and sheared under a 200 psf normal stress.

Americas
GSE Lining Technology, Inc.
Houston, Texas
Phone: 800-435-2008
281-443-8564
Fax: 281-230-8650

Asia/Pacific
GSE Lining Technology Company Ltd.
Bangkok, Thailand
Phone: 66-2-937-0091
Fax: 66-2-937-0097

Europe/Middle East
GSE Lining Technology GmbH
Hamburg, Germany
Phone: 49-40-767420
Fax: 49-40-7674233

A Gundle/SLT Environmental, Inc. Company
www.gseworld.com

Represented by:

BENTOFIX® NW

Thermal Lock NW Geosynthetic Clay Liner (GCL)

Bentofix Thermal Lock "NW" is a needlepunch reinforced GCL comprised of a uniform layer of granular sodium bentonite encapsulated between a scrim reinforced nonwoven and a virgin staple fiber nonwoven geotextile. The needlepunched fibers are thermally fused to the scrim reinforced nonwoven geotextile to enhance the reinforcing bond.

Product Specifications

GEOTEXTILE PROPERTIES	TEST METHOD	MINIMUM TEST FREQUENCY	VALUE (ENGLISH)	VALUE (SI)
Cap Nonwoven - 1 (Mass/Unit Area)	ASTM D 5261	1/200,000 sq ft (1/20,000 sq m)	6.0 oz/yd^2 MARV	200 g/m^2 MARV
Scrim Nonwoven - 2 (Mass/Unit Area)	ASTM D 5261	1/200,000 sq ft (1/20,000 sq m)	6.0 oz/yd^2 MARV	200 g/m^2 MARV
BENTONITE PROPERTIES				
Swell Index	ASTM D 5890	1/100,000 lbs (50,000 kg)	24 ml/2 g min	24 ml/2 g min
Moisture Content	ASTM D 4643	1/100,000 lbs (50,000 kg)	12% max	12% max
Fluid Loss	ASTM D 5891	1/100,000 lbs (50,000 kg)	18 ml max	18 ml max
FINISHED GCL PROPERTIES				
Bentonite (Mass/Unit Area)[1]	ASTM D 5993	1/40,000 sq ft (1/4,000 sq m)	0.893 lb/sq ft MARV	4.34 kg/m^2 MARV
Grab Strength[2]	ASTM D 4632	1/40,000 sq ft (1/4,000 sq m)	150 lbs MARV	667 N MARV
Grab Elongation[2]	ASTM D 4632	1/40,000 sq ft (1/4,000 sq m)	100% Typical	100% Typical
Peel Strength[3]	ASTM D 4632	1/40,000 sq ft (1/4,000 sq m)	15 lbs min	66 N
Permeability[4]	ASTM D 5084	1/100,000 sq ft (1/10,000 sq m)	5 x 10^{-9} cm/sec max	5 x 10^{-9} cm/sec max
Index Flux[4]	ASTM D 5887	1/Week	1 x 10^{-8} m^3/m^2/sec max	1 x 10^{-8} m^3/m^2/sec max
Internal Shear Strength[5]	ASTM D 6243	Periodic	500 psf Typical	24 kPa Typical
DIMENSIONS				
Width x Length	Nominal	Every Roll	15.5 x 150 ft	4.7 x 45.72 m
Area per Roll	Nominal	Every Roll	2325 ft^2	216 m^2
Packaged Weight	Typical	Every Roll	2600 lbs	1179 kg

NOTES:

[1] Oven-dried measurement. Equates to 1.0 lb when indexed to a 12% moisture content.
[2] Measured at maximum peak, in weakest principal direction. Elongation is provided for reference only.
[3] Modified to use a 4-inch wide grip. The maximum peak of five specimens averaged.
[4] De-Aired Tap Water @ 5 psi maximum effective confining stress and 2 psi head.
[5] Typical peak value for specimen hydrated for 24 hours and sheared under a 200 psf normal stress.

Americas
GSE Lining Technology, Inc.
Houston, Texas
Phone: 800-435-2008
281-443-8564
Fax: 281-230-8650

Asia/Pacific
GSE Lining Technology Company Ltd.
Bangkok, Thailand
Phone: 66-2-937-0091
Fax: 66-2-937-0097

Europe/Middle East
GSE Lining Technology GmbH
Hamburg, Germany
Phone: 49-40-767420
Fax: 49-40-7674233

A Gundle/SLT Environmental, Inc. Company
www.gseworld.com

Represented by:

BENTOFIX® NWL

Thermal Lock NWL Geosynthetic Clay Liner (GCL)

Bentofix Thermal Lock "NWL" is a needlepunch reinforced GCL comprised of a uniform layer of granular sodium bentonite encapsulated between a scrim reinforced nonwoven and a virgin staple fiber nonwoven geotextile. The needlepunched fibers are thermally fused to the scrim reinforced nonwoven geotextile to enhance the reinforcing bond.

Product Specifications

GEOTEXTILE PROPERTIES	TEST METHOD	MINIMUM TEST FREQUENCY	VALUE (ENGLISH)	VALUE (SI)
Cap Nonwoven - 1 (Mass/Unit Area)	ASTM D 5261	1/200,000 sq ft (1/20,000 sq m)	6.0 oz./yd^2 MARV	200 g/m^2 MARV
Scrim Nonwoven - 2 (Mass/Unit Area)	ASTM D 5261	1/200,000 sq ft (1/20,000 sq m)	6.0 oz./yd^2 MARV	200 g/m^2 MARV
BENTONITE PROPERTIES				
Swell Index	ASTM D 5890	1/100,000 lbs (50,000 kg)	24 ml/2 g min	24 ml/2 g min
Moisture Content	ASTM D 4643	1/100,000 lbs (50,000 kg)	12% max	12% max
Fluid Loss	ASTM D 5891	1/100,000 lbs (50,000 kg)	18 ml max	18 ml max
FINISHED GCL PROPERTIES				
Bentonite (Mass/Unit Area)[1]	ASTM D 5993	1/40,000 sq ft (1/4,000 sq m)	0.75 lb/sq ft MARV	3.66 kg/m^2 MARV
Grab Strength[2]	ASTM D 4632	1/40,000 sq ft (1/4,000 sq m)	150 lbs MARV	667 N MARV
Grab Elongation[2]	ASTM D 4632	1/40,000 sq ft (1/4,000 sq m)	100% Typical	100% Typical
Peel Strength[3]	ASTM D 4632	1/40,000 sq ft (1/4,000 sq m)	15 lbs min	66 N
Permeability[4]	ASTM D 5084	1/100,000 sq ft (1/10,000 sq m)	5 x 10^{-9} cm/sec max	5 x 10^{-9} cm/sec max
Index Flux[4]	ASTM D 5887	1/Week	1 x 10^{-8} m^3/m^2/sec max	1 x 10^{-8} m^3/m^2/sec max
Internal Shear Strength[5]	ASTM D 6243	Periodic	500 psf Typical	24 kPa Typical
DIMENSIONS				
Width x Length	Nominal	Every Roll	15.5 x 150 ft	4.7 x 45.72 m
Area per Roll	Nominal	Every Roll	2325 ft^2	216 m^2
Packaged Weight	Typical	Every Roll	2160 lbs	980 kg

NOTES:

[1] Oven-dried measurement. Equates to 0.84 lbs when indexed to a 12% moisture content.
[2] Measured at maximum peak, in the weakest principal direction. Elongation is provided for reference only.
[3] Modified to use a 4 inch wide grip. The maximum peak of five specimens averaged.
[4] De-Aired Tap Water @ 5 psi maximum effective confining stress and 2 psi head.
[5] Typical peak value for specimen hydrated for 24 hours and sheared under a 200 psf normal stress.

Americas
GSE Lining Technology, Inc.
Houston, Texas
Phone: 800-435-2008
281-443-8564
Fax: 281-230-8650

Asia/Pacific
GSE Lining Technology Company Ltd.
Bangkok, Thailand
Phone: 66-2-937-0091
Fax: 66-2-937-0097

Europe/Middle East
GSE Lining Technology GmbH
Hamburg, Germany
Phone: 49-40-767420
Fax: 49-40-7674233

A Gundle/SLT Environmental, Inc. Company
www.gseworld.com

Represented by:

GSE GundSeal GCL

Geomembrane Supported Geosynthetic Clay Liner (GCL)

GSE GundSeal GCL composite liner combines the high swelling and sealing characteristics of bentonite clay with the low permeability of a polyethylene geomembrane. GSE GundSeal GCL consists of approximately 0.75 lb/ft^2 (3.7 kg/m^2) of high quality sodium bentonite adhered to a geomembrane. This composite liner allows the installer to conveniently roll out a blanket of clay, replacing or supplementing compacted clay and geomembrane required for liner and cap systems. The polyethylene geomembrane backing for the GSE GundSeal GCL is available in thicknesses ranging from 15 mil (0.4 mm) up to 80 mil (2.0 mm) and may have two textured surfaces for improved slope stability.

Product Specifications

Properties of GSE GundSeal GCL	TEST METHOD	MINIMUM AVERAGE VALUES			
Bentonite Coating, lb/ft^2 (kg/m^2)[1]	ASTM D 5993	≥ 0.75 (3.7)			
Effective Hydraulic Conductivity: GSE GundSeal, m/sec	ASTM D 5887	≤ 4 x 10^{-14}			
Hydraulic Conductivity: Bentonite, m/sec	ASTM D 5887	≤ 5 x 10^{-11}			
Bentonite Moisture Content	ASTM D 2216	25% Typical			
Properties of the HDPE polyethylene geomembrane backing used in the production of GSE GundSeal GCL					
		Smooth Geomembrane[2]		Textured Geomembrane[2]	
Thickness, mil (mm)	ASTM D 5199/D 5994	15 (0.4)	60 (1.5)	30 (0.75)	60 (1.5)
Density, g/cm^3	ASTM D 1505	0.94	0.94	0.94	0.94
Tensile Properties,	ASTM D 638, Type IV				
Strength at Break, lb/in-width (N/mm)	Dumbell, 2 ipm (50 mm/in)	35 (6)	243 (43)	45 (8)	90 (16)
Strength at Yield, lb/in-width (N/mm)		20 (3.5)	130 (23)	63 (11)	130 (23)
Elongation at Break, %	G.L. = 2.0 in (50 mm)	500	700	150	150
Elongation at Yield, %	G.L. = 1.3 in (33 mm)	10	13	13	13
Puncture Resistance, lb (N)	ASTM D 4833	20 (89)	119 (530)	54 (240)	108 (480)
Properties of sodium bentonite used in the production of GSE GundSeal GCL					
Hydraulic Flux: Bentonite, m^3/m^2•sec	ASTM D 5887	≤ 1 x 10^{-10}			
Fluid Loss, ml	ASTM D 5891	≤ 18			
Free Swell, ml/2 g	ASTM D 5890	≥ 24			

NOTES:

[1]0% moisture content.

[2]Available in thicknesses ranging up to 80 mil (2.0 mm). Please see specific GSE geomembrane product data sheets for additional information.

GundSeal Roll Dimensions include 17.5 ft (5.3 m) wide, 170-200 ft (51-61 m) length (depending on geomembrane thickness).

GundSeal material includes a 0.75 oz/yd (25 g/m^2) spunbonded geotextile adhered to the bentonite surface.

Americas
GSE Lining Technology, Inc.
Houston, Texas
Phone: 800-435-2008
281-443-8564
Fax: 281-230-8650

Asia/Pacific
GSE Lining Technology Company Ltd.
Bangkok, Thailand
Phone: 66-2-937-0091
Fax: 66-2-937-0097

Europe/Middle East
GSE Lining Technology GmbH
Hamburg, Germany
Phone: 49-40-767420
Fax: 49-40-7674233

A Gundle/SLT Environmental, Inc. Company
www.gseworld.com

Represented by:

GSE HD

Smooth HDPE Geomembrane

GSE HD is a high quality, high density polyethylene (HDPE) geomembrane produced from specially formulated, virgin polyethylene resin. This polyethylene resin is designed specifically for flexible geomembrane applications. It contains approximately 97.5% polyethylene, 2.5% carbon black and trace amounts of antioxidants and heat stabilizers; no other additives, fillers or extenders are used. GSE HD has outstanding chemical resistance, mechanical properties, environmental stress crack resistance, dimensional stability and thermal aging characteristics. GSE HD has excellent resistance to UV radiation and is suitable for exposed conditions.

Product Specifications

TESTED PROPERTY	TEST METHOD	MINIMUM VALUES				
Thickness, mils (mm)	ASTM D 5199	27 (0.69)	36 (0.91)	54 (1.4)	72 (1.8)	90 (2.3)
Density, g/cm^3	ASTM D 1505	0.94	0.94	0.94	0.94	0.94
Tensile Properties (each direction)	ASTM D 638, Type IV					
Strength at Break, lb/in-width (N/mm)	Dumbell, 2 ipm	122 (21)	162 (28)	243 (43)	324 (57)	405 (71)
Strength at Yield, lb/in-width (N/mm)		63 (11)	84 (15)	130 (23)	173 (30)	216 (38)
Elongation at Break, %	G.L. 2.0 in (51 mm)	700	700	700	700	700
Elongation at Yield, %	G.L. 1.3 in (33 mm)	13	13	13	13	13
Tear Resistance, lb (N)	ASTM D 1004	21 (93)	28 (124)	42 (187)	56 (249)	70 (311)
Puncture Resistance, lb (N)	ASTM D 4833	59 (263)	79 (352)	119 (530)	158 (703)	198 (881)
Carbon Black Content, %	ASTM D 1603	2.0	2.0	2.0	2.0	2.0
Carbon Black Dispersion	ASTM D 5596	+Note 1	+Note 1	+Note 1	+Note 1	+Note 1
Notched Constant Tensile Load, hrs	ASTM D 5397, Appendix	400	400	400	400	400
REFERENCE PROPERTY	**TEST METHOD**	**NOMINAL VALUES**				
Thickness, mils (mm)	ASTM D 5199	30 (0.75)	40 (1.0)	60 (1.5)	80 (2.0)	100 (2.5)
Roll Length (approximate), ft (m)		1120 (341)	870 (265)	560 (171)	430 (131)	340 (104)
Oxidative Induction Time, minutes	ASTM D 3895, 200° C; O_2, 1 atm	>100	>100	>100	>100	>100

NOTES:

+Note 1: Dispersion only applies to near spherical agglomerates. 9 of 10 views shall be Category 1 or 2. No more than 1 view from Category 3.

GSE HD is available in rolls approximately 22.5 ft (6.9 m) wide and weighing about 2,900 lb (1,315 kg).

All GSE geomembranes have dimensional stability of ±2% when tested with ASTM D 1204 and LTB of <-77° C when tested with ASTM D 746.

Americas
GSE Lining Technology, Inc.
Houston, Texas
Phone: 800-435-2008
281-443-8564
Fax: 281-230-8650

Asia/Pacific
GSE Lining Technology Company Ltd.
Bangkok, Thailand
Phone: 66-2-937-0091
Fax: 66-2-937-0097

Europe/Middle East
GSE Lining Technology GmbH
Hamburg, Germany
Phone: 49-40-767420
Fax: 49-40-7674233

A Gundle/SLT Environmental, Inc. Company
www.gseworld.com

Represented by:

GSE HD Textured

Textured HDPE Geomembrane

GSE HD Textured is the textured version of GSE HD. It is a high quality, high density polyethylene (HDPE) geomembrane with one or two coextruded, textured surfaces, and consisting of approximately 97.5% polyethylene, 2.5% carbon black and trace amounts of antioxidants and heat stabilizers; no other additives, fillers or extenders are used. The resin used is specially formulated, virgin polyethylene and is designed specifically for flexible geomembrane applications. GSE HD Textured has excellent resistance to UV radiation and is suitable for exposed conditions. This product allows projects with greater slopes to be designed since frictional characteristics are enhanced.

Product Specifications

TESTED PROPERTY	TEST METHOD	MINIMUM VALUES				
Thickness, mils (mm)	ASTM D 5994	27 (0.69)	36 (0.91)	54 (1.4)	72 (1.8)	90 (2.3)
Density, g/cm^3	ASTM D 1505	0.94	0.94	0.94	0.94	0.94
Tensile Properties (each direction)[1]	ASTM D 638, Type IV					
Strength at Break, lb/in-width (N/mm)	Dumbell, 2 ipm	45 (8)	60 (11)	90 (16)	120(21)	150 (27)
Strength at Yield, lb/in-width (N/mm)		63 (11)	84 (15)	130 (23)	173 (30)	216 (38)
Elongation at Break, %	G.L. = 2.0 in (51 mm)	150	150	150	150	150
Elongation at Yield, %	G.L. = 1.3 in (33 mm)	13	13	13	13	13
Tear Resistance, lb (N)	ASTM D 1004	21 (93)	28 (124)	42 (187)	56 (249)	70 (311)
Puncture Resistance, lb (N)	ASTM D 4833	54 (240)	72 (320)	108 (480)	144 (641)	180 (801)
Carbon Black Content, %	ASTM D 1603	2.0	2.0	2.0	2.0	2.0
Carbon Black Dispersion	ASTM D 5596	+Note 1	+Note 1	+Note 1	+Note 1	+Note 1
Notched Constant Tensile Load[2], hrs	ASTM D 5397, Appendix	400	400	400	400	400
REFERENCE PROPERTY	**TEST METHOD**	**NOMINAL VALUES**				
Thickness, mils (mm)	ASTM D 5994	30 (0.75)	40 (1.0)	60 (1.5)	80 (20)	100 (2.5)
Roll Length (approximate), ft (m)	Standard Textured	830 (253)	700 (213)	520 (158)	400(122)	330 (101)
Oxidative Induction Time, minutes	ASTM D 3895, 200° C; O_2, 1 atm	>100	>100	>100	>100	>100

NOTES:

+Note 1: Dispersion only applies to near spherical agglomerates. 9 of 10 views shall be Category 1 or 2. No more than 1 view from Category 3.

GSE HD Standard Textured is available in rolls approximately 22.5 ft (6.9 m) wide and weighing about 3,700 lb (1,678 kg).

[1]The combination of stress concentrations due to coextrusion texture geometry and the small specimen size results in large variation of test results. Therefore, these tensile properties are minimum average values.

[2]Note: NCTL for HD Textured is conducted on representative smooth membrane samples.

All GSE geomembranes have dimensional stability of ±2% when tested with ASTM D 1204 and LTB of <-77° C when tested with ASTM D 746.

Americas
GSE Lining Technology, Inc.
Houston, Texas
Phone: 800-435-2008
281-443-8564
Fax: 281-230-8650

Asia/Pacific
GSE Lining Technology Company Ltd.
Bangkok, Thailand
Phone: 66-2-937-0091
Fax: 66-2-937-0097

Europe/Middle East
GSE Lining Technology GmbH
Hamburg, Germany
Phone: 49-40-767420
Fax: 49-40-7674233

A Gundle/SLT Environmental, Inc. Company
www.gseworld.com

Represented by:

GSE UltraFlex

Smooth LLDPE Geomembrane

GSE UltraFlex is a high quality, linear low density polyethylene (LLDPE) geomembrane produced from specially formulated, virgin polyethylene with outstanding flexibility. This polyethylene resin is designed specifically for flexible geomembrane applications. Its high uniaxial and multiaxial elongation characteristics make it very suitable for applications where differential or localized subgrade settlements are expected such as leach pads, landfill closure caps, or any application where elongation or puncture resistance is critical. GSE UltraFlex contains approximately 97.5% polyethylene, 2.5% carbon black and trace amounts of antioxidants and heat stabilizers; no fillers or extenders are used. GSE UltraFlex is the only material of its type on the market with many years of proven performance in applications throughout the world.

Product Specifications

TESTED PROPERTY	TEST METHOD	MINIMUM VALUES			
Thickness, mils (mm)	ASTM D 5199	27 (0.69)	36 (0.91)	54 (1.4)	72 (1.8)
Density, g/cm^3	ASTM D 1505	0.92	0.92	0.92	0.92
Tensile Properties (each direction)	ASTM D 638, Type IV				
Strength at Break, lb/in-width (N/mm)	Dumbell, 2 ipm	114 (20)	152 (27)	228 (40)	304 (53)
Elongation at Break, %	G.L. = 2.0 in (51 mm)	850	850	850	850
Tear Resistance, lb (N)	ASTM D 1004	16 (71)	22 (100)	33 (150)	44 (200)
Puncture Resistance, lb (N)	ASTM D 4833	46 (205)	62 (276)	92 (409)	123 (547)
Carbon Black Content, %	ASTM D 1603	2.0	2.0	2.0	2.0
Carbon Black Dispersion	ASTM D 5596	+Note 1	+Note 1	+Note 1	+Note 1
REFERENCE PROPERTY	**TEST METHOD**	**NOMINAL VALUES**			
Thickness, mils (mm)	ASTM D 5199	30 (0.75)	40 (1.0)	60 (1.5)	80 (2.0)
Roll Length (approximate), ft (m)		1120 (341)	870 (265)	560 (171)	430 (131)
Oxidative Induction Time, minutes	ASTM D 3895, 200° C 1 ATM	>100	>100	>100	>100

NOTES:

+Note 1: Dispersion only applies to near spherical agglomerates. 9 of 10 views shall be Category 1 or 2. No more than 1 view from Category 3.

GSE UltraFlex is available in rolls approximately 22.5 (6.9 m) wide and weighing about 2,800 lb (1,270 kg) respectively.

All GSE geomembranes have dimensional stability of ±2% when tested with ASTM D 1204 and LTB of <-77° C when tested with ASTM D 746.

Americas
GSE Lining Technology, Inc.
Houston, Texas
Phone: 800-435-2008
281-443-8564
Fax: 281-230-8650

Asia/Pacific
GSE Lining Technology Company Ltd.
Bangkok, Thailand
Phone: 66-2-937-0091
Fax: 66-2-937-0097

Europe/Middle East
GSE Lining Technology GmbH
Hamburg, Germany
Phone: 49-40-767420
Fax: 49-40-7674233

A Gundle/SLT Environmental, Inc. Company
www.gseworld.com

Represented by:

GSE UltraFlex Textured

Textured LLDPE Geomembrane

GSE UltraFlex Textured is the coextruded textured version of GSE UltraFlex. It is a high quality, linear low density polyethylene (LLDPE) geomembrane with one or two coextruded, textured surfaces, and consisting of approximately 97.5% polyethylene, 2.5% carbon black and trace amounts of antioxidants and heat stabilizers; no other additives, fillers or extenders are used. The resin used is a specially formulated, proprietary virgin polyethylene and is designed specifically for flexible geomembrane applications. GSE UltraFlex Textured has excellent resistance to UV radiation and is suitable for exposed conditions. This product allows projects with greater slopes to be designed since frictional characteristics are enhanced.

Product Specifications

TESTED PROPERTY	TEST METHOD	MINIMUM VALUES	
Thickness, mils (mm)	ASTM D 5994	36 (0.91)	54 (1.4)
Density, g/cm^3	ASTM D 1505	0.92	0.92
Tensile Properties (each direction)[1]	ASTM D 638, Type IV		
Strength at Break, lb/in-width (N/mm)	Dumbell, 2 ipm	100 (18)	132 (23)
Elongation at Break, %	G.L. = 2.0 in (51 mm)	500	500
Tear Resistance, lb (N)	ASTM D 1004	22 (100)	33 (150)
Puncture Resistance, lb (N)	ASTM D 4833	48 (214)	73 (325)
Carbon Black Content, %	ASTM D 1603	2.0	2.0
Carbon Black Dispersion	ASTM D 5596	+Note 1	+Note 1
REFERENCE PROPERTY	**TEST METHOD**	**NOMINAL VALUES**	
Thickness, mils (mm)	ASTM D 5994	40 (1.0)	60 (1.5)
Roll Length (approximate), ft (m)		700 (213)	520 (158)
Oxidative Induction Time, minutes	ASTM D 3895, 200° C O_2, 1 atm	>100	>100

Notes:

+Note 1: Dispersion only applies to near spherical agglomerates. 9 of 10 views shall be Category 1 or 2. No more than 1 view from Category 3.

GSE UltraFlex Textured is available in rolls approximately 22.5 ft (6.9 m) wide and weighing about 3,700 lb (1,678 kg). Other material thicknesses are available upon request.

[1]The combination of stress concentrations due to coextrusion texture geometry and the small specimen size results in large variation of test results. Therefore, these tensile properties are average roll values.

All GSE geomembranes have dimensional stability of ±2% when tested with ASTM D 1204 and LTB of <-77° C when tested with ASTM D 746.

Americas
GSE Lining Technology, Inc.
Houston, Texas
Phone: 800-435-2008
281-443-8564
Fax: 281-230-8650

Asia/Pacific
GSE Lining Technology Company Ltd.
Bangkok, Thailand
Phone: 66-2-937-0091
Fax: 66-2-937-0097

Europe/Middle East
GSE Lining Technology GmbH
Hamburg, Germany
Phone: 49-40-767420
Fax: 49-40-7674233

A Gundle/SLT Environmental, Inc. Company
www.gseworld.com

Represented by:

Serrot HD Geomembranes

Serrot International, Inc. offers High Density Polyethylene (HDPE) and Linear Low Density Polyethylene (LLDPE) smooth and textured geomembranes in thicknesses of 1.0, 1.5, 2.0 and 2.5 mm (40, 60, 80 and 100 mils).
Serrot HD products are manufactured using first quality, high molecular weight resins specifically for containment in hydraulic structures. Serrot HD provides excellent yield strength and seam strength and is ideal for applications requiring high chemical resistance, low permeability and high ultraviolet resistance. HDPE is today's most widely used geomembrane for solid and hazardous waste landfills. Stringent Manufacturing Quality Control is performed on a regular basis. Please refer to the MQC Manual located under the Technical Information section of this web site.

Width: 23'
Color: Black

Features
Chemical Resistance – HDPE, resistant to a wide range of chemicals, is not threatened by typical solid or hazardous waste leachates. It is also suitable for sludge and secondary containment around chemical storage facilities.
Low Permeability – HDPE systems are secure because leachate will not penetrate liners; methane gas will not escape from the cover system; and rainwater will not infiltrate an HDPE cap.
Ultraviolet Resistance – HDPE's resistance to UV exposure is further enhanced by the addition of carbon black to HDPE. Since Serrot HD contains no plasticizers, volatilization is never a problem

Applications
Landfill (primary and secondary
Landfill caps /closures
Lagoon liners
Pond liners
Floating covers
Secondary containment for above ground storage tanks
Solutions ponds for mining applications
Retention ponds
Waste water treatment facilities
Potable water reservoirs
Tank linings
Canal linings
Mining heap leach pads

Serrot LD Geomembranes

Serrot International, Inc. offers High Density Polyethylene (HDPE) and Linear Low Density Polyethylene (LLDPE) smooth and textured geomembranes in thicknesses of 1.0, 1.5, 2.0 and 2.5 mm (40, 60, 80 and 100 mils).
Serrot LD - linear low density polyethylene (LLDPE) geomembranes - are produced from first quality, high molecular weight resins formulated to be chemically resistant, free of leachable additives and resistant to ultraviolet degradation. LLDPE is made specifically for containment in hydraulic structures. Serrot LD provides excellent flexibility and high puncture resistance and is ideal for landfill caps and pond liners. Stringent Manufacturing Quality Control is performed on a regular basis. Please refer to the MQC Manual located under the Technical Information section of this web site.

Width: 23'
Color: Black

Features
Flexibility – Greater flexibility provides increased conformance to subsidence and differential settlement.
Puncture Resistance – High puncture elongation properties make these liners ideal in applications where conforming to subgrade irregularities may puncture other liners.

Applications
Landfill caps /closures
Lagoon liners
Pond liners
Secondary containment
Sludge caps
Mining heap leach pads

Serrot HT and Serrot LT Textured Geomembranes

Serrot International, Inc. offers High Density Polyethylene (HDPE) and Linear Low Density Polyethylene (LLDPE) smooth and textured geomembranes in thicknesses of 1.0, 1.5, 2.0 and 2.5 mm (40, 60, 80 and 100 mils).
Serrot Textured Geomembranes are produced by texturing Serrot HD and Serrot LD geomembranes. By using Serrot Textured Geomembranes, slope angles and factors of safety are increased. This allows for more airspace in the cell, thereby increasing available space for waste. Serrot Textured Geomembranes are manufactured and tested according to the same high standard of Quality Control performed on the smooth products. Please refer to the MQC Manual located under the Technical Information section of this web site.

Width: 23'
Color: Black

Features
Versatility – Serrot Textured Geomembranes are available with a roughened surface on one or both sides of an HDPE or LLDPE geomembrane in thicknesses ranging from 1.0 – 2.5 mm (40 – 100 mils).
High Quality Seaming – Some of Serrot's Textured Geomembranes are producted with a smooth edge on each side of the sheet and along the top and bottom. This ensures that the same high quality welds are achieved as those acheived when welding smooth sheets of geomembrane.
High Coefficient of Friction – When Serrot Textured Geomembranes are used with soils or other geosynthetics, the shear strength is increased resulting in improved slope stability.

Applications
Steep slope applications
Landfills – primary and secondary containment
Landfill caps/closures
Lagoon liners
Pond liners
Sludge caps

Appendix D:

Details for Reliability-Based Design Charts

Internal GCL

$E(t_1)$ =	1	m
$E(t_2)$ =	3	m
s(t) =	0.1	m
$E(\gamma)$ =	20	kN/m^3
$s(\gamma)$ =	1.5	kN/m^3
$s(\psi)$ =	0.5	degrees
$E(\phi_{P})$ =	28.71	degrees
$s(\phi_{P})$ =	3.88	degrees
$E(C_{A,P})$ =	30.43	kPa
$s(C_{A,P})$ =	8.61	kPa
$E(\phi_{LD})$ =	8.96	degrees
$s(\phi_{LD})$ =	2.43	degrees
$E(C_{A,LD})$ =	15.63	kPa
$s(C_{A,LD})$ =	9.49	kPa

$$FS = \frac{C_A}{\gamma t \sin\psi} + \frac{\tan\phi}{\tan\psi}$$

Internal GCL Peak, t = 1 m

E(ψ)	$FS_{MLV,\ Peak}$	t			γ			ψ			C_A			ϕ			$\sigma_{FS,Peak}$	$V_{FS,\ Peak}$	β_{LN}	P_F
		FS_i^+	FS_i^-	ΔFS_i	FS_i^+	FS_i^-	ΔFS_i	FS_i^+	FS_i^-	ΔFS_i	FS_i^+	FS_i^-	ΔFS_i	FS_i^+	FS_i^-	ΔFS_i				
5	23.714	22.128	25.654	-3.526	22.497	25.130	-2.633	21.560	26.348	-4.788	28.656	18.773	9.884	24.762	22.742	2.019	6.001	0.253	12.583	0.000E+00
6	19.764	18.441	21.381	-2.940	18.749	20.944	-2.195	18.245	21.560	-3.315	23.885	15.644	8.241	20.636	18.955	1.681	4.878	0.247	12.149	0.000E+00
7	16.943	15.808	18.330	-2.522	16.072	17.955	-1.883	15.815	18.245	-2.430	20.477	13.409	7.068	17.689	16.251	1.439	4.118	0.243	11.692	0.000E+00
8	14.828	13.834	16.042	-2.208	14.065	15.714	-1.649	13.957	15.815	-1.858	17.922	11.733	6.189	15.479	14.223	1.257	3.569	0.241	11.245	0.000E+00
9	13.182	12.298	14.263	-1.965	12.504	13.971	-1.467	12.490	13.957	-1.467	15.936	10.429	5.506	13.761	12.646	1.115	3.152	0.239	10.821	0.000E+00
10	11.867	11.070	12.840	-1.770	11.255	12.577	-1.322	11.303	12.490	-1.187	14.347	9.386	4.961	12.386	11.384	1.002	2.824	0.238	10.422	0.000E+00
11	10.790	10.065	11.676	-1.611	10.234	11.437	-1.203	10.322	11.303	-0.980	13.047	8.533	4.514	11.262	10.353	0.909	2.560	0.237	10.049	0.000E+00
12	9.893	9.228	10.706	-1.478	9.383	10.487	-1.104	9.499	10.322	-0.823	11.965	7.822	4.143	10.324	9.493	0.831	2.342	0.237	9.699	0.000E+00
13	9.135	8.520	9.886	-1.366	8.663	9.683	-1.020	8.798	9.499	-0.701	11.050	7.220	3.829	9.532	8.767	0.765	2.159	0.236	9.371	0.000E+00
14	8.485	7.913	9.184	-1.270	8.046	8.995	-0.949	8.194	8.798	-0.604	10.265	6.705	3.561	8.852	8.144	0.708	2.004	0.236	9.063	0.000E+00
15	7.922	7.387	8.575	-1.187	7.512	8.398	-0.887	7.667	8.194	-0.526	9.586	6.258	3.328	8.264	7.604	0.659	1.870	0.236	8.772	0.0000
16	7.429	6.927	8.042	-1.115	7.044	7.877	-0.833	7.205	7.667	-0.462	8.992	5.866	3.125	7.749	7.132	0.616	1.753	0.236	8.497	0.0000
17	6.995	6.522	7.573	-1.051	6.632	7.416	-0.785	6.796	7.205	-0.409	8.468	5.521	2.946	7.294	6.716	0.578	1.651	0.236	8.237	0.0000
18	6.608	6.161	7.155	-0.995	6.265	7.008	-0.743	6.431	6.796	-0.365	8.002	5.215	2.788	6.890	6.347	0.544	1.560	0.236	7.991	0.0000
19	6.263	5.838	6.782	-0.944	5.937	6.642	-0.705	6.104	6.431	-0.327	7.586	4.940	2.646	6.529	6.016	0.513	1.480	0.236	7.756	0.0000
20	5.953	5.548	6.447	-0.899	5.642	6.313	-0.671	5.809	6.104	-0.295	7.212	4.693	2.519	6.204	5.719	0.485	1.407	0.236	7.532	0.0000
21	5.672	5.286	6.143	-0.858	5.376	6.016	-0.640	5.541	5.809	-0.268	6.874	4.470	2.404	5.910	5.450	0.460	1.342	0.237	7.318	0.0000
22	5.417	5.047	5.868	-0.820	5.133	5.746	-0.613	5.297	5.541	-0.244	6.566	4.267	2.299	5.643	5.206	0.437	1.283	0.237	7.113	0.0000
23	5.184	4.830	5.616	-0.787	4.912	5.499	-0.587	5.075	5.297	-0.223	6.286	4.081	2.205	5.399	4.983	0.416	1.229	0.237	6.917	0.0000
24	4.970	4.630	5.386	-0.756	4.709	5.274	-0.564	4.870	5.075	-0.204	6.029	3.911	2.118	5.176	4.779	0.397	1.180	0.237	6.728	0.0000
25	4.774	4.447	5.174	-0.727	4.523	5.066	-0.543	4.682	4.870	-0.188	5.793	3.755	2.038	4.971	4.592	0.379	1.135	0.238	6.547	0.0000
26	4.593	4.278	4.979	-0.701	4.351	4.875	-0.523	4.508	4.682	-0.174	5.576	3.611	1.965	4.781	4.419	0.362	1.094	0.238	6.372	0.0000
27	4.426	4.121	4.798	-0.677	4.192	4.697	-0.505	4.347	4.508	-0.161	5.374	3.477	1.897	4.606	4.259	0.347	1.056	0.239	6.204	0.0000
28	4.270	3.976	4.630	-0.655	4.044	4.533	-0.489	4.197	4.347	-0.150	5.188	3.353	1.835	4.443	4.110	0.332	1.021	0.239	6.041	0.0000
29	4.126	3.841	4.475	-0.634	3.907	4.380	-0.473	4.057	4.197	-0.140	5.014	3.237	1.777	4.291	3.972	0.319	0.988	0.239	5.884	0.0000
30	3.991	3.715	4.329	-0.615	3.779	4.238	-0.459	3.927	4.057	-0.130	4.853	3.130	1.723	4.150	3.844	0.306	0.957	0.240	5.733	0.0000
31	3.865	3.597	4.193	-0.597	3.659	4.105	-0.446	3.805	3.927	-0.122	4.701	3.029	1.673	4.018	3.724	0.294	0.929	0.240	5.586	0.0000
32	3.747	3.486	4.066	-0.580	3.547	3.980	-0.433	3.691	3.805	-0.114	4.560	2.934	1.626	3.894	3.611	0.283	0.903	0.241	5.443	0.0000
33	3.636	3.383	3.947	-0.564	3.442	3.863	-0.421	3.584	3.691	-0.107	4.427	2.846	1.582	3.778	3.506	0.272	0.878	0.241	5.305	0.0000
34	3.532	3.285	3.835	-0.550	3.343	3.753	-0.410	3.483	3.584	-0.101	4.303	2.762	1.540	3.668	3.406	0.262	0.855	0.242	5.171	0.0000
35	3.434	3.193	3.729	-0.536	3.249	3.649	-0.400	3.388	3.483	-0.095	4.185	2.683	1.502	3.565	3.313	0.252	0.833	0.243	5.041	0.0000
36	3.342	3.107	3.630	-0.523	3.161	3.552	-0.390	3.298	3.388	-0.090	4.075	2.609	1.466	3.468	3.225	0.243	0.813	0.243	4.915	0.0000
37	3.255	3.025	3.535	-0.511	3.078	3.460	-0.381	3.213	3.298	-0.085	3.970	2.539	1.431	3.376	3.142	0.234	0.793	0.244	4.792	0.0000
38	3.172	2.947	3.446	-0.499	3.000	3.372	-0.373	3.132	3.213	-0.080	3.872	2.472	1.399	3.289	3.063	0.226	0.775	0.244	4.673	0.0000
39	3.094	2.874	3.362	-0.488	2.925	3.290	-0.365	3.056	3.132	-0.076	3.778	2.409	1.369	3.207	2.989	0.218	0.758	0.245	4.556	0.0000
40	3.019	2.804	3.282	-0.478	2.854	3.211	-0.357	2.984	3.056	-0.072	3.689	2.349	1.340	3.129	2.918	0.211	0.742	0.246	4.443	0.0000
41	2.949	2.738	3.206	-0.468	2.787	3.137	-0.350	2.915	2.984	-0.069	3.605	2.292	1.313	3.054	2.851	0.203	0.727	0.246	4.333	0.0000
42	2.882	2.675	3.134	-0.459	2.723	3.066	-0.343	2.849	2.915	-0.065	3.525	2.238	1.287	2.983	2.787	0.196	0.712	0.247	4.225	0.0000
43	2.818	2.615	3.066	-0.451	2.662	2.999	-0.336	2.787	2.849	-0.062	3.449	2.186	1.263	2.916	2.727	0.189	0.698	0.248	4.121	0.0000
44	2.757	2.558	3.000	-0.442	2.604	2.935	-0.330	2.728	2.787	-0.059	3.377	2.137	1.240	2.852	2.669	0.183	0.685	0.249	4.019	0.0000
45	2.699	2.503	2.938	-0.435	2.549	2.873	-0.325	2.671	2.728	-0.057	3.308	2.090	1.218	2.791	2.614	0.177	0.673	0.249	3.919	0.0000
46	2.644	2.451	2.879	-0.427	2.496	2.815	-0.319	2.617	2.671	-0.054	3.242	2.045	1.197	2.732	2.562	0.171	0.661	0.250	3.822	0.0001
47	2.591	2.402	2.822	-0.420	2.446	2.759	-0.314	2.565	2.617	-0.052	3.180	2.002	1.178	2.676	2.511	0.165	0.650	0.251	3.727	0.0001
48	2.540	2.354	2.768	-0.414	2.397	2.706	-0.309	2.516	2.565	-0.049	3.120	1.961	1.159	2.623	2.464	0.159	0.640	0.252	3.635	0.0001
49	2.492	2.309	2.716	-0.407	2.351	2.655	-0.304	2.468	2.516	-0.047	3.062	1.921	1.141	2.571	2.418	0.154	0.630	0.253	3.544	0.0002
50	2.445	2.265	2.666	-0.401	2.307	2.606	-0.300	2.423	2.468	-0.045	3.008	1.883	1.124	2.522	2.374	0.148	0.620	0.254	3.456	0.0003
51	2.401	2.223	2.618	-0.395	2.264	2.560	-0.295	2.379	2.423	-0.043	2.955	1.847	1.108	2.475	2.332	0.143	0.611	0.255	3.370	0.0004
52	2.358	2.183	2.573	-0.390	2.224	2.515	-0.291	2.338	2.379	-0.042	2.905	1.812	1.093	2.430	2.292	0.138	0.603	0.256	3.286	0.0005
53	2.318	2.144	2.529	-0.385	2.185	2.472	-0.287	2.298	2.338	-0.040	2.857	1.778	1.079	2.387	2.253	0.133	0.594	0.256	3.204	0.0007
54	2.278	2.107	2.487	-0.380	2.147	2.431	-0.284	2.259	2.298	-0.038	2.811	1.746	1.065	2.345	2.217	0.128	0.587	0.257	3.123	0.0009
55	2.241	2.072	2.447	-0.375	2.111	2.391	-0.280	2.222	2.259	-0.037	2.766	1.715	1.052	2.305	2.181	0.124	0.579	0.258	3.045	0.0012
56	2.204	2.038	2.408	-0.371	2.076	2.353	-0.277	2.187	2.222	-0.036	2.724	1.685	1.039	2.266	2.147	0.119	0.572	0.260	2.968	0.0015
57	2.170	2.005	2.371	-0.366	2.043	2.317	-0.274	2.153	2.187	-0.034	2.683	1.656	1.027	2.229	2.114	0.115	0.565	0.261	2.894	0.0019
58	2.136	1.973	2.335	-0.362	2.011	2.282	-0.271	2.120	2.153	-0.033	2.644	1.628	1.016	2.193	2.083	0.110	0.559	0.262	2.821	0.0024
59	2.104	1.942	2.301	-0.359	1.980	2.248	-0.268	2.088	2.120	-0.032	2.606	1.601	1.005	2.159	2.053	0.106	0.553	0.263	2.749	0.0030
60	2.073	1.913	2.268	-0.355	1.950	2.215	-0.265	2.058	2.088	-0.030	2.570	1.575	0.995	2.126	2.024	0.102	0.547	0.264	2.680	0.0037
61	2.043	1.885	2.236	-0.351	1.922	2.184	-0.262	2.028	2.058	-0.029	2.535	1.550	0.985	2.094	1.996	0.098	0.541	0.265	2.611	0.0045
62	2.014	1.858	2.206	-0.348	1.894	2.154	-0.260	2.000	2.028	-0.028	2.502	1.526	0.976	2.063	1.969	0.094	0.536	0.266	2.545	0.0055
63	1.986	1.831	2.176	-0.345	1.867	2.125	-0.258	1.973	2.000	-0.027	2.470	1.503	0.967	2.033	1.943	0.090	0.531	0.267	2.480	0.0066
64	1.960	1.806	2.148	-0.342	1.842	2.097	-0.255	1.947	1.973	-0.026	2.439	1.480	0.958	2.004	1.918	0.086	0.526	0.269	2.416	0.0078
65	1.934	1.781	2.120	-0.339	1.817	2.070	-0.253	1.921	1.947	-0.025	2.409	1.459	0.950	1.977	1.894	0.082	0.522	0.270	2.355	0.0093
66	1.909	1.758	2.094	-0.336	1.793	2.044	-0.251	1.897	1.921	-0.024	2.381	1.438	0.943	1.950	1.871	0.079	0.518	0.271	2.294	0.0109
67	1.885	1.735	2.069	-0.334	1.770	2.019	-0.249	1.873	1.897	-0.024	2.353	1.417	0.936	1.924	1.849	0.075	0.514	0.272	2.235	0.0127
68	1.862	1.713	2.044	-0.331	1.748	1.995	-0.248	1.851	1.873	-0.023	2.327	1.397	0.929	1.899	1.828	0.071	0.510	0.274	2.177	0.0147
69	1.840	1.692	2.021	-0.329	1.726	1.972	-0.246	1.829	1.851	-0.022	2.301	1.378	0.923	1.875	1.807	0.068	0.506	0.275	2.121	0.0170
70	1.818	1.671	1.998	-0.327	1.705	1.949	-0.244	1.808	1.829	-0.021	2.277	1.360	0.917	1.852	1.787	0.064	0.503	0.277	2.066	0.0194
71	1.797	1.651	1.976	-0.325	1.685	1.928	-0.243	1.787	1.808	-0.020	2.253	1.342	0.911	1.829	1.768	0.061	0.500	0.278	2.013	0.0221
72	1.777	1.632	1.955	-0.323	1.666	1.907	-0.241	1.768	1.787	-0.020	2.230	1.325	0.906	1.807	1.750	0.057	0.497	0.279	1.961	0.0250
73	1.758	1.614	1.935	-0.321	1.647	1.887	-0.240	1.749	1.768	-0.019	2.209	1.308	0.901	1.786	1.732	0.054	0.494	0.281	1.910	0.0281
74	1.740	1.596	1.915	-0.320	1.629	1.868	-0.239	1.731	1.749	-0.018	2.188	1.292	0.896	1.766	1.715	0.051	0.491	0.282	1.861	0.0314
75	1.722	1.578	1.897	-0.318	1.612	1.849	-0.238	1.713	1.731	-0.018	2.168	1.276	0.892	1.746	1.699	0.047	0.489	0.284	1.812	0.0350
76	1.704	1.562	1.879	-0.317	1.595	1.831	-0.237	1.696	1.713	-0.017	2.148	1.260	0.888	1.727	1.683	0.044	0.486	0.285	1.765	0.0388
77	1.688	1.546	1.861	-0.315	1.579	1.814	-0.236	1.680	1.696	-0.016	2.130	1.246	0.884	1.709	1.668	0.041	0.484	0.287	1.720	0.0427
78	1.672	1.530	1.844	-0.314	1.563	1.798	-0.235	1.664	1.680	-0.016	2.112	1.231	0.881	1.691	1.654	0.038	0.482	0.289	1.675	0.0469
79	1.656	1.515	1.828	-0.313	1.548	1.782	-0.234	1.649	1.664	-0.015	2.095	1.217	0.878	1.674	1.640	0.034	0.481	0.290	1.632	0.0513
80	1.641	1.501	1.813	-0.312	1.534	1.767	-0.233	1.634	1.649	-0.015	2.079	1.204	0.875	1.657	1.626	0.031	0.479	0.292	1.590	0.0559
81	1.627	1.487	1.798	-0.311	1.520	1.752	-0.232	1.620	1.634	-0.014	2.063	1.191	0.872	1.641	1.613	0.028	0.478	0.294	1.549	0.0607
82	1.613	1.474	1.784	-0.310	1.506	1.738	-0.232	1.606	1.620	-0.014	2.048	1.178	0.870	1.626	1.601	0.025	0.476	0.295	1.509	0.0656
83	1.600	1.461	1.770	-0.310	1.493	1.724	-0.231	1.593	1.606	-0.013	2.034	1.166	0.868	1.611	1.589	0.022	0.475	0.297	1.471	0.0706
84	1.587	1.448	1.757	-0.309	1.480	1.711	-0.231	1.581	1.593	-0.012	2.020	1.154	0.866	1.597	1.578	0.019	0.474	0.299	1.434	0.0758
85	1.575	1.436	1.745	-0.308	1.468	1.699	-0.230	1.569	1.581	-0.012	2.007	1.143	0.865	1.583	1.568	0.015	0.473	0.301	1.398	0.0811
86	1.563	1.425	1.733	-0.308	1.457	1.687	-0.230	1.558	1.569	-0.011	1.995	1.132	0.864	1.570	1.557	0.012	0.473	0.302	1.363	0.0865
87	1.552	1.414	1.721	-0.308	1.446	1.676	-0.230	1.547	1.558	-0.011	1.983	1.121	0.863	1.557	1.548	0.009	0.472	0.304	1.329	0.0920
88	1.541	1.403	1.710	-0.308	1.435	1.665	-0.230	1.536	1.547	-0.010	1.972	1.110	0.862	1.545	1.538	0.006	0.472	0.306	1.296	0.0975
89	1.531	1.393	1.700	-0.307	1.425	1.654	-0.230	1.526	1.536	-0.010	1.962	1.100	0.862	1.533	1.530	0.003	0.472	0.308	1.264	0.1031
90	1.521	1.383	1.690	-0.307	1.415	1.645	-0.229	1.517	1.526	-0.010	1.952	1.091	0.861	1.521	1.521	0.000	0.471	0.310	1.234	0.1086
91	1.512	1.374	1.681	-0.307	1.406	1.635	-0.230	1.507	1.517	-0.009	1.943	1.081	0.862	1.510	1.513	-0.003	0.472	0.312	1.204	0.1142
92	1.503	1.365	1.672	-0.308	1.397	1.626	-0.230	1.499	1.507	-0.009	1.934	1.072	0.862	1.500	1.506	-0.006	0.472	0.314	1.176	0.1198
93	1.495	1.356	1.664	-0.308	1.388	1.618	-0.230	1.491	1.499	-0.008	1.926	1.063	0.863	1.490	1.499	-0.009	0.472	0.316	1.149	0.1253
94	1.487	1.348	1.656	-0.308	1.380	1.610	-0.230	1.483	1.491	-0.008	1.918	1.055	0.864	1.480	1.493	-0.012	0.473	0.318	1.123	0.1308
95	1.479	1.340	1.649	-0.308	1.373	1.603	-0.230	1.476	1.483	-0.007	1.911	1.047	0.865	1.471	1.487	-0.015	0.473	0.320	1.098	0.1362
96	1.472	1.333	1.642	-0.309	1.365	1.596	-0.231	1.469	1.476	-0.007	1.905	1.039	0.866	1.462	1.481	-0.019	0.474	0.322	1.074	0.1415
97	1.465	1.326	1.636	-0.310	1.358	1.590	-0.231	1.462	1.469	-0.006	1.899	1.031	0.868	1.454	1.476	-0.022	0.475	0.324	1.051	0.1467
98	1.459	1.320	1.630	-0.310	1.352	1.584	-0.232	1.456	1.462	-0.006	1.894	1.024	0.870	1.446	1.471	-0.025	0.476	0.326	1.029	0.1518
99	1.453	1.313	1.625	-0.311	1.346	1.578	-0.232	1.451	1.456	-0.006	1.890	1.017	0.872	1.439	1.467	-0.028	0.478	0.329	1.008	0.1568
100	1.448	1.308	1.620	-0.312	1.340	1.573	-0.233	1.446	1.451	-0.005	1.885	1.011	0.875	1.432	1.463	-0.031	0.479	0.331	0.988	0.1616

Internal GCL Large-Displacement, t = 1 m

E(ψ)	$FS_{MLV,LD}$	t			γ			ψ			C_d			ϕ			$\sigma_{FS,LD}$	$V_{FS,LD}$	β_{LN}	P_F
		FS_i^+	FS_i^-	ΔFS_i	FS_i^+	FS_i^-	ΔFS_i	FS_i^+	FS_i^-	ΔFS_i	FS_i^+	FS_i^-	ΔFS_i	FS_i^+	FS_i^-	ΔFS_i				
5	10.768	9.953	11.764	-1.811	10.142	11.495	-1.352	9.790	11.963	-2.173	16.211	5.324	10.887	11.267	10.275	0.992	5.687	0.528	4.544	2.768E-06
6	8.976	8.296	9.806	-1.510	8.454	9.582	-1.128	8.286	9.790	-1.504	13.515	4.437	9.078	9.391	8.565	0.826	4.714	0.525	4.199	1.340E-05
7	7.696	7.113	8.408	-1.295	7.249	8.216	-0.967	7.184	8.286	-1.102	11.589	3.803	7.786	8.052	7.345	0.707	4.030	0.524	3.900	4.818E-05
8	6.736	6.226	7.360	-1.134	6.345	7.192	-0.847	6.342	7.184	-0.843	10.146	3.327	6.818	7.047	6.430	0.618	3.521	0.523	3.636	1.385E-04
9	5.991	5.536	6.546	-1.009	5.642	6.396	-0.754	5.677	6.342	-0.665	9.023	2.958	6.066	6.266	5.718	0.548	3.127	0.522	3.401	3.357E-04
10	5.394	4.985	5.894	-0.909	5.080	5.759	-0.679	5.139	5.677	-0.538	8.126	2.662	5.464	5.642	5.150	0.492	2.814	0.522	3.189	7.127E-04
11	4.906	4.534	5.361	-0.827	4.621	5.238	-0.618	4.694	5.139	-0.444	7.393	2.420	4.973	5.131	4.685	0.447	2.559	0.522	2.997	1.362E-03
12	4.500	4.158	4.918	-0.759	4.238	4.805	-0.567	4.321	4.694	-0.373	6.782	2.218	4.564	4.706	4.297	0.408	2.347	0.522	2.821	0.002
13	4.157	3.841	4.543	-0.702	3.914	4.438	-0.524	4.004	4.321	-0.317	6.266	2.047	4.218	4.346	3.970	0.376	2.168	0.522	2.659	0.004
14	3.862	3.569	4.221	-0.653	3.637	4.124	-0.487	3.731	4.004	-0.273	5.824	1.901	3.922	4.038	3.689	0.348	2.015	0.522	2.509	0.006
15	3.608	3.333	3.943	-0.610	3.397	3.852	-0.455	3.493	3.731	-0.238	5.441	1.774	3.666	3.771	3.447	0.324	1.883	0.522	2.368	0.009
16	3.385	3.127	3.700	-0.573	3.187	3.615	-0.428	3.284	3.493	-0.209	5.106	1.663	3.443	3.537	3.234	0.303	1.768	0.522	2.237	0.013
17	3.188	2.945	3.485	-0.540	3.002	3.405	-0.403	3.099	3.284	-0.185	4.811	1.566	3.246	3.331	3.047	0.284	1.666	0.523	2.114	0.017
18	3.014	2.784	3.295	-0.511	2.838	3.219	-0.381	2.934	3.099	-0.165	4.549	1.479	3.071	3.148	2.881	0.267	1.576	0.523	1.998	0.023
19	2.858	2.640	3.125	-0.485	2.691	3.053	-0.362	2.786	2.934	-0.148	4.315	1.401	2.915	2.985	2.733	0.252	1.496	0.523	1.889	0.029
20	2.718	2.510	2.972	-0.462	2.558	2.903	-0.345	2.653	2.786	-0.133	4.105	1.331	2.774	2.838	2.599	0.239	1.423	0.524	1.785	0.037
21	2.591	2.393	2.833	-0.440	2.439	2.768	-0.329	2.532	2.653	-0.121	3.915	1.267	2.648	2.705	2.479	0.226	1.358	0.524	1.686	0.046
22	2.476	2.287	2.708	-0.421	2.331	2.645	-0.315	2.423	2.532	-0.110	3.743	1.210	2.533	2.584	2.369	0.215	1.299	0.525	1.592	0.056
23	2.371	2.189	2.593	-0.404	2.232	2.533	-0.302	2.322	2.423	-0.100	3.586	1.157	2.429	2.474	2.270	0.205	1.245	0.525	1.503	0.066
24	2.275	2.101	2.489	-0.388	2.141	2.431	-0.290	2.230	2.322	-0.092	3.442	1.109	2.333	2.373	2.178	0.195	1.196	0.526	1.417	0.078
25	2.187	2.019	2.393	-0.374	2.058	2.337	-0.279	2.146	2.230	-0.085	3.310	1.064	2.245	2.281	2.095	0.186	1.151	0.526	1.335	0.091
26	2.106	1.944	2.304	-0.360	1.981	2.250	-0.269	2.067	2.146	-0.078	3.188	1.023	2.165	2.195	2.017	0.178	1.110	0.527	1.257	0.104
27	2.031	1.874	2.222	-0.348	1.911	2.170	-0.260	1.995	2.067	-0.072	3.076	0.986	2.090	2.116	1.946	0.170	1.071	0.528	1.182	0.119
28	1.961	1.810	2.146	-0.336	1.845	2.096	-0.251	1.928	1.995	-0.067	2.972	0.950	2.021	2.043	1.880	0.163	1.036	0.528	1.109	0.134
29	1.896	1.750	2.075	-0.326	1.784	2.027	-0.243	1.866	1.928	-0.062	2.875	0.918	1.957	1.975	1.818	0.157	1.003	0.529	1.040	0.149
30	1.836	1.694	2.010	-0.316	1.727	1.963	-0.236	1.807	1.866	-0.058	2.785	0.887	1.898	1.912	1.761	0.150	0.972	0.530	0.973	0.165
31	1.780	1.642	1.948	-0.307	1.674	1.903	-0.229	1.753	1.807	-0.054	2.701	0.858	1.842	1.852	1.708	0.144	0.944	0.530	0.909	0.182
32	1.727	1.593	1.891	-0.298	1.624	1.846	-0.222	1.702	1.753	-0.051	2.622	0.832	1.791	1.797	1.658	0.139	0.917	0.531	0.846	0.199
33	1.678	1.547	1.837	-0.290	1.577	1.794	-0.216	1.654	1.702	-0.048	2.549	0.806	1.742	1.745	1.611	0.134	0.893	0.532	0.787	0.216
34	1.631	1.504	1.786	-0.282	1.534	1.744	-0.211	1.609	1.654	-0.045	2.480	0.783	1.697	1.696	1.567	0.129	0.869	0.533	0.729	0.233
35	1.588	1.464	1.739	-0.275	1.492	1.698	-0.206	1.567	1.609	-0.042	2.415	0.760	1.654	1.650	1.526	0.124	0.847	0.534	0.673	0.251
36	1.546	1.426	1.694	-0.269	1.454	1.654	-0.201	1.527	1.567	-0.040	2.354	0.739	1.614	1.607	1.487	0.119	0.827	0.535	0.619	0.268
37	1.508	1.390	1.652	-0.262	1.417	1.613	-0.196	1.489	1.527	-0.038	2.296	0.719	1.577	1.566	1.450	0.115	0.807	0.536	0.566	0.286
38	1.471	1.356	1.612	-0.256	1.382	1.574	-0.191	1.453	1.489	-0.036	2.242	0.700	1.541	1.527	1.416	0.111	0.789	0.537	0.516	0.303
39	1.436	1.323	1.574	-0.251	1.350	1.537	-0.187	1.420	1.453	-0.034	2.190	0.682	1.508	1.490	1.383	0.107	0.772	0.537	0.467	0.320
40	1.404	1.293	1.539	-0.246	1.319	1.502	-0.183	1.388	1.420	-0.032	2.142	0.665	1.476	1.456	1.352	0.103	0.756	0.538	0.420	0.337
41	1.372	1.264	1.505	-0.241	1.289	1.469	-0.180	1.357	1.388	-0.030	2.096	0.649	1.446	1.423	1.323	0.100	0.740	0.540	0.374	0.354
42	1.343	1.237	1.473	-0.236	1.261	1.438	-0.176	1.329	1.357	-0.029	2.052	0.634	1.418	1.391	1.295	0.096	0.726	0.541	0.329	0.371
43	1.315	1.211	1.442	-0.231	1.235	1.408	-0.173	1.301	1.329	-0.027	2.011	0.619	1.391	1.362	1.269	0.093	0.712	0.542	0.286	0.387
44	1.288	1.186	1.413	-0.227	1.210	1.379	-0.170	1.275	1.301	-0.026	1.971	0.605	1.366	1.333	1.243	0.090	0.699	0.543	0.244	0.404
45	1.263	1.162	1.386	-0.223	1.186	1.352	-0.167	1.250	1.275	-0.025	1.934	0.592	1.342	1.306	1.220	0.087	0.687	0.544	0.204	0.419
46	1.239	1.140	1.359	-0.219	1.163	1.327	-0.164	1.227	1.250	-0.024	1.898	0.579	1.319	1.281	1.197	0.084	0.675	0.545	0.164	0.435
47	1.215	1.118	1.334	-0.216	1.141	1.302	-0.161	1.204	1.227	-0.023	1.864	0.567	1.297	1.256	1.175	0.081	0.664	0.546	0.126	0.450
48	1.193	1.098	1.310	-0.212	1.120	1.279	-0.159	1.183	1.204	-0.022	1.832	0.555	1.277	1.233	1.155	0.078	0.653	0.547	0.089	0.464
49	1.172	1.078	1.287	-0.209	1.100	1.256	-0.156	1.162	1.183	-0.021	1.801	0.544	1.257	1.210	1.135	0.075	0.643	0.549	0.054	0.479
50	1.152	1.060	1.266	-0.206	1.081	1.235	-0.154	1.143	1.162	-0.020	1.772	0.533	1.239	1.189	1.116	0.073	0.634	0.550	0.019	0.492
51	1.133	1.042	1.245	-0.203	1.063	1.215	-0.152	1.124	1.143	-0.019	1.744	0.523	1.221	1.169	1.098	0.070	0.625	0.551	-0.015	0.506
52	1.115	1.025	1.225	-0.200	1.046	1.195	-0.150	1.106	1.124	-0.018	1.717	0.513	1.204	1.149	1.081	0.068	0.616	0.552	-0.048	0.519
53	1.097	1.008	1.206	-0.198	1.029	1.177	-0.148	1.089	1.106	-0.017	1.691	0.503	1.188	1.130	1.065	0.065	0.608	0.554	-0.079	0.532
54	1.080	0.993	1.188	-0.195	1.013	1.159	-0.146	1.072	1.089	-0.016	1.667	0.494	1.173	1.112	1.049	0.063	0.600	0.555	-0.110	0.544
55	1.064	0.978	1.170	-0.193	0.998	1.142	-0.144	1.057	1.072	-0.016	1.644	0.485	1.158	1.095	1.034	0.061	0.592	0.557	-0.140	0.556
56	1.049	0.963	1.154	-0.190	0.983	1.125	-0.142	1.041	1.057	-0.015	1.621	0.477	1.145	1.078	1.020	0.059	0.585	0.558	-0.169	0.567
57	1.034	0.949	1.138	-0.188	0.969	1.110	-0.141	1.027	1.041	-0.014	1.600	0.468	1.131	1.062	1.006	0.056	0.579	0.559	-0.197	0.578
58	1.020	0.936	1.122	-0.186	0.956	1.095	-0.139	1.013	1.027	-0.014	1.579	0.460	1.119	1.047	0.993	0.054	0.572	0.561	-0.224	0.589
59	1.006	0.923	1.108	-0.184	0.943	1.080	-0.138	1.000	1.013	-0.013	1.560	0.453	1.107	1.033	0.980	0.052	0.566	0.562	-0.250	0.599
60	0.993	0.911	1.094	-0.182	0.930	1.066	-0.136	0.987	1.000	-0.013	1.541	0.445	1.096	1.019	0.968	0.050	0.560	0.564	-0.275	0.609
61	0.981	0.900	1.080	-0.180	0.918	1.053	-0.135	0.975	0.987	-0.012	1.523	0.438	1.085	1.005	0.957	0.048	0.555	0.565	-0.300	0.618
62	0.969	0.888	1.067	-0.179	0.907	1.041	-0.134	0.963	0.975	-0.012	1.506	0.431	1.075	0.992	0.946	0.046	0.549	0.567	-0.324	0.627
63	0.957	0.878	1.055	-0.177	0.896	1.028	-0.132	0.952	0.963	-0.011	1.490	0.425	1.065	0.980	0.935	0.044	0.544	0.569	-0.347	0.636
64	0.946	0.867	1.043	-0.176	0.886	1.017	-0.131	0.941	0.952	-0.011	1.474	0.418	1.056	0.968	0.925	0.042	0.540	0.570	-0.369	0.644
65	0.936	0.857	1.032	-0.174	0.876	1.006	-0.130	0.931	0.941	-0.010	1.459	0.412	1.047	0.956	0.916	0.040	0.535	0.572	-0.391	0.652
66	0.926	0.848	1.021	-0.173	0.866	0.995	-0.129	0.921	0.931	-0.010	1.445	0.406	1.039	0.945	0.906	0.039	0.531	0.573	-0.412	0.660
67	0.916	0.839	1.010	-0.171	0.857	0.985	-0.128	0.911	0.921	-0.010	1.431	0.400	1.031	0.934	0.898	0.037	0.527	0.575	-0.432	0.667
68	0.906	0.830	1.000	-0.170	0.848	0.975	-0.127	0.902	0.911	-0.009	1.418	0.395	1.023	0.924	0.889	0.035	0.523	0.577	-0.451	0.674
69	0.898	0.821	0.991	-0.169	0.839	0.965	-0.126	0.893	0.902	-0.009	1.406	0.389	1.016	0.914	0.881	0.033	0.519	0.579	-0.470	0.681
70	0.889	0.813	0.981	-0.168	0.831	0.956	-0.125	0.885	0.893	-0.008	1.394	0.384	1.010	0.905	0.873	0.032	0.516	0.580	-0.488	0.687
71	0.881	0.806	0.973	-0.167	0.823	0.948	-0.125	0.877	0.885	-0.008	1.383	0.379	1.004	0.896	0.866	0.030	0.513	0.582	-0.505	0.693
72	0.873	0.798	0.964	-0.166	0.816	0.939	-0.124	0.869	0.877	-0.008	1.372	0.374	0.998	0.887	0.859	0.028	0.510	0.584	-0.522	0.699
73	0.865	0.791	0.956	-0.165	0.808	0.932	-0.123	0.862	0.869	-0.007	1.361	0.369	0.992	0.879	0.852	0.027	0.507	0.586	-0.538	0.705
74	0.858	0.784	0.948	-0.164	0.801	0.924	-0.123	0.855	0.862	-0.007	1.352	0.365	0.987	0.871	0.846	0.025	0.504	0.588	-0.553	0.710
75	0.851	0.778	0.941	-0.163	0.795	0.917	-0.122	0.848	0.855	-0.007	1.342	0.360	0.982	0.863	0.840	0.023	0.502	0.590	-0.568	0.715
76	0.845	0.771	0.934	-0.163	0.788	0.910	-0.121	0.841	0.848	-0.006	1.334	0.356	0.978	0.856	0.834	0.022	0.500	0.591	-0.582	0.720
77	0.838	0.765	0.927	-0.162	0.782	0.903	-0.121	0.835	0.841	-0.006	1.325	0.351	0.974	0.848	0.828	0.020	0.497	0.593	-0.596	0.724
78	0.832	0.760	0.921	-0.161	0.777	0.897	-0.121	0.829	0.835	-0.006	1.317	0.347	0.970	0.842	0.823	0.018	0.495	0.595	-0.609	0.729
79	0.827	0.754	0.915	-0.161	0.771	0.891	-0.120	0.824	0.829	-0.006	1.310	0.343	0.967	0.835	0.818	0.017	0.494	0.597	-0.621	0.733
80	0.821	0.749	0.909	-0.160	0.766	0.886	-0.120	0.819	0.824	-0.005	1.303	0.339	0.964	0.829	0.814	0.015	0.492	0.599	-0.632	0.736
81	0.816	0.744	0.904	-0.160	0.761	0.880	-0.119	0.814	0.819	-0.005	1.296	0.336	0.961	0.823	0.809	0.014	0.491	0.601	-0.644	0.740
82	0.811	0.740	0.899	-0.159	0.756	0.875	-0.119	0.809	0.814	-0.005	1.290	0.332	0.958	0.817	0.805	0.012	0.489	0.603	-0.654	0.743
83	0.807	0.735	0.894	-0.159	0.752	0.870	-0.119	0.804	0.809	-0.004	1.285	0.329	0.956	0.812	0.801	0.011	0.488	0.605	-0.664	0.747
84	0.802	0.731	0.890	-0.159	0.747	0.866	-0.119	0.800	0.804	-0.004	1.279	0.325	0.954	0.807	0.798	0.009	0.487	0.607	-0.673	0.750
85	0.798	0.727	0.885	-0.158	0.743	0.862	-0.118	0.796	0.800	-0.004	1.274	0.322	0.953	0.802	0.794	0.008	0.486	0.609	-0.682	0.752
86	0.794	0.723	0.881	-0.158	0.740	0.858	-0.118	0.793	0.796	-0.004	1.270	0.319	0.951	0.797	0.791	0.006	0.486	0.612	-0.690	0.755
87	0.791	0.720	0.878	-0.158	0.736	0.854	-0.118	0.789	0.793	-0.003	1.266	0.316	0.950	0.793	0.788	0.005	0.485	0.614	-0.698	0.757
88	0.787	0.716	0.874	-0.158	0.733	0.851	-0.118	0.786	0.789	-0.003	1.262	0.313	0.949	0.789	0.786	0.003	0.485	0.616	-0.705	0.760
89	0.784	0.713	0.871	-0.158	0.730	0.848	-0.118	0.783	0.786	-0.003	1.259	0.310	0.949	0.785	0.784	0.002	0.485	0.618	-0.712	0.762
90	0.781	0.710	0.868	-0.158	0.727	0.845	-0.118	0.780	0.783	-0.003	1.256	0.307	0.949	0.781	0.781	0.000	0.485	0.620	-0.718	0.764
91	0.779	0.708	0.866	-0.158	0.724	0.842	-0.118	0.778	0.780	-0.003	1.253	0.304	0.949	0.778	0.780	-0.002	0.485	0.622	-0.723	0.765
92	0.776	0.705	0.863	-0.158	0.722	0.840	-0.118	0.775	0.778	-0.002	1.251	0.302	0.949	0.775	0.778	-0.003	0.485	0.625	-0.728	0.767
93	0.774	0.703	0.861	-0.158	0.720	0.838	-0.118	0.773	0.775	-0.002	1.249	0.299	0.950	0.772	0.776	-0.005	0.485	0.627	-0.732	0.768
94	0.772	0.701	0.859	-0.158	0.718	0.836	-0.118	0.771	0.773	-0.002	1.248	0.297	0.951	0.769	0.775	-0.006	0.486	0.629	-0.736	0.769
95	0.771	0.699	0.858	-0.158	0.716	0.834	-0.118	0.770	0.771	-0.002	1.247	0.294	0.953	0.767	0.774	-0.008	0.486	0.631	-0.740	0.770
96	0.769	0.698	0.856	-0.159	0.714	0.833	-0.119	0.768	0.770	-0.001	1.246	0.292	0.954	0.765	0.774	-0.009	0.487	0.634	-0.742	0.771
97	0.768	0.696	0.855	-0.159	0.713	0.832	-0.119	0.767	0.768	-0.001	1.246	0.290	0.956	0.763	0.773	-0.011	0.488	0.636	-0.745	0.772
98	0.767	0.695	0.855	-0.159	0.712	0.831	-0.119	0.767	0.767	-0.001	1.246	0.288	0.958	0.761	0.773	-0.012	0.489	0.638	-0.746	0.772
99	0.766	0.694	0.854	-0.160	0.711	0.830	-0.119	0.766	0.767	-0.001	1.247	0.286	0.961	0.759	0.773	-0.014	0.491	0.640	-0.747	0.773
100	0.766	0.694	0.854	-0.160	0.710	0.830	-0.120	0.765	0.766	0.000	1.247	0.284	0.964	0.758	0.773	-0.015	0.492	0.643	-0.748	0.773

Internal GCL Peak, t = 3 m

E(ψ)	$FS_{MLV,\ Peak}$	t			γ			ψ			C_d			ϕ			$\sigma_{FS,Peak}$	$V_{FS,\ Peak}$	β_{LN}	P_F
		FS_t^+	FS_t^-	ΔFS_t	FS_γ^+	FS_γ^-	ΔFS_γ	FS_ψ^+	FS_ψ^-	ΔFS_ψ	$FS_{C_d}^+$	$FS_{C_d}^-$	ΔFS_{C_d}	FS_ϕ^+	FS_ϕ^-	ΔFS_ϕ				
5	12.078	11.891	12.279	-0.388	11.672	12.550	-0.878	10.979	13.422	-2.443	13.725	10.431	3.295	13.125	11.106	2.019	2.336	0.193	12.907	0.000E+00
6	10.062	9.906	10.229	-0.324	9.724	10.455	-0.732	9.286	10.979	-1.692	11.436	8.689	2.747	10.934	9.253	1.681	1.862	0.185	12.488	0.000E+00
7	8.621	8.487	8.765	-0.278	8.331	8.959	-0.628	8.045	9.286	-1.241	9.799	7.443	2.356	9.367	7.929	1.439	1.552	0.180	11.975	0.000E+00
8	7.541	7.423	7.666	-0.243	7.286	7.836	-0.550	7.095	8.045	-0.950	8.572	6.509	2.063	8.192	6.935	1.257	1.332	0.177	11.436	0.000E+00
9	6.699	6.595	6.811	-0.216	6.473	6.962	-0.489	6.345	7.095	-0.750	7.617	5.782	1.835	7.278	6.163	1.115	1.168	0.174	10.901	0.000E+00
10	6.026	5.932	6.127	-0.195	5.823	6.263	-0.441	5.738	6.345	-0.608	6.853	5.199	1.654	6.546	5.544	1.002	1.042	0.173	10.384	0.000E+00
11	5.475	5.389	5.567	-0.177	5.290	5.691	-0.401	5.235	5.738	-0.502	6.228	4.723	1.505	5.946	5.038	0.909	0.940	0.172	9.890	0.000E+00
12	5.016	4.937	5.100	-0.163	4.845	5.213	-0.368	4.813	5.235	-0.422	5.706	4.325	1.381	5.447	4.616	0.831	0.857	0.171	9.421	0.000E+00
13	4.626	4.554	4.704	-0.150	4.469	4.809	-0.340	4.453	4.813	-0.360	5.265	3.988	1.276	5.023	4.258	0.765	0.788	0.170	8.976	0.000E+00
14	4.293	4.225	4.365	-0.140	4.146	4.463	-0.316	4.143	4.453	-0.310	4.886	3.699	1.187	4.660	3.952	0.708	0.729	0.170	8.554	0.000E+00
15	4.003	3.940	4.071	-0.131	3.867	4.162	-0.296	3.872	4.143	-0.271	4.558	3.449	1.109	4.345	3.686	0.659	0.679	0.170	8.155	0.0000
16	3.750	3.690	3.813	-0.123	3.621	3.899	-0.278	3.634	3.872	-0.238	4.271	3.229	1.042	4.069	3.453	0.616	0.635	0.169	7.775	0.0000
17	3.526	3.470	3.586	-0.116	3.405	3.666	-0.262	3.423	3.634	-0.211	4.017	3.035	0.982	3.825	3.248	0.578	0.597	0.169	7.413	0.0000
18	3.327	3.274	3.383	-0.110	3.212	3.460	-0.248	3.235	3.423	-0.188	3.791	2.862	0.929	3.608	3.065	0.544	0.563	0.169	7.069	0.0000
19	3.148	3.098	3.202	-0.104	3.039	3.274	-0.235	3.066	3.235	-0.169	3.589	2.707	0.882	3.414	2.901	0.513	0.533	0.169	6.740	0.0000
20	2.987	2.940	3.038	-0.099	2.884	3.108	-0.224	2.913	3.066	-0.153	3.407	2.568	0.840	3.239	2.754	0.485	0.506	0.169	6.425	0.0000
21	2.842	2.796	2.891	-0.094	2.743	2.956	-0.213	2.774	2.913	-0.139	3.242	2.441	0.801	3.080	2.620	0.460	0.482	0.169	6.123	0.0000
22	2.709	2.666	2.756	-0.090	2.615	2.819	-0.204	2.647	2.774	-0.127	3.092	2.326	0.766	2.936	2.499	0.437	0.460	0.170	5.834	0.0000
23	2.588	2.546	2.633	-0.087	2.498	2.693	-0.196	2.531	2.647	-0.116	2.955	2.221	0.735	2.804	2.388	0.416	0.439	0.170	5.556	0.0000
24	2.477	2.437	2.520	-0.083	2.390	2.578	-0.188	2.425	2.531	-0.107	2.830	2.124	0.706	2.683	2.286	0.397	0.421	0.170	5.288	0.0000
25	2.374	2.336	2.416	-0.080	2.291	2.472	-0.181	2.326	2.425	-0.098	2.714	2.035	0.679	2.571	2.192	0.379	0.404	0.170	5.030	0.0000
26	2.280	2.242	2.320	-0.077	2.199	2.373	-0.174	2.235	2.326	-0.091	2.607	1.952	0.655	2.467	2.105	0.362	0.389	0.171	4.781	0.0000
27	2.192	2.156	2.230	-0.075	2.114	2.282	-0.168	2.150	2.235	-0.085	2.508	1.876	0.632	2.372	2.025	0.347	0.375	0.171	4.540	0.0000
28	2.110	2.075	2.147	-0.072	2.035	2.198	-0.163	2.071	2.150	-0.079	2.416	1.804	0.612	2.282	1.950	0.332	0.361	0.171	4.307	0.0000
29	2.034	2.000	2.070	-0.070	1.961	2.119	-0.158	1.998	2.071	-0.074	2.330	1.738	0.592	2.199	1.881	0.319	0.349	0.172	4.082	0.0000
30	1.963	1.930	1.998	-0.068	1.892	2.045	-0.153	1.929	1.998	-0.069	2.250	1.676	0.574	2.121	1.815	0.306	0.338	0.172	3.863	0.0001
31	1.896	1.864	1.930	-0.066	1.827	1.976	-0.149	1.864	1.929	-0.065	2.175	1.617	0.558	2.049	1.755	0.294	0.327	0.172	3.651	0.0001
32	1.833	1.803	1.866	-0.064	1.767	1.911	-0.144	1.803	1.864	-0.061	2.104	1.562	0.542	1.980	1.697	0.283	0.317	0.173	3.445	0.0003
33	1.774	1.744	1.807	-0.062	1.709	1.850	-0.140	1.746	1.803	-0.057	2.038	1.511	0.527	1.915	1.643	0.272	0.308	0.173	3.245	0.0006
34	1.719	1.690	1.750	-0.061	1.656	1.792	-0.137	1.692	1.746	-0.054	1.976	1.462	0.513	1.855	1.593	0.262	0.299	0.174	3.051	0.0011
35	1.666	1.638	1.697	-0.059	1.605	1.738	-0.133	1.641	1.692	-0.051	1.917	1.416	0.501	1.797	1.545	0.252	0.291	0.174	2.862	0.0021
36	1.617	1.589	1.646	-0.058	1.556	1.686	-0.130	1.593	1.641	-0.048	1.861	1.372	0.489	1.743	1.499	0.243	0.283	0.175	2.677	0.0037
37	1.569	1.542	1.598	-0.056	1.511	1.638	-0.127	1.547	1.593	-0.046	1.808	1.331	0.477	1.691	1.457	0.234	0.276	0.176	2.498	0.0062
38	1.525	1.498	1.553	-0.055	1.467	1.591	-0.124	1.503	1.547	-0.044	1.758	1.291	0.466	1.642	1.416	0.226	0.269	0.176	2.323	0.0101
39	1.482	1.456	1.510	-0.054	1.426	1.547	-0.122	1.462	1.503	-0.042	1.710	1.254	0.456	1.595	1.377	0.218	0.262	0.177	2.153	0.0157
40	1.442	1.416	1.469	-0.053	1.387	1.506	-0.119	1.422	1.462	-0.040	1.665	1.218	0.447	1.551	1.340	0.211	0.256	0.178	1.987	0.0235
41	1.403	1.378	1.430	-0.052	1.349	1.466	-0.117	1.384	1.422	-0.038	1.622	1.184	0.438	1.508	1.305	0.203	0.250	0.178	1.825	0.0340
42	1.366	1.342	1.392	-0.051	1.313	1.428	-0.114	1.348	1.384	-0.036	1.581	1.152	0.429	1.468	1.272	0.196	0.245	0.179	1.666	0.0478
43	1.331	1.307	1.356	-0.050	1.279	1.391	-0.112	1.314	1.348	-0.034	1.541	1.120	0.421	1.429	1.240	0.189	0.239	0.180	1.512	0.0653
44	1.297	1.274	1.322	-0.049	1.246	1.356	-0.110	1.281	1.314	-0.033	1.504	1.090	0.413	1.392	1.209	0.183	0.234	0.181	1.361	0.0867
45	1.265	1.242	1.290	-0.048	1.215	1.323	-0.108	1.249	1.281	-0.032	1.468	1.062	0.406	1.356	1.180	0.177	0.230	0.182	1.214	0.1124
46	1.234	1.211	1.258	-0.047	1.185	1.291	-0.106	1.219	1.249	-0.030	1.433	1.034	0.399	1.322	1.152	0.171	0.225	0.183	1.070	0.1423
47	1.204	1.182	1.228	-0.046	1.156	1.260	-0.105	1.190	1.219	-0.029	1.400	1.008	0.393	1.289	1.125	0.165	0.221	0.183	0.930	0.1763
48	1.175	1.153	1.199	-0.046	1.128	1.231	-0.103	1.162	1.190	-0.028	1.369	0.982	0.386	1.258	1.099	0.159	0.217	0.184	0.792	0.2140
49	1.148	1.126	1.171	-0.045	1.101	1.202	-0.101	1.135	1.162	-0.027	1.338	0.958	0.380	1.228	1.074	0.154	0.213	0.185	0.658	0.2551
50	1.122	1.100	1.144	-0.044	1.075	1.175	-0.100	1.109	1.135	-0.026	1.309	0.934	0.375	1.198	1.050	0.148	0.209	0.187	0.528	0.2989
51	1.096	1.075	1.119	-0.044	1.050	1.149	-0.098	1.084	1.109	-0.025	1.281	0.911	0.369	1.170	1.027	0.143	0.206	0.188	0.400	0.3447
52	1.071	1.051	1.094	-0.043	1.027	1.124	-0.097	1.059	1.084	-0.024	1.254	0.889	0.364	1.143	1.005	0.138	0.202	0.189	0.275	0.3917
53	1.048	1.027	1.070	-0.042	1.003	1.099	-0.096	1.036	1.059	-0.023	1.227	0.868	0.360	1.117	0.984	0.133	0.199	0.190	0.153	0.4392
54	1.025	1.004	1.046	-0.042	0.981	1.076	-0.095	1.014	1.036	-0.023	1.202	0.847	0.355	1.091	0.963	0.128	0.196	0.191	0.034	0.4864
55	1.003	0.983	1.024	-0.041	0.959	1.053	-0.093	0.992	1.014	-0.022	1.178	0.827	0.351	1.067	0.943	0.124	0.193	0.193	-0.082	0.5327
56	0.981	0.961	1.002	-0.041	0.938	1.031	-0.092	0.971	0.992	-0.021	1.154	0.808	0.346	1.043	0.924	0.119	0.190	0.194	-0.196	0.5775
57	0.960	0.941	0.981	-0.040	0.918	1.009	-0.091	0.950	0.971	-0.020	1.131	0.789	0.342	1.020	0.905	0.115	0.188	0.195	-0.306	0.6202
58	0.940	0.921	0.961	-0.040	0.898	0.989	-0.090	0.930	0.950	-0.020	1.109	0.771	0.339	0.997	0.887	0.110	0.185	0.197	-0.414	0.6605
59	0.921	0.902	0.941	-0.039	0.879	0.969	-0.089	0.911	0.930	-0.019	1.088	0.753	0.335	0.976	0.870	0.106	0.183	0.198	-0.519	0.6981
60	0.902	0.883	0.922	-0.039	0.861	0.949	-0.088	0.892	0.911	-0.019	1.068	0.736	0.332	0.955	0.853	0.102	0.180	0.200	-0.621	0.7328
61	0.883	0.865	0.903	-0.039	0.843	0.930	-0.087	0.874	0.892	-0.018	1.048	0.719	0.328	0.934	0.836	0.098	0.178	0.202	-0.721	0.7646
62	0.866	0.847	0.885	-0.038	0.825	0.912	-0.087	0.857	0.874	-0.018	1.028	0.703	0.325	0.914	0.820	0.094	0.176	0.203	-0.818	0.7934
63	0.848	0.830	0.868	-0.038	0.808	0.894	-0.086	0.840	0.857	-0.017	1.009	0.687	0.322	0.895	0.805	0.090	0.174	0.205	-0.913	0.8193
64	0.831	0.813	0.851	-0.038	0.792	0.877	-0.085	0.823	0.840	-0.017	0.991	0.672	0.319	0.876	0.790	0.086	0.172	0.207	-1.004	0.8424
65	0.815	0.797	0.834	-0.037	0.776	0.860	-0.084	0.807	0.823	-0.016	0.973	0.656	0.317	0.858	0.775	0.082	0.170	0.209	-1.094	0.8630
66	0.799	0.781	0.818	-0.037	0.760	0.844	-0.084	0.791	0.807	-0.016	0.956	0.642	0.314	0.840	0.761	0.079	0.169	0.211	-1.180	0.8811
67	0.783	0.766	0.802	-0.037	0.745	0.828	-0.083	0.776	0.791	-0.015	0.939	0.627	0.312	0.822	0.747	0.075	0.167	0.213	-1.264	0.8969
68	0.768	0.751	0.787	-0.037	0.730	0.813	-0.083	0.761	0.776	-0.015	0.923	0.613	0.310	0.805	0.734	0.071	0.165	0.215	-1.346	0.9108
69	0.753	0.736	0.772	-0.036	0.716	0.797	-0.082	0.746	0.761	-0.015	0.907	0.600	0.308	0.789	0.721	0.068	0.164	0.218	-1.424	0.9228
70	0.739	0.722	0.758	-0.036	0.701	0.783	-0.081	0.732	0.746	-0.014	0.892	0.586	0.306	0.772	0.708	0.064	0.163	0.220	-1.501	0.9333
71	0.725	0.708	0.743	-0.036	0.687	0.768	-0.081	0.718	0.732	-0.014	0.877	0.573	0.304	0.756	0.696	0.061	0.161	0.222	-1.574	0.9423

Internal GCL Large-Displacement, t = 3 m

E(ψ)	$FS_{MLV,\ LD}$	t			γ			ψ			C_d			ϕ			$\sigma_{FS,LD}$	$V_{FS,\ LD}$	β_{LN}	P_F
		FS_i^+	FS_i^-	ΔFS_i	FS_i^+	FS_i^-	ΔFS_i	FS_i^+	FS_i^-	ΔFS_i	FS_i^+	FS_i^-	ΔFS_i	FS_i^+	FS_i^-	ΔFS_i				
5	4.791	4.694	4.894	-0.199	4.582	5.033	-0.451	4.355	5.323	-0.968	6.605	2.976	3.629	5.290	4.298	0.992	1.958	0.409	3.790	7.549E-05
6	3.992	3.912	4.078	-0.166	3.818	4.194	-0.376	3.685	4.355	-0.670	5.505	2.479	3.026	4.408	3.582	0.826	1.617	0.405	3.357	3.943E-04
7	3.421	3.352	3.495	-0.143	3.272	3.595	-0.322	3.193	3.685	-0.492	4.719	2.124	2.595	3.777	3.070	0.707	1.379	0.403	2.977	1.454E-03
8	2.993	2.933	3.058	-0.125	2.863	3.145	-0.282	2.817	3.193	-0.376	4.130	1.857	2.273	3.304	2.687	0.618	1.202	0.402	2.641	4.128E-03
9	2.660	2.607	2.718	-0.111	2.544	2.795	-0.251	2.520	2.817	-0.297	3.671	1.650	2.022	2.936	2.388	0.548	1.067	0.401	2.341	9.613E-03
10	2.394	2.346	2.446	-0.100	2.289	2.516	-0.226	2.280	2.520	-0.240	3.305	1.483	1.821	2.642	2.150	0.492	0.959	0.401	2.070	1.922E-02
11	2.176	2.132	2.223	-0.091	2.081	2.287	-0.206	2.081	2.280	-0.199	3.005	1.347	1.658	2.401	1.954	0.447	0.871	0.400	1.824	3.411E-02
12	1.995	1.954	2.038	-0.084	1.907	2.096	-0.189	1.915	2.081	-0.167	2.755	1.234	1.521	2.200	1.792	0.408	0.799	0.400	1.597	0.055
13	1.841	1.803	1.881	-0.077	1.760	1.935	-0.175	1.772	1.915	-0.142	2.544	1.138	1.406	2.030	1.654	0.376	0.737	0.401	1.389	0.082
14	1.709	1.674	1.746	-0.072	1.634	1.796	-0.162	1.650	1.772	-0.123	2.363	1.055	1.307	1.884	1.536	0.348	0.685	0.401	1.195	0.116
15	1.595	1.562	1.629	-0.067	1.525	1.676	-0.152	1.543	1.650	-0.107	2.206	0.984	1.222	1.758	1.434	0.324	0.640	0.401	1.015	0.155
16	1.495	1.464	1.527	-0.063	1.429	1.571	-0.143	1.449	1.543	-0.094	2.069	0.921	1.148	1.647	1.344	0.303	0.600	0.402	0.846	0.199
17	1.407	1.378	1.437	-0.059	1.344	1.479	-0.134	1.366	1.449	-0.083	1.947	0.866	1.082	1.549	1.266	0.284	0.566	0.402	0.688	0.246
18	1.328	1.301	1.357	-0.056	1.269	1.396	-0.127	1.292	1.366	-0.074	1.840	0.816	1.024	1.463	1.195	0.267	0.535	0.403	0.538	0.295
19	1.258	1.232	1.286	-0.053	1.202	1.323	-0.121	1.226	1.292	-0.067	1.744	0.772	0.972	1.385	1.133	0.252	0.507	0.403	0.397	0.346
20	1.195	1.170	1.221	-0.051	1.142	1.256	-0.115	1.165	1.226	-0.060	1.657	0.732	0.925	1.315	1.076	0.239	0.483	0.404	0.263	0.396
21	1.138	1.114	1.163	-0.049	1.087	1.196	-0.110	1.111	1.165	-0.055	1.579	0.696	0.883	1.251	1.025	0.226	0.460	0.405	0.136	0.446
22	1.086	1.063	1.110	-0.046	1.037	1.142	-0.105	1.061	1.111	-0.050	1.508	0.663	0.844	1.194	0.979	0.215	0.440	0.405	0.015	0.494
23	1.038	1.017	1.061	-0.044	0.992	1.092	-0.101	1.016	1.061	-0.045	1.443	0.633	0.810	1.141	0.936	0.205	0.422	0.406	-0.100	0.540
24	0.995	0.974	1.017	-0.043	0.950	1.046	-0.097	0.974	1.016	-0.042	1.383	0.606	0.778	1.093	0.898	0.195	0.405	0.407	-0.210	0.583
25	0.954	0.935	0.976	-0.041	0.911	1.004	-0.093	0.936	0.974	-0.038	1.329	0.580	0.748	1.048	0.862	0.186	0.389	0.408	-0.315	0.624
26	0.917	0.898	0.938	-0.040	0.876	0.966	-0.090	0.900	0.936	-0.036	1.278	0.557	0.722	1.007	0.829	0.178	0.375	0.409	-0.416	0.661
27	0.883	0.865	0.903	-0.038	0.843	0.930	-0.087	0.867	0.900	-0.033	1.232	0.535	0.697	0.969	0.799	0.170	0.362	0.410	-0.512	0.696
28	0.851	0.833	0.870	-0.037	0.813	0.896	-0.084	0.836	0.867	-0.031	1.188	0.514	0.674	0.934	0.770	0.163	0.350	0.411	-0.605	0.727
29	0.822	0.804	0.840	-0.036	0.784	0.865	-0.081	0.808	0.836	-0.029	1.148	0.495	0.652	0.901	0.744	0.157	0.339	0.412	-0.694	0.756
30	0.794	0.777	0.812	-0.035	0.758	0.836	-0.079	0.781	0.808	-0.027	1.110	0.478	0.633	0.870	0.719	0.150	0.328	0.413	-0.779	0.782
31	0.768	0.752	0.786	-0.034	0.733	0.809	-0.076	0.756	0.781	-0.025	1.075	0.461	0.614	0.841	0.696	0.144	0.318	0.415	-0.862	0.806
32	0.744	0.728	0.761	-0.033	0.710	0.784	-0.074	0.732	0.756	-0.024	1.042	0.445	0.597	0.814	0.675	0.139	0.309	0.416	-0.941	0.827
33	0.721	0.706	0.738	-0.032	0.688	0.760	-0.072	0.710	0.732	-0.022	1.011	0.431	0.581	0.788	0.655	0.134	0.301	0.417	-1.017	0.845
34	0.700	0.685	0.716	-0.031	0.667	0.737	-0.070	0.689	0.710	-0.021	0.982	0.417	0.566	0.764	0.636	0.129	0.293	0.419	-1.090	0.862
35	0.679	0.665	0.695	-0.030	0.648	0.716	-0.069	0.670	0.689	-0.020	0.955	0.404	0.551	0.742	0.618	0.124	0.285	0.420	-1.161	0.877
36	0.660	0.646	0.675	-0.030	0.629	0.696	-0.067	0.651	0.670	-0.019	0.929	0.391	0.538	0.720	0.601	0.119	0.278	0.421	-1.229	0.891
37	0.642	0.628	0.657	-0.029	0.612	0.677	-0.065	0.633	0.651	-0.018	0.905	0.379	0.526	0.700	0.585	0.115	0.272	0.423	-1.295	0.902
38	0.625	0.611	0.639	-0.028	0.595	0.659	-0.064	0.617	0.633	-0.017	0.882	0.368	0.514	0.681	0.570	0.111	0.265	0.424	-1.359	0.913
39	0.609	0.595	0.623	-0.028	0.580	0.642	-0.062	0.601	0.617	-0.016	0.860	0.357	0.503	0.663	0.555	0.107	0.259	0.426	-1.420	0.922
40	0.593	0.580	0.607	-0.027	0.565	0.626	-0.061	0.586	0.601	-0.015	0.839	0.347	0.492	0.645	0.542	0.103	0.254	0.428	-1.479	0.930
41	0.578	0.566	0.592	-0.026	0.551	0.611	-0.060	0.571	0.586	-0.014	0.819	0.337	0.482	0.629	0.529	0.100	0.248	0.430	-1.536	0.938
42	0.564	0.552	0.578	-0.026	0.537	0.596	-0.059	0.558	0.571	-0.014	0.801	0.328	0.473	0.613	0.516	0.096	0.243	0.431	-1.591	0.944
43	0.551	0.539	0.564	-0.025	0.524	0.582	-0.058	0.545	0.558	-0.013	0.783	0.319	0.464	0.598	0.505	0.093	0.239	0.433	-1.645	0.950
44	0.538	0.526	0.551	-0.025	0.512	0.569	-0.057	0.532	0.545	-0.012	0.766	0.311	0.455	0.583	0.494	0.090	0.234	0.435	-1.696	0.955
45	0.526	0.514	0.539	-0.025	0.500	0.556	-0.056	0.520	0.532	-0.012	0.750	0.302	0.447	0.570	0.483	0.087	0.230	0.437	-1.745	0.960
46	0.514	0.503	0.527	-0.024	0.489	0.544	-0.055	0.509	0.520	-0.011	0.734	0.294	0.440	0.557	0.473	0.084	0.226	0.439	-1.793	0.964
47	0.503	0.492	0.515	-0.024	0.478	0.532	-0.054	0.498	0.509	-0.011	0.719	0.287	0.432	0.544	0.463	0.081	0.222	0.441	-1.839	0.967
48	0.492	0.481	0.505	-0.023	0.468	0.521	-0.053	0.487	0.498	-0.010	0.705	0.280	0.426	0.532	0.454	0.078	0.218	0.443	-1.884	0.970
49	0.482	0.471	0.494	-0.023	0.458	0.510	-0.052	0.477	0.487	-0.010	0.692	0.273	0.419	0.520	0.445	0.075	0.215	0.446	-1.927	0.973
50	0.472	0.461	0.484	-0.023	0.449	0.500	-0.051	0.468	0.477	-0.010	0.679	0.266	0.413	0.509	0.436	0.073	0.212	0.448	-1.968	0.975
51	0.463	0.452	0.474	-0.022	0.439	0.490	-0.051	0.458	0.468	-0.009	0.666	0.259	0.407	0.498	0.428	0.070	0.208	0.450	-2.008	0.978
52	0.454	0.443	0.465	-0.022	0.431	0.481	-0.050	0.449	0.458	-0.009	0.654	0.253	0.401	0.488	0.420	0.068	0.205	0.453	-2.046	0.980
53	0.445	0.434	0.456	-0.022	0.422	0.471	-0.049	0.441	0.449	-0.009	0.643	0.247	0.396	0.478	0.412	0.065	0.203	0.455	-2.083	0.981
54	0.437	0.426	0.448	-0.021	0.414	0.463	-0.049	0.432	0.441	-0.008	0.632	0.241	0.391	0.468	0.405	0.063	0.200	0.458	-2.119	0.983
55	0.428	0.418	0.439	-0.021	0.406	0.454	-0.048	0.424	0.432	-0.008	0.621	0.235	0.386	0.459	0.398	0.061	0.197	0.460	-2.153	0.984
56	0.421	0.410	0.431	-0.021	0.399	0.446	-0.047	0.417	0.424	-0.008	0.611	0.230	0.382	0.450	0.391	0.059	0.195	0.463	-2.185	0.986
57	0.413	0.403	0.424	-0.021	0.391	0.438	-0.047	0.409	0.417	-0.007	0.602	0.224	0.377	0.441	0.385	0.056	0.192	0.466	-2.217	0.987
58	0.406	0.396	0.416	-0.020	0.384	0.431	-0.046	0.402	0.409	-0.007	0.592	0.219	0.373	0.433	0.379	0.054	0.190	0.469	-2.247	0.988
59	0.399	0.389	0.409	-0.020	0.377	0.423	-0.046	0.395	0.402	-0.007	0.583	0.214	0.369	0.425	0.373	0.052	0.188	0.472	-2.276	0.989
60	0.392	0.382	0.402	-0.020	0.371	0.416	-0.045	0.388	0.395	-0.007	0.574	0.209	0.365	0.417	0.367	0.050	0.186	0.475	-2.304	0.989
61	0.385	0.376	0.395	-0.020	0.364	0.409	-0.045	0.382	0.388	-0.006	0.566	0.204	0.362	0.409	0.361	0.048	0.184	0.478	-2.330	0.990
62	0.379	0.369	0.389	-0.020	0.358	0.403	-0.045	0.376	0.382	-0.006	0.558	0.200	0.358	0.402	0.356	0.046	0.182	0.481	-2.355	0.991
63	0.373	0.363	0.383	-0.020	0.352	0.396	-0.044	0.370	0.376	-0.006	0.550	0.195	0.355	0.395	0.351	0.044	0.181	0.484	-2.380	0.991
64	0.367	0.357	0.377	-0.019	0.346	0.390	-0.044	0.364	0.370	-0.006	0.543	0.191	0.352	0.388	0.346	0.042	0.179	0.488	-2.403	0.992
65	0.361	0.352	0.371	-0.019	0.341	0.384	-0.043	0.358	0.364	-0.006	0.535	0.186	0.349	0.381	0.341	0.040	0.177	0.491	-2.425	0.992
66	0.355	0.346	0.365	-0.019	0.335	0.378	-0.043	0.353	0.358	-0.006	0.528	0.182	0.346	0.375	0.336	0.039	0.176	0.495	-2.445	0.993
67	0.350	0.341	0.360	-0.019	0.330	0.373	-0.043	0.347	0.353	-0.005	0.522	0.178	0.344	0.368	0.332	0.037	0.174	0.498	-2.465	0.993
68	0.345	0.336	0.354	-0.019	0.325	0.367	-0.042	0.342	0.347	-0.005	0.515	0.174	0.341	0.362	0.327	0.035	0.173	0.502	-2.484	0.993
69	0.340	0.331	0.349	-0.019	0.320	0.362	-0.042	0.337	0.342	-0.005	0.509	0.170	0.339	0.356	0.323	0.033	0.172	0.506	-2.501	0.994
70	0.335	0.326	0.344	-0.018	0.315	0.357	-0.042	0.332	0.337	-0.005	0.503	0.166	0.337	0.350	0.319	0.032	0.171	0.510	-2.518	0.994
71	0.330	0.321	0.339	-0.018	0.311	0.352	-0.042	0.327	0.332	-0.005	0.497	0.163	0.335	0.345	0.315	0.030	0.169	0.514	-2.534	0.994

GCL-Geomembrane Interface

$E(t_1)$ =	1	m
$E(t_2)$ =	3	m
s(t) =	0.1	m
$E(\gamma)$ =	20	kN/m^3
$s(\gamma)$ =	1.5	kN/m^3
$s(\psi)$ =	0.5	degrees
$E(\phi_P)$ =	20.60	degrees
$s(\phi_P)$ =	3.25	degrees
$E(C_{A,P})$ =	7.43	kPa
$s(C_{A,P})$ =	5.11	kPa
$E(\phi_{LD})$ =	12.34	degrees
$s(\phi_{LD})$ =	1.78	degrees
$E(C_{A,LD})$ =	5.13	kPa
$s(C_{A,LD})$ =	2.49	kPa

$$FS = \frac{C_A}{\gamma H \sin\psi} + \frac{\tan\phi}{\tan\psi}$$

GCL-GM Peak t = 1 m

E(ψ)	$FS_{MLV,\ Peak}$	t			γ			ψ			C_A			ϕ			$\sigma_{FS,Peak}$	$V_{FS,\ Peak}$	β_{LN}	P_F
		FS_t^+	FS_t^-	ΔFS_t	FS_γ^+	FS_γ^-	ΔFS_γ	FS_ψ^+	FS_ψ^-	ΔFS_ψ	$FS_{C_A}^+$	$FS_{C_A}^-$	ΔFS_{C_A}	FS_ϕ^+	FS_ϕ^-	ΔFS_ϕ				
5	23.714	22.128	25.654	-3.526	22.497	25.130	-2.633	21.560	26.348	-4.788	28.656	18.773	9.884	24.762	22.742	2.019	6.001	0.253	12.583	0.000E+00
6	19.764	18.441	21.381	-2.940	18.749	20.944	-2.195	18.245	21.560	-3.315	23.885	15.644	8.241	20.636	18.955	1.681	4.878	0.247	12.149	0.000E+00
7	16.943	15.808	18.330	-2.522	16.072	17.955	-1.883	15.815	18.245	-2.430	20.477	13.409	7.068	17.689	16.251	1.439	4.118	0.243	11.692	0.000E+00
8	14.828	13.834	16.042	-2.208	14.065	15.714	-1.649	13.957	15.815	-1.858	17.922	11.733	6.189	15.479	14.223	1.257	3.569	0.241	11.245	0.000E+00
9	13.182	12.298	14.263	-1.965	12.504	13.971	-1.467	12.490	13.957	-1.467	15.936	10.429	5.506	13.761	12.646	1.115	3.152	0.239	10.821	0.000E+00
10	11.867	11.070	12.840	-1.770	11.255	12.577	-1.322	11.303	12.490	-1.187	14.347	9.386	4.961	12.386	11.384	1.002	2.824	0.238	10.422	0.000E+00
11	10.790	10.065	11.676	-1.611	10.234	11.437	-1.203	10.322	11.303	-0.980	13.047	8.533	4.514	11.262	10.353	0.909	2.560	0.237	10.049	0.000E+00
12	9.893	9.228	10.706	-1.478	9.383	10.487	-1.104	9.499	10.322	-0.823	11.965	7.822	4.143	10.324	9.493	0.831	2.342	0.237	9.699	0.000E+00
13	9.135	8.520	9.886	-1.366	8.663	9.683	-1.020	8.798	9.499	-0.701	11.050	7.220	3.829	9.532	8.767	0.765	2.159	0.236	9.371	0.000E+00
14	8.485	7.913	9.184	-1.270	8.046	8.995	-0.949	8.194	8.798	-0.604	10.265	6.705	3.561	8.852	8.144	0.708	2.004	0.236	9.063	0.000E+00
15	7.922	7.387	8.575	-1.187	7.512	8.398	-0.887	7.667	8.194	-0.526	9.586	6.258	3.328	8.264	7.604	0.659	1.870	0.236	8.772	0.000E+00
16	7.429	6.927	8.042	-1.115	7.044	7.877	-0.833	7.205	7.667	-0.462	8.992	5.866	3.125	7.749	7.132	0.616	1.753	0.236	8.497	0.000E+00
17	6.995	6.522	7.573	-1.051	6.632	7.416	-0.785	6.796	7.205	-0.409	8.468	5.521	2.946	7.294	6.716	0.578	1.651	0.236	8.237	0.000
18	6.608	6.161	7.155	-0.995	6.265	7.008	-0.743	6.431	6.796	-0.365	8.002	5.215	2.788	6.890	6.347	0.544	1.560	0.236	7.991	0.000
19	6.263	5.838	6.782	-0.944	5.937	6.642	-0.705	6.104	6.431	-0.327	7.586	4.940	2.646	6.529	6.016	0.513	1.480	0.236	7.756	0.000
20	5.953	5.548	6.447	-0.899	5.642	6.313	-0.671	5.809	6.104	-0.295	7.212	4.693	2.519	6.204	5.719	0.485	1.407	0.236	7.532	0.000
21	5.672	5.286	6.143	-0.858	5.376	6.016	-0.640	5.541	5.809	-0.268	6.874	4.470	2.404	5.910	5.450	0.460	1.342	0.237	7.318	0.000
22	5.417	5.047	5.868	-0.820	5.133	5.746	-0.613	5.297	5.541	-0.244	6.566	4.267	2.299	5.643	5.206	0.437	1.283	0.237	7.113	0.000
23	5.184	4.830	5.616	-0.787	4.912	5.499	-0.587	5.075	5.297	-0.223	6.286	4.081	2.205	5.399	4.983	0.416	1.229	0.237	6.917	0.000
24	4.970	4.630	5.386	-0.756	4.709	5.274	-0.564	4.870	5.075	-0.204	6.029	3.911	2.118	5.176	4.779	0.397	1.180	0.237	6.728	0.000
25	4.774	4.447	5.174	-0.727	4.523	5.066	-0.543	4.682	4.870	-0.188	5.793	3.755	2.038	4.971	4.592	0.379	1.135	0.238	6.547	0.000
26	4.593	4.278	4.979	-0.701	4.351	4.875	-0.523	4.508	4.682	-0.174	5.576	3.611	1.965	4.781	4.419	0.362	1.094	0.238	6.372	0.000
27	4.426	4.121	4.798	-0.677	4.192	4.697	-0.505	4.347	4.508	-0.161	5.374	3.477	1.897	4.606	4.259	0.347	1.056	0.239	6.204	0.000
28	4.270	3.976	4.630	-0.655	4.044	4.533	-0.489	4.197	4.347	-0.150	5.188	3.353	1.835	4.443	4.110	0.332	1.021	0.239	6.041	0.000
29	4.126	3.841	4.475	-0.634	3.907	4.380	-0.473	4.057	4.197	-0.140	5.014	3.237	1.777	4.291	3.972	0.319	0.988	0.239	5.884	0.000
30	3.991	3.715	4.329	-0.615	3.779	4.238	-0.459	3.927	4.057	-0.130	4.853	3.130	1.723	4.150	3.844	0.306	0.957	0.240	5.733	0.000
31	3.865	3.597	4.193	-0.597	3.659	4.105	-0.446	3.805	3.927	-0.122	4.701	3.029	1.673	4.018	3.724	0.294	0.929	0.240	5.586	0.000
32	3.747	3.486	4.066	-0.580	3.547	3.980	-0.433	3.691	3.805	-0.114	4.560	2.934	1.626	3.894	3.611	0.283	0.903	0.241	5.443	0.000
33	3.636	3.383	3.947	-0.564	3.442	3.863	-0.421	3.584	3.691	-0.107	4.427	2.846	1.582	3.778	3.506	0.272	0.878	0.241	5.305	0.000
34	3.532	3.285	3.835	-0.550	3.343	3.753	-0.410	3.483	3.584	-0.101	4.303	2.762	1.540	3.668	3.406	0.262	0.855	0.242	5.171	0.000
35	3.434	3.193	3.729	-0.536	3.249	3.649	-0.400	3.388	3.483	-0.095	4.185	2.683	1.502	3.565	3.313	0.252	0.833	0.243	5.041	0.000
36	3.342	3.107	3.630	-0.523	3.161	3.552	-0.390	3.298	3.388	-0.090	4.075	2.609	1.466	3.468	3.225	0.243	0.813	0.243	4.915	0.000
37	3.255	3.025	3.535	-0.511	3.078	3.460	-0.381	3.213	3.298	-0.085	3.970	2.539	1.431	3.376	3.142	0.234	0.793	0.244	4.792	0.000
38	3.172	2.947	3.446	-0.499	3.000	3.372	-0.373	3.132	3.213	-0.080	3.872	2.472	1.399	3.289	3.063	0.226	0.775	0.244	4.673	0.000
39	3.094	2.874	3.362	-0.488	2.925	3.290	-0.365	3.056	3.132	-0.076	3.778	2.409	1.369	3.207	2.989	0.218	0.758	0.245	4.556	0.000
40	3.019	2.804	3.282	-0.478	2.854	3.211	-0.357	2.984	3.056	-0.072	3.689	2.349	1.340	3.129	2.918	0.211	0.742	0.246	4.443	0.000
41	2.949	2.738	3.206	-0.468	2.787	3.137	-0.350	2.915	2.984	-0.069	3.605	2.292	1.313	3.054	2.851	0.203	0.727	0.246	4.333	0.000
42	2.882	2.675	3.134	-0.459	2.723	3.066	-0.343	2.849	2.915	-0.065	3.525	2.238	1.287	2.983	2.787	0.196	0.712	0.247	4.225	0.000
43	2.818	2.615	3.066	-0.451	2.662	2.999	-0.336	2.787	2.849	-0.062	3.449	2.186	1.263	2.916	2.727	0.189	0.698	0.248	4.121	0.000
44	2.757	2.558	3.000	-0.442	2.604	2.935	-0.330	2.728	2.787	-0.059	3.377	2.137	1.240	2.852	2.669	0.183	0.685	0.249	4.019	0.000

Large Displacement, t = 1 m

E(ψ)	$FS_{MLV,\ LD}$	t			γ			ψ			C_d			ϕ			$\sigma_{FS,LD}$	$V_{FS,\ LD}$	β_{LN}	P_F
		FS_i^+	FS_i^-	ΔFS_i	FS_i^+	FS_i^-	ΔFS_i	FS_i^+	FS_i^-	ΔFS_i	FS_i^+	FS_i^-	ΔFS_i	FS_i^+	FS_i^-	ΔFS_i				
5	5.441	5.174	5.768	-0.594	5.236	5.679	-0.444	4.946	6.046	-1.100	6.870	4.012	2.858	5.816	5.071	0.745	1.619	0.298	5.670	7.149E-09
6	4.533	4.310	4.806	-0.495	4.362	4.732	-0.370	4.184	4.946	-0.762	5.725	3.342	2.383	4.845	4.225	0.620	1.325	0.292	5.134	1.419E-07
7	3.885	3.693	4.118	-0.425	3.738	4.055	-0.317	3.625	4.184	-0.559	4.907	2.863	2.044	4.152	3.621	0.531	1.124	0.289	4.644	1.709E-06
8	3.398	3.231	3.603	-0.372	3.270	3.547	-0.278	3.198	3.625	-0.427	4.293	2.503	1.790	3.631	3.168	0.464	0.977	0.287	4.200	1.336E-05
9	3.019	2.871	3.202	-0.331	2.905	3.152	-0.247	2.860	3.198	-0.338	3.816	2.223	1.592	3.227	2.815	0.411	0.865	0.286	3.797	7.337E-05
10	2.717	2.582	2.881	-0.298	2.614	2.836	-0.223	2.587	2.860	-0.273	3.434	1.999	1.435	2.903	2.533	0.370	0.776	0.286	3.429	3.031E-04
11	2.469	2.346	2.618	-0.271	2.375	2.578	-0.203	2.361	2.587	-0.226	3.121	1.816	1.306	2.637	2.302	0.335	0.704	0.285	3.092	9.951E-04
12	2.262	2.150	2.399	-0.249	2.176	2.362	-0.186	2.171	2.361	-0.190	2.861	1.663	1.198	2.416	2.110	0.307	0.645	0.285	2.781	0.003
13	2.087	1.983	2.213	-0.230	2.007	2.179	-0.172	2.009	2.171	-0.162	2.641	1.533	1.107	2.229	1.947	0.282	0.595	0.285	2.493	0.006
14	1.937	1.840	2.055	-0.214	1.863	2.023	-0.160	1.869	2.009	-0.140	2.452	1.422	1.030	2.068	1.807	0.261	0.552	0.285	2.225	0.013
15	1.807	1.717	1.917	-0.200	1.738	1.887	-0.149	1.748	1.869	-0.122	2.288	1.325	0.962	1.929	1.686	0.243	0.515	0.285	1.975	0.024
16	1.693	1.608	1.796	-0.188	1.628	1.768	-0.140	1.641	1.748	-0.107	2.145	1.241	0.904	1.807	1.580	0.227	0.483	0.286	1.740	0.041
17	1.592	1.512	1.690	-0.177	1.531	1.663	-0.132	1.546	1.641	-0.095	2.018	1.166	0.852	1.699	1.486	0.213	0.455	0.286	1.519	0.064
18	1.503	1.427	1.595	-0.168	1.445	1.570	-0.125	1.462	1.546	-0.085	1.906	1.100	0.806	1.604	1.403	0.201	0.430	0.286	1.310	0.095
19	1.423	1.351	1.510	-0.159	1.368	1.486	-0.119	1.386	1.462	-0.076	1.805	1.040	0.765	1.518	1.329	0.189	0.408	0.287	1.112	0.133
20	1.350	1.282	1.434	-0.151	1.298	1.411	-0.113	1.317	1.386	-0.069	1.715	0.986	0.728	1.440	1.261	0.179	0.388	0.288	0.925	0.177
21	1.285	1.220	1.365	-0.145	1.235	1.343	-0.108	1.255	1.317	-0.062	1.633	0.937	0.695	1.370	1.201	0.170	0.370	0.288	0.747	0.228
22	1.226	1.163	1.302	-0.138	1.178	1.281	-0.103	1.198	1.255	-0.057	1.558	0.893	0.665	1.307	1.146	0.161	0.354	0.289	0.577	0.282
23	1.171	1.112	1.244	-0.133	1.126	1.224	-0.099	1.146	1.198	-0.052	1.490	0.853	0.638	1.249	1.095	0.153	0.339	0.290	0.415	0.339
24	1.121	1.064	1.191	-0.127	1.077	1.173	-0.095	1.098	1.146	-0.048	1.428	0.815	0.612	1.195	1.049	0.146	0.326	0.290	0.261	0.397
25	1.076	1.020	1.143	-0.123	1.033	1.125	-0.091	1.054	1.098	-0.044	1.370	0.781	0.589	1.146	1.006	0.140	0.313	0.291	0.113	0.455
26	1.033	0.980	1.098	-0.118	0.992	1.081	-0.088	1.013	1.054	-0.041	1.317	0.749	0.568	1.100	0.967	0.134	0.302	0.292	-0.029	0.512
27	0.994	0.943	1.057	-0.114	0.954	1.040	-0.085	0.975	1.013	-0.038	1.268	0.720	0.549	1.058	0.930	0.128	0.291	0.293	-0.165	0.565
28	0.957	0.908	1.018	-0.110	0.919	1.002	-0.082	0.940	0.975	-0.035	1.223	0.692	0.531	1.019	0.896	0.123	0.281	0.294	-0.295	0.616
29	0.923	0.875	0.982	-0.107	0.886	0.966	-0.080	0.907	0.940	-0.033	1.180	0.666	0.514	0.982	0.865	0.118	0.272	0.295	-0.421	0.663
30	0.891	0.845	0.948	-0.104	0.856	0.933	-0.077	0.876	0.907	-0.031	1.141	0.642	0.498	0.948	0.835	0.113	0.264	0.296	-0.541	0.706
31	0.862	0.816	0.917	-0.101	0.827	0.902	-0.075	0.847	0.876	-0.029	1.104	0.620	0.484	0.916	0.808	0.108	0.256	0.297	-0.657	0.744
32	0.834	0.790	0.887	-0.098	0.800	0.873	-0.073	0.820	0.847	-0.027	1.069	0.599	0.470	0.886	0.782	0.104	0.249	0.298	-0.769	0.779
33	0.807	0.765	0.860	-0.095	0.775	0.846	-0.071	0.795	0.820	-0.026	1.036	0.579	0.457	0.858	0.758	0.100	0.242	0.300	-0.876	0.810
34	0.783	0.741	0.834	-0.093	0.751	0.820	-0.069	0.771	0.795	-0.024	1.005	0.560	0.445	0.831	0.735	0.097	0.235	0.301	-0.980	0.836
35	0.759	0.719	0.809	-0.090	0.728	0.795	-0.067	0.748	0.771	-0.023	0.976	0.542	0.434	0.806	0.713	0.093	0.229	0.302	-1.080	0.860
36	0.737	0.697	0.786	-0.088	0.707	0.772	-0.066	0.727	0.748	-0.022	0.949	0.525	0.424	0.782	0.693	0.090	0.224	0.304	-1.176	0.880
37	0.716	0.677	0.764	-0.086	0.686	0.751	-0.064	0.706	0.727	-0.020	0.923	0.509	0.414	0.760	0.673	0.086	0.218	0.305	-1.269	0.898
38	0.696	0.658	0.743	-0.084	0.667	0.730	-0.063	0.687	0.706	-0.019	0.899	0.494	0.405	0.738	0.655	0.083	0.213	0.306	-1.358	0.913
39	0.677	0.640	0.723	-0.082	0.649	0.710	-0.061	0.668	0.687	-0.018	0.875	0.479	0.396	0.718	0.637	0.080	0.209	0.308	-1.445	0.926
40	0.659	0.623	0.704	-0.081	0.632	0.692	-0.060	0.651	0.668	-0.018	0.853	0.466	0.388	0.699	0.621	0.078	0.204	0.310	-1.528	0.937
41	0.642	0.607	0.686	-0.079	0.615	0.674	-0.059	0.634	0.651	-0.017	0.832	0.452	0.380	0.680	0.605	0.075	0.200	0.311	-1.608	0.946
42	0.626	0.591	0.669	-0.077	0.599	0.657	-0.058	0.618	0.634	-0.016	0.812	0.440	0.372	0.662	0.590	0.072	0.196	0.313	-1.686	0.954
43	0.610	0.576	0.652	-0.076	0.584	0.641	-0.057	0.603	0.618	-0.015	0.793	0.428	0.365	0.646	0.576	0.070	0.192	0.315	-1.760	0.961
44	0.595	0.562	0.636	-0.075	0.570	0.625	-0.056	0.588	0.603	-0.015	0.775	0.416	0.359	0.629	0.562	0.067	0.188	0.316	-1.833	0.967

GCL-GM Peak, t = 3 m

E(ψ)	$FS_{MLV,\ Peak}$	t			γ			ψ			C_d			ϕ			$\sigma_{FS,Peak}$	$V_{FS,\ Peak}$	β_{LN}	P_F
		FS_i^+	FS_i^-	ΔFS_i	FS_i^+	FS_i^-	ΔFS_i	FS_i^+	FS_i^-	ΔFS_i	FS_i^+	FS_i^-	ΔFS_i	FS_i^+	FS_i^-	ΔFS_i				
5	12.078	11.891	12.279	-0.388	11.672	12.550	-0.878	10.979	13.422	-2.443	13.725	10.431	3.295	13.125	11.106	2.019	2.336	0.193	12.907	0.000E+00
6	10.062	9.906	10.229	-0.324	9.724	10.455	-0.732	9.286	10.979	-1.692	11.436	8.689	2.747	10.934	9.253	1.681	1.862	0.185	12.488	0.000E+00
7	8.621	8.487	8.765	-0.278	8.331	8.959	-0.628	8.045	9.286	-1.241	9.799	7.443	2.356	9.367	7.929	1.439	1.552	0.180	11.975	0.000E+00
8	7.541	7.423	7.666	-0.243	7.286	7.836	-0.550	7.095	8.045	-0.950	8.572	6.509	2.063	8.192	6.935	1.257	1.332	0.177	11.436	0.000E+00
9	6.699	6.595	6.811	-0.216	6.473	6.962	-0.489	6.345	7.095	-0.750	7.617	5.782	1.835	7.278	6.163	1.115	1.168	0.174	10.901	0.000E+00
10	6.026	5.932	6.127	-0.195	5.823	6.263	-0.441	5.738	6.345	-0.608	6.853	5.199	1.654	6.546	5.544	1.002	1.042	0.173	10.384	0.000E+00
11	5.475	5.389	5.567	-0.177	5.290	5.691	-0.401	5.235	5.738	-0.502	6.228	4.723	1.505	5.946	5.038	0.909	0.940	0.172	9.890	0.000E+00
12	5.016	4.937	5.100	-0.163	4.845	5.213	-0.368	4.813	5.235	-0.422	5.706	4.325	1.381	5.447	4.616	0.831	0.857	0.171	9.421	0.000E+00
13	4.626	4.554	4.704	-0.150	4.469	4.809	-0.340	4.453	4.813	-0.360	5.265	3.988	1.276	5.023	4.258	0.765	0.788	0.170	8.976	0.000E+00
14	4.293	4.225	4.365	-0.140	4.146	4.463	-0.316	4.143	4.453	-0.310	4.886	3.699	1.187	4.660	3.952	0.708	0.729	0.170	8.554	0.000E+00
15	4.003	3.940	4.071	-0.131	3.867	4.162	-0.296	3.872	4.143	-0.271	4.558	3.449	1.109	4.345	3.686	0.659	0.679	0.170	8.155	0.000E+00
16	3.750	3.690	3.813	-0.123	3.621	3.899	-0.278	3.634	3.872	-0.238	4.271	3.229	1.042	4.069	3.453	0.616	0.635	0.169	7.775	3.775E-15
17	3.526	3.470	3.586	-0.116	3.405	3.666	-0.262	3.423	3.634	-0.211	4.017	3.035	0.982	3.825	3.248	0.578	0.597	0.169	7.413	0.000
18	3.327	3.274	3.383	-0.110	3.212	3.460	-0.248	3.235	3.423	-0.188	3.791	2.862	0.929	3.608	3.065	0.544	0.563	0.169	7.069	0.000
19	3.148	3.098	3.202	-0.104	3.039	3.274	-0.235	3.066	3.235	-0.169	3.589	2.707	0.882	3.414	2.901	0.513	0.533	0.169	6.740	0.000
20	2.987	2.940	3.038	-0.099	2.884	3.108	-0.224	2.913	3.066	-0.153	3.407	2.568	0.840	3.239	2.754	0.485	0.506	0.169	6.425	0.000
21	2.842	2.796	2.891	-0.094	2.743	2.956	-0.213	2.774	2.913	-0.139	3.242	2.441	0.801	3.080	2.620	0.460	0.482	0.169	6.123	0.000
22	2.709	2.666	2.756	-0.090	2.615	2.819	-0.204	2.647	2.774	-0.127	3.092	2.326	0.766	2.936	2.499	0.437	0.460	0.170	5.834	0.000
23	2.588	2.546	2.633	-0.087	2.498	2.693	-0.196	2.531	2.647	-0.116	2.955	2.221	0.735	2.804	2.388	0.416	0.439	0.170	5.556	0.000
24	2.477	2.437	2.520	-0.083	2.390	2.578	-0.188	2.425	2.531	-0.107	2.830	2.124	0.706	2.683	2.286	0.397	0.421	0.170	5.288	0.000
25	2.374	2.336	2.416	-0.080	2.291	2.472	-0.181	2.326	2.425	-0.098	2.714	2.035	0.679	2.571	2.192	0.379	0.404	0.170	5.030	0.000
26	2.280	2.242	2.320	-0.077	2.199	2.373	-0.174	2.235	2.326	-0.091	2.607	1.952	0.655	2.467	2.105	0.362	0.389	0.171	4.781	0.000
27	2.192	2.156	2.230	-0.075	2.114	2.282	-0.168	2.150	2.235	-0.085	2.508	1.876	0.632	2.372	2.025	0.347	0.375	0.171	4.540	0.000
28	2.110	2.075	2.147	-0.072	2.035	2.198	-0.163	2.071	2.150	-0.079	2.416	1.804	0.612	2.282	1.950	0.332	0.361	0.171	4.307	0.000
29	2.034	2.000	2.070	-0.070	1.961	2.119	-0.158	1.998	2.071	-0.074	2.330	1.738	0.592	2.199	1.881	0.319	0.349	0.172	4.082	0.000
30	1.963	1.930	1.998	-0.068	1.892	2.045	-0.153	1.929	1.998	-0.069	2.250	1.676	0.574	2.121	1.815	0.306	0.338	0.172	3.863	0.000
31	1.896	1.864	1.930	-0.066	1.827	1.976	-0.149	1.864	1.929	-0.065	2.175	1.617	0.558	2.049	1.755	0.294	0.327	0.172	3.651	0.000
32	1.833	1.803	1.866	-0.064	1.767	1.911	-0.144	1.803	1.864	-0.061	2.104	1.562	0.542	1.980	1.697	0.283	0.317	0.173	3.445	0.000
33	1.774	1.744	1.807	-0.062	1.709	1.850	-0.140	1.746	1.803	-0.057	2.038	1.511	0.527	1.915	1.643	0.272	0.308	0.173	3.245	0.001
34	1.719	1.690	1.750	-0.061	1.656	1.792	-0.137	1.692	1.746	-0.054	1.976	1.462	0.513	1.855	1.593	0.262	0.299	0.174	3.051	0.001
35	1.666	1.638	1.697	-0.059	1.605	1.738	-0.133	1.641	1.692	-0.051	1.917	1.416	0.501	1.797	1.545	0.252	0.291	0.174	2.862	0.002
36	1.617	1.589	1.646	-0.058	1.556	1.686	-0.130	1.593	1.641	-0.048	1.861	1.372	0.489	1.743	1.499	0.243	0.283	0.175	2.677	0.004
37	1.569	1.542	1.598	-0.056	1.511	1.638	-0.127	1.547	1.593	-0.046	1.808	1.331	0.477	1.691	1.457	0.234	0.276	0.176	2.498	0.006
38	1.525	1.498	1.553	-0.055	1.467	1.591	-0.124	1.503	1.547	-0.044	1.758	1.291	0.466	1.642	1.416	0.226	0.269	0.176	2.323	0.010
39	1.482	1.456	1.510	-0.054	1.426	1.547	-0.122	1.462	1.503	-0.042	1.710	1.254	0.456	1.595	1.377	0.218	0.262	0.177	2.153	0.016
40	1.442	1.416	1.469	-0.053	1.387	1.506	-0.119	1.422	1.462	-0.040	1.665	1.218	0.447	1.551	1.340	0.211	0.256	0.178	1.987	0.023
41	1.403	1.378	1.430	-0.052	1.349	1.466	-0.117	1.384	1.422	-0.038	1.622	1.184	0.438	1.508	1.305	0.203	0.250	0.178	1.825	0.034
42	1.366	1.342	1.392	-0.051	1.313	1.428	-0.114	1.348	1.384	-0.036	1.581	1.152	0.429	1.468	1.272	0.196	0.245	0.179	1.666	0.048
43	1.331	1.307	1.356	-0.050	1.279	1.391	-0.112	1.314	1.348	-0.034	1.541	1.120	0.421	1.429	1.240	0.189	0.239	0.180	1.512	0.065
44	1.297	1.274	1.322	-0.049	1.246	1.356	-0.110	1.281	1.314	-0.033	1.504	1.090	0.413	1.392	1.209	0.183	0.234	0.181	1.361	0.087

GCL-GM Large -Displacement, t = 3m

E(ψ)	$FS_{MLV,\ LD}$	t			γ			ψ			C_d			ϕ			$\sigma_{FS,LD}$	$V_{FS,\ LD}$	β_{LN}	P_F
		FS_i^+	FS_i^-	ΔFS_i	FS_i^+	FS_i^-	ΔFS_i	FS_i^+	FS_i^-	ΔFS_i	FS_i^+	FS_i^-	ΔFS_i	FS_i^+	FS_i^-	ΔFS_i				
5	3.480	3.449	3.514	-0.065	3.412	3.560	-0.148	3.163	3.868	-0.705	3.957	3.004	0.953	3.855	3.110	0.745	0.705	0.202	6.122	4.634E-10
6	2.898	2.872	2.926	-0.055	2.841	2.965	-0.123	2.674	3.163	-0.488	3.295	2.501	0.794	3.210	2.590	0.620	0.564	0.195	5.424	2.926E-08
7	2.482	2.460	2.507	-0.047	2.433	2.539	-0.106	2.316	2.674	-0.358	2.823	2.142	0.681	2.749	2.219	0.531	0.471	0.190	4.740	1.072E-06
8	2.170	2.150	2.191	-0.041	2.127	2.220	-0.093	2.041	2.316	-0.274	2.468	1.872	0.597	2.404	1.940	0.464	0.405	0.187	4.094	2.123E-05
9	1.927	1.909	1.946	-0.036	1.889	1.971	-0.082	1.825	2.041	-0.217	2.192	1.662	0.531	2.134	1.723	0.411	0.356	0.185	3.492	2.394E-04
10	1.732	1.717	1.749	-0.033	1.698	1.772	-0.074	1.649	1.825	-0.176	1.972	1.493	0.478	1.918	1.549	0.370	0.317	0.183	2.935	1.670E-03
11	1.573	1.559	1.588	-0.030	1.542	1.609	-0.068	1.504	1.649	-0.145	1.791	1.355	0.435	1.742	1.406	0.335	0.286	0.182	2.417	7.825E-03
12	1.440	1.427	1.454	-0.027	1.411	1.473	-0.062	1.381	1.504	-0.122	1.640	1.240	0.399	1.594	1.288	0.307	0.261	0.181	1.936	0.026
13	1.327	1.315	1.340	-0.025	1.301	1.358	-0.057	1.277	1.381	-0.104	1.512	1.143	0.369	1.469	1.187	0.282	0.240	0.181	1.487	0.068
14	1.230	1.219	1.243	-0.024	1.206	1.259	-0.053	1.187	1.277	-0.090	1.402	1.059	0.343	1.362	1.101	0.261	0.222	0.181	1.067	0.143
15	1.146	1.136	1.158	-0.022	1.123	1.173	-0.050	1.108	1.187	-0.079	1.307	0.986	0.321	1.269	1.026	0.243	0.207	0.180	0.673	0.250
16	1.073	1.063	1.083	-0.021	1.051	1.098	-0.047	1.039	1.108	-0.069	1.223	0.922	0.301	1.187	0.960	0.227	0.194	0.180	0.303	0.381
17	1.008	0.998	1.018	-0.020	0.987	1.031	-0.044	0.978	1.039	-0.061	1.150	0.866	0.284	1.115	0.902	0.213	0.182	0.180	-0.047	0.519
18	0.950	0.941	0.959	-0.018	0.930	0.972	-0.042	0.923	0.978	-0.055	1.084	0.815	0.269	1.051	0.850	0.201	0.171	0.180	-0.378	0.647
19	0.898	0.889	0.907	-0.018	0.879	0.919	-0.040	0.874	0.923	-0.049	1.025	0.770	0.255	0.993	0.804	0.189	0.162	0.181	-0.692	0.756
20	0.851	0.843	0.859	-0.017	0.833	0.871	-0.038	0.829	0.874	-0.045	0.972	0.729	0.243	0.941	0.762	0.179	0.154	0.181	-0.991	0.839
21	0.808	0.800	0.816	-0.016	0.792	0.828	-0.036	0.788	0.829	-0.041	0.924	0.692	0.232	0.894	0.724	0.170	0.146	0.181	-1.275	0.899
22	0.769	0.762	0.777	-0.015	0.754	0.788	-0.034	0.751	0.788	-0.037	0.880	0.659	0.222	0.851	0.689	0.161	0.140	0.181	-1.547	0.939
23	0.734	0.727	0.741	-0.015	0.719	0.752	-0.033	0.717	0.751	-0.034	0.840	0.628	0.213	0.811	0.658	0.153	0.133	0.182	-1.806	0.965
24	0.701	0.695	0.709	-0.014	0.687	0.718	-0.032	0.686	0.717	-0.031	0.803	0.599	0.204	0.775	0.629	0.146	0.128	0.182	-2.054	0.980
25	0.671	0.665	0.678	-0.013	0.657	0.688	-0.030	0.657	0.686	-0.029	0.769	0.573	0.196	0.742	0.602	0.140	0.123	0.183	-2.292	0.989
26	0.643	0.637	0.650	-0.013	0.630	0.659	-0.029	0.630	0.657	-0.027	0.738	0.549	0.189	0.711	0.577	0.134	0.118	0.183	-2.520	0.994
27	0.617	0.611	0.624	-0.013	0.604	0.633	-0.028	0.605	0.630	-0.025	0.709	0.526	0.183	0.682	0.554	0.128	0.113	0.184	-2.739	0.997
28	0.593	0.587	0.600	-0.012	0.581	0.608	-0.027	0.582	0.605	-0.023	0.682	0.505	0.177	0.655	0.532	0.123	0.109	0.184	-2.950	0.998
29	0.571	0.565	0.577	-0.012	0.559	0.585	-0.027	0.560	0.582	-0.022	0.656	0.485	0.171	0.630	0.512	0.118	0.105	0.185	-3.153	0.999
30	0.550	0.544	0.556	-0.011	0.538	0.564	-0.026	0.540	0.560	-0.020	0.633	0.467	0.166	0.607	0.494	0.113	0.102	0.185	-3.348	1.000
31	0.530	0.525	0.536	-0.011	0.518	0.543	-0.025	0.520	0.540	-0.019	0.611	0.449	0.161	0.584	0.476	0.108	0.099	0.186	-3.535	1.000
32	0.511	0.506	0.517	-0.011	0.500	0.524	-0.024	0.502	0.520	-0.018	0.590	0.433	0.157	0.564	0.459	0.104	0.095	0.187	-3.716	1.000
33	0.494	0.489	0.499	-0.010	0.483	0.506	-0.024	0.485	0.502	-0.017	0.570	0.417	0.152	0.544	0.444	0.100	0.093	0.188	-3.890	1.000
34	0.477	0.472	0.482	-0.010	0.466	0.489	-0.023	0.469	0.485	-0.016	0.551	0.403	0.148	0.526	0.429	0.097	0.090	0.188	-4.058	1.000
35	0.461	0.457	0.466	-0.010	0.451	0.473	-0.022	0.454	0.469	-0.015	0.534	0.389	0.145	0.508	0.415	0.093	0.087	0.189	-4.220	1.000
36	0.446	0.442	0.451	-0.010	0.436	0.458	-0.022	0.439	0.454	-0.015	0.517	0.376	0.141	0.492	0.402	0.090	0.085	0.190	-4.376	1.000
37	0.432	0.428	0.437	-0.009	0.422	0.444	-0.021	0.425	0.439	-0.014	0.501	0.363	0.138	0.476	0.389	0.086	0.083	0.191	-4.527	1.000
38	0.419	0.414	0.424	-0.009	0.409	0.430	-0.021	0.412	0.425	-0.013	0.486	0.351	0.135	0.461	0.377	0.083	0.080	0.192	-4.671	1.000
39	0.406	0.401	0.411	-0.009	0.396	0.417	-0.020	0.400	0.412	-0.013	0.472	0.340	0.132	0.446	0.366	0.080	0.078	0.193	-4.811	1.000
40	0.394	0.389	0.398	-0.009	0.384	0.404	-0.020	0.388	0.400	-0.012	0.458	0.329	0.129	0.433	0.355	0.078	0.076	0.194	-4.945	1.000
41	0.382	0.378	0.386	-0.009	0.373	0.392	-0.020	0.376	0.388	-0.011	0.445	0.319	0.127	0.420	0.345	0.075	0.075	0.195	-5.074	1.000
42	0.371	0.366	0.375	-0.009	0.362	0.381	-0.019	0.365	0.376	-0.011	0.433	0.309	0.124	0.407	0.335	0.072	0.073	0.196	-5.198	1.000
43	0.360	0.356	0.364	-0.008	0.351	0.370	-0.019	0.355	0.365	-0.011	0.421	0.299	0.122	0.395	0.325	0.070	0.071	0.198	-5.318	1.000
44	0.349	0.346	0.354	-0.008	0.341	0.359	-0.019	0.344	0.355	-0.010	0.409	0.290	0.120	0.383	0.316	0.067	0.070	0.199	-5.432	1.000